SPATIAL MAPPING OF HEAT VULNERABILITY IN ABUJA, THE CAPITAL CITY OF NIGERIA

Joshua, Jonah Kunda

B.Sc., PgD, M.Sc.

A thesis submitted to the School of Geography The University of Nottingham, for the degree of Doctor of Philosophy

August, 2023

Abstract

Urbanisation alters land surface features by replacing natural environments with artificial impervious surfaces (AIS). Such changes modify the thermal properties of cities, making cities more vulnerable to heat, with growing threats to human health. This study mapped the heat vulnerability for human health in Nigeria's capital, Abuja. Landsat imagery and gridded population and socioeconomic variables from the WorldPop database and demographic and health surveys were combined to develop 9 heat vulnerability indicators for a spatial mapping: maps of land surface temperature, AIS, Normalised Difference Vegetation Index, the vulnerable population comprising those aged below 14 and over 65 years, the women population, population density, poverty level, literacy rate, and dwelling quality. The attributes of each indicator were first reclassified based on their relative influence on heat vulnerability using a fundamental scale of 1 to 5, where '1' was designated very low influence and '5' indicated very high influence. The weighted overlay was used for the spatial mapping of the heat vulnerability using an expert's judgment as an input. The study's results reveal a significant relationship between AIS, LST, and NDVI ($p<0.05$). The association between maximum temperature and heat-related mortality was statistically significant as its *p*-value is less than 0.05 in all six locations of the research area, with the informal settlement having a larger correlation (r^2: 0.62) than the city centre (r^2:0.28). 12% and 30% of the map areas are high and very highly heat-vulnerable, while 27% are moderately heat-vulnerable. Low and very low vulnerability regions occupied 23% and 8% of the map. The projections of heat vulnerability to the middle and end of the 21st century using temperature projections from 5 selected CMIP6 GCMs for the low and high forcing scenarios, and demographic and socioeconomic variables show a consistent increase in spatial patterns and temporal trends of the heat vulnerability compared to the heat vulnerability map at present. The study's findings indicate the existence of informal settlements within the high and very high heat-vulnerability areas. Most urban areas with surrounding vegetation cover are moderately vulnerable to heat. Low or very low heat vulnerability exists in regions with water bodies and natural cover, supporting the importance of Blue-Green infrastructures in heat reduction. The heat vulnerability projections could considerably influence heat-related risk in the future, highlighting the need for risk assessments incorporating long-term climatic and socioeconomic indicators. The heat vulnerability maps produced by this research have the potential to serve as a baseline for long-term climate resilience and adaptation plan. The thesis contributes to developing a better understanding of the impacts of extreme temperatures on human health.

Acknowledgment

This research work would not have been possible without the guidance, critical review, and constructive comments of my supervisors, Professor Giles Foody and Professor Simon Gosling. I owe them a debt of gratitude. I am equally grateful to my internal Assessor, Professor Suzanne McGowan for her useful comments and suggestions throughout my studies. My thanks also go to the International Society of Biometeorology's Student and New Partnership, Professor Colin Thorne, Professor Marcus Danjuma, Dr. Istifanus Dafub, and the management of the Nigerian Meteorological Agency and the Federal Ministry of Environment for completing the Heat Vulnerability Survey for this study. Thank you to Environment and Climate Change Canada and WorldClim for providing the downscaled temperature projections used in this study, Gong et al. for providing the global maps of artificial impervious surfaces, WorldPop for providing the gridded socioeconomic data, and the United States Geological Survey for providing the Landsat images used in this study. Lastly, I would like to express my gratitude to my family and friends for their moral support throughout my studies.

Table of Contents

Abstract……..…ii

Acknowledgement…….……....iii

Table of Contents…….....iv

List of Figures ……xi

List of Tables……xvi

List of abrreviation……..xvii

CHAPTER ONE: BACKGROUND TO THE STUDY

1.0 Introduction……1

1.1 The urban thermal environment……..3
1.2 Types of urban heat island…….4
1.2.1 The surface urban heat island (SUHI)……..4
1.2.2 The canopy layer heat island (CLHI)…….…….6
1.2.3 Boundary layer heat island (BLHI)…….….6

1.3 The effects of urban heat island…….....8

1.4 The relationship between air and land surface temperatures…….....9

1.5 Statement of the research problem……11

1.6 Research aim…….13

1.7 Research objectives……...14

1.8 Thesis outline……14

CHAPTER TWO: A SYSTEMATIC LITERATURE REVIEW ON THE EFFECTS OF EXTREME HEAT ON HUMAN HEALTH AND THE SPATIAL MAPPING OF HEAT VULNERABILITY

2.0 Introduction..……...15

2.1 Extreme temperature and human health…….…….15

2.2 The regional focus of the review…….21

2.3 Method……22

2.4 Results…….24

2.4.1 The effects of extreme heat on human health in tropical Africa….....24

2.4.1.1The study duration and the temporal resolution of the data used.....26

2.4.1.2 The technology and procedures used for data collection……26

2.4.1.3 Approaches for data analysis...……..27

2.4.1.4 Summary of the review findings……...27

2.4.1.5 Distribution of studies based on urban and rural settlements……....48

2.4.2 Spatial mapping of heat vulnerability to human health……51

2.4.2.1 Indicators for heat vulnerability…….....54

2.4.2.2 Spatial scale of mapping……59

2.4.2.3 Techniques for data analysis……..59

2.4.2.3 Validation of heat HVIs and maps…….……75

2.5 The role of remote sensing and GIS for understanding the relationship between the UHI and human health ……77

2.5.1 Limitations of remotely sensed data…….....82

2.6 Conclusion……...85

CHAPTER THREE: THE STUDY AREA

3.0 Introduction…….89

3.1 Geographical location…….89

3.2 Population……...90

3.3 Weather and climate……91

3.4 Vegetation……...94

3.5 Relief and geology……..96

3.6 Land use/cover……96

CHAPTER FOUR: RESEARCH METHODS

4.0 Introduction…….. 100

4.1 Research objective 1: Mapping spatio-temporal change of AIS……100

4.1.1 Computation of land use/cover area from Gong *et al*. (2020) datasets…100

4.1.2 Mapping the AIS from Landsat datasets…….102

4.1.3 Data pre-processing technique…..……...103

4.1.4 Classification scheme design…….……103

4.1.5 Description of land use/cover classes…….104

4.1.6 Supervised/unsupervised classification……..105

4.1.7 Testing/accuracy assessment and area estimation……..106

4.1.8 Reference data sampling design…….106

4.1.9 Conclusion……..108

4.2 Research objective 2: Investigate the high-resolution spatio-temporal changes in the magnitude of UHI in response to urbanisation…….……108

4.2.1 Computation of LST…….……..108

4.2.2 Procedures for the computation of LST……109

4.3 Research objective 3: Assessment of the influence of Tmax (^{o}C) on heat-related mortality…….....111

4.3.1 Description of in-situ meteorological and morality data collection……111

4.3.2 The nature and accessibility of health data……..112

4.3.3 Empirical statistical heat-mortality modelling……114

4.3.4 Computation of excess mortality count……..114

4.3.5 Seasonal cycle of mortality and the contrasting patterns of excess mortality across the 6 hospitals…….117

4.3.6 Temperature threshold……....121

4.3.7 Model selection for regression……...122

4.4 Research objective 4: Mapping of heat vulnerability……....122

4.4.1 Heat vulnerability indicators……...122

4.4.2 Justification for choosing the 3 primary indicators that constitute this study's heat exposure index…….126

4.4.2.1 Land surface temperature……126

4.4.2.2 Artificial impervious surface……...126

4.4.2.3 Normalized difference vegetation index…….127

4.4.2.4 Generating the 3 primary indicators that constitute this study's heat exposure index…….....l28

4.4.3 Justification for choosing the 3 primary indicators that constitute this study's heat sensitivity index……...130

4.4.3.1 Vulnerable population (below 14 and above 65 years old)…….……130

4.4.3.2 Women population……..130

4.4.3.3 Population density……...131

4.4.3.4 Generating the primary indicators that constitute this study's heat sensitivity and adaptive capacity index……132

4.4.4 Justification for choosing the 3 primary indicators that constitute this study's heat adaptive capacity index……135

4.4.4.1 Population living in poverty as define by $1.25 per day threshold…..135

4.4.4.2 Literacy level of the population above 15 years……..135

4.4.4.3 Household dwelling quality…….....136

4.4.5 Reclassification of the attributes of the HVIs……..…138

4.4.5.1 Reclassification of LST…...……138

4.4.5.2 Reclassification of AIS……139

4.4.5.3 Reclassification of NDVI……140

4.4.5.4 Reclassification of vulnerable population……...141

4.4.5.5 Reclassification of women population……142

4.4.5.6 Reclassification of poverty level……..……143

4.4.5.7 Reclassification of literacy rate……...…….144

4.4.5.8 Reclassification of dwelling quality……145

4.4.5.9 Reclassification of population density…….145

4.4.6 Creation of heat exposure, sensitivity, and adaptive capacity index…..148

4.4.7 Incorporating expert's judgment into the heat vulnerability mapping….149

4.4.8 Expert's judgement on the 9 primary indicators…….…...149

4.4.9 Expert's Judgement on the 3 secondary indicators……..150

4.4.10 Construction of heat vulnerability maps……..151

4.4.11 Validation of heat vulnerability maps……..152

4.5 Research objective 5: Heat vulnerability projections for the middle and end of the 21st century under low and high forcing scenarios……...152

4.5.1 Temperature data from the 5 selected CMIP6 GCMs……...152

4.6 Conclusion..……..153

CHAPTER FIVE: MAPPING SPATIO-TEMPORAL CHANGE OF ARTIFICIAL IMPERVIOUS SURFACE

5.0 Introduction……...156

5.1 Spatio-temporal mapping of AIS…….....156

5.2 The error-adjusted area assessment……162

5.3 Area estimation and uncertainty……165

5.4 Error-adjusted area estimation……..…….168

5.5 Computation of confidence intervals…….170

5.6 The relationships between UHI and AIS ……..……173

5.7 NDBI…….……....177

5.8 NDVI…….181

5.9 The relationship between AIS, UHI, and the NDVI……..189

5.9 Conclusion……191

CHAPTER SIX: ASSOCIATIONS BETWEEN TEMPERATURE AND HEAT-RELATED MORTALITY

6.0 Introduction……...192

6.1 Justification for the choice of 4-month moving average baseline ……192

6.2 Rationale for the use of a polynomial model of the 3rd order…….195

6.3 The association between *Tmax* (°C) and excess mortality…….....208

6.4 Analysis of model residuals……...213

6.5 Model simulation of heat-related mortality at 1°C temperature intervals…..214

6.5 Conclusion…….220

CHAPTER SEVEN: MAPPING OF HEAT VULNERABILITY

7.0 Introduction……...221

7.1 Reclassified maps of HVIs……...…….221

7.2 Heat exposure, sensitivity and adaptive capacity index……227

7.3 The heat vulnerability maps……..231

7.4 Sensitivity analysis……233

7.5 Comparison of heat vulnerability maps derived from DHS and WorldPop datasets……236

7.6 Site-specific comparison of heat vulnerability maps generated from WorldPop and DHS datasets……239

7.7 Limitations of census data at the ward level for sensitivity analysis……..242

7.8 Validation using data on heat-related mortality……..243

7.9 Confirmation of heat vulnerability on a high-resolution satellite image……248

7.10 Conclusion……..254

CHAPTER EIGHT: PROJECTIONS OF HEAT VULNERABILITY WITH TEMPERATURE RISE

8.0 Introduction……..255

8.1 The Coupled Model Intercomparison Project (CMIP)...……..255

8.2 Shared Socio-economic Pathways (SSPs)……....255

8.2.1 Tier 1: Top priority scenario……..259

8.2.2 Tier 2: Additional scenarios of interest……..260

8.3 Representative Concentration Pathways……261

8.4 Justification for the choice of Tier 1 (SSP1-2.6 and SSP5-8.5)……263

8.5 Mean annual temperature projections……264

8.6 Monthly average temperature projections…….267

8.6.1 Monthly temperature change (°C) based on SSP1-2.6……...267

8.6.1.1 The HadGEM3-GC31-LL model…….267

8.6.1.2 The MPI-ESM1-2-HR model……..268

8.6.1.3 The MIROC6 model……268

8.6.1.4 The ACCESS CSM2 model……269

8.6.1.5 The GISS-E2-1-H model…….269

8.6.2 Monthly temperature change (°C) based SSP5-8.5……270

8.6.2.1 The HadGEM3-GC31-LL model……....270

8.6.2.2 The MPI-ESM1-2-HR model…….…….....270

8.6.2.3 The MIROC6 model…….……..….271

8.6.2.4 The ACCESS CSM2 model……....271

8.6.2.5 The GISS model…….…….272

8.7 Seasonal temperature change……....274

8.8 Spatial variations of temperature over Abuja and its environs…….287

8.9 Heat vulnerability projections…….……..290

8.10 Preparation of indicators for the projections of heat vulnerability……291

8.11 Heat vulnerability projections from the HadGEM3-GC31-LL model…296

8.12 Heat vulnerability projections from the MPI model……297

8.13 Heat vulnerability projections from the MORIC6 model……298

8.14 Projections of heat vulnerability from the ACCESS model……299

8.15 Projections of heat vulnerability from the GISS-E2 model…….301

8.16 Conclusion……...309

CHAPTER NINE: SUMMARY, DISCUSSION, AND CONCLUSION

9.0 Introduction……...311

9.1 Research objective 1: mapping the spatiotemporal change in the study area's AIS……..312

9.2 Research objective 2: Investigate high-resolution spatial and temporal changes in the magnitude of UHI in the study area as a result of urbanisation…….313

9.3 Research objective 3: Determine the effect of *Tmax* (°C) on heat-related mortality in the study area……315

9.4 Research objective 4: Perform spatial mapping of heat vulnerability in the research area…….....317

9.5 Research objective 5: heat vulnerability projections for the middle and end of the 21st century under low and high forcing scenarios……...320

9.6 Conclusion…….325

9.7 Recommendations…….327

9.8 Limitations of the research……329

9.9 Future research direction……...331

References……...334

List of Figures

Figure 1.1: The number of people living in urban areas worldwide……2

Figure 1.2: The percentage of urban residents, population by size category, and population growth……..……2

Figure 1.3: UHI profile……4

Figure 1.4: Illustration describing the components of the urban atmosphere (Modified after Voogt, 2004)……..7

Figure 1.5: Daytime/night-time surface and air temperature…….…...11

Figure 2.1: Member Countries of tropical Africa and their sub-regions……22

Figure 2.2: spatial distribution of the 59 cited studies on the effects of extreme heat on human health in tropical Africa……25

Figure 2.3: Annual distribution of heat vulnerability studies……54

Figure 2.4: Global distribution of studies on the spatial mapping of heat vulnerability……..58

Figure 3.1: Location of the study area…….…..90

Figure 3.2: The seasonal pattern of rainfall in the study area from 1990 to 2019.....92

Figure 3.3: Seasonal distribution of maximum temperatures in the study area from 1990 to 2019…….……93

Figure 3.4: Seasonal distribution of minimum temperatures in the study area from 1990 to 2019……..93

Figure 3.5: The city centre of Abuja, the Nigeria's capital city (Authors fieldwork, 2019).....…..99

Figure 3.6: Traffic congestion along Abuja - Karu expressway (Authors fieldwork, 2019).....…..99

Figure 3.7: Mpape informal settlement around Maitama District, Abuja. (Authors fieldwork, 2019)…….……99

Figure 3.8: Maraba informal settlement in Karu area of Nasarawa State. (Authors fieldwork, 2019).....…..99

Figure 4.1: Classified Landsat and Google Earth image used as reference data for obtaining sample points for accuracy assessment…….107

Figure 4.2: The reference points collected by stratified random sampling….108

Figure 4.3: Location of hospitals and weather station in the study area……..112

Figure 4.4: Time series graphs for the six hospitals participating in this study showing the expected mortality and excess mortality for the monthly average

approach (left panel) and the 4-months moving average method (right panel)……...120

Figure 4.5: Framework of heat vulnerability based on the 3 secondary indicators modified after Zhu *et al*. (2014). ……124

Figure 4.6: (a) The LST map of March 2020 from Landsat 8 image, (b) AIS map of 2020 from Landsat 8 sensor, and (c) NDVI map of 2020 derived from bands 4 and 5 of Landsat 8 image ……....129

Figure 4.7: (a) Vulnerable population of 2020 generated from WorldPop datasets, (b) Total number of women of childbearing age (15-49) per grid square in 2020, derived from WorldPop datasets, and (c) Population density of 2020 derived from WorldPop datasets…….....134

Figure 4.8: (a) 2020 poverty level generated from the WorldPop dataset, (b) Literacy rate of 2020 generated from the WorldPop dataset, and (c) dwelling quality of 2020 derived from WorldPop datasets ……...137

Figure 4.9: Conceptual procedures for the constructions of the 3 secondary indicators…….148

Figure 4.10: Respondent's areas of interest…….149

Figure 4.11: Experts' opinions on the relative importance of the 9 primary HVIs……150

Figure 4.12: Expert's judgement on the relative importance of the 3 secondary HVIs.....…...151

Figure 4.13: Schematic representation of the research methodology…….155

Figure 5.1: Land use/cover maps (1985-2019) produced using Gong *et al*. (2020) GAIA maps (a), (b), and (c), as well as Landsat 5 TM (d), Landsat 7 ETM (e), (f), and Landsat 8 OLI-TIRS (g), and (h)…….……160

Figure 5.2: Land use/cover trend of change from 1985 – 2019……..161

Figure 5.3: AIS area showing the urban expansion of Abuja (1985 – 2019)…161

Figure 5.4: Temporal change in the AIS area between 1985 and 2019……162

Figure 5.5: LST generated from the thermal bands of Landsat images……176

Figure 5.6: LSTs of the study area generated from Landsat 5 TM, Landsat 7 ETM, and Landsat 8 OLI-TIRS acquired at 09:15Z……177

Figure 5.7: NDBI of the study area generated from the Near-infrared and shortwave- infrared bands of Landsat images.. 180

Figure 5.8: NDVI of the study area generated from the Near-infrared and red bands of Landsat images……..183

Figure 5.9: Scatterplots of LST, NDVI and NDBI……..188

Figure 6.1: Regression plots of Tmax (°C) and Excess mortality count of the University of Abuja Teaching Hospital from 4-month moving average and monthly average baseline……...…….197

Figure 6.2: Regression plots of Tmax (°C) and Excess mortality count of General Hospital Kwali from the 4-month moving average and monthly average baseline…….……...199

Figure 6.3: Regression plots of Tmax (°C) and Excess mortality of National Hospital Abuja from 4-month moving average and monthly average baseline……....201

Figure 6.4: Regression plots of Tmax (°C) and Excess mortality of General Hospital Abaji from 4-month moving average and monthly average baseline…….…...203

Figure 6.5: Regression plots of Tmax (°C) and Excess mortality of specialist Hospital Mararaba from 4-month moving average and the monthly average baseline…….…...205

Figure 6.6: Regression plots of Tmax (°C) and Excess mortality of General Hospital Kuje from 4-month moving average and monthly average baseline……207

Figure 6.7: The 95% confidence interval for the third-order polynomial regression function output from the four-month moving average baseline for the relationship between Tmax (°C) and excess mortality…….211

Figure 6.8: Residual plots of regression output from the four-month moving average baseline for the relationship between Tmax (°C) and excess mortality…….213

Figure 6.9: Model simulation of maximum temperature and excess mortality at 1°C temperature intervals……216

Figure 7.1: (a) Reclassified LST map generated from the thermal bands of Landsat 8 image of March 2020, (b) reclassified AIS map generated from Landsat 8 image of March 2020 …….223

Figure 7.2: (a) Reclassified NDVI map generated from bands 4 and 5 of Landsat 8 image of 2020, (b) reclassified Vulnerable population of 2020 generated from WorldPop datasets ……..224

Figure 7.3: (a) Reclassified women population at childbearing age (15-49 years old) of 2020 generated from WorldPop datasets, (b) reclassified poverty level of 2020 generated from WorldPop datasets……..…….…..225

Figure 7.4: (a) Reclassified literacy level of 2020 generated from WorldPop datasets (b) reclassified dwelling quality of 2020 generated from WorldPop datasets……...…….226

Figure 7.5: Reclassified population density of 2020 derived from WorldPop datasets……...227

Figure 7.6: Heat exposure index (a), sensitivity index (b), adaptive capacity index (c)……..230

Figure 7.7: Heat vulnerability map from the 9 primary indicators (a) and the 3 secondary indicators (b)……..……232

Figure 7.8: Reclassified heat vulnerability indicators of Abuja and its environs from the DHS datasets, (a) vulnerable population, (b) women population, (c) poverty level, (d) literacy rate, (e) dwelling quality, (f) population density…….....235

Figure 7.9: Heat vulnerability maps of Abuja and environs from the WorldPop datasets (a) and the DHS datasets (b)……..238

Figure 7.10: Sample points from the heat vulnerability maps from the WorldPop and DHS datasets…….....240

Figure 7.11: Heat vulnerability and regression plot of the Gwagwalada area council (a); Municipal area council (b); Kuje area council (c); Kwali area council (d); Karu area of Nasarawa state (e), and Abaji area council (f)……..247

Figure 7.12: Heat vulnerability map and Google image……..252

Figure 8.1: Matrix showing Tie 1: Top Priority and Tie 2: Additional Scenarios of interest……...……..260

Figure 8.2: The socioeconomic parameters used in SSPs projections….……262

Figure 8.3: Estimates of global GHGs emissions and concentrations……262

Figure 8.4: Assumptions underlying the RCPs used to drive future climate projections…….……..….263

Figure 8.5: Mean annual temperature change (°C) in Abuja and its surrounds from the five selected CMIP6 models for the middle and end of the century, based on the low forcing scenario SSP1-2.6 and the strong forcing scenario SSP5-8.5……..267

Figure 8.6: Seasonal temperature change from the HadGEM3-GC31-LL model……...278

Figure 8.7: Seasonal temperature change from the MPI-ESM1-2-HR model……...280

Figure 8.8: Seasonal temperature change from the MIROC6 model……..…282

Figure 8.9: Seasonal temperature change from the ACCESS-CSM2 model…284

Figure 8.10: Seasonal temperature change from the GISS-E2-1-H model….286

Figure 8.11: Spatial variations in temperature due to the elevations……290

Figure 8.12: Heat vulnerability projections from the HadGEM3-GC31-LL model under low and high forcing scenarios for the middle and the end of the 21st century…….…….303

Figure 8.13: Heat vulnerability projections from the MPI model under low and high forcing scenarios for the middle and the end of the 21st century……..…304

Figure 8.14: Heat vulnerability projections from the MIROC6 model under low and high forcing scenarios for the middle and the end of the 21st century ……..…305

Figure 8.15: Heat vulnerability projections from the ACCESS model under low and high forcing scenarios for the middle and the end of the 21st century ……..…306

Figure 8.16: Heat vulnerability projections from the GISS-E2 model under low and high forcing scenarios for the middle and the end of the 21st century ……..…307

Figure 8.17: Heat vulnerability ensemble for the 5 selected CMIP6 GCMs for the low forcing scenarios and high forcing scenarios…….……208

List of Tables

Table 1.1: Surface temperature change (°C) in some tropical African cities…..8

Table 2.1: List of heat events by region and country in 2000–2021 …….16

Table 2.2: Classification of tropical climates……22

Table 2.3: Keywords search terms in the Web of Science database……...22

Table 2.4: Number of studies on the heat-human health by country…….……24

Table 2.5: Summary of studies on the effects of extreme heat on human health in tropical Africa……30

Table 2.6: The distribution of studies by settlement type……..48

Table 2.7: Classification of studies based on urban and rural areas….....50

Table 2.8: Summary of studies on the spatial mapping of heat vulnerability...61

Table 2.9: Studies that validated the heat vulnerability maps outputs……..75

Table 2.10: Summary of methodologies and results for the validation…….76

Table 2.11: Satellite sensors used for the spatial mapping of HVIs…….79

Table 4.1: Gong *et al.*'s (2020) GAIA classification system ……....101

Table 4.2: Satellite images used to update the maps of Gong *et al.* (2020)…..102

Table 4.3: The average monthly mortality for the six hospitals in Abuja……115

Table 4.4: Association between the time series analysis of excess mortality from the monthly average baseline and the 4-month moving average baseline…..116

Table 4.5: Characteristics of the 9 HVIs used for this study and some studies that used similar indicator……125

Table 4.6: Reclassification of the 9 HVIs used in this study……146

Table 4.7: Characteristics of the 5 CMIP6 GCMs used in this study……..153

Table 4.8: Summary of the data types used in this study……154

Table 5.1: Area estimates of land use/cover of Abuja from 1985 to 2019 ……157

Table 5.2: Land use/cover classification producer's, user's, and overall classification accuracy…….157

Table 5.3: Error matrix sample counts derived from Landsat and Google Earth images……...…….163

Table 5.4: The error matrix populated to estimate the proportions of the map area……..166

Table 5.5: Error-adjusted area of map class…….……169

Table 5.6: The standard error of area estimates and 95% CI.…….....171

Table 5.7: Classification of LST, NDBI, and NDVI index values based on their land use/cover type……..184

Table 6.1: Regression output from the 4-months moving average and the monthly average baseline……194

Table 6.2: Summary of polynomial regression output of Tmax (°C) and excess mortality count for the six hospitals in the study area……..212

Table 6.3: Simulated deaths of Gwagwalada and Municipal area council using 1°C temperatures Intervals……..217

Table 6.4: Simulated deaths of Kuje and Kwali area council using 1°C temperatures Intervals…….218

Table 6.5: Simulated deaths of Maraba and Abaji area council using 1°C temperatures Intervals…….219

Table 7.1: Heat exposure, sensitivity, and adaptive capacity index by map area (%)……...229

Table 7.2: Area (%) of heat vulnerability maps from WorldPop and DHS datasets……237

Table 7.3: Site-specific comparison of the heat vulnerability maps from the WorldPop and DHS datasets……241

Table 7.4: Summary of regression output of heat vulnerability map and excess mortality for the 6 simulated hospitals…….245

Table 8.1: Summary of the SSPs scenarios storylines……..256

Table 8.2: Summary of the RCPs scenario storylines ……..262

Table 8.3: Mean-annual temperature change across Abuja and its environs from the 5 selected CMIP6 GCMs for 2041-2060 and 2081-2100 ….....265

Table 8.4: The monthly average maximum temperature changes from the 5 selected CMIP6 GCMs.....…...273

Table 8.5: Projected seasonal temperature changes from the 5 GCMs……276

Table 8.6: Spatial change in the heat vulnerability area from the low forcing scenarios……..293

Table 8.7: Spatial change in the heat vulnerability area from the high forcing scenarios……..294

List of abbreviations

AIS	Artificial impervious surfaces
CMIP5	Coupled Model Intercomparison Project Phase 5
CMIP6	Coupled Model Intercomparison Project Phase 6
CRU	Climate Research Unit
DEM	Digital Elevation Model
DHS	Demographic and Health Survey
EROS	Earth Resources Observation and Science
FGD	Focus Group Discussion
FROM-GLC	Finer Resolution Observation and Monitoring of Global Land Cover
GAIA	Global Artificial Impervious Area
GCM	Global Climate Model
GDP	Gross Domestic Product
GHGs	Greenhouse Gases
HVIs	Heat Vulnerability Indicators
IPCC	Intergovernmental Panel on Climate Change
LST	Land Surface Temperature
NCDC	National Climate Data Centre
NOAA	National Oceanic and Atmospheric Administration
OLI	Operational Land Imager
RCPs	Representative Concentration Pathways
SDG	Sustainable Development Goal
SRTM	Shuttle Radar Topography Mission
SSPs	Sheared Socioeconomic Pathways
TIRS	Thermal Infrared Sensor
UHI	Urban Heat Island
UNFCCC	United Nations Framework Convention on Climate Change
USGS	United State Geological Survey
WBGT	Wet Bulb Globe Temperature
WCRP	World Climate Research Programme
WMO	World Meteorological Organisation

CHAPTER ONE: BACKGROUND TO THE STUDY

1.0 Introduction

The last quarter of the twentieth century saw a massive increase and migration of the human population from rural to urban areas, owing primarily to natural growth and improvements in the global economy (Kabisch *et al.,* 2017; Ramyar *et al*., 2021). According to UN estimates (2018), urban areas house more than 55.3% of the world's human population, and is expected to house more than 60% by 2030. The World Bank projected an annual growth rate of 1.1% in 2019, with an average increase of 82 million people per year in urban areas. These factors are expected to add 2.5 billion people to the world's urban areas by 2050, with Africa and Asia accounting for roughly 90% of this growth (United Nations, 2019). Urbanisation is a global trend with substantial environmental consequences primarily characterised by population growth and increased urban density.

Typically, urbanisation is associated with faster economic growth and higher Greenhouse Gas (GHG) emissions (O'Neill *et al*., 2012; IPCC, 2019; Raihan & Tuspekova, 2022). Because urbanisation indirectly impacts income growth, consumption patterns, and energy efficiency, it is defined as a broader socioeconomic phenomenon that includes not only population concentrations in urban areas but also changes in consumption and production structure that occur during the urbanisation transition. The United Nations Department of Economic and Social Affairs Population Division's Figure 1.1 illustrates the regional distribution of urban population. Figure 1.2 shows the percentage of urban residents, population by size category, and population growth from the Population Division of the United Nations Department of Economic and Social Affairs, Prospects for Global Urbanization.

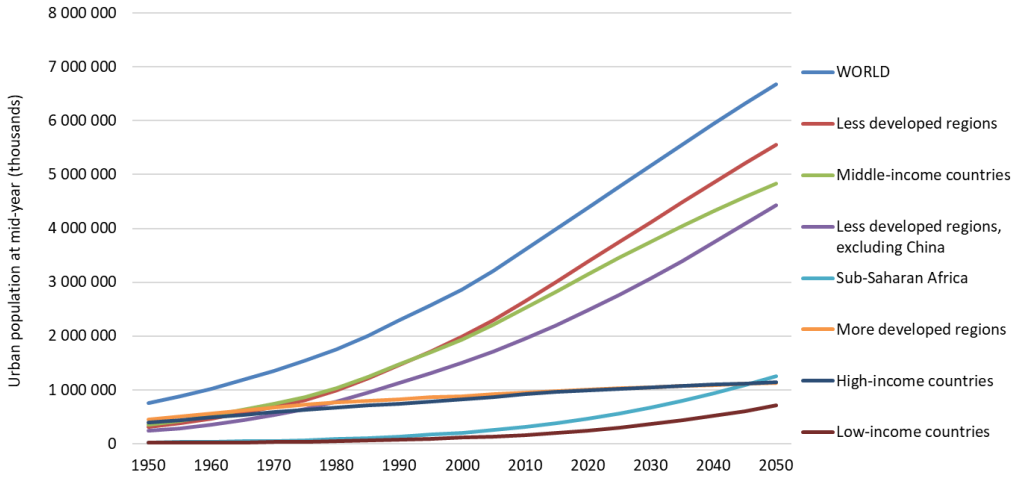


Figure 1.1: The number of people living in urban areas worldwide, in thousands, for each region from 1950 to 2050 (UNDESA, 2018).

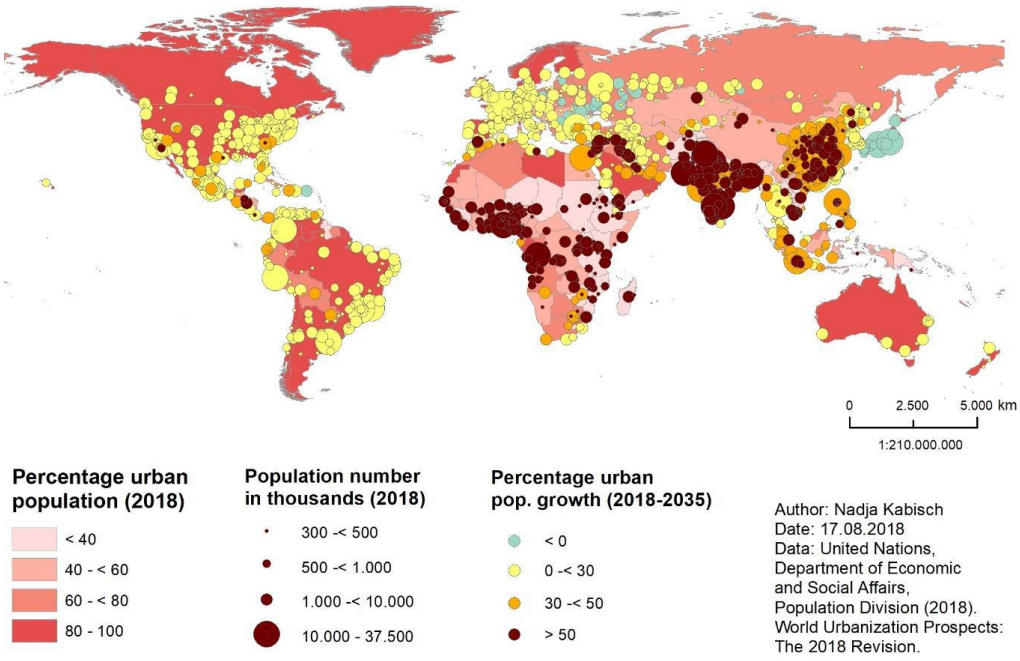


Figure 1.2: The percentage of urban residents, population by size category, and population growth from 2018 to 2035 (UNDESA, 2018).

Urban areas typically have more AIS than rural areas. Understanding the effects of urbanisation on human society and the environment necessitates understanding the degree of change in AIS. AIS are primarily human-made structures made of any material that blocks or prevents water from penetrating the soil naturally. They are most commonly found on major highways, paved areas, hardened ground, and urban roofs (Bounoua *et al.*, 2018; Gong *et al.*, 2020). AIS are an important surrogate for built-up areas, influencing energy and

material flow and reflecting various levels of human activity (Solecki *et al.,* 2013; Zhu *et al.,* 2019; Zhu *et al.,* 2022). The effects of urbanisation on agricultural productivity, environmental quality, biodiversity loss, and microscale circulations (urban canyon effects, effects on convection) are important (Seto *et al.,* 2012; Chen *et al.,* 2020). Surface radiation effects (less albedo, more surface area, and different emissivity) and surface energy partitioning (less evaporation, different ground heat flux) (Oke, 1982; Arnfield, 2003) all have a long-term impact on human health and well-being (Guo *et al.*, 2016; Yang *et al*., 2021; Ingole *et al*., 2022).

1.1 The urban thermal environment

Urban areas can have a distinctive micro-climate often characterised as an urban heat island (UHI). The UHI is now a well-documented instance of urbanisation causing atmospheric change (Yao *et al*., 2020; Wang *et al*., 2022). The UHI is a climatological and environmental phenomenon in which urban areas have higher surface and atmospheric temperatures than rural areas. UHI is a major environmental problem in urban areas, affecting climatic and ecological processes, particularly during the hot summer months (Landsberg, 1981; Oke, 1987; Liu *et al*., 2022).

The magnitude of the UHI is influenced by building materials' thermal and physical properties, surface roughness, evapotranspiration surface, and daily and seasonal synoptic conditions (Oke *et al.,* 1991; Arnfield, 2003). A consequence of anthropogenic alteration of the natural environment is the tendency of urban areas to initiate a UHI. Thermal variations in the properties of AIS, which account for the storage of solar radiation and its conversion to sensible heat are essential characteristics of the urbanisation process. The thermal characteristics of cities are important components of the energy balance that affect UHI, which is the primary factor influencing global warming and climate change (Oke, 1987; Xian & Crane, 2006; Haass *et al*., 2018; Hayes *et al.,* 2022). Figure 1.3 shows the profile of a UHI modified from the United States Environmental Protection Agency (USEPA, 2014).

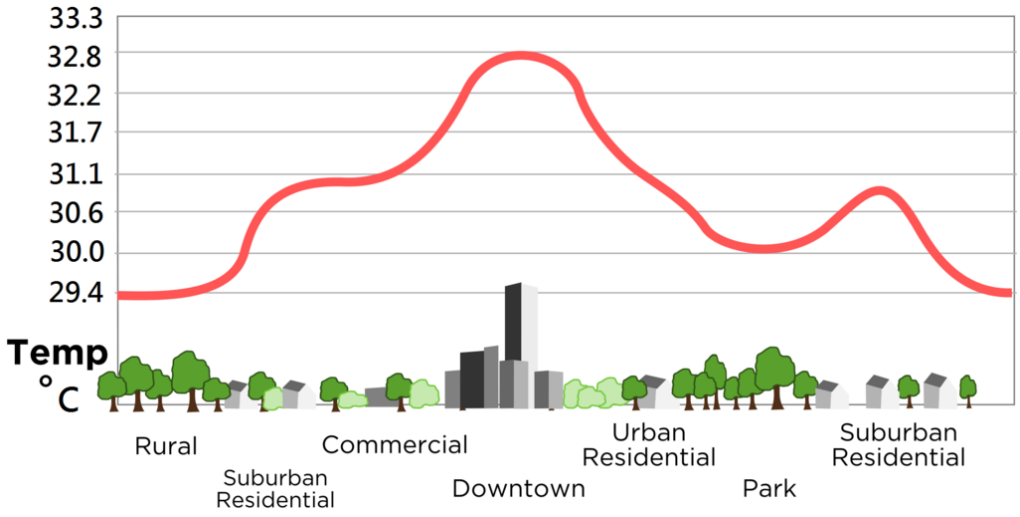


Figure 1.3: UHI profile modified from the USEPA (2014).

1.2 Types of urban heat island

Depending on where it occurs, UHI types include surface heat island (SUHI), canopy layer heat island (CLHI), and boundary layer heat island (BLHI) (Oke, 1987, Fernando, 2012, Kim & Brown, 2021). These classifications are based on the vertical position of UHI and their measurement elevations.

1.2.1 The surface urban heat island (SUHI)

The surface urban heat island (SUHI) is a phenomenon in which metropolitan regions have greater temperatures than adjacent rural or natural areas. It is the outcome of various causes related to urbanisation and human activity. The SUHI occurs over the surface envelope and is caused by temperature differences between urban and rural areas (Alves *et al.*, 2020; Marconcini *et al.*, 2023). Meteorological measurements from mobile transects, near-surface networks (Amorim *et al.*, 2015), and climate classifications (Steward and Oke, 2012) were used to calculate the SUHI. Using remote sensing data (e.g., satellite images) to research SUHI has expanded as geospatial technologies have advanced (Alves *et al.*, 2020). Satellite remote sensing covers enormous areas and allows for a direct and consistent examination of the thermal environment of large cities. SUHI is described as LST. The thermal bands of airborne sensors offer a synoptic means of studying LST effects on UHI, morbidity and mortality. LST measured from Satellite is a fundamental factor in SUHI developments, not only performing as a gauge for climate change, nonetheless owing to its regulator of the rising

terrestrial radiation, and subsequently, the regulator of the surface sensible and latent heat flux exchange in the atmosphere (Sun and Pinker, 2003). Among the key factors influencing the SUHI are:

Urbanisation and heat: Urban areas have considerably distinct characteristics compared to rural areas. The presence of buildings, concrete, bitumen, and other infrastructure materials influences solar heat absorption and retention. These surfaces, referred to as "urban heat sinks," tend to absorb and store more heat throughout the day, resulting in higher temperatures in urban areas (Gong *et al.,* 2020).

Heat retention and release: Urban areas typically have less vegetation than rural areas. Through evapotranspiration, which releases moisture into the air and helps lower temperatures, vegetation plays a crucial role in cooling. In contrast, urban surfaces retain heat and release it slowly at night, resulting in higher temperatures. The SUHI intensified at night-time than in the daytime and is influenced mainly by solar radiation reflected within AIS recurrently, which is the main reason for the heat island in cities (Roth and Chow, 2012; Marconcini *et al.,* 2023).

Human activities and heat production: Urban areas are hubs of human activity and have many sources of heat production. For instance, Transportation, industrial processes, and energy consumption contribute to the discharge of waste heat, thereby increasing the temperature in urban areas (Oke, 1987, Wang *et al*., 2022).

Effects on microclimates: The SUHI affects the microclimate of urban areas, influencing human comfort, energy consumption, air quality, and ecological systems. Higher temperatures can increase the energy required for cooling, increasing GHG emissions and air pollution. Urban populations may also experience an increase in heat stress and heat-related morbidity (Gosling *et al.,* 2009, Li *et al*., 2021).

Mitigation strategies: Various mitigation strategies are used to combat SUHI. One example is increasing vegetation through urban greening initiatives, such

as tree cultivation and creating green spaces. Urban planning and design can also include cool roofs, reflective pavements, and the strategic placement of buildings to maximise shade and airflow. Moreover, increasing energy efficiency, promoting sustainable transportation, and reducing heat can help mitigate the SUHI effect (Kabano *et al*., 2022).

Climate change co**nsequences:** Due to rising global temperatures, the SUHI effect may intensify due to ongoing climate change. The combination of urbanisation and global warming can result in substantial temperature increases in cities. Future emphasis will increase on adapting cities to these changes and implementing sustainable urban design and planning practices.

1.2.2 The canopy layer heat island (CLHI).

The CLHI are accountable for heating the atmosphere of cities and ranges from the Earth's Surface to the approximate mean building summit. Generally, CLHI data is derived from in-situ weather stations. CLHI is measured at an elevation that extends from the ground's surface to the top of the roof and is suitable for a microscale study (Voogt, 2007). CLHI studies have analysed UHIs by further dividing them into an urban canopy layer (UCL) and a building canopy layer (BCL). This classification also relates to the vertical position of the fixed weather station. A UCL is a layer formed at the height of the roof of a building in a city, usually calculated by the average height or defined by connecting the rooflines of buildings (Oke *et al.*, 2017). However, UCL has a high position and is unsuitable for studying the effects of UHIs on people's thermal comfort or health. To compensate for these limitations, BCL has been defined and reflected in several studies as a climatic range of how people feel closer to the surface (Ching 2013). BCLs are also directly related to the height at which equipment is installed on a mobile platform to measure mobile traverse or the installation location of AW**Ss.**

1.2.3 Boundary layer heat island (BLHI)

The BLHI is measured starting at the height of the rooftop to the atmosphere and is derived using radiosondes. BLHI are used to examine the consequence of UHI

at the mesoscale, i.e.1–10,000 km^2. They are accountable for warming the urban atmosphere (Mirzaei *et al*., 2012). The atmospheric layers of BLHI are dome shapes of hot air over cities that substantially affect the regional winds and temperature. The warmer air can spread by winds beyond to influence adjoining regions. Great attention is devoted to the urban canopy layer since it encompasses air adjoining the urban surface and expands to the mean structure elevation, causing the most substantial impact on the population through instantaneous temperature variations. Temperature upsurges within this medium have constantly been associated with anthropogenic influence (Voogt and Oke, 2003). Figure 1.4 presents the schematic components of the urban atmosphere modified after Voogt (2004).

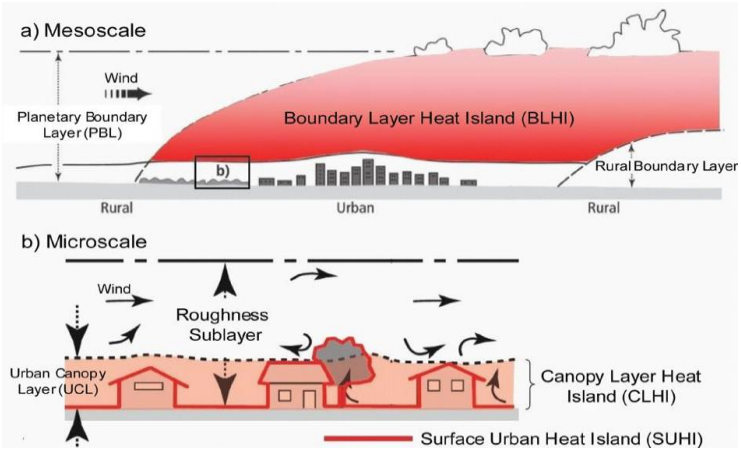


Figure 1.4: Illustration describing the components of the urban atmosphere (Modified after Voogt, 2004).

This study focuses on SUHI using LST from the thermal band of satellite remote sensing, which encompasses vast areas and enables a comprehensive examination of Abuja's thermal environment. Several urbanisation-related processes have been identified as crucial variables that may contribute to developing and enhancing the SUHI in urban settings of tropical Africa at different dimensions and through the use of different technologies. This study demonstrates that the magnitude of the SUHI's spatial extent varies by city and is influenced by geographic location, urban structure, building materials, vegetation cover, anthropogenic heat, and pollutants. Table 1.1 summarises previous studies that evaluated the magnitudes of SUHI in several tropical African cities.

Table 1.1: Surface temperature change (°C) in some tropical African cities

Reference	Country	Cities	Study period	Magnitude of UHI (°C)
Odongo (2016)	Kenya	Nairobi	2013-2014	3.5
Appian (2017)	Ghana	Bosomtwe, Kumasi	2002-2014	7.0
Koudahe *et al.* (2018)	Togo	Lomé	1970-2014	0.7
Kabanda & Kabanda (2019)	Tanzania	Dar es Salaam	2018	8.0
Nwilo *et al.* (2019)	Chad	Lake Chad	1973-2017	3.8
Ige *et al.* (2017)	Nigeria	Abuja	1987-2014	4.8
Awuh *et al.* (2019)	Nigeria	Abuja	1986-2016	6.7
Bosco & Thomas (2019)	Rwanda	Kigali	2015	2.1
Haggag *et al.* (2016)	Rwanda	Karama Gahororo Rubona	1964-2010	1.5 1.7 1.3
Feyissa *et al.* (2018)	Ethiopia	Addis baba	2020-2080	2.1
Osima *et al.* (2018)	Eritrea	Eritrea	1971-2000	2.0
Dissanayake *et al.* (2019)	Ethiopia	Addis baba	1986-2016	4.4
Aondoaseer *et al.* (2018)	Nigeria	Abuja	1987-2001	6.3
Ajayi (2018)	Nigeria	Abuja	1987-2014	6.2
Ifatimehin *et al.* (2013)	Nigeria	Lokoja	2001-2010	3.2
Littaye *et al.* (2018)	Mauritania	Nouadhibou	1945-2016	3.3
Efe & Eyefia (2014)	Nigeria	Benin-City	1980-2012	5.5
Ayanlade (2016)	Nigeria	Lagos	2002-2014	5.0
Linden (2011)	Burkina Faso	Ouagadougou	2003-2004	1.9
Offerle *et al.* (2005)	Burkina Faso	Ouagadougou	2002-2003	5.0
Di Leo *et al.* (2016)	Burkina Faso	Bobo-Dioulasso	2003-2013	3.4
Awuh *et al.* (2018)	Nigeria	Calabar	2002-2016	2.3
Nguemhe Fils *et al.* (2018)	Cameroon	Douala	1986-2016	3.5
Linda & Oluwatola 2015)	Nigeria	Ibadan	1972-2014	1.6
Umar & Satish (2014)	Nigeria	Kano	1986-2014	11.0
Henninger (2009)	Rwanda	Kigali	1971-2008	1.6
Lindley *et al.* (2015)	Tanzania	Dar es Salaam	2012-2013	2.0
Tarawally *et al.* (2018)	Sierra Leone	Freetown Bo	1998-2015	1.8 3.3
Christian & Ugoyibo (2013)	Nigeria	Enugu	2008	4.0
Hummel (2016)	Senegal	Dakar	2016	4.0
Balogun & Balogun (2014)	Nigeria	Akure	1986-2006	9.9
Mensah (2017)	Ghana	Accra	2005-2017	0.8

1.3 The effects of surface urban heat islands

Several processes influence the formation of an SUHI in cities. Pavements and buildings, for instance, considerably contribute to SUHI by absorbing and

storing heat before releasing it back into the urban environment. Moreover, urban operations such as industrial operations, electricity generation, and anthropogenic factors emit heat directly into the urban environment, with harmful effects on the urban climates and environment (Kim *et al*., 2018; Hayes *et al.*, 2022; Yao *et al*., 2022). The degree of influence varies between cities based on the intensity of the SUHI. Some of the effects of the SUHI can be summarised as follows: The SUHI plays a crucial role in the increasing frequency of convective precipitation and lightning and the decreasing frequency of freezing precipitation and snowfall (Han *et al*., 2015). Lavoie & Lachance (2006) uncovered the major effects of SUHI on plant phenology, earlier flowering dates, and the lengthening of the growing season. However, these effects have been amplified by global warming. Wilby & Perry (2006) reported that SUHI and global warming could considerably alter the ranges of plant and animal pathogens, species, and pests.

SUHIs are a major factor in the thermal characterisation of urban layers and are recognised as the most influential factor in global warming and climate change. For instance, SUHI increases the frequency and intensity of urban storms, causing urban flooding (Dixon & Mote, 2003; Bornstein & Lin, 2000; Deilami *et al*., 2018); increases the demand and consumption of energy in urban areas for heating during the cold season and cooling during the warm season (Mideksa & Kallbekken, 2010; Santamouris *et al.*, 2015). The increased number of hot days and warm spells caused by SUHI has increased the frequency of morbidity and mortality associated with extreme temperatures (Tan *et al*., 2010; Hayes *et al*., 2022). Other effects of SUHI are the observed increase in the degree and hours of thermal discomfort; the production of ozone at the lower level of the troposphere in the form of mesoscale wind; and the per capita increase in the quantity of water consumed during the summer period (Almusaed, 2011; Han *et al*., 2022; Naikoo *et al*., 2022).

1.4 The relationship between air and land surface temperatures

The use of remote sensing data to investigate SUHIs requires understanding the relationship between surface and air temperatures. Different methods are employed to quantify SUHI. Satellite-based land surface temperature (LST)

measurements have been the widely used method. While weather station-reported air temperatures have served as the basis for research into atmospheric UHI (Streutker, 2002; Jiang *et al.*, 2022), LST has a major effect on air temperatures, especially in the canopy layer closest to the ground. Zhou & Wang, (2011) and Almadrones-Reyes & Dagamac, (2022) have demonstrated that the LST is directly proportional to the nature and characteristics of land use/land cover surfaces. Consequently, the emissivity properties of urban surfaces and the heat capacity of human-made structures considerably influence the temperature patterns in an urban region. According to EPA (2014), Lindén *et al*. (2015), and He *et al*., (2022) surface property influences the surface energy balance of urban areas (for example, emissivity, albedo, and surface roughness). Therefore, surface and air temperature relationships vary over time and across land use/cover surfaces, and LST is influenced by changing surface conditions, resulting in greater spatial and temporal variability than the air temperature.

LST has a major impact on the atmosphere of urban-rural areas. When rural areas begin to cool rapidly at sunset, the urban-rural differential cooling rates are at their highest; however, urban areas remain warmer for longer period and cool at a slower rate (Goward, 1981). The temperature difference was discovered to be most substantial after sunset and least before sunrise (Tzavali *et al*., 2015; Stewart *et al*., 2021). The vitiations could be attributed to the impact of AISs in cities, which absorb and store heat during the day before releasing it into the atmosphere at night. Population density and built-up density, which have been used to differentiate between urban and rural areas, also influence temperature patterns in an urban region. Surface temperatures are higher than air temperatures during the day but converge at night, as shown in Figure 1.5.

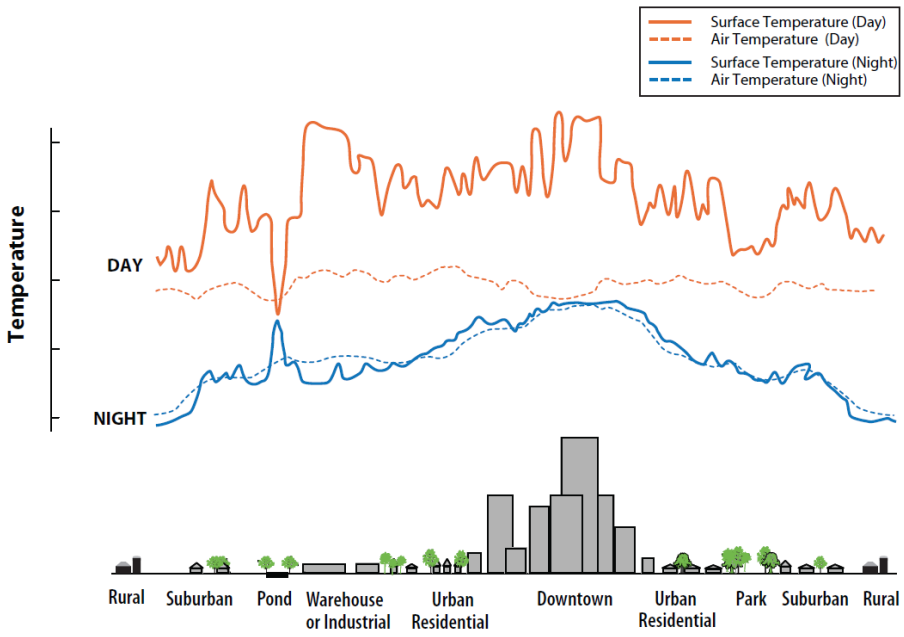


Figure 1.5: Daytime and night-time surface and air temperature (EPA, 2014).

1.5 Statement of the research problem

The primary goal of sustainable development is to meet current needs without jeopardising future generations (Brundtland, 1985). Sustainable development has emerged as the primary policy goal when evaluating the effects of interventions such as policies, programmes, strategies, and initiatives. The 2030 Sustainable Development Goals (SDGs) include fundamentals such as eradicating poverty (SDG 1), ensuring healthy lives and encouraging well-being (SDG 3), promoting growth and the creation of meaningful employment (SDG 8), and addressing the escalating effects of climate change (SDG 13) (United Nations, 2015). Climate change and worsening socioeconomic and heat vulnerability are expected to thwart complacent efforts to achieve the SDGs (Kjellstrom *et al*., 2016; Borg *et al*., 2021).

Climate change has become the most serious environmental issue, with potentially disastrous consequences. Human activities considerably impact the composition of the atmosphere by increasing the concentration of GHGs. Higher GHG concentrations can cause global warming and temperature rises, which can have various consequences (IPCC 2013). Working Group I of the IPCC reported in its sixth assessment report in 2022 that climate change affects ecological and societal structures, contributing to sea-level rise and an increase in the

frequency, duration, and severity of natural disasters such as cold and heat waves, floods, droughts, and storms. Carbon dioxide (CO_2), methane (CH_4), nitrous oxide (N_2O), hydrofluorocarbons (HFCs), perfluorocarbons (PFCs), and sulphur hexafluoride (SF6) are examples of anthropogenic GHGs emissions whose concentrations are increasing and have an impact on average temperatures, precipitation, and wind patterns. Their concentrations are often attributed to direct and indirect human actions such as using fossil fuels, industrialisation, deforestation, and urbanisation increasing GHG concentrations in the atmosphere and causing temperature and sea levels to rise. GHGs absorb and release heat from the earth's surface into the atmosphere. As GHG concentrations rise, more heat is trapped, resulting in warmer climates (UNFCCC, 2010).

Health and social issues may arise due to the interaction between global warming and the LST effect. Heat-related stress has been cited by the World Health Organization as one of the urban health problems (WHO, 2020). When the body's physiological capacity to withstand excessive heat from the inside and the outside is compromised, heat-related morbidity can occur (Kjellstrom *et al*., 2016; Berker *et al*., 2018). Extreme heat is caused by exposure to three broad contexts: the environment, the individual, and the workplace. Radiant heat, latent heat, and relative humidity are all components of the environment that can affect thermal comfort (Schulte & Chun, 2009; Parsons, 2014; Naffum *et al*., 2019; Tewari & Vinay, 2022). Prolonged exposure to high heat, especially at temperatures above 35°C and with inadequate dehydration, causes heat-related morbidity and mortality. Heat-related diseases include but are not limited to: rashes, cramps, excessive sweating, headaches, dizziness, nausea, confusion, weakness, and heat stroke (Parsons, 2014; Gauer & Meyers, 2019). Chronic diseases, clinical organ damage, accidents, and premature death have all been linked to prolonged exposure to extreme heat (Centers for Disease Control & Prevention, 2008; Lucas *et al*., 2014; Fatima *et al*., 2021).

Several international frameworks, conventions, protocols, and agreements have been made to combat the effects of climate change. Several reports and conferences have emerged due to much research into the consequences of heat on human health (UNFCCC, 2010; McMichael *et al.*, 2006; Field & Barros,

2014). Many of these studies have concentrated on the high income countries across different climatic regions (Sheridan & Allen, 2015; Ryti *et al.*, 2016; Green *et al*., 2019). Studies have shown that when a thermal metric exceeds a locally relevant threshold, human mortality and morbidity rates rise nearly everywhere in the world (Gosling *et al*., 2009). Studies tend to congregate around a thermal measure that exceeds this threshold, and the research findings in temperate locations cannot be directly relevant to countries with tropical climates (Green *et al.*, 2019). Many studies have already been conducted on climate change, extreme heat, and SUHI in tropical Africa. However, environmental impact and UHI intensity have received more attention than the effects of heat on human health in tropical African cities (Agan, 2017; Akomolafe *et al*., 2020; Salmamza *et al*., 2022). This research seeks to fill this knowledge gap by mapping of heat vulnerability for heat-related mortality in Abuja, Nigeria's capital. Given its rapid population growth (2.64 % annually), its status as one of Africa's most rapidly urbanising cities (3.5% annually), and its proximity to the world's fastest-expanding informal settlements (UN Habitat 2012; Rikko & Wapwera, 2016), Abuja was chosen as the study area. In addition, the Nigerian Meteorological Agency (NiMet, 2021) identified Abuja as one of the states in Nigeria at risk of heat waves.

Reducing GHG emissions and planning for extreme heat are two strategies needed to lessen the adverse effects of heat exposure and encourage actions that make people less vulnerable to and more resilient in the face of such extremes. Identifying heat vulnerability areas and their socioeconomic and demographic characteristics is the first step in achieving the Sustainable Development Goals to prevent and control heat-related morbidity and mortality. When planning to make the environment safer, healthier, and more liveable, remote sensing and GIS are practical tools for mapping heat vulnerability hotspots towards achieving a more resilient environment and lessening their exposure to extreme weather related to climate change by 2030.

1.6 Research aim

This study intends to investigate the association between temperatures and human health, taking into consideration heat vulnerability, and generate high-

resolution spatiotemporal maps of the LST in Abuja to better understand the impact of temperature variability on human health.

1.7 Research objectives

In order to achieve the research aim, specific objectives are:

i. mapping the spatiotemporal change in the study area's artificial impervious surface

ii. investigate high-resolution spatial and temporal changes in the LST in the study area as a result of urbanisation

iii. determine the effect of maximum temperature on heat-related mortality in the study area

iv. perform spatial mapping of heat vulnerability in the research area

v. perform spatial mapping of heat vulnerability projections for the middle and end of the 21st century under low and high forcing scenarios.

1.8 Thesis outline

The outline of this thesis is as follows:

Chapter 1 describes the study's background and provides the rationale for the research, purpose, objectives, and format. Chapter 2 provides a systematic literature assessment on the regional mapping of heat vulnerability and the effects of extreme heat on human health in tropical Africa. Chapter 3 presents a comprehensive overview of the study area, including its geography and historical context, weather, and climate, population and land use, terrain and geology, vegetation, soil and land use. Chapter 4 discusses the research methodology, including data types and sources, data collection, pre-processing, processing, and validation. Chapter 5 discusses the spatial and temporal evolution of AISs. Generating AIS maps and the trend in land use/cover change from 1985 to 2019 examines the driving force for urbanisation and settlement expansion, as well as accuracy evaluation and area estimation. Chapter 6 examines the effect of maximum temperature on heat-related mortality. Chapter 7 examines the mapping of heat vulnerability concerning heat exposure, heat sensitivity, and adaptive capability. Using low and high forcing scenarios CMIP6 GCMs, Chapter 8 provides spatial projections of heat vulnerability for the middle and end of the twenty-first century. The 9th chapter provides a summary of the study's findings, limitations, and recommendations.

CHAPTER TWO: A SYSTEMATIC LITERATURE REVIEW ON THE EFFECTS OF EXTREME HEAT ON HUMAN HEALTH AND THE SPATIAL MAPPING OF HEAT VULNERABILITY

2.0 Introduction

This chapter identifies, evaluates, and synthesises all the high-quality research evidence related to the scope of this thesis. Relevant literature on the effects of extreme heat on human health in tropical Africa and the spatial mapping of heat vulnerability to human health anywhere else were reviewed. Findings from this review were systematically extracted, investigated, and discussed to identify this research's needs, argument, and empirical findings.

2.1. Extreme temperature and human health

Worldwide, higher-than-normal diurnal temperatures and heat waves are being experienced as a result of global warming. Because of the predictable consequences of climate change, there is renewed concern about the effects of extreme heat on human health (IPCC, 2021; Goshua *et al*., 2021). To date, most studies on this topic have focused on high income countries in comparison to low and middle income countries (LMICs), for which few studies have been conducted (Basu, 2009; Green *et al*., 2018; Ebi *et al.,* 2021; Kotharkar & Ghosh, 2022). Temperatures in tropical African cities are frequently near the upper limit of human comfort (Sherwood & Huber, 2010). The occurrence of hot days in tropical Africa has been increasing since the 1980s as a result of anthropogenic effects and GHG emissions, which continue to alter the region's summer temperatures (Mahlstein *et al*., 2011; Harrington *et al*., 2017; Herold *et al*., 2017; Ntoumos *et al*., 2022). According to Niang *et al*. (2014), surface temperatures over tropical Africa could rise by a degree faster than the estimated global average.

Many extreme heat events in tropical Africa continually go unreported. Nonetheless, the World Meteorological Organisation (2018) has reported extreme heatwave events in some low African cities, with temperatures over 50.6^{o}C during the summer. Similar occasions have been reported by the

Emergency event database (EM-DAT 2021), where an incident at extreme temperatures of 51.0°C and 60.0°C in Morocco and Nigeria killed non in

Morocco but over 60 people in Nigeria (Table 2.1). The effects of extreme heat on human health are often exacerbated by socioeconomic and demographic characteristics of the population, for example, poverty, literacy, infants and aging group. The IPCC (2022) reported that low-income countries had limited adaptive capacity to extreme heat due to scarce resources, fragile political institutions, and socio-cultural practices. There has been very little research on the spatial mapping of heat vulnerability to human health in tropical Africa (Omonijo *et al*., 2013; Agan, 2017; Leal Filho *et al*., 2018; Niu *et al*., 2021). Yet, such studies can enhance the resilience of a region in response to climate change-enhanced extreme heat occasions.

Recent studies indicate that some high-income counties have observed a decline in the sensitivity of health outcomes to extreme heat, which implies an increase in adaptive capacity to extreme heat (Coates *et al*., 2014; Bobb *et al*., 2014; Sheridan & Allen, 2018; Laranjeira *et al*., 2021). Unlike the high-income countries, vulnerability to extreme heat in low-income cities is on the rise due to their increase in sensitivity and low adaptive capacity to extreme heat (Hajat *et al*., 2010; Azhar *et al*., 2017; Green *et al*., 2019; Ncongwane *et al*., 2021; Chen *et al*., 2022). The purpose of this systematic review is to assemble a rigorous assessment of the peer-reviewed literature on the relationship between extreme heat and human health; and the spatial mapping of heat vulnerability.

Table 2.1: List of heat events by region and country in 2000–2021 (EM-DAT, 2021)

Region	Country	Date	*Tmax* (°C)	Number of the people affected	Total mortality
West Africa	Nigeria	June 2002	60		60
Southern Africa	South Africa	January 2016	45		11
Northern Africa	Sudan	August 2015	47		16
	Algeria	01 July 2003	47		40
	Morocco	August 2000	51		

Western Asia	Cyprus	July 2000	43	400	5
	Israel	July 2000	45		
	Jordan	July 2000	43	12	
	Turkey	June- July 2000	46	300	11
	Cyprus	June - July 2007	42		4
	Turkey	June - July 2007	43		3
Southern Asia	Pakistan	June 2000	46		24
	India	May 2002	50		1030
	Pakistan	May 2002	50	24	113
	India	May - June 2003	49		1210
	Bangladesh	May - June 2003	40		62
	Pakistan	May - June 2003	50		200
	Bangladesh	July 2005			
	India	June 2005	49		329
	India	May 2006			47
	Pakistan	June 2005	50	200	106
	Pakistan	May 2006	50	100	84
	India	April - June 2007	45		72
	India	March- May 2010	49		250
	India	April - May 2013	46		557
	Pakistan	Jan - April 2014			139
	India	May 2015	48		2248
	India	April - May 2016	51		300
	India	June 2019	42		90
	India	June 2019		450	22
	Pakistan	May 2018	42		180
	India	April - June 2017	48	490	264
Eastern Asia	China	July 2003	43	3500	7
	China	July 2004	39		39
	Japan	Jul - Aug 2004	40	300	10
	China	July 2005	39	200	
	Japan	August 2007	41	3000	62
	Japan	July 2008			47
	Japan	July 2009			16
	Japan	July 2010	35	15000	170

	China	Jul - Aug 2013			40
	Japan	Jul - August 2011	35	22000	36
	Japan	Jul - Sept 2013	41	54000	338
	Japan	July 2014	39	17000	27
	Japan	August 2015		11187	32
	Japan	May 2015		480	2
	Japan	July 2015		3200	5
	Japan	August 2016		490	3
	Korea	Jul - August 2018	38	13768	
	Japan	July 2018	41	49000	119
	Korea	July 2018			
	Japan	July - August 2019	30	18347	162
	Japan	July 2019		5600	11
Western Europe	Austria	Jul- Aug 2003			345
	Belgium	August 2003			1175
	Switzerland	July 2003			1039
	Germany	August 2003			9355
	France	August 2003	43		19490
	Luxembourg	July 2003			170
	Netherlands	Jul- Aug 2003			965
	Belgium	June-July 2006			940
	Germany	July 2006			2
	France	July 2006	37		1388
	Netherlands	July 2006	34		1000
	Austria	July 2007	39		5
	Belgium	Jun-Jul 2015			410
	France	Jun-Aug 2015	40		3275
	Belgium	July 2018			
	Germany	July 2018	38		
	France	July 2018	38		
	Austria	July 2019			1
	Belgium	Jun-Jul 2020	35		128
	Belgium	July 2019	41		400

	Germany	June 2019	39		4
	Germany	July 2019	42		
	France	Jun- Jul 2019	46		567
	France	July 2019	44		868
	Netherlands	July 2018			
	Netherlands	July 2019	40		400
	Belgium	August 2019	35		188
	Belgium	August 2020			1460
	France	Jul- Aug 2020			1924
	Netherlands	August 2020			400
Southern Europe	Albania	July 2004	38		3
	Spain	August 2003	40		15090
	Croatia	July 2003			788
	Serbia Montenegro	July 2000	42	70	3
	Italy	Jul- Aug 2003			20089
	Spain	July 2004			26
	Slovenia	Jul- Aug 2003			289
	Portugal	August 2003			2696
	Macedonia	July 2004	43		15
	Canary Is	July 2004	42	113	13
	Spain	Jul- Aug 2006	40		21
	Portugal	Jun-Aug 2005			462
	Portugal	July 2006			41
	Greece	Jun-Jul 2007	46		16
	Albania	July 2007		150	
	Bosnia and Herzegovina	July 2007			
	Italy	July 2007	45		6
	Macedonia	July 2007	45	202	
	Serbia	July 2007	45		
	Italy	August 2011	47		10
	Spain	August 2018	47		9
	Spain	June 2019			2
	Italy	August 2018	40		
	Portugal	August 2018	45		

	Italy	June 2019			3
Eastern Europe	Bulgaria	Jun- Jul 2000	43		7
	Romania	July 2000	43	100	6
	Russian Federation	July 2001	30		276
	Czech Republic	July 2003			418
	Slovakia	Jul - Aug 2003			
	Romania	July 2004	38		27
	Romania	Jul- Aug 2005	36	500	13
	Romania	Jun- Jul 2006	36	200	26
	Bulgaria	Jun- Jul 2007	46	50	2
	Hungary	July 2007	42		500
	Romania	Jun-Jul 2007	45		30
	Slovakia	July 2007	40	89	1
	Russian Federation	Jun- Aug 2010	40		55736
Northern Europe	UK	July 2003			301
	UK	July 2018	33		
	UK	June 2019			5
	UK	July 2019	39		
	UK	Jun-Aug 2020			2556
Northern America	USA	July 2000	38		35
	USA	August 2001			56
	USA	June 2002			14
	USA	July 2005	47	31	33
	USA	Jul - Aug 2006	50		164
	USA	Jul - Aug 2006	44		24
	USA	July 2011	50		22
	USA	June- July 2012	40		123
	Canada	June - July 2018	37		70
	Canada	June- July 2021	50		486
	USA	June-July 2021	47		138
South America	Brazil	February 2010	46		32
	Bolivia	August 2013		17490	18

Australia and New Zealand	New Zealand	Jan – April 2001			
	Australia	Jan- Feb 2009	49	2000	347
	Australia	January 2014	52		139
	Australia	Dec 2018-Jan 2019	49		

2.2 The regional focus of the review

Tropical regions lie between latitudes 23.5° north and south of the equator. Tropical Africa consists of 48 nations that make up five sub-regions: West Africa (16 countries), East Africa (9), Central Africa (10), part of Southern Africa (7), and the Indian Ocean islands, and Madagascar (6). Figure 2.1 presents the sub-regions and member countries of tropical Africa. The Köppen-Geiger system classified the climate of tropical Africa as Type 'A,' characterised by constant, elevated temperatures, and generally humid (Af) with high amounts of precipitation because of their closeness to the equator (Burkart *et al.,* 2014). There is, however, the emergence of drier climatic areas with declining rainfall towards latitude 23.5° north and south away from the equator due to the influence of the subtropical high-pressure system (Aw) and transition from type 'A' to type 'B' arid climates. Generally, regions located at high altitudes have lower temperatures, typical of warm temperate-type 'C' climates (Kottek *et al.,* 2006). Table 2.2 presents the climate types of tropical Africa.

Table 2.2: Classification of tropical Climates (Köppen, 1900)

Type	Description	Criterion
A	Equatorial climates	$T_{min} \geq +18\ ^{\circ}C$
Af	Equatorial rainforest, fully humid	$P_{min} \geq 60$ mm
Am	Equatorial monsoon	$P_{ann} \geq 25(100-P_{min})$
As	Equatorial savannah with dry summer	$P_{min} < 60$ mm in summer
Aw	Equatorial savannah with dry winter	$P_{min} < 60$ mm in winter
C	Warm temperate climates	$-3^{o}C < T_{min} < +18\ ^{o}C$

Note: T_{min} is the annual mean air temperature near-surface (2m); P_{min} is the precipitation of the driest month; P_{ann} is the accumulated annual precipitation.

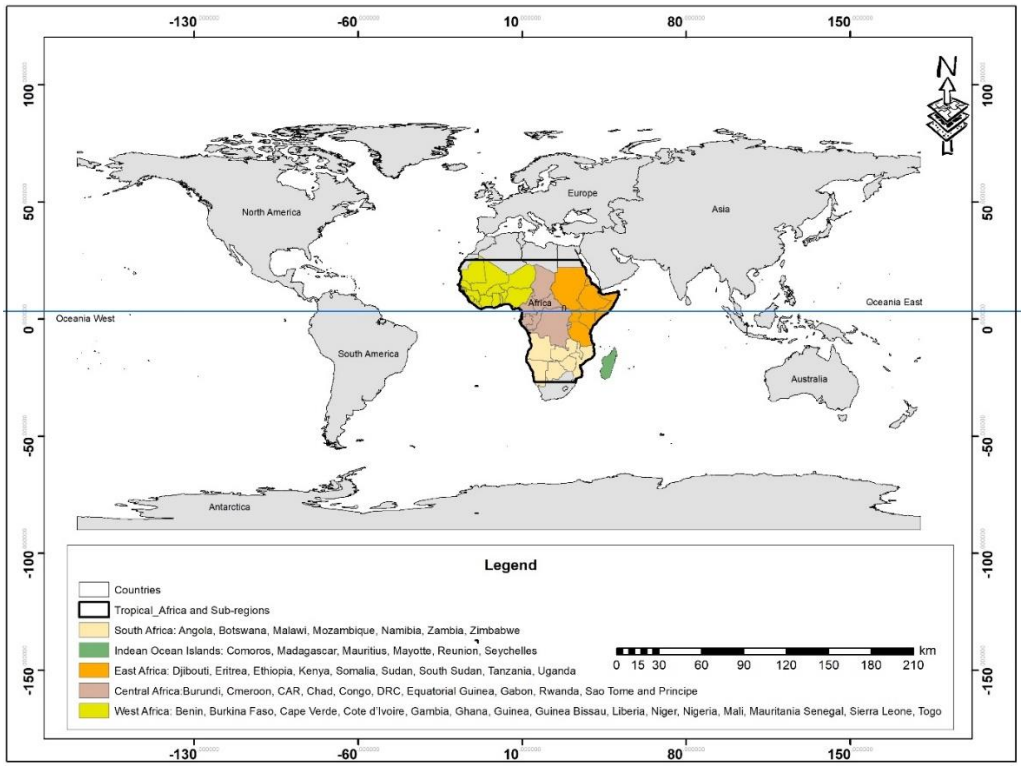


Figure 2.1: Member Countries of tropical Africa and their sub-regions

2.3 Method

For this review, literature searches were performed in Web of Science (WoS) to retrieve research papers on the 2 topics of interest, on (i) the association between extreme heat and human health; and (ii) the spatial mapping of heat vulnerability. Both searches were narrowed to peer-reviewed articles written in English. Table 2.3 provides the keywords and the search terms across all fields in the WoS database.

Table 2.3: Keywords search terms across all fields in the WoS database

S/N	Keywords searched	Results from the search terms (WoS)
1.	extreme heat and heat-related morbidity and mortality	229
3.	extreme heat on human health	1,396
4.	extreme heat on heat-related mortality	578
5.	extreme heat on heat-related morbidity	194
6.	extreme heat on thermal comfort	659
7.	extreme heat on heat stress	4281
8.	extreme heat on heat rashes	5
9.	Heat vulnerability	249

10.	heat vulnerability and human health	645
11.	Heat vulnerability mapping	301
13.	Spatial mapping of heat vulnerability on human health	21
14.	heat vulnerability mapping for human mortality	40
15.	human health vulnerability to heat	638
16.	mapping of human health vulnerability to extreme temperature	26
17.	Heat vulnerability mapping for human health	62
18.	vulnerability mapping of extreme temperature to human health	26

No publication date were set in both searches for publications extending to December 2022. A preliminary scan was applied to eliminate studies that examine non-human impacts such as those on plants and animals. A manual check on the articles' title, abstract, and body was made for further screening using the criteria listed below.

1. Studies carried out in any tropical African country that has informed the influence of extreme heat or heatwaves on human health using data from post-mortem questionnaires and or Modified British Medical Research Council (MRC) questionnaire, interviews, Focus Group Discussion (FGD), and household survey. Verbal autopsy, hospital records, clinical data, crude death, vital event registration, and quarterly relative risk were included in the review.

2. Studies carried out in any tropical African country that informed and or projected the influence of extreme heat or heatwaves on human health using a climate model data repository were included in the review.

3. Studies carried out in tropical African countries that have considered the effects of heat as modifiers of deaths/infections from malaria, Trypanosomiasis, Schistosomiasis, *etc*., were included in the review.

4. Studies not just in tropical Africa but anywhere else that have combined spatial mapping of heat vulnerability on human health with vulnerability due to flooding, air pollution, *etc*. were excluded from the review, except for these studies that have contained within a section with an in-depth

result on heat vulnerability mapping using heat vulnerability indicators and a specified methodology and results.

5. Studies in tropical Africa and anywhere else from government reports and projects on the spatial mapping of heat vulnerability for human health were included in the review**.** After removing duplicate entries and articles due to study area location, and the 5 criteria listed above, 59 articles on the influence of extreme heat on human health in tropical Africa, and 76 articles on the spatial mapping of heat vulnerability anywhere met the requirement for this review.

2.4 Results

2.4.1 The effects of extreme heat on human health in tropical Africa

The systematic review identified 59 studies on the impact of heat on human health in tropical Africa, 12 articles were conducted in Nigeria, and 11 in Ghana. Kenya has 8 studies, while Tanzania has 6. The number of studies conducted in Burkina Faso is 5, while the Gambia has 4. 3 articles were for Zambia and Senegal, including Zimbabwe, DRC, Uganda, and Cameroon, each with 2 studies. Countries with 1 study were Mozambique, Malawi, Burundi, Rwanda, Sudan, Mali, Gabon, and Guinea as shown in Figure 2.2, indicating that Central, East, and South Africa have a shortage of literature on the effects of extreme heat on human health. The number of studies on the effects of heat on human health, broken down by country in tropical Africa is shown in Table 2.4.

Table 2.4: The number of studies on the effects of heat on human health, broken down by country

Study location	Number of studies
Nigeria	12
Ghana	11
Kenya	8
Tanzania	6
Burkina Faso	5
Gambia	4
Zambia	3
Senegal	3
Zimbabwe	2

Democratic republic of Congo	2
Uganda	2
Cameroon	2
Mozambique	1
Malawi	1
Burundi	1
Rwanda	1
Sudan	1
Mali	1
Gabon	1
Guinea	1

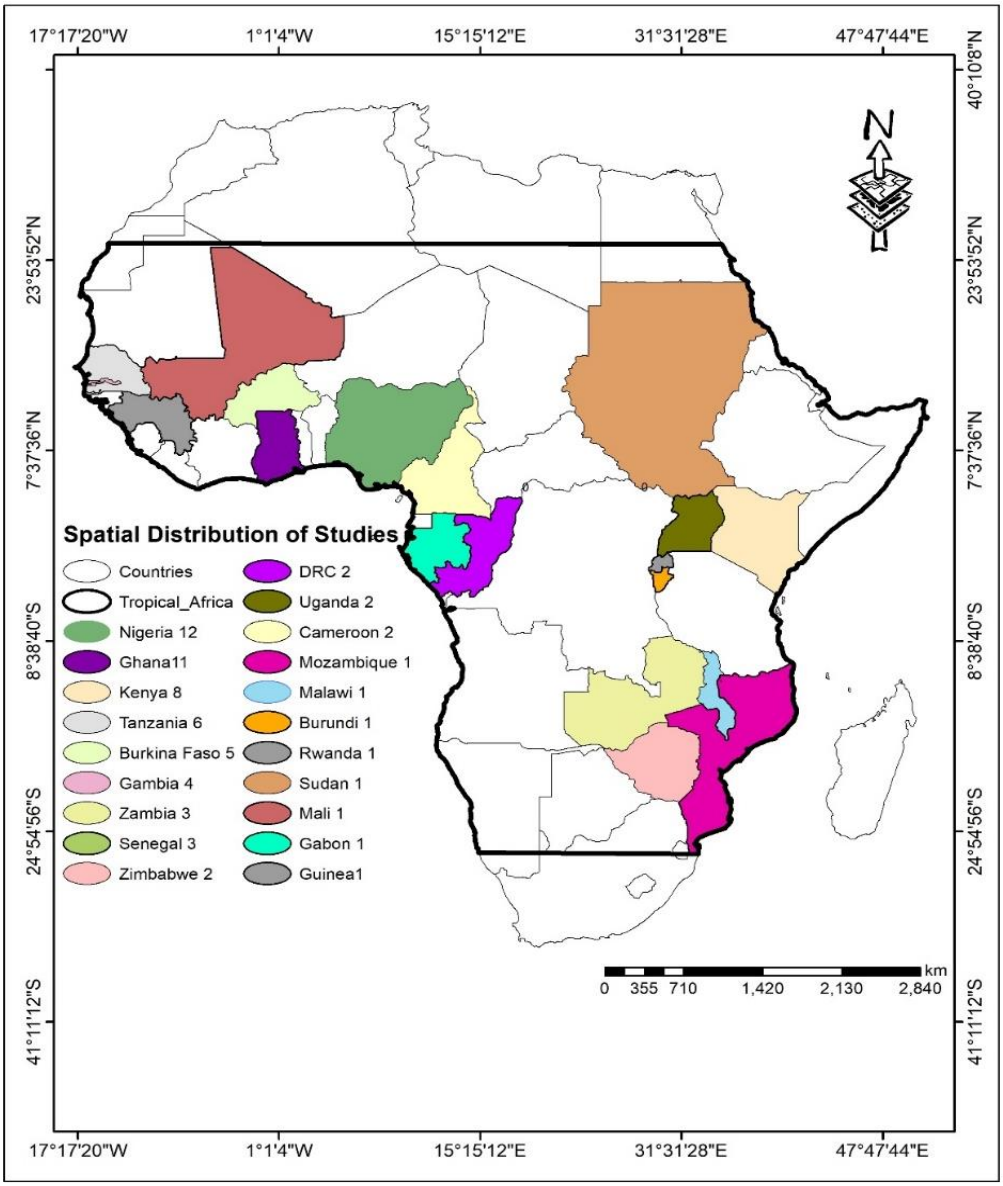


Figure 2.2: Spatial distribution of the 59 cited studies on the effects of extreme heat on human health in tropical Africa. Note: Some studies cut across more than one country; as a result, the number of studies by country may not necessarily tally with the number of studies by author.

2.4.1.1 The study duration and the temporal resolution of the data used

Concerning the temporal resolution of the data, e.g., daily, monthly, or decadal time scale, many studies have applied various timeframes for assessing heat effects on human health. 2 (3%) of the studies used long-time projections (Lorena *et al.,* 2018; Ragatoa *et al.,* 2018). 14 (24%) performed a short-time investigation; for example, Azongo *et al*. (2012) and Faye *et al.* (2021) studied heat exposure on a daily scale. Brewwster & Greenwood (1993) and Frimpong *et al*. (2014) concentrate on seasonal scale variations. However, studies that focus on long-time variances, for instance annual scale reduce uncertainties due to a small number of observations. Although the lag period depend on the scope of the study, for example, a short-time investigation by Nunfam (2021) used a survey and FGD to understand workers' sensitivities to extreme heat and occupational practices on human wellbeing, efficiency, and social comfort. 42 (72%) of the studies identified in this review are based on long-time scales that study variations between heat and human health for over 5 years. For example, studies by Etard *et al*. (2004) and Faye *et al*. (2021) cover a duration of 11 and 39 years, respectively. It was argued that studies founded on a temporal scale, for example over five years offer a better extrapolation of the association between extreme heat and human health (McGregor *et al.,* 1961) because it enables a more accurate assessment of the effects and changes over time, where long-term and short-term variations may be readily identified.

2.4.1.2 The technology and procedures used for data collection

On the technologies used for data collection, systematic data collection from weather stations managed by meteorological agencies and departments owned by the government are often used (Olatunde, 2016; Azongo *et al.*, 2012; Luque *et al.*, 2009). Several studies used recent technologies for data collection. For example, Wiru *et al*. (2020), Mutai (2013), and Paz (2009) used satellite data from the National Climate Data Centre of the National Oceanic and Atmospheric Administration. Herold *et al.* (2017), Lorena *et al*. (2018), and Ragatoa *et al*. (2018) used climate data from the GCMs or reanalysis, for example, CORDEX-AFRICA, ERA-Interim, and data from the UAE Climate Research Unit (CRU). Balogun & Balogun (2014), Kwasi *et al*. (2014), and Balogun & Daramola

(2019) used a Shielded portable Lascar EL-USB-2 data logger for collecting observed temperature and relative humidity data. There is a correlation between the years covered by a study i.e. duration, the data type, and the data analysis processes. Some studies, for instance, spanned more than 30 years (1980-2020), while others spanned less than five years (2015-2020), and still, others spanned less than a year (for example, January to October). Some experiments utilised technological data observations concerning the data type, such as temperature and relative humidity, from a weather station or a Shielded portable Lascar EL-USB-2 data recorder. Other research methods include questionnaires, surveys, and FGD. Nevertheless, some studies rely on hospital health data. Both factors influence the choice of models and data analysis procedures.

2.4.1.3 Approaches for data analysis

Over 47 (80%) of the identified studies employed descriptive and inferential statistics to analyse short-term or duration data, such as studies that covered less than a year and utilised data from field surveys, FGD, questionnaires, and interviews (Alaigba *et al.,* 2018; Ngwenya *et al*., 2018; Nunfam 2021). Due to their cost, portability, and convenience of use, the use of Lascar USB temperature and humidity sensors with a calibrated Questemp heat stress monitor for short-duration research has increased in recent years (Balogun & Balogun, 2014; Kwasi *et al*., 2014; Frimpong *et al*., 2016). Long-term or long-duration studies, such as 30 years, frequently employ time series, regression, and correlation designs to directly compare health data with biometeorological factors (Scott *et al*. 2017; Asamoah *et al*. 2018; Wiru *et al*., 2020). To this end, a more detailed investigation of the discrepancies concerning the approaches can contribute to a better understanding of the relationship between extreme heat and human health, which might offer valuable assistance from targeted intervention procedures.

2.4.1.4 Summary of the review findings

Even though the majority of studies in this review showed an increase in morbidity and mortality in the hot/rainy season compare to the cool season (e.g., Kynast-Wolf *et al*., 2006; Mutisya *et al*., 2010; Diboulo *et al*., 2012; Scott *et al*., 2017), studies in Bono village of Ghana revealed an increased risk of death at

the lowest Apparent Temperature (18°C). In Botswana, Alexander *et al*. (2013) found that minimum temperatures were related to an increase in Diarrhea occurrence. Before 1975, a study by Rayco-solon *et al*. (2004) revealed seasonality in death rates, with more deaths occurring during the "hungry" season. However, seasonal incidence-related mortality has reduced in recent years. There are, however, variations in the results from these studies in terms of the scale of the observed temperature thresholds, and the exposure metrics which could impede the conclusion of the expected consequence across the studies. For instance, Diboulo *et al*. (2012) noted a substantial increase in deaths with heat intensification at lag 0 – 1 as in lagged temperature days. A temperature rise of 1.0°C at lag 0 - 1 was related to a 2.6% rise in mortality for all ages and 3.7% for under five years with people aged over 60 most vulnerable to extreme heat. Asamoah *et al*. (2018) found a 42% rise in the likelihood of suffering a miscarriage with every degree rise in Wet Bulb Globe Temperature (WBGT), suggesting a connection between atmospheric heat exposure and adverse pregnancy outcomes in Accra. Lorena *et al*. (2018) found an increase in non-communicable diseases in children and deteriorating mental health and occupational hazard in adults of informal residences with low income due to extreme temperature. It was also discovered that an increase in temperature to over 40°C during summer could affect the population who spend long hours in the heat, such as street vendors (Ngwenya *et al*., 2018).

Frimpong *et al*. (2020) found that heat stress considerably influences farmers in Bawku East of Northern Ghana, with Malaria and heat cramps identified among the recurring diseases. Nunfam *et al.* (2019a) established a relationship ($p < 0.05$) between historical climate change threat awareness and work-related heat stress and the variance in educational accomplishment in the dissemination of coping approaches to work-related pressure from extreme temperatures. This is in agreement with the conclusions of Nunfam *et al*. (2019b), who found a major variation in temperature-related morbidity with the type of mining activities among workforces in five mining spots in Western Ghana. Some studies have shown a decline in the spread of malaria due to high temperatures and a decline in precipitation in west Africa owing to climate change (Ermert *et al.*, 2012), temperature and rainfall have influenced the growth rates and the survival of malaria pathogens. This finding was supported by McGregor *et al*. (1961);

Lawoyin (2001); Reyburn *et al*. (2011) and Ifatimehin & Ujoh (2014) who reported an increase in morbidity and or mortality in the rainy/hot season. Daniel (2015) reported a significant relationship between maximum temperature, rainfall, and heat rash. Table 2.5 presents the Summary of studies on the effects of extreme heat on human health in tropical Africa ordered by first author surname.

Table 2.5: Summary of studies on the effects of extreme heat on human health in tropical Africa ordered by first author surname

Reference	Country	Location	Study period	Hardware and Software Technologies used	Type and method of Data collection	Techniques of data analysis	Summary of findings
Sy *et al.*, (2022)	Senegal	Senegal	2009-2019	Weather station, climate model projections, and household survey	Temperatures, and health (morbidity, mortality), households' surveys	univariate and bivariate analyses	Morbidity and mortality affected women (57%), but men (43%). Health hazards are linked to age, drinkable water availability, fuel type, habitation and construction materials, fans and air conditioners, and medical history.
Faye *et al*. (2021)	Senegal	Bandafassi	1973 2012	- Weather station	Mortality, temperatures (˚C), dew point temperature (˚C), wind speed, and rainfall	Poisson generalized additive and distributed lag non-linear model	Extreme heat has led to a rise in the relative risk (RRs 1.4, (95% CI: 1.2–1.6, and 1.5 (95% CI: 1.3–1.8 among women and persons over 55 years at greater threats
Diouf *et al*. (2013)	Senegal	Ferlo	2003	- FORTRAN, MATLAB and xmgrace, GrADS and FERRET - TRMM and ERA-Interim.	- Clinical data - Rainfall and temperature	Liverpool Malaria Model, Spectral and Filtering analysis	Temperature and rainfall influence the epidemiology of malaria through their development

						rates, survival of pathogens, and changes in land surface characteristics
Etard *et al*. (2004)	Senegal	Niakhar	1989-2000	- Monthly mortality rate - Verbal autopsy, Post-mortem interview, and questionnaire.	Independent review by two physicians to assign the principal reason for demise. Discordant diagnoses were discussed by the panel of clinicians and a consensus cause was reached.	Diarrhoeal, malaria, and acute respiratory infections called for 30% and 70% of the death earlier than 10 years of age in the warming time
Nunfam *et al*. (2021)	Ghana	Western Region of Ghana	2017	Descriptive cross-sectional survey	Confirmatory factor and invariance analysis	Extreme heat has a major effect on well-being and behavioral efficiency.
Nunfam (2021)	Ghana	5 mining locations in the Western Area of Ghana.	October 2017 to December 2017	Surveys and FGD	Descriptive statistical techniques involving frequency and percent, and inferential statistical	Workers' are sensitive to extreme heat due to their occupational practices, which affects their well-being and safety, psychological behaviour,

							efficiency, and social comfort
Wiru *et al*. (2020)	Ghana	Bono	2005 - 2015	Meteorological station and the United Stat National Oceanic and Atmospheric Administration's (NOAA) National Climate Data Centre.	Mortality, Tmax, Tmin, relative humidity	Over dispersed Poisson regression and distributed lag nonlinear models	Rise in mortality at the lowest apparent heat (18°C) from lag 2 to 4 with the maximum relative risk of death (RR 1.61, 95% CI: 1.2, 2.15, *p-value 0.001*) happening 3 days when exposed to heat.
Frimpong *et al*. (2020)	Ghana	Bawku East	Jan-Jun 2013		Household survey and FGD	Descriptive and inferential statistics (chi-square)	Malaria and heat cramps are repeated illnesses among farmers due to heat stress.
Nunfam *et al.* (2019)	Ghana	Ghana	2017		Questionnaires and interview	Descriptive statistics, chi-square, and Fisher's exact tests	A significant association between educational attainment and adaptation strategies to occupational heat stress ($p < 0.05$).
Nunfam *et al.* (2019)	Ghana	5 mining spots in Western Ghana	2019		Questionnaires and FGD	Descriptive and inferential statistics. E.g. frequency and percent, chi-	Temperature-connected illnesses varied with the type of mining activity ($p < 0.001$).

						square, fisher exact test	
Frimpong *et al.* (2016)	Ghana	Bawku	January to December 2013	Lascar USB temperature and humidity sensors and a calibrated Questemp heat stress monitor	- Household survey - FGD	- Correlation test	94 % of farmers' health are affected by heat with older farmers directly vulnerable to heat-related illnesses
Frimpong *et al.*(2014)	Ghana	Manga, Garu, Binduri, Pusiga	1961 to 2012		Mean seasonal *Tmin*, *Tmax*, and relative humidity	- Regression and Durbin-Watson statistical test	1^{o}C increase in *Tmax* with effects on the health of outdoor farmers who spend many hours doing manual work.
Kwasi *et al*. (2014)	Ghana	Pusiga, Binduri, and Manga	January to June 2013	- Lascar EL USB temperature and humidity loggers	- WBGT	Correlation test	93.5% of respondents expressed concern about the effects of heat on their health, 49% expressed that the increase in heat has affected their income
Asamoah *et al.* (2018)	Ghana	Upper East and West regions, Greater Accra, and Central regions	2004-2007	- WBGT - HOTHAPS-Soft database and SPSS version 22	- Maternal morbidity and mortality, temperature, humidity, heat radiation, and wind speed	Logistic regression and the Liljegren method	42% rise in the odds of suffering a miscarriage with each degree rise in WBGT (crude OR 1.42 95% CI 1.00–2.03).

					- The survey, verbal autopsy, and questionnaire		
Azongo *et al.* (2012)	Ghana	Kassena-Nankana	1995-2010	Thermometer and rain gauge from a weather station	Daily mortality, temperature and mean precipitation	Time-series Poisson regression and correlation between lagged weather predictors	Rise in death due to an increase in heat at lag days 01 was detected at 25^{th} and 75^{th} percentiles (0.19%; 95% CI: 0.05%, 0.21%) and (1.14%; 95% CI: 0.12%, 1.54%). Relationship of heat above 75^{th} percentile at lag days 26 and lag days 713 (0.32%; 95% CI: 0.16%, 0.25%) and (0.31% 95% CI: 0.14%, 0.26%).
Trærup *et al.* (2011)	Tanzania	Tanzania	1998–2004	Weather station	Temperature, Cholera cases, and deaths	Time series, regression, and Correlation model	A 1.0°C rise in *Tmax* rises the relative risk for cholera cases by 29% ($\beta = 0.256$, $p = 0.02$; IRR = 1.29) and 15% ($\beta = 0.141$, $p = 0027$; IRR = 1.15
Lorena *et al.* (2018)	Tanzania	Dar es Salaam	2018-2040	Heat forecasting models	Temperature and health data	Forecasting and modeling	Heat-related mortality from non-

							communicable diseases in children. Declining mental and occupational health in adults of low-income residents.
Mrema *et al*. (2012)	Tanzania	Rufiji	1999 – 2010	-Thermometer and rain gauge from the Tanzania Meteorological Authority - Intercooled Stata 11 and MGCV package in R2.14.2	Health and vital events registration system, mortality, rainfall, and temperature data	Time-series Poisson regression models	A strong association between *Tmax* and death in all ages. Age group < 4 = (*RR*0.93, 95% CI0.8940.974), age group > 60 (*RR*0.946, 95% CI 0.91 0.98).
Ndetto & Matzarakis (2013)	Tanzania	Dar es Salaam	2001–2011	Synoptic meteorological data station	- Air temperature, relative humidity, wind speed, and global radiation	- Rayman model	December to February is the most thermal stressful period for human beings with PET < 35 °C.
Reyburn *et al*. (2011)	Tanzania	Unguja, Zanzibar	2002–2008	Weather station	Temperature, cholera surveillance record, rainfall, humidity, ocean environmental variables	Time series, correlation, and autoregressive integrated moving averages model	A 1°C rise in temperature at a 4-month lag occasioned a 2-fold rise in cholera. Heat and precipitation interface conceded a positive relationship (*P* <

							0.04) with cholera at a 1-month lag.
Adeniyi (2009)	Nigeria	Ibadan	1997-2001	-Thermometer, Hygrometer, and anemometer from weather station *of* International Institute for Tropical Agriculture (IITA) Ibadan.	Temperature Humidity Index and Wind Chill Index	Thom (1959)'s discomfort index, Fourier analysis, modified Civitan's (1995) method of harmonic analysis.	Uncomfortable conditions in the afternoon of March and June due to high temperature and humidity Index values.
Lawoyin (2001)	Nigeria	Lagun	1993-1997	EPI Info	- Infant birth and death information - Voluntary Health Workers and Traditional Birth Attendants	Fisher's exact test and relative risk (RRs)	More neonatal deaths occurred during the warm and rainy seasons than in the dry season (p=0.02) predominantly among womens (p=0.01).
Daniel (2015)	Nigeria	Akure	2003-2012	Thermometer and rain gauge from the weather station of NiMet	Temperature, Precipitation, and incidence of heat rashes	Line graph and correlation analysis	A positive relationship between *Tmax*, rainfall, and heat-rash during Jan-Feb (0.95), Mar (0.67), Apr (0.65), Jul (0.67), Aug (0.87), Sept (0.74), and Dec (0.86)
Ragatoa *et al.* (2018)	Nigeria	Five Climatic zones of Nigeria	2018-2100	- Replications based on Weather Research and Forecasting at ~ 44 km	Temperature and Precipitation	Spatio-temporal trend analysis, Annual	The hottest days of heatwaves vary from 26 to 45.0°C

				under CORDEX-AFRICA and ERA-Interim 0.1°/0.1° - R-statistics and NetCDF Operators		Aggregated time series	with impacts on human health
Olatunde (2016)	Nigeria	Lokoja	2016	Thermometer and hygrometer from weather station of NiMet	Monthly Temperature and relative Humidity	Thom's Discomfort Index and the Humidex Calculator	Thermal discomfort varied from under 50% to over 50% between "noticeable" discomfort and "evident" discomfort
Alaigba *et al.* (2018)	Nigeria	Akure		Garmin GPS etrex 30	- A questionnaire, Temperature, relative humidity, wind speed	- Rayman model	*Tmax* of 35.0°C – 55.0°C has led to thermal discomforts and heat stress with heart-related diseases such as fatigue, sunstroke, muscle cramps, heat stroke, and heat exhaustion
Ifatimehin & Ujoh (2014)	Nigeria	Lokoja	2012-2013	- Satellite imagery - ILWIS 3.3 and Idrisi software	Nigeriasat-1 and Landsat imageries (Land use, LST, and NDVI) Hospital records for malaria infectious data	correlation and buffer analysis	The temporal increase in LST for sand bars, vacant land, and built-up area results in a rising incidence of malaria during the rainy season.

Omonijo *et al*. (2013)	Nigeria	Ondo	1998–2008	Synoptic meteorological station	- Temperature, RH, radiation, and wind velocity	- Rayman model	Moderate heat stress 57.5%, strong heat stress 32.6%, and minor heat stress 9.8%; no thermal stress 0.02%.
Balogun & Balogun (2014)	Nigeria	Akure	2010	- Shielded portable Lascar EL-USB-2 data loggers - Digital camera (Nikon Coolpix 950 with a 183-degree field of view fisheye lens)	- Thermohygrometric index (THI), discomfort index (DI), and relative strain index (RSI) defined by Temperature and humidity - Hemispherical images	Descriptive statistics with a one-way analysis of variance, Hemispherical images calculations using *Chapman et al*. (2001) method.	Urban core signifying major heat stress and health risk ($p < 0.05$).
Oloukoi *et al*. (2014)	Nigeria	Iseyin, Okeho and Shaki, Oke-Ogun	12/2008–2/2009		Temperature, rainfall, and cases of diseases. Correlational study Household survey, FGD, Key informant interviews	- Pearson's R correlation test	The occurrence of Diarrhea, measles, and malaria was in the dry season. Increase cases of flu at the onset of Harmattan and the monsoon season.
Omonijo (2017)	Nigeria	Ibadan	1991 - 2015	Synoptic meteorological data station	- Air temperature, relative humidity, wind speed, and solar radiation	Rayman model	43.5% moderate heat stress, 30% strong heat stress, 18.1% slight heat stress, 6.5% is under no thermal

							stress and extreme heat stress accounted for 1.3% and 0.6% .
Balogun & Daramola (2019)	Nigeria	Akure	January to December 2009	Shielded portable Lascar EL-USB-2 temperature/humidity data loggers	- Air temperature, relative humidity, and dew point temperature	Thermal comfort index developed by Thom (1959)	March is the most thermally stressful of the year
Ye *et al.* (2009)	Kenya	Nairobi	2003-2005	Digital meteorological stations	Temperature, humidity, and rainfall	Logistic regression	Pneumonia was the top reason for mortality causing 25.7% of deaths over < 5 years between April and June
Scott *et al*. (2017)	Kenya	Kibera, Mathare and Mukuru	1984-2014	- Thermometer/hygrometers from the network of Ibutton sensors and Kenya Meteorological Department. - Satellite imagery	- Temperature, humidity, and heat index - Landsat 8 imagery	Time-series, single-channel algorithm	Death at age 0-4 and <50 yrs. rise by 1% for every 1.0˚C rise in mean daily temperature above 20.0˚C
Mutai (2013)	Kenya	Nairobi	1980-2002	- Thermometer and Rain gauge from the weather station. - MODIS	Temperature, rainfall, aerosol optical depth, and respiratory-related diseases	Time series, Pearson's correlation, and multivariate linear regression analysis	The strong correlation between temperature and Aerosol Optical Depth than rainfall with a high rate of respiratory diseases.
Grace *et al*. (2012)	Kenya	Kenya	1998–2008	- Meteorological stations Remotely sensed data	- Rainfall, temperature, maternal data,	Cluster analysis Multi-	No influence of heat on inhibiting disparity (β =

					educational level, household water source, floor material, livelihood zones/strategy	level linear regression	−0.03, p N 0.1 for average temperature, and β = 0.09, p N 0.1 for heat inconsistency)
Egondi *et al.* (2012)	Kenya	Nairobi	2003-2008	Thermometer and rain gauge from a weather station	Temperature, rainfall, and mortality	Time series distributed lag approach model	1.0°C rise in temperature over the 75th percentile was related to death in under 5 years from non-communicable disease. 1.0°C reduction in temperature below the 25th percentile (threshold = 17.9 °C) was related to a 3%, 9%, and 13% rise in all-cause death in <50 years at lag 0–1 day
Mutisya *et al.* (2010)	Kenya	Nairobi	2003-2005		Quarterly relative risk	Poison regression	Mortality is highest in rainy/hot season among new-borns and age < 5 years (RR = 1.6, CI:1.3–2.2 and RR = 1.5, CI: 1.1–2.0)

Alexander *et al.* (2013)	Botswana	Botswana	1974–2003	- CRU TS 3.10	- Rainfall, temperature, vapour pressure, Diarrhea occurrence	Time series and Autoregressive analysis	Increase in Diarrhea occurrence in the dry season (proportion deviation from the yearly seasonal mean [Pmy] = 0.07) but in the wet season (Pmy = −0.01)
Kynast-Wolf *et al.* (2010)	Burkina Faso	Nouna	1999-2003	- Thermometer from a weather station - Statistical Analysis System Analytics (SAS Institute)	- Cardiovascular and all-cause death by month and season and temperature - Verbal autopsy	Time series, Poisson regression	High mortality for all-cause death, > 65 yrs was highly significant (β = 0.07, p b 0.00). Between 40 and 64 years (β = 0.03, p = 0.09) For CVD death, the influence were not statistically significant (β = 0.01, p = 0.3 and β = 0.06, p = 0.2 for 40–64 and <65 years.
Diboulo *et al.* (2012)	Burkina Faso	Nouna	1999-2009	- Thermometer and rain gauge from a weather station - Health and Demographic Surveillance System - MGCV package in R	- Mortality, temperature, and rainfall - Verbal Autopsy	Time series Poisson regression models	A 1.0°C rise in temperature at lag 0–1 was related to a 2.6% increase in the danger of death in all age

							groups. Increase in danger of 3.7% (95% CI: 0.3, 7.3). For lags 2–6 and 7–13 among under 5 years. The old <60 years are vulnerable to extreme low and high temperatures in lag strata 0–1
Hammer *et al.* (2006)	Burkina Faso	Nouna	1999-2003	SAS 9.1 software	- All-cause and cause-specific mortality in children - Verbal Autopsy	Poisson regression	Malaria remained the common diagnosis (42%) with the highest death rates in new-borns 6– 11 months in the rainy and warm period
Kynast-Wolf *et al.* (2006)	Burkina Faso	Nouna	1993-2001	PROC GENMOD	The month of birth and death	Floating relative risk model and Poison regression	High mortality in the dry period in all age groups except babies at the end of the wet period.
Sankoh *et al.* (2003)	Burkina Faso	Nouna	1993-1998		- Crude death - Verbal Autopsy	Poison regression	Malaria and Diarrhea accounted for 21% of total deaths in adults and 22% in older people in the dry and warm period

Jankowska *et al*. (2012)	Mali	Mali	1960–2009	Global Positioning Systems, Global Historical Climatology Network, NASA Thermal infrared data NOAA/CPC Geostationary Meteosat	- Temperature, precipitation, livelihood, and malnutrition	Cluster analysis Multivariate linear regression, spatial correlations	Temperature and rainfall index b−100 zone was related to stunting (β = −0.17, p b 0.00), underweight (β = −0.159, p b 0.00) and anaemia (β = −0.15, p b 0.01) for all clusters
Enete *et al*. (2013)	Cameroon	Douala	2012	Digital thermometer (KT300) and hygrometer, pyrometer, anemometer, and luminance meter from the weather station	Air temperature, humidity, solar radiation wind speed, and global luminance	Descriptive and inferential statistics, comfort analysis, and Spearman rank correlation	Discomfort from heat stress results in stroke, cramps, exhaustion, fatigue, headache, nausea, fainting, and mortality. A strong connection between land-use/cover and heat-related signs.
Dapi *et al*. (2010)	Cameroon	Yaounde´ and Douala	2010	Lascar data loggers	- Indoor air temperature, humidity, and dew point. - Interview and Questionnaire administered to school children	Descriptive statistics, linear regression, and Pearson correlation coefficient	High Occurrence in girls than boys for headaches (58 /39%), feeling 'very hot overall' (37/21), and 'very hot in the head' (21/18).
Luque *et al*. (2009)	Zambia	Lusaka	2003–2006	- Meteorological station	- *Tmax*, Cholera Medical registers	Time series, and Poisson regression	A 1.0°C rise in temperature 6 weeks before the onset of the

						outbreak clarified 5.2% of the rise in cholera cases (RR = 1.05, 95% CI: 1.04, 1.06) The associated hazard was 4.7%
Jaffar *et al.* (1997)	Gambia	Upper river division	1989-1993	- The monthly and annual mortality rate - Post-mortem questionnaires		56% of mortality from acute respiratory infections, malaria, acute gastroenteritis, and septicaemia in the rainy/heat season between July-October
McGregor *et al.* (1961)	The Gambia	Keneba	5 years period	Monthly mortality counts	Descriptive analysis	The high mortality rate in rainy/heat season in children above 7 years (July-October).
Rayco-solon *et al*. (2004)	Gambia	Keneba, Manduar and Kantong Kunda	1950-1997	Odds dying in rainy/hungry season	Cox regression and likely test model	Seasonality in mortality with more losses in the 'hungry' season prior to1975 (odds ¼ 1.87; 95% CI ¼ 1.62–2.17) and from 1975 to 1984 (odds ¼ 1.84; 95% CI ¼ 1.34–2.53).

Brewwster & Greenwood (1993)	The Gambia	Banjul	1988-1990		Seasonal mortality rate	Odds ratio	Peak mortality in meningitis, pneumonia, and malnutrition in the rainy/hot season (July-December).
Longo-Mbenza *et al*. (1991)	DRC	Kinshasa	1987–1991	Weather station	- Temperature, Haematocrit, stroke Patients admitted	Correlation and regression	Temperature was linked to haematocrit (r = 0.12, p b 0.00 and r = 0.1, p b 0.01) Temp. < 28°C increased hazard of stroke death by 21 (OR = 21; 95% CI: 15, 29)
Pasquini *et al.,* (2020)	Dar es Salaam	Dar es Salaam	1981-2010		Climate analyses, semi-structured interviews, and an engagement workshop with stakeholders.	Mixed techniques.	Heat and health are currently a low-priority policy issue, although informal settlement residents have high exposure, sensitivity, and low adaptability to heat.
Ngwenya *et al.* (2018)	Zimbabwe	Bulawayo	October - and November 2015		FGD	Grounded theory	*Tmax* < 40 °C in summer affects the health of vendors who spend long hours in the street under the sun.

Chang *et al.* (2004)	Kenya, Zambia, and Zimbabwe	1989–1995		- Temperature, Women aged 15–49 years experiencing cardiovascular events, venous thrombo-embolism, arterial stroke, and acute myocardial infarction	Time series, binomial regression, and Sensitivity analysis	5.0°C change in *Tmean* Kenya: VTE, 0.43 (95% CI: 0.14, 1.27); stroke, 0.65 (95% CI: 0.11, 3.89) Zambia: VTE, 1.16 (95% CI: 0.21, 6.47); stroke, 0.89 (95% CI: 0.45, 1.75) Zimbabwe: VTE, 0.70 (95% CI: 0.49, 1.01); stroke, 0.91 (95% CI: 0.62, 1.34)
Ng & Cowling (2014)	Guinea, Gabon, DRC, South Sudan, Uganda	1976–2014	Climate Research Unit	Temperature, Absolute humidity Lag effects, 8 reported Ebola virus disease	Time series and regression models	Cumulative ORs of EVD outbreaks related to deviations (−1, −2, and −3.0°C) from the monthly average temperature were significant with a regular dose-response relation across the lag period from 1.20 to 1.71, 1.43 to 2.93, and 1.71 to 5.00.
Paz (2009)	Kenya, Uganda, Rwanda,	1971–2006	-NOAA NCEP-NCAR	Air temperature, Cholera cases	Time series and Poisson regression	A 0.1°C increase in the annual *Tmean* increases

	Burundi, Tanzania, Zambia, Malawi, Mozambique					the yearly total of cholera cases by 1.87 ($\beta = 0.63$, $p = 0.18$) for recent year and 2.78 ($\beta = 1.02$, $p = 0.03$) for the preceding year.
Batté *et al*. (2018)	West Africa	1993-2016	- Météo-France seasonal System 5 based on the CNRM-CM global coupled model: experimental contribution to the World Weather Research Programme/World Climate Research Programme (WWRP/WCRP) ERA-Interim data	- Temperature HWDI. - Relative humidity by computing a heatwave index grounded on daily average apparent temperature threshold exceedance.	- Pearson time correlation, the ensemble and index probabilistic forecast - NCEP reanalysis - The statistical–dynamical forecasting approach	High possibilities of heatwave indices above the top quintile of 1993–2014 in utmost parts of West Africa.
Ermert *et al*. (2012)	West Africa	1960-2000	REMO data from the Climatic Research Unit (version CRU TS	Temperature and rainfall	Liverpool Malaria Model and integrated weather-disease model	A declined spread of malaria for a simulated rise in temperatures and a reduction in precipitation.
Herold *et al*. (2017)	Poorer countries in Africa, Asia, and Latin America	1958-2010	56 ensemble members.	20th Century Reanalysis warm nights frequency index (TX90p) and daily *Tmin* (TN90p)	Numerical weather forecast models	10% increase in hot days during 1961–1990 to 26% in 2010 with a rise in heat-associated death

Note DRC, Democratic Republic of Congo; FGD, focus group discussion; CI, Confidence interval; CVD, cardiovascular disease; Lag, a period between one event and another; RR, relative risk.

2.4.1.5 Distribution of studies based on urban and rural settlements

Urban settlements refer to areas with a population density of over 10,000 and substantial human-built infrastructure (Pateman, 2011, Li *et al.*, 2019). Various amenities, services and industries characterise these areas. Urban settlements often serve as economic, cultural, and administrative centres. Among the features of urban areas include paved roads, public transportation systems, commercial establishments, educational institutions, and recreational facilities. Rural settlements, on the other hand, are areas with limited human-made infrastructure and a lower population density of fewer than 10,000 people (Bibby & Shepherd, 2004, Li *et al.*, 2019). Rural settlements include small villages, hamlets, and isolated houses, often found in the countryside. Natural landscapes, agricultural activities, and smaller communities characterise rural areas. Housing in rural settlements is typically dispersed with limited access to amenities.

33 of the studies identified in the literature review (58%) focused solely on urban areas. 14 studies (22%) were conducted in rural areas. 12 studies (20%) assessed the association between ambient temperature or heat waves and mortality in urban and rural areas. Some studies compared urban and rural populations based on their sensitivity to extreme heat (Nunfam *et al.*, 2021; Jankowska *et al.*, 2012; Alexander *et al.*, 2013). Fewer studies were carried out in the rural areas compared with urban, with the rural areas of West Africa having more studies relative to other regions. Together these studies revealed a harmful influence of heat on human health, behaviour, and productivity among farmers, labourers, and mining workers in rural communities (Nunfam, 2021). Even while populations have diverse responses and coping mechanisms to heat exposure, these are inefficient in preventing heat-related morbidity and mortality at both the household and farm levels (Frimpong *et al.*, 2020). The distribution of studies by settlement type is shown in Table 2.6.

Table 2.6: The distribution of studies by settlement type

S/N	Type of settlements	No. of studies	%

1.	Urban areas	33	58
2.	Rural areas	14	22
3.	Both urban and rural areas	12	20

Urban centers are known for their heat impacts on human health due to heat islands. The UHI, whereby temperatures of towns are often higher than the surrounding rural regions, will worsen the influences of heat on human health (Sheridan & Allen, 2015). Urbanisation is the leading cause of urban sprawl. Urban sprawl has led to the growth of informal settlements that harbour low and middle-income populations of cities. The informal settlements are densely-packed housing with poor building materials that lacks access to public services and amenities—making their population particularly vulnerable to heat (Scott *et al*., 2017). The disparities in the designs of built-up expansion, vegetation and construction materials in cities can differentially affect the threat of heat-related morbidity and mortality. Urban centers in tropical Africa could be highly vulnerable to heat because cities and informal settlements are connected, leading to a substantial proportion of low-income earners of cities residing in informal settlements.

Egondi *et al*. (2012) found that the extreme heat experienced in the neighbourhood of informal settlements was greater than the ambient temperature recorded in the nearest weather station by several ^{o}C. A recent study by Scott *et al*. (2017) employed iButtons – an in expensive device for measuring temperature and relative humidity, to investigate heat variations in an informal settlement in Nairobi. Both studies recognised poor populations at risk of extreme heat. There are very few empirical studies on the vulnerability of human health to heat, particularly in the informal settlements of tropical Africa (Pasquini *et al*., 2020). Even though climate threat is projected for the African continent (Dosio, 2017), studies in Zimbabwe have recommended that informal settlements and urban outdoor workers are more vulnerable to extreme heat (Ngwenya *et al*., 2018). To this end, very little is known about the vulnerability to heat in tropical Africa. Table 2.7 presents the classification of studies based on urban and rural areas.

Table 2.7: Classification of studies based on urban and rural areas ordered by first author surname

Sub-region	Urban and rural	Urban	Rural
West Africa	**Nigeria** (Olatunde 2016; Adeniyi, 2009, Balogun & Daramola, 2019, Omonijo 2017, Balogun & Balogun, 2014, Ragatoa *et al*., 2018); **Ghana** (Kwasi *et al*., 2014, Asamoah *et al*., 2018, Nunfam *et al*., 2019, Nunfam *et al*., 2021); **Mali** (Jankowska *et al*., 2012); **Botswana** (Alexander *et al*., 2013).	**Nigeri**a (Ifatimehin & Ujoh 2014; Omonijo *et al*., 2013; Daniel 2015; Alaigba *et al*., 2018; Olatunde 2016; Lorena *et al*., 2020); **Gambia** (Brewwster & Greenwood, 1993; Jaffar *et al*., 1997); **Senegal** (Faye *et al*., 2021); **Burkina Faso** (Sankoh *et al*., 2003, Kynast-Wolf *et al*., 2006, Hammer *et al*., 2006, Kynast-Wolf *et al*., 2010, Diboulo *et al*., 2012); **Ghana** (Azongo *et al*., 2012).	Nigeria (Lawoyin 2001; Oloukoi *et al*., 2014); **Senegal** (Diouf *et al*., 2013, Etard *et al*., 2004); **Gambia** (McGregor *et al*., 1961, Rayco-solon *et al*., 2004); **Ghana** (Nunfam *et al*., 2021, Frimpong *et al*., 2014, Frimpong *et al*., 2016, Nunfam *et al*., 2019, Frimpong *et al*., 2020, Wiru *et al*., 2020, Nunfam, 2021).
Central Africa		**Democratic Republic of Congo** (Longo-Mbenza *et al*., 1991, Ng & Cowling 2014); **Cameroon** (Dapi *et al*., 2010, Enete *et al*., 2013).	
South Africa		**Zambia** (Chang *et al*., 2004, Paz, 2009, Luque *et al*., 2009); **Zimbabwe** (Chang *et al*., 2004, Ngwenya *et al*., 2018).	
East Arica	**Kenya** (Scott *et al*., 2017).	**Kenya** (Ye *et al*., 2009, Mutisya *et al*., 2010, Thaddaeus *et al*., 2012, Grace *et al*., 2012, Mutai, 2013); **Tanzania** (Trærup *et al*., 2011, Ndetto & Matzarakis, 2013, Lorena *et al*., 2018, Paz, 2009; Reyburn *et al*., 2011).	**Tanzania (**Mrema *et al*., 2012)
Indian Ocean Island			

2.4.2 Spatial mapping of heat vulnerability for human health

One common way to study human health vulnerability during extreme heat is to describe the heat in terms of its measurable threat. Although heat and temperature are often conflated to mean the same thing, in strict definitional terms, heat and temperature differ. Heat is energy transferred from one substance or object to another (moving from hot to cold). Heat is stored as internal energy in the receiving object following its transfer. A change in the level of stored energy can be recorded as a temperature change. In a human health context, energy or heat can be transferred to the human body from the surrounding environment by conduction, convection and radiation. Therefore, a rise in body core temperature (BCT) occurs if the environment imposes substantial heat gain on the human body that cannot be offset by heat loss (e.g. evaporation) (McGregor and Vanos, 2018).

In the framework of social vulnerability and the measured extent to which a population is resistant to heat threats, the studies on the vulnerability of heat to human health have grown in prominence (Cutter *et al*., 2003; Flanagan *et al*., 2011). Whereas heat vulnerability for human health can be defined in several ways, the definition often includes environmental, demographic, and population-specific health and socioeconomic variables (Cutter *et al*., 2003; Fussel, 2007; Conlon *et al*., 2020). Vulnerability is generally defined as the risk of losing property or life due to environmental threats (Cutter *et al*., 2012). Heat vulnerability is the likelihood of being adversely affected by heat hazards (Maragno *et al.*, 2020). The Intergovernmental Panel on Climate Change (2022) define vulnerability as "the extent to which a system is sensitive to or incapable of adapting to detrimental impacts of climate change, encompassing climate variation and extreme weather events. McCarthy *et al*., (2001) and Boa *et al*. (2015) define heat vulnerability as the degree to which a system experience harm due to exposure to heat threat. Heat vulnerability refers to the physical, social, economic, environmental, and organisational systems and procedures that define a systems or element's susceptibility and capacity for coping with and adapting to heat threats, such as the consequences of climate change (Leal Filho *et al*., 2018).

The environment, the individual, and the workplace all contribute to extreme temperatures. Radiant heat, latent heat, and relative humidity are all environmental factors that influence thermal comfort (Schulte & Chun, 2009; Parsons, 2014; Naffum *et al*., 2019; Tewari & Vinai, 2022). Heat-related morbidity and mortality are caused by prolonged exposure to extreme heat, particularly at temperatures above 35 °C and with insufficient dehydration. Extreme temperatures pose a substantial health risk to humans. High temperatures can cause heat stroke, exhaustion, cramps, and even fatality (Kovats and Hajat 2008, Gosling *et al*. 2009, Sy *et al*. 2022). The vulnerability of a population to environmental hazards is a function of their exposure, sensitivity, and adaptive capacity to extreme heat.

In the context of fatalities caused by excessive heat, exposure refers to elevated temperatures' intensity and spatial distribution. Extreme heat exposure can vary temporally due to a warming climate, as temperatures rise consistently over time, or spatially due to the UHI effect, which causes some areas of a city to be considerably hotter than others. Heat exposure functions are increasingly utilised in studies on heat vulnerability to estimate the health effects of environmental exposures that are difficult to directly measure (Bobb *et al.,* 2014; Gasparrini *et al*., 2015; Stone *et al.*, 2014; Millan *et al.,* 2019). For instance, it is difficult to determine the number of deaths caused by a heat wave because the cause of death listed on death certificates may be attributable to an underlying health condition exacerbated by extreme heat, such as a cardiovascular or respiratory illness (Harlan *et al*., 2013; Millan *et al*., 2019).

Health researchers increasingly develop heat exposure-response functions as an alternative to direct attribution approaches to quantify heat-related mortality (Bobb *et al*., 2014; Kalkstein *et al*., 2011, Millan *et al*., 2019). These functions are based on the association between observed temperature and all-cause mortality over time (Bobb *et al*., 2014; Kalkstein *et al*., 2011, Millan *et al*.**,** 2019). Exposure-response functions for heat mortality are statistically derived from the relationship between temperature and total mortality over a predetermined period. Therefore, heat vulnerability consists of exposure,

sensitivity, and adaptive capacity (Turner *et al.*, 2003; Leal Filho *et al*., 2018, Tran *et al*., 2020). The IPCC utilises this three-component strategy in its reports (IPCC, 2022). Wilhelmi & Hayden (2010) provide one concept of heat vulnerability, defining it as a complex top-down and bottom-up framework based on populations' exposure, sensitivity, and adaptive capability. Heat vulnerability is commonly perceived as composed of components such as heat exposure and sensitivity to perturbations or external stresses and the ability to adapt extreme heat (Adger & Kelly, 1999). In this regard, heat exposure and sensitivity can create a conceivable influence, interacting with adaptive capacity to generate heat vulnerability.

Heat vulnerability is the component of risks (exposure), the extent to which a population can absorb influences without suffering long-term damage (sensitivity), and the possibility of a population adjusting its features and behaviour to enhanced cope with prevailing and expected pressures (adaptive capacity) (Turner *et al*., 2003). Adaptive capacity, perceived as gross vulnerability, combines heat exposure and sensitivity, allowing a population to regulate a climate event by moderating the potential damage or surviving with the consequence (Rathi *et al*., 2021; Adnan *et al.*, 2022). Predicting the locations and hot spots of heat vulnerability will lead to timely interventions to mitigate the effects of extreme heat in advance. Recent concerns over the global rise in temperatures and their impact on human health have led to increased research on the spatial mapping of heat vulnerability (Rinner, 2009). The literature review identified 76 articles on the spatial mapping of heat vulnerability which are discussed here.

The earliest studies were conducted in the United States (for example, Vescovi *et al*., 2005; Reid *et al*., 2009; Rinner *et al*.,2010; Johnson *et al*., 2012). This review found a rise in studies on heat vulnerability to 9 publications per year from 2018 (Figure 2.3). The increase in research on the spatial mapping of heat vulnerability is partly due to the improvements in technology and data portals, cloud computing, and web tools on access to reliable data at a finer resolution (Gamble *et al.,* 2018). Over 39 (49%) of the identified studies on the spatial mapping of heat vulnerability included in this review are in the United

States. 16 of the identified studies (20%) were in Asian countries. The number of studies conducted in each continent is presented in Figure 2.4, indicating that 12 of the identified studies (14%) were in Europe, 5 of the identified studies (6%) were in Australia, and 6 of the identified studies (8%) were in Latin America. 2 of the identified studies (3%) were in Africa (Table 2.3). Studies on the spatial mapping of heat vulnerability to human health are concentrated in high-income countries, with only a few studies conducted in the LMICs as shown in Figure 2.4.

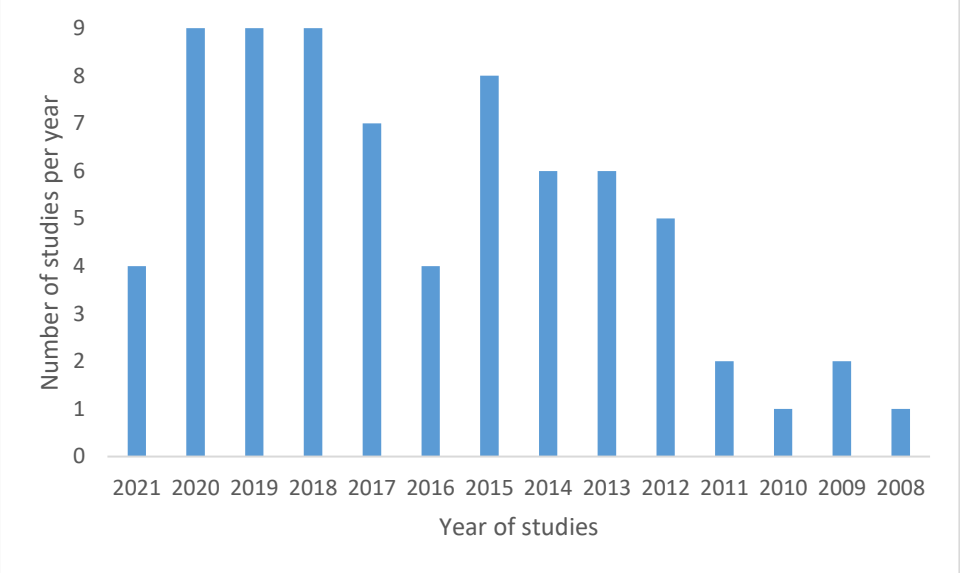


Figure 2.3: Annual distribution of heat vulnerability studies.

2.4.2.1 Indicators for heat vulnerability

The social determinants of health are the conditions under which a person is born, raised, resides, works, and ages, influencing health outcomes. Social determinants of vulnerability can also influence heat-related health outcomes, including heat exhaustion, dehydration, and other heat-related illnesses (Conlon *et al*., 2020; Ray *et al*., 2023). Approach required to address the social determinants of heat-related vulnerability factors include plans to:

- enhancing access to healthcare and social services,
- enhancing housing conditions,
- providing targeted support to vulnerable populations during heatwaves,
- Increasing awareness of heat-related risks and preventative measures.

Collaboration between healthcare providers, social service agencies, urban planners, and community organisations is essential for mitigating these vulnerabilities and fostering heat resilience in the community. The social vulnerability index is the result of daily activities and events or their adjustments (Hewitt, 2014). Inadequate access to resources such as knowledge and data, limited political power and involvement, unique traditions and beliefs, weak institutions or slow personalities and facilities, for example, have a substantial impact on a number of the underlying causes of social vulnerability (Blaikie *et al*., 1994; Cutter, 1997; Mileti, 1999). While these determinants vary over space and time, studies show that specific demographic and living conditions characteristics—age, race/ethnicity, income levels, gender, building quality, and public infrastructure—have an impact on amplifying or decreasing overall vulnerability to heat exposures (Blaikie *et al.*, 1994; Hewitt, 1997; Tobin & Montz, 1997). Based on these findings, Cutter *et al*. (2003) created the social vulnerability index, which incorporates demographic, residential, and environmental characteristics that contribute to social vulnerability. While these variables may not fully explain the fundamental reasons for social vulnerability, they provide a starting point for operationalising the concept.

The Cutter *et al*. (2003) social vulnerability and the concept of social determinants of heat-related health outcomes are the basis from which the identified literatures in this review formulate their heat vulnerability indices. The commonly used indices are air temperature, LST, dwelling quality, and impervious surface. Certain geographical areas, such as UHI, are especially vulnerable to heat waves. These places may have greater ambient temperatures due to the dense concrete infrastructure, lack of green space, and less air circulation. Residents of such areas may face heightened heat-related dangers. Others are demographic and socioeconomic variables, including population density, ethnicity, gender, age, level of literacy, and poverty level. Individuals with lower socioeconomic levels have limited access to facilities that reduce the impacts of heat, such as air conditioning, cooling centres, and appropriate housing. They may work in jobs that expose them to high heat or be unable to afford cooling measures, increasing their exposure. Heat can be exacerbated by

inadequate insulation and overpopulation in homes. People living in inadequate housing may struggle to maintain a healthy indoor temperature or lack access to ventilation and cooling systems, leaving them more vulnerable to heat-related health concerns. The older population is particularly vulnerable to heat-related health effects due to physiological changes associated with ageing. Older people may be more vulnerable to the adverse effects of heat due to reduced thermoregulatory ability, chronic health issues, or limited mobility. People who have pre-existing health diseases such as cardiovascular disease, respiratory disorders, or diabetes are more likely to suffer from heat-related illnesses. These problems may limit their ability to control body temperature or respond effectively to thermal stress. Isolated socially Individuals with limited social networks, such as the elderly, may lack the required support systems to withstand severe temperatures. During heat waves, they may be less likely to receive timely assistance, resulting in increased susceptibility and the likelihood of adverse health outcomes. A lack of access to healthcare services, such as preventive treatment and immediate medical response, can increase heat-related health concerns. This could include having difficulty obtaining vital medications, receiving proper heat management advice, or gaining access to healthcare facilities during heat emergencies. Cultural practices and individual behaviours can influence individual sensitivity to heat-related health problems. Certain cultural norms, for example, may prohibit cooling measures or protective clothing in hot weather. Inadequate knowledge of heat-related risks and preventive measures can also contribute to vulnerability.

The number of heat vulnerability indicators used by studies varies due to data access in some locations. For instance, most heat vulnerability studies in advanced countries have an average of eight indicators compared with studies in developing countries where fewer indicators are used due to the difficulties in accessing data. For example, Wolf & McGregor (2013) employed 10 indicators in their heat vulnerability study in London, whereas Uejio *et al*. (2011) utilised 11 indicators in their investigations in Philadelphia and Phoenix. Mushore *et al.* (2018) employed proxy variables from Landsat-8-derived bio-physical surface features and socio-demographic parameters to assume their representation of heat vulnerability indicators in Harare, Zimbabwe (Table 2.8). Virtually all the

studies included in this review used indices related to exposure to heat hazards - impervious surface, air temperature, LST and urban heat islands, with socioeconomic and demographic indices. Few studies included health-related indicators (Loughnan *et al*. 2014; Wolf *et al.* 2014; He *et al*. 2019), language (Mortensen *et al*. 2018), employment as a proxy for poverty and inequality (Hulley *et al*. 2019), and immigrant status (Yu *et al*. 2021). Figure 2.4 shows the spatial distribution of heat vulnerability studies to human health included in this review.

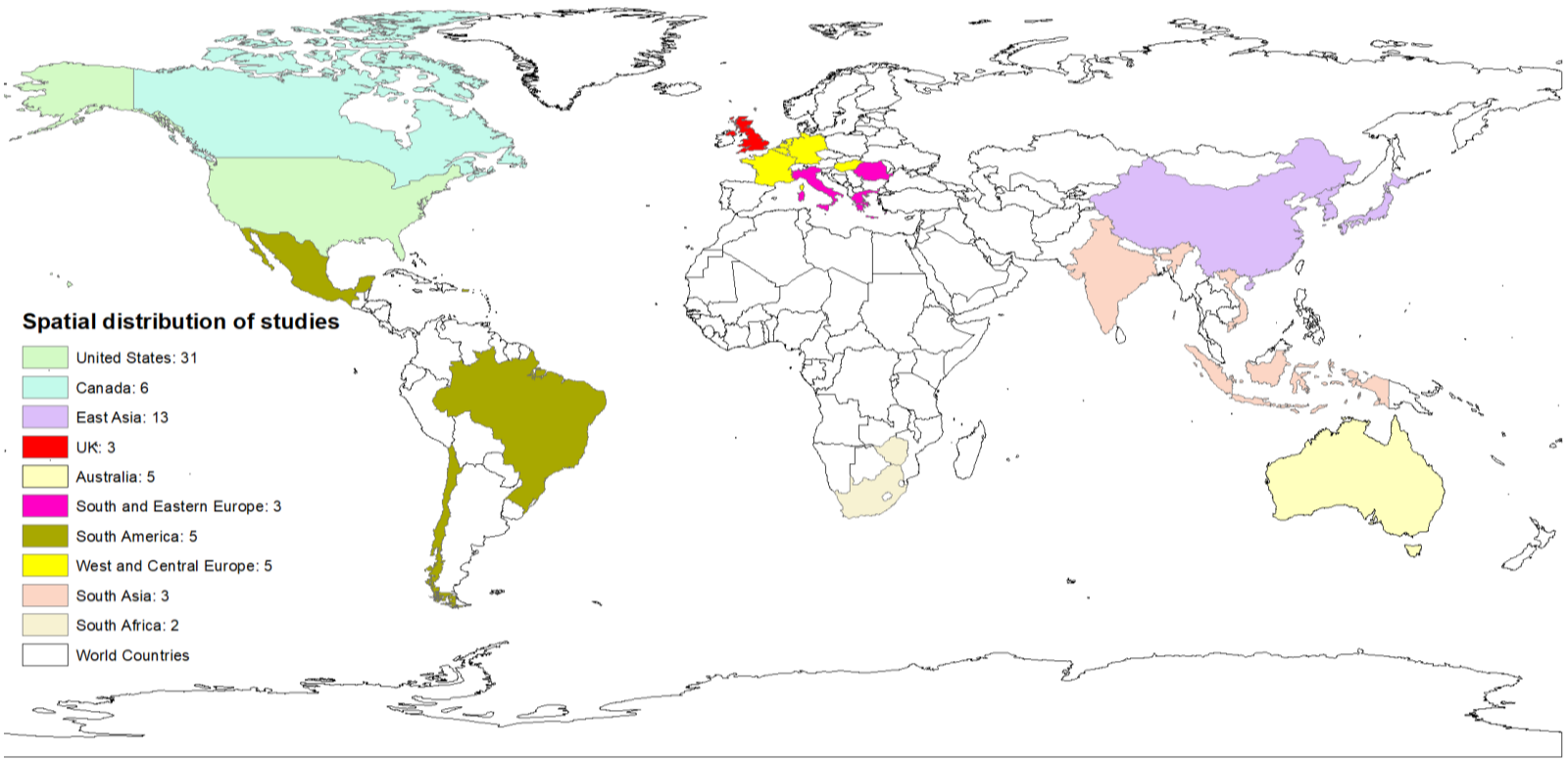


Figure 2.4: Global distribution of studies on spatial mapping of heat vulnerability.

2.4.2.2 Spatial scale of mapping

The spatial scale of mapping used by the studies identified in this review ranges from pixel to census track, district to sub-district, and administrative boundaries to country level. Census and sub-census blocks and wards were utilised as a mapping scale in 47 (59%) of the identified studies. 6 (8%) of the identified studies are at the district level. Grids and pixel spatial unit data were used in 7 (9%) of the identified research. Administrative, postal unit and zip code were used in 8 (10%) of the identified studies. 14 (18%) of the identified studies use municipalities, countries, and local government areas (LGAs) as mapping scales. In all cases, the scope of study and data accessibility often define the spatial scale of the heat vulnerability mapping. In some cases, the census tract can be relatively coarse, and the demographics may not match the tract-level boundaries (Weber *et al*., 2015; Guo *et al*., 2019). A proxy indicator that offers a worthy substitute can be used when an index is not accessible at the required spatial scale, for example, literacy level, and poverty and inequality indices. For instance, Gronlund *et al*. (2016) used high school education as a proxy for income level. There is no conclusive procedure for the spatial mapping of heat vulnerability to human health. It is, however, essential to use the approach that is best suitable to the requirements of the study, which will be contingent on data accessibility and the knowledge of what defines heat vulnerability for a specific exposure in a location and how to represent them on maps (Gamble *et al*., 2018).

2.4.2.3 Techniques for data analysis

On methods, principal component analysis (PCA) or factor analysis and overlay is the predominant procedure used by over 56 (71%) of the identified studies included in this review. For example, in their study, Zhu *et al*. (2014) combined PCA and overlay. Tran *et al*. (2020) and Zhang *et al*. (2019) combined PCA, AHP, and weighted overlay. Loughnan *et al*. (2012) and Wolf *et al*. (2014) integrated PCA, regression model, and weighted overlay. Large datasets are increasingly becoming standard indices for heat vulnerability mapping. For instance, Azhar *et al*. (2017) used over 12 indicators for their mapping. The use of multiple and complex indices is often challenging to interpret. The PCA reduces the dimensionality and redundancy of datasets to increase

interpretability while reducing information loss (Jolliffe & Cadima, 2016). Since the PCA grouped heat vulnerability indicators to generate indicators, it becomes difficult to isolate the magnitude of the impacts related to separate indices (Jagarnath *et al*., 2020). In this regard, overlay operation is often used to integrate the indicators to form vulnerability maps. The overlay analysis is an operation that superimposes several layers of datasets that represent diverse themes to identify the relationship. By merging datasets from two or more attributes and geometry, new geometries and units of change entity in a visual form are created.

Expert judgment has been used in some studies for mapping the vulnerability mapping of health to heat. For example, Zhu *et al*. (2015) and Tran *et al*. (2020) invited experts from public health, meteorology, and social sciences to rank the heat vulnerability indicators included in their study. AHP and PCA were used to weigh each index based on their relative influence. The use of expert judgment is a valuable component of the spatial mapping of heat vulnerability for human health, even though this component was missing in over 75 (95%) of the indicated papers included in this review. Table 2.8 presents the summary of the cited papers on the spatial mapping of heat vulnerability for human health.

Table 2.8: Summary of studies on the spatial mapping of heat vulnerability for the whole world ordered by first author surname

Region	Location	Authors	Summary of heat vulnerability indicators used	Mapping methodology	Institutional/Spatial scale of data	Validation Data
Australia	Melbourne	Loughnan *et al.* (2012)	Aged, care facilities, ethnicity, aged people living alone, infants and elderly, urban density	Regression analysis, weighted overlay	Postal area	Morbidity and mortality
	Australian capital cities	Loughnan *et al*. (2014)	Demographic, environmental, and health. Vulnerability variables	Regression analysis, Overlay	SA, LGA	Morbidity
	Sydney	El-Zein & Tonmoy (2015)	*Tmax* days, *Tmin*, land cover, population density/ > 12yrs/ requiring financial assistance, road density, elderly/ and living alone, children, multiunit dwellings, not English speaking, home loan repayment, homeownership, household income, internet access, assets to liabilities of the local council, business rates, residential rates, community service expenses, environmental and health expenses	Multi-criteria outranking, overlay	15 LGA	
	Port Phillips	Norton *et al*. (2015)	heat exposure (daytime and night-time heat) % population of elderly, very young, and socially disadvantaged Land use/cover/Public Use Zones	Overlay		
	Sydney	Zhang *et al*. (2018)	LST, infants, elderly persons, ethnicity, low education people, new arrival, language barrier, low-income people, persons	Spatial statistics and Analysis, Overlay	Raster-based subdividing indicator	

			with disability, isolated people, traffic convenience, internet access, proximity to woody vegetation, proximity to a water body			
UK	Birmingham	Tomlinson *et al.* (2012)	LST, elderly population, ill, the density of households, flat	Normalization, equal weight, overlay	Census areas	
	London	Wolf *et al*. (2014)	Daily mortality and ambulance callout, daily *Tmin/Tmax*, elderly population above 65 years	PCA, regression analysis	Census tracts	Mortality and Ambulance callout
	London	Wolf & McGregor (2013)	LST, households in rented tenure/ without central heating/ single pensioner, flat, ethnicity, population density, elderly, self-report bad health status, receiving a social benefit	PCI, spatial clustering analysis, overlay	Census tracts	Satellite image of surface temperature for a single day embedded in a long heatwave event
Eastern Asia	Tibet, China	Bai *et al*. (2016)	Old age, low income, illiteracy, physical/mental disability, small living spaces, and living alone	PCA	County-level	
	Shanghai, China	He *et al*. (2019)	Heatwave duration, frequency, and intensity, the density of roads, vegetation coverage, night-time light value, and availability of medical resources.	FA	Grid	Mortality
	Guangdong Province/China	Zhu *et al*. (2014)	Elderly, infant/mortality rate, immigrant, unemployment, agricultural population, health worker, GDP per capita, living space, harmless sanitary latrines, illiteracy rate,	AHP, PCA, overlay	Districts level	

			temperature growth, heatwave day count			
	Osaka City, Japan	Macnee & Tokai, (2016).	Population density/ over 65 yrs, receiving home care, unemployed, didn't graduate high school, Single-person households/ Over 65 single, Greenspace/open water	PCA, overlay	Census districts	
	Beijing. China	Dong *et al*. (2014)	LULC, heatwave/high temp. days, population density, elderly ratio, income level,	Normalization, equal weight, overlay	Sub-districts	
	Korea	Kim *et al*. (2017)	Heatwave/deaths, population, elderly/living alone, agricultural workers, labourer, poverty, urbanization rate, *Tmax*, tropical night, hospitals	Zero-inflated Poisson regression analysis, overlay	Administrative areas	Mortality
	Zhejiang Province	Hu *et al*. (2017)	Land Cover, temperature, % of elderly (≥65 years), % of elderly (≥60 years) living alone, air conditioners per 100 households, illiteracy rates of population (≥15 years), per capita GDP, vegetation index, high fractional settlements, DEM	Weighted overlay	Sub-district level	Qualitative assessments, spatial variations in heat-related deaths
	Beijing	Zhang *et al*. (2019)	Heatwave days/public awareness, the capacity of an earlier warning, high-rise buildings concentration, Paved area, Population density, % > 65 yrs, green areas, Capacity of infrastructure	AHP, weighted overlay	Districts level	
	Chongqing, China	Zhang *et al*. (2019)	LST, air quality, vegetation, DEM, water bodies, Night-time, hospital visits, lights, the total	PCA, Pearson correlation, z-score method	County-level	Pearson correlation/ monthly

		elderly population (60+); elderly people with disability; elderly people with low income; dwellings without bathing facilities; dwellings built, the density of highways, total beds of health institutions,			hospital visits in the summer period
Beijing	Guo *et al*. (2019)	LST, NDVI, % population > 65/< 5yrs, < high school, above college, illiterate, living alone, unhealthy > 60, income, AC /100 households	PCA, EWI	Census units	
Hong Kong	Song *et al*. (2020)	Elderly, Lower education, Attainment, Foreigners, English-speaking People, Labour force participation rate, Poverty, vulnerable occupation, elderly living alone, household size, nuclear households, people living alone, building density, unvegetated open space, transport land, daytime surface temperature, night-time surface temperature	PCA	Community level	Multivariate analyses were conducted to construct a parsimonious set of metrics for further analysis
Hangzhou	Liu *et al*. (2020)	Several elderly (≥65 years), unhealthy seniors, elderly (≥60 years) living alone, illiteracy (≥15 years), Populations less than high school education, disposable income, cooling facilities, and Lack of green space.	EWA and PCA	30m, sub-district level.	Linear regression, death data
China	Zhang *et al*. (2021)	LST, elderly dependency, maternal mortality, perinatal mortality, the morbidity of	PCA, correlation analysis	Provincial-level administrative divisions	

			infectious diseases, the proportion of households with > 5 persons, air temperature, % of people living alone, per capita GDP, electricity demand, air quality			
North America	Quebec, Canada	Vescovi *et al.*(2005)	Isolation, income, hot days/repeated hot days with *Tmax* > 30°C and *Tmin* > 22°C, education, aged	Normalization, equal weight, Overlay	Census subdivision	
	Philadelphia	Weber *et al.*(2015)	NDVI, LST, % population < poverty line, < high school, households with single person > 65 living alone, % of housing units built before 1960	EW, Overlay	Census block	
	United States	Reid *et al.(2009)*	Vegetation, poverty, ethnicity, aged/living alone, education, living alone, diabetes, central AC/AC	PCA, Overlay	Census tracts	
	Toronto, Canada	Rinner *et al.(2010)*	Vegetation, LST, old residence/density residence without AC, behaviour, disease, aged, cognitive impairment, babies/young children, insufficiency, rental households, isolation, homeless, education, non-English speaking, recent immigrants, cooling centers, ethnicity, home cooling, drop-in centers, participating in community outreach centers	Ordered weighted averaging, overlay	Census tracts	
	Washington, California	Reid *et al.(2012)*	Poverty, race non-white, < high school diploma, non-green	PCA	ZIP code	Morbidity and mortality

Massachusetts, Oregon, New Mexico		space, living alone, > 65 yrs/live alone, homes without central AC/with no AC, diabetes			
Chicago Illinois	Johnson *et al*.(2012)	LST, NDVI, NDBI, Womens > 65/living alone, Males < 65 yrs/living alone, race, family income in 1989, > 25 yrs </>25yrs with high school	PCA, overlay	Census blocks	Mortality
Chicago, Illinois, Dayton, Ohio, Indianapolis, Indiana	Johnson *et al*.(2013)	LST, NDVI, NDBI, total population, race, age, sex, educational, income, and poverty status	PCA, overlay	Census block group	
Maricopa County Arizona	Harlan *et al*.(2013)	Ethnicity, immigrant, poverty, education, central AC, elderly/living alone, living alone, unvegetated area, LST	PCA, overlay	Census blocks	Mortality
Georgia	Maier *et al*. (2014)	Poverty, education, ethnicity, living alone, elderly, elderly and living, diabetes, land use	PCA, overlay	Administrative areas	Mortality
Georgia	Manangan *et al*. (2015)	Impervious surface, % 65 yrs/living alone, poverty level, heat event, % dialysis patients covered by Medicare, hospital insufficiency	Overlay analysis	Census tracts	
Phoenix Arizona	Chuang & Gober, (2015)	NDVI, Poverty line, Race/non-Hispanic white, <high school diploma, Age > 65 yrs/living alone, No central AC, No AC, Living alone, Diabetes	FA, overlay	Census tracts	Hospital admission
Travis County, Texas	Prudent *et al*. (2016)	Health, built environment, and social factors	PCA	Census tracts	Mortality
Greater Vancouver	Krstics *et al*. (2017)	Temperature exposure, Social vulnerability, Population distribution, Urban form	HEID approaches,	Postal code	Mortality

British Columbia			summation model		
Phoenix	Chow *et al.* (2012)	NDVI, mean summer *Tmax/Tmin*, elderly, income, foreign-born noncitizens, immigrants	Normalization, equal weight	Census tracts	
New York State	Nayak *et al*. (2018)	Elderly/social isolation; social/language; socioeconomic; and environmental/urban vulnerability	PCA, Overlay	Census tracts	Emergency department visits and admissions
National Capital Region	Aubrecht *et al.* (2013)	Heatwave count, elderly, living alone, poverty, poor English skills, education, vegetation	Normalization, equal weight, overlay	Census blocks	
Philadelphia	Hammer *et al*. (2020)	LST, sociodemographic, health status, community assets, locations of city-operated pools and spray grounds, health centers, and community schools	PCA, overlay	Census block group	
Phoenix, Arizona	Watkins *et al*. (2021)	9 Adaptive resources to mitigate the impact of extreme heat (e.g. AC unit, trees in a yard). 22 Adaptive behaviours to reduce the impact of extreme heat (e.g., using central AC, changing one's schedule). 9 Proximate sensitivity to extreme heat impacts (e.g., cost of electricity, health status). 3 The health outcome related to self-reported experience with symptoms of heat-related illness or thermal discomfort	Kendall's tau-b correlation	Census block group	
Dallas, Texas	Mallen *et al.* (2019)	Non-green space, aged 65yrs/living alone, Diabetes	PCA	Census tracts	Mortality

			prevalence, Race, Living below the poverty line, Less than high school education, access to AC			
	Philadelphia	Hondula *et al.*(2012)	LST, residential density, land use, commercial, building coverage, race, education, income, below the poverty line, aged/living alone, living alone	PCA, overlay	Zip code area	
	Detroit Michigan	Conlon *et al*. (2020)	Aged 65/living alone, living alone, Minority, < than HS education, poverty level, impervious surface, Non-tree canopy, non-vegetated/water, No trees, distance to water	PCA	Census tracts	Mortality
	Pittsburgh, Pennsylvania	Bradford *et al*. (2015)	% aged > 65yrs/living alone, poverty, with poor English skills, level of education, ethnic diversity, with diabetes, accessible to AC, green space	Factor analysis	Census block	
	Chicago, Illinois	Wilson & Chakraborty (2019)	Level of education, income level, substandard housing units, aged under 18 years, the population in homes for the aged and dependent, race	Maximum likelihood, factor analysis	Census tracts	
	Portland, Oregon	Voelkel *et al*. (2018)	Income level; race; level of education; age and English speaking ability, housing quality, surface temperature, and UHI	Student's t-test, network distance, and covariance analysis	Census block group	
	Canada	Ho *et al*. (2018)	Ages, infants, people in old houses and bad living environments, low education population, people living alone,	Multi-criteria analysis	Census tracks	

			Low-income population, unemployed			
	Philadelphia and Phoenix	Uejio *et al*. (2011)	Heat exposure and the built environment: vegetal health/density, nigh surface temperature, impervious surface, housing density, poverty level, household renting, aged 65 yrs/ living alone, disabilities, linguistically isolated, a household with 7 or more residents, race, neighbourhood stability: residents changed household by 5 yrs., vacant household	Generalized Linear and Mixed Models	Census groups	block
	British Columbia, Canada	Yu *et al*. (2021)	Climate, age, pre-existing health, socioeconomic, race/ethnicity, immigration status, built environment, social cohesion, institutional	PCA	Census tracts	
	Texas	Heaton *et al*. (2014)	Excess non-accidental mortality counts, weather simulations, Socio-economic and demographic	A hierarchical model with spatial varying	Census groups	block
	Houston, Texas	Mortensen *et al*. (2018)	Temperature, density of persons>65/<5 yrs, %black, % Hispanic, without AC, % low-quality buildings, emergency call data, mortality data	Hierarchical marked point process model	Census groups	block
	Vancouver, Canada	Ho *et al*. (2015)	Seniors; infants; living in old housing, multi-story apartment, mobiles homes; living alone; low income; low education; and the unemployed	Raster-based multi-criteria decision analysis	60 m pixel	

	Gwynns Falls Watershed, Baltimore Counties, Maryland	Huang *et al*. (2011)	LST, income, poverty, having a bachelor's degree, receiving < 9 years of education, % of White people, aged> 65yrs/ living alone, total crime	Correlation analysis, GIS mapping	Census-based unit, block group	
	Cambridge	Williams *et al*. (2019)	Demographics, pre-existing medical diagnoses, and indoor, and environmental quality	The generalized additive mixed, regression model	Two public housing units	
	Dallas, Texas	French, (2018)	Heat events, aged >65 living alone, poverty line, Prevalence of diabetes, impervious surface, number of medical infrastructure facilities	Overlay and spatial regression	Census tracts	HVI outcomes with the modelled mortality at the census tract level compared
	United States	Lay *et al*. (2021)	Temperature and mortality, AC, coverage, total population, and population aged 65 years or older	Regressions model	208 US cities	
	Milwaukee and Wisconsin	Christenson *et al*. (2017)	Population density, health, demographic, socioeconomic, natural, and built environment factors	Overlay/EW	Census block groups	
	Camden, New Jersey	Sabrin *et al*. (2020)	DEM, PM, Vegetation, Water Fraction, building footprint and height, PM, ozone, imperviousness, income, population density, and ages <5 &>65yrs	The normalization, regression model, overlay	Census tracts	
	Vancouver, Canada	Aminipouri *et al*. (2016)	Demographic/socioeconomic and environmental exposure factors, infrastructure conditions	Overlay/RA	105 census areas	

	Los Angeles County, California	Hulley *et al*. (2019)	LST, aged population, density, poverty level, NDVI, disabled, unemployment, building height, education, income, NDVI	PCA, correlations	Sub-city block scale	
	United States	Gronlund *et al*. (2016)	*Tmax*, aged > 78 yrs, black race, sex, home ZIP-code, non-green space, high school education, housing built before 1940), AC prevalence	Regression model	Census tracts	
Southern Europe	Italy/Milan	Bhattacharjee *et al*. (2019)	UHI, vulnerable population index, healthcare accessibility, housing quality NDVI	Overlay and correlation		
	Athens, Greece	Keramitsoglou *et al*. (2013)	LST, NDVI, DEM, population density, non-proper, sub-standard, and houses made of inexpensive building materials with no plan	Artificial intelligence fuzzy logic, urban climate model	Census block	Meteorological data, mean temporal correlation
	Padova, Italy	Maragno *et al*. (2020)	Built area, impervious surface, roofs, and streets incoming solar radiation, trees, and green areas, land use, and population aged 0-10 and 65+	Overlay	District level	
South America	Santiago, Chile	Inostroza *et al*. (2016)	Urban area, LST, aged, infant, disabled, family structure, literacy, NDVI, road, access to medicals, water and communication services, unemployment, material index,	Cluster analysis, PCA	Census tracts	
	San Juan, Puerto Rico	Méndez-Lázaro *et al*. (2018)	LST, land cover, demographic and socioeconomic data; age, income level, educational level, access to health service	PCA/ factor analysis, overlay	Census tracts	
	Porto, Alegre, Curitiba, São	Lapola *et al*. (2019)	LST, Aged >65-yrs, human development index	Heat stress vulnerability and risk index	Census tracts	

	Paulo, Vitória, Natal, Manaus					
	Mexico City, Mexico; Sa˜o Paulo, Brazil; Santiago, Chile	Bell *et al*. (2008)	Weather and pollution, % population characteristics, educational attainment at death, age at death, cause of death (%)	Regression model	City Level	
	Rio de Janeiro	Prosdocimi & Klima, (2020)	Multiple socioeconomic, environmental, and urban forms/characteristics	Factor analysis	Census block group	Distance to hospital/clinics and health record data
Eastern Europe	Bucharest, Romania	Grigorescu *et al*. (2021)	Permanent resident, agricultural area, climate conditions, impervious surfaces, green areas, water resources, vulnerable age groups, ethnic diversity, dependency on the primary sector for livelihood, agricultural income, access to clean water, cultivated and inhabited environment, connectivity to drinking water infrastructure, health care services provided by high-level medical infrastructure, pharmacies, early warning/intervention services, education level, heat management & adaptation in agriculture, blue areas, forest areas, protected areas	Multi-criteria vulnerability assessment, Hull's score and standard deviation	Administrative-territorial units	
Western Europe	Liege, Belgium	Stephenne *et al*. (2017)	Total population, elderly population (over 65 years, women population over 65, male population over 65, gender ratio, UHI	Overlay	Spatial units	

	France	Rey *et al*. (2009)	Temperature, Ozone concentration, age, gender, and mortality observed during the 2003 heatwave	Poisson model	Small spatial units	
	Amsterdam, The Netherlands	Van den Hoeven & Wandel (2015)	Surface temperature, impervious surface, the energy efficiency of buildings, aged and infants, population and workforce, and Quality of life in the neighbourhoods.	GIS mapping	Municipality	
	Cologne area, Germany	Depietri *et al*. (2013)	UHI, LULC, unemployed, aged > 65yrs/living alone, immigrants, forest cover	Equal weight, overlay	85 districts	Sensitivity analysis
Central Europe	HUNGARY	Uzzoli *et al*. (2018)	Heat day, socio-economic development, quality of life, average life expectancy at birth, education level, income base income per resident	Normalization	District level	
Southern Asia	India	Azhar *et al*. (2017)	Land cover, vegetation fraction, NDVI, aged, under 5, sex ratio, Ethnic group, and Scheduled castes, workers, lowest wealth quintile and literacy, children fully immunize, household amenities	PCA/Kaiser-Meyer-Olkin test	District level	
	Jakarta and Bandar Lampung	Manik & Syarifah (2017)	Community knowledge of climate change, climate variability water availability, health-related to air temperature, energy consumption social relationships, education, income, house adaptation	Balanced weighted average	Community-level	
	Vietnam	Tran *et al*. (2020)	Aged > 65 &<5, % low access to safe water, population	AHP, overlay	Province	

			density, poverty, % population in urban, % women population, % illiterate, % unemployment, % households with AC, health-related status, vegetation index		
South Africa	Harare, Zimbabwe	Mushore *et al*. (2018)	Biophysical surface properties and socio-demographic factors	Overlay/EW	30 m pixel
	Durban metropolitan	Jagarnath *et al*. (2020)	Population density, age, gender, women, urban land use, pre-existing medical conditions, income, vegetal cover, education, poverty, ethnicity, acclimatization, access to AC/pool, and home tenure	PCA, weighted variance approach, overlay	Ward scale

2.4.2.3 Validation of heat vulnerability indicators and maps

The validation of heat vulnerability indicators and maps is essential for establishing the accuracy of the heat vulnerability maps. Unfortunately, only 19 (24%) of the papers identified in this review performed validation (Table 2.9).

Table 2.9: Studies that validated the heat vulnerability maps outputs

Validation datasets	No. of studies	Reference(s)
Heat-related mortality	(9)	(Wolf & McGregor, 2013; He *et al*., 2019; Kim *et al*., 2017; Johnson *et al*., 2012; Harlan *et al*., 2013; Maier *et al*., 2014; Prudent *et al*., 2016; French, 2018; Mallen *et al*., 2019)
All-cause mortality	(2)	(Krstic *et al*., 2017; Conlon *et al*., 2020)
Heat-related morbidity	(1)	(Loughnan *et al*., 2014)
Heat-related morbidity and mortality	(1)	(Reid *et al*., 2012)
Mortality data and Ambulance callout	(1)	(Wolf *et al*., 2014)
Hospital admission for heat-related stress	(1)	(Chuang & Gober, 2015)
Emergency department visits and admissions	(1)	(Nayak *et al*., 2018)
Distance to hospital/clinics and health records	(1)	(Prosdocimi & Klima, 2020)
Satellite images of surface temperature	(2)	(Wolf & McGregor, 2013; Keramitsoglou *et al*., 2013)

Most studies validate their vulnerability maps by comparing the maps to health data and investigating the relationship between them. Regression modelling appears to be the widely used technique in the identified papers in this review, as it was used by n=7 (38%) of the recognised studies that validated their map outputs. For instance, Liu *et al*. (2020) and Song *et al*. (2020) used the heat vulnerability indicators and morbidity and mortality data for their validation using linear and multivariate regression. Loughnan *et al*. (2014) used stepwise regression to choose the best heat vulnerability indicators for Australia's capital city. Other studies used heat vulnerability maps and morbidity and or mortality data with bivariate correlation (Loughnan *et al*., 2012; Hu *et al*., 2017; Kim *et al*., 2017; Zhang *et al*., 2019). In their study, Wolf *et al*. (2014) used mortality and ambulance call-out and heat vulnerability indicators in a contingency table or cross-classification analysis, usually used to validate whether predictions validate heat vulnerability maps. The Table measures dichotomous results (i.e.,

"yes, a vulnerability hotspot does have higher health impacts than its counterpart areas" or "no, the vulnerability hotspot is not a real hotspot as validated using health outcome data"). In this regard, the vulnerability score for an individual location is linked to the aggregated morbidity and mortality result measure. When the contingency tables are generated, statistical methods can be considered to define the prediction detail and performance of the validation. Table 2.10 presents a summary of methods and results of heat vulnerability validation. It becomes evident that the statistical techniques and health datasets used for validation makes it challenging to compare the effectiveness of the validation results. Some studies showed low R^2 values (Conlon *et al*., 2020; Kim *et al*., 2017), which could be due to the incompatibility of the spatial scale of the indicators and validation datasets, for instance, a combination of higher and lower resolution datasets can lead to a loss of information. The use of an inappropriate index, the non-inclusion of essential indicators, and unfair weighting structures.

Table 2.10: Summary of methodologies and results for the validation

Reference(s)	Study location	Methodology	Validation equation	Results
Song *et al.* (2020)	Hong Kong	Heat-related Health Risk Index (x)was used to regress heat-related mortality data (y)	y =0.79x-0.12	R^2=0.60, n=91
Wolf *et al.* (2014)	London	Skill scores were computed for the dichotomous (yes/no) on HVI performance as a predictor of levels of mortality and ambulance callout	Skill scores were calculated for the dichotomous (yes/no) outcome	The vulnerability score and health outcomes matched in 65% of geographical areas
Zhang *et al.* (2019)	Chongqing, China	Heat health risk (x) was used to correlate the summer hospital visit (y)	y = 3E-05x^2 – 0.00x+0.52	R^2 = 0.924
Liu *et al.* (2020)	Hangzhou	Total heat-related deaths (x) were used to regress Heat Vulnerability Indicators (y)	y = 80.77x – 18.18 y = 28.29x + 8.24	R^2 = 0.58-EWA R^2 = 0.32-PCA
Loughnan *et al*. (2014)	Australia	Vulnerability indicators (x) were used to correlate the Emergency Service demand on hot days (y).		R^2 0.04 - 0.62

Hu *et al*. (2017)	Zhejiang, China	Risk assessment results (*x*) were used to correlate health outcomes (*y*)	y= 175.02x0.428	R^2 = 0.61
Loughnan *et al.* (2012)	Australia	Heat vulnerability factors (*x*) were correlated with mortality and morbidity across hot days (*y*)		R^2 = 0.03
Kim *et al.* (2017)	Korea	Scatterplot of the detected total of heatwave linked mortality (*x*) and the projected heatwave vulnerability index (HVI) (*y*)		R^2 = 0.32
Chuang and Gober (2015)	Phoenix, Arizona	Geographic variances of the vulnerability map and the heat-related hospitalization were compared	Evaluated the index developed by Reid *et al.* (2009)	54% accurate
Wolf and McGregor (2013)	London	Heat vulnerability hotspots", were overlaid on the MODIS surface temperature	Assess the degree to which areas of high heat vulnerability coincide with areas of high heat exposure.	Getis Ord z-score 41.96 and surface temperature 19^{o}C or greater.
He *et al.* (2019)	Shanghai, China	The spatial distribution of all grids with high mortality risk was used to regress the identified number of sensitive residents in these grids		

2.5 The role of remote sensing and GIS for understanding the relationship between the UHI and human health

Extreme heat in the form of air temperature, LST, UHI atmospheric temperature and WBGT was the primary heat exposure index used in the papers identified in this review. The contributions of AIS and vegetation cover as measured by the NDVI are important and utilised by a number of research. The NDVI is the measure of vegetation amount in an area often used in urban studies as an inverse measure of impervious surface (Ghorbani *et al.*, 2012; Evangelides & Nobajas, 2020), which are perceived to intensify the effects of heat or offer relief by decreasing the temperature effects on human health (Gascon *et al*., 2016; Guo *et al*., 2019).

The literature shows temperature, impervious surface, and NDVI are commonly used in heat vulnerability mapping (Zheng *et al*., 2020). LST from airborne or satellite remote sensing is the primary tool for the measurement of temperature in vulnerability mapping studies due to its spatio-temporal scale relative to measurements of in situ data from meteorological station networks, automobile transects, or specialised sensor platforms. The use of remote sensing images and GIS techniques for mapping impervious surfaces and NDVI has been a vital component of vulnerability mapping. Among the commonly used satellite sensors for heat, and human health studies are Landsat MSS, TM, ETM+, OLI, MODIS, and national land cover databases. For instance, daytime and night-time surface temperatures acquired from Landsat and MODIS sensors are prevalent in the literature (Uejio *et al*., 2011; Buscail *et al*., 2012; Dong *et al*., 2014; Hu *et al*., 2017; Conlon *et al*., 2020; Zheng *et al*., 2020). Table 2.11 presents satellite sensors widely used for heat-human health studies.

Some studies obtain vegetation height using point clouds from light detection and ranging (LiDAR) (Maragno *et al*., 2020). Other studies combined satellite data with air temperature, humidity, and air quality indices acquired from weather stations and national monitoring systems such as the US EPA and China National Environmental Monitoring Centre (Vescovi *et al*., 2005; Sabrin *et al*., 2020; Zhang *et al*., 2019). Due to their detrimental impact on human health, a few studies have included the concentration of PM2.5 and ozone using tapered element oscillating microbalance (Kalisa *et al*., 2018; Yang *et al.,* 2019). The dwelling quality, such as housing type and surface material are connected to thermal stress and influences the adaptive capacity. For instance, some ancient and lower-quality buildings are deficient in thermal insulation (Rinner *et al*., 2010; Salamanca *et al*., 2013). In this review, Voelkel *et al*. (2018) included dwelling quality as an index for heat vulnerability. Other socio-demographic and health indices incorporated in most studies cited in this review were often acquired from national census statistics, household surveys, or open data from the national disease control bureaus database and health centres. GIS and statistical techniques are often used for data preparation and spatial analysis.

Table 2.11: Satellite sensors commonly used for the mapping of heat vulnerability indicators and maps

Sensor	Satellite	Spatial resolution	Revisit Time	Thermal Spectral band(µm)	Local time of Image acquisition	Temporal coverage	Data Available at
PHyTIR	ECOSTRESS	60m	Varies/every few days	8.28µm, 8.79µm 9.06µm, 10.05 µm 12.05 µm	Varying	06/2018 – present	https://ecostrss.jpl.nasa.gov/data
SLSTR	ESA - Sentinel 3A & 3B	1km	12 hours	10.45µm – 11.25 µm 11.57 µm – 12.48 µm	1000am/pm	02/2016 – present 04/2018 – present	http://scihub.copernicus.eu/dhus/#/c
Landsat TIRSI	Landsat 8	100m	16 days	Band 10 (10.6 - 11.19 µm) Band 11 (11.5 - 12.51 µm)	0949	02/2013 - present	EarthExplorer, GloVis, and LandLook Viewer.
Landsat ETM+	Landsat 7	60m	16 days	Band 6 (10.4 -12.5 µm)	0939	4/1999- present	EarthExplorer, GloVis and LandLook Viewer.
Landsat ETM	Landsat 6	120m	16 days	Band 6 (10.40 - 12.50 µm)	0942	1993	EarthExplorer or GloVis
Landsat MSS & TM	Landsat 5	120m	16 days	Band 6 (10.40 - 12.50 µm)	0915	3/1984 – 01/2013	EarthExplorer, GloVis, and LandLook Viewer.
Landsat MSS	Landsat 4	120m	16 days	Band 6 (10.40 - 12.50 µm)	1000	7/1984 - 12/1993	EarthExplorer, GloVis and LandLook Viewer.
MODIS	Aqua	1km	Twice Daily	(31) 10.78 – 11.28 (32) 11.77 – 12.27	1330 0130	04/2002 - present	http://modis.gsfc.nasa.gov/ https://lpdaac.usgs.gov/lpdaac/products/modisoverview
MODIA	Terra	1km	Twice daily	(31) 10.78 – 11.28 (32) 11.77 – 12.27	1030 2230	2000 2000	http://modis.gsfc.nasa.gov/ https://lpdaac.usgs.gov/lpdaac/products/modisoverview

ASTER	Terra	90m	Twice daily	(10) 8.125 – 8.475 (11) 8.475 – 8.825 (12) 8.925-9.275 (13) 10.25-10.95 (14) 10.95-11. 65	Request only	12/1999 - present	http://asterweb.jpl.nasa.gov/index.asp
AVHRR	Multiple NOAA	1.1km	Twice daily	(4) 10.3.11.3 (4) 11.5- 12.5	2:00am/pm	1979 – present	http://noaasis.noaa.gov/NOAASIS/ml/avhrr.html http://eros.usgs.gov/Find Data/Products and Data Available/AVHRR
AVHRR	MetOP	1.1km	29 Days	(4) 10.3.11.3 (4) 11.5- 12.5	0930	2006	http://www.esa.int/esaLP/ESA7USVTYWC LPmetop 0.html
AASTER	Envisat	1km	35 days	11-12	1000	2014	http://envisat.esa.int/instruments/aatsr/
SEVIRI	Meteosat 8	3km	Geostationary	10.8 -12	Every 15mins	2005	http://landsaf.meteo.pt/
GEOS Imager	GEOS Network	4km	Geostationary	(4) 4.2 – 11.2 (5) 11.5- 12.5	Every 3hrs (full disc)	1974 - present	http://goespoes.gsfc.nasa.gov/goes/index.html
VIIRS	Join polar satellite system (NOAA 20)	750m	12hours	10.26 µm- 11.26 µm 11.54 µm – 12.29 µm		11/2018 – present	https://ladsweb.modaps.eosdis.nasa.gov/
VIIRS	Soumi national polar partnership (SNPP)	1km	12hours	10.10 µm- 10.60 µm 10.80 µm- 11.60 µm 11.80 µm – 12.80 µm 13.0 µm – 13.6 µm		10/2011-Present	https://ladsweb.modaps.eosdis.nasa.gov/

Note: Landsat 1, 2, and 3 had a multispectral scanner that did not have thermal infrared bands, International Space Station/ECOsystem space-borne Thermal Radiometer Experiment on Space Station (ECOSTRESS).

In heat-health investigations such as heat vulnerability research, the map overlay incorporates multiple heat indices across spatial scales by rating the layers differently. The overlay procedure integrates heat vulnerability indices associated with hat exposure, sensitivity, and adaptability to provide heat vulnerability-based region classification maps. Wolf & McGregor (2013), for instance, utilised overlay and spatial clustering analysis to integrate heat vulnerability indicators and surface temperature from Moderate Resolution Imaging Spectroradiometer (MODIS) images to determine the correlation between "hot spots" of vulnerability and regions of high temperature. It is intriguing to discover whether zones of high social vulnerability intersect with regions of high heat exposure or, in the case of heat events, regions that may experience temperature spikes.

An overlay operation is an essential tool for merging heat vulnerability indices such as land use, poverty and inequality, literate level, population density, and pre-existing medical issues for spatial mapping of heat vulnerability for human health. Remote sensing data and GIS techniques have aided in the spatial mapping of environmental exposures due to extreme heat, such as UHI, artificial impervious surfaces, and the presence or absence of green space, as well as the sensitivity mapping of demographic and socioeconomic indices associated with heat-related morbidity and mortality, such as poverty, literacy, age, and gender. In heat vulnerability investigations, two ways of weighing heat vulnerability indicators were frequently used: equal and weighted overlay analysis. Most research utilises Normalisation and equal weight overlay to combine the heat vulnerability indices and generate heat vulnerability maps. For example, Vescovi *et al*. (2005); Tomlinson *et al*. (2012); Chow *et al*. (2012); Aubrecht *et al.* (2013); Depietri *et al*. (2013); Dong *et al*. (2014); Christenson *et al*. (2017); Mushore *et al.* (2018). The equal weight overlay processes are based on the assumption that all the heat vulnerability indicators have equal influence on heat vulnerability. The weighted overlay assigns a weight to each raster layer based on its relative influence on heat vulnerability. The raster data are reclassified to a single vulnerability scale in this approach. A vulnerability value is obtained by multiplying each raster cell's vulnerability value by its layer weight and adding the results (Zhu *et al.*, 2014; Tran *et al.*, 2020; Grigorescu *et al*., 2021). Other

research used Overlay of ordered weighted averaging, such as Rinner *et al.* (2010). Manik & Syarifah (2017) employed a balanced weighted average in their investigation. Jagarnath *et al.* (2020) use PCA and weighted variance to overlay their heat vulnerability indices for the metropolitan area of Durban. Usually, the heat vulnerability maps should be easy to understand by individuals, policymakers, and the community to visualise the vulnerable areas and apply the appropriate adaptive measure

2.5.1 Limitations of remotely sensed data

The advancement in satellite technology has made remote observation of urban environments promising using sensors on-board satellite, airborne and aircraft platforms. Remotely sensed data from these platforms are suitable for measuring and monitoring the urban thermal environment. Aside from their extensive applications, remote sensing data for heat human health studies has some limitations. Firstly, the Landsat sensor, the famous satellite for UHI mapping, with an overpass time of approximately 10 am, is a sub-optimal time for UHI studies (between 9:15 to 9:49 am- depending on the Landsat sensor instead of about 2 pm). The estimation accuracy of LST is contingent on the influence of atmospheric corrections for a precise estimation of the surface emissivity (Tomlinson *et al*., 2011). The LST measurement from space is often affected by superficial radiative and properties of thermodynamic - surface emissivity, moisture, and albedo; the irradiative contribution at the external, and the influence of the atmosphere near the surface - the transfer of turbulent from the surface (Arnfield, 2003). There is, therefore, an extensive gap between the LST data retrieved from remote and air temperature measurements from the ground weather station, on which winds and instability have a substantial influence (Mirzaei & Haghighat, 2010).

Heat-health investigations benefit from the accurate measurement of air temperatures from weather stations. Satellite images in recent times can provide spatial estimates of LST at high temporal and spatial resolution (e.g. 100 meters). One often recorded meteorological observation with high precision, and temporal resolution, is air temperature, as measured at standard meteorological shelter height in weather stations (Stisen *et al*., 2007; Hooker *et al*., 2018). However, because these data are obtained as point samples, they cannot

accurately capture spatial variability of air temperature, particularly in locations where the distribution of meteorological stations is poor. Satellite remote sensing offers unprecedented global coverage of crucial land surface metrics, including surface temperature and vegetation indices, (Carlson, 2007; Emida *et al*., 2020).

LST is one of the most critical parameters for many satellite-based approaches to estimating air temperature. According to Vancutsem *et al*. (2010), two ways to estimate air temperature from LST may be distinguished: (i) the minimum air temperature and (ii) the maximum air temperature. Because solar radiation does not affect the thermal infrared signal throughout the night, retrieving the minimum air temperature is more accessible. The LST and minimum air temperature have an excellent association (Mostovoy *et al.*, 2006; Doshi *et al*., 2020). According to Vancutsem *et al*. (2010), MODIS nighttime outputs give a fair estimate of minimum air temperature, with root mean square error (RMSE) ranging from 2.1°C to 2.8°C. Many parameterization procedures have been devised to predict daytime air temperature using LST.

Some research has used LST from remote sensing as a proxy for near-surface air temperature. However, LST can only be used as a proxy for air temperature in applications where the algorithm's sensitivity to temperature is very low (Tang *et al*., 2010). The empirical technique is commonly used since it is based on the practical link between LST and air temperature. For example, Cresswell *et al*. (1999) computed the air temperature from Meteosat LST using an experimental solar zenith angle technique. Jang *et al.* (2004) used a neural network technique to predict air temperature using the five bands of the Advanced Very High-Resolution Radiometer (AVHRR), surface altitude, solar zenith angle, and Julian day. Jasim *et al*. (2020) model air temperature from LST estimation from MODIS and Landsat 8 images using Duration Day Length and DEM.

The empirical methods mentioned above are limited by the difficulty of spatial and temporal generalisation and the need for a training dataset (Stisen *et al*., 2007). The temperature-vegetation index technique was first introduced by Nemani & Running (1989) to overcome these constraints. It is based on the idea that LST and vegetation index have an inverse relationship and that the

temperature of a fully vegetated canopy is in equilibrium with the temperature of the air within the canopy (Goetz *et al*., 2000; Prihodko & Goward, 1997; Stisen *et al*., 2007; Liu *et al*., 2018; Kim 2020). A temperature-vegetation index approach has been established to estimate air temperature using various remotely sensed data, ranging from AVHRR to MSG SEVIRI data. However, only a few studies have successfully used the temperature-vegetation index method for MODIS and Landsat data, despite being a viable alternative for providing high spatial and temporal resolution air temperature estimation. Vancutsem *et al.* (2010) tested the temperature-vegetation index method. However, they failed since there is no clear link between them. When the criterion for the negative correlation coefficient between NDVI and LST was lowered to 0.1 in research by Stisen *et al*. (2007), the performance of the temperature-vegetation index algorithm did not suffer. This study focuses on LST as opposed to UHI, which indicates the urban thermal regime.

The viewing geometry influences the radiances collected by satellite sensors. The instruments may miss a substantial amount of the building surface. The three-dimensional city building blocks part of the surface from observation may cause the troposphere to absorb substantial energy. Some radiation from the atmosphere may be recorded by remote sensing instruments straight devoid of relating to the targeted objects (Voogt & Oke, 2003). The interpretation of LST derived from the satellite is disadvantaged because the land cover in urban areas is typically highly fragmented and heterogeneous. A consequence of this is that the image pixels often have mixed composition, especially in thermal wavebands that are typically relatively coarse. Inaccuracies of remote sensing devices and celestial-related noise in the satellite image pixel are also evident (Lillesand *et al*., 2015). The disparities in spatial resolution of the remote sensing bands are unsuitable for comprehensive thermal mapping. Fusion and downscaling are usually needed to improve the data, a rigorous process (Atkinson, 2003). The effects of topography, horizontal and vertical surfaces often result in an extensive variant in the thermal and radiative components of road surfaces and dark top-of- roofs measurements due to variations in the azimuth angle of the satellite, which make the accuracy of LST mapping contingent on the position of the satellite during the radiances measuring. A considerable part of the urban environment cannot be captured using remote

sensing because of its three-dimensional nature (Voogt & Oke, 2003). They capture cloudless imagery in tropical Africa, where most of the year is cloudy. Problems from missing pixels constitute a major limitation of LST mapping from the remote sensor (Ho *et al*., 2014).

2.6 Conclusion

Several studies identified in this systematic literature review observed negative effects of extreme heat on human health among which include declining mental health in adults of low-income residents (Lorena *et al*., 2018); a rise in the odds of suffering a miscarriage with each degree rise in temperature (Asamoah *et al*., 2018), effects on the wellbeing and safety, psychological behaviour, efficiency, and social comfort of outdoor occupation who spend many hours doing manual work (Nunfam, 2021). The main effects are however connected to heat-related morbidity and mortality from non-communicable diseases. The impact of extreme heat on human health is governed by the season, the socio-economic and demographic status of the population, and the region's environmental quality such as green space, and lakes, and tree-lined avenues, and other Blue-Green infrastructure. Green spaces are important contributor to human well-being. Notably, urban green space has been related to declines in heat-related diseases that are especially prevalent in several cities and are frequently the focus of expensive, extensive preventative campaigns (Maas *et al*., 2009; Amano *et al*., 2018; Marando *et al*., 2022). Therefore, there is a great deal of opportunity to shape cities for improved health outcomes. However, most evidence of the health advantages of urban green spaces comes from wealthy nations (Van den Berg *et al*. 2015). Given that over 90% of urban population growth would be centred in Asia and Africa (United Nations, 2014), it is necessary to assess the global urban green areas' importance.

A study by Amano *et al*. (2018) found a correlation between urban public health and green space and the interplay between these variables. Consequently, the association between green space and health must be understood for places with differing degrees of affluence. In keeping with a large body of data supporting the good impacts of green space on health mediated by direct psychological benefits, higher physical activity, and enhancement in the environment, green space was related to improved health in wealthy cities (Ihtisham *et al*., 2020; Janik, 2022).

Human exposure to extreme heat can lead to an increase in heat-related morbidity and mortality. Most of the studies cited in this review reported an increase in heat-related morbidity and mortality during the dry/hot season and the heat/rainy season relative to the dry/cold season. For example, the prevalence of infectious diseases, such as malaria and diarrhoea, increased mortality in coastal towns of tropical Africa during the hot/wet season (Greenwood, 1993; Ifatimehin & Ujoh, 2014). The common reasons for excess mortality in these seasons are extreme heat and hygienic environments. For instance, extreme heat influenced rainfall in tropical Africa. The increased rain usually overstretches the sewage and drainage systems, leading to stagnant water and a wet environment. Moreover, the stagnant water and a damp environment offer numerous disease agents decent breeding and surviving grounds. In addition, the heat/rainy season, which is characterised by planting and growing crops, often coincides with the time of least food supply and poor nutritional status of the population (Rayco-solon *et al*., 2004).

The dry/hot season is the transition period between Harmattan and the heat/rainy season in tropical African cities that border the Sahara desert. The dry/hot season exhibits excess mortality due to extreme heat, increasing the time spent outdoors to try and cool down. The poor population that cannot afford air conditioning spends more time outside, making them vulnerable to disease pathogens (Pasquini *et al*., 2020). Moreover, their dwelling is usually overcrowded and poorly ventilated, leading to indoor air pollution, a major cause of mortality peak in informal settlements (Oloukoi *et al*., 2014). There is a further increased risk of airborne disease and meningitis due to the Harmattan dust from the Sahara desert during the dry/hot season (Aara'L 2020; Laryae *et al.*, 2022). A common observation in most identified studies in tropical Africa was the age dependency of morbidity seasonality. Older people in the population are at a higher risk of dying during the hot/dry season (Daniel, 2015; Scott *et al*., 2017) while children below 9 years are most vulnerable to death in the heat/rainy season (Kynast-Wolf *et al.*, 2006).

Human exposure and sensitivity, and their ability to adapt to the effects of extreme heat are dependent on the socioeconomic and environmental quality of the population. Generally, there is a link between the human dwelling environment, economic, and social characteristics with the adverse effects of heat-related morbidity and mortality. Informal settlements are an important feature of tropical African cities, commonly-identified as unplanned and densely-packed low-rise buildings that experience extreme heat (Yahia *et al*., 2018). The dwellers of informal settlements are highly exposed and sensitive to the impact of extreme heat due to their low adaptive capacity, e.g. unable to afford air-conditioning or building insulation. Uncontrolled rapid urbanisation in tropical Africa has led to the growth of informal settlements. The UN-Habitat (2014) stated that over 55% of Sub-Saharan Africa lived in informal settlements. Informal settlements are hazardous environments that expose the inhabitants to heat vulnerability. The inhabitants of informal settlements are highly vulnerable to heat because of their living in densely-populated conditions and poor-quality homes (Scott *et al*., 2017).

To prevent urban sprawl and informal settlements, the future urban expansion of Abuja must build satellite towns to integrate low-income inhabitants into the city. Satellite towns can be built based on their unique characteristics since they can absorb urban population growth. A satellite town can produce jobs and has a solid relationship with its parent city and the surrounding countryside. During the design phase of a satellite town, residential and industrial development should be considered concerning travel time and distance to the central city. New satellite settlements in Abuja will relieve congestion in the central city. If adequately implemented, satellite cities are an effective method for controlling urbanisation in metropolitan areas. Therefore, combining land use, transportation, urban design, and local plans must take precedence if these initiatives serve as models for future growth. The open areas and bodies of water must be conserved—implementing a sustainable solution for wastewater treatment and solid waste management in satellite communities.

The spatial mapping of heat vulnerability is aiming to recognise the locations and precise inhabitants vulnerable to heat threats. There is a scarcity of such

studies in tropical Africa relative to other world regions, probably because the heat effects are not recognised as an important health threat in tropical Africa (Ngwenya *et al*., 2018; Pasquini *et al*., 2020). More studies are required to advance the knowledge of heat vulnerability in the region and the use of vulnerability maps in urban planning and policy making. Although there are discrepancies among studies in the choice of datasets as heat vulnerability indicator, it is recommended that studies select indicators that suit their local environment. The studies considered in this literature review focused on air temperature WBGT, atmospheric temperature, heat index and LST in the daytime. Since the magnitude of the UHI is generally larger at night, it would be fascinating for future studies to look into the impact of night-time heat on human health, knowing that night is usually warmer than day-time in tropical Africa (Herold *et al*., 2017).

Urbanisation and the growth of informal settlements are causing green spaces to disappear. Recent studies have found that people dwelling in areas with less vegetation cover are more vulnerable to heat-related morbidity and mortality (Schinasi *et al*., 2018). These overcrowded regions with poor physical infrastructure have little greenery, trees, parks, and shade to reduce the UHI effect and aid night-time cooling. Night-time cooling is essential for people to secure a good night's sleep and recuperate from the day's heat. The study has revealed a strong association between amplified night-time heat and inadequate sleep. The consequence is prevalent among lower-income persons and aging (Obradovich *et al*., 2017). A broad understanding of heat interactions between land components and human activities can promote the choice of heat vulnerability indicator and mapping. Even though fewer studies in this review used health data for validating heat vulnerability maps, validation determines the efficiency of the maps. The systematic review presented in this chapter serves as the guide for choosing the appropriate data and the procedures for investigating the study's objectives presented in chapter four.

CHAPTER THREE: THE STUDY AREA

3.0 Introduction

This chapter provides a description of the area of research. The chapter covers Abuja's geographical location, weather and climate, vegetation, population, relief and geology and the land use/cover.

3.1 Geographical location

This research was conducted in Nigeria's Federal Capital Territory (FCT), Abuja, and its environs, which are centrally located in the country's middle belt. The area is located between latitudes 9°4′ North and 7°29′ East of the Greenwich Meridian, with an estimated land area of approximately 8000 km^2 (Enoguanbhor *et al*., 2019). Nasarawa state borders the area on the east, Niger state on the west, Kaduna state on the north, and Kogi state on the southwest (Figure 3.1). The FCT, Abuja, was established on 3rd February 1976 by the Nigerian Federal Military Government in response to a recommendation that Lagos, the country's former capital city since 1914, could no longer effectively serve as the Federal Capital due to its proximity to the Atlantic Ocean and scarce land for expansion which resulted in enduring problems with housing, dilapidated infrastructure, traffic congestion, and an unsanitary environment. The requirement for a central location with sufficient land resources as the national capital to enable urban development, economic growth, and prosperity has necessitated the choice of Abuja (Abubakar, 2014). Abuja, the current FCT, was carved out of the central states of Nigeria: Niger, Kaduna, Plateau, and Kwara, with the Federal Capital Development Authority (FCDA) serving as the regulating agency charged with planning, developing, and controlling the FCT. The master plan for Abuja was completed in 1979, and infrastructure development began in 1980. In 1991, Government agencies, ministries, departments, international diplomatic missions, firms, and businesses relocated from Lagos and other parts of the country to Abuja, resulting in a high rate of urbanisation (Abdul *et al*., 2018).

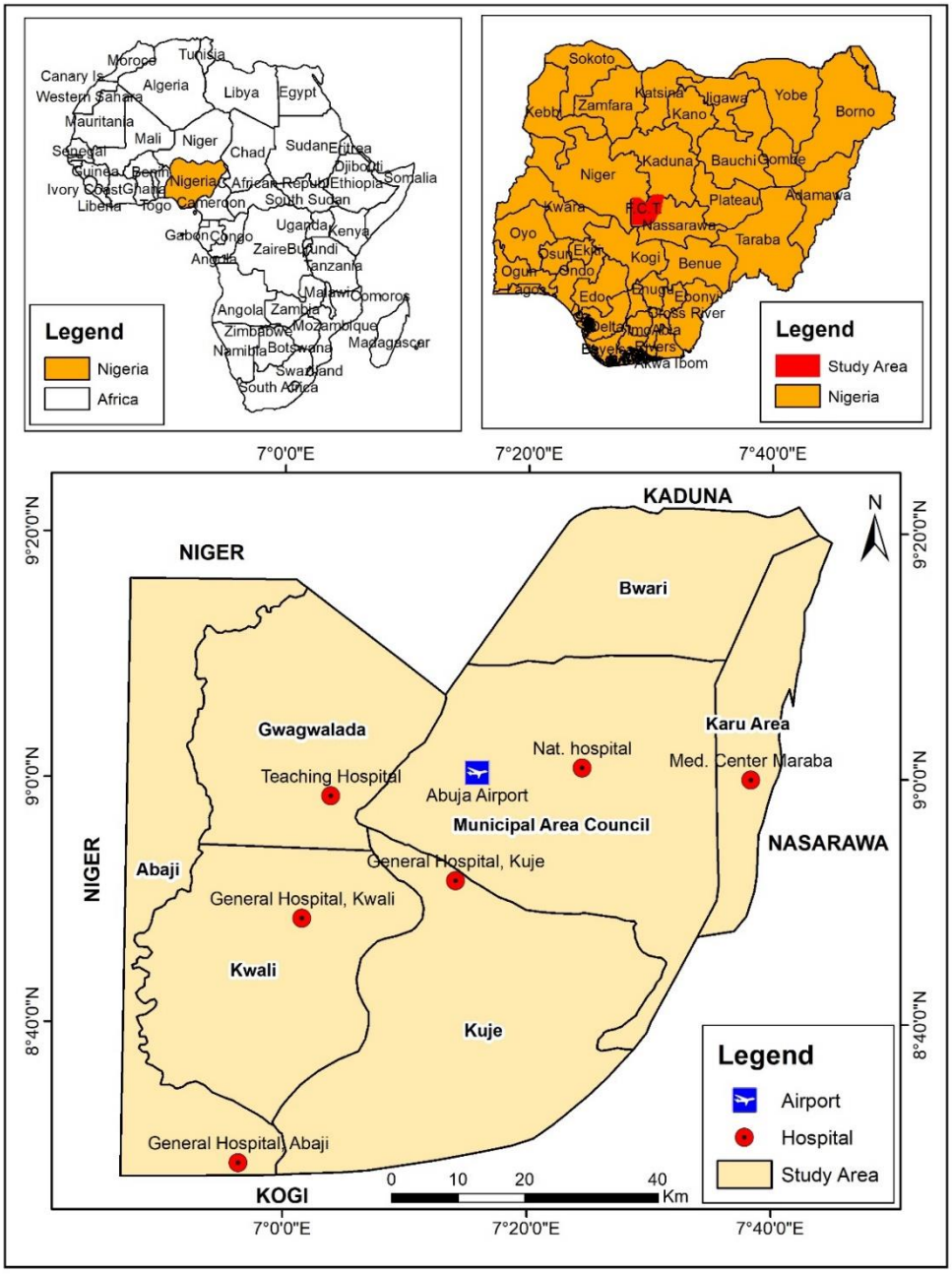


Figure 3.1: Location of the study area.

3.2 Population

Messrs International Planning Associates (IPA) - a consortium of architects, city planners, and engineers based in the United States, was tasked with developing a Master Plan for the new Capital City's 3 million-person capacity (Obiadi & Onochie, 2018). However, Abuja's population increased from about 300,000 in 1976 to over 2.75 million in 2012 (Obiadi & Nzewi, 2018). The area is home to the indigenous Gbagyi people and others who relocate from various walks of life in search of a better life. Since 1991, the population of Abuja and its environs have continued to grow with rapid urbanisation due to the relocation of Federal

Agencies, Ministries, Government offices, International Diplomatic missions, businesses, from Lagos or the establishment of branches; making Abuja one of the world's fastest-growing cities, with approximately 6 million people in 2016. In the absence of critical social infrastructure and services required to support the increased population, rapid urbanisation has resulted in the formation of informal settlements (Dawam, 1994). Informal dwellings lack essential infrastructure and services such as water, motorable roads, efficient electricity supply, adequate sewage and sanitation facilities, solid waste management facilities, and a structured urban management system (Zubair *et al*., 2015).

3.3 Weather and climate

As in the tropics, the FCT is subject to two major weather events each year. These are referred to as the rainy and dry seasons. The rainy season lasts from April to October. The FCT's rainfall pattern is determined by its location on the windward side of the Jos Plateau and within the zone of rising air masses. Annual rainfall totals between 1100mm and 1600mm. Due to the area's hilly and mountainous terrain, with isolated hills and inselbergs, convective and orographic rainfall is frequently encountered. Convective and orographic rain are characterized by line squalls, cumulonimbus clouds, and heavy rain that may last several minutes accompanied by long-lasting drizzles (Ahmed *et al*., 2021). During the rainy season, daytime temperatures range between 28.0 ^{o}C and 30.0^{o}C, while night-time temperatures are typically between 22.0 ^{o}C and 23.0^{o}C. Although a brief Harmattan season is experienced between December and February caused by the North-East Trade Wind, which is laden with dust haze, increased coldness, and dryness. The dry seasons usher in a season of high temperatures ranging from 37.0°C to 44.0°C during the day and sinking to 12.0°C at night (Orisakwe *et al*., 2017). The monthly precipitation for the past 29 years has been analysed and displayed in Figure 3.1. The graph depicts a rise in precipitation between 1993 and 1994. Similarly, a precipitation decline was observed in 2000, followed by a significant increase in 2002. Also, a notable downward trend began between 2006 and 2008. This cyclic pattern of Abuja's precipitation persisted throughout the study period. Figure 3.2 presents the seasonal distribution of rainfall from 1990-2019 in the study area.

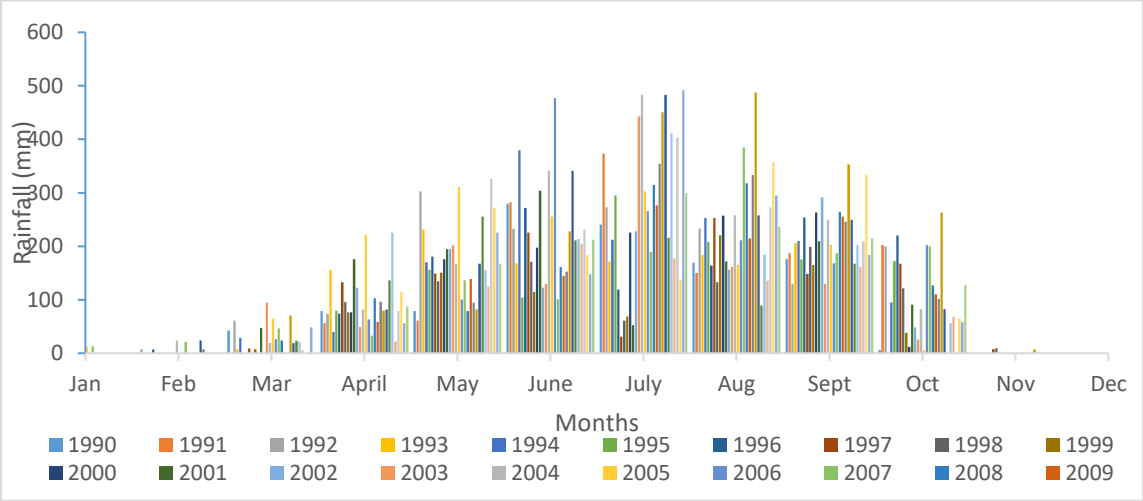


Figure 3.2: The seasonal pattern of rainfall in the study area from 1990 to 2019.

Abuja's relative humidity has been steadily increasing since late February, reaching a high of 88% in July. Consistent rains begin in April, when the relative humidity is 75% within this timeframe. The entire area will be under the influence of the tropical maritime wind by August when the Inter Tropical Discontinuity (ITD) reaches its northernmost position (*mT*) (Binbol & Uzochukwu, 2008; Ige *et al.*, 2017). This high relative humidity will last until December. From October to January, it will go down a lot. During the summer months, relative humidity can fall to as low as 15% in the afternoon. The combination of low relative humidity and high afternoon temperatures creates a desiccating effect during the dry season and a heat trap effect during the rainy season (Elemo *et al*., 2021). During the dry season, the region typically had low temperatures and humidity. Their patterns closely resemble those of two dominating tropical air masses, resulting in the establishment of the following distinct climate regimes (Ekwe *et al*., 2014):

i. Hot and humid period: April – June
ii. Cool and humid period: July – October
iii. Cool and dry period: November - January
iv. Hot and dry period: February – March.

Sunshine hours are a critical component of the climate that is essential to human health. Abuja benefits from the double passage of the sun above due to its location in the tropical climate. This means that insolation is rather steady and

sunlight hours are abundant. In general, sunshine hours in the area are high, averaging around nine hours in the dry season but a little lower in the wet season due to the effect of cloud cover (Binbol & Uzochukwu, 2008; Okundamiya & Nzeako, 2010). Abuja possesses a tropical continental climate. Because the sun seems to move through the tropics, the relative stability of the inter-tropical convergence zone (ITCZ) is what keeps the temperature stable, even though the seasons change (Binbol & Uzochukwu, 2008). Figure 3.3 and 3.4 present's Seasonal distribution of maximum and minimum temperatures in the study area from 1990 to 2019.

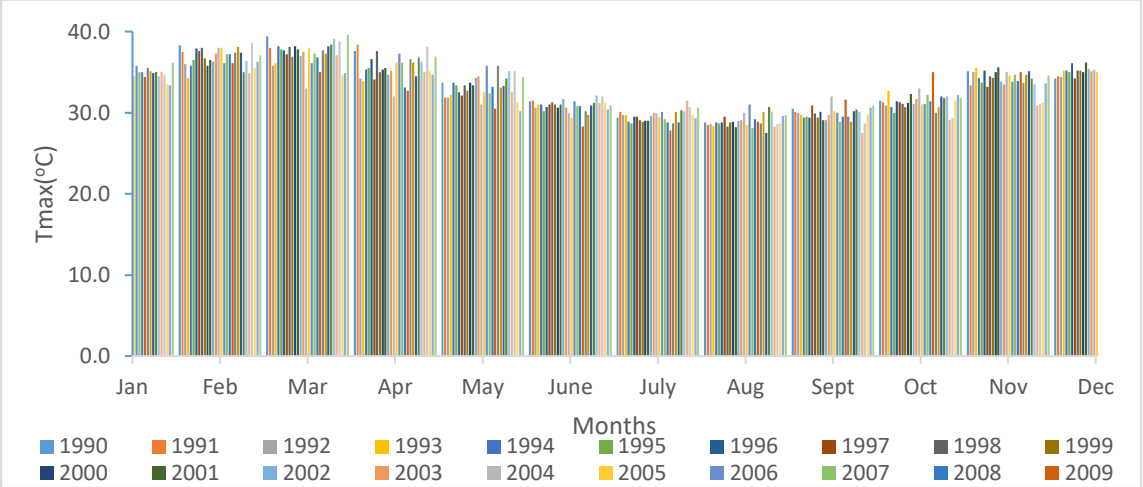


Figure 3.3: Seasonal distribution of maximum temperatures in the study area from 1990 to 2019.

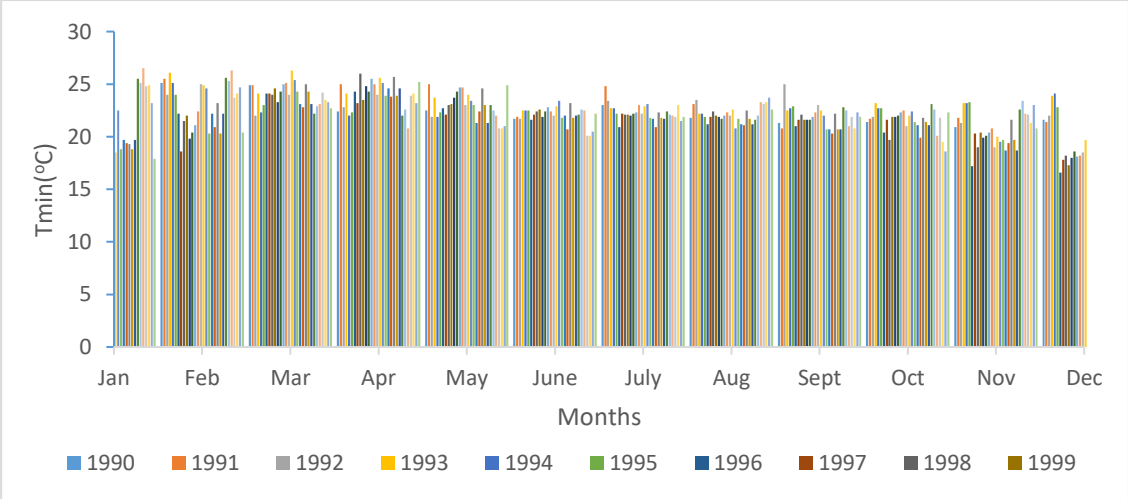


Figure 3.4: Seasonal distribution of minimum temperatures in the study area from 1990 to 2019.

3.4 Vegetation

Abuja is located in the Southern Guinean Savannah of the West African sub-region, which is characterized by trees, shrubs, and grasses that are usually seen as clusters of rainforest greenery on plains lands and steep terrain (Ezeamaka & Oluwole, 2016). The vegetation cover comprised of parks, the largest and most populous of which is Millennium Park in the Maitama District (Chibuike *et al*., 2018). Grasslands, shrubs, and deciduous, and tropical trees are preserved in their natural state in Abuja. Flowers are frequently grown for aesthetic purposes across residential and commercial areas (Agbelade *et al*., 2017; Oyewole *et al*., 2019). In the FCT of Abuja, there are many parks, green areas, and open spaces which can be divided into three fundamental categories: (i) The neighbourhood parks, (ii) district parks, and (iii) the city parks. The neighbourhood parks are found in residential areas and are usually within walking distance of the majority of households. District parks are more extensive than neighbourhood parks but contain fewer amenities than the city parks. They are often developed near major thoroughfares and are not always within walking distance of residential neighbourhoods (Ihuma *et al*., 2016). In terms of the size and diversity of park elements, city parks are the largest parks. Parking facilities are given because city parks are typically accessed by vehicle.

Abuja's growing population has created a slew of issues, putting a strain on land and forest resources, and green spaces, as well as exposing the city to a variety of environmental threats. Environmental dangers such as air pollution, wind erosion, and water erosion are on the rise as a result of deforestation and population growth in the FCT, and this is visible in urban centres throughout Nigeria (Agbelade *et al*., 2017). The conservation and development of urban vegetation cover are among the problems of sustainable urban planning in our expanding urbanised surroundings (Dar *et al*., 2021; Marando *et al.,* 2022). Parks and recreation areas provide a variety of leisure and entertainment opportunities for people's relaxation, pleasure, and amusement. Parks enable residents to relax and play, thereby supporting a healthy lifestyles. However, there is a lack of understanding of the socio-ecological implication of these green areas and management practices that could lead to sustainable management

(Agbelade *et al*., 2017; Enoguanbhor, 2022). The presence of vegetation contributes to lower surface temperatures than in non-vegetated places. Furthermore, tree maturity is important in lowering temperatures in urban areas through shadow and evapotranspiration. Other advantages of urban vegetation include a better environment, which corresponds to healthier residents, the attractiveness of the landscape and scenery, reduced ultraviolet radiation, and social and environmental advantages. (Chibuike *et al*., 2018; Park *et al.*, 2021). The composition and arrangement of urban parks can influence the degree of cooling observed. Park size, park border, park design, percentage of woodland regions, and percentage of water bodies, for example, can all have a substantial impact on cooling effect intensity (Feyisa *et al*., 2014; Liao *et al*., 2021). Urban parks are an effective way to mitigate the UHI problem. Trees can lessen the adverse impacts of air pollution and noise pollution in the areas surrounding the park, in addition to lowering the effects of temperature. The observed severity of the cooling effect is attributed mostly to the density of green spaces, rather than the size of the park (Qiu & Jia, 2020). Urban vegetation and green spaces could be an additional effective way of biodiversity preservation and ecological capacity in terms of physiological, sociological, socioeconomic, and aesthetic advantages (Farid *et al*., 2022). Urban woods may also be used to address urbanisation issues, such as food shortages, energy scarcity, worsening air quality, extreme heat, health risks, and excessive noise levels (Agbelade *et al*., 2017).

Albizia, zygia, Butyrospernum paradoxam, Anniellia oliveri, and *Parkia clappertoniana* are among the tree species found in the Park or Grassy Savannah. The Savannah Woodland is comprised of the plains of Gurara, Robo, and Rubochi, and the hills that surround them. *Afzelia africana, Anogeissus leiocarpus, Butyroscarpus paradoxim, Daniella oliveri, Khaya senegalensis, Prosopis africana, Uapaca togoensis, Albizia, zygia, vitex doniant, Bombox costatum,* and *Ptrecarpuserinaceus* are just a few of the trees that grow in this area. Shrub Savannah is found throughout the territory, particularly in rugged terrain near hills and ridges. Among the tree species found there are *Antiaris africana, Anthocleista nobilis, Ceiba pentandra, Cola gigantean, Celtis spp., Chlorophora excelsa (iroko), Khaya grandifolia (Benin Mahogany), Terminalia*

Superba (afara), Triplochiton scleroxylon, and *Dracacna arborea.* Certain tree species such as *Piptadeniatrum africanum (agboin), Lophira alata (ekki),* and *Terminalia ivorensis*, are also common in some of the forest patches. Major tree species found in the savannah wood areas are *Anogeissus leiocarpus, Daneilla oliveri, Khaya senegalensis,* and *Pterocarpus arenaceous*, they produce high-quality lumber.

3.5 Relief and geology

The FCT and its environs are characterised by isolated hills, highlands, and inselbergs, all of which contribute to the area's beauty. The area's dominant terrain is hilly and dissected, with various summits exceeding 760m above sea level (Malomo *et al*., 1983; Sadiya *et al*., 2014). The hills in the FCT are formed by clusters that form long ranges, the most notable of which are the Bwari-Aso and Gwagwa ranges in the northeast corner of Abuja. The Gurfata range is southwest of Suleja, while the Idon-Kasa range is northwest of Kuje (Ibrahim *et al*., 2016). The study area's lowlands are situated to the extreme southwest, around the Guraja River's flood plain, and the Gwagwa plains, which are elevated 70m above sea level (Mallo & Mgbanyi, 2013). The Gwagwa plains are home to most of the Federal Capital City's infrastructure development. The relief pattern in the study area influences the city's local climate. The area's geology is characterised by basement complex rocks and primarily alluvial and luvisol soils, making the area fertile for agriculture and vegetation growth. However, its soil's high sand content makes it prone to erosion (Agunleti & Arikawe, 2014).

3.6 Land use/cover

Abuja, the Federal Capital Territory, is home to indigenous and migrants, resulting in various human activities defining land use in the city. Initially, the regional and city master plans were produced to guide the development of the new capital territory, but this quickly ran into challenges, particularly in the areas of infrastructure provision and city management (Abuja development control, 2007). The land use in the study area includes commercial hubs, multinational corporations and offices, marketplaces, shopping malls, hotels, and residential

layouts. Notable among these are the general post office, Abuja international conference centre, Herbert Macauley way Garki, Wuse market, Wuse general hospital, Sheraton hotel and towers, foreign affairs ministry headquarters Wuse, Transcorp Hilton hotel (Maitama), and the British high commission along Agui-Ironsi way (Maitama). The transportation network is pooled together with urbanised regions because they are composed of the same materials, the most fundamental of which is the artificial impervious surfaces. These highways, including the ring road, are the FCC's four district roads. Other land uses and land covers include flower gardens, bare/open areas, and water. The vast majority of the land inside the municipality has been developed to suit the population boom.

Abuja's informal settlements expansion is a response to the Federal Capital City's (FCC) stringent planning and development laws. The FCC has effectively implemented development control as a technique for sustainable development. The Urban and Regional Planning Department of the Federal Capital Development Authority (FCDA) developed planning requirements and oversight to ensure sustained physical planning and monitoring of land use management in the nation's capital. This has given an aesthetically pleasing atmosphere, habitable and useful for Abuja FCC's sustainable expansion. Nonetheless, the stringent procedures (time, money, and agent requirements) involved in getting title papers for property and building design approval make development processes in FCT lengthy and stressful. As a result, the surrounding communities served as an alternate and desirable location for those developments that were denied FCC authorization. The evacuation of illegal colonies from the FCT in 2003 considerably aided the unplanned and illegal growth of informal settlements in the surrounding territories. More than 2 million individuals have been displaced due to demolition activity since 2003 (UN-HABITAT, 2012; Rikko *et al*., 2019). The Karu area of Nasarawa state is one of the closest to Abuja, and it has many low- and middle-income employees from Abuja. This impacts the physical growth and extension of the towns, as well as the region's demographic and environmental degradation.

Unauthorised land developments or illegal subdivisions are standard on the outskirts of the FCT. They are illegal because they violate zoning restrictions; the land subdivision frequently fails to fulfil planning standards for right-of-way, road access, and public space provision, and the infrastructure standard is very inadequate (UN-Habitat, 2007; Sulyman & Danladi 2021). Informal settlements are frequently prone to spreading diseases and criminal activity, causing discomfort to residents and the surrounding metropolitan environment (French & Gardner, 2012). However, it is vital to highlight that informal settlements are now one of the defining features of the Nigerian urban landscape, as they house the vast majority of lower-income households and serve as the primary source of new housing. The informal settlements surrounding the Federal Capital Territory (FCT) of Abuja are the primary source of cheap, unskilled, and semi-skilled labour in the construction and transportation industries; security guards; operators of small and medium-scale commercial enterprises; restaurant operators and food vendors; street cleaners and waste pickers; gardeners; babysitters and domestic aids, among others.

The increase in demand for shelter and fuelwood by the low-income earners around the FCT, Abuja, and its environs has damaged the natural habitat by clearing vegetation cover for the AIS. Fuelwood is the traditional energy source used by indigenous peoples and low-income residents of informal settlements. It is the primary source of cooking in homes and the catering business, bakeries, and restaurants. Access to fuelwood is obtained by physically cutting trees from neighbouring vegetation or clearing vegetation for construction sites and agricultural development. This contributed to the loss of natural vegetation in the area. To this end, the main takeaways from this goal are that: as proven by Wang *et al*. (2022); Ma & Peng (2022); and Gao *et al*. (2022), a considerable increase in the area covered by AIS and bareland could lead to the growth of the UHI problem in Abuja and its environs. Furthermore, previous studies have established the AIS map as a crucial indicator of heat vulnerability (Uejio *et al*., 2011; Kim *et al*. (2018; French, 2018; Conlon *et al.,* 2020; Sabrin *et al*., 2020). Figures 3.8 - 3.8 presents the land use type of the city centre and the informal settlements of Abuja and its environs.



Figure 3.5: The city centre of Abuja, the Nigeria's capital city (Authors fieldwork, 2019).



Figure 3.6: Traffic congestion along Abuja - Karu expressway (Authors fieldwork, 2019).

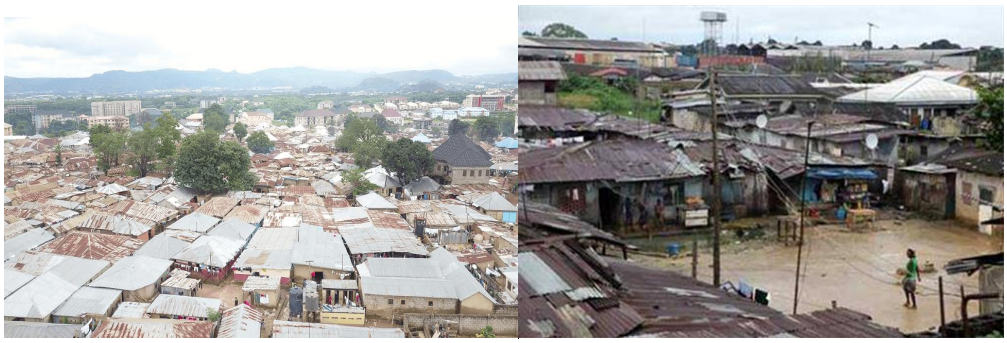


Figure 3.7: Mpape informal settlement around Maitama District, Abuja. (Authors fieldwork, 2019).



Figure 3.8: Maraba informal settlement in Karu area of Nasarawa State. (Authors fieldwork, 2019).

CHAPTER FOUR: RESEARCH METHODS

4.0 Introduction

In this chapter, the research methodology is described. The chapter discusses the types, sources, and characteristics of datasets used to achieve the study's objectives and the data analysis procedures.

4.1 Research objective 1: Mapping spatio-temporal change of artificial impervious surface

This section's primary objective was to map the spatiotemporal change in artificial impervious surface area in Abuja and its environs using Gong *et al*. (2020)'s global artificial impervious area (GAIA) maps. Due to incomplete or missing data in the Gong *et al*. (2020) GAIA datasets, it becomes impossible to access all of the artificial impervious surface maps required for this study. Due to the requirement of this study to detect spatiotemporal changes in the artificial impervious surface, Landsat images were utilised to fill in the missing years and accomplish this objective. The study area's land use/cover categories include artificial impervious surfaces, cropland, forestland, shrubland, grassland, waterbody, and bareland.

4.1.1 Computation of land use/cover area from Gong *et al.* (2020) datasets

Gong *et al*. (2020)'s classification system for Finer Resolution Observation and Monitoring of Global Land Cover (FROM-GLC-Hierarchy) is presented in Table 4.1. Level 1 type represents land use/cover categories such as crops, while level 1 is the code for the level 1 type. The level 1 code crop, for example, is 10. Level 2 type, 3 types, and so on are the names of the sub-classes that comprise the level 1 class. The level 1 crop type was composed of rice with level code (10/11), greenhouse (10/12), others (10/13), crop in urban (10/19), and bare crop (10/94). To calculate the land use/cover area for class level 1 type crop, all the pixels of level code 10 were merged to estimate their area.

Table 4.1: Gong *et al.*'s (2020) GAIA classification system for (FROM-GLC-Hierarchy)

Level 1 Type	Level 1 Code	Level 2 Type	Level 1/2 Code	Level 2 Type	Level 1/2 Code	Level 2 Type	Level 1/2 Code	Level 2 Type	Level 1/2 Code	Level 2 Type	Level 1/2 Code	Level 2 Type	Level 1/2 Code	Level 2 Type	Level 1/2 Code
Crop	10	Rice	10/11	Greenhouse	10/12	Others	10/13	Crop in urban	10/19						
Forest	20	Broadleaf	20/21	Needle leaf	20/22	Mixed	20/23	Orchard	20/24	Forest in urban	20/29				
Grass	30	Managed	30/31	Nature	30/32	Grass in urban	30/39								
Shrub	40	Shrub in urban	40/49												
Wetland	50	Grass	30/51	Silt	90/52	Wetland in urban	50/59								
Water	60	Lake	60/61	Pond	60/62	River	60/63	Sea	60/64	Water in urban	60/69				
Tundra	70	Shrub	40/71	Grass	30/72										
Impervious	80	High albedo	80/81	Low albedo	80/82										
Bareland	90	Saline-alkaline	90/91	Sand	90/92	Gravel	90/93	Bare - crop	10/94	Dry river/lake bed	90/95	Other	90/96	Bareland in urban	90/99
Snow/ice	100	Snow	100/101	Ice	100/102										
Cloud	120														

4.1.2 Mapping the artificial impervious surface from Landsat datasets

The Earth Resources Observation and Science (EROS) archive of the United States Geological Survey (USGS) was used to acquire satellite imagery for the missing years of the Gong *et al*. (2020) datasets, which were then used to fill in the missing years of the artificial impervious surface maps. Due to the poor quality of Landsat images for some periods, it took much work to have consistent images with the Gong *et al*. (2020) datasets. The problem is related to Landsat 7 Enhanced Thematic Mapper Plus (ETM+) data scan-line corrector off (SLC-off) since 2003, which results in about 22% of its image pixels not being scanned due to a failed SLC (Scaramuzza & Barsi, 2005). The SPOT image with the finer spatial resolution was acquired from Google Earth Pro for accuracy assessment.

The Landsat Thematic Mapper (TM) is a multispectral sensor with 7 bands, the 6th of which is thermal infrared (TIR). Bands 1–3 are visible, 4–5 are near-infrared (NIR), and band 7 is in the mid-infrared (MIR). Bands 1-3 of the ETM+ sensor are visible, band 4 is NIR, bands 5 and 7 are short-wave infrared (SWIR), band 6 is TIR, and band 8 is a panchromatic band with a spatial resolution of 15 m. The sensor Operational Land Imager (OLI) and Thermal Infrared Sensor (TIRS) has 11 bands. The first is a coastal aerosol band, followed by visible bands 2-4 and NIR and SWIR bands 6-7. Bands 8 and 9 are panchromatic, while bands 10 and 11 are TIR. Table 4.2 contains a detailed list of sensor names, acquisition dates and times, spatial resolution, and other characteristics of the satellite images used to fill in the missing GAIA from Gong *et al.* (2020).

Table 4.2: Satellite images used to update the datasets of Gong *et al.* (2020).

Scanner	Date of data acquisition	Time of data acquisition	Path/row	Spatial resolution (m)	Source
Landsat 5 TM	07/12/1999	09:42am	189/054	30/120	USGS
Landsat 7 ETM+	03/12/2004	09:39am	189/054	30/60	USGS
Landsat 7 ETM+	03/04/2009	09:40am	189/054	30/60	USGS
Landsat 8 OLI	04/12/2014	09:49am	189/054	30/100	USGS
Landsat 8 OLI	26/02/2019	09:49am	189/054	30/100	USGS

Bands 1 through 5 and 7 of Landsat 5 (TM) images have a spatial resolution of 30 metres. Band 6 (thermal infrared) spatial resolution is 120 metres. Landsat 7 (ETM+) images are made up of eight spectral bands, each having a spatial resolution of 30 metres for Bands 1, 2, 3, 4, 5, and 7. Bands 6 (thermal) and 8 (panchromatic) have resolutions of 60 and 15 metres, respectively. Landsat 8 (OLI-TIRS) images include 9 spectral bands with spatial resolutions of 30 metres for Bands 1, 2, 3, 4, 5, 6, 7, and 9. Band 8 (panchromatic) has a spatial resolution of 15 metres. Thermal bands 10 and 11 are collected at 100 metres and are effective for providing LST data.

4.1.3 Data pre-processing technique

Landsat images for mapping artificial impervious surfaces were imported into Erdas Imagine, where a layer stacking to combine the bands into a single image was achieved. In this regard, the bands for each Landsat scene (except the thermal bands) were combined. A shapefile for the study area was created covering the administrative boundary of the FCT, Abuja, and part of the Karu area of Nasarawa state, which was used to clip out the Area of Interest (AOI) from the Landsat scenes, acquired from the path/row: 189/054, where the study area falls within. The USGS had geometrically and radiometrically corrected all the Landsat images used in this study.

4.1.4 Classification scheme design

For this research, a land use/cover classification method was used based on the Gong *et al*. (2020) classification scheme (Table 4.2) and the author's prior knowledge of the study area. In addition, literature from Idoko & Bisong (2010), Ibrahim *et al*. (2016), and Akomolafe *et al*. (2020) was also used to improve the image classification for this study. The snow/ice cover classes designed by Gong *et al*. (2020) data were not available in a tropical African city like Abuja and its environs, so they were adjusted to a local level using Google Earth and fieldwork. In this study, seven land use/cover classes were considered, similar to the classes generated by Gong *et al*. (2020) classification scheme. (1) Impervious surfaces, (2) cropland, (3) forestland, (4) shrubland, (5) grassland,

(6) waterbody, and (7) bareland are the land use/cover categories evaluated. The following sections provide detailed descriptions of these land use/cover classes.

4.1.5 Description of land use/cover classes

Impervious surface: Mostly artificial structures made of any substance that obstructs or inhibits water from naturally penetrating the earth. They primarily exist on major highway surfaces, paved areas, hardened ground, and rooftops in human settlements like urbanised areas.

Cropland: This category includes areas that are cultivated and used for grazing and orchards. Physical boundaries are not based on precise field boundaries but are broadly defined to include the main agricultural activity areas. According to field observations and the cropping calendar, most of the agricultural land in the study area was fallow during the dry season. This made it more difficult to distinguish between agricultural areas and rocky, unpaved, and bare land on the satellite image.

Forestland: Comprises densely forested areas with natural vegetation, where the canopy and forest trees taller than 5 m. Riverine vegetation with scattered grasses, primarily perennial species, is also included in this category.

Shrubland: Sparse vegetation or trees spaced about 100 meters apart. This class also includes a variety of small shrubs and bushes with varying densities.

Grassland: Because there is little canopy cover, the grass cover is well-established and consistent, especially during the wet season. This class also includes pastureland.

Water bodies: locations of major surface water concentration, such as rivers, streams, ponds, reservoirs, and marshy areas.

Bareland: Land devoid of vegetation, such as exposed rocks or areas with only a thin layer of vegetation (apart from agricultural fields devoid of crop cover). Quarries, mine dumping grounds, and construction zones are also included in this category.

4.1.6 Supervised/unsupervised classification

Typically, training samples are generated through fieldwork, also known as reference data, aerial photographs, and historical map extraction (Lillesand Kiefer & Chipman, 2015). For this study, the initial supervised maximum likelihood classification using training areas derived from prior knowledge of the area, Google Earth image, and the elements of image interpretation techniques such as the shape of the feature, size, tone, texture, pattern, colour, and association for all land use/cover classes revealed a severe problem resulting from spectral confusion. For instance, urban areas were misclassified as agricultural areas or, conversely. On closer inspection, it was discovered that settlement surfaces dominated by untarred roads and bareland produced the same radiometric response as bareland with the same soil composition. To address the difficulty caused by spectrum confusion, a hybrid supervised/unsupervised classification technique was adopted. In this manner, every pixel for every scene was classified using a hybrid classification algorithm. This process comprises building spectral signature files from supervised training sets and unsupervised (ISODATA) techniques. The unsupervised classification was applied to every image to generate training data, which were then used to generate training sets for the supervised classifier. The clusters were categorised with visual interpretation, nearest neighbourhood, and the Google Earth image. Training samples were chosen from the outcomes of the unsupervised classification for validation to fully understand the spectral signatures of the various land use/cover categories.

It is recommended that a minimum of 10–30 samples per class be used for training when selecting training and validation sets of pixels from Landsat images (Petropoulos *et al*., 2011). In this study, a method called "stratified random sampling" was used to get about 500 training pixels from each image for all classes. While allocating each cell to a particular class represented in the signature file, the maximum likelihood classification tool takes into account both the variances and covariance of the category signatures. The Maximum Likelihood Classifier tool's algorithm depends on Bayes' decision-making theory, which states that the cells in each class sample in the multidimensional

space are evenly distributed. On the premise that the allocation of a class sample is normally distributed, the average vector and covariance matrix can be used to classify a class. Based on these two features for each cell value, the statistical probability for each class is determined to identify the cells' membership in the class. Once a precondition option is supplied, each cell is assigned the category to which it is most likely to belong (Richards & Jia, 2006; Srivastava *et al*., 2012; Lillesand *et al*., 2015).

4.1.7 Testing/accuracy assessment and area estimation

To support confidence in the evidence produced and conclusions reached, using remote sensing maps for scientific applications necessitates reporting classification accuracy. It is recommended that the classification accuracy of the remote sensing image be validated before using the classification result for scientific investigation or policy decision. It is critical to assess the accuracy of changes in land information and estimate the area of change (Olofsson *et al*., 2014). Stehman & Foody (2019) acknowledged the relevance of obtaining high-quality reference data to compare the map, the importance of sampling to obtain these reference data, and the role of an error matrix and accuracy measures derived from the error matrix in summarising the accuracy information. This study performed an accuracy assessment for the land use/cover maps derived from the supervised classification scheme based on Olofsson *et al*. (2013) recommended methods for assessing the accuracy of land use/cover and calculating their area change. The error-adjusted estimates and confidence intervals approach of representing land use/cover area was used since an accuracy assessment was conducted using the generated error matrix. This is owing to the uncertainties involved with map classification error, which can cause the area of land use/cover change determined from a map to deviate substantially from the genuine area of change. Errors like these should be corrected.

4.1.8 Reference data sampling design

For manual classifications of the sample pixels, high spatial resolution images from Google Earth were used as reference data. The Google Earth images used

as reference data for this study were from the same period as the Landsat imagery used to create the study's land use/cover maps. Figure 4.1 shows a classified Landsat 8 image (left panel) and a Google Earth image from 2019 (right panel) used as reference data to obtain sample points for accuracy assessment.

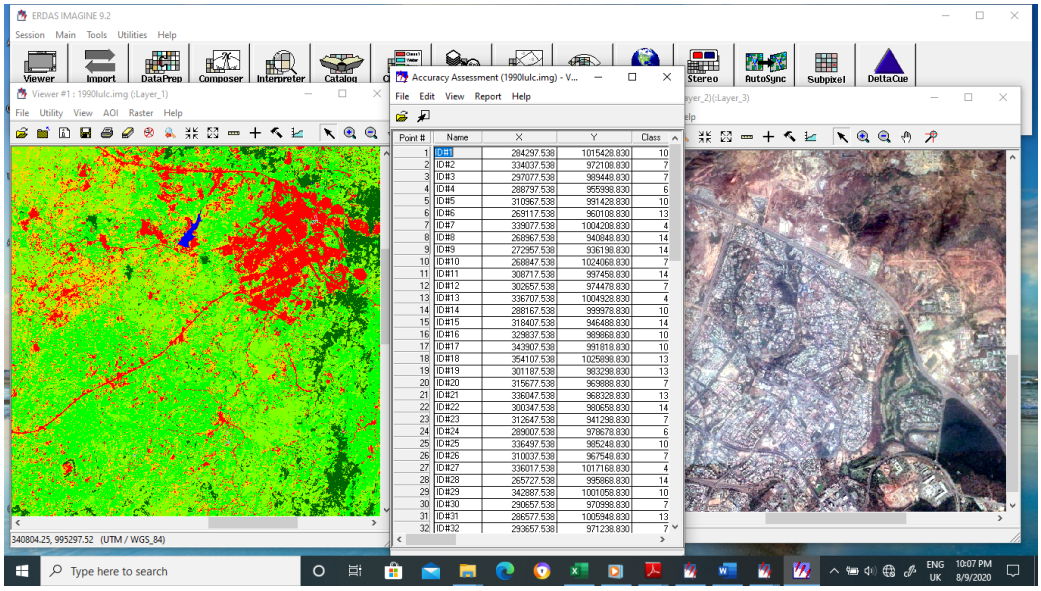


Figure 4.1: Classified Landsat 8 image (left panel) and Google Earth image of 2019 (right panel) used as reference data for obtaining sample points for accuracy assessment.

Sampling design defines how to select the subset of the map that forms the basis for the accuracy assessment. A stratified random sampling design was used for sample testing, where the seven map classes that served as strata were selected for obtaining the sample points. An arbitrary sample size of 500 pixels was distributed with a minimum sample size of 70 pixels to each of the seven map classes of the output Land use/cover map for 1999, 2004, 2009, 2014, and 2019. The stratified random sample approach uses probability sampling design methods, which are crucial for proving statistically sound analysis. The randomly generated points were applied to compare the classified maps using the reference data to the actual land use/cover. Figure 4.2 presents the stratified random sampling points of the accuracy assessment.

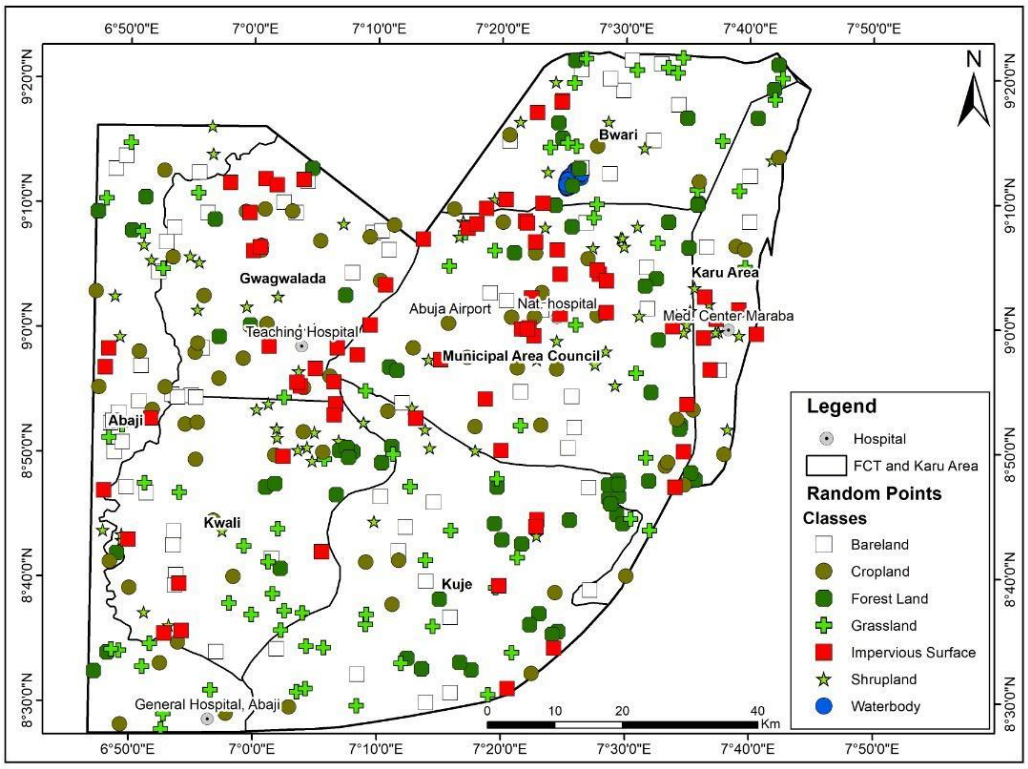


Figure 4.2: The reference points collected by stratified random sampling.

4.1.9 Conclusion

This section covers data types, collection techniques, sample strategies, pre-processing, and data analysis. The objective was to create a spatiotemporal map of artificial impervious surfaces. Gong *et al*. (2020)'s global artificial impervious area maps were the primary data source for this section. Due to the lack of data in 2000, 2004, 2009, 2014, and 2019, Landsat images from the thematic mapper, enhanced thematic mapper, and operational land imager was utilised to generate artificial impervious surface maps. The purpose was to appreciate the spatial and temporal variations of the artificial impervious surface of Abuja.

4.2 Research objective 2: investigate the high-resolution spatio-temporal changes in the magnitude of UHI in response to urbanisation

4.2.1 Computation of land surface temperature

Land surface temperature (LST) mapping is a crucial component of environmental modelling due to the trend of a growing world population, the

expansion of urban areas, and the impact of artificial impervious surfaces on urban heat islands (UHI). From satellite images, LST measures temperature at the Earth's surface and atmosphere's boundary, typically between the ground surface and an altitude of 2-3 metres (Dash *et al*., 2002). Therefore, knowledge of the interaction between urban land use/cover and the local atmospheric conditions requires scientific understanding. This section examines how remote sensing can estimate LST and identify UHI.

For this section, 7 temporal Landsat data sets were downloaded. Initially, only data from the summer months (late February to early May) were of interest for inclusion in the study; however, accessing cloud-free data for all of these months proved difficult. The LST mapping spectral bands are visible, near-infrared, and mid-infrared observations with a spatial resolution (pixel size) of 30 m. Landsat 5 TM has a spatial resolution of 120m in the thermal infrared spectrum, Landsat 7 ETM+ has a resolution of 60m, and Landsat 8 OLI has a spatial resolution of 100 m. This study computed LST using band 6 for Landsat 4, 5, and 7 and bands 10 and 11 for Landsat 8. The Landsat bands were supplemented with the near-infrared band (Band 5 for Landsat 8) and the red band (Band 4 for Landsat 5 and 7) (Band 3 for Landsat 5 and 7). The rescaling constant and K_1 and K_2 - band-specific thermal conversion constants contained in the metadata file of the Landsat image downloaded from the USGS website - are other auxiliary information used for LST computations. The LST was calculated using equations 4.1 and the ArcGIS raster processing tools.

4.2.2 Procedures for the computation of LST

The initial step for LST extraction from satellite data is the conversion of the image digital number (DN) to Top of Atmosphere radiance values (ToAr) using the spectral radiance scaling method given in equation 4.1 (Zhang *et al*., 2017; Wang *et al.*, 2019; Khan *et al*., 2022).

$$ToAr = L\lambda = M_L * Qcal + A_L\text{-}Oi \quad (4.1)$$

where

M_L= is the band-specific multiplicative rescaling factor

Qcal = Band image (band 10 for Landsat 8 and band 6 for Landsat 5 and 7)

A_L= is the band-specific additive rescaling factor, and

Oi= is the correction for Band 10.

After the conversion of DNs to reflection, the TIRS bands data were further converted from spectral radiance to brightness temperature (BT) using equation 4.2.

$$BT = K_2 / \ln [(K_1/L\lambda) + 1] - 273.15 \quad (4.2)$$

where

K_1 and K_2 are the band-specific thermal conversion constants obtained from the metadata. For obtaining the LST in degrees Celsius, the radiant temperature is revised by adding the absolute zero (−273.15). Further components for LST mapping are the computations of the Normalized Difference Vegetation Index (NDVI) using equation (4.3).

$$NDVI = \frac{NIR - Red}{NIR + Red} \quad (4.3)$$

where

NIR- denotes the near-infrared band: Band 5 for Landsat 8 and Band 4 for Landsat 5 and 7.

Red - denotes Band 4 for Landsat 8 and Band 3 for Landsat 5 and 7. The maximum and minimum NDVI values were further used to compute the proportion of vegetation (PV) using equation 4.4.

$$Pv = \frac{[NDVI - NDVI_S]^2}{[NDVI_v + NDVI_s]} \quad (4.4)$$

where

The $NDVI_s$ and $NDVI_v$ are the thresholds of soil and vegetation pixels. While the conversion of satellite brightness temperature into LST required the use of emissivity, this has been calculated from NDVI using the error correction equation and P_V as presented in equation 4.5.

$$E = 0.004Pv + 0.986 \quad (4.5)$$

where

E - Is the emissivity calculated from the proportion of vegetation (P_V)

Using the single-channel method, the LST was converted to Satellite BT using equation 4.6.

$$Ts = BT / \{1 + \lambda (BT/\rho) \ln \varepsilon\lambda]\} \quad (4.6)$$

where

Ts - is the LST in Degrees Celsius (^oC)

BT - is at sensor BT (^oC)

λ - is the wavelength of emitted radiance (λ = 11.5 μm)

$\varepsilon\lambda$ - is the emissivity.

4.3 Research objective 3: Assessment of the influence of maximum temperature on heat-related mortality

4.3.1 Description of in-situ meteorological and morality data collection

The University of Abuja Teaching Hospital, Gwagwalada (UATH), National Hospital, Abuja (NHA), General Hospital Kwali (GHK), General Hospital Abaji (GHA), General Hospital Kuje (GHKU), and the specialist Hospital Maraba, Karu area of Nasarawa State (SHM) provided the mortality data used in this study (Figure 4.3). The data contained mortality record at a monthly scale. The characteristics of the data varied by the hospital from which they were collected. For instance, the UATH data were categorised by gender (male and women) and age: 0-5 years, 6-17 years, 18-30 years, 31-45 years, and over 46 years. The NHA data were obtained for the monthly summary of heat-related mortality. The GHA, GHKU, and GHK data included mortality records from health centres in their catchment areas' settlements. Except for the UATH, mortality data for the study were collected on paper and then converted to digital format.

The cause of death and in-patient admission rates for the following diseases were obtained from hospitals and health centres: cardiovascular disease, respiratory disease, cerebrovascular disease, diabetes, psychiatric disorder, myocardial

infarction, ischemic heart disease, congestive heart failure, malaria, measles, cholera, meningitis, and pneumonia. The causes of death from cardiovascular, respiratory, cerebrovascular, and ischemic heart disease were not included in the GHA and GHK data. The periods for the health data vary, with the UATH covering the years 2000 - 2019 and the GHA covering the years 2005 - 2019. The Nigerian Meteorological Agency (NiMet) weather station at Nnamdi Azikiwe International Airport in Abuja provided the daily maximum temperature (*Tmax*) from 1990 to 2019. The acquired data were computed on a monthly scale similar to the mortality data obtained from health centres. Figure 4.3 shows the locations of the hospitals and weather stations from which data for this study was collected.

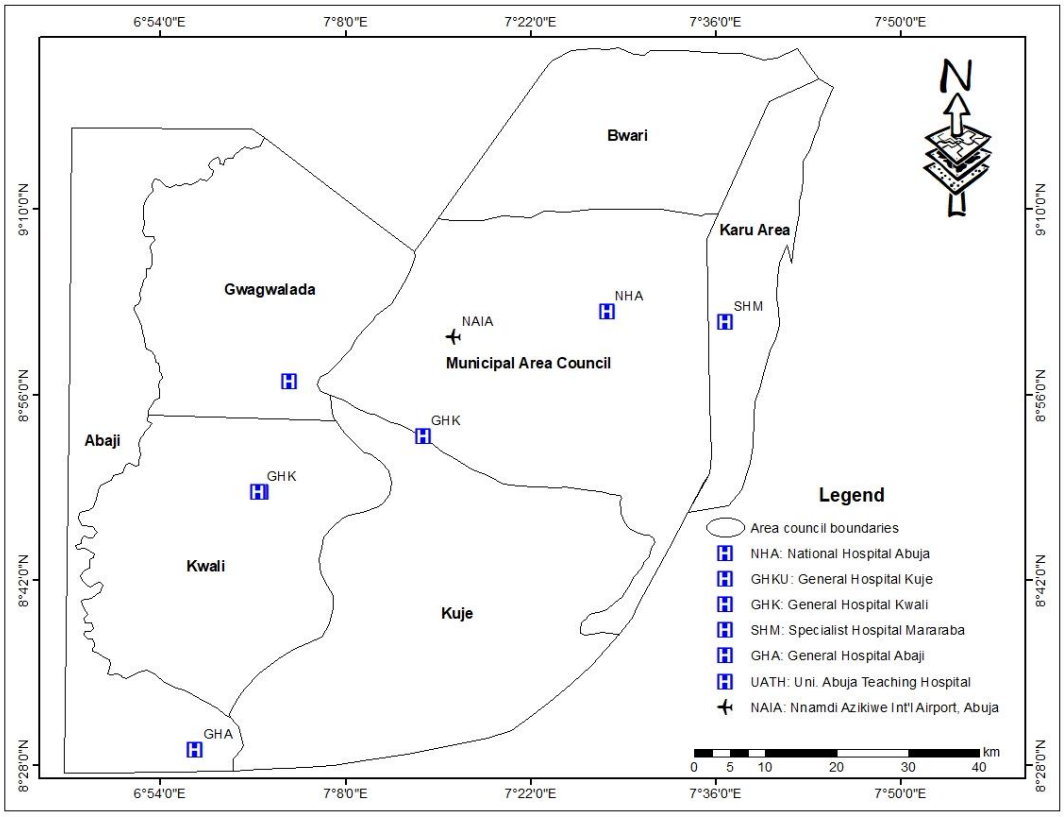


Figure 4.3: Location of hospitals and weather station in the study area.

4.3.2 The nature and accessibility of health data

The data for this study are in-hospital mortality, which are deaths that happened and were recorded in the hospital and for whom the cause of death was known. The study did not include deaths that occurred at home or for which the cause was unknown. The University of Abuja Teaching Hospital, Gwagwalada Area

Council, Abuja, Nigeria; National Hospital, Municipal Area Council, Abuja; General Hospital Kwali Area Council, Abuja; and Specialist Hospital Maraba, Karu region of Nasarawa state, Nigeria, provided health data for this study. Health data applications were submitted to each institution's administrative secretary between September 30th and October 14th, 2019, along with a research proposal and ethical approval from the University of Nottingham, United Kingdom. Individually, the research proposals were tailored to the needs of each facility. The applications were followed up on and forwarded to the Chief Medical Directors and the hospitals' health research ethics committee for approval. These activities took place between the 17th and 24th of October 2019.

The review sessions for the assessment of data applications were held individually by the health research ethics committees of each hospital between November 1st and 4th, 2019. All of the applications were approved without any problems. The committee recommends that data extraction begin when the committee's suggested corrections have been implemented. The health research ethics committee of the National Hospital, Abuja, made the following suggestions on the research proposals for correction:

1. The need to revise the study's objectives requires more information than is supplied on the National Hospital death certificate types.
2. More detail was requested on how the investigator intends to secure the hospital's health information to avoid future legal issues.
3. Errors in spelling and grammar.

All the issues noted were corrected, and the document was resubmitted to the Department of Statistics and Records for data extraction. Each hospital received two separate payments for the ethical and data extraction fees. The processes for acquiring health data from the speciality hospital Maraba in the Karu district of Nasarawa state are slightly different from those of the other hospitals. Applications for health data and subsequent authorization were sought from the head medical director of the Hospitals Management Board in Lafia, Nasarawa State's capital city. Furthermore, the approval letter was submitted to the office of the chief medical director of the specific hospital where the health data was required (specialist hospital, Maraba) for further approvals, along with other

relevant documents such as the application letter requesting the health data, the research proposal, payment receipt at the hospital management board, Lafia, and ethical clearance from the University of Nottingham, United Kingdom. To that end, an ethical charge was paid at both the hospital management board Lafia and the specialist hospital Karu. These events took place between September 27th and December 17th, 2019.

The hospital's mortality total varies greatly, which can be linked to the hospital's location, the type of equipment in the hospital, the socioeconomic status of the population, and the catchment hospital. For example, the mortality numbers from the general hospital Kuje and the specialist hospital Maraba were high because the data included death from other catchment hospitals in the wards. Furthermore, the data from these hospitals cover malaria, measles, and cholera mortality. The mortality figures from the National Hospital Abuja were low because the facility is expensive, located in the city centre, and has sophisticated equipment that the wealthy can only afford.

4.3.3 Empirical statistical heat-mortality modelling

Empirical statistical modelling was employed to explore the relationship between observed monthly *Tmax* and mortality data. Linear regression was used to understand the data and help elucidate any relationships between the *Tmax* and mortality. In this regard, the monthly observed *Tmax* and mortality were plotted using a scatter graph to fit a linear function in the arrangement (*x,y*), where *x (Tmax)* is the 'independent' variable and *y* (observed mortality) is the 'dependent' variable.

4.3.4 Computation of excess mortality count

The term "excess mortality" is used in epidemiology and public health to describe the overall death toll during a crisis that is higher than expected under "normal" conditions (Checchi & Roberts, 2008). In this instance, excess mortality concerns the number of fatalities during heat waves and extreme heat events compared to the number of fatalities that would have been expected if the extreme heat had not occurred. Due to industrial strike actions by health organisations in the study area, the mortality statistics gathered for this study are

incomplete for certain months. The AVERAGEIFS function, which is a simple logical expression that works with cells with missing data, was used to compute the months for which there was missing data.

The computation of excess mortality was performed using the observed/expected method, similar to one of the approaches used by Guest *et al*. (1999); Dessai (2002); Gosling *et al*. (2007) Babalola *et al*. (2018); Li & Tang (2019). The term "expected mortality" refers to the total number of deaths over a given period. The expected mortality count in this study estimates the likely number of deaths based on observed mortality data using a monthly average and a four-month moving average approach. For this study, two methods were used to calculate the excess mortality. Firstly, the average mortality for each month was used to calculate the expected mortality. For instance, this approach computed January's average mortality as expected mortality and used it for each January month throughout the data. Table 4.3 shows the average monthly mortality for the six hospitals included in this investigation.

Table 4.3: The average number of deaths per month for the six hospitals involved in this study

Hospital	**The average monthly deaths**											
	Jan.	Feb.	Mar	Apr	May	Jun	Jul	Aug	Sep	Oct.	Nov	Dec
UATH	49.7	53.6	54.5	52.6	51.3	46.8	48.7	46.2	44.7	45.2	44.8	49.7
NHA	20.3	25.1	20.3	18.7	19.1	18.7	19.8	17.4	24.1	17.1	19	15.8
GHKU	59.8	59.5	60.1	57.6	61.1	61.8	63.3	64.1	60.4	63.1	59.2	67.9
GHK	134.3	136.9	134	123.5	126.9	127.8	128	121.4	117.5	117	120.6	125.7
SHM	132.5	133.4	149.2	146.8	126.5	117	109.65	106.4	107.45	111.1	121.4	131.6
GHA	52.9	48.2	48.8	42.8	48.3	43.6	42.1	37.4	38.9	36.1	39.3	42.7

Secondly, a 4-months moving average was used for the calculating the expected mortality - January 2000 to December 2019 was computed as the expected mortality. The second method appears to smooth the variations in the data. The association between the time series analysis of excess mortality from the 4-month moving average and the monthly average baseline is shown in Table 4.4. The excess mortality from the 4-month moving average baseline was used as the independent variable, while the monthly average baseline was used as the

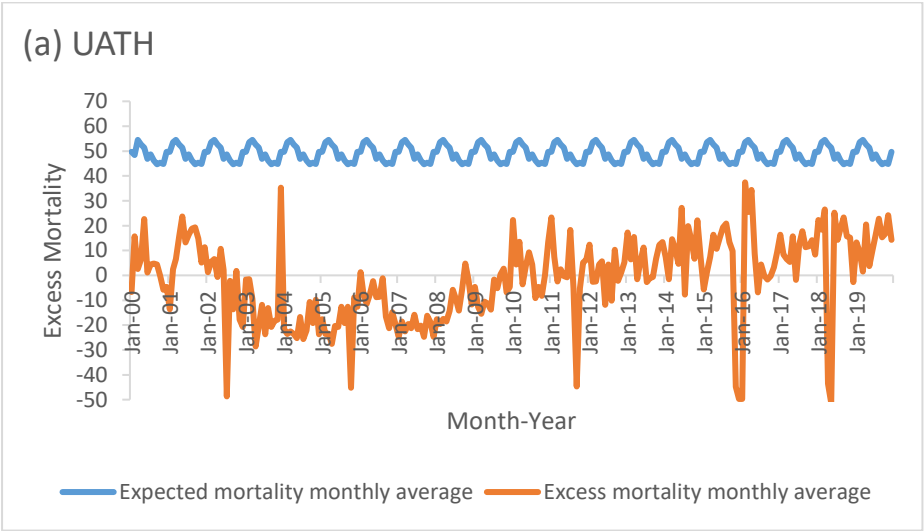
dependent variable. According to results from the University of Abuja Teaching Hospital and the National Hospital Abuja, the time series models from the 4-month moving average baseline and the monthly average baseline have a correlation coefficient of 0.63 and 0.72, with a *p*-value of 0.06 and 0.88, signifying no significant relationship. There is no significant association between the time series model from the 4-month moving average baseline and the monthly average baseline for the General Hospital Kuje since the *p*-value is greater than 0.05 (*p*-value: 5.64) with a correlation coefficient of: 0.007. The correlation coefficients of the time series model from the 4-month moving average baseline and the monthly average baseline for general hospital Kwali, specialist hospital Maraba, and general hospital Kwali are 0.47, 0.46, and 0.40, with a *p*-value of 1.23, 0.98 and 1.60, signifying no significant relationship as shown in Table 4.4.

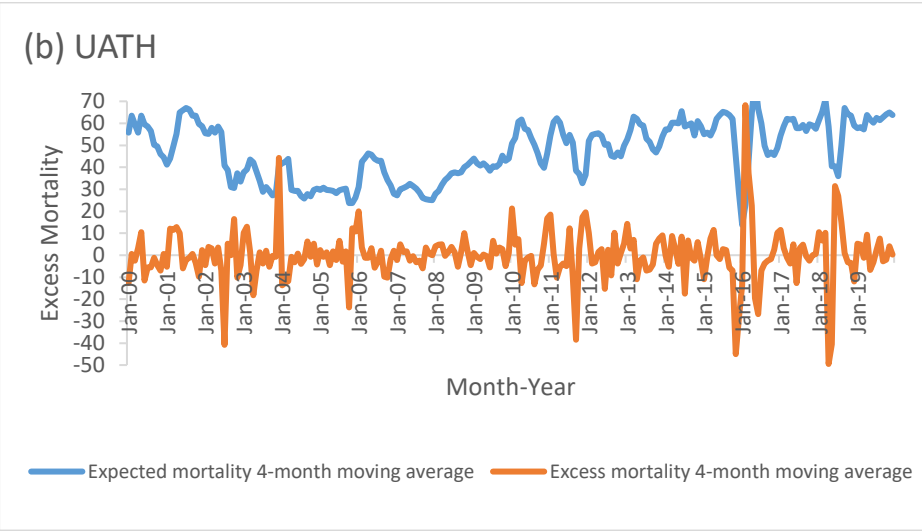
Table 4.4: Association between the time series analysis of excess mortality from the monthly average baseline and the 4-month moving average baseline.

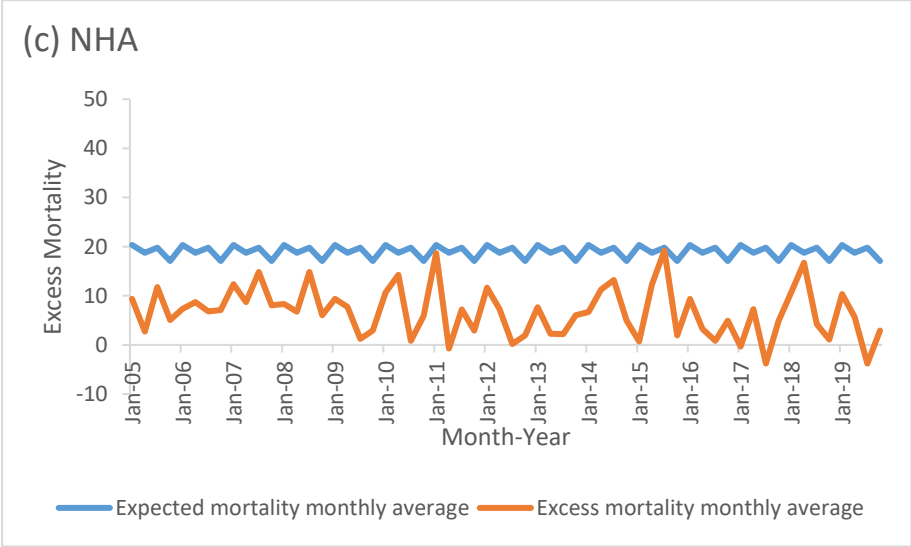
Uni. Abuja Teaching Hospital	*Excess mortality 4-month moving average*	Excess mortality monthly average	*p-value*
(x) Excess mortality 4-month moving average	1		
(y) Excess mortality monthly average	0.63	1	0.06
National Hospital Abuja	*Excess mortality 4-month moving average*	Excess mortality monthly average	*p-value*
(x) Excess mortality 4-month moving average	1		
(y) Excess mortality monthly average	0.72	1	0.88
General Hospital Kuje	*Excess mortality 4-month moving average*	Excess mortality monthly average	*p-value*
(x) Excess mortality 4-month moving average	1		
(y) Excess mortality monthly average	0.007	1	5.64
General Hospital Kwali	*Excess mortality 4-month moving average*	Excess mortality monthly average	*p-value*
(x) Excess mortality 4-month moving average	1		
(y) Excess mortality monthly average	0.47	1	1.23
Specialist hospital Maraba	*Excess mortality 4-month moving average*	Excess mortality monthly average	*p-value*
(x) Excess mortality 4-month moving average	1		
(y) Excess mortality monthly average	0.46	1	0.98
General Hospital Abaji	*Excess mortality 4-month moving average*	Excess mortality monthly average	*p-value*
(x) Excess mortality 4-month moving average	1		
(y) Excess mortality monthly average	0.40	1	1.60

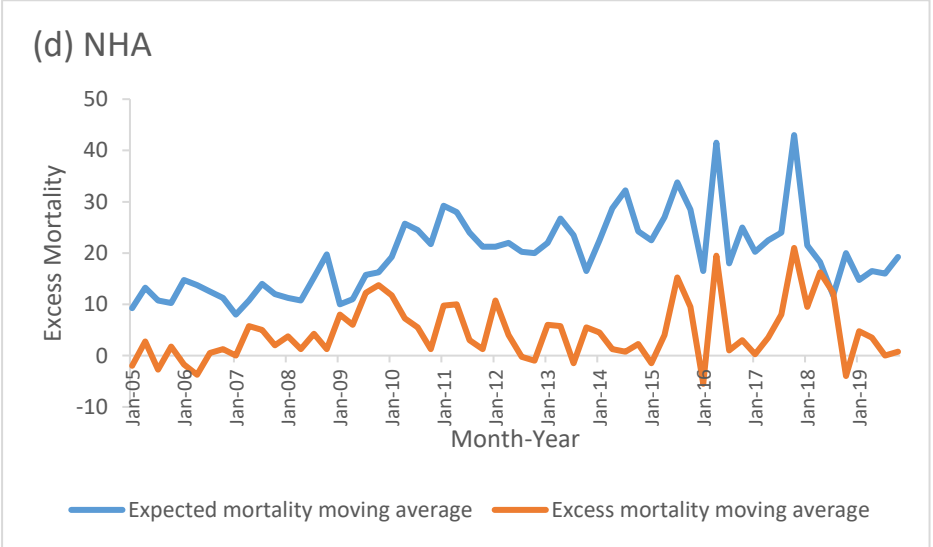
4.3.5 Seasonal cycle of mortality and the contrasting patterns of excess mortality across the 6 hospitals

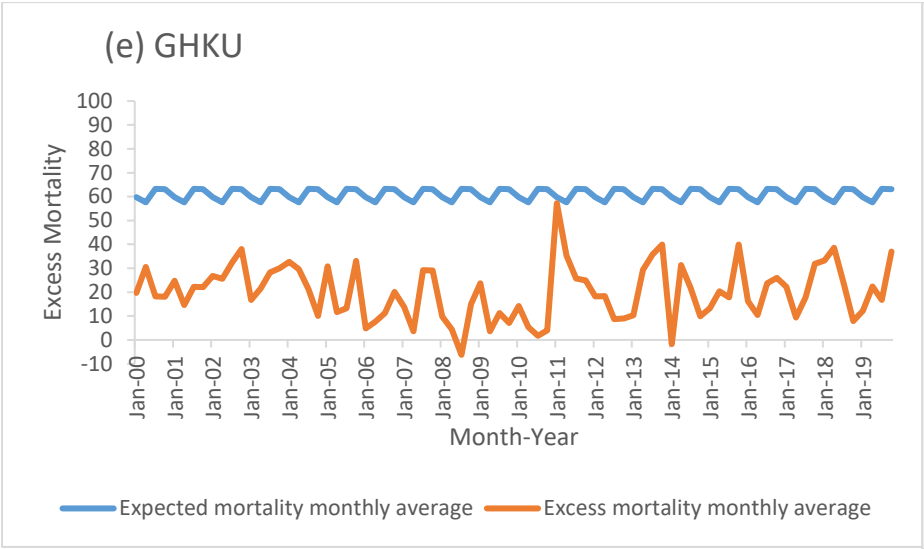
Mortality rates in the six hospitals exhibit seasonal fluctuations. For example, heat-related mortality at the University of Abuja teaching hospital and the General Hospital Abaji increases during the dry, hot season (December, January, February, March, April, and May) relative to the remaining months of the year, which is characterised by the warm/wet season. Mortality statistics from the National Hospital in Abuja indicate a high mortality rate during the hot/dry season, despite September being the month with the most significant mortality rate. There are no significant differences in mortality rates between the hot/dry and warm/wet seasons in the general hospital Kuje and the specialist hospital Maraba, which could be attributed to the fact that mortality data from these hospitals included deaths from malaria, measles, and cholera--all of which are common in the warm/wet season in tropical Africa. However, the specialist hospital Maraba, located in the research region's informal settlement, had the highest mortality in March and April, the hottest months in the study area. Hospitals that gave data on heat-related mortality had a high mortality rate during the hot/dry season. However, hospitals that provided data on total mortality had little or no seasonal differences in mortality. Similarly, the substantial peaks in mortality that occurred at the same time in some hospitals across the study hospitals could be attributed to insufficient data archiving methods in the past and the gradual improvement in recent times, as well as the absence of data in some months due to industrial strike actions, and the subsequent increase in mortality in the months following the suspensions of the industrial strike actions. Figure 4.4 shows the time series graphs of the expected mortality and the excess mortality for the monthly average method (left panel) and the 4-month moving average method (right panel).

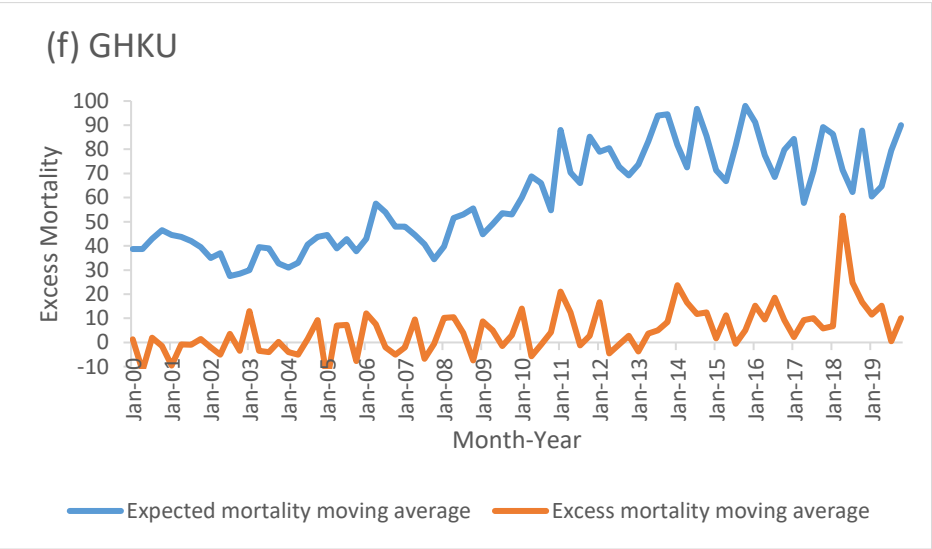

(a) UATH
Excess Mortality
Month-Year
Expected mortality monthly average
Excess mortality monthly average

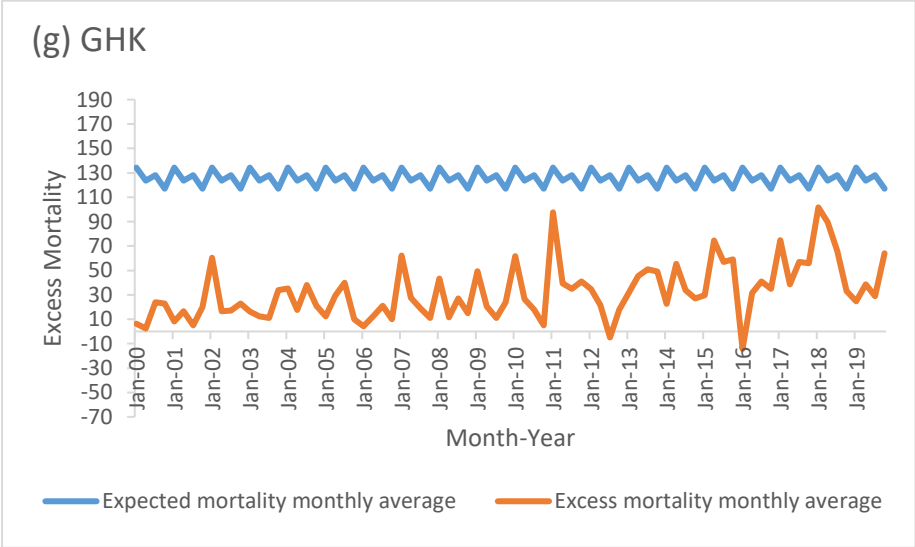

(b) UATH
Excess Mortality
Month-Year
Expected mortality 4-month moving average
Excess mortality 4-month moving average

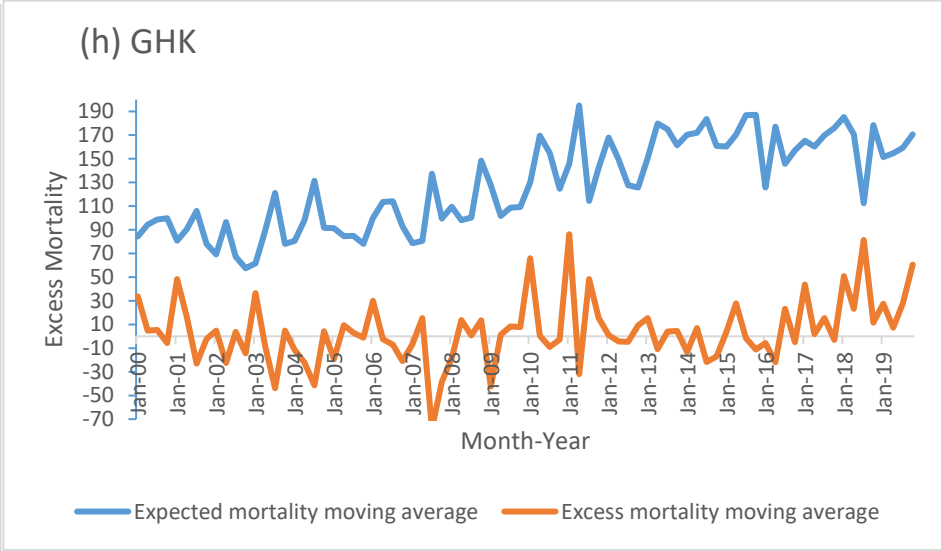

(c) NHA
Excess Mortality
Month-Year
Expected mortality monthly average
Excess mortality monthly average


(d) NHA
Excess Mortality
Month-Year
Expected mortality moving average
Excess mortality moving average


(e) GHKU
Excess Mortality
Month-Year
Expected mortality monthly average
Excess mortality monthly average


(f) GHKU
Excess Mortality
Month-Year
Expected mortality moving average
Excess mortality moving average


(g) GHK
Excess Mortality
Month-Year
Expected mortality monthly average
Excess mortality monthly average


(h) GHK
Excess Mortality
Month-Year
Expected mortality moving average
Excess mortality moving average

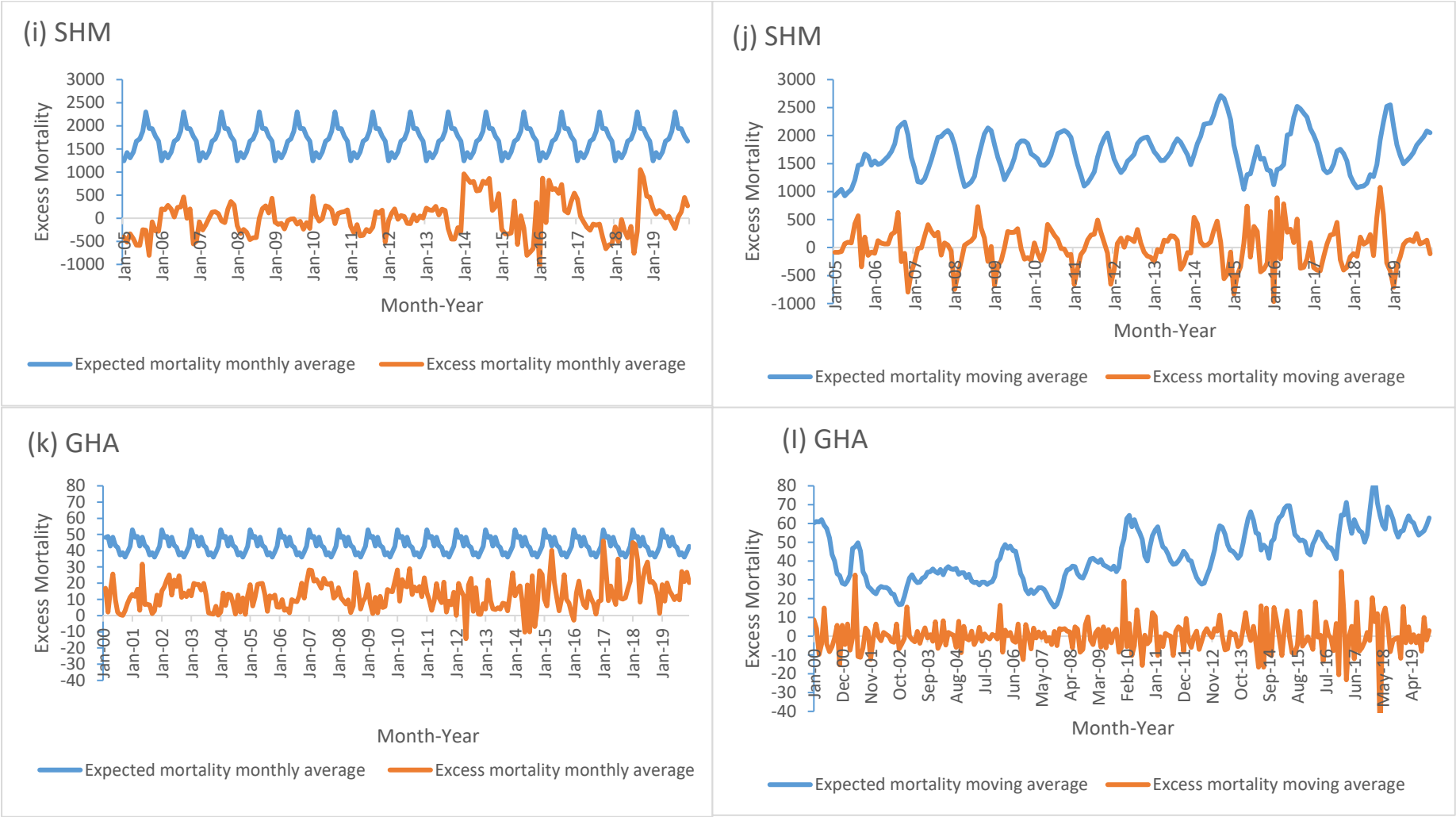


Figure 4.4: Time series graphs for the six hospitals participating in this study showing the expected mortality and excess mortality for the monthly average approach (left panel) and the 4-month moving average method (right panel).

In each instance, excess mortality was calculated by subtracting the expected values from the observed values. For the monthly average baseline, subtractions were made from the average mortality that occurred in, for instance, January from the observed mortality of each January for every year of the study period. That meant subtracting every observed death in January from the (expected) average death of January (49.7), every observed death in February from the (expected) average death of February (53.6), every observed death in March from the (expected) average death of March (54.5), every observed death in April from the (expected) average death of April (52.6) and so on. For the 4-months moving average baseline, the observed mortality value for each month was subtracted from the 4-months average of the preceding month. The excess mortality was computed by subtracting the expected death count in each month from the corresponding month of the observed number of deaths. The *Tmax* (^{o}C) data utilised in this investigation were precise to 1 decimal place, making it easy to categorise the computed excess mortality into 0.5^{o}C *Tmax* categories, e.g. 31-31.4 ^{o}C, 31.5-31.9 ^{o}C, 32.-32.4 ^{o}C, 32.5-32.9^{o}C. This For instance, in January of the year 2000, the monthly *Tmax* (^{o}C) recorded was 35.9°C, and there were 7 excess mortality counts. 7 was therefore assigned to 35.5–35.9 °C intervals. The average mortality counts in each 0.5°C temperature interval were computed to arrive at the monthly excess mortality.

4.3.6 Temperature threshold

The threshold temperature is the temperature above which excess mortality begins to rise above zero. Temperature thresholds vary with location, as does the population's sensitivity to heat. For instance, the UK Met Office's Heat–Health Watch System's temperature thresholds for issuing health warnings in London are 32.0^{o}C (day) and 18 ^{o}C (night), while in North East England, they are 28.0^{o}C (day) and 15.0^{o}C (night) for at least two consecutive days and the prevailing night (Gosling *et al*., 2009). For the National Weather Service's extreme heat watch and warning system in the USA to be issued, daytime temperatures must be greater than or equal to 40.6°C, and night-time temperatures must be less than or equal to 26.7°C for two consecutive days

(Robinson, 2001). Similarly, the Royal Netherlands Meteorological Institute defines a heatwave as a period with a *Tmax* of 25.0 to 30.0°C or higher for three to five days (Huynen *et al*., 2001). Heat warnings are issued by the Chinese Meteorological Administration in Shanghai when extreme temperatures are predicted to exceed 35.0°C. (Tan *et al*., 2007). In Nigeria, the Nigerian Meteorological Agency issued a heatwave warning when temperatures exceeded 35.0°C (NiMet, 2021). For this study, only temperatures above 30.0°C were included in the model because there was no excess mortality at temperature intervals of 25.0-30.0°C.

4.3.7 Model selection for regression

Tmax (°C) and excess mortality were modelled using linear and nonlinear regression from the 4-month moving average and the monthly average baseline going forwards, assuming two baselines. This is to enable a comparison of the sensitivity of the estimates to the chosen baseline. In this case, the calculated excess mortality was regressed against the *Tmax* (°C). The statistical output of the preliminary analysis was aimed at determining the strength of the relationship between *Tmax* (°C) and mortality. The outputs of the linear and nonlinear models, as well as those from the two different baselines, were examined to determine whether one or both models should be used in the future. The most important components for comparison were the R^2 and *P*-value, as well as the nonlinear regression at the second, third, and fourth polynomial orders that best fit the data. The curves for each regression model were plotted in 1.0°C increments. For each regression model, a 95% confidence interval was derived around the curve to determine the level of certainty and uncertainty associated with the sampling technique.

4.4 Research objective 4: Mapping of heat vulnerability

4.4.1 Heat vulnerability indicators

This study's heat vulnerability indicators (HVIs) were chosen based on prior research (Cutter *et al*., 2003; Turner *et al.*, 2003; Campbell *et al.*, 2018) and data availability. 9 primary HVIs are included for the mapping of heat vulnerability:

LST, AISs, the NDVI, population density, poverty level, literacy rate, housing quality, women population, and vulnerable population, defined as those aged below 4 and over 65 years. They are primary HVIs since they were derived from the source data using various mapping techniques. The 9 primary HVIs included in this mapping are used to generate three secondary HVIs based on the framework developed by the IPCC (2021), which considers vulnerability as a function of a population's exposure to extreme heat events, its sensitivity to extreme heat events, and its adaptation capacity to extreme heat events.

(1) Heat exposure index: In this context, the heat exposure index is the severe climatic anomalies, such as excessive temperatures, to which a population is exposed. Human health was affected by the degree, variation, and temperature distribution. Heat exposure can alter over time as temperatures increase or in space due to the UHI. This occurs when urban areas are warmer than other areas due to the presence or absence of AIS and vegetation cover (Karimi *et al*., 2018; Mallen *et al*., 2019; Sabrin *et al*., 2020). The heat exposure index is composed of environmental factors that can increase heat capacity. UHI is a major cause of heat exposure (Oke, 1987; Stone, 2012). Frequently, the heat exposure index is calculated utilising proxies such as LST, AIS, or the absence or presence of vegetative cover (Reid *et al*., 2009; Bao *et al*., 2015). Heat exposure may be exacerbated by factors such as the dwelling quality, with all structures accumulating more heat on upper levels as heat rises, or by the roofing material, with dark, absorbent materials storing more thermal energy than reflective materials (Stone, 2012).

(2) Heat sensitivity index: The rate at which a population is positively or negatively affected by a climate event is considered as sensitivity (Tran *et al*., 2020). Sensitivity relates to the extent to which a person may be impacted by heat, given the physiological factors that may promote or prevent these effects. Young or elderly individuals may find it more challenging to regulate their body temperature (Reid *et al*., 2009; Hulley *et al*., 2019; Sabrin *et al*., 2020). Sensitivity refers to how effectively a population can cope with additional exposure, or how much greater exposure may adversely impact the population.

For instance, the population with heat-sensitive pre-existing diseases, such as diabetes, will be more sensitive to heat than individuals who do not have an existing health problem (Reid *et al*., 2009; Sabrin *et al*., 2020).

(3) The adaptive capacity index: The adaptive capacity index measures a population's ability to regulate a climate incident, mitigate potential effects, or withstand the consequences (Zhu *et al*., 2014). Adaptive capacity is defined by Cutter *et al*. (2008) and KC *et al*. (2015) as "the capabilities or possessions that a person or population has access to in order to control exposure to extreme heat." The ability of a population to effectively reduce or survive with greater personal exposure is referred to as "adaptive capacity" (Mallen *et al*., 2019). Individuals who have access to air conditioning, for example, have a stronger adaptive capacity than those who do not, regardless of their heat sensitivity. These factors—heat exposure, sensitivity, and adaptive capacity—have been shown to affect heat-related morbidity and mortality, hence they are considered as the three secondary indicators of heat vulnerability. Figure 4.5 presents a framework of heat vulnerability based on the secondary indicators. Table 4.5 presents the characteristics of this study's nine heat vulnerability indicators and some studies that used similar indicators.

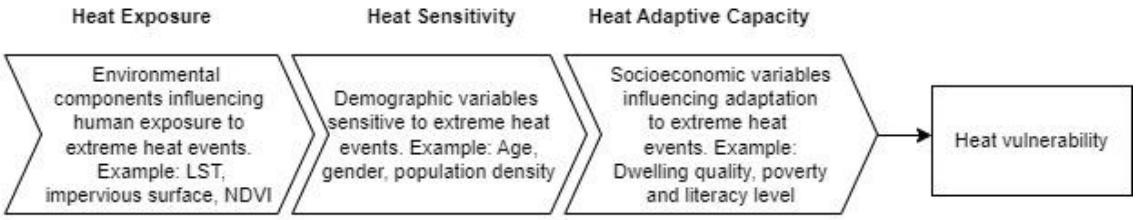


Figure 4.5: Framework of heat vulnerability based on the 3 secondary indicators modified after Zhu *et al*. (2014) and Tran *et al*., (2020).

Table 4.5: Characteristics of the 9 heat vulnerability indicators used for this study and some studies that used similar indicator

Items	Heat Vulnerability Indicators	Descriptions of Datasets	Data Source	Year of data collection	Method of data capture	Studies that used similar indicators
Exposure index	LST	LST map generated using Band 10 & 11 of the March 2020 Landsat 8 image with a 100m spatial resolution	USGS website	2020	Single channel method	Wolf & McGregor (2013); Tomlinson *et al.* (2012); Johnson *et al*.(2012); Weber *et al*.(2015); Hulley *et al*. (2019)
	Impervious Surfaces	30 m spatial resolution Landsat 8 Bands 1-9 sensor-generated map of artificial impervious surfaces.	USGS website	2020	Supervised and unsupervised classification	Maier *et al*. (2014); Manangan *et al.* (2015); Sabrin *et al*. (2020); Grigorescu *et al*. (2021)
	NDVI	NDVI map with a spatial resolution of 30m derived from bands 4 and 5 of the 2020 Landsat 8 image.	USGS website	2020	Standardized index	Chow *et al.* (2012); Johnson *et al.*(2012); Weber *et al*.(2015); Guo *et al*. (2019); Prosdocimi & Klima (2020)
Sensitivity index	Population below 14 years and above 65 years	Grid-based estimates of the male/women population under 4 and over 65 years of age at a spatial resolution of 92m	https://www.worldpop.org/about Demographic & health survey	2020	Sub mapped, re-projection, resampled and reclassified	Johnson *et al.* (2012); Loughnan *et al.* (2012); Wolf *et al*. (2014); Sabrin *et al*. (2020); Prosdocimi & Klima (2020).
	Women population	Estimates of the total number of women (15-49 years old) at a spatial resolution of 92m based on gridded estimates.	https://www.worldpop.org/about Demographic & health survey	2020	Sub mapped, re-projection, resampled and reclassified	Cutter *et al*. (2003); *Johnson et al*.(2013); Aminipouri *et al.* (2016); Reckien (2018); *Tran et al.* (2020)
	Population Density	Gridded estimates of the total population divided by the number per pixel at a spatial resolution of 92m	https://www.worldpop.org/about Demographic & health survey	2020	Sub mapped, re-projection, resampled and reclassified	Tomlinson *et al.* (2012); Keramitsoglou *et al*. (2013); Macnee & Tokai (2016); Hulley *et al.* (2019); Sabrin *et al*. (2020)
Adaptive capacity	Poverty level	923m resolution poverty and inequality gridded estimates of male/women population living on less than $1.25 per day.	https://www.worldpop.org/about Demographic & health survey	2020	Sub mapped, re-projection, resampled and reclassified	Hondula *et al.*(2012); Bradford *et al*. (2015); Bai *et al*. (2016); Hulley *et al*. (2019); Jagarnath *et al*. (2020).
	Literacy rate	Gridded estimates of the male/women literate population (Over 14 years old) at a spatial resolution of 923m	https://www.worldpop.org/about Demographic & health survey	2020	Sub mapped, re-projection, resampled and reclassified	Zhu *et al*. (2014); Bai *et al*. (2016); Manik & Syarifah (2017); Voelkel *et al*. (2018); Wilson & Chakraborty (2019)
	Dwelling Quality	Floating point raster image of dwelling quality at a spatial resolution of 92m.	https://www.worldpop.org/about Google image	2020	Sub mapped, re-projection, resampled and reclassified	Christenson *et al*. (2017); Mortensen *et al*. (2018); Bhattacharjee *et al*. (2019); Yu *et al*. (2021).

4.4.2 Justification for choosing the 3 primary indicators that constitute this study's heat exposure index

The heat exposure index in this study is comprised of 3 primary indicators: LST, artificial impervious surface, and NDVI. There are various other heat exposure index indicators that are not included in this study due to data availability. The selection of the 3 primary indicators that constitute the heat exposure index was based on existing literature, as presented below.

4.4.2.1 Land surface temperature

The land surface is the interface between the atmosphere and biosphere for material and energy exchange and has a pronounced effect on the temperature. LST is the temperature at the Earth's surface from the sun's energy and heat being reflected, reradiated, and absorbed by the Earth's surface (Equere *et al.,* 2020; Sabrin *et al*., 2020). LST change as a result of change in climate and human activities, such as the conversion of land use through urbanisation. The alteration of natural land cover to AIS has a massive influence on both LST and UHI. Due to its substantial influence on human health, LST has been a primary indicator of heat vulnerability (Garland *et al*., 2015; Russo *et al*., 2016; Coffel *et al*., 2017; Abrar *et al.,* 2022). Human exposure to extreme heat affects well-being, and the spatial distributions of LST varies with land use/cover (Stewart & Oke, 2012; Loughnan *et al.,* 2015). Urban areas with AIS behave differently from natural surfaces in terms of shortwave and longwave radiation absorption, evapotranspiration, the release of anthropogenic heat, and the blocking of the prevailing wind. As a result, urban areas experience heat islands than their adjacent areas (Bokaie *et al*., 2016). Figure 4.6(a) presents the LST map for this study.

4.4.2.2 Artificial impervious surface

Urbanisation has posed a major threat to the natural environment by displacing vegetation with AIS. Gong *et al*. (2019) stated that urbanisation has resulted in changes in AIS and loss of vegetation cover, thereby increasing the intensity of UHI. In this regard, land areas with a high proportion of AIS and densely packed

neighbourhoods exhibit a high heat intensity (Chithra *et al*., 2015; Yahia *et al*., 2018). Due to its influence on the UHI, AIS, which include land areas covered in stone, pavements, parks, rooftops, bricks, concrete, asphalt, or sand, are recognised as essential indicators of heat vulnerability. AIS and bare land store more heat than vegetation and water bodies, effectively replacing the cooling effect of evapotranspiration (Buyantuyev & Wu, 2010; Cobbinah *et al*., 2015; Scott *et al*., 2017). Water bodies such as rivers, lakes, ponds, reservoirs, and streams have a major influence on regional climate that usually reaches tens of kilometres from the coastline (Scott & Huff, 1996; Wang *et al.*, 2022). One of the most critical effects of water bodies on climate is that they can lower temperatures and cut down on summer thunderstorms (Scott & Huff, 1996). The AIS map for this study is shown in Figure 4.6(b). The land cover classes of grassland, shrubs and forest land were combined for heat vulnerability mapping to form the class vegetation cover.

4.4.2.3 Normalised difference vegetation index

NDVI measures the difference between near-infrared (which vegetation strongly reflects) and red light (which vegetation absorbs) to quantify vegetation. NDVI represents vegetation density and is an inverse measure of bare/impervious surface (Rongming *et al*., 2018; Hu *et al.*, 2018). Higher NDVI values typically indicate a more substantial proportion of vegetation in a pixel. Typically, LST is low in regions with a high NDVI. This negative correlation between NDVI and LST is helpful for urban climate studies. Vegetation absorbs carbon dioxide for photosynthesis and heat to cool the environment. With the annihilation of plant life, the cooling system's efficiency declines, resulting in the rise of LST (Halder *et al*., 2022). The density and quality of vegetation can mitigate the effect of UHI, and the UHI effect is exacerbated by the absence of green space caused by urban expansion, which may expose residents to heat-related health risks (Reid *et al.*, 2009; Zhou *et al.*, 2007). Extreme heat exacerbates morbidity and mortality associated with heat exposure (Jin *et al.*, 2020; Nwilo *et al.*, 2020). A reasonable proportion of vegetation cover can moderate the environment by cooling, serving as a carbon sink, and mitigating the effects of UHI on human health (Guha *et al.*, 2019; Zhao *et al.*, 2020). Figure 4.6(c) presents the NDVI map generated for this study.

4.4.2.4 Generating the 3 primary indicators that constitute this study's heat exposure index

For this study, the LST, NDVI, and AIS were derived from the Landsat sensor. LST can be calculated using various techniques, including land-cover dynamic monitoring centred on brightness temperature, the single-channel approach, and the split-window procedure (Jimenez-Munoz *et al.,* 2014; Yu *et al*., 2014; Sabrin *et al*., 2020). The single-channel method was used for LST mapping in this study because it was among the approved method by the USGS (Yu *et al*., 2014; Zhang *et al*., 2016; Cristóbal *et al.,* 2018**)**. The inputs for the LST from the Landsat 8 image were bands 4 (red), 5 (infrared), and 10 and 11 (thermal infrared). On a pixel-by-pixel basis, NDVI is computed as the normalised difference between the near-infrared band 5 (0.85–0.88 m) and the red band 4 (0.64–0.67 m) of the electromagnetic spectrum. The NDVI values are then used to calculate the proportionate vegetation (Pv), an estimate of the proportion of vegetation in each pixel. Pv is computed using Equation 4.4. The AIS were generated using supervised and unsupervised classification. Sections 4.1 and 4.2 describe the methodologies for mapping the LST, NDVI, and the AIS.

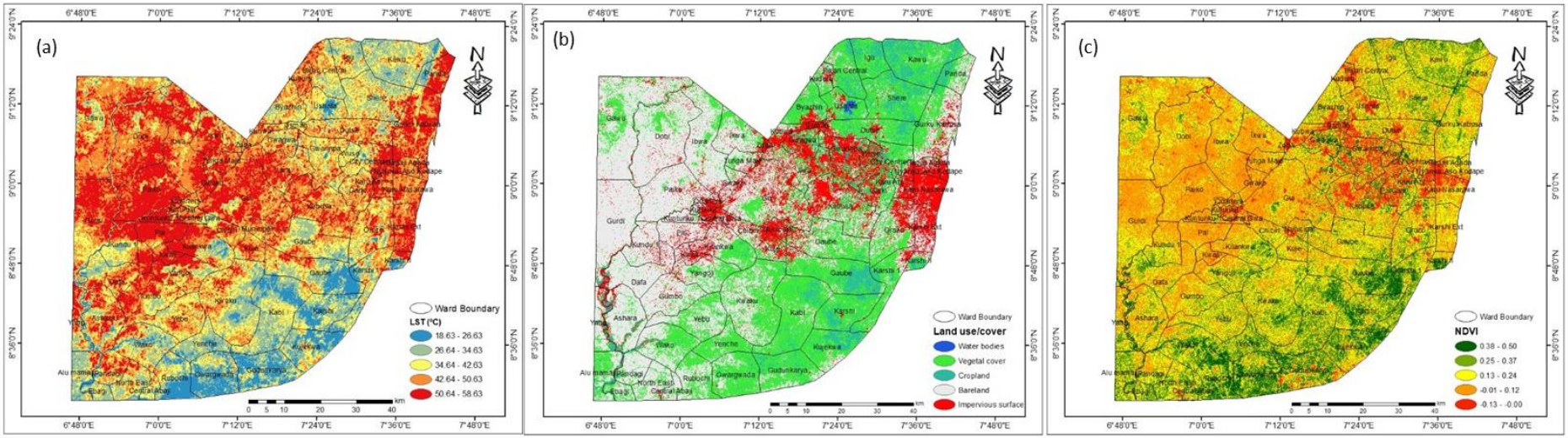


Figure 4.6: (a) The LST map generated from bands 10 and 11 of Landsat 8 image of March 2020 with a spatial resolution of 100m; (b) AIS of 2020 generated from Landsat 8 sensor with a spatial resolution of 30 m; (c) NDVI map of 2020 derived from bands 4 and 5 of Landsat 8 image with a 30m spatial resolution.

4.4.3 Justification for choosing the 3 primary indicators that constitute this study's heat sensitivity index

This study's sensitivity index covers three primary indicators: population density, the vulnerable population, and the women population. The selection of the three primary indicators comprising the heat sensitivity index was based on existing literature, as detailed below.

4.4.3.1 Vulnerable population (those below 14 years and over 65 years old)

Reid *et al*. (2009), Wolf & McGregor (2013), and Arsenovi *et al.* (2019) identify age as a crucial indicator of heat vulnerability, with the elderly over 65 and the young population under the age of 14 being the most vulnerable groups to heat-related morbidity and mortality. Kenny *et al*. (2010), Di Napoli *et al.* (2018), and Shih *et al*. (2022) found that older and younger populations have a greater rate of hospital admission and mortality during heat waves because they are the marginalised populations in society, which could enhance their risk of heat-related morbidity and mortality. Because of severe medical conditions and health issues, adults over 65 years are more prone to heat sensitivity (de Schrijver *et al*., 2022). Living alone puts people at greater risk since there are fewer people to check on them in an emergency, they are more prone to disregard heat risks, and they lack resources to deal with the heat (Semenza *et al.,* 1999; Reid *et al.*, 2009; Malmquist *et al*., 2022). Due to their propensity for chronic diseases and increased likelihood of social exclusion, elderly populations are often thought to be at higher risk (Robinson, 2001; Meade *et al*., 2020). Young children under 14 years are more sensitive to heat than adults because they sweat less and have a lower body-mass ratio (Chen *et al.*, 2015). The vulnerable population of 0 to 14-year-olds and over-65s used for this study is depicted in Figure 4.7(a).

4.4.3.2 Women population

Extreme heat can considerably affect women between 0-14 years old and over 65 years old. Women respond differently to heat than men because they have higher body fat (BF %) and physical strength. Younger women are more

vulnerable to dehydration during heat waves due to their smaller body size and higher water requirements. They may be unable to recognise or communicate their thirst effectively, leading to increased risk (Yang *et al*., 2019; Abrar *et al*., 2022). Because of their lower incomes, sector-specific occupations, household care, and limits imposed by cultural norms in some communities, women may have a more difficult time recovering from heat-related morbidity than males (Cutter *et al*., 2003; Reid *et al*., 2009; Zhu *et al*., 2014). Due to safety issues, several coping mechanisms for dealing with heat, particularly in some cultures of LMICs, such as natural coolness outdoors during hot days/nights, may not be possible for women. This may limit the number of times women can spend outdoors at night (Pasquini *et al*., 2020). Staying indoors during hot weather, particularly for the poor who lack access to air conditioning and fans, may raise their risk of heat-related morbidity and discomfort. Younger women from low-income families with limited air conditioning or adequate shelter may be at a higher risk during heat waves. Heatwaves can create stress and discomfort, affecting the mental well-being of children and adolescents. Pregnant women were only recently added to the list of people most vulnerable to heat stress (UNFCCC, 2017; USAID, 2019; Chersich *et al*., 2020).

Pregnancy makes women more vulnerable to extreme heat because of the changes in anatomy and physiology during pregnancy that makes thermoregulation difficult. Younger women have a less developed thermoregulatory system, making them more vulnerable to heat-related illnesses such as heat exhaustion and heatstroke (Laburn, 1996). Findings by Van der Hoeven & Wandl (2015) show that pregnant women exposed to extreme heat may give birth to a child with a low body weight, which may enhance the infant's vulnerability to heat. Mothers who are breastfeeding may experience challenges maintaining hydration and proper milk supply during heat waves. Air pollution levels can increase during heat waves, worsening air quality. This can exacerbate respiratory conditions in children, especially those with asthma or other respiratory problems (Sharma *et al.,* 2023). Prolonged exposure to high temperatures and sunlight can cause sunburns, rashes, and other skin irritations in young children (Reis-Mansur *et al.,* 2023). For this study, it should be stated that women of non-childbearing age, such as those aged 0-14, were already

included in the vulnerable population indicators as dependent populations. Including this age group in the women population indicator will amount to redundancy. The map of the women population for this investigation is shown in Figure 4.7(b).

4.4.3.3 Population density

Even though heat vulnerability is spatially variable, there is an important association between population density areas and heat vulnerability (Wolf & McGregor, 2013). According to Reid *et al*. (2009) and Hanberry (2022), the most vulnerable locations to heat are those with the highest densities of people living in metropolitan areas. High population concentration is frequently found in inner city areas that are also affected by the UHI, which is expected considering that dense population concentration has been demonstrated to correspond with regions with higher temperatures (Count *et al.*, 2007; Apriana & Syahrani, 2022). In examining exposure to heat stress in Quebec, Vescovi *et al.* (2005) found that areas with high population density on Montreal Island, which are geographically adjacent, have higher heat-related fatality rate than other locations. Johnson & Wilson (2009) for Philadelphia, USA, Tomlinson *et al*. (2011) for Birmingham, UK, Gabriel & Endlicher (2011) for Berlin, and Loughnan *et al*. (2012) for Melbourne all take into account the spatial concentration of higher than usual mortality rates during heatwave events in densely populated areas. Figure 4.7(c) shows the population density of Abuja and its environs.

4.4.3.4 Generating the primary indicators that constitute this study's heat sensitivity and adaptive capacity index

This study's sensitivity index (population density, vulnerable, and women populations) and adaptive capacity index (dwelling quality, poverty and literacy level) were generated from demographic and socioeconomic datasets using the WorldPop program, available at www.worldpop.org. The WorldPop series is a free, open-access collection of high-resolution sociodemographic spatial databases focusing on low- and middle-income nations. The WorldPop datasets were derived from population counts, household surveys, census data, satellite

images, and cell phone data to generate gridded demographic and socioeconomic datasets using Stevens *et al.'s* (2015) innovative random forest prediction tree-based modelling approach. The Stevens *et al.* (2015) random forest method is a semi-automated geostatistical modelling approach that accommodates population count and a wide variety of open access auxiliary datasets, *e.g.*, settlement places, settlement proportions, land use, roadways, housing maps, healthcare facility locations, satellite nightlights, vegetative cover, landscape, and refugee camps, to develop a gridded estimation of the concentration of human population and socioeconomic variables such as poverty level, and literacy rate at 100 m and 1000 m spatial resolution (Bondarenko *et al.,* 2020).

Gridded population and socio-demographic data from the WorldPop repository were downloaded in Geotiff format for this investigation. The WorldPop's estimation of socio-demographic characteristics was based on two techniques, resulting in two types of datasets in their archive: unconstrained and constrained top-down methods. The unconstrained datasets based their estimates on the demographic and socioeconomic survey and census data for the entire polygon, including uninhabited areas. This method provides estimates that include vacant land and forest reserve areas that were typically devoid of human habitation. Because estimates from constrained top-down approaches were based on settlement and footprints of human habitation areas extracted from satellite imagery, this study downloaded demographic and socioeconomic data from a constrained top-down method. The downloaded datasets for Nigeria were subsets for Abuja and its surroundings. The datasets were reprojected to WGS 1984 UTM Zone 32N. Due to the coarse nature of the WorldPop datasets, a resampling procedure was employed to convert the raster grid's cell values to a higher resolution compatible with the 30 m Landsat image. When classifying the datasets, the natural break was used to divide the attribute values using an equal interval into five equal-sized groups.

Primary heat vulnerability indicators for the research area were also acquired ward-by-ward from the demographic and health survey (DHS). This DHS source includes indicators such as population under 14 and over 65, women population,

poverty level, literacy rate, and population density. Spatial categorisation and proportional comparison at the ward level were used to transform the DHS statistics into percentages. Each indicator class's percentage was calculated by dividing the demographic target, such as the women population, by the total population and then multiplying the result by 100 to convert it to a percentage. These calculations were done so that the percentage of each indicator for each polygon (ward) region under consideration could be found so that more calculations could be done in the ArcGIS environment. There are various methods for representing quantity on a map. For this study, the percentages of each class of DHS heat vulnerability indicators were plotted on a map in graduated colours. In this instance, the DHS heat vulnerability indicators were classified into five classes, each defined by a particular colour. For classifying the % statistics, an equal interval was used to divide the range of attribute values into five equally-sized subranges. ArcGIS may now automatically calculate class breaks based on the value range. It should be noted that this method highlights the proportion of an attribute's value to other values. Each shapefile map indicator was converted to a raster format, allowing the features of each indicator to be reclassified based on their relative influence on heat vulnerability.

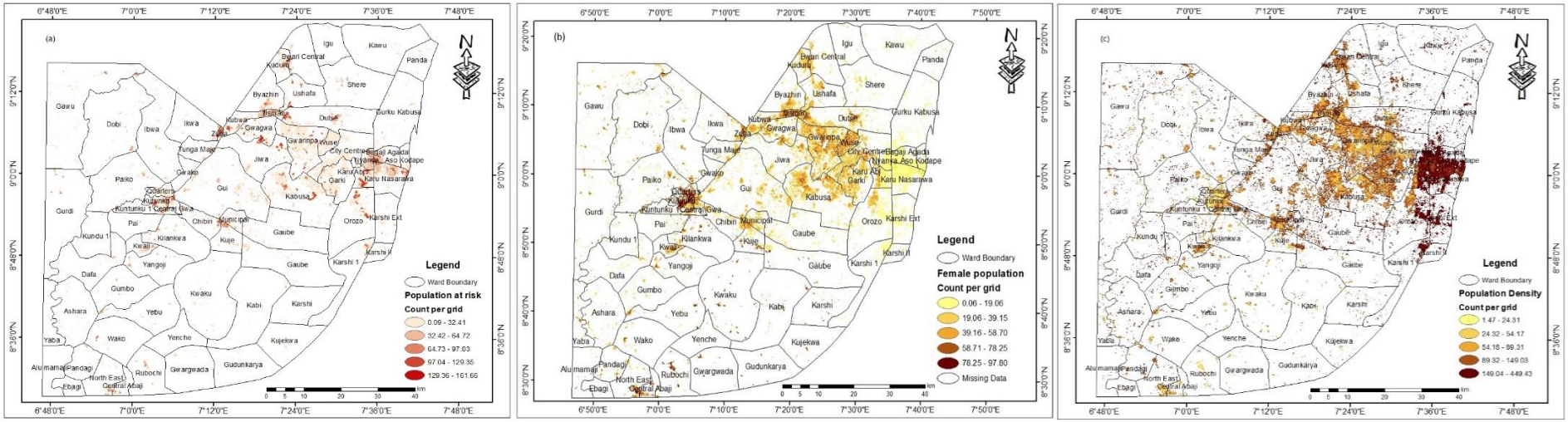


Figure 4.7: (a) Vulnerable population of 2020 generated from WorldPop datasets at a spatial resolution of 92m, (b) Total number of women of childbearing age (14-49) per grid square in 2020, derived from WorldPop datasets with a spatial resolution of 92m, (c) Population density of 2020 at a spatial resolution of 92m derived from WorldPop datasets.

4.4.4 Justification for choosing the 3 primary indicators that constitute this study's heat adaptive capacity index

Limiting personal heat exposure through socioeconomic status is a valuable indicator of heat risk (Sheridan & Allen, 2018; De Cian *et al*., 2019; Guardaro *et al*., 2022). Socioeconomic status, such as the levels of education, and poverty, are widely used as components of the adaptive capacity index in heat vulnerability mapping (Reid *et al*., 2009; Santacroce *et al*., 2022), which inform the inclusion of poverty, literacy rate, and dwelling quality as the components of the adaptive capacity index of this study.

4.4.4.1 Population living in poverty as define by $1.25 per day threshold

The international poverty line is a monetary threshold of $1.90 per day below which an individual is considered to be living in poverty (World Bank, 2022). The financial level of a household was thought to be the most effective measure of adaptation capacity for reducing the effects of extreme heat (Tran *et al.,* 2020). Low income impacts the population by making them more vulnerable to heat threats (Harlan *et al*., 2007; Johnson *et al.,* 2020). People below the poverty line are more vulnerable to heat because they have a lower adaptation capacity (Cutter *et al.,* 2003). They may be unable to afford air conditioning, fans, refrigeration, and adequate healthcare services (Gronlund, 2014; Voelkel *et al*., 2018). Because of the scarcity of shaded and vegetated areas, they may need more cooling spaces, whether indoors or outdoors. The people below the poverty line have little control over their working conditions; they have a low quality of life and appear more vulnerable to heat-related morbidity and mortality (Pasquini *et al*., 2020). Kim & Joh (2006) discovered that low-income people died at a higher rate during hot weather in Seoul, Korea. Access to wealth is a critical component of heat adaptive ability to reduce risk through early-warning systems (Du Toit *et al.,* 2018). Figure 4.8(a) presents an estimate of the proportion of poverty level per grid square in 2020.

4.4.4.2 Literacy level of the population above 15 years

Low education is crucial in heat vulnerability. In their study on county-level heat exposure of urban and rural residents in Tibet, China, Bai *et al*. (2016) included

illiteracy as a vulnerability indicator, where illiterate individuals were more vulnerable to heat-related morbidity than literate individuals. According to O'Neill *et al.* (2003), people with low levels of education are more vulnerable to heat, and the proportion of people who have never attended school is exceptionally high among rural residents. Higher educational attainment was associated with greater lifetime earnings (Cutter *et al.*, 2003). The amount of literacy influences morbidity and mortality associated with heat. People with less than a high school diploma are more vulnerable to heat because they cannot comprehend warning signals and gain access to recovery knowledge (Reid *et al*., 2009; Zhu *et al*., 2014; Tran *et al.*, 2020). To combat excessive heat, it is crucial to have current knowledge and comprehension of heat risks and adaption options. Essential components of heat vulnerability include appropriate adaptation strategies such as public messaging (radio, television), mobile phone-based text messages, automated phone calls, and amber alerts, as well as conventional adaptation habits such as remaining indoors, wearing comfortable clothing, and dieting. Due to a poor understanding of adaption measures, such as access to temperature information on hot days or nights, the population's vulnerability to heat may increase, which could be detrimental to human health (Pasquini *et al*., 2020). Figure 4.8(b) presents the study's literacy map.

4.4.4.3 Household dwelling quality

The type and quality of homes and neighbourhoods considerably affect the heat vulnerability (Jenerette *et al*., 2011; du Toit *et al*., 2018). People in poor infrastructure are more likely to die from heat than in traditional homes (Harlan *et al*., 2006; du Toit *et al*., 2018). Living in poor dwellings increase the risk of heat-related mortality through inadequate infrastructure, densely populated buildings with inadequate ventilation, and a lack of green space. Socioeconomic status is crucial since many disadvantaged communities lack the institutional capacity for education, health care, and employment. Due to their degraded ecosystems and high poverty levels, regions with poor housing may be more vulnerable to heat than those that reside in high-quality housing connected with high-income earners and have the infrastructure to manage extreme heat (Pasquini *et al.*, 2020). Figure 4.8(c) shows the residential quality of the area of investigation.

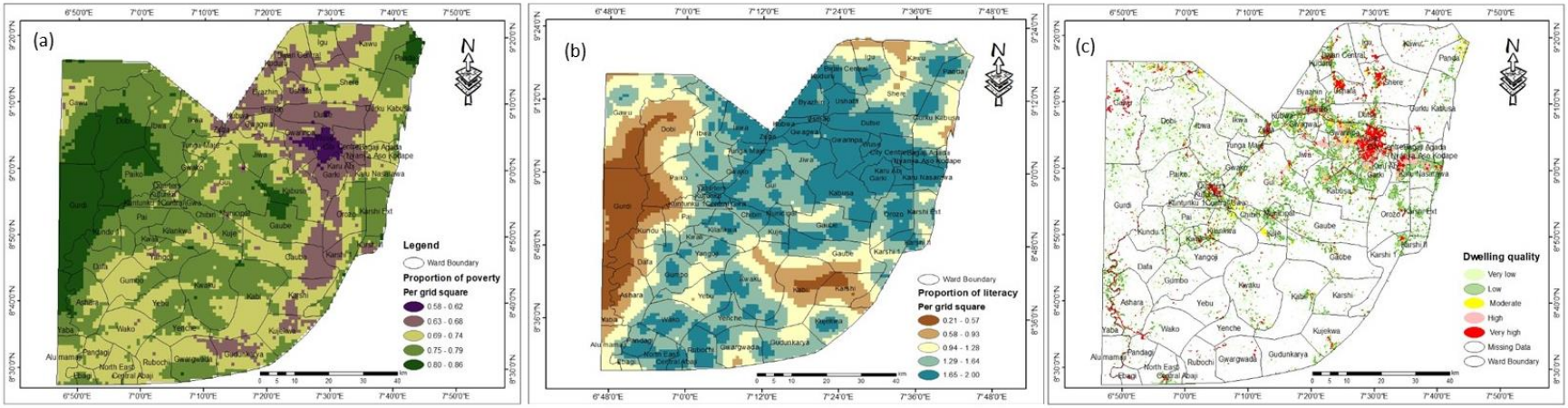


Figure 4.8: (a) 2020 poverty level of people living on less than $1.25 per day generated from the WorldPop dataset at a 923m resolution, (b) Literacy level of 2020 at a spatial resolution of 923m generated from the WorldPop dataset, (c) 2020 dwelling quality derived from Worldpop datasets at a spatial resolution of 92m.

4.4.5 Reclassification of the attributes of the heat vulnerability indicators

This section describes the heat vulnerability maps used in this study and explains why they were reclassified. Several earlier studies on heat vulnerability based their technique on principal component analysis (PCA), which is the most frequent yet most complex method for creating a heat vulnerability map, and with which the Reid *et al.* (2009) study was initially conducted (Wolf *et al*. 2014; Bai *et al.* 2016; Mallen *et al*. 2019; Song *et al*. 2020; Zhang *et al*. 2021). Even though PCA and overlay were employed by over 56 (71%) of the recognised papers included in the systematic literature review of this study, only Zhu *et al*. (2014) combined PCA and overlay in their work. Zhang *et al*. (2019) and Tran *et al.* (2020) integrated PCA, AHP, and weighted overlay. Loughnan *et al*. (2012) and Wolf *et al.* (2014) combined PCA, a regression model, and a weighted overlay. While PCA reduces the dimensionality and redundancy of datasets to improve their interpretability and reduce information loss (Jolliffe & Cadima, 2016), the PCA grouped heat vulnerability indicators to generate the heat vulnerability map, making it difficult to isolate the influence of individual heat vulnerability indicators (Jagarnath *et al*., 2020). This study's heat vulnerability mapping method is based on a methodology that emphasises the relative influence of the attributes for each heat vulnerability indicator based on literature and expert opinions. For this reason, the attributes of each map HVIs were reclassified based on their relative influence on heat-related mortality using previous studies. A scale of 1 to 5 was used, with '1' denoting very low influence and '5' representing very high influence. This was done for each of the 9 primary HVIs and the 3 secondary indicators.

4.4.5.1 Reclassification of LST map

Studies by Van der Hoeven & Wandl (2015), Anderson *et al.* (2018), and Tran *et al***.** (2020) have shown that places with a high surface temperature produce sensible heat that makes heat-health problems worse compared to places with a low LST. In their study on weighting the mechanics and spatial distribution of composite heat vulnerability metrics in Atlanta and Georgia, Karanja *et al.* (2022) classified the LST map into 5-equal interval classes to demonstrate the spatiotemporal variation of heat vulnerability in the cores of cities. Lissner

et al. (2012) and Depietri *et al*. (2013) classified LST into five groups based on how they affect human health: very low, low, moderate, high, and very high. For this study, the LST map of Abuja was reclassified into five classes of equal intervals, similar to Karanja *et al.* (2022).

Map areas with very low surface temperatures, 18.6 – 26.6^{o}C, were reclassified as (1) signifying very low influence on human health relative to other classes. They occupied 6.7% of the map area. Areas with temperatures between 26.64 - 34.6^{o}C were reclassified as (2), signifying low influence on human health. This land area comprises 17.71% of the map's area. In their investigation of the relationship between land-use/cover change and LST in Dongting Lake, China, Tan *et al*. (2020) found that the class with very low and low surface temperatures are found near forests, rice fields, and water bodies. These land use/cover play a critical regulatory role in reducing heat effects. Land areas with temperatures between 34.6 – 42.6^{o}C were reclassified as (3), signifying moderate influence on human health. They comprised 22.90 % of the study region. The map areas with temperatures between 42.6 – 50.6^{o}C and 50.6 – 58.6^{o}C were reclassified as (4) and (5), signifying high and very high influence on human health because of their relatively harmful effects on human health. They occupied an estimated 28.85% and 24.07 % of the map area. High temperatures have been linked to adverse health effects by Bi *et al*. (2011), Revich *et al*. (2015), and Cohen & Dechezleprêtre (2022). Extreme heat can precipitate acute disorders, such as heat stroke and dehydration, and worsen various underlying diseases. As a result, in the absence of adaptation, mortality is expected to rise in areas with extreme temperatures, particularly among vulnerable groups such as the elderly, children, and people performing manual labour in extreme heat. Table 4.5 presents the reclassified LST map of this study.

4.4.5.2 Reclassification of artificial impervious surfaces

This study's AIS surface map was reclassified based on the estimates of their thermal variabilities and contributions to heat islands. According to Farina (2012), Bokaie *et al*. (2016), and Jain *et al*. (2020), extreme heat is associated with AIS and bare lands, such as artificial features related to industrial, commercial, residential, and transportation networks. Heat absorption is a

common occurrence on AIS. A bare surface is a good conductor of heat. Because of evaporative cooling, areas with water bodies and vegetation surfaces have relatively low temperatures. Following the confirmations from Jain *et al*. (2020) and Kamali Maskooni *et al*. (2021), the AIS were reclassified into five classes based on how much of a contribution they made to the formation of heat islands. Areas of water bodies like rivers, lakes, streams, and ponds were reclassified as (1), accounting for 0.20% of the study area. Forest, shrubs, and grassland have been reclassified as (2) because they have little influence on heat islands. These areas accounted for 17.71% of the map's area. Cropland has a moderate impact on temperature (3), accounting for 26.59% of the study area. The bare surface was reclassified as (4), whereas AIS were reclassified as (5) due to their high thermal characteristics, which highly influence the LST. They occupied an estimated 30.73% and 24.77% of the map area, respectively, as shown in Table 4.5.

4.4.5.3 Reclassification of NDVI

The NDVI maps typically range from –1 to +1, with higher values indicating more vigorous and healthy vegetation and lower to negative values indicating unhealthiest and lack of vegetation cover. The NDVI for this study was reclassified using the thresholds established by Gross (2005), Gandhi *et al*. (2015), Bokaie *et al*. (2016) and Sun *et al*. (2022), who stated that negative NDVI values are associated with clouds, snow covers, and water bodies, while very low NDVI values of less than 0.1 are associated with AIS and bare land. Grass and shrubland have moderate NDVI values between 0.2 and 0.3. Forestland is characterised by a high NDVI value >0.6. In this regard, the NDVI map for this study was reclassified into five classes, with (1) representing areas with negative NDVI values, such as water bodies; they have very little influence on heat islands. These areas accounted for 8% of the map's area. Areas with very high NDVI values have little influence on heat islands and are reclassified as (2), representing shrubland and forestland, respectively. They took up 21% of the map. High-NDVI-valued areas are reclassified as 3. These are grassland and farmland areas, accounting for 31% of the map area. Areas with low and very low NDVI values, such as bareland and AIS, are reclassified as (4) and (5) due

to their strong influence on heat islands. They occupy 35% and 5% of the map area, respectively. Table 4.5 shows the reclassified NDVI map from this study.

4.4.5.4 Reclassification of vulnerable population

In their study on mapping the heat vulnerability index based on different urbanisation levels in Nebraska, USA, Jalalzadeh Fard *et al*. (2021) classified vulnerable populations into five ordinal classes based on the number of vulnerable people per unit area. The vulnerable population was then reclassified according to their level of vulnerability (a value from 1 and 5), with (1) representing the least vulnerable and (5) the most vulnerable. In their study examining health vulnerability to climate change, Manangan *et al.* (2015) classified vulnerable populations into four classes based on percentile, with a score of 1 indicating less than the 25^{th} percentile and a score (4) indicating more than the 75^{th} percentile. This way, regions with many vulnerable people are more likely to have more heat-related illnesses and deaths than regions with fewer vulnerable people. Similar to Jalalzadeh Fard *et al*. (2021), the vulnerable population for this study was reclassified into five classes based on their relative influence on heat vulnerability. Consequently, locations with the lowest count of younger and older populations (0.09–32.41 population count per grid cell) are reclassified as (1), indicating a very low influence on heat vulnerability. These regions comprised 4.94% of the map area. Locations with a vulnerable population of 32.42-64.72 per grid cell are reclassified as (2), suggesting a relatively low influence on heat vulnerability. They occupy 5.50% of the map's area. Areas with a vulnerable population between 64.73 - 97.03 persons per grid cell are reclassified as (3), suggesting a moderate influence on heat vulnerability. They occupied 13.64 % of the map's area. Areas with a vulnerable population (97.04–129.35 per grid cell) have been reclassified as (4), indicating a high influence on heat vulnerability. They covered 26.54% of the map. The reclassification of map areas with a vulnerable population count between 129.36 and 161.66 per grid cell to category (5) indicates a comparably very high influence on heat vulnerability. They occupied 49.36% of the map's area. Table 4.5 show the reclassified population at risk for this study.

4.4.5.5 Reclassification of women population

Chanana-Nag *et al*. (2020) used Jenk's natural break categorisation in ArcGIS to classify women participants into five groups (very low, low, medium, high, and very high) to identify the districts where women farmers are mostly affected by climate risk. The overlay approach gave the "high" and "very high" classes for the parameter priority. These areas were deemed hotspots because they had "high" or "extremely high" levels of women engagement and climatic threats. Although the people in the other categories (very low to moderate) are also exposed to climatic risks, they are much less intense and affect a far smaller percentage of women who work in agriculture than they do in hotspots. Like Chanana-Nag *et al*. (2020), this study reclassified the women population of childbearing age into five classes based on the Jenks natural break classification. Jenk's "natural breaks" classifying technique generates categories centred on the data's natural groups. In this regard, the map areas with a very low and low women population count per grid (0.06-19.60 and 19.61-39.15) were reclassified as (1) and (2), indicating very low and low influence to heat vulnerability. These populations occupied 2.69 and 2.10 % of the map's area. This is consistent with Snyder *et al*. (2006) and Driskell & Embry (2007), who revealed that the low concentrations of women populations among women-headed residents of racial and ethnic minorities might contribute to a low poverty rate. A sizeable section of the population can afford to adapt to the heat threat and its associated morbidity and death due to the low prevalence of poverty. Women population counts per grid of 39.16 - 58.70 have been reclassified as a moderate influence (3). These regions were deemed to have a moderate influence on heat vulnerability due to their comparatively moderate concentration of the women population. They occupied 21.86% of the map area. Areas with 58.71–78.25 and 78.26–97.80 counts per grid cell of the women population were reclassified as (4) and (5) because of their high and very high concentrations of women population count per grid. They occupied 30.64 and 42.71% of the map area. Reckien (2018) found that high-density neighbourhoods of African-American communities and households headed by women are especially prone to heat-related morbidity and mortality. Binita *et al*. (2015) found that the absence of

job options may cause poverty among local women. Table 4.5 presents the reclassified women population of childbearing age for this study.

4.4.5.6 Reclassified poverty level as define by $1.25 per day threshold

In their study on poverty and inequality in Vietnam, Minot *et al.* (2006) classified poverty into five classes based on an equal interval to develop a spatially targeted intervention plan. Jalalabad Fard *et al.* (2021) classified poverty scores into five ordinal groups in their study on mapping the heat vulnerability index based on different urbanisation levels in Nebraska, USA. To determine acceptable break values for classifications, Fard *et al.* (2021) classify poverty level using computed absolute deviation around class medians (ADCM) for five of the most common classification techniques used to generate choropleth maps. Tatem *et al*. (2014), Steele *et al.* (2017), and März (2018) in their studies also classified poverty and inequality into five classes based on their influence on heat vulnerability. This study reclassifies the poverty map into five equal classes, similar to Minot *et al*. (2006) and Jalalabad Fard *et al*. (2021), based on their relative influence on heat vulnerability.

In this regard, map areas with a very low and low proportion of people living below the poverty line (0.58-0.62 and 0.63-0.68 persons per grid square) were reclassified as (1) and (2) due to their relatively very low and low influence on heat vulnerability. This implies that the map areas with very low proportions of people living below the poverty line have a high proportion of the wealthy population. Wealthy households have enough resources to access the air conditioning and good medical facilities and thus have a greater adaptive capacity to heat vulnerability (Du Toit *et al.,* 2018; Pasquini *et al*., 2020). Areas with a very low proportion of people living below the poverty line occupied 1.29% and 9.7% of the study area. Areas with 0.69 - 74 proportions of people living in poverty per grid square are reclassified as (3) because of their moderate influence on heat vulnerability. They occupied 31.97% of the map area.

Due to their high and very high impact on heat vulnerability, areas with (0.75 – 0.79) and (0.80 – 0.86) proportions of people per grid square living in

poverty were reclassified as (4) and (5). They took up 46.22 and 10.77 % of the study area. This implies that most households in these grids are poor. Poverty and low income influence the population by making them more vulnerable to heat threats (Harlan *et al*., 2007; Johnson *et al.,* 2020). People below the poverty line are more vulnerable to heat-related illness and mortality because they have a lower adaptation capacity (Cutter *et al.,* 2003). People below the poverty line lead miserable life with poor nutrition, poor housing conditions, and obstructive socioeconomic situations that lead to heat exposure (Uddin *et al.,* 2019). The reclassified poverty level for this study is shown in Table 4.5.

4.4.5.7 Reclassification of literacy level

In their study on the heat vulnerability index to improve urban public health management in San Juan, Puerto Rico, Méndez-Lázaro *et al.* (2018) classified literacy level into five categories based on its influence on heat vulnerability: very high, high, moderate, low, and very low. The literacy level in this study was reclassified using the literary population classifications suggested by Bosco *et al*. (2017) and Méndez-Lázaro *et al*. (2018). Map areas with a very low (2.0–1.65) and low (1.64–1.29) proportion of illiterate households per grid square were reclassified as (1) and (2), indicating a very low and low influence on heat vulnerability. These populations have many people who can read and interpret a wide range of literature on heat-related warnings and precautions. They take up 30 and 31.56% of the map's area, respectively, and are made up of grids with educated families with timely access to information on heat risks and adaptation alternatives. Educational status influences population awareness, and those with a high school diploma have a lower fatality rate from heat-related dangers (Reid *et al.* 2009; Portier *et al*. 2013; Basu & Malig 2011). Because of their relatively moderate literacy rate, areas with 1.28–0.94 people per grid square are reclassified as (3), indicating a moderate influence on heat vulnerability. They took up 19.33% of the study area. Areas with a high (0.21–0.57) and very high (0.58–0.93) proportion of illiterate population per grid square were reclassified as (4) and (5) due to their high and very high influence on heat vulnerability. These classes have high proportions of illiterate people who cannot read and comprehend a variety of heat-related warnings and precautions. Many people in these groups lack the knowledge necessary to

obtain temperature information on hot days or nights, which could be hazardous to their health. They occupied 10.81 % and 7.61% of the map area, respectively. The reclassified literacy level for this investigation is presented in Table 4.5.

4.4.5.8 Reclassification of household housing quality

Tusting *et al*. (2019) classify the quality of rural and urban dwellings based on construction materials and dwelling quality. In this study, the dwelling map was reclassified, with areas of very high and high-quality infrastructures classified as (1) and (2) due to their low impact on heat vulnerability. These regions comprised 79.91% and 10.25% of the study area and are dominated by wealthy households. Because of their moderate influence on heat vulnerability, map areas with moderate-quality housing are reclassified as (3); they occupy 0.45% of the map area. Areas with very low and low-quality housing consist of compacted and naturally small terraced buildings with few or no layout plans. Lower-income households in the study area typically occupy these homes. Very low and low-quality dwellings occupied 9.08% and 0.31% of the map area, respectively. They were reclassified as (4) and (5) due to their high and very high influence on heat vulnerability. Rinner *et al.* (2010) and Wang *et al.* (2021) found that high heat exposure locations were concentrated in less-urbanised regions with low-quality buildings and low socioeconomic status. Most households are poor and live in a clustered environment with little or no access to facilities that would increase their adaptation to excess heat. The reclassified dwelling quality for this study is shown in Table 4.5.

4.4.5.9 Reclassification of population density

A dense population has been linked to higher temperatures (Count *et al*., 2007), and it is expected that dense populations are common in inner-city areas also affected by UHI. Several studies on heat hazards have found that higher population density increases human risk (Béguin *et al*., 2011; Harlan *et al.*, 2006; Tomlinson *et al.*, 2011). As a result, people living in densely populated areas are more vulnerable to heat compared to people living in areas of low population density. In their study towards sectoral and standardised

vulnerability assessments, Lissner *et al*. (2012) classify the population density into five classes based on its vulnerability threshold (a number between 1 and 5). Class (1) is the least vulnerable, while class (5) is the most vulnerable. This study's population density map was reclassified into five categories. The map areas with very low population density (1.47–24.31 persons per grid) were reclassified as (1). This is because areas of low population density have been linked to relatively low temperatures (Count *et al*., 2007) and thus have a lower influence on heat-related morbidity and mortality. These areas cover 1.16% of the study area. Areas of low population density (24.32–54.17 persons per grid area) have been reclassified as (2). These regions have a relatively low influence on heat vulnerability; they account for 9.57 % of the map's total area. Because of their relatively moderate influence on heat vulnerability, areas with moderate population density per grid 54.18–89.311) are reclassified as (3). These areas accounted for 20.48% of the map's total area. Harlan *et al*. (2006), Tomlinson *et al*. (2011) Wheeler *et al*. (2015) established that increasing population density increases human risk of heat-related health risks. This study reclassifies densely populated areas as the most vulnerable to heat-related morbidity and mortality. Areas with a population count of 89.32 to 149.03 people per grid cell were classed as (4), which indicates high influence. They took up 33.74% of the map. Areas having a population count of 149.04–449.43 people per grid cell were classed as (5), indicating a very high influence on heat vulnerability. They took up 35.03% of the map. Table 4.6 shows the reclassified population density of this research.

Table 4.6: Reclassification of the 9 heat vulnerability indicators used in this study.

LST	**Influence**	**LST (°C)**	**Reclassified value**	**% of the map area**
	Very Low	18.63-26.63	1	6.79
	Low	26.64-34.63	2	17.38
	Moderate	34.64-42.63	3	22.90
	High	42.64-50.63	4	28.85
	Very High	50.64-58.63	5	24.07
Artificial Impervious surface	Influence	Land use/cover categories	Reclassified value	% of the map area
	Very Low	Waterbodies	1	0.20
	Low	Vegetal cover	2	17.71
	Moderate	Cropland	3	26.59
	High	Bareland	4	30.73

	Very High	Impervious surface	5	24.77
NDVI	Influence	Index values	Reclassified values	% of the map area
	Very Low	-0.13 – - 0.01	1	8.08
	Low	0.38–0.51	2	20.74
	Moderate	0.25 – 0.37	3	30.53
	High	0.13 – 0.24	4	35.42
	Very High	-0.01– 0.12	5	5.24
Vulnerable population	Influence	Population count per grid	Reclassified value	% of the map area
	Very Low	0.09 - 32.41	1	4.94
	Low	32.42 - 64.72	2	5.50
	Moderate	64.73 - 97.03	3	13.64
	High	97.04 - 129.35	4	26.55
	Very High	129.36 - 161.66	5	49.37
Women population	Influence	Population count per grid	Reclassified value	% of the map area
	Very Low	0.066 - 19.60	1	2.69
	Low	19.61 - 39.15	2	2.10
	Moderate	39.16 - 58.70	3	21.86
	High	58.71 - 78.25	4	30.64
	Very High	78.25 - 97.80	5	42.71
Income level	Influence	Proportion per grid	Reclassified value	% of the map area
	Very Low	0.13 - 0.24	1	1.29
	Low	0.25 - 0.35	2	9.73
	moderate	0.36 - 0.47	3	31.97
	High	0.47 - 0.58	4	46.22
	Very High	0.58 - 0.69	5	10.77
Literate level	Influence	Gridded population count	Reclassified value	% of the map area
	Very Low	1.609 - 2	1	30.64
	Low	1.37 - 1.60	2	31.56
	Moderate	1.07 - 1.37	3	19.33
	High	0.70 - 1.07	4	10.81
	Very High	0.21- 0.70	5	7.66
Dwelling quality	Influence	area per grid	Reclassified value	% of the map area
	Very Low	very high-quality	1	79.91
	Low	High quality	2	10.25
	Moderate	Moderate quality	3	0.45
	High	Low quality	4	9.08
	Very High	Very low-quality	5	0.31
Population density	Influence	Population count per grid	Reclassified value	% of the map area
	Very Low	1.47 - 24.31	**1**	1.16
	Low	24.32 - 54.17	2	9.57
	Moderate	54.18 - 89.31	3	20.48
	High	89.32 - 149.03	4	33.74
	Very High	149.04 - 449.43	5	35.03

4.4.6 Creation of heat exposure, sensitivity, and adaptive capacity index

The 9 primary HVIs were used to calculate the three secondary HVIs for this study, using an equal weight overlay with the assumption that each indicator has an equal influence on heat vulnerability. In this regard, the heat exposure index was constructed by equally weighting the three primary indicators that make it up: the LST, AIS, and NDVI. The three primary indicators that comprise the heat sensitivity index—population density, vulnerable population, and women population—were combined, assuming they would each have an equal influence. The three primary indicators that comprise the adaptive capacity index—poverty level, literacy level, and housing quality—were also used in constructing the adaptive capacity index by overlaying the three indicators at equal weight. The conceptual processes for building the three secondary indicators are shown in Figure 4.9.

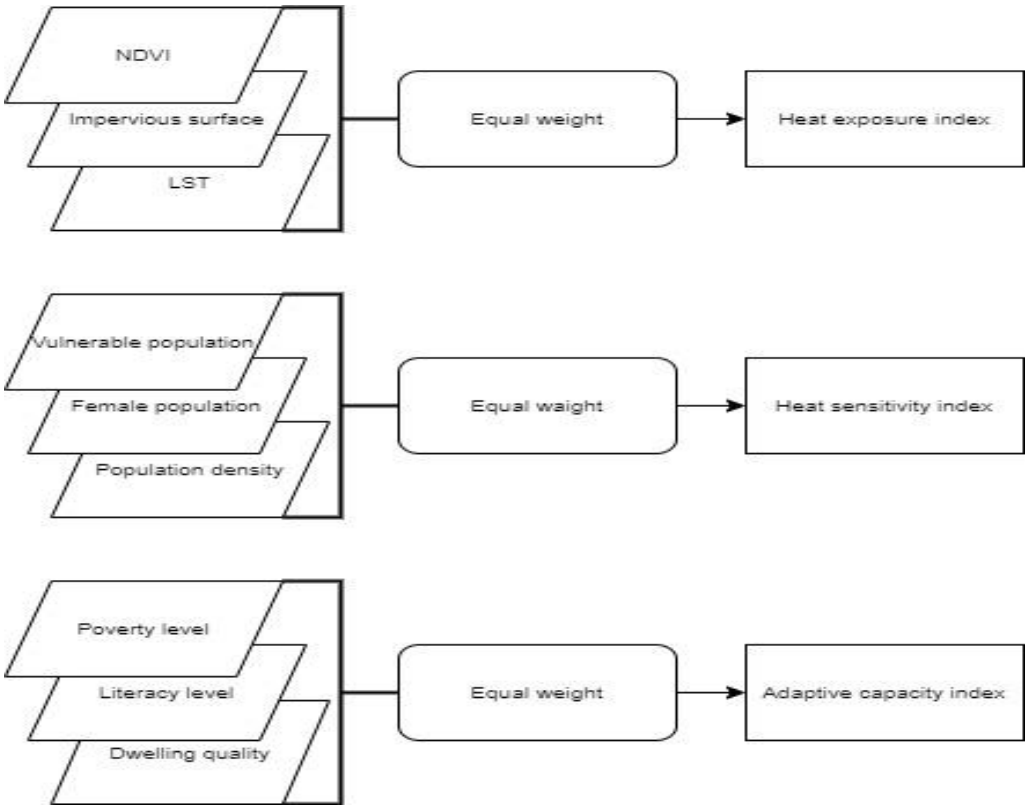


Figure 4.9: Conceptual procedures for the constructions of the 3 secondary heat vulnerability indicators.

4.4.7 Incorporating expert judgments into the heat vulnerability mapping

A survey was created in Google Drive that asked experts how they would rank the relative influence of the 9 primary HVIs and the 3 secondary HVIs. Fifteen experts in biometeorology, public health, environmental science, and social science from the Students and New Professionals of the International Society for Biometeorology, the Ministry of Health Abuja, the Nigerian Meteorological Agency Abuja, the Ministry of Environment, and the Nasarawa State University, Keffi, Nigeria, were invited to participate in the study. A judgment matrix was obtained for each measurement using a 1-9 scale, where 0 indicates no influence, 1-2 indicates very low influence, 3-4 indicates low influence, 5-6 indicates moderate influence, 7-8 indicates strong influence, and 9 and above indicates very strong influence. Ten experts participated in the survey. Of the participants, n = 2 (20%) were from the field of public health, n = 3 (30%) were from the field of environmental sciences, n = 5 (50%) were from the field of biometeorology, and n = 0 (0%) were from the field of social sciences. The specialisations of the experts who participated in the survey are shown in Figure 4.10.

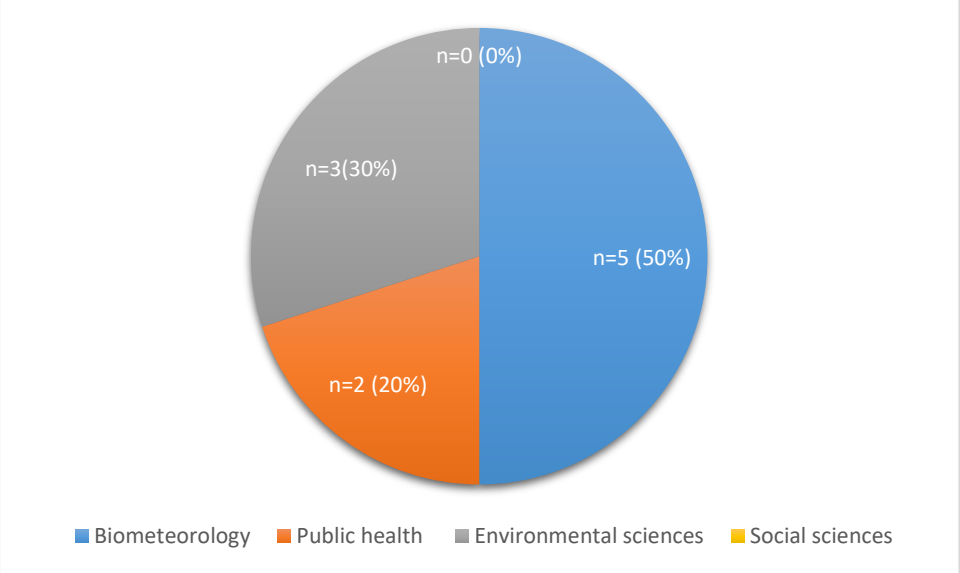


Figure 4.10: Respondent's areas of interest

4.4.8 Expert's judgements on the 9 primary HVIs used in this study

Based on the results of the heat vulnerability survey, which asked experts to rank the relative importance of the 9 primary indicators of heat vulnerability, n = 7 (13%) of the experts believe that LST has the greatest influence on heat

vulnerability relative to the other primary indicators used in this study. n = 6 (11%) of the experts believe that the AIS is the most influential indicator of heat vulnerability. In contrast, n = 7 (13%) of the experts believe that the NDVI has the greatest influence on heat vulnerability relative to the other indicators included in this study. n = 6 (11%) experts ranked the vulnerable population as the most influential indicator of heat vulnerability, while n = 2 (4%) respondents believe that the women population is the most influential indicator of heat vulnerability. n = 5 (9%) of the experts consider population density the most influential indicator of heat vulnerability. Compared to the other primary indicators used in this study, n=7 (13%) experts believe that poverty influences heat vulnerability. According to n = 5 (9%) of experts, literacy is the most influential indicator of heat vulnerability. n = 8 (15%) experts who responded to the survey believe that dwelling quality is the essential indicator influencing heat vulnerability. Expert judgments on the relative importance of the 9 primary HVIs included in this investigation are presented in Figure 4.11.

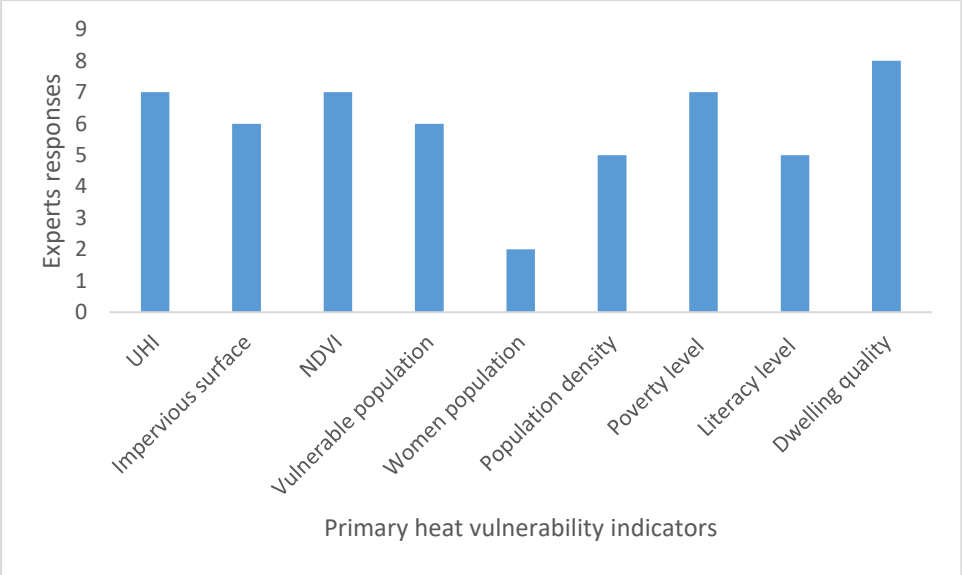


Figure 4.11: Experts' opinions on the relative importance of the 9 HVIs.

4.4.9 Experts Judgement on the 3 secondary HVIs

Using the findings of the heat vulnerability survey, which asked experts to rank the relative importance of heat exposure, sensitivity, and adaptive capacity index, n = 7 (41%) of the experts indicated that the exposure index was the most crucial factor affecting heat vulnerability. The sensitivity index was chosen as

the leading indicator influencing heat vulnerability by n = 6 (35% of the experts). n = 4 (24%) of the experts who answered the survey believe that the adaptive capacity index is the essential indicator influencing heat vulnerability. Figure 4.12 presents experts' judgement on the relative importance of the 3 secondary HVIs used in this study.

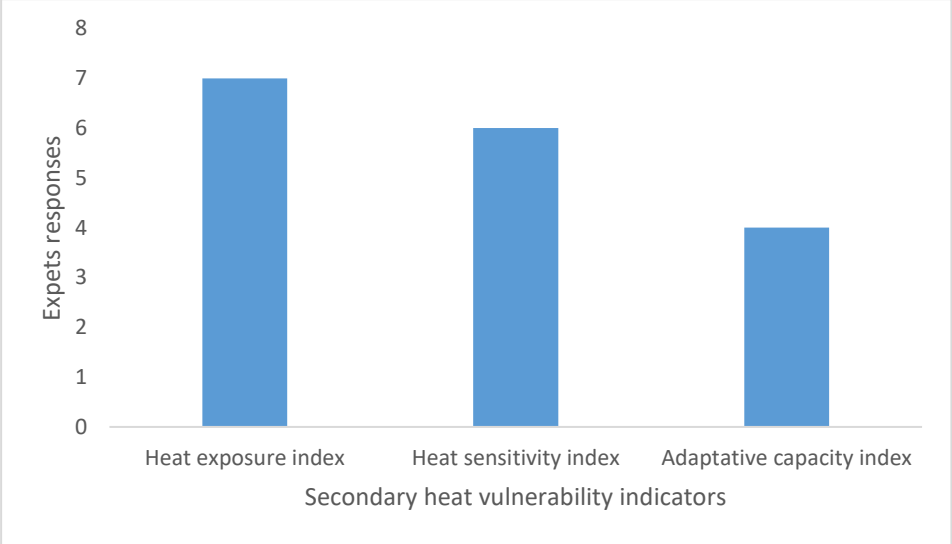


Figure 4.12: Expert's judgement on heat exposure, sensitivity, and adaptive capacity index.

4.4.10 Construction of heat vulnerability maps

The heat vulnerability map for this study was created using a weighted overlay tool in ArcGIS and expert judgments. The weighted overlay model performs a multiple-criterion analysis on a set of the raster. Two heat vulnerability maps for Abuja were constructed. First, a heat vulnerability map was created by overlaying the 3 secondary HVIs, using influences from the expert's judgements as input. Second, the study's 9 primary HVIs were used to construct a heat vulnerability map. In this regard, the heat vulnerability map's weighted input criteria were the expert's rating of the relative influence of the 9 reclassified primary HVIs. To be able to integrate all of the data, the weighted overlay function was used with an evaluation scale of "1 to 5 by 1." Influence weights were assigned to all 9 layers (LST: 13%, AIS: 13%, NDVI: 13%, vulnerable population: 11%, women population: 4%, population density: 9%, poverty level: 13%, literacy level: 9%, and dwelling quality: 15% each, equalling 100% as a total) for this specific case (values). The heat vulnerability maps used the same

five classes as Méndez-Lázaro *et al.* (2018): very low, low, moderate, high, and very high.

4.4.11 Validation of heat vulnerability maps

Morbidity and mortality statistics were adequate data for validating heat vulnerability maps (Reid *et al.*, 2012). The validation for this study was done using heat-related mortality data and heat vulnerability maps. In this regard, the independent variable was the excess mortality count generated from health data acquired from the six hospitals in the study area. In contrast, the dependent variable was the heat vulnerability index calculated from the maps. A linear regression model compared the excess mortality count to the heat vulnerability index. A sensitivity analysis was also performed. A comparison was made between the heat vulnerability map generated from the WorldPop datasets and those derived from the DHS datasets.

4.5 Research objective 5: Heat vulnerability projections for the middle and end of the 21st century under low and high forcing scenarios

4.5.1 Temperature data from CMIP6 Global Climate Models

The CMIP6 climate projections utilised in this study were obtained from the WorldClim archive. The data have been downscaled and biad-adjusted in the WorldClim v2.1 dataset. The CMIP6 models (mentioned in Table 4.7) were used to investigate projected yearly, monthly, seasonal, and spatial temperature changes. Five models were selected at random. The maximum temperature data for the baseline period (2001–2020), the near term (2041–2060), and the future long-term projections (2081–2100) were analysed at 20-year intervals. The monthly maximum temperature measurements at 30-second spatial resolutions were averaged over two 20-year periods (2041-2060 and 2081-2100) and compared to the bassline (2001-2020) to assess temperature change.

As seasonal variance in tropical Africa is essential, temperature projections for four seasons were examined: Harmattan (DJF), summer (MAM), rainy (JJA),

and winter (SON). The digital elevation model and mean temperature anomalies were used to understand better the rise in temperature with altitude. The ensemble of 5 CMIP6 models for the present and projected climates was evaluated for temperature variations under two future SSP scenarios: a low forcing scenario SSP1-2.6 and a strong forcing scenario SSP5-8.5. Five narratives describing alternative socioeconomic advancements are the foundation for every SSP (Gidden *et al.*, 2019). This included sustainable development (SSP1), moderate advancement (SSP2), territorial dispute (SSP3), unequal distribution (SSP4), and improvement based on fossil fuels (SSP5) (SSP5). Comprehensive explanations of SSPs are accessible in chapter seven. Table 4.7 presents a list of CMIP6 climate projections with spatial resolutions of 30 seconds used in this study.

Table 4.7: WorldClim-downscaled list of CMIP6 GCM future climate projections with spatial resolutions of 30 seconds used in this study.

Model	Country	Modeling Institution	Horizontal Resolution (Lon. x lat.)
HadGEM3-GC31-LL	UK	Met Office Hadley Centre	1.25° × 1.87°
MPI-ESM1-2-HR	Germany	Max Planck Institute for Meteorology	0.94° × 0.94°
MIROC6	Japan	Studies and Japan Agency for Marine-Earth Science and Technology	1.4° × 1.4°
ACCESS-CSM2	Australia	Australian Community Climate and Earth System Simulator Coupled Model	1.1° × 1.1°
GISS-E2-1-G	USA	NASA Goddard Institute for Space Studies	2.5° × 2.5°

4.6 Conclusion

This chapter describes the nature, source, and technique of this research's data analysis. The chapter includes a summary of the data types, sources, and graphical representations used in the research technique. The first chapter of the study results is presented in the next chapter. The chapter examines the spatiotemporal growth of AIS due to urbanisation.

Table 4.8: Summary of the data types and sources utilised in this investigation.

S/N	Type of data	Description	Period	Spatial resolution	Source of data
1.	Global Artificial Impervious Area maps	Change detection of artificial impervious surface	1985, 1990, 1995	30m	Gong *et al*. (2020) annual maps of global artificial impervious area: http://data.ess.tsinghua.edu.cn/.
2.	Landsat TM, ETM+ and OLI	Change detection of artificial impervious surface	1999, 2004, 2009, 2014 and 2019.	30m	USGS website: http://pubs.usgs.gov/fs/2010/3026/ http://landsat.gsfc.nasa.gov/
3.	Thermal, red and infrared bands of Landsat TM, ETM+ and OLI	- LST mapping - Normalised difference vegetation index mapping - Normalised difference built-up index mapping	1985-2020	120m, 60m, and 100m 30m 30m	USGS website: http://pubs.usgs.gov/fs/2010/3026/ http://landsat.gsfc.nasa.gov/
4.	Meteorological data	Maximum Temperature	1990-2019	Monthly	Nigerian Meteorological Agency, Abuja, Nigeria.
5.	Mortality data	Respiratory, cerebrovascular, diabetes, pre-existing psychiatric disorders, myocardial infarction, ischemic heart disease, and congestive heart failure	2000-2019	Monthly	- University Teaching Hospital, Gwagwalada, Abuja - National Hospital Abuja, Nigeria - Specialist Hospital Karu, Nasarawa State - General Hospital Kwali, Abuja - General hospital Kuje - General hospital Abaji
6.	Population and socioeconomic data	- Poverty level - Literacy rate - Population <15 and older > 65 years - Women population - Population density - Dwelling quality	2019/2020	923.47m/ward 923.47m/ward 92.35m/ward 923.47m/ward 92.35m/ward 92.35m /ward	- National Population Commission Abuja Nigeria - National Bureau of Statistics, Abuja, Nigeria - WorldPop datasets
7.	Maximum temperature projections	SSP1-2.6: Low forcing scenario and SSP5-8.5: strong forcing scenario	2001-2020 2041-2060 2081-2100	HadGEM3: 1.25° × 1.87° MPI: 0.94° × 0.94° MIROC6: 1.4° × 1.4° ACCESS: 1.1° × 1.1° GISS: 2.5° × 2.5°	- WorldClim datasets - Environmental and climate change Canada datasets

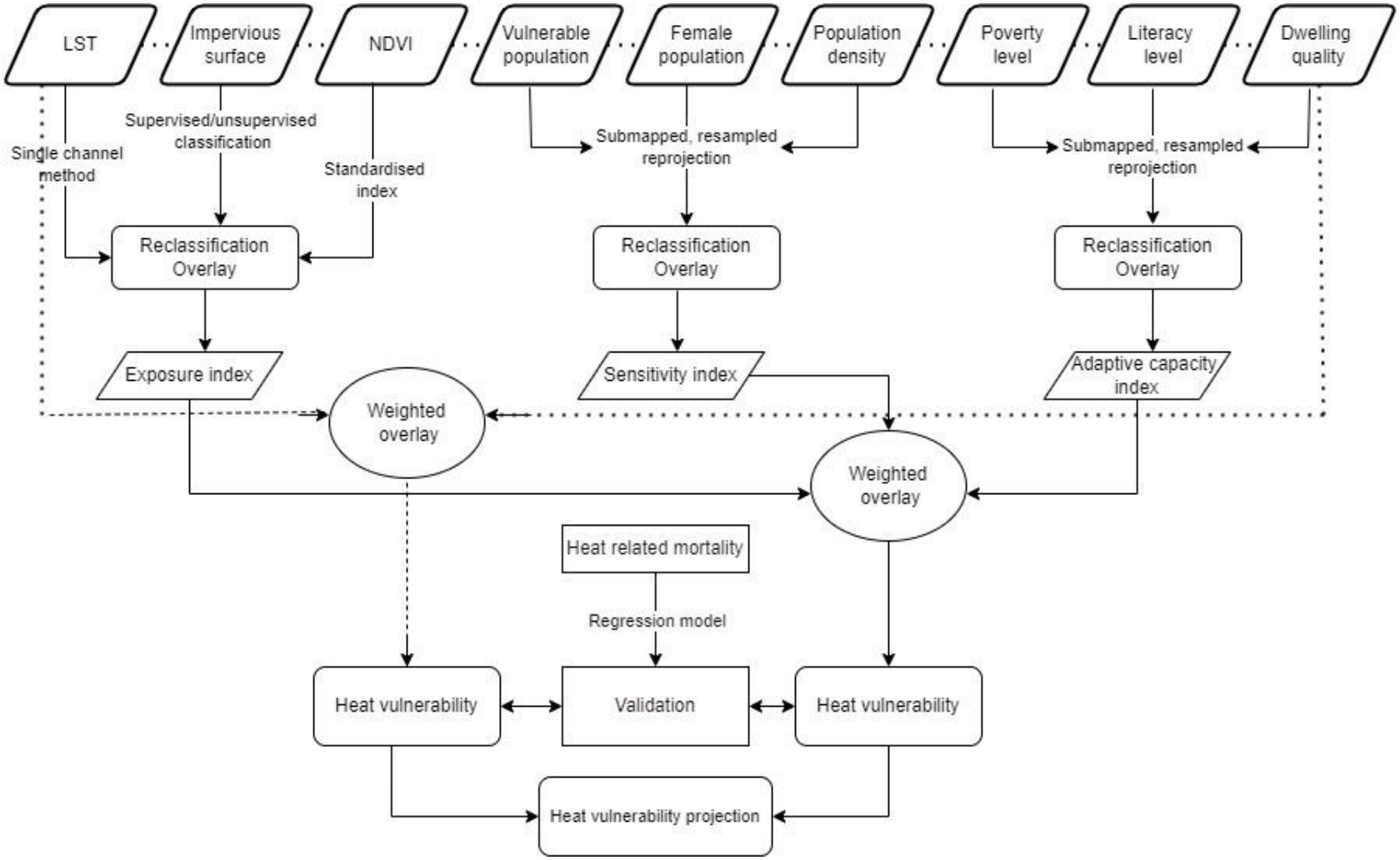


Figure 4.13: Schematic representation of the research methodology from the 2 methods used for mapping heat vulnerability

CHAPTER FIVE: MAPPING SPATIO-TEMPORAL CHANGE OF ARTIFICIAL IMPERVIOUS SURFACE

5.0 Introduction

The urban transformation affects both land use/cover and urban climate. Rapid urbanisation has resulted in substantial changes in land cover/cover. Environmental changes caused by urbanisation often result in warmer weather in urban areas than in the surrounding, non-urbanised areas. This chapter examines the link between urban growth and thermal features by mapping AIS and evaluating their impacts on the thermal environment of Abuja and its environs from 1985 to 2019. Landsat images were used to calculate spatial variations of AIS and LST and their temporal influence associated with growing AIS.

5.1 Spatio-temporal mapping of artificial impervious surface

AISs, such as buildings and roads, are a major feature of urban areas and alter local hydrology. For example, artificial surfaces act to reduce water infiltration. Incoming solar radiation is absorbed by built materials and stored as heat, contributing to UHI. When the urban environment is warmer than the surrounding rural areas, the UHI effect occurs (Oke, 1987; Bounoua *et al*., 2018; Gong *et al.*, 2019). The pattern of distribution and density of AIS considerably influence the creation of UHI (Ma & Peng, 2022; Mallen *et al*., 2020; Wang *et al*., 2019). Timely, dependable, and consistent information on AIS is critical for planning and mitigating UHI effects. The classification of land use/cover over Abuja and its environs at various dates was required to detect changes in AIS since the FCT's move from Lagos in 1990. In the study region, 7 land use/cover categories have been identified-bare land, shrubland, water bodies, forest land, AIS, grassland, and cropland. The study area's land use/cover varied among classes and years. Table 5.1 and Figures 5.1(a-h) show the spatiotemporal area of land use/cover in 1985, 1990, 1995, 1999, 2004, 2009, 2014, and 2019.

Table 5.1: Estimates of land use/cover area from 1985 to 2019 using data from Landsat sensors and Gong *et al.* (2020).

Land use/cover Categories	1985 (Gong *et al.*,2020)		1990 (Gong *et al.*,2020)		1995 (Gong *et al.*,2020)		1999 (Landsat TM)		2004 (Landsat ETM+)		2009 (Landsat ETM+)		2014 (Landsat OLI)		2019 (Landsat OLI)	
	(km^2)	(%)	(km^2)	(%)	(km^2)	(%)	(km^2)	(%)	(km^2)	(%)	(km^2)	(%)	(km^2)	(%)	(km^2)	(%)
Bareland	2532.03	31.80	1284.90	16.14	771.06	9.68	463.61	5.83	591.21	7.43	413.68	5.20	164.58	2.07	553.24	6.95
Shrubland	996.04	12.51	560.64	7.04	791.12	9.93	1100.50	13.83	113.73	1.43	694.84	8.73	884.71	11.12	543.46	6.83
Waterbody	61.80	0.78	36.72	0.46	19.58	0.25	5.51	0.07	5.09	0.06	8.15	0.10	9.96	0.13	2.80	0.04
Forest Land	2060.30	25.87	1398.57	17.56	1190.47	14.95	556.69	7.00	251.16	3.16	242.73	3.05	115.49	1.45	216.80	2.72
Impervious Surface	21.00	0.26	71.97	0.90	113.48	1.43	153.76	1.93	145.51	1.83	165.00	2.07	353.00	4.44	671.30	8.44
Grassland	2286.22	28.71	2060.28	25.87	2183.25	27.42	2486.45	31.25	2639.46	33.17	2734.00	34.36	2154.09	27.07	2492.68	31.32
Cropland	5.72	0.07	2550.04	32.02	2894.16	36.34	3190.03	40.09	4210.34	52.92	3699.32	46.49	4275.39	53.73	3477.50	43.70
Total	7963.12	100.00	7963.12	100.00	7963.12	100	7956.55	100.00	7956.50	100.00	7957.73	100.00	7957.22	100.00	7957.78	100.00

Table 5.2: Land use/cover classification producer's, user's, and overall classification accuracy.

Year	1999		2004		2009		2014		2019	
Class name	Producer's accuracy	User's accuracy	Producer's accuracy	User's accuracy	Producer's accuracy	User's accuracy	Producer's accuracy	User's accuracy	Producer's accuracy	User's accuracy
Bareland	84.75%	70.42%	78.87%	78.87%	87.69%	80.28%	86.89%	75.71%	80.00%	78.87%
Shrubland	85.07%	80.28%	81.67%	70.00%	84.85%	78.87%	83.58%	78.87%	85.07%	80.28%
Water bodies	100.00%	84.29%	100.00%	100.00%	100.00%	100.00%	100.00%	92.86%	100.00%	95.71%
Forestland	78.79%	73.24%	83.82%	81.43%	89.55%	85.71%	81.33%	87.14%	92.65%	90.00%
Impervious surface	84.93%	88.57%	87.10%	77.14%	83.56%	87.14%	81.08%	84.51%	84.85%	78.87%
Grassland	64.21%	83.56%	74.67%	75.68%	73.08%	78.08%	76.25%	83.56%	68.29%	76.71%
Cropland	77.78%	85.14%	68.09%	85.33%	75.64%	78.67%	67.95%	70.67%	70.00%	75.68%
Overall classification accuracy	80.80%		81.27%		84.00%		81.80%		82.20%	

Land use/cover mapping is one of the most commonly used analyses for detecting urban expansion. The AIS created in Abuja, and its environs reflect the city's urban growth since its relocation in 1990. Before the 1990s, in 1985, dwellings were primarily concentrated around the city centre (Wuse district) and a smattering of farming communities throughout the region. They eventually led to urban-dwelling, especially after 2000, to the present urbanised areas. Figure 5.1(a) indicates that the city core (Wuse district) with pockets of development and farming settlements in Bwari, Gwagwalada, and Nyanya occupied 10.14 km^2 of the study in 1985. With the government's ministries, agencies, embassies, and other cooperative firms shifting to Abuja in 1990, more infrastructures were developed, and AIS increased. 1990 saw an increase in AIS to 71.97 km^2 (Figure 5.1(b)). Since then, urban growth has expanded, with 113.48 km^2 added in 1995 and 153.76 km^2 added in 1999 (Figure 5.1(c) and (d)). Figure 5.1(e) depicts that the AIS declined to 145.51 km^2 in 2004 but increased to 165.00 km^2 in 2009. (Figure 5.1(f)). Between 2014 and 2019, it was confirmed that AIS covered 353. 00 km^2 and 671. 30 km^2, respectively. The spatial distribution of AIS of Abuja and its environs in 2019 is shown in Figures 5.1(g) and (h), demonstrating that pockets of urban parks and gardens are becoming increasingly ubiquitous as urbanisation advances in the city's core.

'Bare surface' refers to underdeveloped lands and exposed areas. These include a parade and sports grounds for the armed services, playgrounds for institutions, open spaces between buildings, rocky outcrops of the study area, and rural and suburban arable land that is uncultivated during the dry season and cultivated during the wet season. As illustrated in Figures 5.1 (a) and (b), the bare surface decreased from 2553.03 km^2 in 1985 to 1284.90 km^2 in 1990. Between 1995 and 1999, the area of bare surface decreased from 771.06 km^2 to 463.64 km^2 (Figure 5.1(c) and (d)). In 2004, the area of barre surface increased to 591.21 km^2 before shrinking to 416.8 km^2 in 2009. (Figure 5.1(e)). Table 5.1 and Figure 5.1(g) demonstrate a further decline of bare surface in 2014 to 164.58km^2 and a substantial increase in 2019 to 553.24km^2 (Figure 5.1(h)).

Abandoned farmland that has remained fallow for several years is replete with Shrublands. According to the findings of this study, Shrubland covered 996.04km^2 of the map area in 1985 (Figure 5.1(a)), but only 566.44km^2 in 1990. (Figure 5.1(b)). Between 1995 and 1999, Shrubland expanded by 791.12 km^2 and 1,100.50km^2, respectively (Figure 5.1(c) and (d)). Figure 5.1(e) illustrates that shrubland coverage declined substantially to 113.73km^2 in 2004 before increasing to 694.84km^2 and 887.71km^2 in 2009 and 2014, respectively (Figure 5.1(f) and (g)). As depicted in Figure 5.1(h), the area of Shrubland dropped to 543.46 km^2 in 2019.

The study area's forest land comprises recreation centres, wooded areas, and a forest reserve. According to the analysis, forest land covered a large amount of the studied region in 1985, covering 2060.30km^2 (Figure 5.1(a)). This had drastically decreased to 1398.57 km^2 by 1990 (Figure 5.1(b)). In 1995, 1999, 2004, and 2009, the area of forestland was reduced by 1190.47km^2, 556.95km^2, 251.16km^2, and 242.73km^2. (Figures 5.1(c), (d), (e) and (f)). In 2014, forestland was reduced by an additional 115.49 km^2 (Figure 5. 1(g)) but increased to 216.80 km^2 in 2019 (Figure 5. 1(h)). The variation in grassland land area from 2286.22km^2 in 1985 to 2060.28km^2 in 1990 and 2183.25km^2 in 1995 may be explained by the research area's seasonality of rainfall (Figures 5.1(a), (b), and (c)). From 2486.45km^2 in 1999 to 2639.26km^2 and 2734km^2 in 2004 and 2009, the grassland area expanded rapidly until declining to 2154.09km^2 in 2014. (Figures 5.1(d), (e), (f) and (g)). Figure 5.1(h) shows there were 2492.68 km^2 more grasslands in 2019. Cropland area rose from 5.72km^2 in 1985 to 2550.04km^2 in 1990 (Figure 5.1(a) and (b)). There was an additional rise in 1995, 1999, and 2004 to 2894.16km^2, 3190.03km^2, and 4210.34km^2 (Figure 5.1(c), (d) and (e)). However, the cropland area declined in 2009 to 3699.32km^2 (Figure 5.1(f)). Land use/cover area estimates were derived directly from the map; ideally, they would have been error adjusted, but this could not be done because there is no accuracy assessment information for Gong *et al.* (2020) maps. Figure 5.1(g) and (h) and Table 5.1 indicate an increase to 4275.39km^2 and a decline to 3477.50km^2 of cropland area between 2014 and 2019.

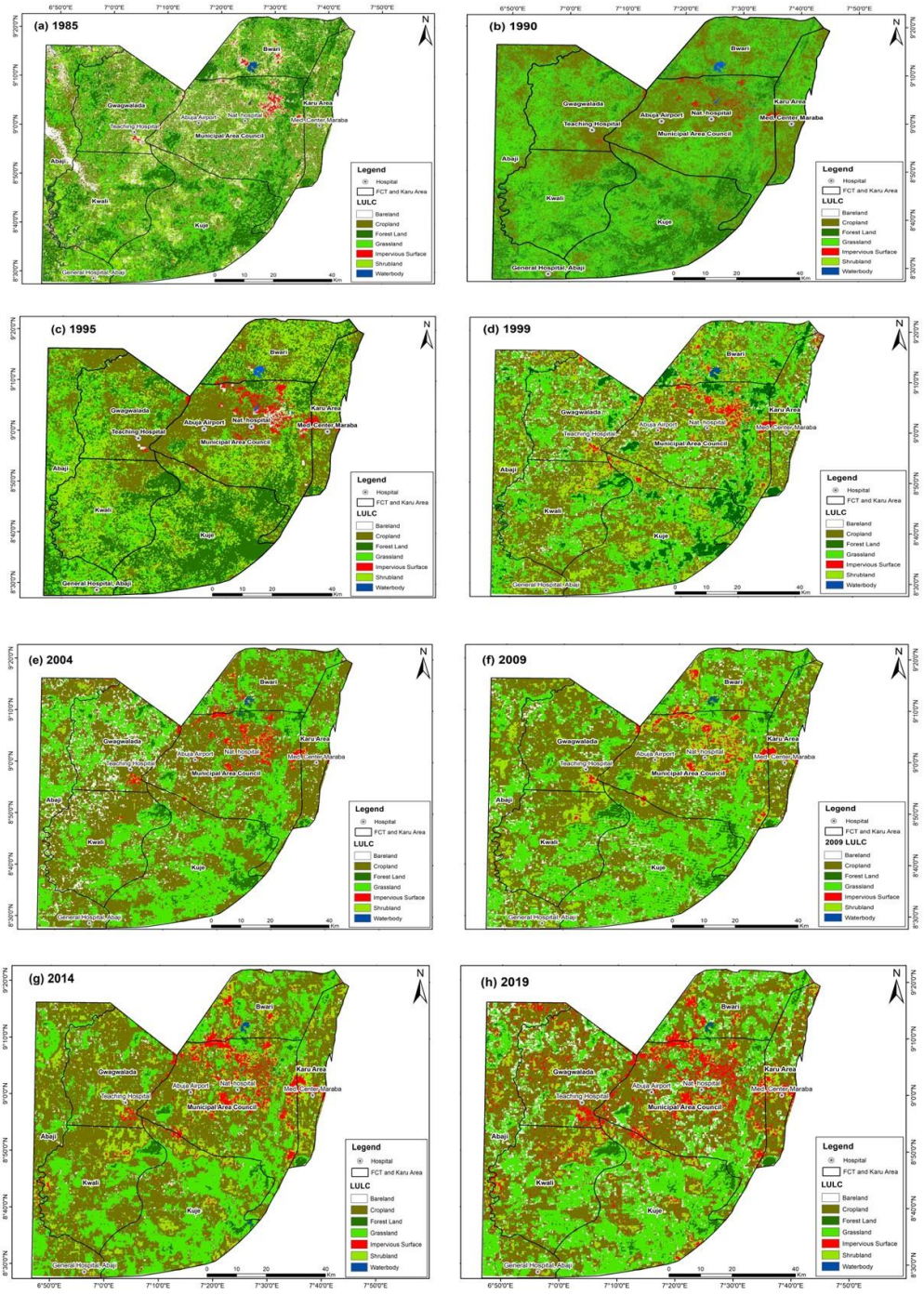


Figure 5.1: Land use/cover maps (1985-2019) produced using Gong *et al*. (2020) global artificial impervious area maps (a), (b), and (c), as well as Landsat 5 TM (d), Landsat 7 ETM (e), (f), and Landsat 8 OLI-TIRS (g), (h).

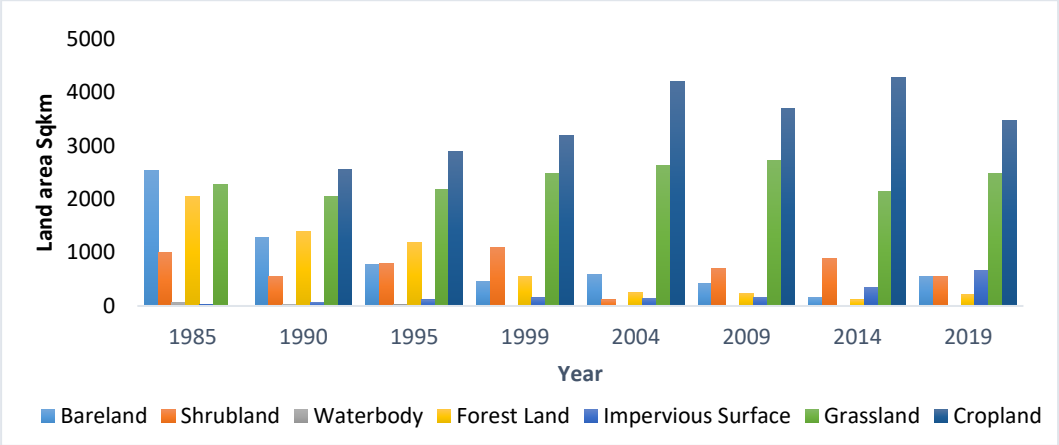


Figure 5.2: Land use/cover trend of change from 1985 – 2019.

Figures 5.2 and 5.3 show the spatial and temporal evolution of Abuja's AIS from 1985 to 2019. AISs are a crucial determinant of environmental change and a major indicator of urbanisation. Since the turn of the century, Abuja has undergone considerable urbanisation, with the most noticeable developments coming between 2009 and 2019. As a result of the move of the government's headquarters from Lagos, there has been an increase in population and expansion of the economy. Between 2000 and 2010, removing informal settlements in the city to restore Abuja's Master Plan reduced the spread of Abuja's AIS.

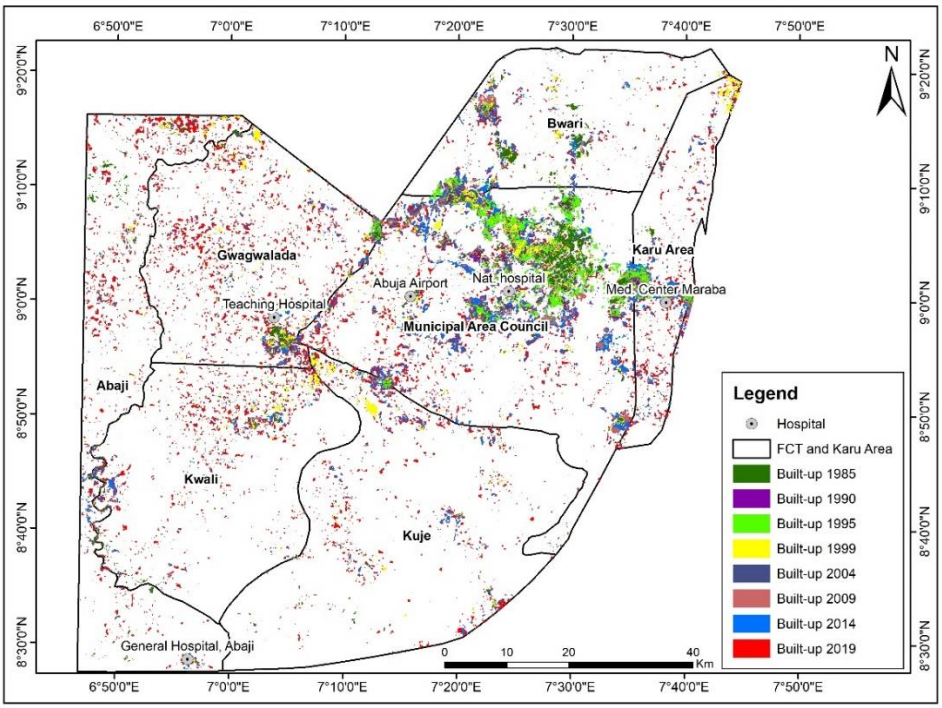


Figure 5.3: AIS area showing the urban expansion of Abuja and its environs (1985 – 2019).

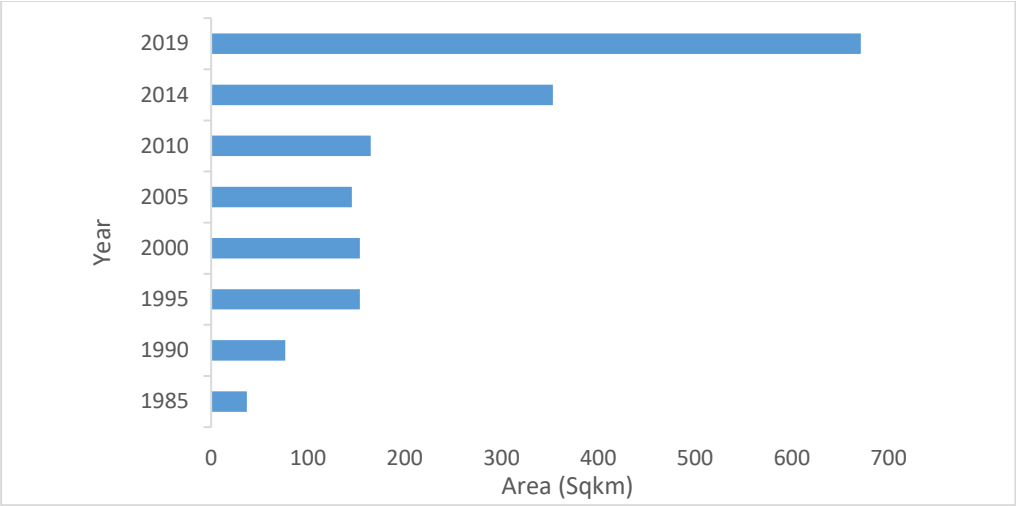


Figure 5.4: Temporal change in the AIS area between 1985 and 2019.

5.2 The error-adjusted area assessment

The error matrix is a cross-tabulation of the class labels allocated by the map and reference data. The diagonal of the error matrix represents correct classifications, whereas the off-diagonal components indicate errors of omission and commission. These were built based on the pixel-by-pixel assessment of the map and reference classifications for the accuracy assessment sample. The error matrix's cell items and marginal values are central to area estimation and computation of accurate assessment of the maps produced for this study, as presented in Table 5.3. The error matrix cell entries for the land use/cover maps were constructed from the accuracy assessment reports generated by Erdas imagine, which was founded on the sample set generated. The row totals for the error matrix class in Table 5.3 present the map areas, whereas the column totals provide the areas according to reference data. The map area was derived from the classified imagery in a kilometre square (km^2). The area proportion of the mapped class (W_i) was computed by dividing the number of pixels per stratum, *i.e.*, the class of map area (i), by the total number of pixels, which is the total area of the map as presented in Table 5.3.

Table 5.3: Error matrix sample counts. The cell entries (pij) represent the proportion of area derived from Landsat 7 ETM+ of 1999, 2004, and 2009, and Landsat 8 OLI of 2014 and 2019, respectively. Google Earth images from similar years were used to collect reference data. Note: BL: Bareland; SL: Shrubland; WB: Water Body; FL: Forestland; IS: Impervious surface; GL: Grassland; CL: Cropland.

		Reference Data(i)									
Map 1999	Class	FL	WB	SL	CL	BL	GL	IS	Row Total	Map Area(km^2)	W_i
	BL	1	0	2	5	50	6	7	71	463.61	0.06
	SL	4	0	57	3	0	7	0	71	1100.50	0.14
	WB	7	59	0	0	2	2	0	70	5.51	0.00
	FL	52	0	3	5	0	11	0	71	556.69	0.07
	IS	2	0	0	0	3	3	62	70	153.76	0.02
	GL	0	0	3	5	2	61	2	73	2486.45	0.31
	CL	0	0	2	63	2	5	2	74	3190.03	0.40
	Column Total	66	59	67	81	59	95	73	500	7956.50	1
Map 2004	Class	CL	WB	SL	FL	BL	GL	IS	Row Total	Map Area(km^2)	W_i
	BL	6	0	3	0	56	4	2	71	591.21	0.07
	SL	7	0	49	4	3	4	3	70	113.73	0.01
	WB	0	70	0	0	0	0	0	70	5.09	0.00
	FL	4	0	0	57	2	5	2	70	251.16	0.03
	IS	5	0	2	2	3	4	54	70	145.51	0.02
	GL	8	0	4	3	3	56	0	74	2639.46	0.33
	CL	64	0	2	2	4	2	1	75	4210.34	0.53
	Column Total	94	70	60	68	71	75	62	500	7956.50	1
Map 2009	Class	IS	WB	SL	FL	BL	GL	CL	Row Total	Map Area(km^2)	W_i
	BL	3	0	0	1	57	5	5	71	413.68	0.05

	SL	4	0	56	1	2	4	4	71	694.84	0.09
	WB	0	70	0	0	0	0	0	70	8.15	0.00
	FL	1	0	4	60	0	3	2	70	242.73	0.03
	IS	61	0	3	1	2	0	3	70	165.00	0.02
	GL	3	0	2	2	4	57	5	73	2734.00	0.34
	CL	1	0	1	2	0	9	62	75	3699.32	0.46
	Column Total	73	70	66	67	65	78	81	500	7956.50	1

Map 2014	Class	BL	WB	SL	FL	GL	CL	IS	Row Total	Map Area(km^2)	W_i
	BL	53	0	4	1	4	6	2	70	164.58	0.02
	SL	0	0	56	5	4	4	2	71	884.71	0.11
	WB	2	65	0	3	0	0	0	70	9.96	0.00
	FL	0	0	0	61	3	3	3	70	115.50	0.01
	IS	3	0	3	0	0	5	60	71	353.00	0.04
	GL	0	0	0	2	61	7	3	73	2154.09	0.27
	CL	3	0	4	3	8	53	4	75	4275.39	0.54
	Column Total	61	65	67	75	80	78	74	500	7956.50	1

Map 2019	Class	WB	BL	SL	FL	GL	CL	IS	Total	Map Area (km^2)	W_i
	BL	0	56	3	0	4	5	3	71	553.24	0.07
	SL	0	3	57	0	5	4	2	71	543.46	0.07
	WB	67	0	0	3	0	0	0	70	2.80	0.00
	FL	0	0	0	63	4	3	0	70	216.80	0.03
	IS	0	4	3	0	3	5	56	71	671.30	0.08
	GL	0	4	4	0	56	7	2	73	2492.68	0.31
	CL	0	3	0	2	10	56	3	74	3477.51	0.44
	Column Total	67	70	67	68	82	80	66	500	7956.50	1

5.3 Area estimation and uncertainty

For this study, area estimations were performed to express the error matrix as proportions of the estimated area. The area estimates were calculated using equation 5.1 as an illustration for estimating the proportion of impervious surface class area (pij) (Olofsson *et al*., 2014).

$$\widehat{\boldsymbol{p}}_{\boldsymbol{ij}} = \boldsymbol{W}_{\boldsymbol{i}} \frac{\boldsymbol{n}_{\boldsymbol{ij}}}{\boldsymbol{n}_{\boldsymbol{i}\cdot}} \qquad (5.1)$$

Where;

$\boldsymbol{W}_{\boldsymbol{i}}$ = The proportion of area mapped as class i

$\boldsymbol{p}_{\boldsymbol{ij}}$ = is indicated as $\widehat{\boldsymbol{p}}_{\boldsymbol{ij}}$

Where i signifies the row and j represents the column in the error matrix.

$\boldsymbol{n}_{\boldsymbol{i}}$. is the number of samples for map class i, $\frac{\boldsymbol{n}_{\boldsymbol{ij}}}{\boldsymbol{n}_{\boldsymbol{i}\cdot}}$ is the summed over j.

To this end, each row element (nij) in Table 5.3 was multiplied by the area proportion of the map class (W_i) divided by the total number of samples for the map class (ni). Table 5.4 presents the error matrix of estimated area proportions for the study area's land use/cover map, produced using the error matrix sample count.

Table 5.4: The error matrix populated by estimated proportions of the area. Note: BL: bareland; SL: shrubland; WB: water Body; FL: forestland; IS: impervious surface; GL: grassland; CL: cropland.

		Reference data 1999									
Map 1999	Class	FL	WB	SL	CL	BL	GL	IS	Row Total	Map Area (km^2)	W_i
	BL	0.00082	0.00000	0.00164	0.00410	0.04103	0.00492	0.00575	0.05827	463.60	0.05827
	SL	0.00779	0.00000	0.11104	0.00584	0.00000	0.01364	0.00000	0.13831	1100.50	0.13831
	WB	6.93050	0.00058	0.00000	0.00000	1.98050	1.98050	0.00000	0.00069	5.51	0.00069
	FL	0.05124	0.00000	0.00296	0.00493	0.00000	0.01080	0.00000	0.06997	556.70	0.06997
	IS	0.00055	0.00000	0.00000	0.00000	0.00083	0.00083	0.01712	0.01933	153.80	0.01932
	GL	0.00000	0.00000	0.01284	0.02140	0.00856	0.26113	0.00856	0.31250	2486.50	0.31250
	CL	0.00000	0.00000	0.01084	0.34133	0.01084	0.02709	0.01084	0.40093	3190.00	0.40093
	Column Total	0.06048	0.00058	0.13932	0.37761	0.06128	0.31847	0.04226	1.00000	7956.50	1.00000
Map 2004	Class	CL	WB	SL	FL	BL	GL	IS	Row Total	Map Area(km^2)	W_i
	BL	0.00628	0.00000	0.00314	0.00000	0.05861	0.00419	0.00209	0.07431	591.20	0.07431
	SL	0.00143	0.00000	0.01001	0.00082	0.00061	0.00082	0.00061	0.01429	113.70	0.01429
	WB	0.00000	0.00060	0.00000	0.00000	0.00000	0.00000	0.00000	0.00064	5.10	0.00064
	FL	0.00180	0.00000	0.00000	0.02570	0.00090	0.00226	0.00090	0.03157	251.20	0.03157
	IS	0.00131	0.00000	0.00052	0.00052	0.00078	0.00105	0.01411	0.01829	145.50	0.01829
	GL	0.03586	0.00000	0.01793	0.01345	0.01345	0.25104	0.00000	0.33174	2639.50	0.33174
	CL	0.45156	0.00000	0.01411	0.01411	0.02822	0.01411	0.00706	0.52917	4210.30	0.52917
	Column Total	0.49824	0.00064	0.04571	0.05460	0.10258	0.27346	0.02477	1.00000	7956.50	1.00000
Map 2009	Class	IS	WB	SL	FL	BL	GL	CL	Row Total	Map Area(km^2)	W_i
	BL	0.00220	0.00000	0.00000	0.00073	0.04173	0.00366	0.00366	0.05199	413.70	0.05198
	SL	0.00492	0.00000	0.06887	0.00123	0.00246	0.00492	0.00492	0.08732	694.80	0.08732
	WB	0.00000	0.00102	0.00000	0.00000	0.00000	0.00000	0.00000	0.00102	8.20	0.00102
	FL	0.00044	0.00000	0.00174	0.02615	0.00000	0.00131	0.00087	0.03050	242.70	0.03050

	IS	0.01807	0.00000	0.00089	0.00030	0.00059	0.00000	0.00089	0.02074	165.00	0.02074
	GL	0.01412	0.00000	0.00941	0.00941	0.01883	0.26826	0.02353	0.34357	2734.00	0.34357
	CL	0.00620	0.00000	0.00620	0.01240	0.00000	0.05579	0.38429	0.46487	3699.30	0.46487
	Column Total	0.04594	0.00102	0.08711	0.05021	0.06361	0.33394	0.41817	1.00000	7956.50	1.00000
		BL	WB	SL	FL	GL	CL	IS	Row Total	Map Area(km^2)	W_i
Map 2014	BL	0.01570	0.00000	0.00118	0.00030	0.00118	0.00177	0.00059	0.02068	164.60	0.02068
	SL	0.00000	0.00000	0.08769	0.00783	0.00626	0.00626	0.00313	0.11118	884.70	0.11118
	WB	0.00000	0.00116	0.00000	0.00005	0.00000	0.00000	0.00000	0.00125	10.00	0.00125
	FL	0.00000	0.00000	0.00000	0.01265	0.00062	0.00062	0.00062	0.01452	115.50	0.01452
	IS	0.00190	0.00000	0.00187	0.00000	0.00000	0.00312	0.03749	0.04436	353.00	0.04436
	GL	0.00000	0.00000	0.00000	0.00742	0.22621	0.02596	0.01113	0.27071	2154.10	0.27071
	CL	0.02150	0.00000	0.02866	0.02149	0.05731	0.37969	0.02866	0.53730	4275.40	0.53730
	Column Total	0.03910	0.00116	0.11941	0.04974	0.29159	0.41743	0.08162	1.00000	7956.50	1.00000
	Class	WB	BL	SL	FL	GL	CL	IS	Total	Map Area(km^2)	W_i
Map 2019	BL	0.00000	0.05483	0.00294	0.00000	0.00392	0.00490	0.00294	0.06952	553.20	0.06952
	SL	0.00000	0.00289	0.05483	0.00000	0.00481	0.00385	0.00192	0.06829	543.50	0.06829
	WB	0.00034	0.00000	0.00000	0.00002	0.00000	0.00000	0.00000	0.00035	2.80	0.00035
	FL	0.00000	0.00000	0.00000	0.02452	0.00156	0.00117	0.00000	0.02724	216.80	0.02724
	IS	0.00000	0.00475	0.00356	0.00000	0.00356	0.00594	0.06654	0.08436	671.30	0.08436
	GL	0.00000	0.01716	0.01716	0.00000	0.24029	0.03004	0.00858	0.31324	2492.70	0.31324
	CL	0.00000	0.01772	0.00000	0.01181	0.05905	0.33070	0.01772	0.43699	3477.50	0.43699
	Total	0.00034	0.09735	0.07849	0.03635	0.31319	0.37659	0.09770	1.00000	7956.50	1.00000

5.4 Error-adjusted Area Estimation

The error-adjusted area estimates the mapped area according to the reference data. For this study, the computation of error-adjusted area for each land use/cover class was carried out by multiplying the column total of the map class by the total map area. The computed error-adjusted area for the classified Landsat images used in this study is presented in Table 5.5.

Table 5.5: Error-adjusted area of map class. Note: WB: Water Body; BL: Bareland; SL: Shrubland; FL: Forestland; GL: Grassland; CL: Cropland; IS: Impervious surface; EAJ=Error adjusted Area.

		Reference data								
Map 1999		BL	SL	WB	FL	IS	GL	CL	Row Total	Map Area(km^2)
	Column Total	0.061	0.139	0.001	0.061	0.042	0.319	0.378	1.00	7956.55
	EAJ	487.570	1108.480	4.644	481.190	336.230	2533.930	3004.490	7956.50	
Map 2004		BL	SL	WB	CL	IS	GL	FL	Row Total	Map Area(km^2)
	Column Total	0.103	0.046	0.001	0.498	0.025	0.273	0.055	1.00	7956.50
	EAJ	816.150	363.698	5.090	3964.250	197.092	2175.766	434.453	7956.50	
Map 2009		BL	SL	WB	IS	CL	GL	FL	Row Total	Map Area(km^2)
	Column Total	0.064	0.087	0.001	0.046	0.418	0.334	0.050	1.00	7957.72
	EAJ	506.200	693.213	8.150	365.559	3327.650	2657.367	399.577	7956.50	
Map 2014		GL	SL	WB	BL	IS	CL	FL	Row Total	Map Area(km^2)
	Column Total	0.292	0.119	0.001	0.039	0.082	0.417	0.049	1.00	7957.23
	EAJ	2320.230	950.140	9.249	310.826	649.429	3321.591	395.763	7956.50	
Map 2019		GL	SL	BL	WB	IS	CL	FL	Row Total	Map Area(km^2)
	Column Total	0.31320	0.078	0.097	0.000	0.098	0.377	0.036	1.00	7957.78
	EAJ	2492.320	624.630	774.710	2.680	777.430	2996.790	289.230	7956.50	

5.5 Computation of confidence intervals

Confidence intervals were computed to estimate the precision of the map area. Firstly, the standard error for the column total of class number 1 was computed using the square root of the estimated area proportion (W_i). Furthermore, the sample counts were multiplied by the correct sample count divided by the total column sample as shown in Equation 5.2 (Olofsson *et al.*, 2014).

$$\boldsymbol{S(p.1)} = \sqrt{\sum_{i-1}^{7} \boldsymbol{W^2} \frac{\frac{n_{ij}}{ni}\left(1-\frac{n_{ij}}{ni}\right)}{n_i - 1}} = \boldsymbol{SE}\left(\hat{\boldsymbol{p}}_j\right) = \sqrt{\sum_i \frac{\boldsymbol{W_i}\hat{\boldsymbol{p}}_{ij} - \hat{\boldsymbol{p}}_{ij}^{\,2}}{\boldsymbol{n_i - 1}}} \qquad (5.2)$$

For impervious surfaces, S (p.1) was computed as = $\left((0.084^2 \frac{\mathbf{56}}{\mathbf{71}}\left(\mathbf{1} - \frac{\mathbf{56}}{\mathbf{71}}\right)\right)$ / $\mathbf{71 - 1}$

$\boldsymbol{S(p.1)}$= 0.0041

The standard error of the map class impervious surface was computed by multiplying the standard error of the column class by the total map area as shown in Equations 4.3 (Olofsson *et al.*, 2014).

$$\boldsymbol{SE}\left(\hat{\boldsymbol{A}}_{\boldsymbol{1}}\right) = \boldsymbol{SE}(\hat{\boldsymbol{p}}_{\boldsymbol{1}}) \times \boldsymbol{A_{tot}} \qquad (5.3)$$

SE (A_1) = 0.0041x 7957.78 = 32.75km^2

The margin error of confidence intervals was further computed by multiplying the standard error of the map class by 1.96. The margin of error for map class impervious surface was therefore computed as: A_1=32.75 x 1.96 = 65.51km^2. The upper 95% confidence intervals were computed by multiplying the standard error of the map class by 1.96 added to the error-adjusted area of the class. For the lower 95% confidence intervals, the multiplied standard error by 1.96 was subtracted from the error-adjusted area of the map class. For example, the upper 95% CIs of impervious surface was computed as: Upper 95% CI= 777.43 + (1.96 x 32.75) =842.94; Lower 95% CI=777.43 - (1.96 x 32.75) =711.93.

Table 5.6: The standard error of area estimates and 95% confidence intervals. Note: WB: BL: Bareland; SL: Shrubland; Water Body; FL: Forestland; IS: Impervious surface; GL: Grassland; CL: Cropland. EAJ: Error-adjusted Area; S(P.1): Standard Error for column total of Class; S(A.1): Standard Error of map Class.

The standard error of area estimates and 95% confidence intervals 1999.						
Class	EAJ (km^2)	$S(P_{.1})$	$S(A_{.1})$	The margin of error of CI	Upper 95% CI	Lower 95% CI
BL	487.57	0.00318	25.29	50.58	538.15	436.99
SL	1108.48	0.00658	52.33	104.67	1213.15	1003.81
WB	4.64	3.03805	0.24	0.48	5.13	4.16
FL	481.19	0.00370	29.46	58.91	540.10	422.28
IS	336.23	0.00074	5.89	11.78	348.01	324.46
GL	2533.93	0.01365	108.60	217.21	2751.14	2316.73
CL	3004.49	0.01669	132.82	265.64	3270.14	2738.85
Column Total	7956.50	0.04457	354.64	709.27	8665.82	7247.28
The standard error of area estimates and 95% confidence intervals 2004.						
BL	816.15	0.00363	28.85	57.69	873.84	758.46
SL	363.69	0.00079	6.27	12.55	376.25	351.15
WB	5.09	0.00000	0.00	0.00	5.09	5.09
FL	434.45	0.00148	11.76	23.52	457.97	410.94
IS	197.09	0.00092	7.36	14.71	211.80	182.38
GL	2175.77	0.01666	132.54	265.08	2440.85	1910.68
CL	3964.25	0.02176	173.15	346.30	4310.55	3617.95
Column Total	7956.50	0.04524	359.93	719.85	8676.35	7236.65
The standard error of area estimates and 95% confidence intervals 2009.						
BL	506.20	0.00247	19.67	39.35	545.55	466.86
SL	693.21	0.00426	33.90	67.80	761.02	625.41
WB	8.15	0.00000	0.00	0.00	8.15	8.15
FL	399.58	0.00129	10.23	20.45	420.03	379.13
IS	365.56	0.00084	6.65	13.29	378.86	352.26

GL	2657.37	0.01675	133.29	266.59	2923.95	2390.78
CL	3327.65	0.02032	161.69	323.39	3651.04	3004.26
Column Total	7956.50	0.04592	365.44	730.87	8688.59	7226.85
The standard error of area estimates and 95% confidence intervals 2014.						
BL	310.83	0.00107	8.49	16.99	327.82	293.83
SL	950.14	0.00546	43.17	86.33	1036.47	863.81
WB	9.25	3.88505	0.31	0.62	9.87	8.63
FL	395.76	0.00059	4.65	9.31	405.07	386.45
IS	649.43	0.00192	15.27	30.53	679.96	618.89
GL	2320.23	0.01182	94.09	188.17	2508.41	2132.06
CL	3321.59	0.02844	226.28	452.56	3774.15	2869.02
Column Total	7956.50	0.04929	392.26	784.52	8741.75	7172.71
The standard error of area estimates and 95% confidence intervals 2019.						
BL	774.71	0.00339	26.99	53.99	828.69	720.72
SL	624.63	0.00325	25.84	51.69	676.31	572.94
WB	2.68	8.57911	0.07	0.14	2.82	2.54
FL	289.23	0.00098	7.83	15.66	304.89	273.57
IS	777.43	0.00411	32.75	65.51	842.94	711.93
GL	2492.32	0.01560	124.16	248.33	2740.65	2243.99
CL	2996.79	0.02194	174.62	349.25	3346.04	2647.54
Total	7956.50	0.04929	392.28	784.55	8742.33	7173.23

It should be stated that evaluating the pixel count matrices with the error-adjusted matrix indicated a slight discrepancy between the mapped and estimated land use/cover area classifications. For all categories, the generated maps are within a 95% confidence interval of the estimated area, demonstrating the maps' robustness and dependability (Olofsson *et al.*, 2014).

5.6 The relationships between UHIs and artificial impervious surfaces

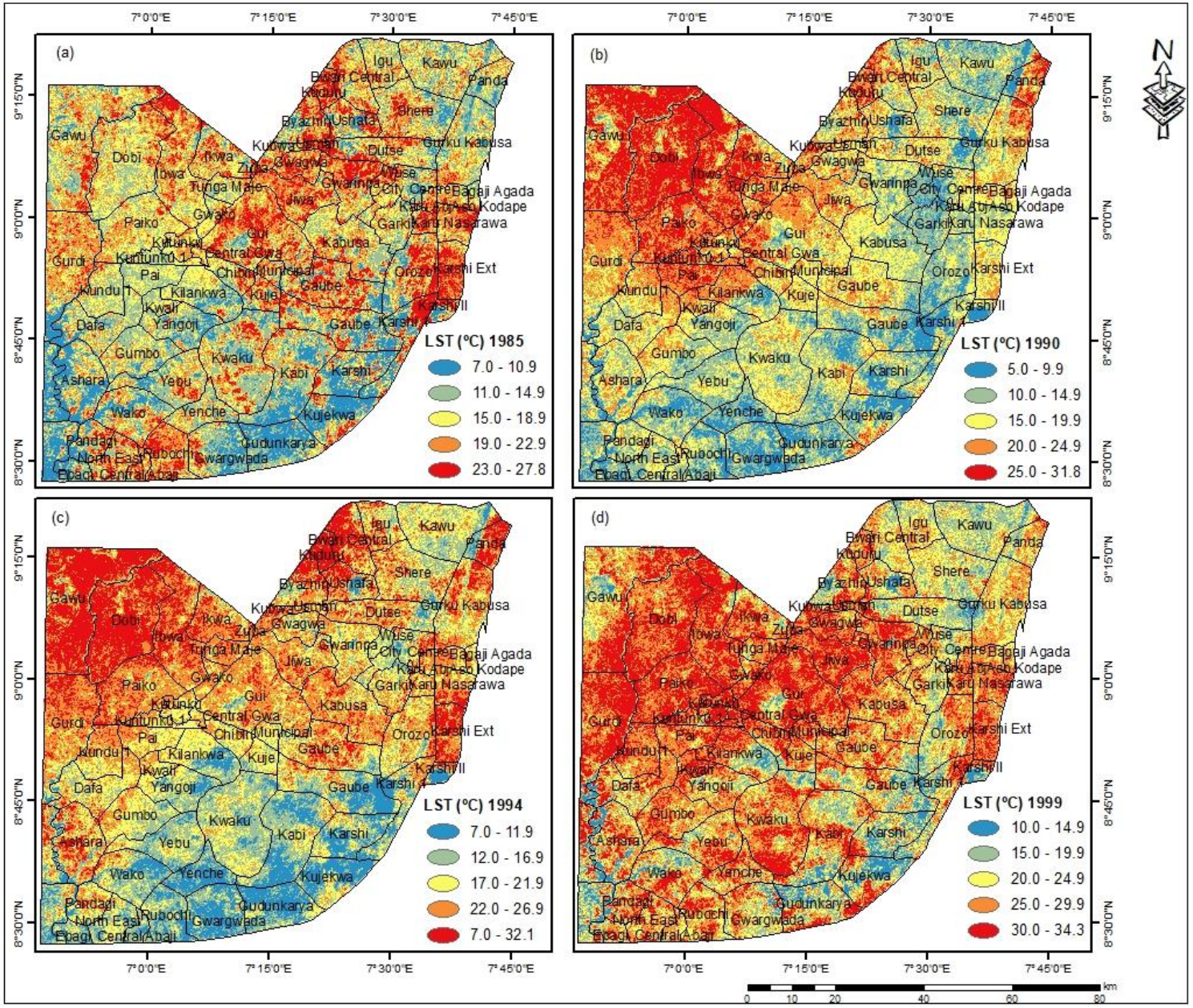
In Abuja, there is only one weather station that measures temperature. Consequently, it is unable to offer temperature data on a spatiotemporal scale. Remote sensing can obtain data on the thermal environment to enhance comprehension and understanding of the relationship between the AIS resulting from urbanisation, LST, and other pertinent biophysical indices such as the NDVI. These environmental components were computed for this investigation using Landsat images in this section. In addition, the effect of AIS on the development of UHI and the impact of the green cover was revealed.

LST is a helpful indicator for investigating the spatiotemporal variation of UHI. Figure 5.5 shows the thermal environment of the study area, signifying the effects of urbanisation on LST. Figure 5.5(a), for example, shows that areas with higher LST were more evenly distributed in the northern part of the study area in 1986, albeit in a more fragmented distribution than in the southern part of Abuja. The municipal, Gwagwalada, Bwari area council, and Karu areas experienced the most intense urban warming. LST was exceptionally high in GUI, Gwarimpa, and Nyanya, peaking at 27.8°C on 13 March 1986, with the lowest surface temperatures recorded in Ashara, Alu Mama, and Kujekwa, at 7.9°C, 11.7°C, and 12.1°C.

The metropolitan area's land conversion zone experienced the most substantial increase in LST during 1990, particularly in the city centre, Wuse, Jiwa, Zuba, and Dobe in the north-eastern and north-western parts of the study area. The LST in this region can reach 31.8^{o}C. When compared to the northern settlements, the surrounding areas in the southern part of the study do not show patterns associated with major warming this year. Figure 5.5(b) shows that LST in the southern region ranged from 5.0^{o}C to 10.0^{o}C. Since 1994, the Kwali, quarters, Gwarimpa, and Nyanya regions have been among the hottest in the study area, with maximum LSTs ranging from 26.7^{o}C to 32.1^{o}C. (Figure 5.5(c)). The hottest spots were distributed along a strip parallel to traffic lines. Figure 5.5(d) shows a momentous rise in LST in the study region's north-western half, with temperatures ranging from 29.4°C to 34.3°C in central Giwa, Kutunku, and

part of Gurdi. Except for Jabi Lake, Lower Usman Dam in Bwari, and some mountainous areas with high vegetation coverage in the north-eastern part of the study area, the high LST area spread across the northern part of the study area in 1999, with a contiguous and concentrated distribution and a major heat island in the central city centre, compared to the earlier years. LST increased by 2.7ºC in 2004 (Figure 5.5(e)), with the north-central part of the study area experiencing the highest LST. The LST increased from 38.1ºC in 2009 to 45.8ºC in 2014 (Figures 5.5(f) and (g)), with the northern region experiencing the most substantial increase. Figure 5.4(h) represents the 2019 LST, with surface temperatures ranging from 34.9ºC to 51.5ºC. During fallow periods, the traces of seasonal variations and farmlands are sometimes left as bare areas, conferring a high LST to such locations. The lowest heat island is found in the city centre's parks and garden areas, particularly the dense riparian areas around the southern part of the study area (18.1ºC to 29.3ºC). In Kwali Area Council, the lowest LST of 7.0°C was recorded near the Yaba boundaries. Other locations with the lowest LST included Ushafa, Gudunkarya, Kujekwa, and a portion of Ashara. They are frequently seen in the southern part of the study area, which has much vegetation. Large open spaces and farmlands surrounded by nucleated settlements are prevalent away from Abuja's city centre. This vegetation helps to keep the temperatures down in these areas.

It is worth noting that a long-warming band runs along the River Gwagwalada and its tributaries near the western border of the study area. The Lower Usman Dam water treatment plant, the primary source of public water supply in Abuja's FCT, contributes to the cooler temperatures in the Ashara ward. The difference in the intensity of the LST experienced in the study area's northern and southern parts represents the difference in LST between Abuja's urban, suburban, and rural areas. LST over the central business district has been increasing. Furthermore, the LST area decreased in the late 1990s but increased by more than 15.7ºC from 2014 to 2019, establishing the last ten years as a period of rapid heating. Even though the heat island's intensity has increased, the Karu area has always been dominant at different times as shown in Figure 5.5.


(a)
LST (°C) 1985
7.0 - 10.9
11.0 - 14.9
15.0 - 18.9
19.0 - 22.9
23.0 - 27.8
(b)
LST (°C) 1990
5.0 - 9.9
10.0 - 14.9
15.0 - 19.9
20.0 - 24.9
25.0 - 31.8
(c)
LST (°C) 1994
7.0 - 11.9
12.0 - 16.9
17.0 - 21.9
22.0 - 26.9
7.0 - 32.1
(d)
LST (°C) 1999
10.0 - 14.9
15.0 - 19.9
20.0 - 24.9
25.0 - 29.9
30.0 - 34.3
7°0'0"E
7°15'0"E
7°30'0"E
7°45'0"E
9°15'0"N
9°0'0"N
8°45'0"N
8°30'0"N
N
km
0
10
20
40
60
80

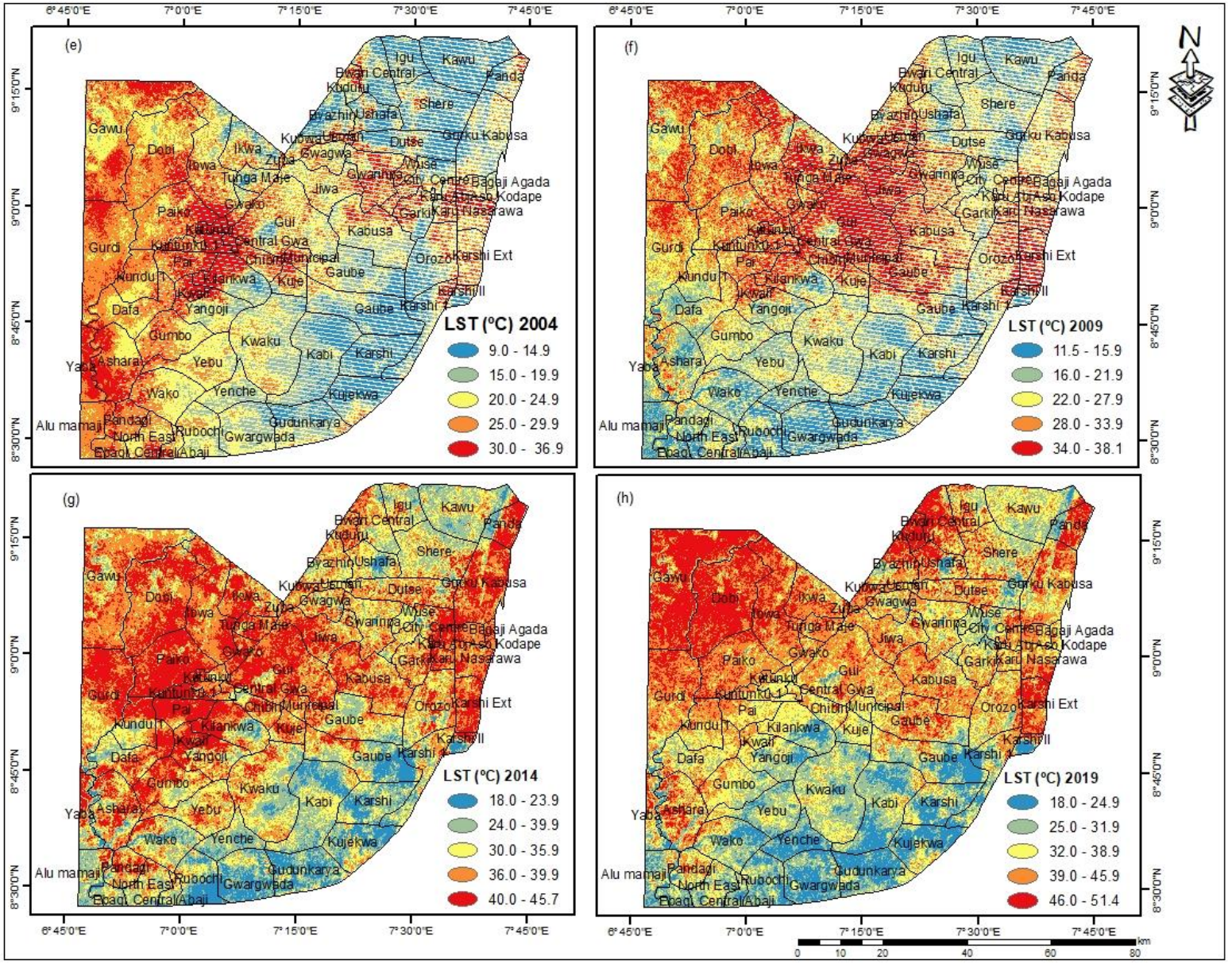

(e)
LST (°C) 2004
9.0 - 14.9
15.0 - 19.9
20.0 - 24.9
25.0 - 29.9
30.0 - 36.9
(f)
LST (°C) 2009
11.5 - 15.9
16.0 - 21.9
22.0 - 27.9
28.0 - 33.9
34.0 - 38.1
(g)
LST (°C) 2014
18.0 - 23.9
24.0 - 39.9
30.0 - 35.9
36.0 - 39.9
40.0 - 45.7
(h)
LST (°C) 2019
18.0 - 24.9
25.0 - 31.9
32.0 - 38.9
39.0 - 45.9
46.0 - 51.4
6°45'0"E
7°0'0"E
7°15'0"E
7°30'0"E
7°45'0"E
9°15'0"N
9°0'0"N
8°45'0"N
8°30'0"N
N
0 10 20 40 60 80 km

Figure 5.5: LST of the study area generated from the thermal bands of Landsat images. (a) Landsat 4 TM acquired at 09:15Z of November 27, 1986; (b) Landsat 5 TM acquired on February 16, 1990, (c) May 12, 1994, and (d) December 6, 1999, at 09:15Z; (e) Landsat 7 ETM of April 21, 2004, and (f) March 30, 2009, acquired at 09:38Z; (g) Landsat 8 OLI-TIRS of December 4, 2014, and (h) February 26th, 2019 acquired at 09:49Z. Note: Because the Landsat images were collected too early in the day, the LST may not depict the ideal surface temperature in the area.

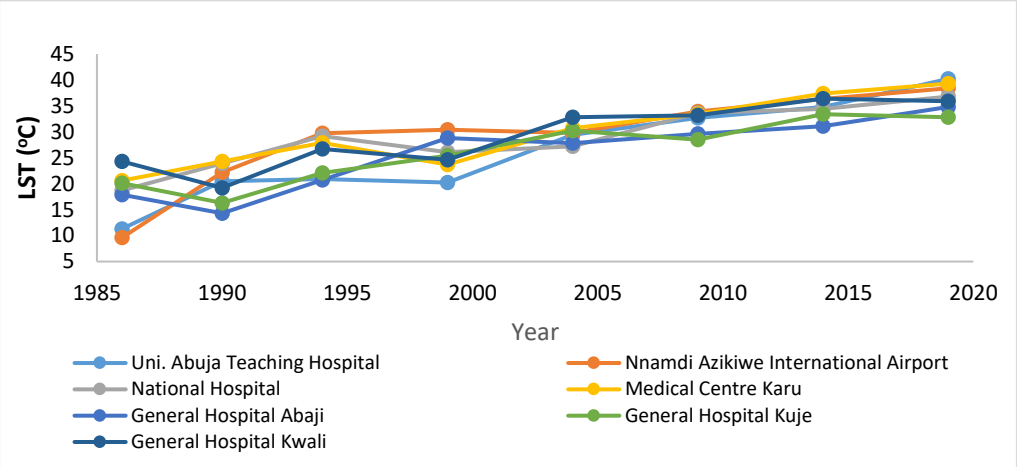
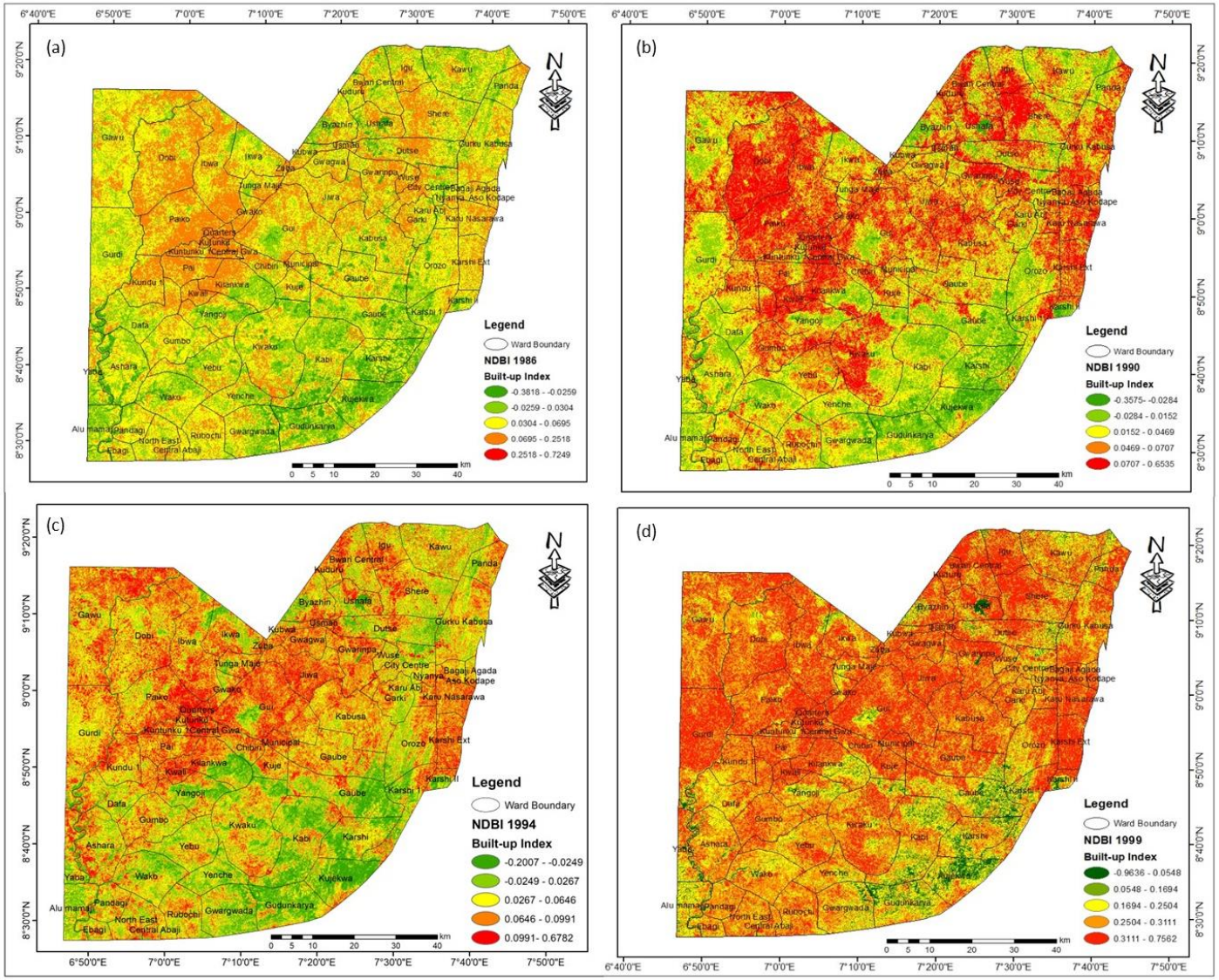


Figure 5.6: LSTs were extracted from the LST map of the study area generated from Landsat 5 TM, Landsat 7 ETM, and Landsat 8 OLI-TIRS acquired at 09:15Z. Note: The area councils were compared based on the characteristics of the settlements in terms of their extent of urbanization and level of imperviousness to depict the spatial patterns of UHI such as areas with urban features (University of Abuja Teaching Hospital Gwagwalada, National Hospital Abuja); areas with suburban features (General Hospital Kuje, Medical Centre Karu), and rural characteristics (General Hospital Kwali, General hospital Abaji).

5.7 Normalized Difference Built-up Index

LST is not uniformly spread throughout the city. Heat dispersion and fluctuation are often influenced by vegetation cover and impermeable surfaces (Oke, 2006; Yue *et al*., 2019). The NDVI and NDBI are commonly used to assess vegetation greenness and heat island sensitivity. The NDBI is a binary image-based index used to analyse urban patterns. NDBI is one of the most commonly used indexes for exploring built-up areas due to its sensitivity to the thermal environment. The NDBI can be used to extract AIS such as asphalt and concrete where the reflectivity values are in the SWIR and near-infrared bands of the image. Near-infrared spectrum reflection is more critical than SWIR spectrum reflection on

a green surface. The NDBI enables automatic mapping of built-up areas, with higher positive values indicating built-up areas and lower positive values indicating barren regions. Figure 5.7 depicts the NDBI index results, which show built-up areas in red and vegetation cover in green. Other land use/cover classes, such as bare land and water bodies, appeared between the two colours in light red, green, and yellow. The index values of the NDBI maps generated for this study varied with the proportion and density of the location's land use/cover feature. The NDBI map of Abuja, as shown in Figure 5.7, has index values ranging from -0.3818 to 0.7249 in 1986 (Figure 5.7(a.)) and index values ranging from -0.2780 to 0.6616 in 2019. (Figure 5.7(h)). Positive NDBI values are found in areas with higher AIS and little or no vegetation, such as built-up areas and barren land. High NDBI values indicate a lack of vegetation in the area. Green, densely vegetation areas, on the other hand, have NDBI values ranging from negative to zero. Cells with the lowest NDBI have been fully vegetated. Pixels with NDBI values ranging from 0.3 to 0.4 are mixed in with vegetation cover and cropland. The locations with positive NDBI values are commonly observed in the study area's AIS; they are more visible in areas dominated by built-up areas, whereas the light red colours depict high to moderate imperviousness, such as bare surface areas. Riparian vegetation and other green covers, such as croplands, had the lowest and most negative NDBI values.


(a)
Legend
Ward Boundary
NDBI 1986
Built-up Index
-0.3818 - -0.0259
-0.0259 - 0.0304
0.0304 - 0.0695
0.0695 - 0.2518
0.2518 - 0.7249
(b)
Legend
Ward Boundary
NDBI 1990
Built-up Index
-0.3575- -0.0284
-0.0284 - 0.0152
0.0152 - 0.0469
0.0469 - 0.0707
0.0707 - 0.6535
(c)
Legend
Ward Boundary
NDBI 1994
Built-up Index
-0.2007 - -0.0249
-0.0249 - 0.0267
0.0267 - 0.0646
0.0646 - 0.0991
0.0991- 0.6782
(d)
Legend
Ward Boundary
NDBI 1999
Built-up Index
-0.9636 - 0.0548
0.0548 - 0.1694
0.1694 - 0.2504
0.2504 - 0.3111
0.3111 - 0.7562
N
km
0 5 10 20 30 40

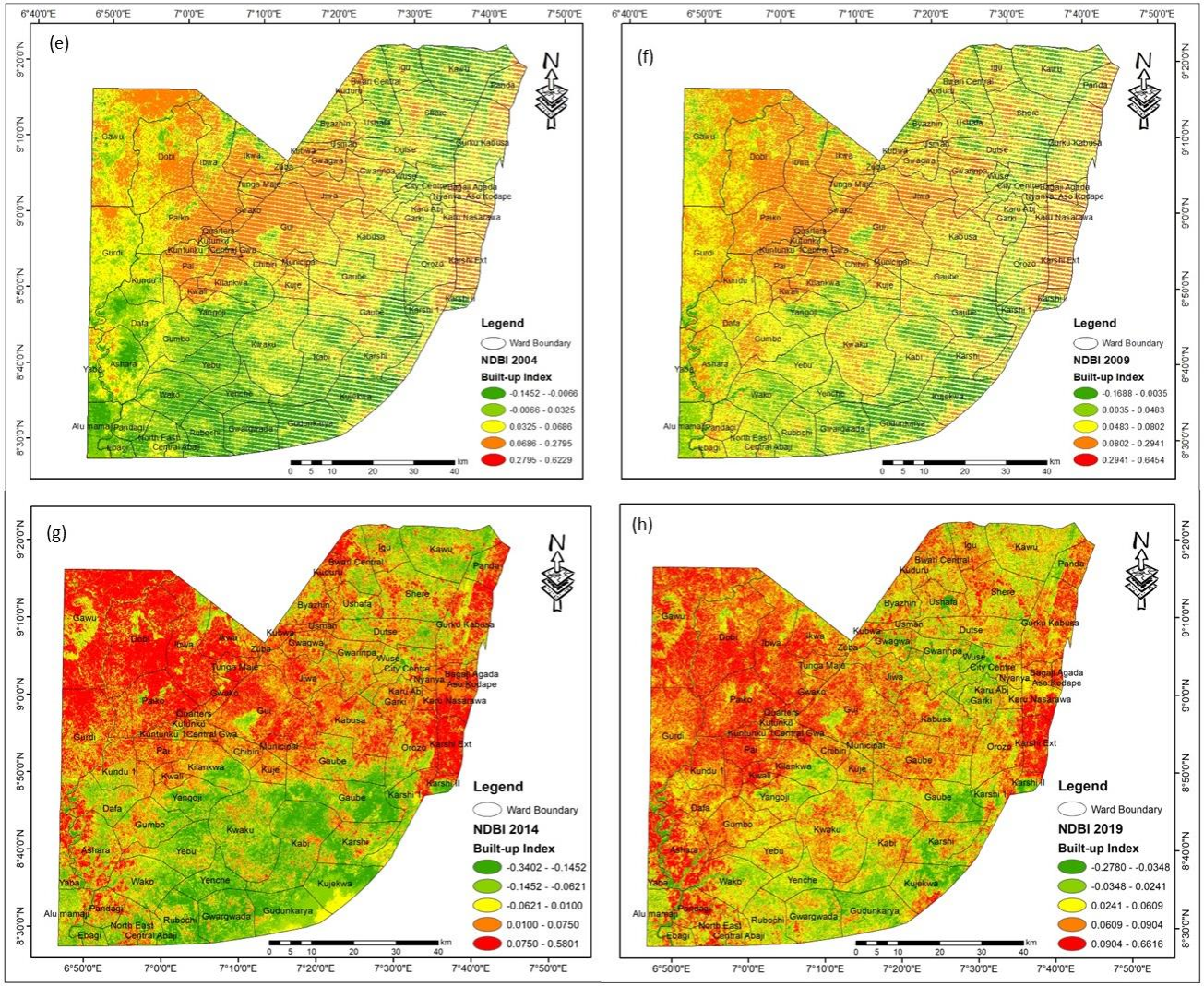
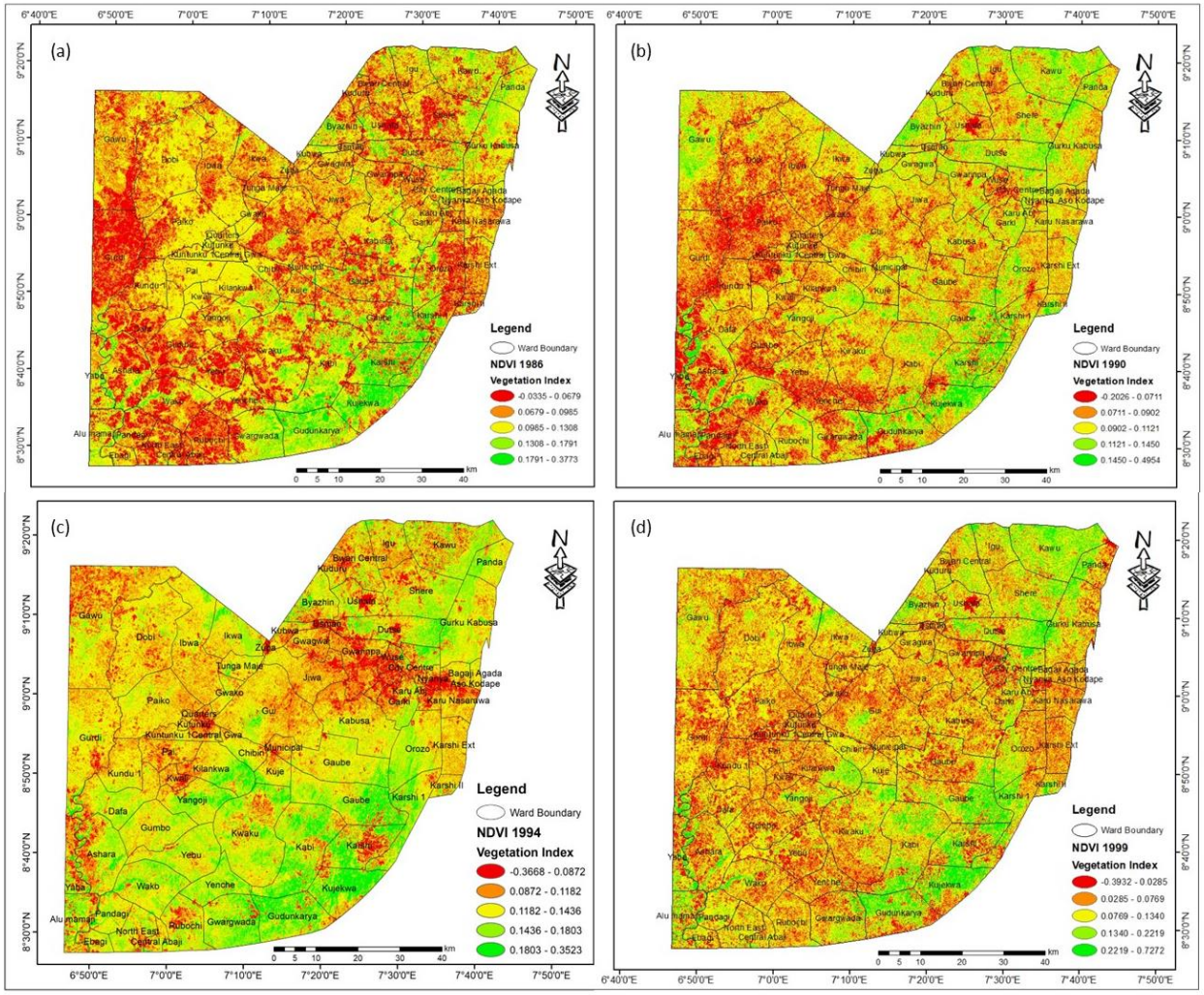

(e)
Legend
Ward Boundary
NDBI 2004
Built-up Index
-0.1452 - -0.0066
-0.0066 - 0.0325
0.0325 - 0.0686
0.0686 - 0.2795
0.2795 - 0.6229
(f)
Legend
Ward Boundary
NDBI 2009
Built-up Index
-0.1688 - 0.0035
0.0035 - 0.0483
0.0483 - 0.0802
0.0802 - 0.2941
0.2941 - 0.6454
(g)
Legend
Ward Boundary
NDBI 2014
Built-up Index
-0.3402 - -0.1452
-0.1452 - -0.0621
-0.0621 - 0.0100
0.0100 - 0.0750
0.0750 - 0.5801
(h)
Legend
Ward Boundary
NDBI 2019
Built-up Index
-0.2780 - -0.0348
-0.0348 - 0.0241
0.0241 - 0.0609
0.0609 - 0.0904
0.0904 - 0.6616

Figure 5.7: NDBI of the study area generated from the Near-infrared and shortwave-infrared bands of Landsat images. (a) Landsat 4 TM was acquired at 09:15Z of November 27, 1986; (b), (c), and (d) Landsat 5 TM was acquired on February 16, 1990, May 12, 1994, and December 6, 1999, at 09:15Z; (e) and (f) Landsat 7 ETM of April 21, 2004, and March 30, 2009, acquired at 09:38Z; (g) and (h) Landsat 8 OLI-TIRS of December 4, 2014, and February 26th, 2019 acquired at 09:49Z.

5.8 The Normalized Difference Vegetation Index

The NDVI results for this study range between -1 and 1. A small NDVI close to 1 indicates the highest potential density of green leaves, whereas a large NDVI close to -1 indicates no or unhealthy vegetation. Figure 5.8 depicts the NDVI maps for this investigation, with index values ranging from -0.0336 to 0.3776. (See Figure 5.8(a)) Built-up areas and barren land in Abuja have low or slightly positive NDVI values because they have more AIS and little or no vegetation. Locations having an NDVI of less than 0.2 are called vegetation-free. On the other hand, agricultural and green areas with a lot of vegetation have NDVI values that are near to 1. Fully vegetated cells, for example, have an NDVI greater than 0.3. Pixels that are blended with plants and other objects have NDVI values between 0.1 and 0.2. Healthy vegetation absorbs the most visible light and reflects a considerable part of near-infrared light, as illustrated in Figure 5.8. Poor or sparse vegetation with an NDVI of 0.3 reflects more visible light and less near-infrared radiation.


(a)
Legend
Ward Boundary
NDVI 1986
Vegetation Index
-0.0335 - 0.0679
0.0679 - 0.0985
0.0985 - 0.1308
0.1308 - 0.1791
0.1791 - 0.3773
(b)
Legend
Ward Boundary
NDVI 1990
Vegetation Index
-0.2026 - 0.0711
0.0711 - 0.0902
0.0902 - 0.1121
0.1121 - 0.1450
0.1450 - 0.4954
(c)
Legend
Ward Boundary
NDVI 1994
Vegetation Index
-0.3668 - 0.0872
0.0872 - 0.1182
0.1182 - 0.1436
0.1436 - 0.1803
0.1803 - 0.3523
(d)
Legend
Ward Boundary
NDVI 1999
Vegetation Index
-0.3932 - 0.0285
0.0285 - 0.0769
0.0769 - 0.1340
0.1340 - 0.2219
0.2219 - 0.7272
N
km
0 5 10 20 30 40

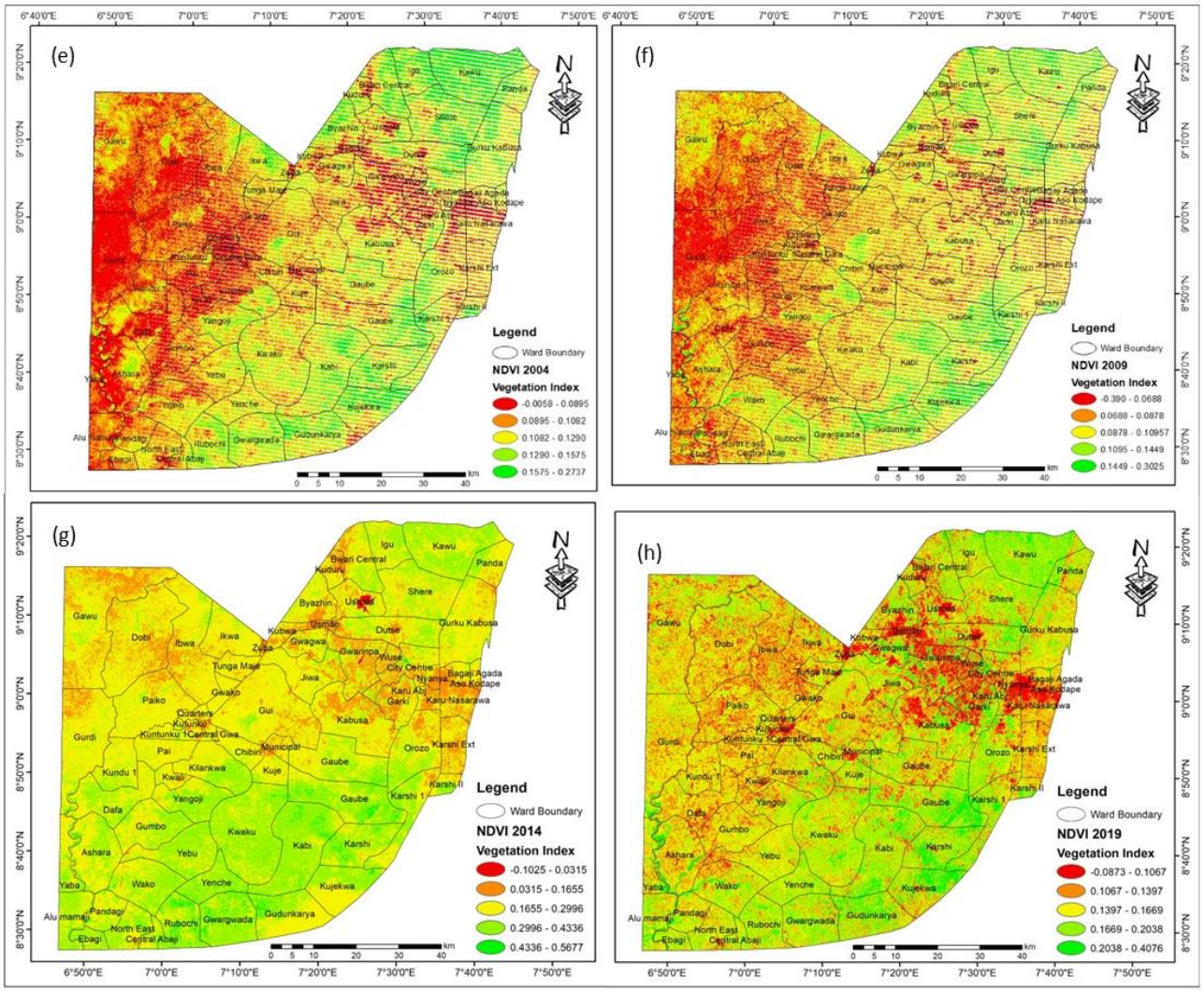
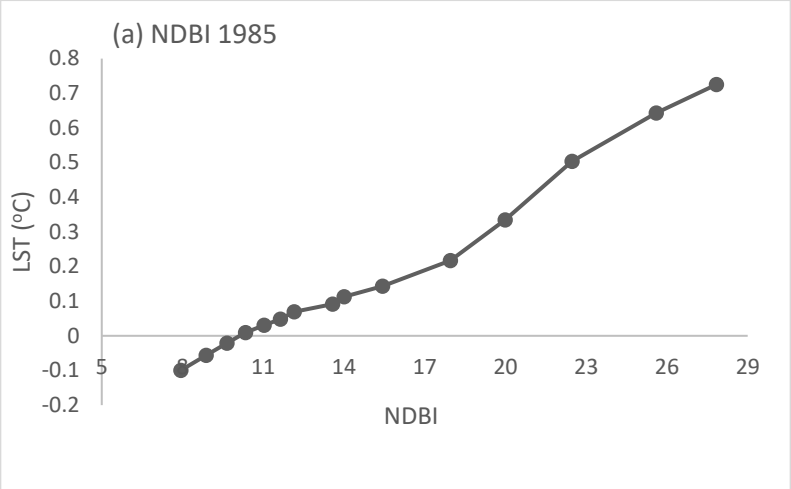


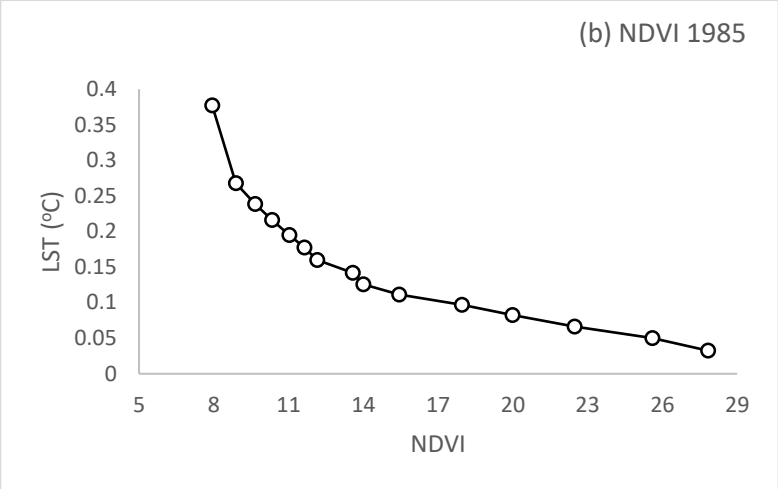
Figure 5.8: NDVI of the study area generated from the Near-infrared and red bands of Landsat images (a) Landsat 4 TM was acquired at 09:15Z of November 27, 1985; (b), (c), and (d) Landsat 5 TM acquired on February 16, 1990, May 12, 1994, and December 6,

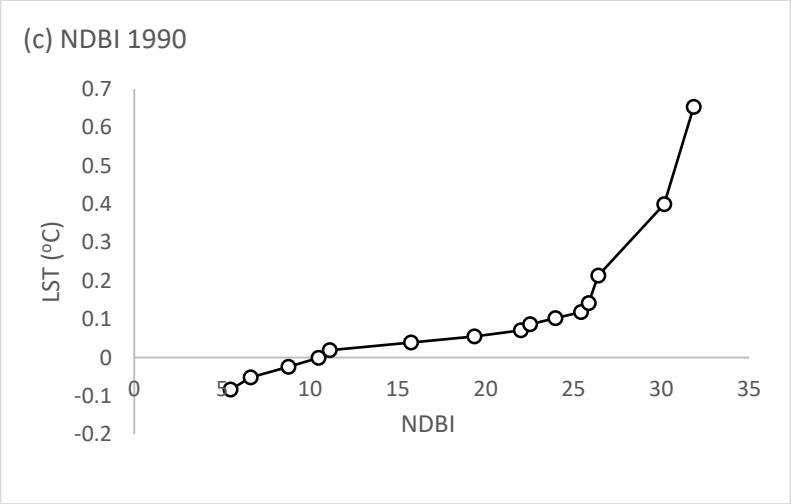
1999, at 09:15Z; (e) and (f) Landsat 7 ETM of April 21, 2004, and March 30, 2009, acquired at 09:38Z; (g) and (h) Landsat 8 OLI-TIRS of December 4, 2014, and February 26th, 2019 acquired at 09:49Z.

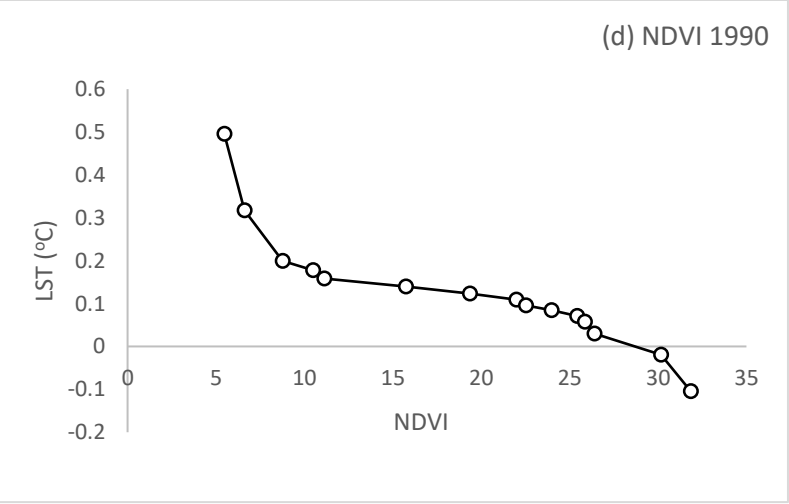
Table 5.7: Classification of LST, NDBI, and NDVI index values based on their land use/cover type

Land use/cover	1986			1990			1994			1999			2004			2009			2014			2019		
	LST	NDBI	NDVI	LST	NDBI	NDVI	LST	NDBI	NDVI	LST	NDBI	NDVI	LST	NDBI	NDVI	LST	NDBI	NDVI	LST	NDB1	NDVI	LST	NDBI	NDVI
Forest land	7.93	-0.10	0.38	5.47	-0.08	0.50	5.32	-0.09	0.35	12.82	-0.51	0.73	9.48	-0.07	0.27	11.62	-0.07	0.30	15.71	-0.23	0.57	23.18	-0.13	0.41
	8.88	-0.06	0.27	6.61	-0.05	0.32	5.55	-0.06	0.25	13.70	-0.18	0.37	10.21	-0.04	0.21	11.97	-0.03	0.21	18.07	-0.20	0.52	26.19	-0.08	0.28
	9.65	-0.02	0.24	8.77	-0.02	0.20	6.75	-0.02	0.23	14.95	-0.09	0.31	10.79	-0.02	0.19	12.10	0.00	0.19	20.43	-0.16	0.48	27.50	-0.05	0.25
Shrubs/Grassland	10.34	0.01	0.22	10.49	0.00	0.18	8.95	0.01	0.20	16.52	-0.04	0.26	11.37	0.00	0.18	12.11	0.02	0.16	22.93	-0.13	0.43	28.55	-0.02	0.23
	11.03	0.03	0.20	11.11	0.02	0.16	10.15	0.03	0.18	17.77	0.01	0.22	11.96	0.02	0.16	13.01	0.04	0.14	25.44	-0.09	0.39	29.59	0.01	0.21
	11.63	0.05	0.18	15.74	0.04	0.14	11.32	0.05	0.16	19.02	0.07	0.17	12.47	0.04	0.15	14.79	0.06	0.13	27.50	-0.05	0.34	30.77	0.04	0.19
Cropland	12.14	0.07	0.16	19.36	0.05	0.12	15.48	0.07	0.14	20.26	0.12	0.13	14.98	0.05	0.14	16.58	0.07	0.11	29.12	-0.02	0.30	31.82	0.05	0.18
	13.57	0.09	0.14	21.99	0.07	0.11	16.65	0.09	0.13	21.51	0.18	0.10	16.42	0.07	0.13	18.26	0.09	0.10	30.60	0.02	0.25	32.87	0.07	0.16
	14.00	0.11	0.13	22.52	0.09	0.10	17.80	0.10	0.12	22.45	0.22	0.08	18.78	0.09	0.12	20.04	0.10	0.08	32.07	0.05	0.21	33.78	0.09	0.15
Bareland	15.43	0.14	0.11	23.97	0.10	0.08	18.94	0.12	0.10	23.70	0.26	0.05	20.15	0.10	0.11	22.72	0.12	0.07	33.55	0.08	0.17	34.70	0.11	0.13
	17.95	0.22	0.10	25.42	0.12	0.07	18.08	0.13	0.08	25.31	0.30	0.02	22.51	0.11	0.10	24.28	0.13	0.06	35.02	0.10	0.12	35.48	0.12	0.12
	19.98	0.33	0.08	25.86	0.14	0.06	20.25	0.16	0.07	26.56	0.32	-0.02	25.95	0.15	0.09	27.84	0.19	0.03	36.35	0.11	0.08	36.27	0.13	0.10
impervious surface	22.47	0.50	0.07	26.40	0.21	0.03	24.45	0.23	0.05	28.80	0.35	-0.05	28.12	0.28	0.08	30.40	0.35	-0.02	37.67	0.13	0.03	37.06	0.19	0.08
	25.59	0.64	0.05	30.17	0.40	-0.02	28.15	0.44	0.01	30.67	0.39	-0.13	32.18	0.53	0.07	34.19	0.56	-0.06	39.15	0.15	-0.01	38.10	0.34	0.05
Impervious surface/Water bodies	27.83	0.72	0.03	31.84	0.65	-0.10	32.10	0.68	-0.25	34.31	0.76	-0.27	36.26	0.62	0.05	38.13	0.65	-0.09	45.78	0.58	-0.06	51.46	0.66	0.00

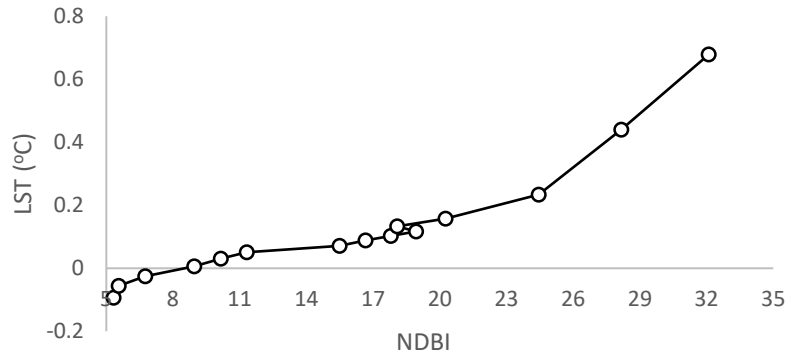

(a) NDBI 1985
LST (ºC)
NDBI
0.8
0.7
0.6
0.5
0.4
0.3
0.2
0.1
0
-0.1
-0.2
5
11
14
17
20
23
26
29


(b) NDVI 1985
LST (ºC)
NDVI
0.4
0.35
0.3
0.25
0.2
0.15
0.1
0.05
0
5
8
11
14
17
20
23
26
29

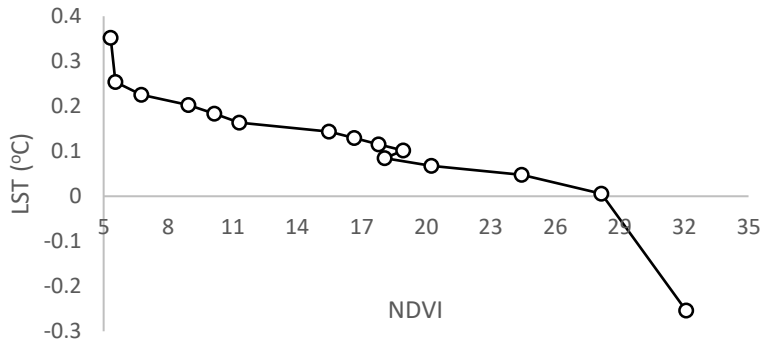

(c) NDBI 1990
LST (ºC)
NDBI
0.7
0.6
0.5
0.4
0.3
0.2
0.1
0
-0.1
-0.2
0
5
10
15
20
25
30
35


(d) NDVI 1990
LST (ºC)
NDVI
0.6
0.5
0.4
0.3
0.2
0.1
0
-0.1
-0.2
0
5
10
15
20
25
30
35

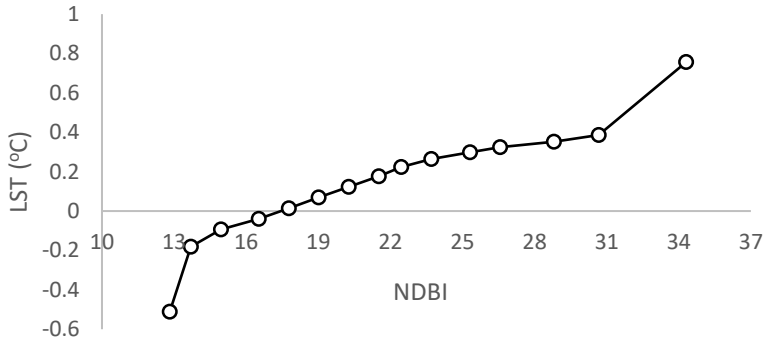
(e) NDBI 1994



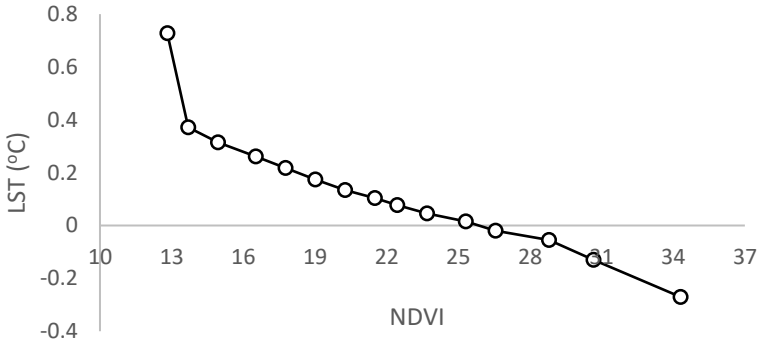
(f) NDVI 1994

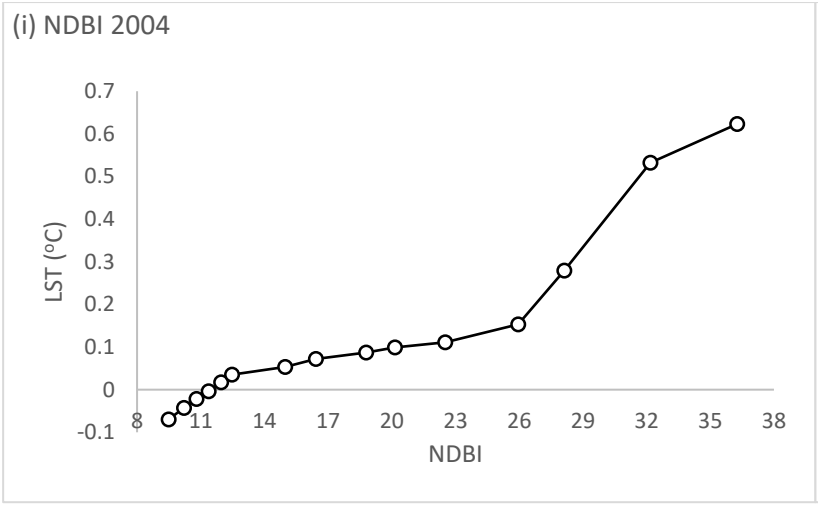


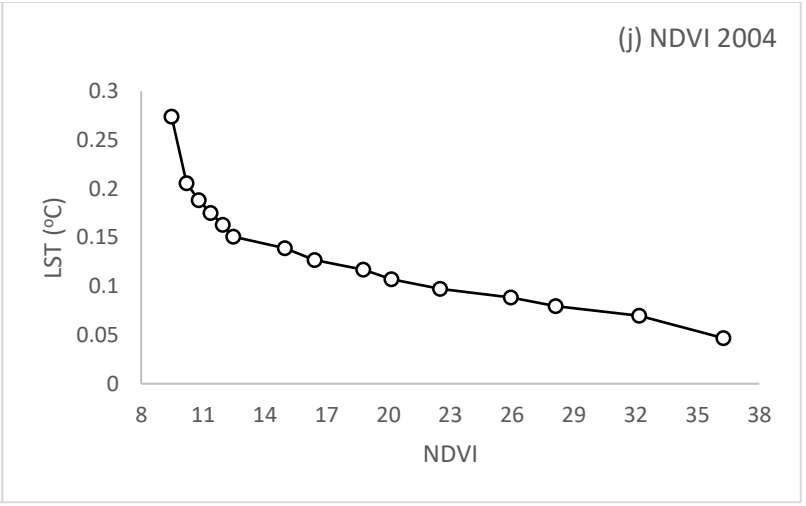
(g) NDBI 1999

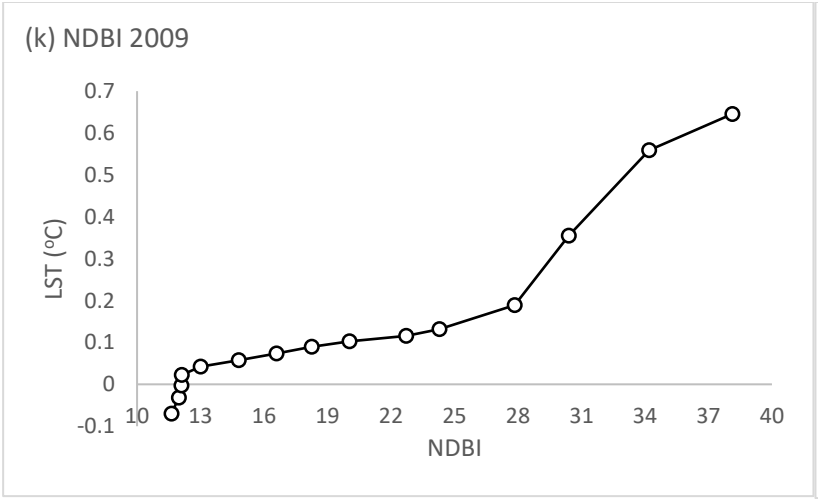


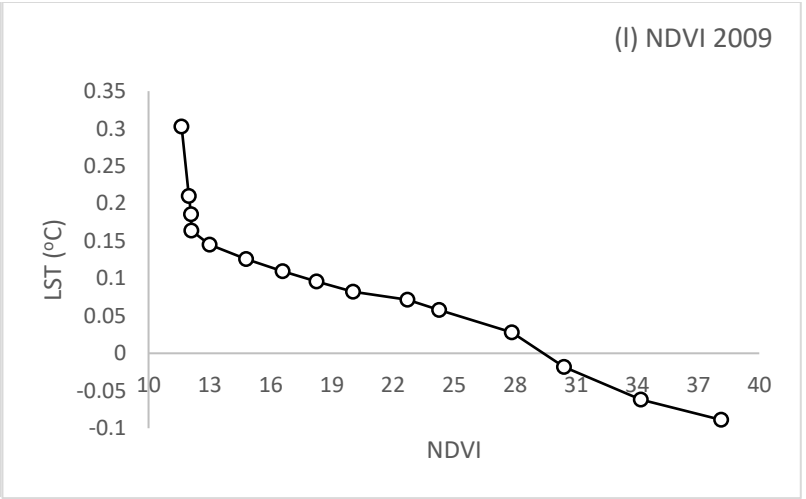
(h) NDVI 1999




(i) NDBI 2004
LST (°C)
NDBI
0.7
0.6
0.5
0.4
0.3
0.2
0.1
0
-0.1
8 11 14 17 20 23 26 29 32 35 38


(j) NDVI 2004
LST (°C)
NDVI
0.3
0.25
0.2
0.15
0.1
0.05
0
8 11 14 17 20 23 26 29 32 35 38


(k) NDBI 2009
LST (°C)
NDBI
0.7
0.6
0.5
0.4
0.3
0.2
0.1
0
-0.1
10 13 16 19 22 25 28 31 34 37 40


(l) NDVI 2009
LST (°C)
NDVI
0.35
0.3
0.25
0.2
0.15
0.1
0.05
0
-0.05
-0.1
10 13 16 19 22 25 28 31 34 37 40

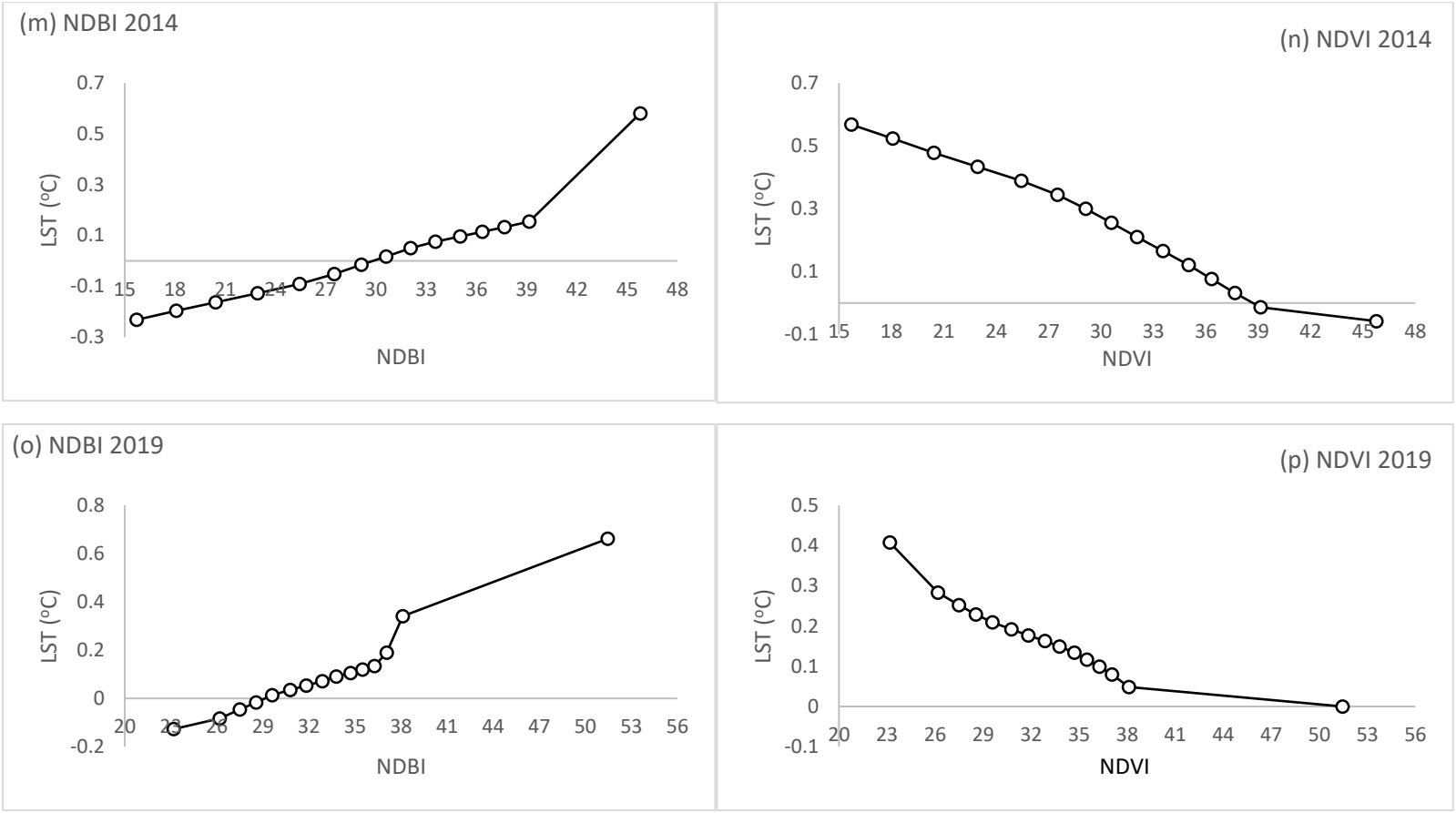


Figure 5.9: Scatterplots of LST, NDVI and NDBI (a) 1986 LST and NDBI, (b) 1986 LST and NDVI, (c) 1990 LST and NDBI, (d) 1990 LST and NDVI, (e) 1994 LST and NDBI, and (f) 1994 LST and NDVI (g) 1999 LST and NDBI (h) 1999 LST and NDVI (i) 2004 LST and NDBI (j) 2004 LST and NDVI (k) 2009 LST and NDBI (l) 2009 LST and NDVI (m) 2014 LST and NDBI (n) 2014 LST and NDVI (o) 2019 LST and NDBI (p) 2019 LST and NDVI. Note: The dependent variable was LST, while the independent variables were NDBI and NDVI.

5.9 The relationship between AIS, UHI, and the NDVI

The thermal and index values of the LST, NDBI, and NDVI were investigated using a regression model to spatially characterise their quantitative relationship as shown in Figures 5.9, and Table 5.7. Built-up areas were observed to have the highest index value compared to other land use/cover classes, followed by bare land. Cultivated lands and vegetation cover had the lowest to moderate NDBI index values. As measured by the NDVI index, water bodies are expected to have a negative index value. For the study period (1986 to 2019), comparing the relationship between LST, NDBI, and NDVI, implies that urban expansion has led to an increase in the thermal environment of Abuja, which is linked to environmental changes such as the removal of vegetation cover in place of AIS (e.g., concrete, metal, and asphalt). Standard deviation values between the LST and NDVI indicated heterogeneity and propositional differences in the abundance of vegetation in all surface materials. The regression model revealed that the regression coefficient between LST, NDBI, and NDVI in the eight (8) Landsat images shows that the urban expansion has an intensifying effect on the surface temperature of Abuja that enhances the UHI effect.

Remote sensing data are an essential resource for researching environmental dynamics at the local or global scale. The normalised difference built-up index (NDBI) is one of the various indexes for built-up area analysis. Zha *et al*. (2003) introduced the NDBI to map urban built-up areas automatically. The approach exploits the distinct spectral responses of urban and other land cover types. Through the mathematical manipulation of recorded NDVI and NDBI images produced from satellite data, urban areas are effectively mapped. However, the method provided by Zha *et al.* (2003) recodes the NDBI and NDVI images to construct binary images based on the idea that a positive NDBI value should represent urbanised regions and a positive NDVI value should show vegetation. This recording procedure cannot distinguish metropolitan regions from the barren and bare ground (Bhatti & Tripathi, 2014).

The study quantifies the link between LST and green areas by demonstrating how LST changes by land use/cover. The presence of vegetation is one factor that distinguishes land use/cover. The relationship between LST, AIS, and the

vegetation cover was investigated using a regression model. This research used satellite images to calculate NDVI as a proxy for photosynthetic activity, which can be used to detect the presence of vegetation. There is a relationship between LST, NDVI, and NDBI. Despite the wide range of variability and overlap within the land use/cover categories, the data show that the most developed land has the greatest LST and NDBI and the lowest NDVI values.

These results suggest that urbanisation and land use/cover changes have severely diminished vegetation, resulting in increased surface UHI (Simwanda *et al*., 2019; Halder *et al*., 2021). UHI influences the environment by increasing energy consumption, harming life quality and human health (Rinner *et al*., 2010; Wu *et al*., 2022). According to Lin *et al*. (2011), Doick *et al*., (2014), and Karakus (2019), evapotranspiration by plants and water bodies cools the environment while enhancing albedo by 15% over artificial impervious surfaces due to lower heat energy absorption and more reflected longwave radiation. Similarly, vegetation reduces incident shortwave radiation, cools the environment, and lowers carbon levels in the atmosphere, making it a viable approach for reducing UHIs (Ming *et al*., 2014; Adeyeri *et al*., 2017). Findings from this study show that the vegetation cover of Abuja and its environs tends to diminish with the environmental transformation, as seen in other rapidly rising cities (Kumar & Shekhar, 2015; Pal & Ziaul, 2017; Kafy *et al*., 2022). Due to their relative similarity in pixel value, using the NDVI to determine the effects caused by bare and impermeable surfaces can be challenging (Khanal *et al*., 2019; Zhu *et al*., 2021). Similar findings were found in Anshun City, China (Deng *et al.*, 2017), Hoshangabad, India (Malik & Shukla, 2019), and Ibadan, Nigeria (Fashae *et al*., 2020). According to their findings, the cool-island effect from vegetation covers such as forests, Shrublands, and green areas have lower LST within cities. Substantial LST hot spots were detected in built-up regions and bare surfaces, while substantial cold spots were on vegetated surfaces and water bodies. This suggests that important clusters of high LST correspond to places void of vegetation. On vegetated surfaces, however, substantial clusters of low LST were identified. This implies that vegetation considerably impacts surface temperature change. This study found that the rate of land use/cover changes

poses a major environmental hazard. The manifestations of these changes are the rapid disappearance of vegetation cover, leading to soil erosion, loss of biodiversity, and hydrological changes. In recent years, essential progress has been made in quantifying urban expansion-driven land use/cover changes in tropical Africa. However, more research is needed to estimate the future importance of land use/cover change in the functioning of the earth system and define prerequisites for sustainable land use. Anthropogenic activities have been discovered to cause changes that substantially interact with natural environmental variability, resulting in environmental damage in locations where urban land use is not effectively planned. These are the general implications of the trend identified in Abuja.

5.10 Conclusion

This chapter examined the spatiotemporal change of urban expansion and its effects on the LST and UHI of Abuja over the study periods. When comparing the LST of AIS from 1986 to 2019, it is clear that the severity of LST has increased, with settlement development being the primary cause. As a result, higher LSTs are recorded in the informal settlements. There is also a low potential for UHI formation in settlements away from the city centre, characterised by suburban and rural settings. The LST model for urban thermodynamics was developed using relevant remote sensing indices and spatial statistics such as NDBI and NDVI. The chapter concludes that built-up areas and vegetation affect LST. It should be noted that the satellite images and resulting LST and NDVI depictions in this study are snapshots in time and do not represent systematic, consistent depictions of surface conditions in a longitudinal study. For example, it was intended that the Landsat image for this study would be consistent during the hot/dry season to compare the images spatially and temporally to detect changes. However, the difficulty in obtaining consistent cloud-free images during the summer months makes it impossible to compare the images and detect LST hotspots, which in most cases, have disappeared over time due to seasonal timing inconsistencies. The sixth chapter of this study will assess the effects of maximum temperatures on heat-related mortality.

CHAPTER SIX: ASSOCIATIONS BETWEEN TEMPERATURE AND HEAT-RELATED MORTALITY

6.0 Introduction

The effect of extreme heat on human health is influenced by the age structure of the population, season, geographic location, and other potential confounding factors, such as the adaptive capacity of the population to climate change and their socioeconomic status (Kouis *et al.,* 2019; Ebi *et al*., 2021). This chapter presents the relationship between maximum temperature and heat-related mortality in Abuja and its environs. Excess mortality was assessed in each of the research area's six sub-regions to understand their spatial variations. Empirical statistical models that describe the relationship between excess mortality and maximum temperature at a monthly scale were developed. Only maximum temperatures were considered in this study. The relationships between maximum temperature and heat-related mortality provided in this chapter are based on a 3rd order polynomial regression utilising a 4-month moving average baseline.

6.1 Justification for the choice of 4-month moving average baseline

Using the temperature intervals and the excess mortality count computed from the observed-expected mortality, the regression was plotted for the 4-month-moving average and the monthly average baseline. This was aimed at understanding the models' strength and their significance level. The temperature intervals are the independent variable (x), whereas the excess mortality count is the dependent variable (y). Six regression plots were performed for each of the hospitals of the six area councils. The model output from the 4-month-moving average and the monthly average baselines were presented in Table 6.1 and Figure 6.1.

From the 4-month-moving average baseline, the regression output for the University of Abuja Teaching Hospital, Gwagwalada, shows an R^2 value of 0.49. The model result from the monthly-average baseline suggested an R^2 of 0.14. Comparing the *p*-value from the two baselines at a confidence level of 0.05

reveals that the *p*-value from the 4-month-moving average baseline was *p*: 0.0016, while the *p*-value from the monthly-average baseline was 0.13, as shown in Table 6.1.

When compared to the R^2 and *p*-value from the National Hospital Abuja, the R^2 from the 4-month-moving average baseline is more potent (R^2:0.26) compared to the monthly average baseline (R^2:0.10). Both the 4-month-moving average and the monthly average baseline model were significant at the 95% confidence level, with the 4-month-moving average producing the more significant results (*p*-value: 0.048 vs *p*-value: 0.24). The model output from the 4-month-moving average and the monthly average baseline from the Kuje general hospital are both significant at the 0.05 level (*p*-values: 0.00045 and *p*-value: 0.010). However, the 4-month-moving average's R^2 value: 2: 0.57 is more robust than the monthly average baseline's R^2 value: 2:0.36).

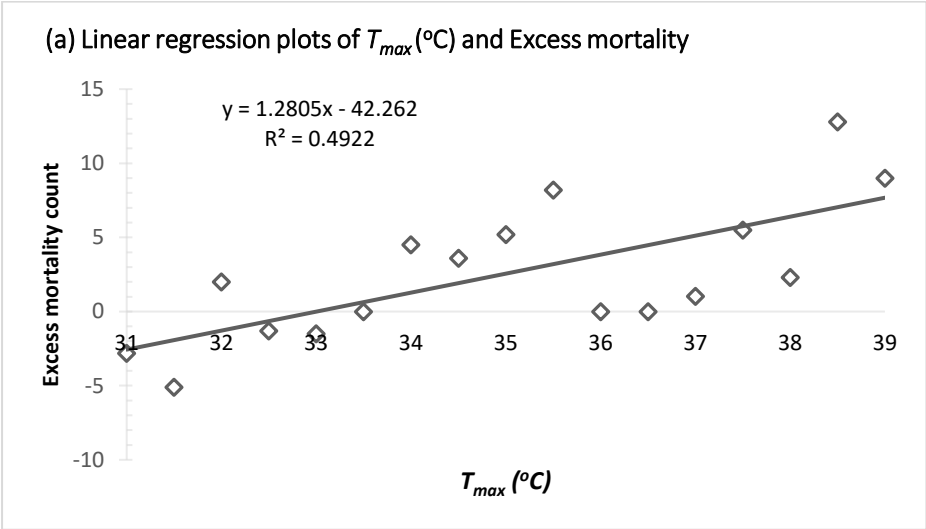
The result of the model based on a 4-month-moving average and a monthly average baseline is shown in Table 6.1. The output from the 4-month-moving average baseline has an R^2: 0.56 and a *p*-value: 0.00019, whereas the output from the monthly average baseline has an R^2: 0.41 and a *p*-value: 0.0027. The model output from the specialist hospital Mararaba indicates that the 4-month-moving average has an R^2: 0.58 and a *p*-value: 0.00012. The monthly average baseline has a R^2: 0.27and a *p*-value: 0.022. The Abaji general hospital's R^2 from the 4-month-moving average baseline was R^2: 0.36, with a *p*-value: 0.010. The R^2 and *p*-value for the monthly average baseline were R^2: 0.27 and *p*-value: 0.031, respectively.

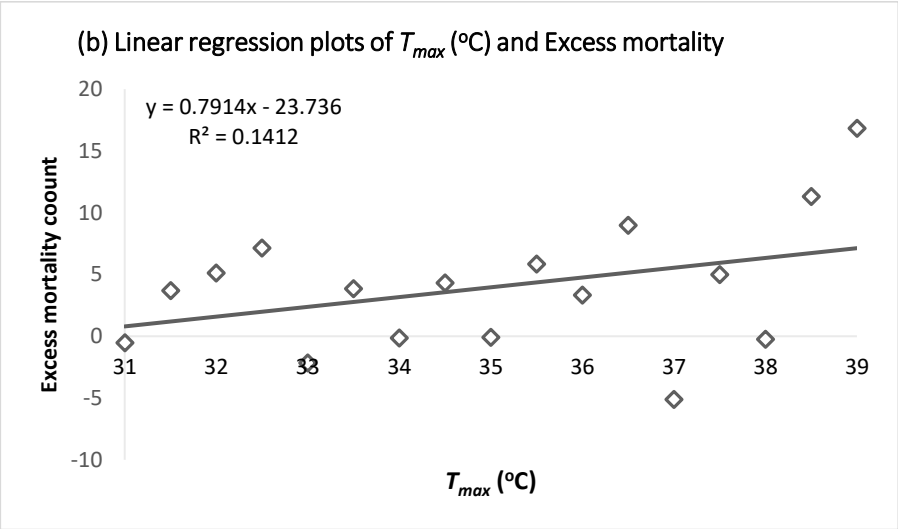
Table 6.1: Regression output from the 4-months-moving average and the monthly average baseline.

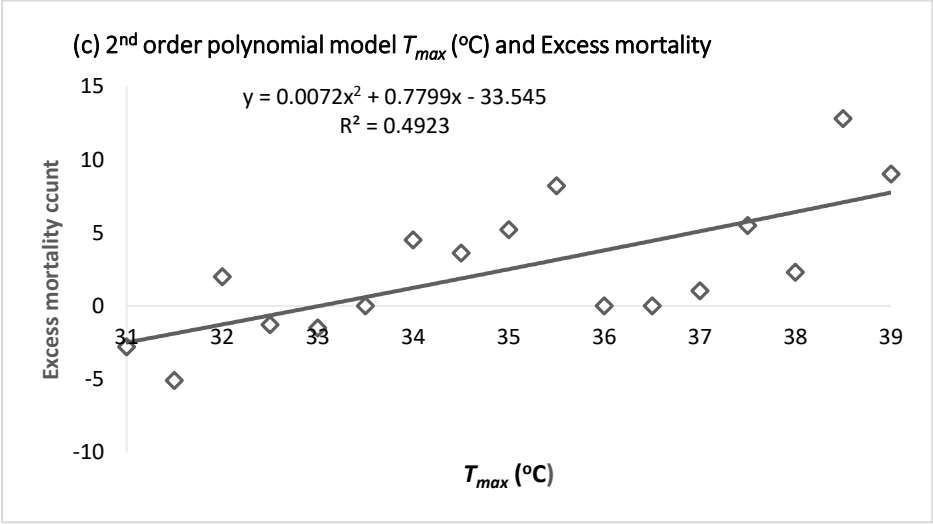
Location	4-month-moving average baseline					Monthly average baseline				
	R^2	Regression equation	Significance level	*p*-value	Standard error	R^2	Regression equation	Significance level	*p*-value	Standard error
Teaching Hospital Gwagwalada	0.49	$y = 1.2805x - 42.262$	0.05	0.0016	3.39	0.14	$y = 0.7914x - 23.736$	0.05	0.13	5.09
National Hospital Abuja	0.26	$y = 0.2821x - 2.6561$	0.05	0.048	1.08	0.10	$y = 0.2707x - 2.0037$	0.05	0.24	1.85
General Hospital Kuje	0.57	$y = 0.8324x - 23.832$	0.05	0.00045	1.88	0.36	$y = 0.7961x - 21.698$	0.05	0.010	2.74
General Hospital Kwali	0.56	$y = 25.506x - 721.72$	0.05	0.00019	64.50	0.41	$y = 24.475x - 605.24$	0.05	0.0027	83.61
Specialist Hospital Mararaba	0.58	$y = 18.829x - 455.98$	0.5	0.00012	45.58	0.27	$y = -5.0667x + 321.69$	0.05	0.022	24.00
General Hospital Abaji	0.36	$y = 0.876x - 24.489$	0.05	0.010	3.02	0.27	$y = 0.7696x - 20.113$	0.05	0.031	3.28

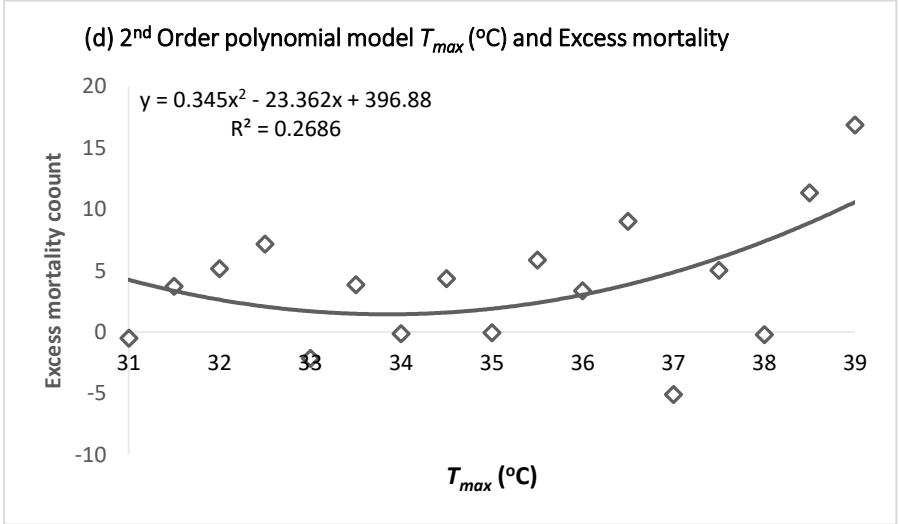
6.2 Rationale for the use of a polynomial model of the third order

Quadratic functions are widely used to construct curves that describe the temperature-mortality association. The temperature-mortality curves' various shapes show the temperatures based on risk elements. Much prior research has revealed the most common shapes as U-, J-, V-, and W-shaped. To select whether to employ one or two going forward models, both models were examined by studying the 2^{nd}, 3^{rd}, and 4^{th} orders of polynomial models. This will aid in comparing and selecting the models that best suit the data. Non-linear regression at the second, third, and fourth polynomial orders demonstrated a stronger association. Compared to the other models, the 3-rd order polynomial model with a 4-month-moving average baseline shows a better relationship between maximum temperature and mortality. The R^2 value for the 3-rd order regression model from the 4-months moving average baseline shows a strong positive correlation between maximum temperature and mortality. The model also offers a progressive increase in excess mortality as temperature rises. These are compared to other models from the second and fourth polynomial orders, which appear to underestimate the genuine relationship when the temperature is low and overestimate the true relationship when the temperatures are high. Figure 6.1 (a) shows the linear regression plots of maximum temperature and excess mortality count from the 4-month moving average baseline at the University of Abuja Teaching Hospital Gwagwalada, and (b) from the monthly average baseline, (c) second-order polynomial model from the 4-month-moving average baseline, (d) second-order polynomial model from the monthly average baseline, (e) third order polynomial model from the 4-month-moving average baseline, (f) monthly average baseline from third order polynomial model, (g) fourth order polynomial model from the 4-month-moving average baseline, (h) fourth order polynomial model from the monthly average baseline. Figures 6.2-6.6 show linear and nonlinear regressions for the association between maximum temperature and excess mortality count for the remaining five hospitals in the study area.


(a) Linear regression plots of T_{max} (°C) and Excess mortality
y = 1.2805x - 42.262
R² = 0.4922
Excess mortality count
T_{max} (°C)


(b) Linear regression plots of T_{max} (°C) and Excess mortality
y = 0.7914x - 23.736
R² = 0.1412
Excess mortality coount
T_{max} (°C)


(c) 2nd order polynomial model T_{max} (°C) and Excess mortality
y = 0.0072x² + 0.7799x - 33.545
R² = 0.4923
Excess mortality ccunt
T_{max} (°C)


(d) 2nd Order polynomial model T_{max} (°C) and Excess mortality
y = 0.345x² - 23.362x + 396.88
R² = 0.2686
Excess mortality coount
T_{max} (°C)

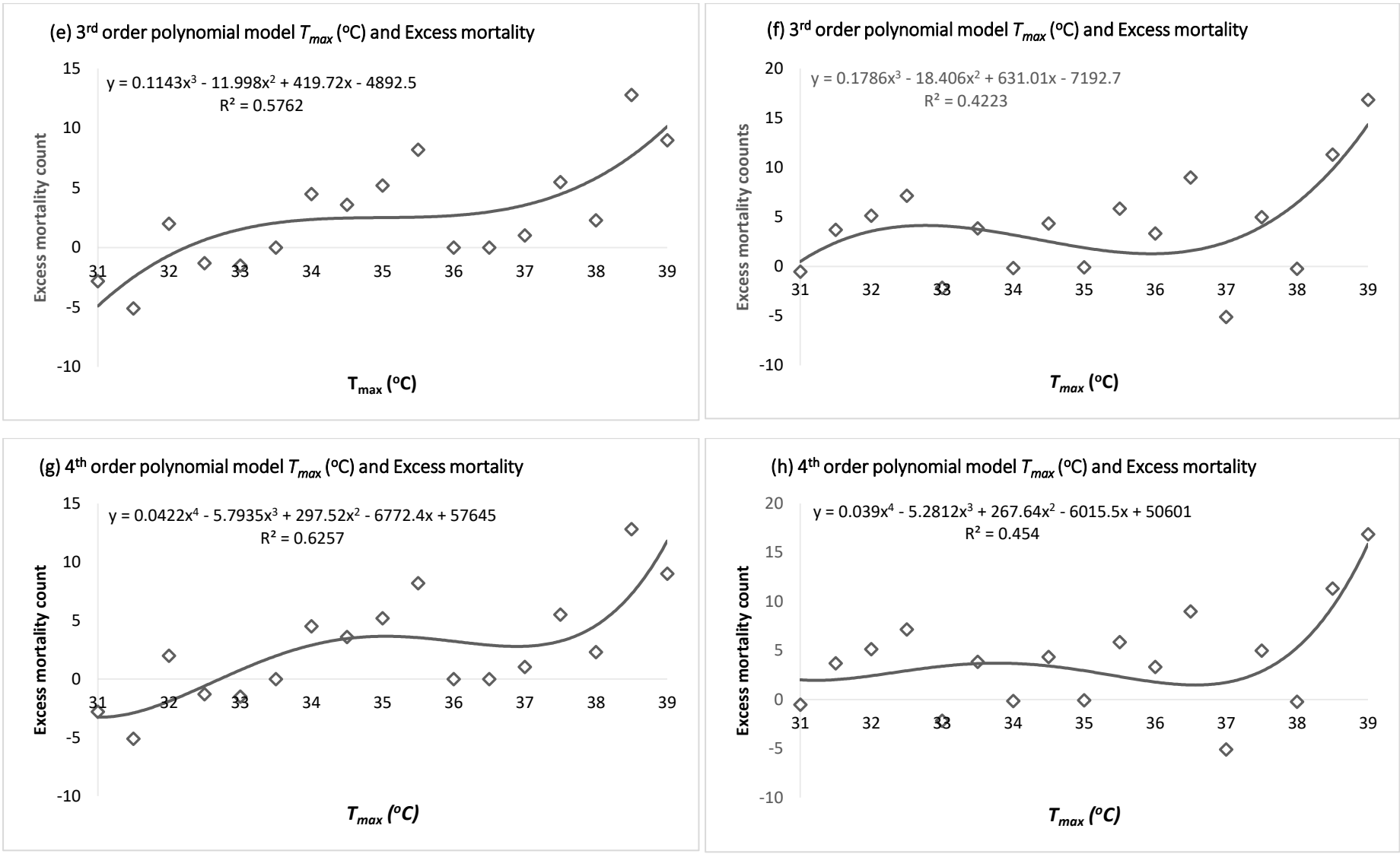
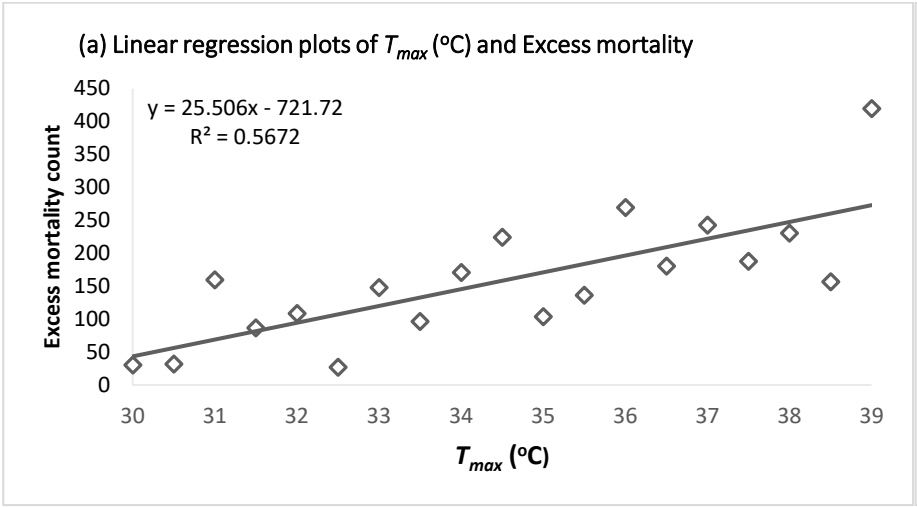
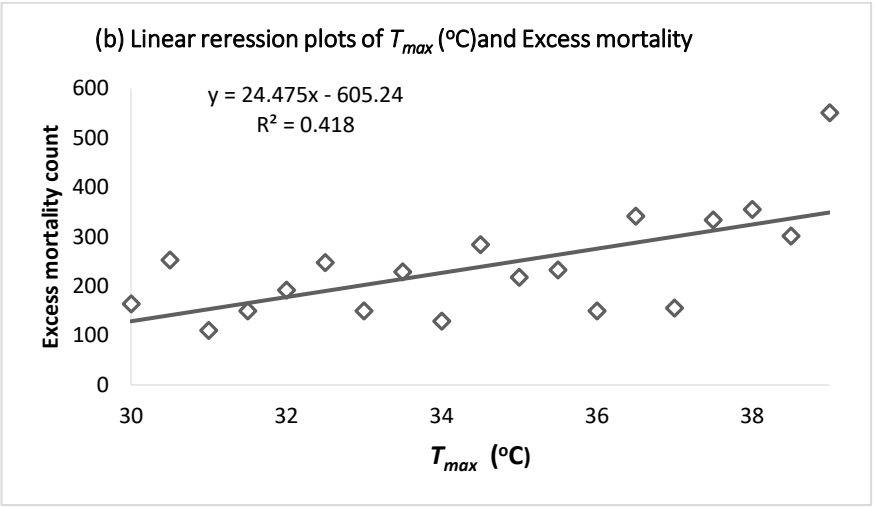
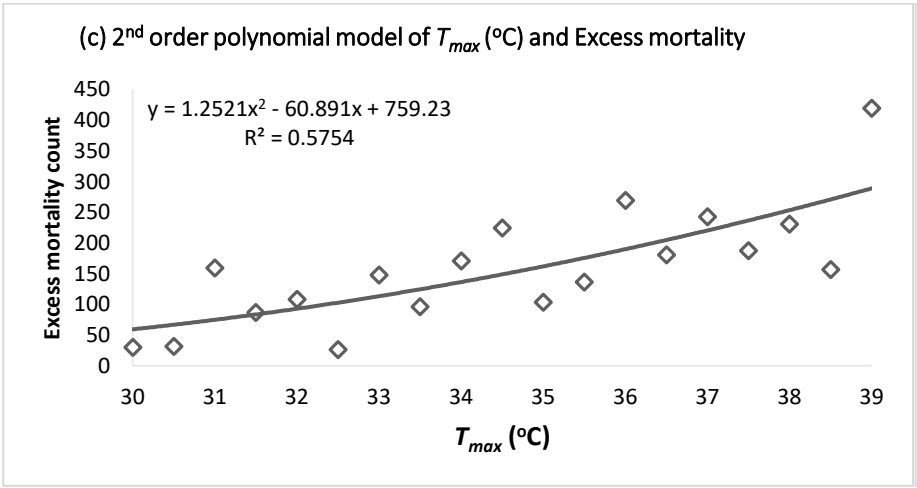
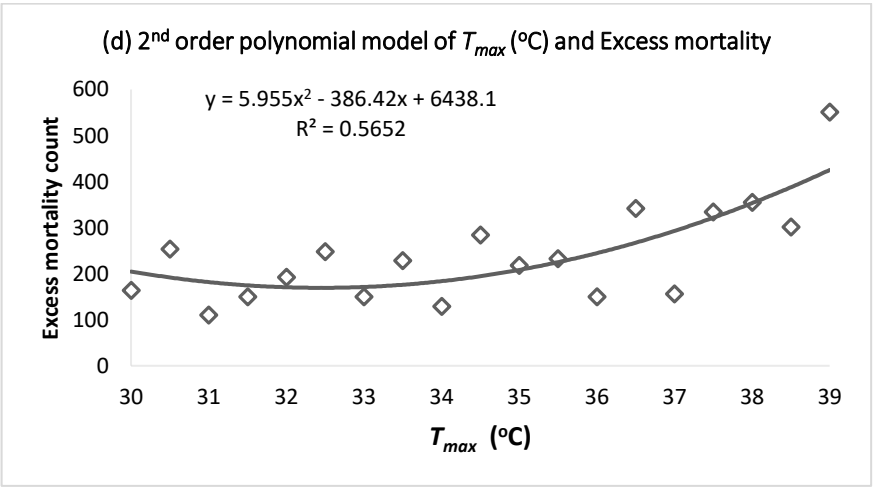


Figure 6.1: Regression plots of *Tmax* (°C) and Excess mortality count of the University of Abuja Teaching Hospital from 4-month moving average (left column) and monthly average baseline (right column).


(a) Linear regression plots of T_{max} (°C) and Excess mortality
y = 25.506x - 721.72
R² = 0.5672
Excess mortality count
T_{max} (°C)


(b) Linear reression plots of T_{max} (°C)and Excess mortality
y = 24.475x - 605.24
R² = 0.418
Excess mortality count
T_{max} (°C)


(c) 2nd order polynomial model of T_{max} (°C) and Excess mortality
y = 1.2521x² - 60.891x + 759.23
R² = 0.5754
Excess mortality count
T_{max} (°C)


(d) 2nd order polynomial model of T_{max} (°C) and Excess mortality
y = 5.955x² - 386.42x + 6438.1
R² = 0.5652
Excess mortality count
T_{max} (°C)

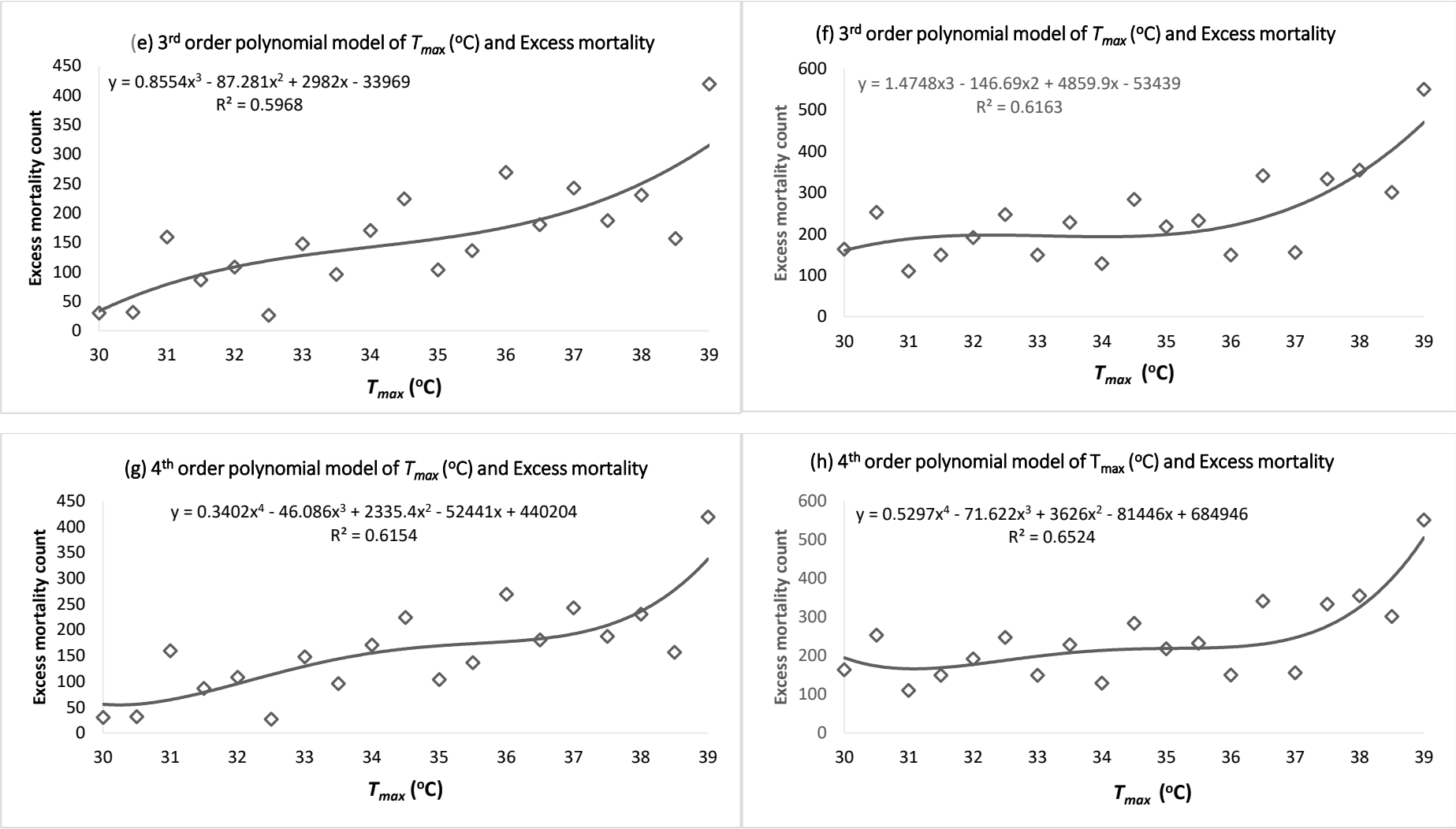
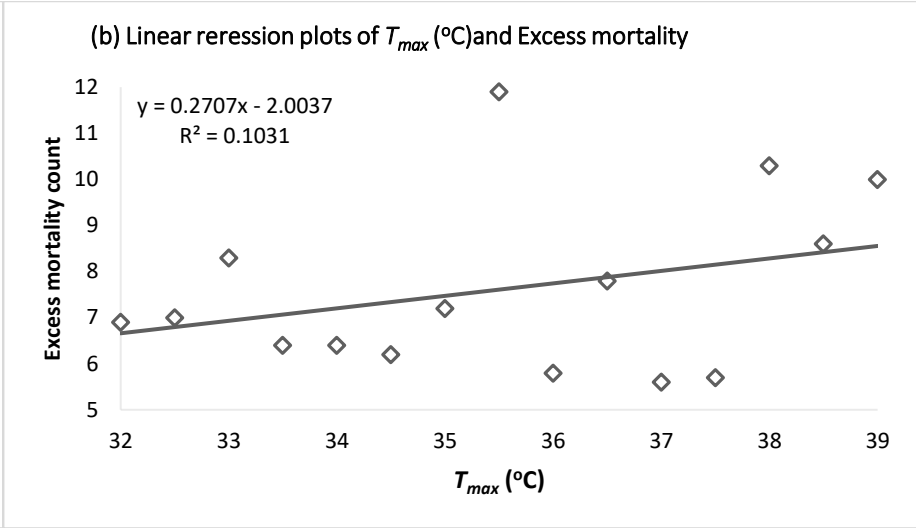
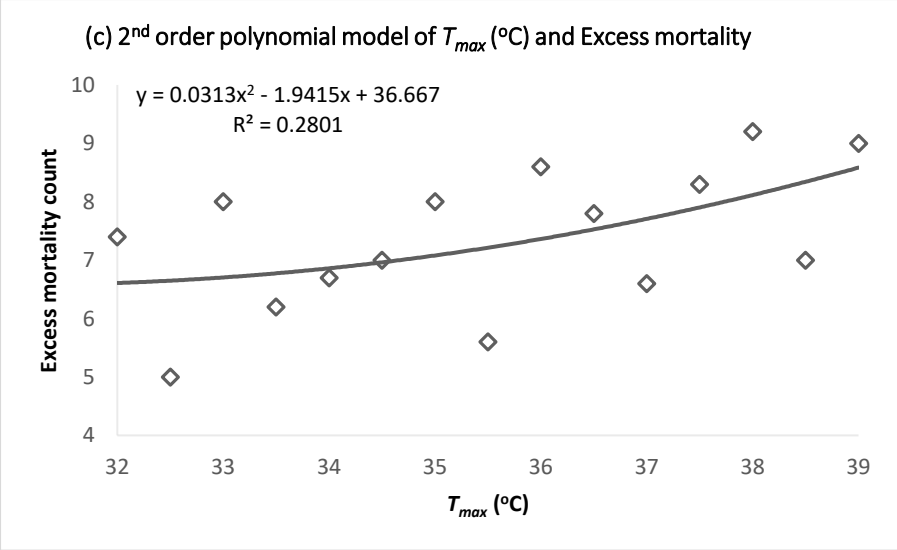
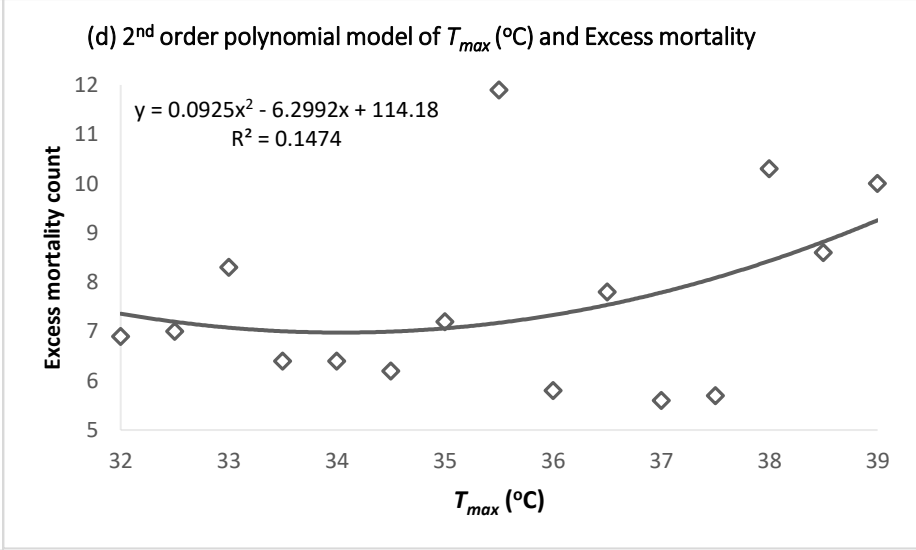


Figure 6.2: Regression plots of *Tmax* (°C) and Excess mortality count of General Hospital Kwali from the 4-month moving average (left column) and monthly average baseline (right column).


(a) Linear regression plots of T_{max} (°C) and Excess mortality
y = 0.2821x - 2.6561
R² = 0.268
Excess mortality count
T_{max} (°C)


(b) Linear reression plots of T_{max} (°C)and Excess mortality
y = 0.2707x - 2.0037
R² = 0.1031
Excess mortality count
T_{max} (°C)


(c) 2nd order polynomial model of T_{max} (°C) and Excess mortality
y = 0.0313x² - 1.9415x + 36.667
R² = 0.2801
Excess mortality count
T_{max} (°C)


(d) 2nd order polynomial model of T_{max} (°C) and Excess mortality
y = 0.0925x² - 6.2992x + 114.18
R² = 0.1474
Excess mortality count
T_{max} (°C)

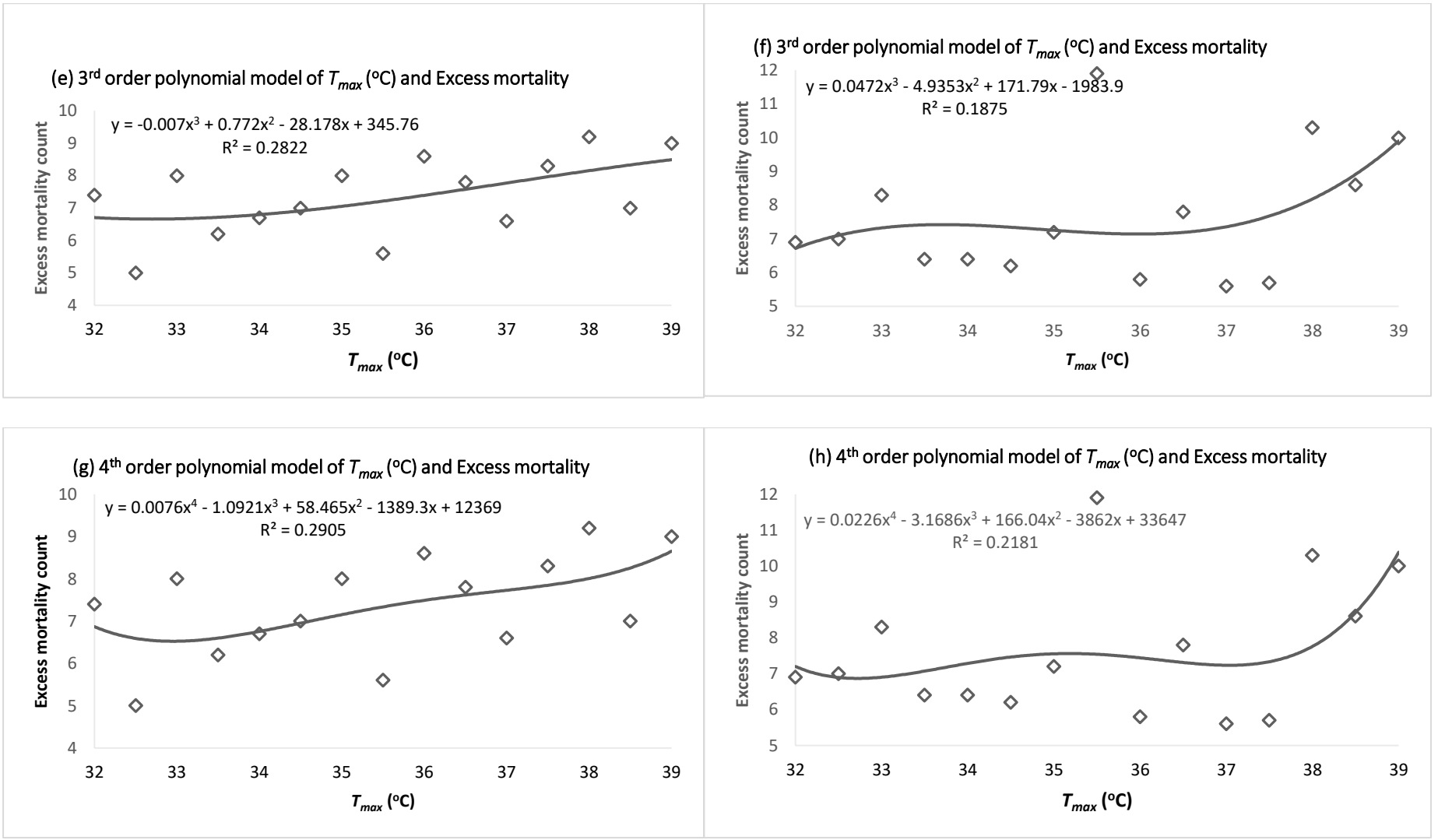
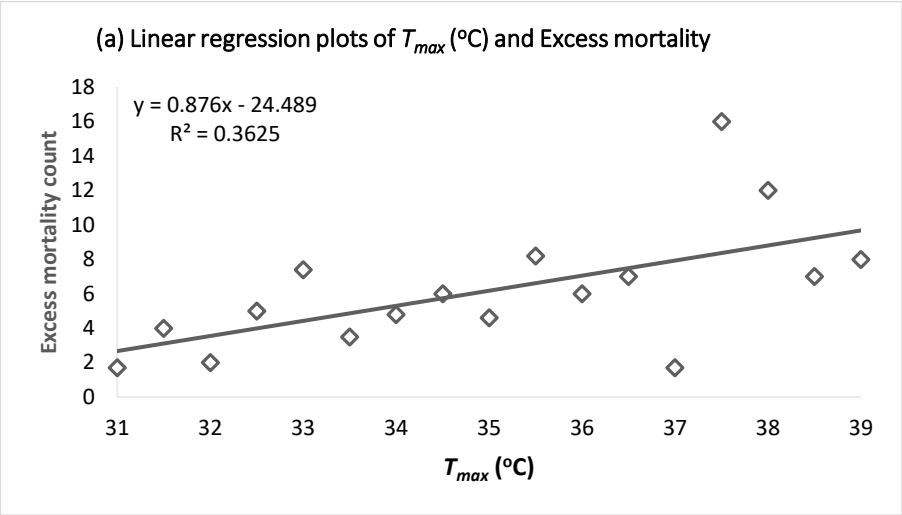
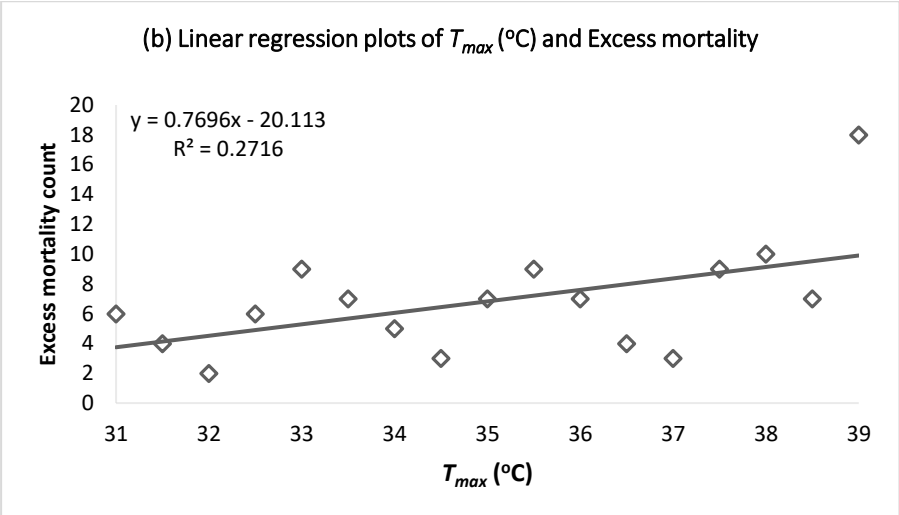
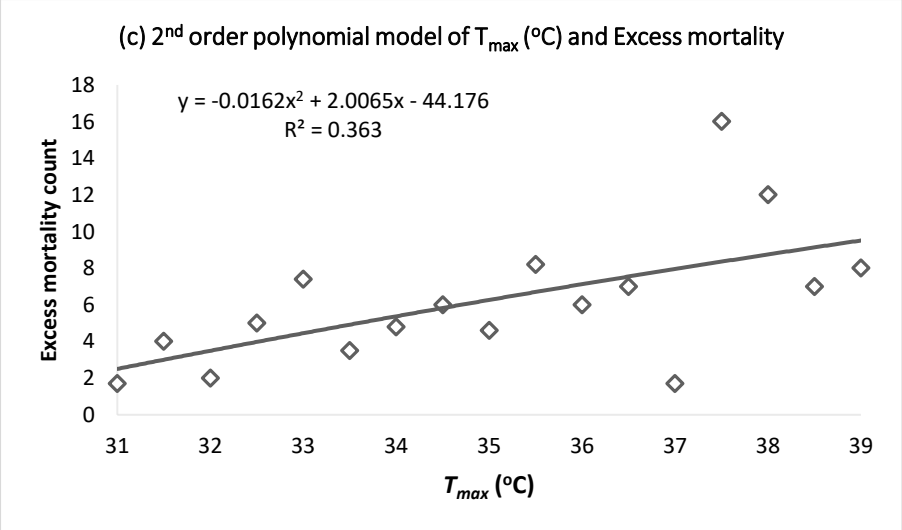
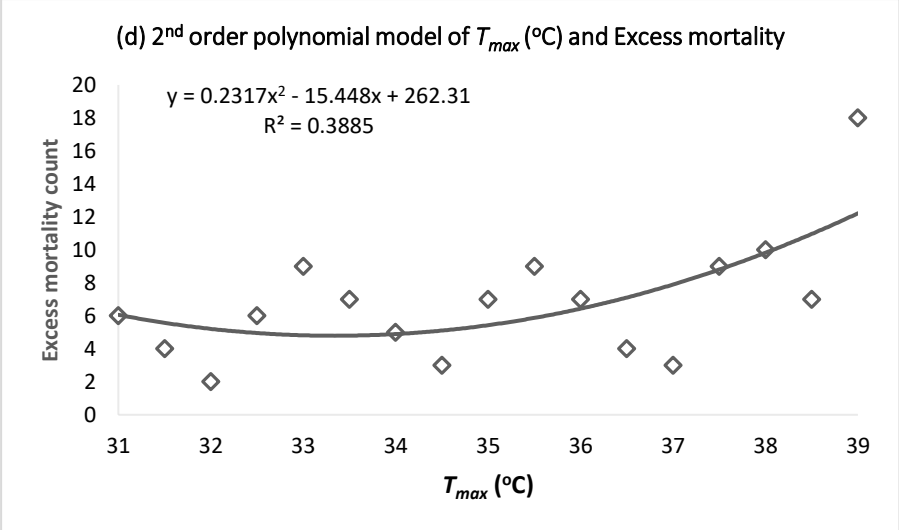


Figure 6.3: Regression plots of *Tmax* (°C) and Excess mortality of National Hospital Abuja from 4-month moving average (left column) and monthly average baseline (right column).


(a) Linear regression plots of T_{max} (°C) and Excess mortality
y = 0.876x - 24.489
R² = 0.3625
Excess mortality count
T_{max} (°C)


(b) Linear regression plots of T_{max} (°C) and Excess mortality
y = 0.7696x - 20.113
R² = 0.2716
Excess mortality count
T_{max} (°C)


(c) 2nd order polynomial model of T_{max} (°C) and Excess mortality
y = -0.0162x² + 2.0065x - 44.176
R² = 0.363
Excess mortality count
T_{max} (°C)


(d) 2nd order polynomial model of T_{max} (°C) and Excess mortality
y = 0.2317x² - 15.448x + 262.31
R² = 0.3885
Excess mortality count
T_{max} (°C)

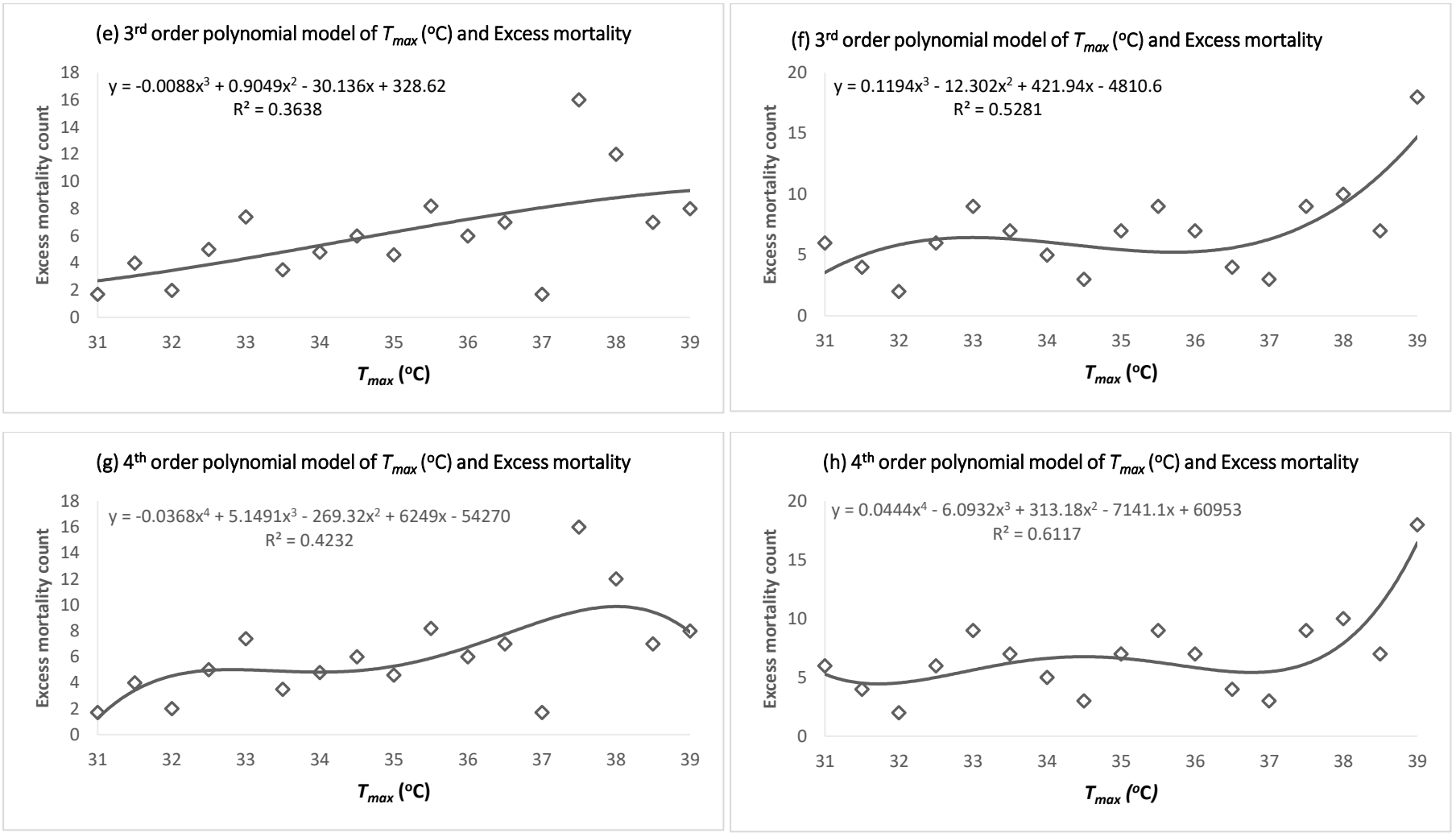
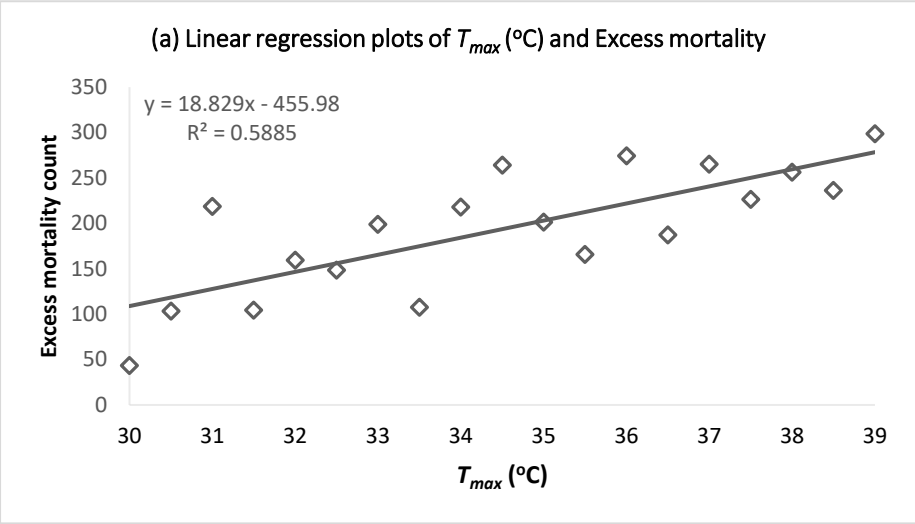
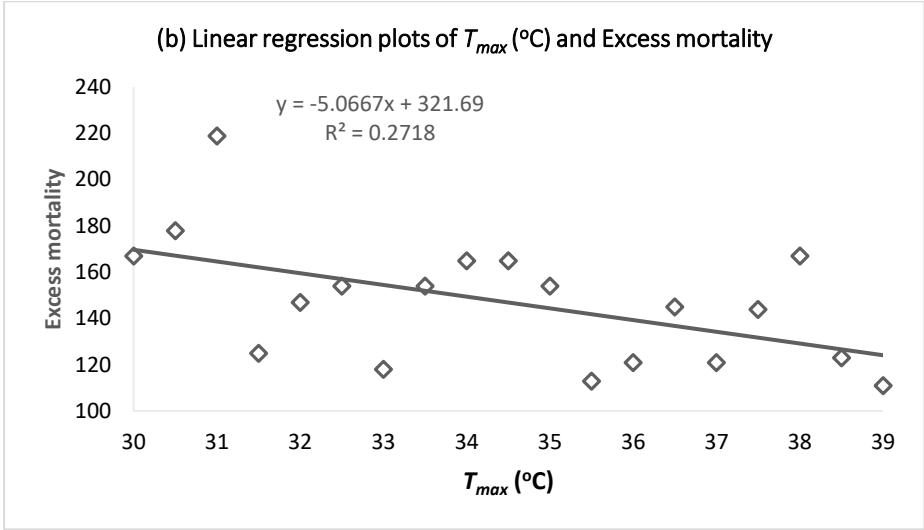
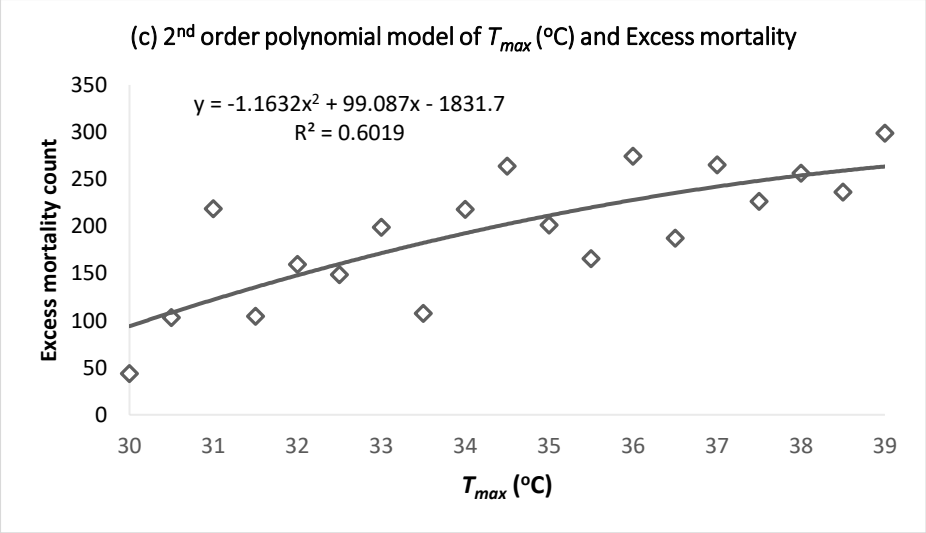
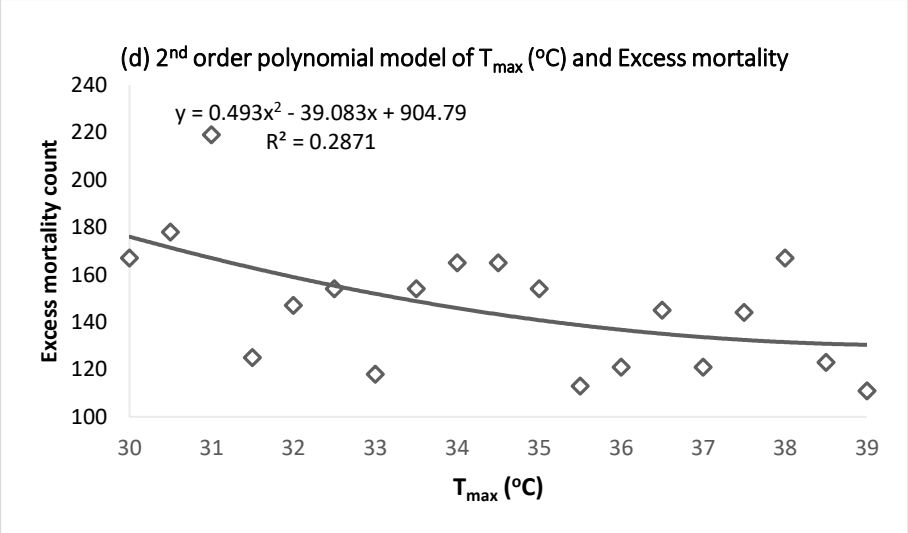


Figure 6.4: Regression plots of *Tmax* (°C) and Excess mortality of General Hospital Abaji from 4-month moving average (left column) and monthly average baseline (right column).


(a) Linear regression plots of T_{max} (°C) and Excess mortality
y = 18.829x - 455.98
R² = 0.5885
Excess mortality count
T_{max} (°C)


(b) Linear regression plots of T_{max} (°C) and Excess mortality
y = -5.0667x + 321.69
R² = 0.2718
Excess mortality
T_{max} (°C)


(c) 2nd order polynomial model of T_{max} (°C) and Excess mortality
y = -1.1632x² + 99.087x - 1831.7
R² = 0.6019
Excess mortality count
T_{max} (°C)


(d) 2nd order polynomial model of T_{max} (°C) and Excess mortality
y = 0.493x² - 39.083x + 904.79
R² = 0.2871
Excess mortality count
T_{max} (°C)

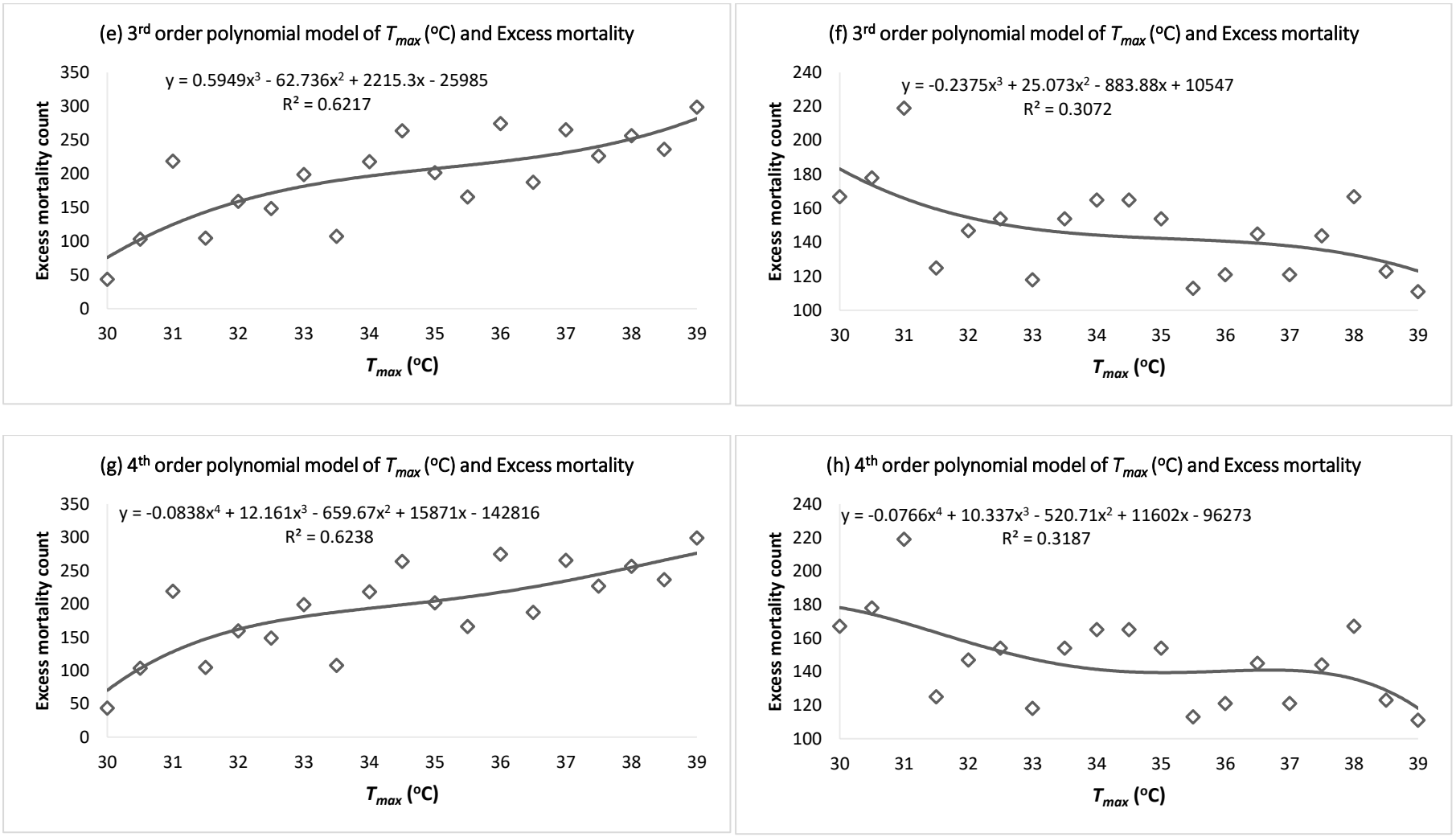
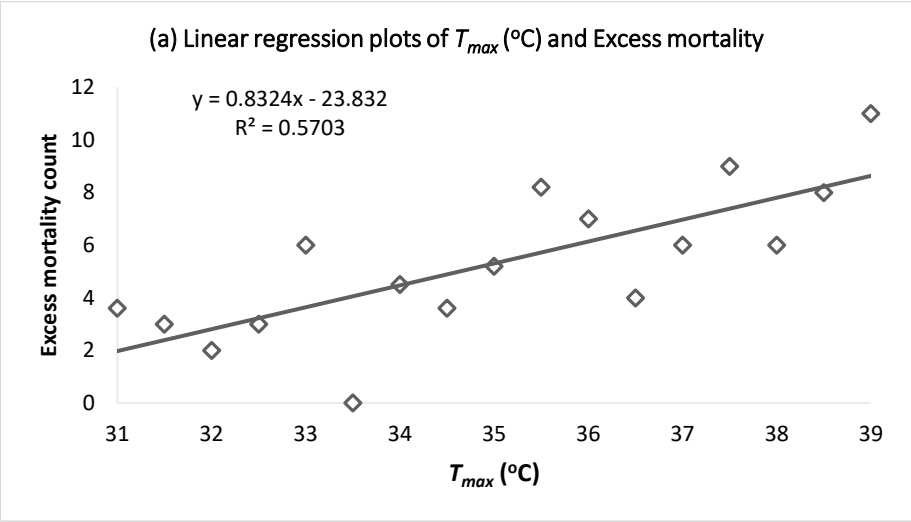
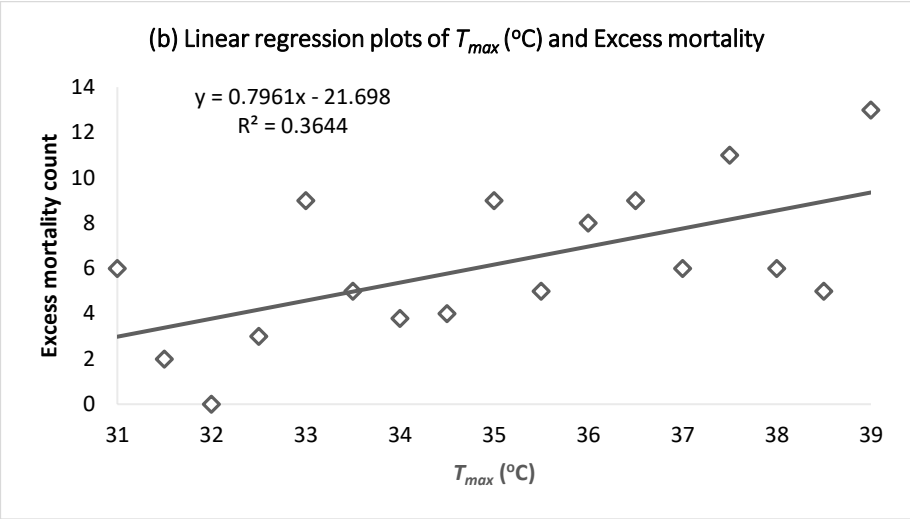
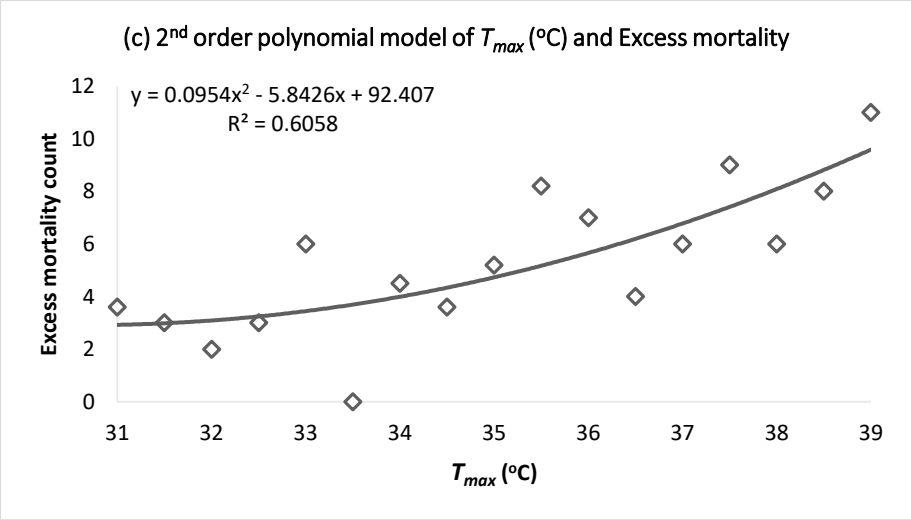
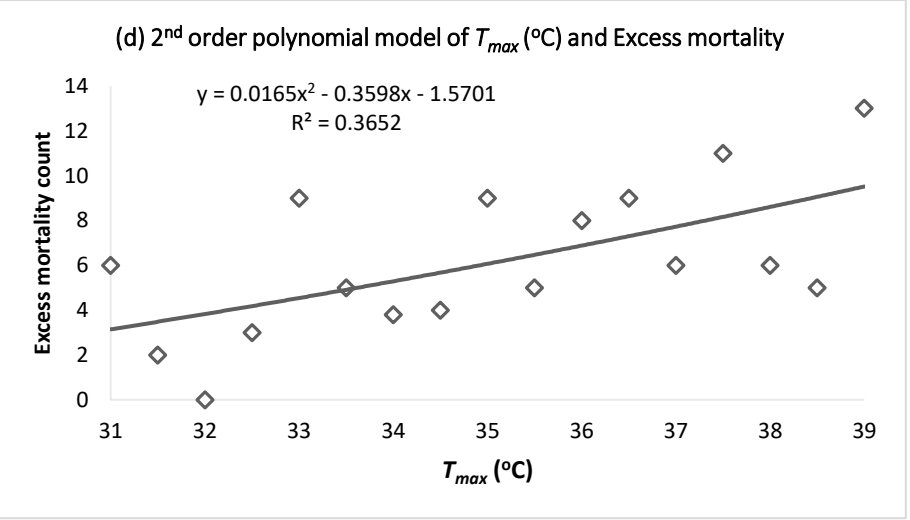


Figure 6.5: Regression plots of *Tmax* (°C) and Excess mortality of specialist Hospital Mararaba from 4-month moving average (left column) and the monthly average baseline (right column).


(a) Linear regression plots of T_{max} (°C) and Excess mortality
y = 0.8324x - 23.832
R² = 0.5703
Excess mortality count
T_{max} (°C)


(b) Linear regression plots of T_{max} (°C) and Excess mortality
y = 0.7961x - 21.698
R² = 0.3644
Excess mortality count
T_{max} (°C)


(c) 2nd order polynomial model of T_{max} (°C) and Excess mortality
y = 0.0954x² - 5.8426x + 92.407
R² = 0.6058
Excess mortality count
T_{max} (°C)


(d) 2nd order polynomial model of T_{max} (°C) and Excess mortality
y = 0.0165x² - 0.3598x - 1.5701
R² = 0.3652
Excess mortality count
T_{max} (°C)

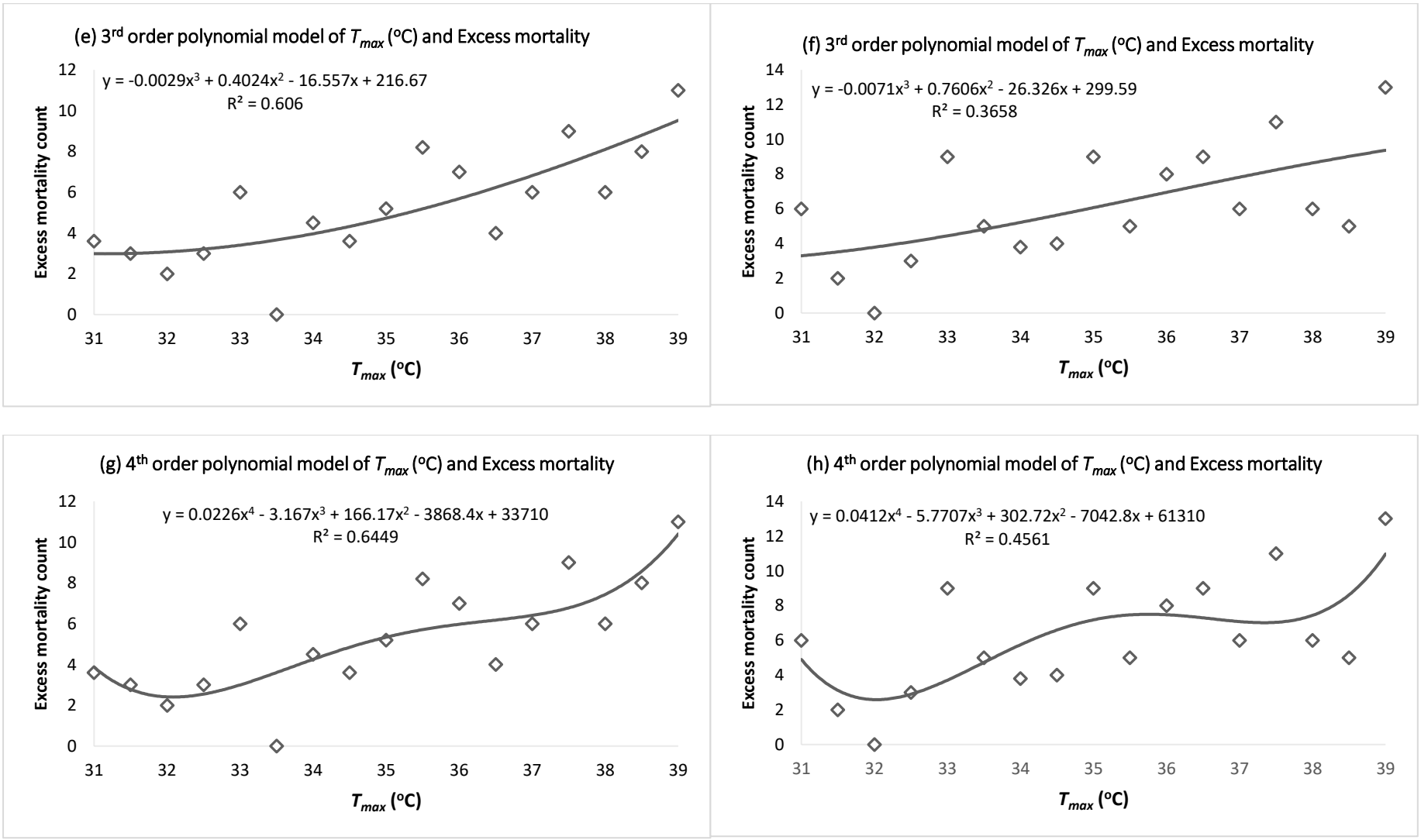


Figure 6.6: Regression plots of *Tmax* (°C) and Excess mortality of General Hospital Kuje from 4-month moving average (left column) and monthly average baseline (right column).

The temperature threshold for this study varies with location. For instance, only temperatures above 30.0^{o}C were regressed on excess mortality count from the national hospital, Abuja, general hospital Kwali, and the specialist hospital Mararaba. The temperature threshold for the University of Abuja Teaching Hospital, Gwagwalada, the general hospital Abaji and the general hospital Kuje were 31.0^{o}C. These temperature thresholds were chosen since no meaningful association could be demonstrated when lower temperature intervals were plotted against the excess mortality count.

6.3 The association between maximum temperature and excess mortality

Figure 6.7 depicts the relationship between temperature and excess mortality in the six area councils of Abuja and the Karu area of Nasarawa state from the 4-month-moving average of the 3rd order polynomial regression. The association between maximum temperature and excess mortality in the highly urbanised regions of Abuja is depicted in Figures 6.7(a) and (b). This consists of the temperature intervals and mean mortality for each interval calculated from the actual maximum temperature and heat-related mortality data collected on a monthly scale. The Municipal Area Council is in the city centre. Gwagwalada Area Council is the second-largest urban area in Abuja, about 55 kilometres away from the city centre. The regression model for both locations shows an increase in heat-related mortality as temperature rises. Figure 6.7(a) depicts a gradual increase in heat-related mortality starting at 30.0^{o}C. However, the rate of mortality increase with temperature gradually slows and stabilises at temperatures ranging between 34.0^{o}C to 37.0^{o}C before an abrupt increase is observed. Figure 6.7(b) depicts a sustained gradual increase in heat-related mortality at temperatures ranging from 32.0^{o}C to 39.0^{o}C. The regression statistics of the relationship between maximum temperature and excess mortality count in Table 6.7 are weaker in the Municipal area council (R^2: 0.28; *P*-value =0.048) than in the Gwagwalada area council (R^2 0.59: *p*-value =0.0017), even though the model output from both location are significant at 0.05 level. This could imply that heat-related mortality in the city centre is lower than in Gwagwalada urban areas. The increased UHI may have only a minor impact on human health in the city centre which is dominated by a wealthy population that

can afford mitigations such as air conditioning. The relationship in the Municipal and Gwagwalada models is represented by elongated U-shaped curves (Figure 6.7(a)) and flatter, broad J-shaped curves (Figure 6.7(b)).

Figures 6.7(c) and (d) depict the relationship between maximum temperature and excess mortality for Kuje area council, a suburban settlement 39 kilometres southwest of Abuja city centre, and Kwali area council, a rural settlement 75 kilometres from Abuja city centre. The non-linear elongated shallow U-shaped curve in Figure 6.7(c) and the more distinct S-shaped curve in Figure 6.7(d) imply that heat-related mortality increases as temperature rises in both locations. The nonlinear curves for temperature and excess mortality for the Kwali area council are relatively flat, with a rapid increase in mortality at temperatures above 36.0^{o}C and (R^2: 0.596; *p*-value: 0.00019) indicating a stronger relationship than for the Kuje area council (R^2: 0.60: 0.00046), where the relationships become smaller and less scattered. It is worth noting that Figure 6.7(d) has the highest excess mortality count in comparison to other locations because the model was created using total mortality data from both the Kwali General Hospital and the health centre in the ten wards that comprise the Kwali Area Council (Ashara, Dafa, Gumbo, Kilankwa, Kundu, Kwali, Pai, Wako, Yangoji, and Yebu).

Figure 6.7(e) presents the relationship between maximum temperatures and heat-related mortality in the Karu area, Nasarawa state-an informal settlement located 30 kilometres away from Abuja's centre. The Karu model has the typical "inverted flat U-shaped" form of polynomial functions. The model showed that the excess mortality from heat-related mortality increases with increasing temperature, firstly excess mortality is moderates at temperatures below 30.0^{o}C but later begins to increase at temperatures of 30.0^{o}C, then gradually slows down at 36.0^{o}C, and later increases to the maximum value at 39.0^{o}C, indicating a progressive increase in mortality with increasing temperature with a *p*-value =0.00012, signifying a strong association. Abaji is Abuja's most remote area council, with primarily rural settlements located 174 kilometres from the city centre. The Abaji area council regression model was found to be statistically significant. Figure 6.7(f) shows a regression curve shaped like an elongated

linear model with a *p*-value of 0.01055, indicating a progressive increase in mortality with increasing temperature. Table 6.2 summarises the linear regression output of *Tmax* (^{o}C) as an independent variable and excess mortality count as a dependent variable for the six hospitals in the study area. The 95% confidence intervals (CI) are used to assess estimate precision, with a narrower CI around the best fit line indicating a more precise estimate.

A confidence interval is a range surrounding a measurement that indicates its precision. Confidence intervals aid in navigating the uncertainties over how effectively a sample estimates a population-wide value. In this investigation, the margin of error reported was the 95% confidence interval. The degree of significance is the statistical phrase for the willingness to be incorrect. A confidence interval of 95% has a 5% chance of being incorrect. A consistent estimation would remain relatively constant if the survey were repeated. A variable estimation varies from each sample. For instance, the confidence intervals for the national hospital in Abuja and the general hospital in Abaji are wider than the estimates, indicating instability. In this aspect, the interval is broad, the error margin is substantial, and the accurate measurement is most likely to be within the broader range, indicating an inaccurate estimation. Conversely, relatively narrow confidence intervals relative to the point estimate indicate that the estimated value at The University of Abuja Teaching Hospital, Gwagwalada, General Hospital Kuje; Specialist Hospital Mararaba, General Hospital Kwali, and General Hospital Abaji is generally consistent. The range is limited, the margin of error is minimal, and there is only a minuscule range of conceivable numbers, implying an accurate estimation. Figure 6.7 The presents the 95% confidence interval for the third-order polynomial regression function output from a four-month moving average baseline for the relationship between maximum temperature and excess mortality

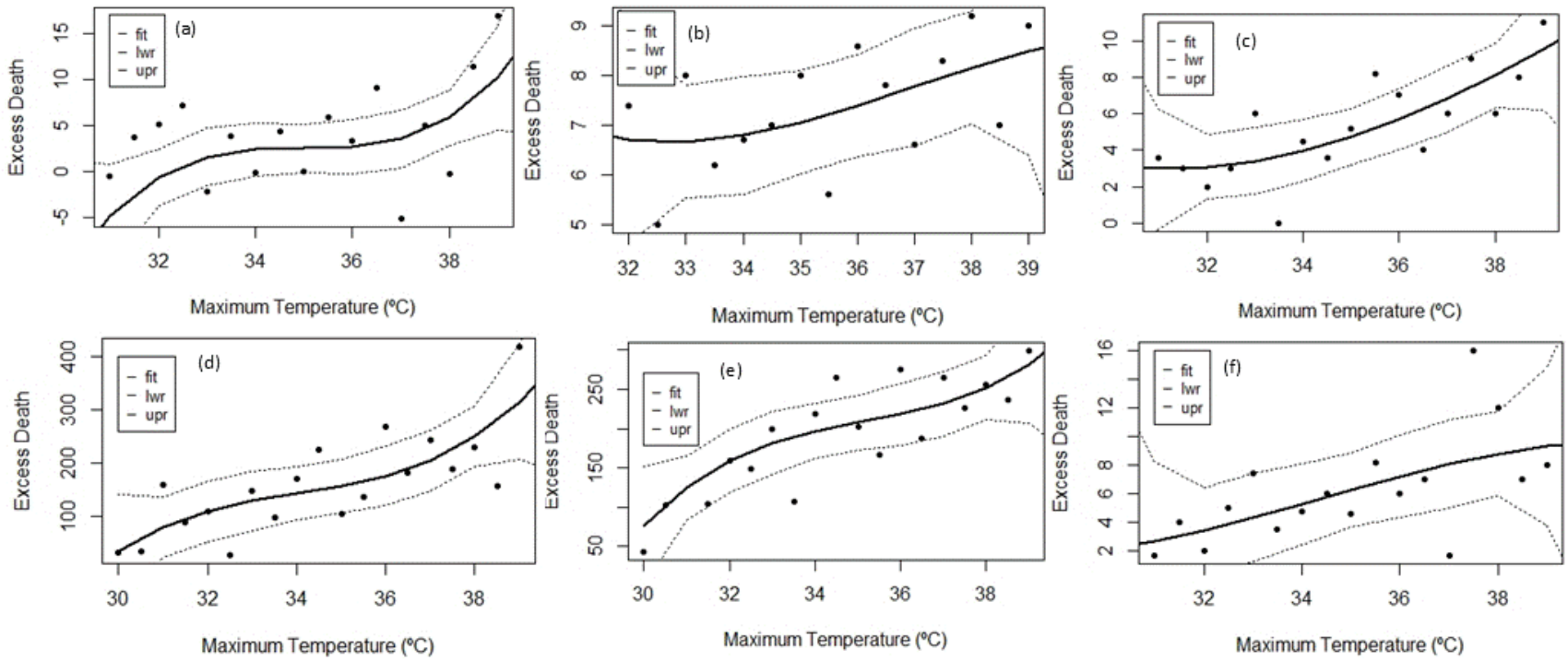


Figure 6.7: The 95% confidence interval for the third-order polynomial regression function output from a four-month moving average baseline for the relationship between maximum temperature and excess mortality. (a) The University of Abuja Teaching Hospital, Gwagwalada; (b) National Hospital Abuja; (c) General Hospital Kuje; (d) General Hospital Kwali; (e) Specialist Hospital Mararaba; and (f) General Hospital Abaji is shown.

Table 6.2: Summary of polynomial regression output of *Tmax* (°C) and excess mortality count for the six hospitals in the study area

Location	R^2	Regression equation	Standard error	Significant level	*P* value
Teaching Hospital Gwagwalada	0.596	$y = 0.1143x^3 - 11.998x^2 + 419.72x - 4892.5$	3.391	0.05	0.00169
National Hospital Abuja	0.2822	$y = -0.007x^3 + 0.772x^2 - 28.178x + 345.76$	1.082	0.05	0.0481
General Hospital Kuje	0.606	$y = -0.0029x^3 + 0.4024x^2 - 16.557x + 216.67$	1.884	0.05	0.00046
General Hospital Kwali	0.596	$y = 0.8554x^3 - 87.281x^2 + 2982x - 33969$	64.502	0.05	0.00019
Specialist Hospital Mararaba	0.621	$y = 0.5949x^3 - 62.736x^2 + 2215.3x - 25985$	45.581	0.05	0.00012
General Hospital Abaji	0.363	$y = -0.0088x^3 + 0.9049x^2 - 30.136x + 328.62$	3.029	0.05	0.01055

6.4 Analysis of model residuals

Checking the residuals of the regression is an effective technique for inspecting the inconsistency of the dependent variable using the independent variable. The residuals were investigated in this study using regression tools and scatterplots. Figure 6.8 shows that the regression model's residuals were small and unstructured *i.e*. there was no heteroscedasticity, indicating that the regression model effectively described a significant portion of the dependent variable's disparity. The residual structure also revealed that the relationship between the variables could be nonlinear.

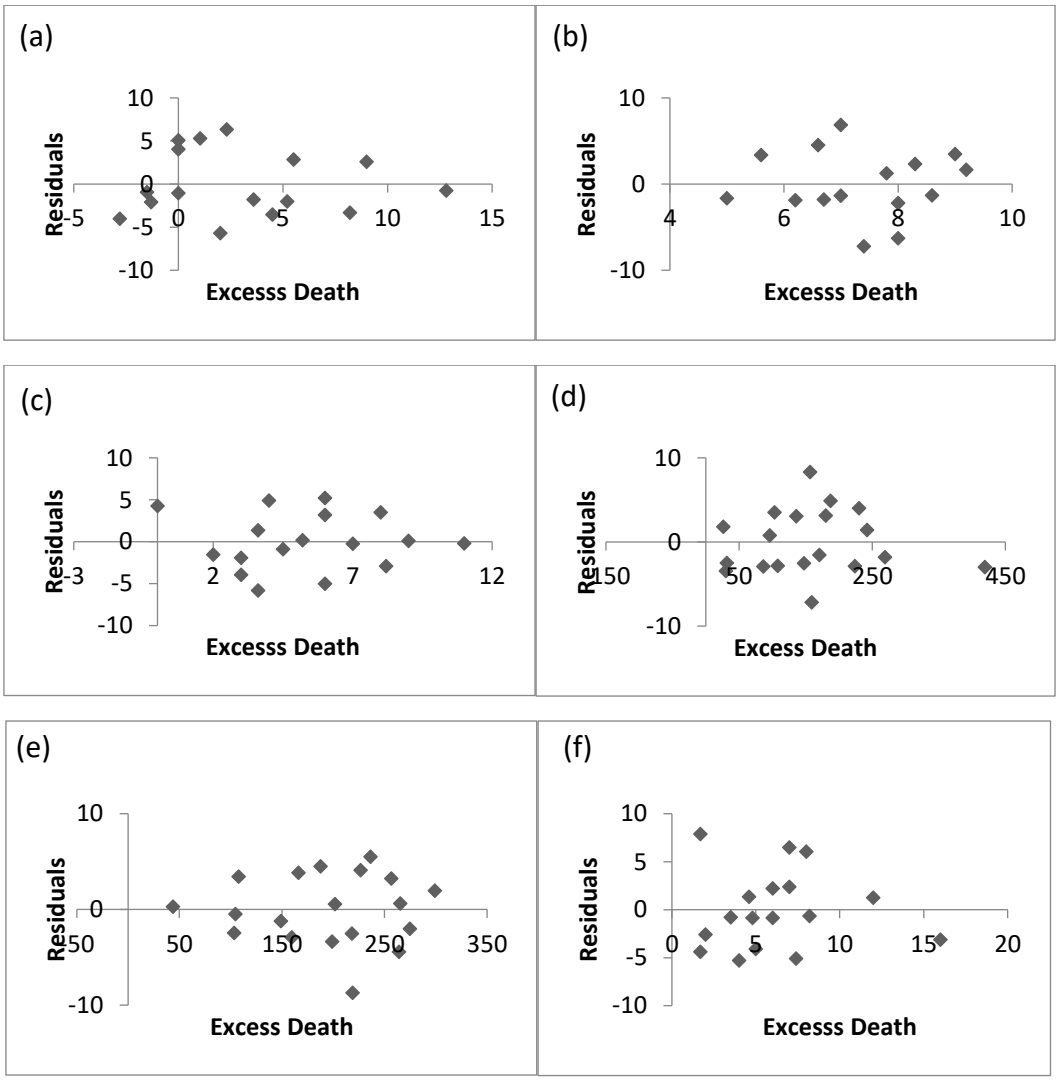
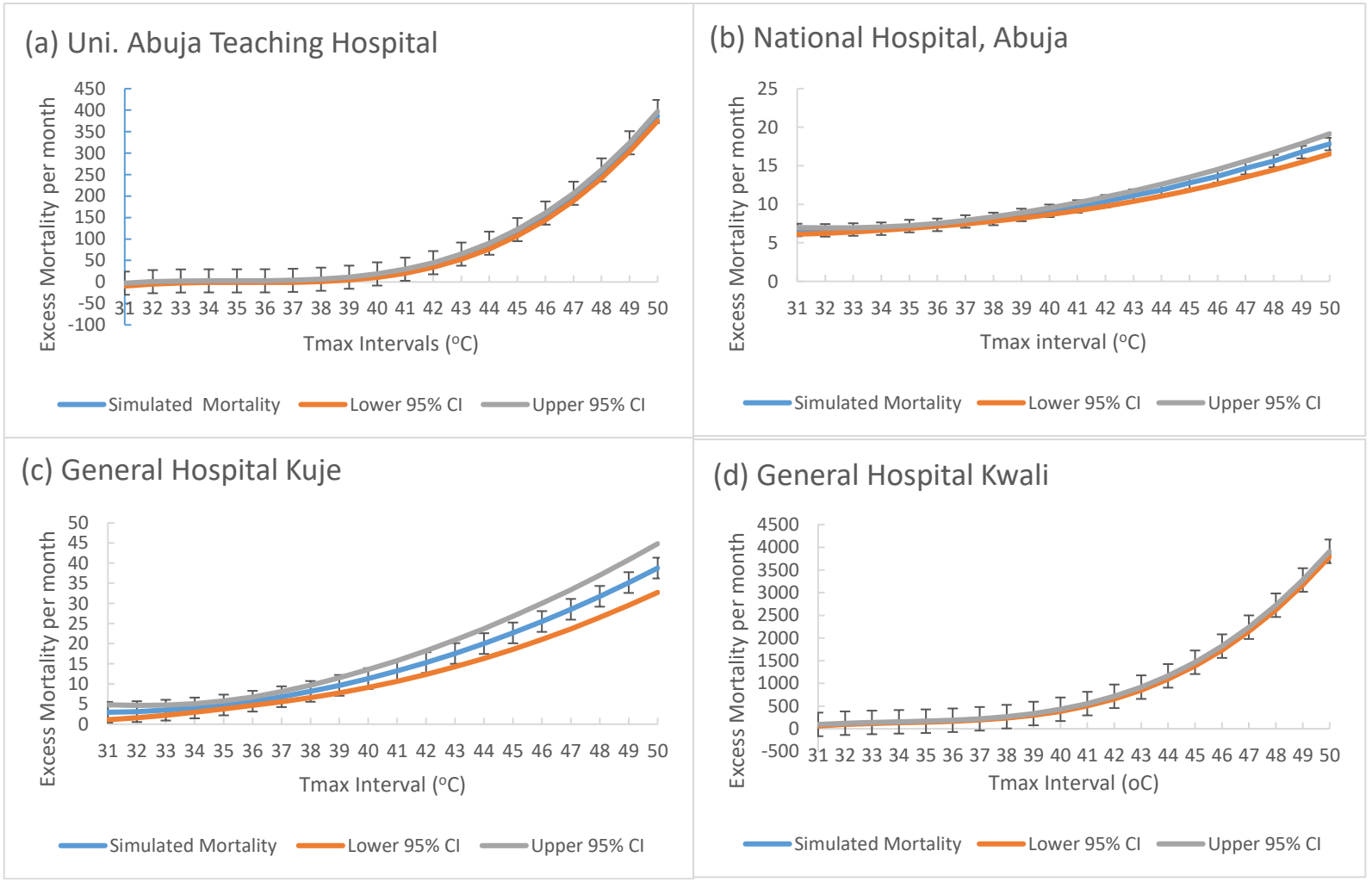


Figure 6.8: Residual plots of regression output from a four-month moving average baseline for the relationship between maximum temperature and excess mortality (a) The University of Abuja Teaching Hospital, Gwagwalada; (b) National Hospital Abuja; (c) General Hospital Kuje; (d) General Hospital Kwali; (e) Specialist Hospital Mararaba; and (f) General Hospital Abaji.

6.5 Model simulation of heat-related mortality at 1ºC temperature intervals

Tables 6.3, 6.4, and 6.5 show the simulated increased mortality for each of the six research locations as a function of temperature. The 95% lower and upper confidence intervals for each band are given beside the best-fit curves. The simulated death indicates the excess mortality for the expected association in these plots. This means that monthly mortality will increase at each place for every 1°C increase in maximum temperature. For instance, in the urban settlements of the study area (Table 6.3), a rise in maximum temperature to 40°C in the settlements of the Gwagwalada area will result in 14.70 excess monthly death in the population. A further increase in maximum temperature to 50°C will result in 386 deaths per month. In the Municipal area council located at the city centre, increasing the maximum temperature to 40°C will lead to 9.7 monthly excess death in the population. A further increase in maximum temperature to 50°C will result in 17.8 monthly deaths.

A rise in maximum temperature to 40°C in the Kuje area council will result in 11.34 monthly deaths in the population (Table 6.4), and 38.78 deaths per month will result from raising the maximum temperature to 50°C. A rise in maximum temperature to 40°C will result in 407 monthly deaths in the Kwali area council and surrounding villages. A further increase in maximum temperature to 50°C would result in 3853.5 monthly deaths. Settlements dominated by rural characteristics (Table 6.4), for example, Maraba in Nasarawa state's Karu area and Abaji area council, will record 323 and 10.551 deaths per month for an increase in maximum temperature to 40°C, and 2302.5 and 19.311 deaths for an increase in maximum temperature to 50°C as shown in Figure 6.9.


(a) Uni. Abuja Teaching Hospital
Excess Mortality per month
450 400 350 300 250 200 150 100 50 0 -50 -100
31 32 33 34 35 36 37 38 39 40 41 42 43 44 45 46 47 48 49 50
Tmax Intervals (°C)
Simulated Mortality
Lower 95% CI
Upper 95% CI
(b) National Hospital, Abuja
Excess Mortality per month
25 20 15 10 5 0
31 32 33 34 35 36 37 38 39 40 41 42 43 44 45 46 47 48 49 50
Tmax interval (°C)
Simulated Mortality
Lower 95% CI
Upper 95% CI
(c) General Hospital Kuje
Excess Mortality per month
50 45 40 35 30 25 20 15 10 5 0
31 32 33 34 35 36 37 38 39 40 41 42 43 44 45 46 47 48 49 50
Tmax Interval (°C)
Simulated Mortality
Lower 95% CI
Upper 95% CI
(d) General Hospital Kwali
Excess Mortality per month
4500 4000 3500 3000 2500 2000 1500 1000 500 0 -500
31 32 33 34 35 36 37 38 39 40 41 42 43 44 45 46 47 48 49 50
Tmax Interval (oC)
Simulated Mortality
Lower 95% CI
Upper 95% CI

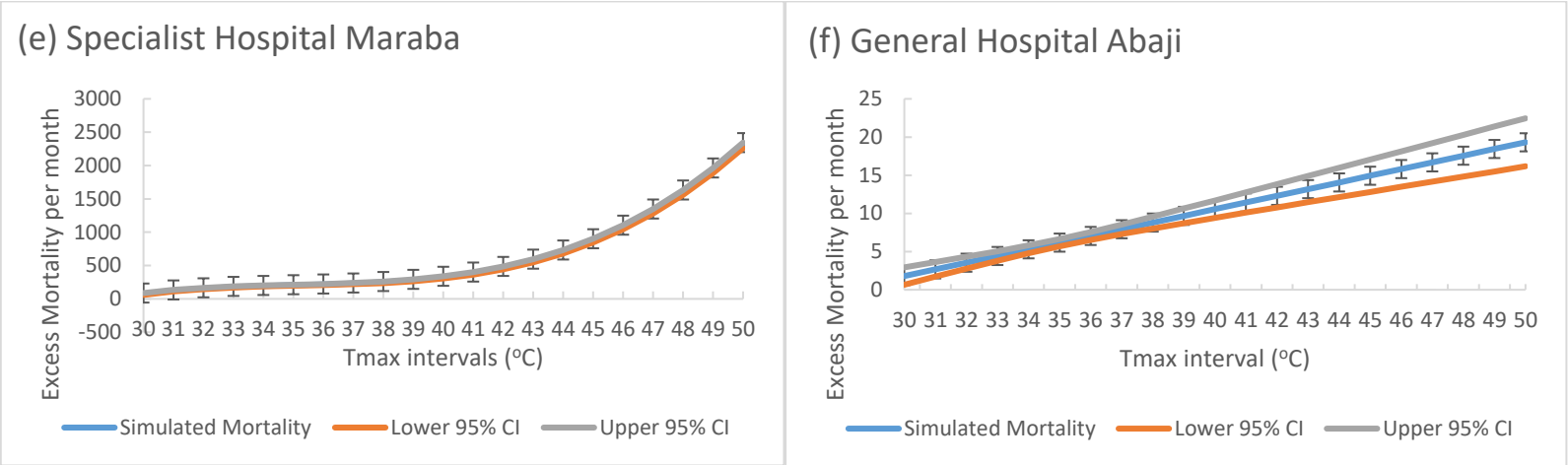


Figure 6.9: Model simulation of maximum temperature and excess mortality at 1°C temperature intervals (a) The University of Abuja Teaching Hospital, Gwagwalada; (b) National Hospital Abuja; (c) General Hospital Kuje; (d) General Hospital Kwali; (e) Specialist Hospital Mararaba; and (f) General Hospital Abaji.

Table 6.3: Simulated deaths of Gwagwalada and Municipal area council using 1ºC temperatures Intervals

	Uni. Teaching Hospital Gwagwalada				National Hospital Abuja			
T_{max}(ºC)	Simulated Death	Lower 95% CI	Upper 95% CI	conf se	Simulated Death	Lower 95% CI	Upper 95% CI	conf se
31	-6.152	-9.507	-2.793	1.575	6.665	6.124	6.996	0.633
32	-2.037	-4.802	0.742	1.301	6.619	6.234	6.946	0.516
33	0.041	-2.223	2.303	1.062	6.726	6.402	6.964	0.408
34	0.749	-1.154	2.634	0.888	6.832	6.622	7.056	0.315
35	0.766	-0.993	2.513	0.8223	7.176	6.880	7.234	0.257
36	0.798	-1.104	2.684	0.888	7.332	7.161	7.515	0.257
37	1.524	-0.743	3.783	1.062	7.771	7.464	7.898	0.315
38	3.621	0.848	6.392	1.301	8.101	7.806	8.368	0.408
39	7.788	4.423	11.137	1.575	8.618	8.199	8.912	0.516
40	14.703	10.715	18.685	1.869	9.156	8.651	9.523	0.633
41	25.055	20.411	29.688	2.1762	9.721	9.162	10.200	0.753
42	39.535	34.222	44.838	2.490	10.387	9.733	10.941	0.877
43	58.810	52.822	64.798	2.809	11.129	10.366	11.746	1.001
44	83.581	76.904	90.256	3.132	11.843	11.061	12.615	1.127
45	114.546	107.171	121.909	3.457	12.776	11.818	13.546	1.254
46	152.362	144.294	160.426	3.784	13.621	12.637	14.540	1.381
47	197.736	188.964	206.496	4.112	14.687	13.519	15.598	1.508
48	251.338	241.862	260.798	4.442	15.615	14.463	16.718	1.636
49	313.861	303.687	324.033	4.772	16.767	15.469	17.900	1.764
50	386.004	375.122	396.878	5.104	17.822	16.538	19.146	1.892

Table 6.4: Simulated deaths of Kuje and Kwali area council using 1°C temperatures Intervals

	General Hospital Kuje				General Hospital Kwali			
T_{max}(°C)	Predicted Death	Lower 95% CI	Upper 95% CI	conf se	Predicted Death	Lower 95% CI	Upper 95% CI	conf se
31	2.972	1.108	4.833	0.875	79.248	62.630	95.730	24.013
32	3.131	1.593	4.672	0.722	109.021	95.194	122.812	20.036
33	3.496	2.234	4.758	0.589	128.565	116.872	140.129	16.872
34	4.045	2.997	5.095	0.493	142.865	132.438	153.172	15.042
35	4.782	3.812	5.769	0.456	157.017	146.682	167.417	15.042
36	5.719	4.663	6.766	0.493	176.443	164.738	187.994	16.872
37	6.834	5.589	8.091	0.589	205.968	192.078	219.696	20.036
38	8.155	6.614	9.695	0.722	250.702	234.195	267.294	24.013
39	9.651	7.782	11.514	0.875	316.112	296.4542	335.689	28.464
40	11.346	9.138	13.567	1.038	407.067	384.119	429.880	33.199
41	13.232	10.651	15.802	1.209	528.742	502.395	554.929	38.112
42	15.304	12.354	18.259	1.383	686.229	656.457	715.925	43.142
43	17.577	14.246	20.907	1.560	884.765	851.462	917.975	48.253
44	20.032	16.329	23.741	1.740	1129.481	1092.559	1166.196	53.422
45	22.681	18.582	26.773	1.920	1425.338	1384.891	1465.71	58.633
46	25.517	21.036	30.005	2.102	1777.654	1733.595	1821.642	63.876
47	28.544	23.677	33.412	2.284	2191.591	2143.811	2239.119	69.144
48	31.765	26.501	37.024	2.468	2672.065	2620.675	2723.271	74.431
49	35.187	29.529	40.831	2.651	3224.339	3169.321	3279.226	79.734
50	38.783	32.733	44.825	2.835	3853.543	3794.884	3912.116	85.050

Table 6.5: Simulated deaths of Maraba and Abaji area council using 1ºC temperatures Intervals

	Specialist Hospital Maraba				General Hospital Abaji			
$T_{max}(^oC)$	Predicted Death	Lower 95% CI	Upper 95% CI	conf se	Predicted Death	Lower 95% CI	Upper 95% CI	conf se
30	73.914	60.037	87.763	20.115	1.791	0.651	2.930	1.653
31	122.732	110.974	134.365	16.969	2.667	1.711	3.622	1.386
32	156.676	146.861	166.377	14.159	3.543	2.759	4.326	1.137
33	179.319	171.100	187.534	11.923	4.419	3.786	5.051	0.918
34	194.342	187.007	201.660	10.630	5.295	4.773	5.816	0.756
35	205.287	197.9114	212.564	10.630	6.171	5.692	6.649	0.695
36	215.617	207.381	223.816	11.923	7.047	6.525	7.568	0.756
37	229.086	219.227	238.744	14.159	7.923	7.290	8.555	0.918
38	249.019	237.273	260.664	16.969	8.799	8.015	9.582	1.137
39	279.176	265.254	292.980	20.115	9.675	8.719	10.630	1.386
40	323.048	306.831	339.169	23.460	10.551	9.411	11.690	1.653
41	384.287	365.625	402.749	26.932	11.427	10.097	12.756	1.929
42	466.222	445.235	487.259	30.487	12.303	10.778	13.827	2.211
43	572.865	549.249	596.251	34.099	13.179	11.457	14.901	2.498
44	707.316	681.247	733.284	37.752	14.055	12.133	15.976	2.787
45	873.443	844.806	901.919	41.434	14.931	12.808	17.053	3.079
46	1074.687	1043.501	1105.720	45.139	15.807	13.483	18.130	3.372
47	1314.659	1280.903	1348.254	48.862	16.683	14.156	19.209	3.666
48	1596.816	1560.587	1633.087	52.598	17.559	14.829	20.288	3.960
49	1925.054	1886.121	1963.787	56.345	18.435	15.501	21.368	4.256
50	2302.598	2261.078	2343.922	60.101	19.311	16.173	22.448	4.552

6.5 Conclusion

This chapter presents the findings on the relationship between temperature and mortality in Abuja and its environs. The results from the chapter show a positive relationship between temperature and heat-related deaths in all the six hospital in the area. The R^2 of the regression, however, shows spatial diversity in the heat-health association. For instance, the National and general hospitals in Abaji show a weaker relationships than the University of Abuja Teaching Hospital, Gwagwalada, General Hospital Kuje, General Hospital Kwali, and Specialist Hospital Mararaba. The temperature thresholds at the University of Abuja Teaching Hospital, Gwagwalada, the general hospital Abaji, and the general hospital Kuje were higher (31.0^{o}C) than those at the national hospital, Abuja, the general hospital Kwali, and the specialist hospital Mararaba with temperature thresholds of 30.0^{o}C. The findings can be used to project the effects of climate change on future mortality rates and improve early warning systems and heat-health action strategies.

The primary function of epidemiology is to compare the incidence of disease among two or more populations. Age, for instance, is an essential factor in determining mortality. An older population will have a greater overall mortality rate than a younger population. Consequently, age differences will confound any comparison between people with distinct age structures. The comparison of heat-related mortality rates for the six hospitals chosen for this study could be misleading because the populations being compared may differ considerably regarding specific underlying characteristics, such as age and gender, affecting the study's results. Population standardisation requires comprehensive and reliable data on the entire population. Missing information for specific age groups can lead to biased estimates and potentially misrepresent disease incidence. The lack of information on the total population can introduce biases and inaccuracies, leading to flawed conclusions. Hospitals might use varying methods for data collection, diagnostic criteria, and reporting practices, which can introduce inconsistencies and inaccuracies in the standardised data, affecting the overall analysis and interpretation of disease incidence.

CHAPTER SEVEN: MAPPING OF HEAT VULNERABILITY

7.0 Introduction

Urbanisation has often increased temperature and intensified features such as the UHI, making the urban population vulnerable to heat. Abuja and its environs have been more heat-sensitive due to increased LST during the last few decades. This chapter aims to map heat vulnerability in Abuja and the surrounding area using heat vulnerability indicators associated with environmental, demographic, and socioeconomic characteristics. The HVIs used in this chapter include maps of (i) artificial impervious surface cover, (ii) LST, (iii) NDVI, (iv) population under 14 and over 65 years, (v) the proportion of the women population, (vi) population density, (vii) poverty level, (viii) literacy rate, and (ix) dwelling quality.

7.1 Reclassified maps of heat vulnerability indicators

The reclassified LST map indicates regions with high temperatures in the western and northeastern regions of the research area compared to locations in the south and southeast, where temperatures are relatively low. Primarily due to bare surfaces, regions in the southwest also significantly impact heat vulnerability. As indicated in Figure 7.1(a) and (b), regions to the north and southeast were characterised mainly by low temperatures, which can be linked to the high proportion of vegetation cover and water bodies. According to the reclassified NDVI map, the absence of healthy vegetation cover influenced the northeast and western regions considerably influenced heat vulnerability. In contrast, the southern region's much healthier vegetation cover contributed to its low influence on heat vulnerability. Figure 7.2(a) presents the reclassified NDVI for this research. Figure 7.2(b) indicates the population at risk, which consists of individuals younger than 14 and older than 65. Compared to other regions such as Gwarinpa, the city centre, and Wuse, the northeastern region of Karu, Dutse, Usman, and Quarters has a disproportionately high population at risk. Relative to settlements in the city centre, vulnerable populations are concentrated outside the city centre. The towns on the city's outskirts have a greater influence on heat vulnerability- than the settlements in the city's centre.

The reclassified women population map reveals that the quarters, Usman, Zuba, and Dutse have the largest women population proportion compared to other regions. As indicated in Figure 7.3(a), these regions were classified as having the greatest influence on heat vulnerability compared to the settlements of Nyanya, Aso, and Karshi, where the low proportion of the women population accounts for their low influence. Figure 7.3(b) shows the reclassified proportion of people living in poverty. When compared to households in the city centre, Wuse, Gwarimpa, and a portion of Dutse, which have a high influence on heat vulnerability- the settlements of Dobi, Gurdi, and Panda in the northwest and northern extent of the study area have the highest proportion of poor households. These regions in the study area have the lowest morbidity and mortality rates associated with heat. The high influence of Gurdi, Dobi, and part of Karshi, and Kabi on heat vulnerability could be attributed to their high proportion of illiterate and low-educated residents, as compared to the population in the city centre, Wuse, Garki, Gwarimpa, and Dutse, which has a high concentration of literate and highly educated residents. Compared to regions with a high population concentration and a low educational qualification, regions with a low educational level were reclassified as having a high influence on heat vulnerability. Figure 7.4(a) presents the reclassified literacy level of the study area.

The reclassified map of dwelling quality shown in Figure 7.4(b) indicates that the city centre, Wuse, a portion of Garki, and Gwarimpa were among the settlements with the highest proportions of high-quality buildings compared to Dafa, Waka, Yebu, and Yangoji, among others, where the majority of settlements are of low quality. The influence of low-quality buildings on heat vulnerability is greater than that of high-quality buildings. The reclassified population density of the research region is shown in Figure 7.5. The eastern region of the study area has a higher population density than other regions. Highly inhabited areas considerably influence heat vulnerability compared to the sparsely populated areas in the city centre, including the Wuse, Kutunku, and Garki areas. They have little influence on the morbidity and mortality caused by heat.

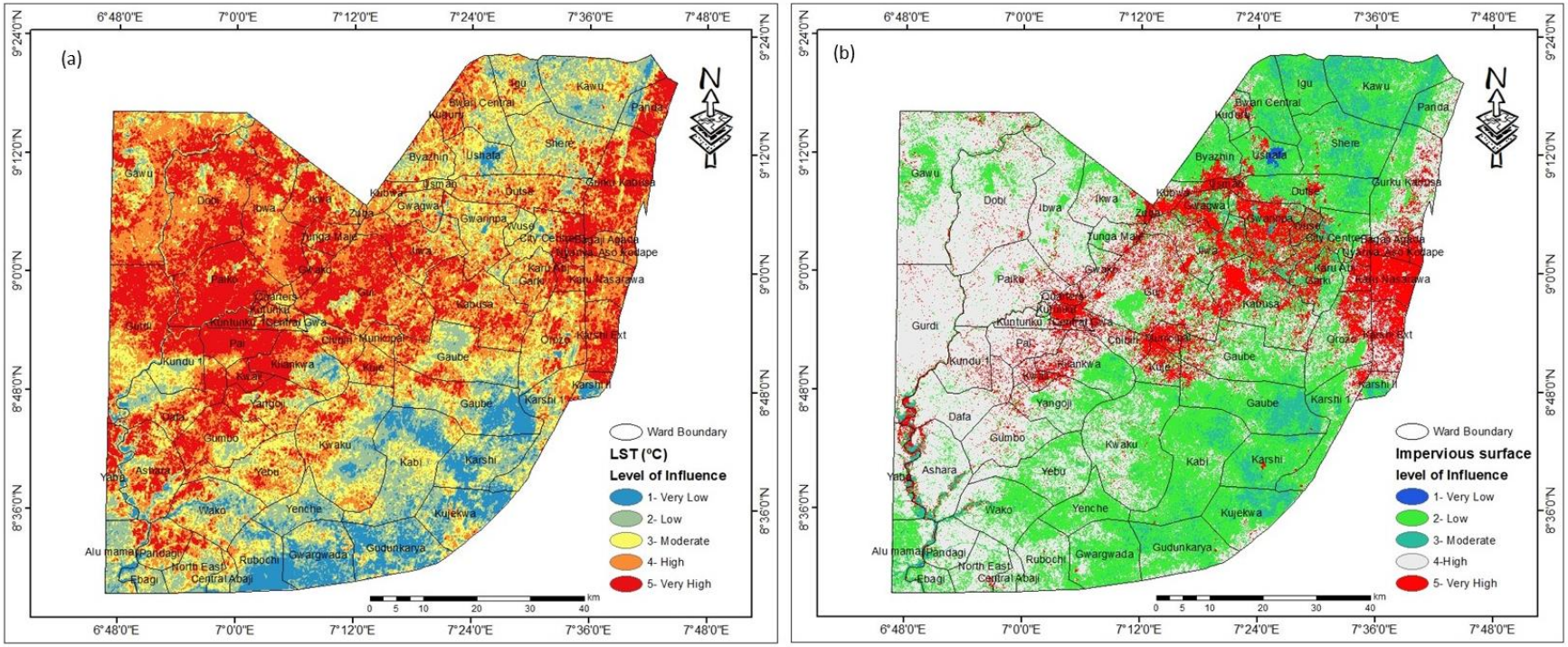


Figure 7.1: (a) Reclassified LST map generated from the thermal bands of Landsat 8 image of March 2020 at a spatial resolution of 100m; (b) Reclassified AIS map generated from Landsat 8 image of March 2020 at a spatial resolution of 30m.

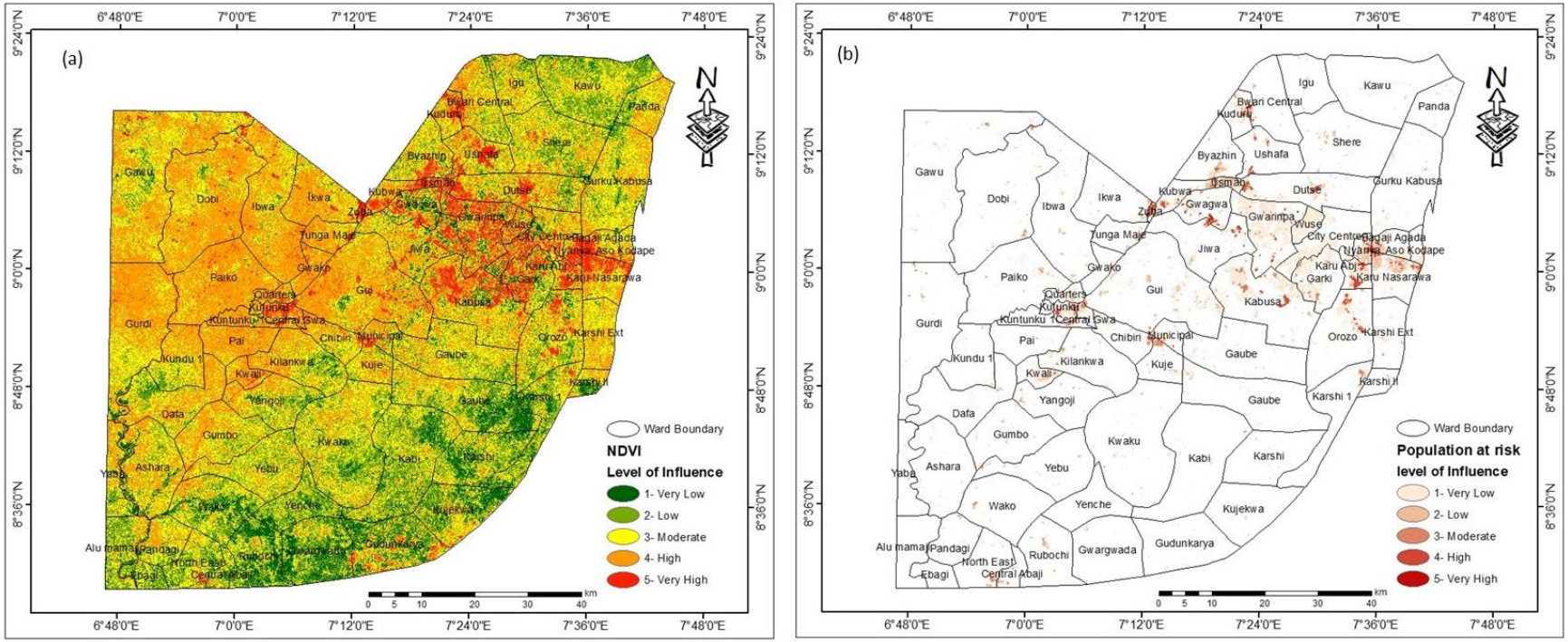


Figure 7.2: (a) NDVI generated from bands 4 and 5 of Landsat 8 image of 2020 at a spatial resolution of 30m; (b): Reclassification Vulnerable population of 2020 generated from WorldPop datasets at a spatial resolution of 92m.

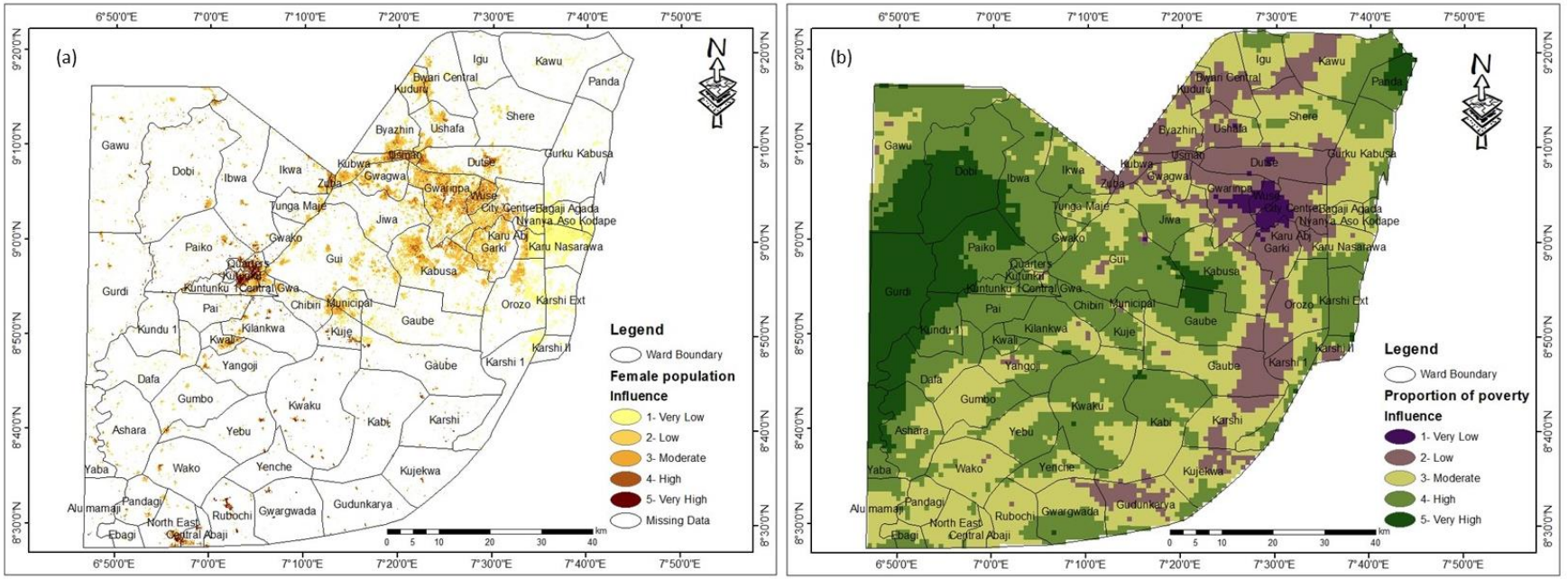


Figure 7.3: (a) 2020 proportion of women at childbearing age (15-49 years old) per grid square at a spatial resolution of 923m; (b) 2020 poverty level of people living below $1.25 a day at a spatial resolution of 923m.

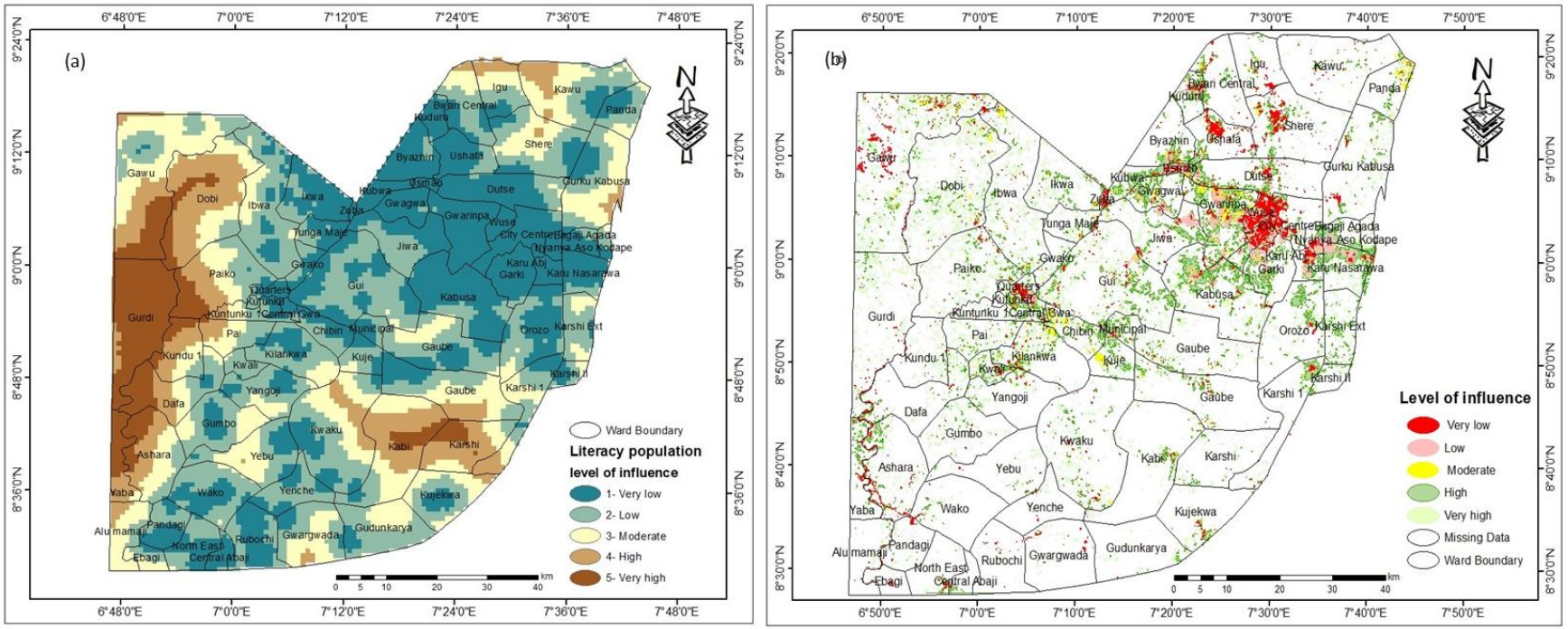


Figure 7.4: (a) Literacy level of 2020 at a spatial resolution of 923m generated from Worldpop datasets; (b): Dwelling quality of 2020 generated from Worldpop datasets at a spatial resolution of 92m.

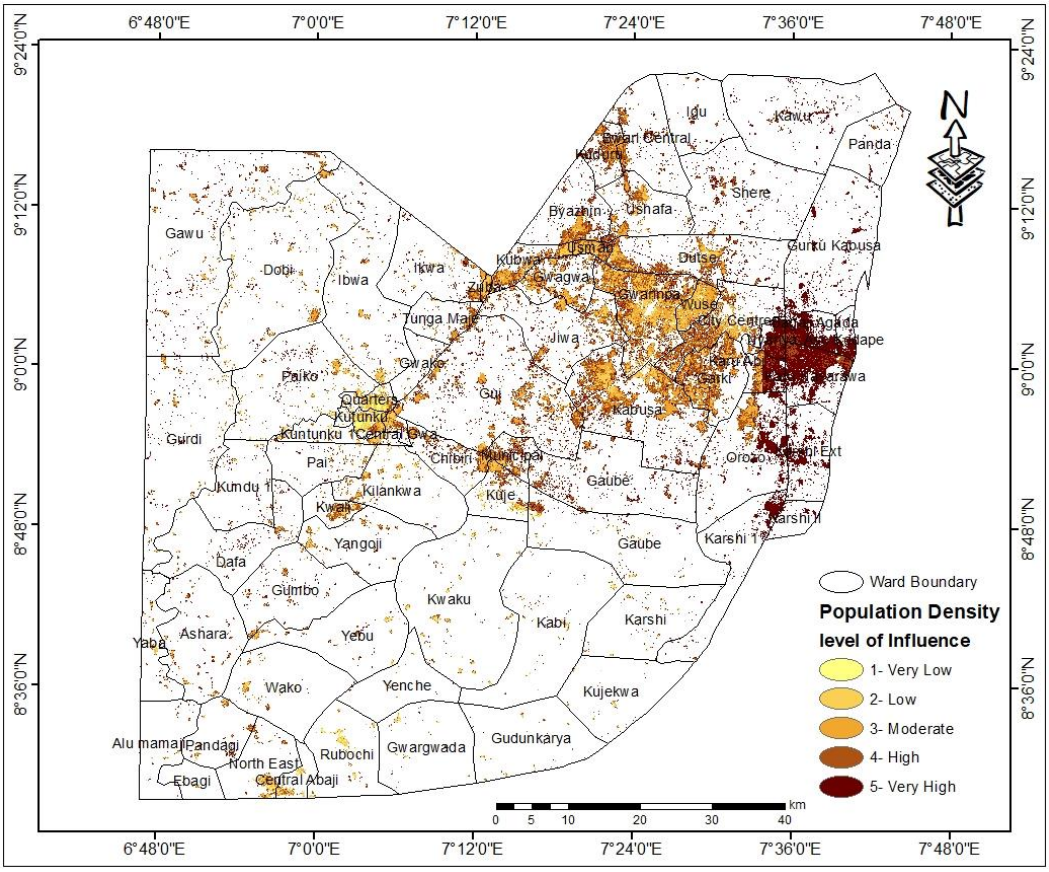


Figure 7.5: Population density of 2020 at a spatial resolution of 92m derived from WorldPop datasets.

7.2 Heat exposure, sensitivity and adaptive capacity index

Figure 7.6(a) depicts the heat exposure index, which indicates locations in the study area that are highly exposed to heat. The study area's north-western and north-south towns have been identified as having very high and high heat exposure levels. They accounted for 26.78% and 14.18% of the study area, respectively, and are distinguished by concentrations of AIS, particularly in the Municipal Area Council, Gwagwalada, and Karu areas. Areas with moderate heat exposure made up 25.06% of the study area. They are commonly seen in the study area's northern and southwestern reaches. Low and very low heat-exposed areas occupied 14.76% and 19.20% of the map area. They are more common in the study's southern region. This means that the heat hotspots are typical in areas with primarily AIS and nucleated settlements, often with less vegetation cover. In comparison, areas dominated by farming communities with dispersed settlements and much vegetation cover are less exposed to heat.

Figure 7.6(b) illustrates the sensitivity index of Abuja and its environs. 37.92% and 21.16 % of the map area are very low and low sensitivity to heat. These areas can be found throughout the study area, accumulating in the northeastern area. For example, Zuba, Gwagwa, Chibiri, Kabusa, and Orozo, have the highest concentration of low sensitivity to heat. Moderate sensitivity areas occupied 15.62% of the map area and can also be found throughout the map area, with high concentrations at quarters, Kutunku, Aso, and Wuse, among others. Areas of high and very high heat sensitivity are concentrated in the study area's eastern settlements, with a higher prevalence in Gwarimpa, Kubwa, Kabusa, and Garki, among other places. They cover 18.85 and 6.75% of the map, respectively.

The adaptive capacity index map shown in Figure 7.6(c) revealed that settlements in the Municipal area council comprising the city centre in the eastern part of the study area were more adaptable to heat vulnerability than settlements on the study area's periphery. This could be attributed to the households' imbalanced economic status; residents of the Municipal area council had better economic development than residents of the other area councils on the outskirts of the study area, resulting in potentially higher adaptive capacity. For example, most households in Garki, Wuse, Gwarimpa, Kabusa, Jiwa, and Dutse, among others, had a higher number of wealthy residents who could afford better-living conditions. The very high and high adaptations cover 18.85% and 48.03 % of the map area. Most households in Gawu, Gurdi, Gudunkarya, Karshi, Gurku Kabusa, and Panda, among other settlements away from the Municipal Area Council, are dominated by middle and low-income earners. These households have less income to afford a better life, such as better health care or air conditioning during the hot season. Because of the poor living conditions in these areas and the inadequate provision and maintenance of sewage and waste disposal systems, they have a moderate to low adaptive capacity to heat.

These areas cover 25.29%, 6.97%, and 0.77% of the map area. There is a large correlation between education and poverty, with higher education often resulting in higher income. However, correlation does not imply causation, and there is

no guarantee that more education will result in wealth. Many other factors may be at work, such as natural ability, family environment, inheritances, and even health. Although air conditioning is one of the most effective measures for mitigating the health effects of heat, it can also increase electricity consumption, discard condensing heat to the air, raise street temperatures, and thus exacerbate the heat island effect. Heat exposure combined with the sensitivity index indicates prospective consequences or gross vulnerability. To provide an estimate of net vulnerability, influence or gross vulnerability is mediated by adaptive capacity. To translate this into a knowledge of how vulnerability to extreme heat influences various areas of populations, an emphasis on the spatial heterogeneity of vulnerability and its separate components are required. Table 7.1 present the % of the map area's heat exposure, sensitivity and the adaptive capacity index of the study area.

Table 7.1: Heat exposure, sensitivity, adaption, and vulnerability by map area (%)

Vulnerability scale	Level of Exposure by map area (%)	Level of Sensitivity by map area (%)	Level of Adaptation by map area (%)
(1) Very Low	19.20	37.92	0.77
(2) Low	14.79	21.16	6.96
(3) Moderate	25.06	15.62	25.39
(4) High	14.18	18.53	48.03
(5) Very High	26.78	6.76	18.85

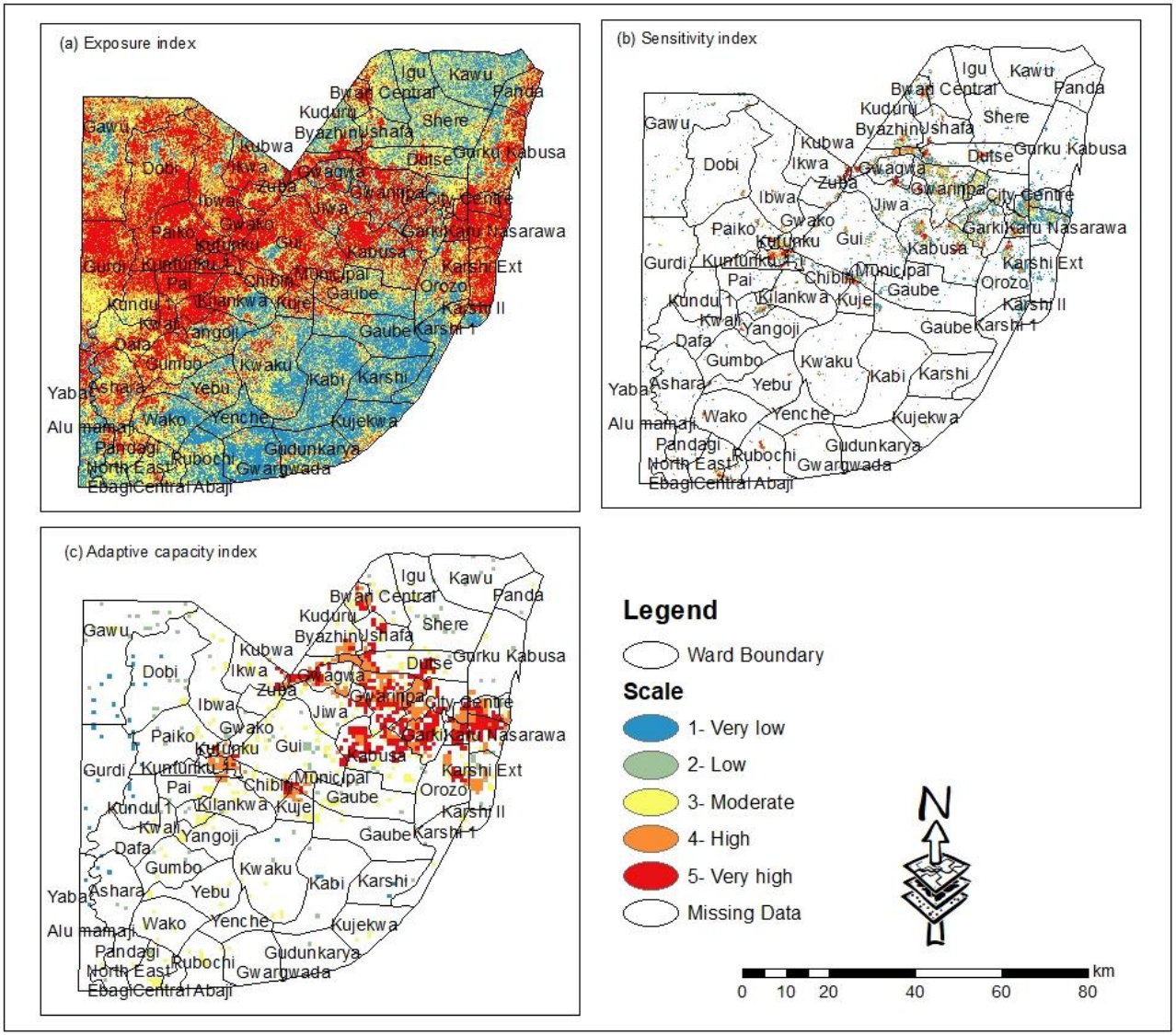


Figure 7.6: Heat exposure index (a), sensitivity index (b), adaptive capacity index (c).

7.3 The heat vulnerability maps

Based on expert judgments, the weighted overlay tool in ArcGIS was used to construct the heat vulnerability maps for this investigation. There were two heat vulnerability maps created for Abuja and its surroundings. First, a heat vulnerability map was made by experts ranking the three secondary indicators' relative importance. The three layers' influence weights (exposure index: 41%, sensitivity index: 35%, and adaptive capacity index: 24%) were determined using these metrics. Second, using the nine primary indicators from the study, heat vulnerability was created. Concerning this, the weighted input criteria for the heat vulnerability map were based on an expert's assessment of the relative influence of the nine reclassified primary indicator maps (LST: 13%, impervious surface: 13%, NDVI: 13%, vulnerable population: 11%, women population: 4%, population density: 9%, poverty level: 13%, literacy level: 9%, and dwelling quality: 15% each, equating 100% as a total). Figures 7.7 (a) and (b) present the heat vulnerability maps of Abuja and its environs. Both maps confirm that the study area's north-eastern and north-western parts have very high and high vulnerability to heat-related morbidity and mortality. Paiko, Ikwa, Gawu, and the western part of Kilankwa, Karu, Aso Kadope, Karshi extension, Dutse, Gwarimpa, Usman, Chibiri, a portion of Garki, Nyanya, Yaba, and Ashara are among the settlements in these areas. Patches of highly vulnerable areas are scattered throughout the study area, indicating that heat-related morbidity and mortality are not limited to urban areas. Areas with moderate vulnerability to heat are well distributed in parts of Gwarimpa, Garki, Kabusa, Jiwa, Orozo, and Kwali. Both maps emphasise moderate vulnerability in Gwarimpa, part of Karu and Kabusa. The city centre, Wuse, part of Garki and part of Gwarimpa has low and very low heat vulnerability. Usman and Bwari in the northern part of the study area were characterised by low vulnerability to heat (Figure 7.7(a)), likely due to the presence of water bodies in the area. However, as shown in Figure 7.7(b), these locations are highly vulnerable. Similarly, the northern part of Kabusa is characterised by a low vulnerability in Figure 7.7(a), but the exact location was characterised by a high vulnerability in Figure 7.7(b). Both heat vulnerability maps from the two methods produce similar results with minor differences. Figure 7.7(a) and (b) presents the two methods' heat vulnerability maps of Abuja and its environs.

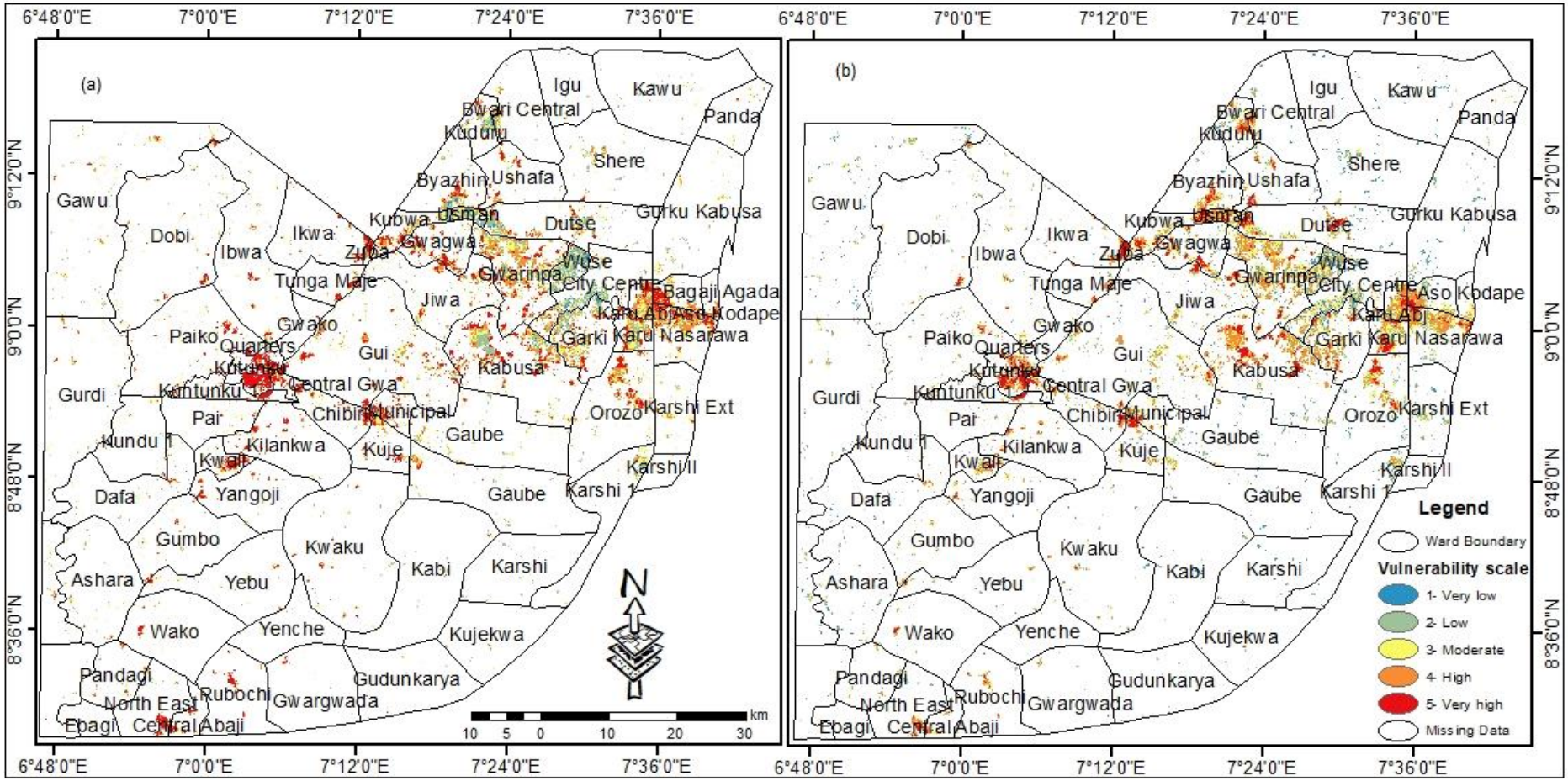


Figure 7.7: Heat vulnerability map from the 2 methods (using 3 secondary indicators (a) and the 9 primary HVIs (b)).

7.4 Sensitivity analysis

Sensitivity analysis examines the degree to which findings are impacted by variations in datasets, methodologies, models, and estimates of unquantified parameters or hypotheses to assess the validity of research findings (Schneeweiss, 2006; de Souza *et al.,* 2016). Sensitivity analysis determines which outcomes depend most on problematic or unproven hypotheses. Conlon *et al.* (2020) have shown that minor modifications to HVI construction can result in quantifiable differences in the performance of the heat vulnerability map. If planners want to use HVIs as policy guides, they must comprehend the consequences of these HVIs' design decisions. Consequently, datasets and methodology-based sensitivity analysis would assist in addressing an effective heat vulnerability data gap. In order to gain a guide to the quality of the heat vulnerability maps developed for this study, a heat vulnerability map was further generated using a similar approach, but from a real-time datasets-demographic and health survey at a ward level. In this regard, nine HVIs were employed for mapping purposes. The LST, impervious surface, and NDVI remain unchanged. Population under 14 and over 65 years, women population, poverty level, literacy rate, population density, and dwelling quality were derived from ward-level demographic and health survey (DHS) statistics. This is done to determine the map's quality by comparing it to other relevant maps from this study using WorldPop data sets.

Figure 7.8(a) presents the reclassified population at risk, comprising a population below 14 years and over 65 years old. Similar to the population at risk map from the WorldPop datasets, the population at risk from the DHS also show a very low influence to heat vulnerability in the urbanised areas compared to settlements away from the city, where a high proportion of vulnerable population contributed to their high influence to heat vulnerability. On the DHS map (Figure 7.8(b)), the women population has a low influence on heat vulnerability in Kawu, Gaube, Dobi, Kujekwa and Gwarimpa relative to the other wards of the study area. The maps of the poverty level, literacy rate and dwelling quality show very low to low influence on heat vulnerability in the

most urbanised part of the study area, such as the city centre, Wuse, Gwarimpa, Garki, and part of Jiwa. Areas of high to very high influence on heat vulnerability were commonly observed in the suburban and informal settlements away from the urban centre. They include settlements of Gawu, Gurdi, Pandagi, and Kujekwa, among others, as shown in Figure 7.8(c), (d) and (e). The population density map from the DHS shows that the settlements close to the city centre of Abuja are more densely populated than settlements away from the city centre. For instance, Karu, Kabusa, Dutse, Zuba, and Pai were among the densely populated settlements that highly influenced heat vulnerability. Areas of low population density were characterised by low influence to heat vulnerability. These areas are common on the outskirt of the city. Among these wards were Kawu, Gawu, Wako, and Panda. Figure 7.8 presents the reclassified HVIs from the DHS datasets.

Using the 6 HVIs from the DHS presented in Figure 7.8, in addition to the LST, artificial impervious surface and NDVI maps, a weighted overlay tool in ArcGIS was used to create the heat vulnerability map for DHS datasets. The weighted overlay map was calculated using the expert's judgements on the relative influence of the 9 primary HVIs, similar to Figure 7.6(a). In this regard, the model weighted input criteria were the UHI, artificial impervious surface, NDVI, vulnerable population, women population, the poverty level, literacy rate, dwelling quality and population density. The heat vulnerability map from the DHS datasets for this study expresses the spatial variations of the vulnerability on an ordinal scale. When the spatial units of the heat vulnerability map were quantified, the areas comprised very low, low, moderate, high and very highly vulnerable areas, respectively.

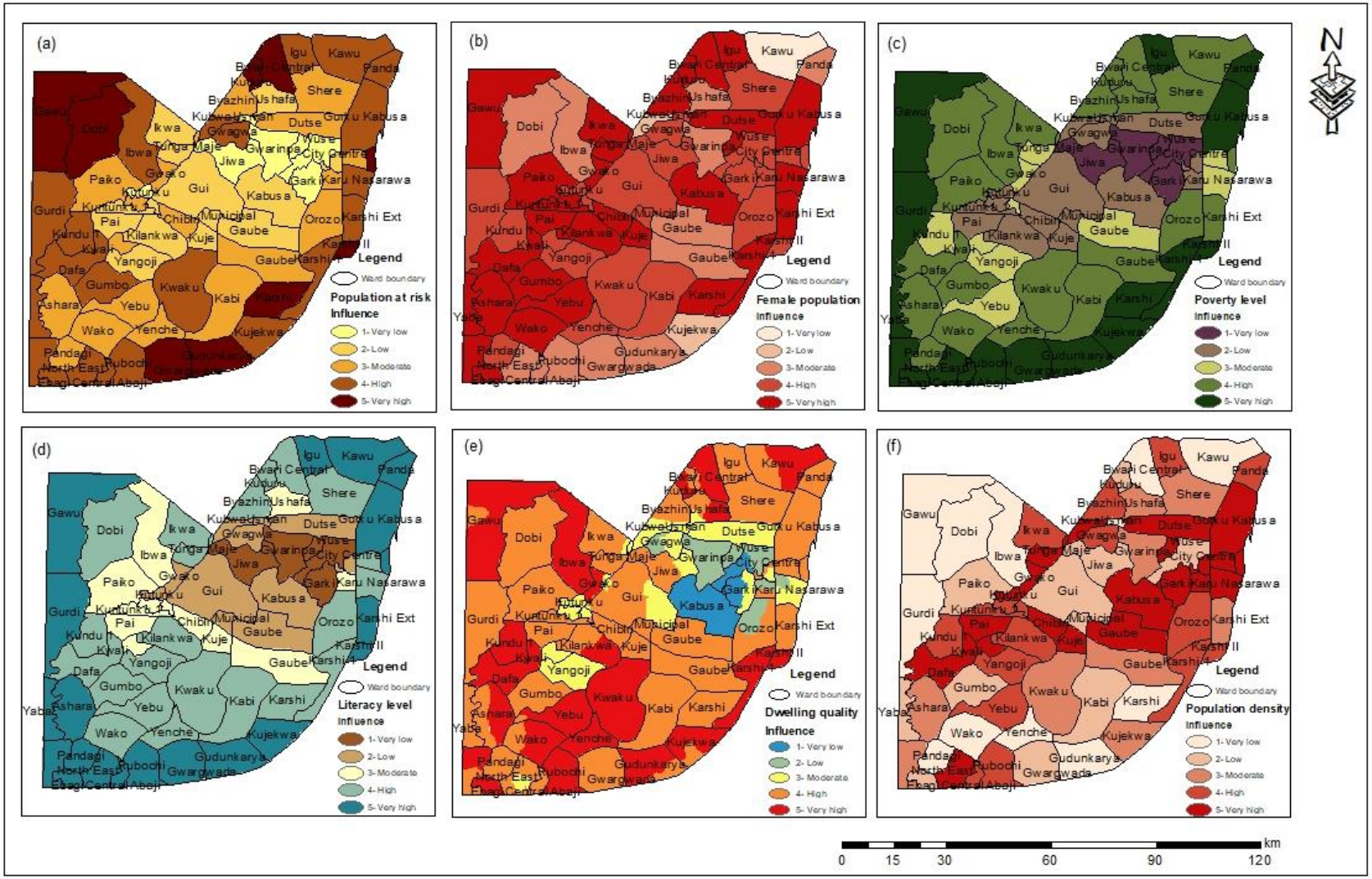


Figure 7.8: Reclassified heat vulnerability indicators of Abuja and its environs from the Demographic and Health Survey Datasets, (a) population at risk, (b) women population, (c) poverty level, (d) literacy rate, (e) dwelling quality, (f) population density.

7.5 Comparison of heat vulnerability maps derived from DHS and WorldPop datasets

Table 7.2 compares map areas from the WorldPop and the DHS datasets to ascertain their level of agreement, which revealed that the very high and highly vulnerable locations to heat occupied 12.19% and 30.01% of the map area generated from the WorldPop data. In contrast, the very high and highly vulnerable areas on the map generated by the DHS occupied 23.58 and 22.95% of the map area, respectively. Both maps revealed a reasonable proportion of increased vulnerability to heat in the northern wards of Zuba, Kubwa, Gwagwa, Kuduru, and part of Bwari. A substantial portion of the Usman ward exhibits low heat vulnerability on the DHS map. This is most likely due to the presence of the Usman dam in the area. Both maps show high vulnerability to heat in Bagaji Agada, Kabusa, Garki, Karu, and Nyanya wards in the eastern part of the study area. In both maps, areas of informal settlements in this region, such as Bagaji and Karu, appear to have a higher proportion of high vulnerability to heat. Increased heat vulnerability in the southwestern part of the study area includes quarters, Kutunku, Paiko, a portion of Kuje, and Kwali. However, as illustrated in Figure 7.8, there is a spatial variation in the proportion of heat vulnerability in these wards.

Throughout the map area, there are areas of moderate heat vulnerability. On the WorldPop and DHS models, they occupied 26.65% and 24.36% of the map area. The reasonable proportions of areas with low heat vulnerability in some urbanised parts of the study area with high proportions of imperviousness are intriguing for both models. This may be due to trees, parks, gardens, and surface water in these areas. Settlements, including Gwarimpa, GUI, the city centre, and a substantial portion of Dutse in the north to the north-eastern part of the study area, have very low to low heat vulnerability. However, on the DHS map, Wuse ward, a busy commercial and shopping hub in the Municipal area council, appears to have a high proportion of areas highly vulnerable to heat. On the WorldPop map, regions of very low and low vulnerability to heat occupied 8.14% and 22.99 % of the map area and 12.88% and 15.24% on the DHS map. In both maps, the southern part of the study area appears to have a high

proportion of low heat vulnerability. Figure 7.9(a) and (b) depict the two maps derived from the WorldPop and DHS datasets. The percentage of land covered by each map is presented in Table 7.2.

Table 7.2: Area (%) of the heat vulnerability maps from WorldPop and DHS datasets

Vulnerability scale	Heat vulnerability % map area	
	DHS	WorldPop
(1) Very Low	12.88	8.14
(2) Low	15.24	22.99
(3) Moderate	24.36	26.65
(4) High	22.95	30.01
(5) Very High	23.58	12.19

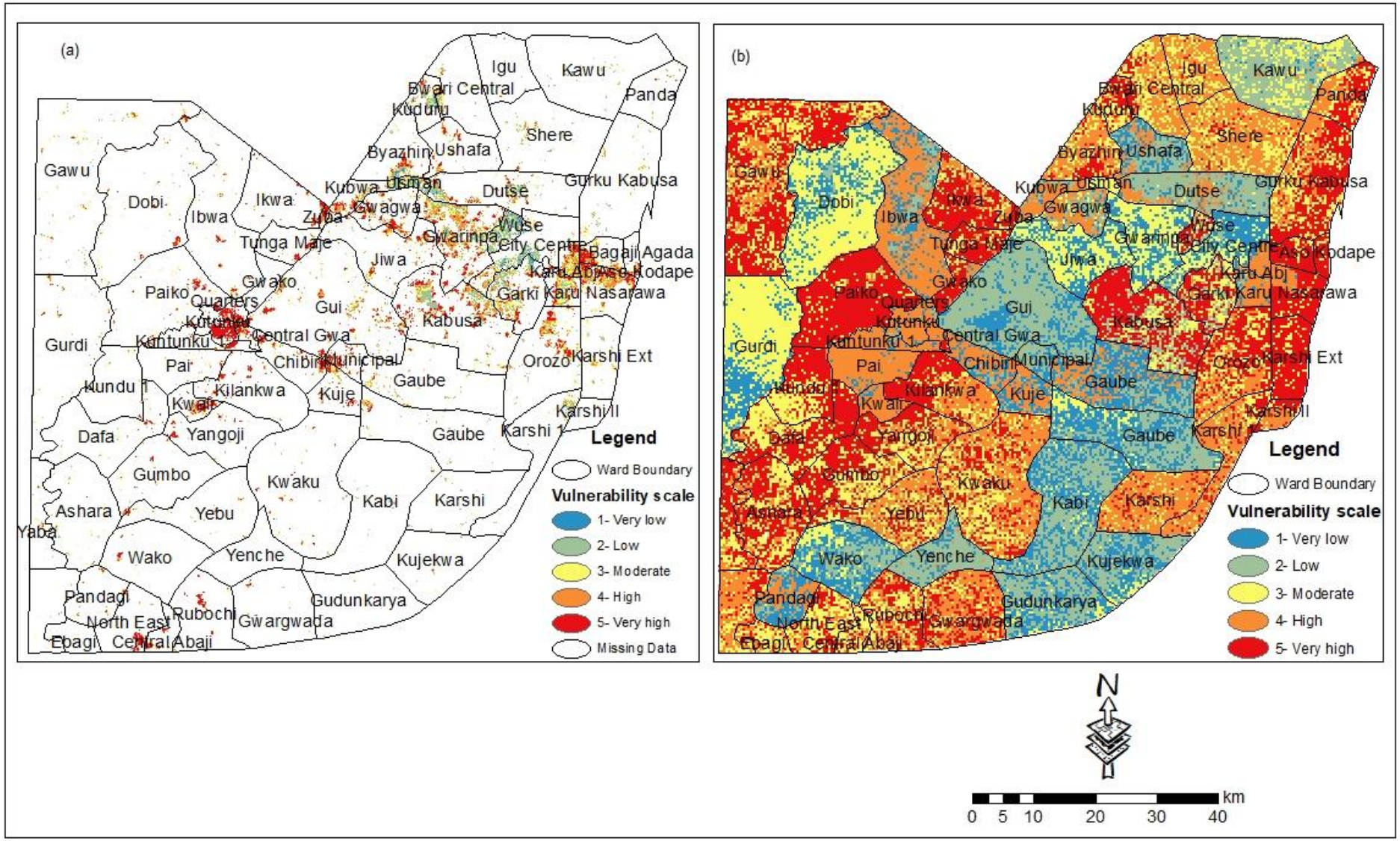


Figure 7.9: Heat vulnerability maps of Abuja and environs from the WorldPop datasets (a) and the Demographic and Health Survey Datasets (b)

7.6 Site-specific comparison of heat vulnerability maps generated from WorldPop and DHS datasets

Table 7.3 presents a pivot table for a site-specific comparison of the heat vulnerability maps from the WorldPop and DHS datasets. True positive (TP): An observation that is both predicted and observed to be positive on both maps. False positive (FP): An observation that was projected to be positive but turned out to be negative. True negative (TN): An observation that is anticipated to be negative but turns out to be negative. As can be seen from column 4 of Table 7.3, representing sample points of map class of very low vulnerability, 22621 sample points were true positive because the observations from both maps from the WorldPop and DHS datasets identified these locations as very low heat vulnerability areas. 7952 sample points were misclassified as low vulnerable areas, 3059 sample points were misclassified as moderate areas, and 9487 sample points were misclassified as highly vulnerable. The overall accuracy of the very low vulnerability class was 46.29%, as shown in column 9 of Table 7.3.

For the low vulnerable scale, 16773 sample points were misclassified as very low vulnerable on the WorldPop map. 70964 sample points were the true positive because they accurately classified as low vulnerability areas on both maps from the WorldPop and DHS datasets. 17709 sample points were misclassified as moderate vulnerability, 9439 sample points were misclassified as high vulnerability areas, and 23076 sample points were misclassified as very high vulnerability areas. In comparison, 5741 sample points were misclassified as very highly vulnerable. The overall accuracy of the low vulnerability class was 51.44%, as shown in column 9 of Table 7.3. For the moderate vulnerability scale presented in column 6 of Table 7.3, 13424 sample points were misclassified as very low heat vulnerability areas, 15233 sample points were misclassified as low heat vulnerability areas, 76124 sample points were correctly classified as moderate vulnerability areas, 40124 sample points were misclassified as high vulnerability areas, and 15032 sample points were misclassified as very high vulnerability areas. The accuracy of the moderate vulnerability areas is 47.59%, as shown in column 9 of Table 7.3.

For the high vulnerability areas, 8775 sample points were misclassified as very low vulnerable areas, 15570 sample points were misclassified as low vulnerability areas, 20797 sample points were misclassified as moderate vulnerability areas, 94649 sample points were correctly classified as high vulnerability areas on both maps of heat vulnerability from the WorldPop datasets and the DHS datasets, whereas 40330 sample points were misclassified as highly vulnerable areas. The overall accuracy of the high vulnerability class is 52.55%, as shown in column 9 of Table 7.3. For the very high vulnerability class, 1096 sample points were misclassified as very low vulnerability class, and 3159 sample points were misclassified as low vulnerability areas. 4973 sample points were misclassified as moderate vulnerability areas. 16204 sample points were misclassified as high vulnerability areas. 47625 sample points were correctly classified as very high heat vulnerability areas on both maps from the WorldPop and DHS datasets. The overall accuracy of the very highly vulnerable class is 65.20%, as shown in column 9 of Table 7.3**.** Figure 7.10 presents the sample points of the heat vulnerability maps from the WorldPop and DHS datasets. The Site-specific comparison of the heat vulnerability maps from the WorldPop and DHS datasets is presented in Table 7.3.

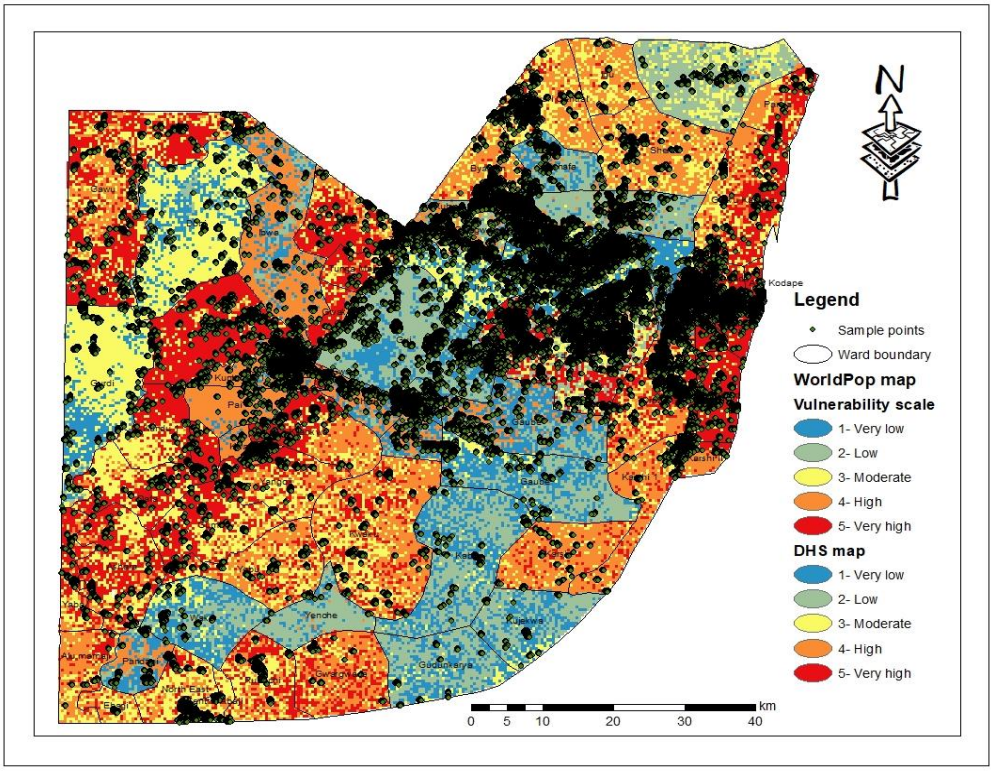


Figure 7.10: sample points of the heat vulnerability maps from the WorldPop and DHS datasets.

Table 7.3: Site-specific comparison of the heat vulnerability maps from the WorldPop and DHS datasets

	Vulnerability scale	vulnerability scale	1-very low	2-Low	3-Moderate	4-High	5-Very High	(%)Accuracy
1- Very low	1-very low	1	22621	0	0	0	0	46.29
	2-low	1	7952	0	0	0	0	
	3-moderate	1	3058	0	0	0	0	
	4-high	1	9487	0	0	0	0	
	5-very high	1	5741	0	0	0	0	
2-Low	1-very low	2	0	16773	0	0	0	
	2-low	2	0	70964	0	0	0	51.44
	3-moderate	2	0	17709	0	0	0	
	4-high	2	0	9439	0	0	0	
	5-very high	2	0	23076	0	0	0	
3- Moderate	1-very low	3	0	0	13424	0	0	
	2-low	3	0	0	15233	0	0	
	3-moderate	3	0	0	76124	0	0	47.59
	4-high	3	0	0	40124	0	0	
	5-very high	3	0	0	15032	0	0	
4-High	1-very low	4	0	0	0	8775	0	
	2-low	4	0	0	0	15570	0	
	3-moderate	4	0	0	0	20797	0	
	4-high	4	0	0	0	94649	0	52.55
	5-very high	4	0	0	0	40330	0	
5-Very High	1-very low	5	0	0	0	0	1096	
	2-low	5	0	0	0	0	3159	
	3-moderate	5	0	0	0	0	4973	
	4-high	5	0	0	0	0	16204	
	5-very high	5	0	0	0	0	47652	65.20

7.7 Limitations of census data at the ward level for sensitivity analysis

Census data at the ward level has limited spatial resolutions, which can restrict its utility and accuracy. Among the limitations of using census data at the ward level for sensitivity analysis of the WorldPop data-generated vulnerability maps are:

1. Census data at ward level lack detailed geographical information: Low-resolution census data provides limited information about the spatial distribution of population characteristics. It typically uses large geographic units, such as census blocks or tracts, which can mask variations within these units. This lack of detail makes it challenging to accurately analyse localized patterns and trends.

2. Inability to capture fine-scale variations: Low-resolution spatial mapping fails to capture fine-scale variations in population characteristics. For instance, it might not accurately represent demographic patterns within neighbourhoods, urban areas, or rural regions, where there could be significant variations in socioeconomic factors, ethnic composition, or housing patterns.

3. Difficulty in identifying small population groups: Low-resolution census data may need to capture small population groups or subgroups with distinct characteristics adequately. This can result in underrepresentation or misrepresentation of marginalized or minority populations, making it challenging to address their specific needs or develop targeted policies.

4. Limited accuracy in spatial analysis: Low-resolution mapping can introduce errors when conducting spatial analysis. Aggregating data into larger units can lead to the ecological fallacy, where conclusions based on aggregated data do not accurately reflect individual-level characteristics. This can affect local policy decisions, resource allocation, and planning at local levels.

5. Challenges in monitoring spatial changes over time: Low-resolution census data might need to provide more granularity to monitor spatial changes and trends accurately. Identifying shifts in population distributions, urban growth patterns, or changes in demographic characteristics at a localized level becomes difficult, hindering effective long-term planning.

6. Reduced ability for small-area comparisons: Low-resolution spatial mapping restricts the ability to make meaningful comparisons between small geographic areas. When the data is aggregated into larger units, assessing disparities, identifying clusters, or understanding specific neighbourhood-level dynamics becomes challenging.

7.8 Validation using data on heat-related mortality

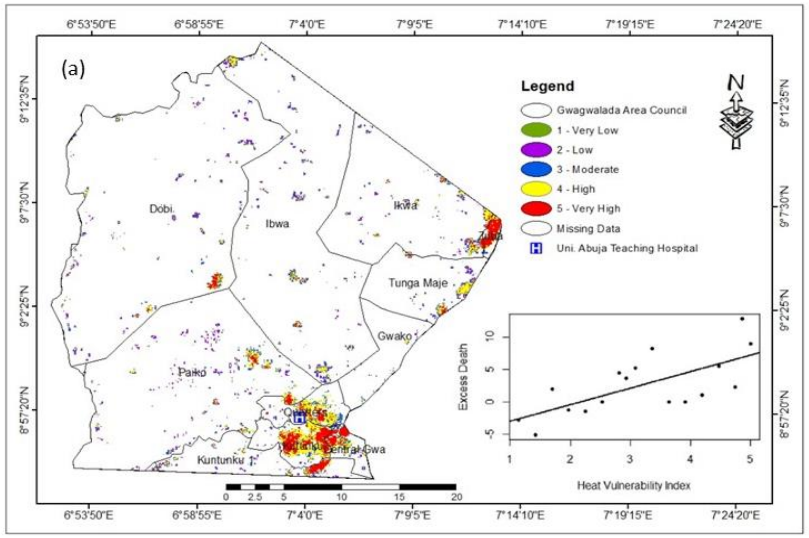
One of the most common techniques for validating heat vulnerability maps is the use of heat-related morbidity or mortality data. For example, Reid *et al.* (2012) were among the earlier study that used mortality data to validate heat vulnerability maps. Using a regression model, the relationship between observed heat-related mortality and the heat vulnerability categories index was determined. In this regard, the initially computed excess mortality in chapter six was used for the validation of heat vulnerability maps in this section. Heat-related mortality from six hospitals in the study area (Specialist hospital Mararaba, Karu area of Nasarawa state, National Hospital Abuja, General hospital Kuje, General hospital Abaji, General Hospital Kwali, and the University of Abuja Teaching Hospital Gwagwalada) were used as the dependent variable, while the heat vulnerability index for the corresponding map in Figure 7.11(a), (b), (c), (d), (e) and (f) were used as the independent variable. In this regard, the heat vulnerability score for the specific location of the hospitals were used for the validation.

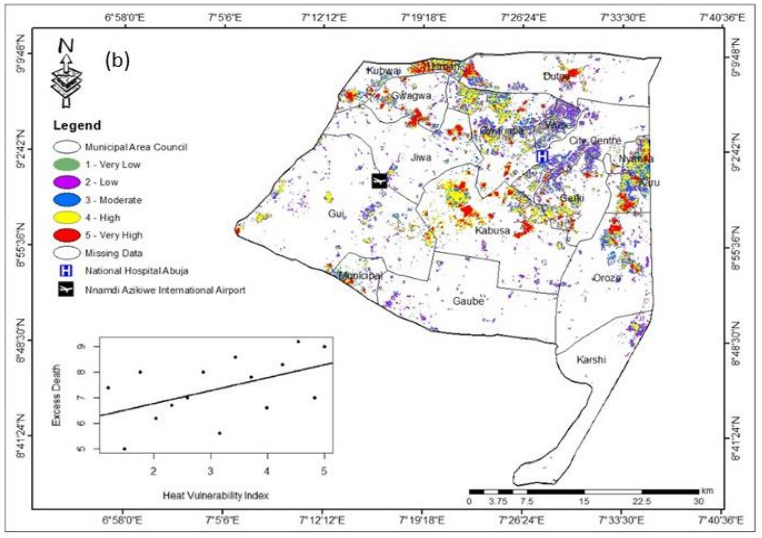
Even though the relationship between observed heat-related mortality and heat vulnerability maps is significant, the regression model in Table 7.4 shows a

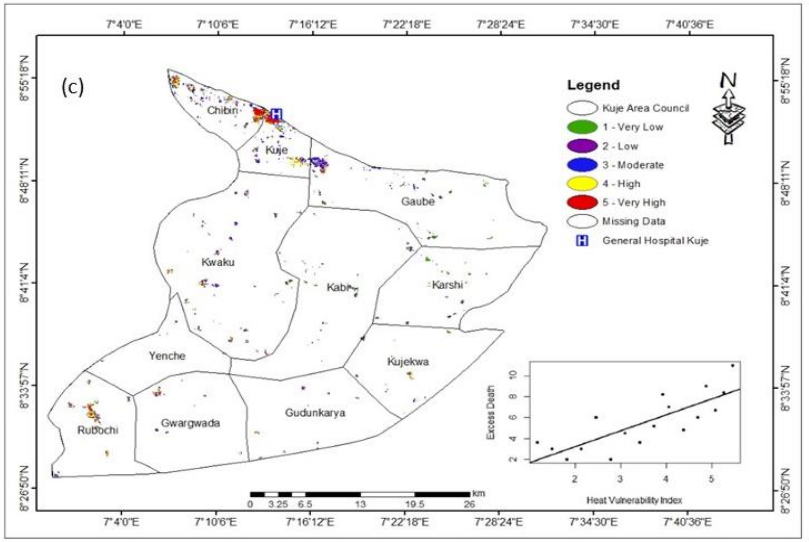
weak statistical relationship between the heat vulnerability map and excess mortality for the National hospital Abuja municipal area council (R^2 = 0.26, *p*-value = 0.05) and the general hospital Abaji municipal area council (R^2 = 0.36, *p*-value = 0.01). In Table 7.4, there was a moderate to strong relationship between observed heat-related mortality and heat vulnerability maps at the specialist hospital Mararaba, Karu area (R^2 = 0.58, *p*-value = 0.00,.05); general hospital Kuje area council (R^2 = 0.56, *p*-value = 0.00,.05); general hospital Kwali area council (R^2 = 0.55, *p*-value = 0.00,.05); and the University of Abuja Teaching hospital Gwagwalada (R^2 = 0.48, *p*-value = 0.00, .05). The regression result for the six hospitals in the study area is summarised in Table 7.4.

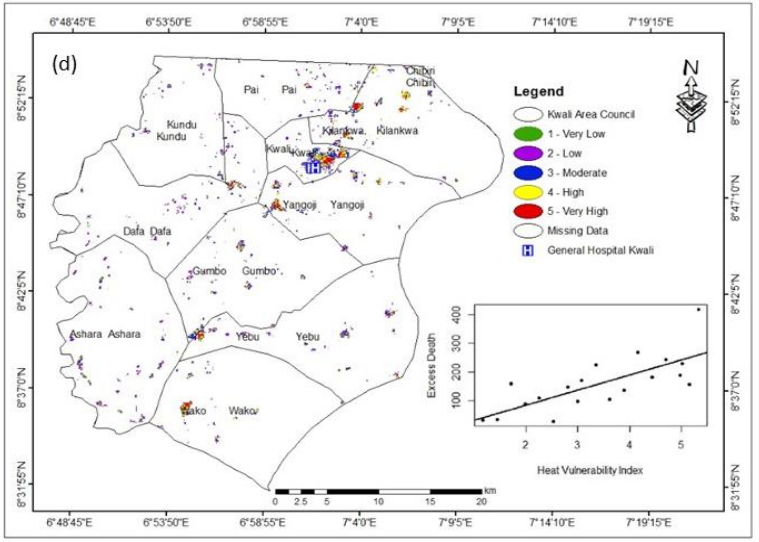
Table 7.4: Summary of regression output of Heat vulnerability map and excess mortality for the (6) simulated hospitals

No. Location	R^2	Regression equation	F value	Coefficients	Standard error	Significant level	*p*-value
1. Teaching Hospital Gwagwalada	0.49	$y = 0.6311x - 12.8$	14.34	0.63	0.17	0.05	0.001
2. National Hospital Abuja	0.26	$y = 0.1385x + 3.8398$	4.62	0.14	0.06	0.05	0.050
3. General Hospital Kuje	0.56	$y = 0.408x - 4.6552$	19.10	0.41	0.09	0.05	0.000
4. General Hospital Kwali	0.55	$y = 12.429x - 132.36$	21.04	12.43	2.71	0.05	0.000
5. Specialist Hospital Mararaba	0.59	$y = 9.2678x - 23.058$	24.01	9.27	1.89	0.05	0.000
6. General Hospital Abaji	0.37	$y = 0.4356x - 4.4571$	8.67	0.44	0.147	0.05	0.010


(a)
Legend
Gwagwalada Area Council
1 - Very Low
2 - Low
3 - Moderate
4 - High
5 - Very High
Missing Data
Uni. Abuja Teaching Hospital
Dobi
Ibwa
Ikwa
Tunga Maje
Gwako
Paiko
Kuntunku
Excess Death
Heat Vulnerability Index


(b)
Legend
Municipal Area Council
1 - Very Low
2 - Low
3 - Moderate
4 - High
5 - Very High
Missing Data
National Hospital Abuja
Nnamdi Azikiwe International Airport
Kubwa
Gwagwa
Dutse
Jiwa
Gui
Kabusa
Gaube
Karshi
Orozo
Excess Death
Heat Vulnerability Index


(c)
Legend
Kuje Area Council
1 - Very Low
2 - Low
3 - Moderate
4 - High
5 - Very High
Missing Data
General Hospital Kuje
Chibiri
Kuje
Gaube
Kwaku
Kabi
Karshi
Yenche
Kujekwa
Gudunkarya
Gwargwada
Rubochi
Excess Death
Heat Vulnerability Index


(d)
Legend
Kwali Area Council
1 - Very Low
2 - Low
3 - Moderate
4 - High
5 - Very High
Missing Data
General Hospital Kwali
Pai
Chibiri
Kundu
Kilankwa
Kwali
Yangoji
Dafa
Gumbo
Ashara
Yebu
Wako
Excess Death
Heat Vulnerability Index

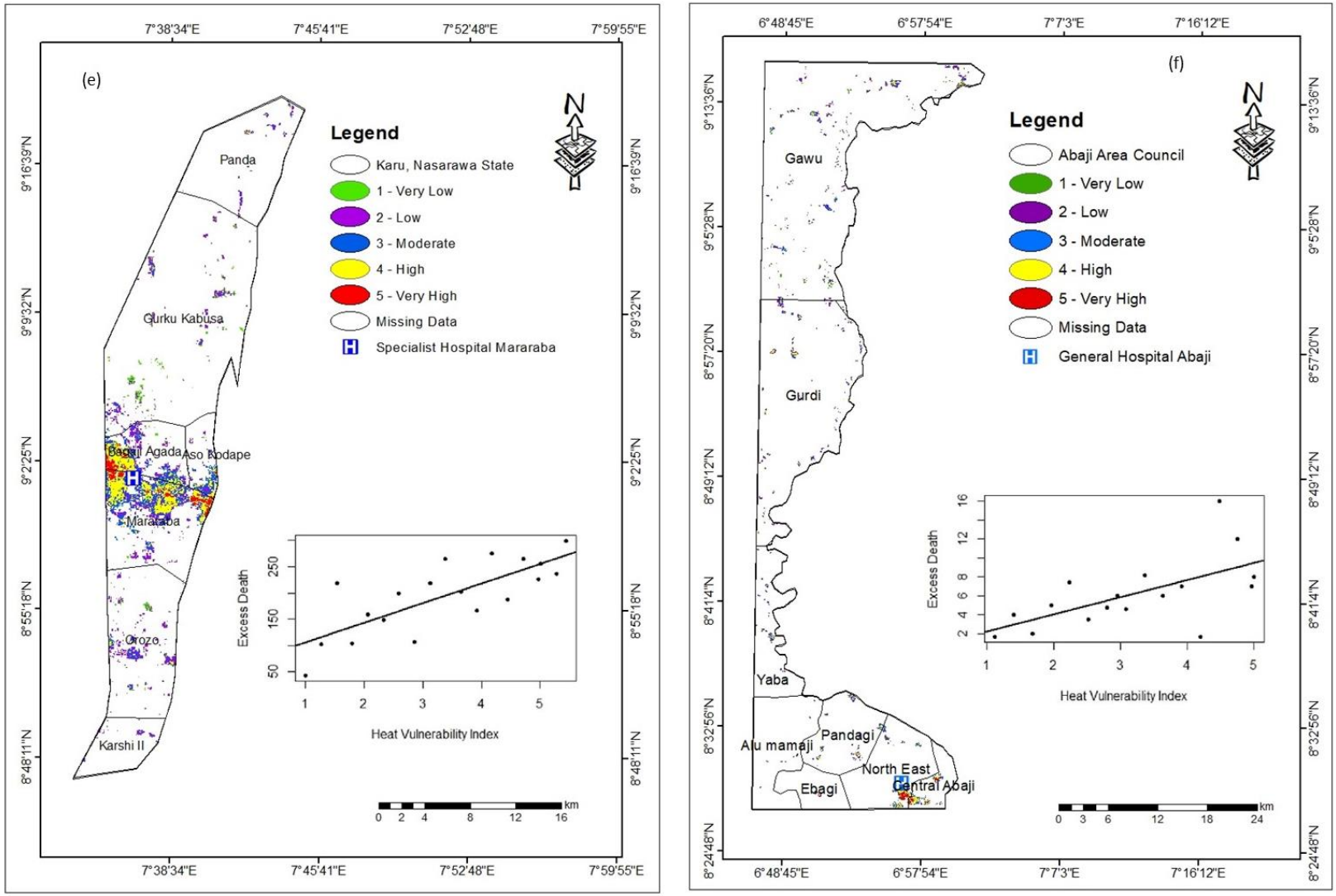
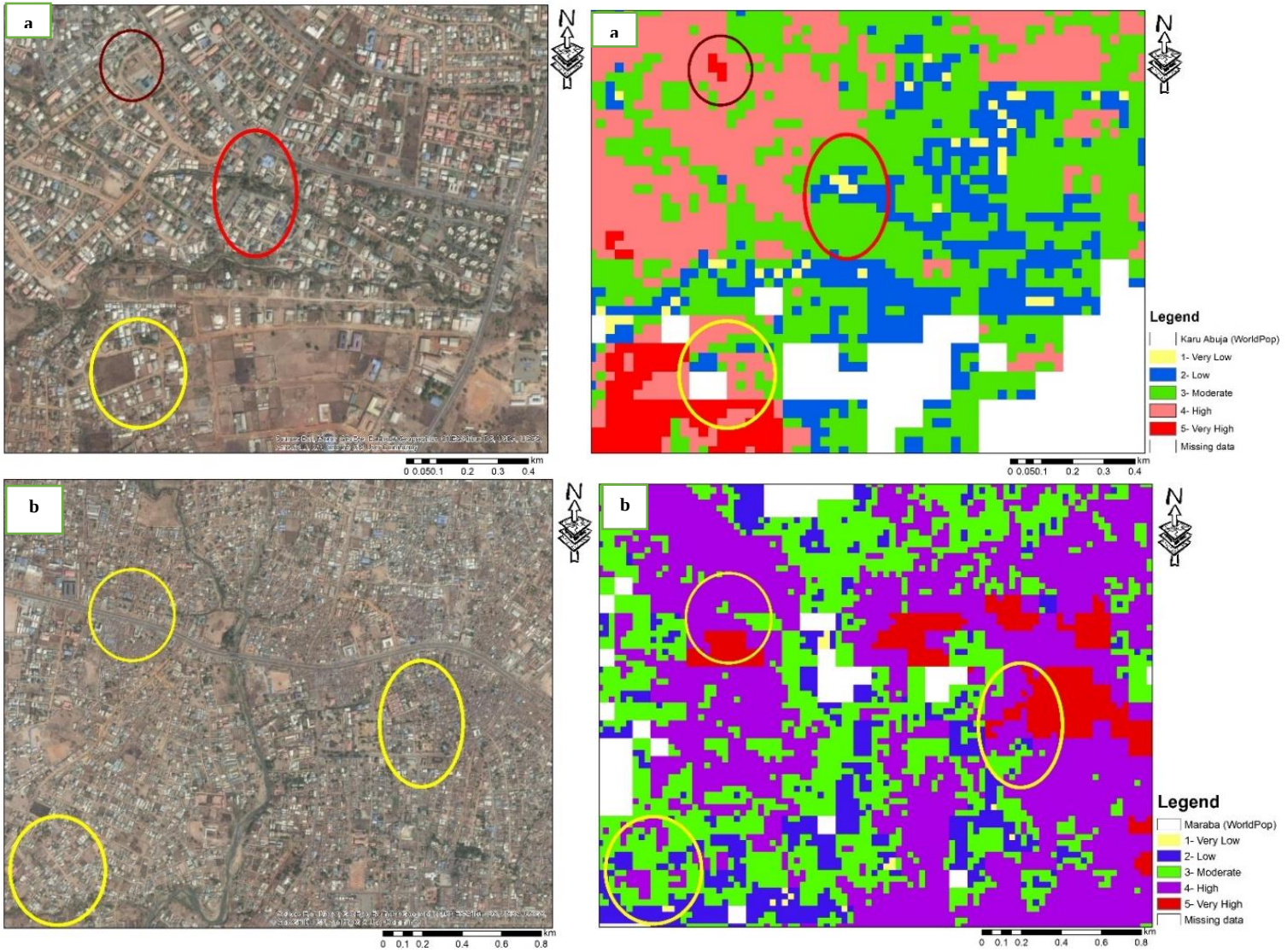
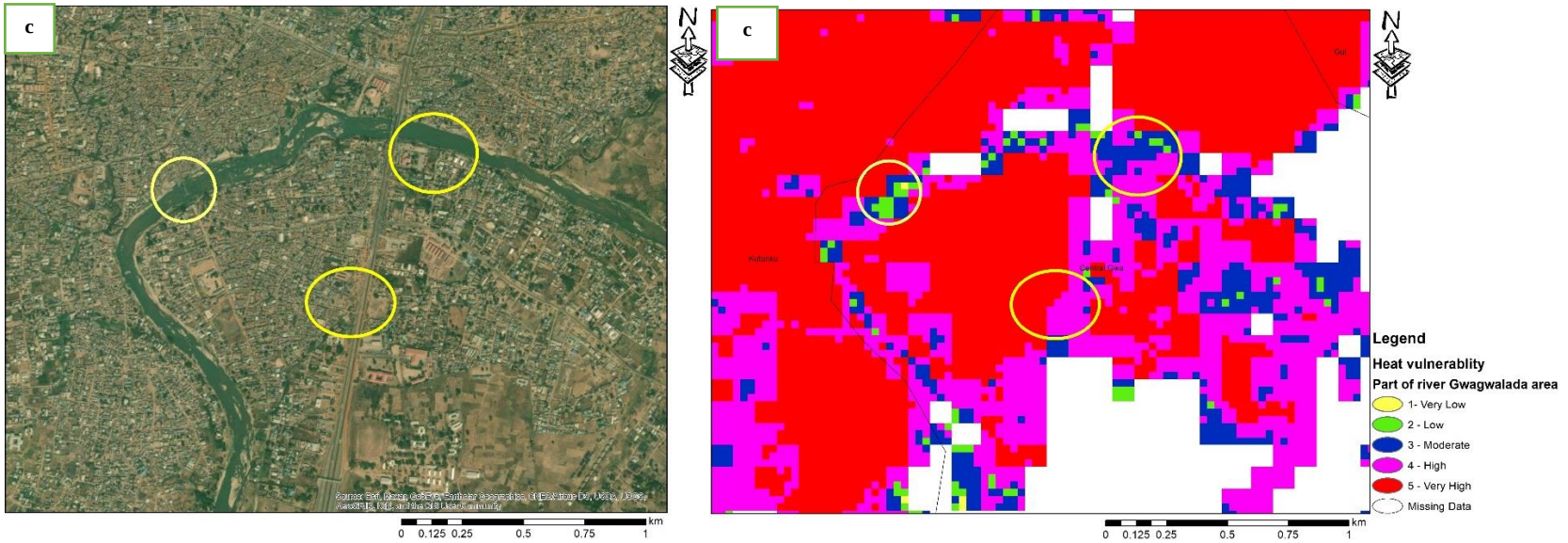


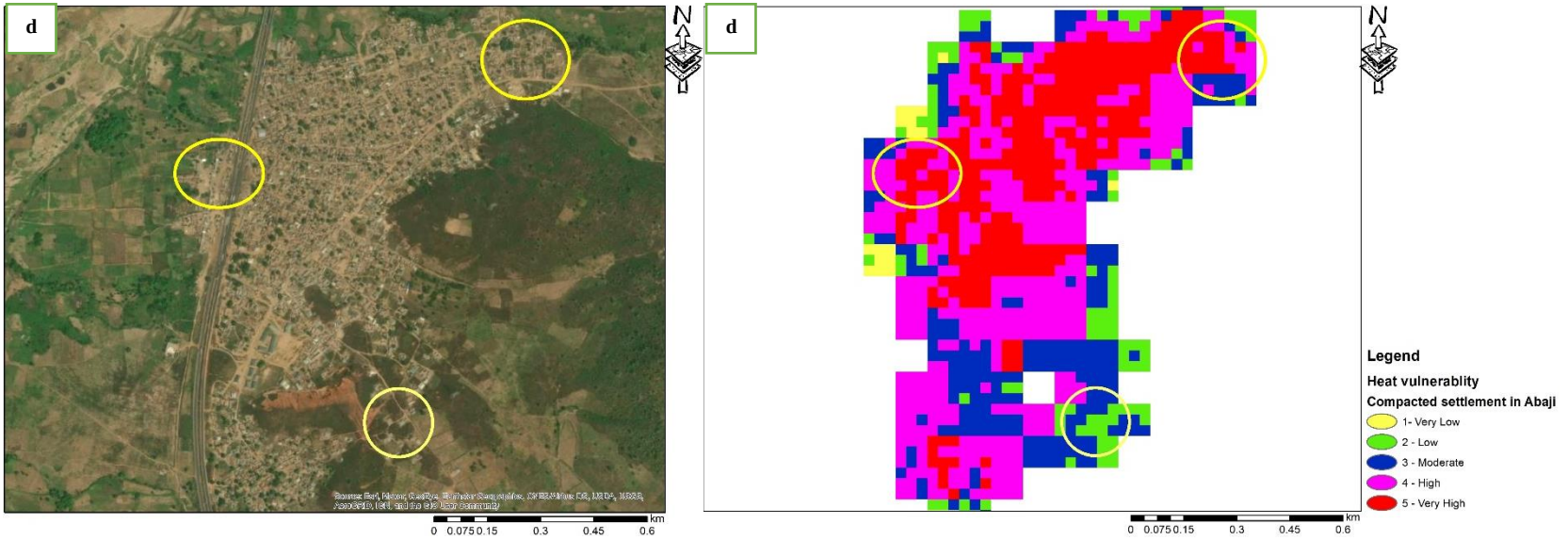
Figure 7.11: Heat vulnerability and regression plot of the Gwagwalada area council (a); Municipal area council (b); Kuje area council (c); Kwali area council (d); Karu area of Nasarawa state (e), and Abaji area council (f).

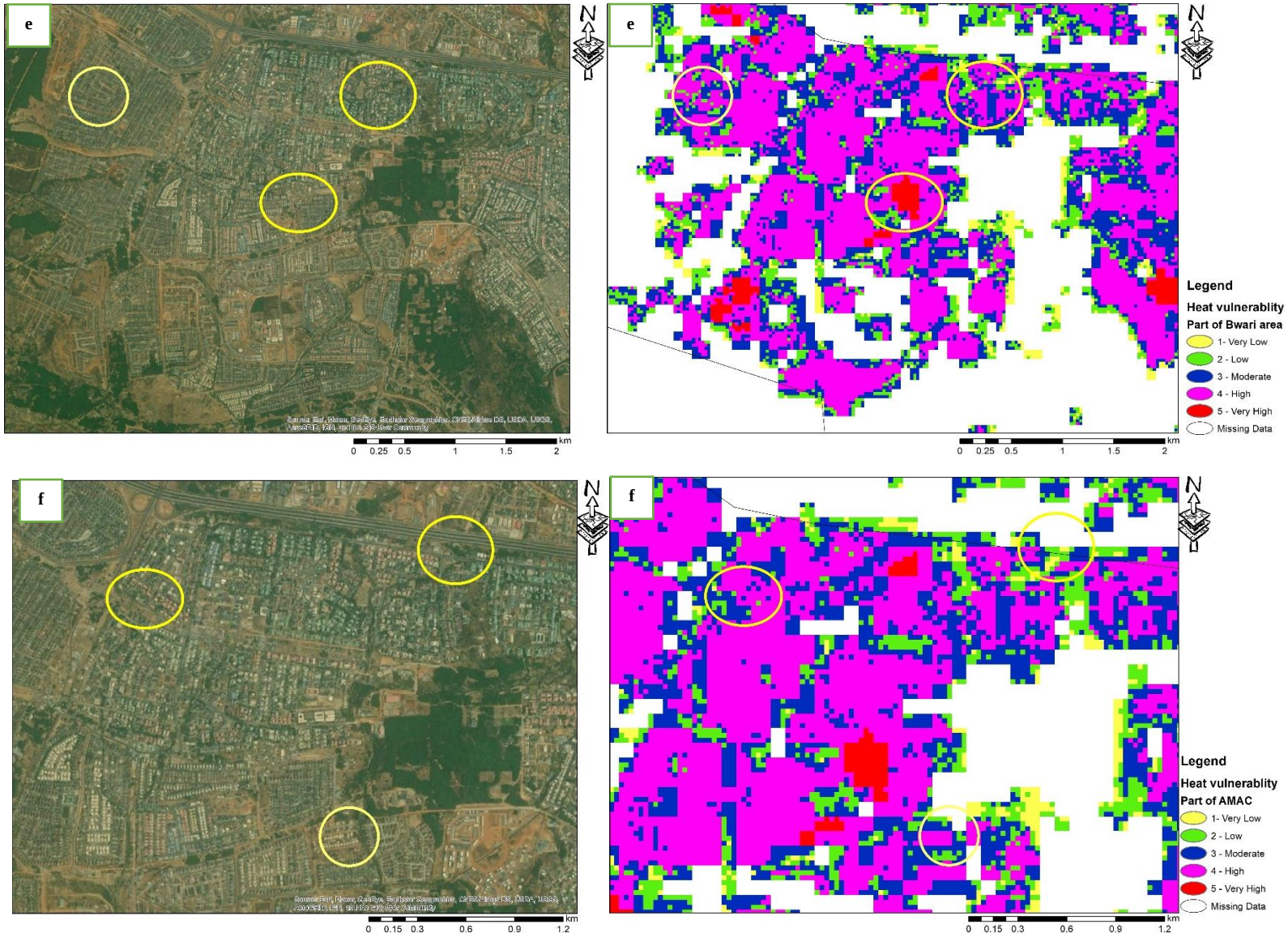
7.9 Confirmation of heat vulnerability locations on a high-resolution satellite image

For this investigation, the heat vulnerability map was overlaid on a high-resolution image to check the features at the sites and their association with a low, moderate, or high level of heat vulnerability. Prominent features on the heat vulnerability maps were zoomed in for verification on a high-resolution image, as shown in Figure 7.12. The confirmation shows that areas of vegetation cover and water bodies appear to have a very low and low vulnerability to heat on the satellite image, as shown in Figures 7.12 (a), (b), and (c). Similarly, the yellow circle in Figure 7.12 (d), (g), and (h) shows areas with a mixture of bare surfaces, artificial impervious surfaces, water bodies, and trees. This confirmed the relationship between the heat vulnerability scale and the land use/cover of the locations. It became obvious that the areas with impervious and bare surfaces show a high heat vulnerability compared to the adjacent places of trees and, rivers, streams, lakes, and ponds that offer low to moderate vulnerability on the map. The presence of industry was recognised in a highly urbanised settlement in the northern-western part of Figure 7.12(a), which could attribute to the high level of heat vulnerability in the location as indicated by a smaller circle. Further comparison shows that areas of the informal settlements characterized by increased population density, low quality, unplanned, and compacted buildings are highly vulnerable to heat, as shown in Figure 7.12(a), (d), (e), and (f).


a
N
0 0.050.1 0.2 0.3 0.4
km
a
N
Legend
Karu Abuja (WorldPop)
1- Very Low
2- Low
3- Moderate
4- High
5- Very High
Missing data
0 0.050.1 0.2 0.3 0.4
km
b
N
0 0.1 0.2 0.4 0.6 0.8
km
b
N
Legend
Maraba (WorldPop)
1- Very Low
2- Low
3- Moderate
4- High
5- Very High
Missing data
0 0.1 0.2 0.4 0.6 0.8
km


c
N
0 0.125 0.25 0.5 0.75 1
km
c
N
Legend
Heat vulnerablity
Part of river Gwagwalada area
1- Very Low
2 - Low
3 - Moderate
4 - High
5 - Very High
Missing Data
0 0.125 0.25 0.5 0.75 1
km


d
N
0 0.075 0.15 0.3 0.45 0.6
km
d
N
Legend
Heat vulnerablity
Compacted settlement in Abaji
1- Very Low
2 - Low
3 - Moderate
4 - High
5 - Very High
0 0.075 0.15 0.3 0.45 0.6
km


e
N
0 0.25 0.5 1 1.5 2 km
e
N
0 0.25 0.5 1 1.5 2 km
Legend
Heat vulnerablity
Part of Bwari area
1- Very Low
2 - Low
3 - Moderate
4 - High
5 - Very High
Missing Data
f
N
0 0.15 0.3 0.6 0.9 1.2 km
f
N
0 0.15 0.3 0.6 0.9 1.2 km
Legend
Heat vulnerablity
Part of AMAC
1- Very Low
2 - Low
3 - Moderate
4 - High
5 - Very High
Missing Data

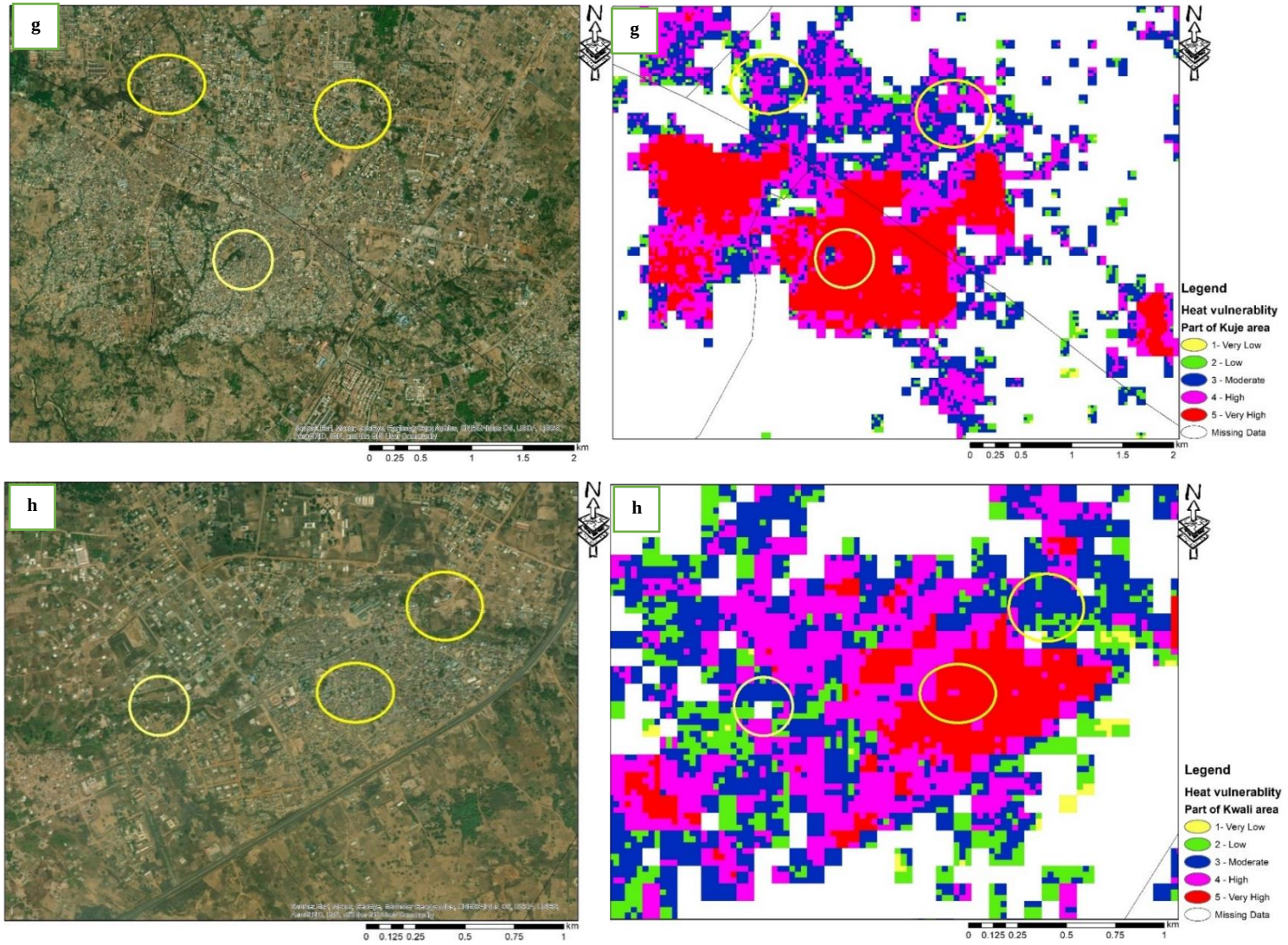


Figure 7.12: Heat vulnerability map and Google image of part of (a) AMAC, (b) Karu, (c) Gwagwalada, (d) Abaji, (e) Bwari, (f) Kuje, and (g) Kwali area council.

Figure 7.12 shows that informal settlements in Abuja are more vulnerable to heat, which may be attributable to the area's high population density, and compacted low-quality buildings. According to Ndetto & Matzarakis (2017), informal community people are prone to extreme heat, similar to the northern slice of Abuja, where the high intensity of heat prevails more than those in the southern region. In addition to the Karu district, Mpape, Quarters, Zuba, and Gwarimpa are vulnerable communities surrounding the city centre. Often, these informal settlements consist of poorly constructed, closely packed little structures. Residents in these neighbourhoods are more likely to endure heat stress and discomfort due to poor planning and a lack of green infrastructure. According to Naicker *et al*. (2017), residents of South Africa's informal settlements are the most vulnerable to extreme heat, with temperatures up to 5°C higher than the adjacent city.

This research shows that more people are relocating to the study area, resulting in the growth of informal settlements in and around Abuja and the disappearance of green spaces. This finding is consistent with what Roy *et al*. (2018) discovered in their study of the association between heat and fatalities as evaluated by microclimate indices. People who live in locations with less vegetation are more likely to become ill or die. In densely populated areas with poor infrastructure, there are insufficient green spaces to lessen the LST and assist cool the evening air (Rehan, 2016; Schinasi *et al*., 2018; Tian *et al.*, 2021). People need night-time cooling to have decent night-time sleep and recuperate from the day's temperature. Higher night-time temperatures have been linked to decreased sleep in studies, with the effect being most important for low-income people and the aged (Obradovich *et al*., 2017). A current study comparing overnight heat and fatalities in a metropolitan region shows that high-night heat plays a major role in heat-related deaths. When the days and nights are hot, the effect is most evident (Murage *et al*., 2017; Royé *et al.*, 2021).

During extreme heat events, people with less income are more likely to die outside of a hospital. Most people who live in informal settlements have low incomes and do not know about all the health problems that come with heat, which may limit their ability to adapt. Their lack of knowledge about

temperature levels shows that they do not use weather forecasts or reports, making it harder for them to get ready. It could also be because there are no early warning systems, programmes to help people stay healthy in hot weather. This is probably true for most people who live in informal settlements.

7.10 Conclusion

In a changing climate, communities must develop strategic plans to safeguard vulnerable people from heat-related morbidity and mortality. This chapter combines maps of AIS, LST, and the NDVI with socioeconomic and demographic variables to map heat vulnerability. The goal was to identify regions vulnerable to heat for heat mitigation policy and adaptation strategies. Results from the study revealed a spatial variation of heat vulnerability in the study area with zones with a high concentration of AIS more vulnerable to heat. The heat capacity of these materials is high, and they cool off slowly at night, contributing to UHI. High heat vulnerability locations can also be found where bare lands, scant vegetation, construction sites, and rural pastures. There is less heat vulnerability where there is water, shade, and green foliage, particularly in locations with dense canopy cover. The statistical validation using the regression model revealed a relatively weak relationship between the heat vulnerability map and excess mortality in the Municipal and Abaji area councils compared to results from Gwagwalada, Kuje, Kwali, and Karu areas. The spatial variations of heat vulnerability in Abuja and its environs can be attributed to the spatial variations in economic level, the efficiency of health facilities, literacy level, and proximity to health facilities, among other population and environmental factors. Mortality has varied because of these factors; otherwise, everyone in the study area would be equally vulnerable to heat. Results from this chapter can assist urban planners and health authorities in improving their emergency response plans and communication strategies for higher heat resilience in urban settings by focusing on immediate and long-term responses by neighbourhood. The following chapter examines future heat vulnerability based on average annual maximum temperature estimates from the CMIP6 for SSPs 1-2.6 and 5-8.5 for the periods 241-2060 and 2081-2100. Under the premise of a rise in temperature, the sensitive population, and the socioeconomic level, the future development of heat vulnerability was projected over Abuja and its environs.

CHAPTER EIGHT: PROJECTIONS OF HEAT VULNERABILITY WITH TEMPERATURE RISE

8.0 Introduction

Extreme heat and socioeconomic factors may exacerbate the harmful effects of climate change on human health. This chapter aims to explore the spatial patterns of temperature change at monthly, seasonal and annual timescales. Five Shared Socioeconomic Pathways (SSPs) models from the Coupled Model Intercomparison Project Phase 6 (CMIP6) were used. The projection models chosen were based on low forcing scenarios (1-2.6) and high forcing scenarios (5-8.5) for 2041-2060 and 2081-2100. The chapter intends to develop future projections of heat vulnerability for Abuja and its surroundings based on the assumption of rising temperatures in the middle and end of the 21st century, while leaving the demographic and socioeconomic variables at present.

8.1 The Coupled Model Intercomparison Project

In the sixth phase of the CMIP6, the partners and modelling teams were organised and coordinated by the World Climate Research Programme (WCRP). Over time, as participation in CMIP increased and the number and complexity of climate models increased, so did the need for more thorough and organised experiments. Due to this, CMIP eventually developed into a comprehensive framework within which various separate Model Intercomparison Projects (MIPs) are structured (Eyring *et al*., 2016). MIPs are assemblages of experiments and simulations developed to assess and compare specific aspects of climate models. Each MIP describes an experimental approach to improve comprehension of the fundamental physical processes that shape the climate system or the way the climate system reacts to outside factors like increasing GHG concentrations. There are 23 different MIPs in CMIP6. The "ScenarioMIP," which incorporates information from about 30 climate models, coordinates future climate change simulations (O'Neill *et al*., 2016).

8.2 Shared Socio-economic Pathways (SSPs)

The most recent version of CMIP6 (2016-2021) and the IPCC Sixth Assessment Report (AR6) is the Shared Socioeconomic Pathways (SSPs) (IPCC, 2021). The

SSP scenarios are based on anticipated concentrations of GHGs that range from aggressive emission reduction to continued emissions growth. The Paris Agreement's goal of keeping the global temperature rise well below 2.0°C and pursuing efforts to keep it to 1.5°C inspired the development of the most combative mitigation scenario. SSPs combine components from the Special Report on Emissions Scenarios (SRES) and Representative Concentration Pathways, the two previous scenarios (RCPs). If climate control is not implemented, the SSPs show alternative scenarios for how the world might change over the following century.

Five SSPs were created using human development assumptions, including those related to population, education, urbanisation, GDP, economic growth, rate of technological advancement, emissions of GHGs and aerosols, energy supply and demand, and land-use changes, among others. The SSPs were developed to work in conjunction with a more advanced version of the RCPs (Riahi *et al*., 2017; Meinshausen *et al.,* 2020). The new RCPs specify the stabilised radiative forcing (the difference between solar energy entering the earth's atmosphere and solar energy leaving it) at the end of the century and the degree of climate change mitigation necessary for a given SSP to achieve this forcing. SSPs show global trends and the state of the world, but they also show how challenging it is to put any international regulations, mitigation measures, or adaptation plans into effect (Chen *et al*., 2021; Stern & Stiglitz, 2021). Following Riahi *et al*., (2017). Table 8.1 summarises the five scenario storylines for the SSPs. It should be noted that the radiative force labels, such as "5.8" in the SSP5-8.5 scenario, are mere "name tags" that approximate the total radiative forcing levels at the end of the 21st century. Because there are major uncertainties in radiative forcing, those labels are only informative.

Table 8.3: Summary of the 5 scenario storylines of the SSPs after Riahi *et al.* (2017).

SSP1	**Sustainability: "The green route" (low challenges to mitigation and adaptation).** 1. The globe is slowly shifting toward a more sustainable course, stressing more inclusive growth that respects perceived natural constraints.

	2. The governance of the global commons gradually gets better, expenditures in education and healthcare speed up the demographic change, and the focus turns from economic growth to a broader emphasis on human well-being. 3. Inequality is decreasing between and within countries due to a growing commitment to accomplishing development objectives. 4. The consumption is geared toward low material growth and decreased energy and resource intensity.
SSP2	**"Middle of the road"**: **moderate difficulties in mitigation and adaptation.** 1. The world is moving down a path where social, economic, and technological tendencies do not deviate significantly from past patterns. 2. Productivity and income development are unequal, with some nations making important progress while others falling short of expectations. 3. Institutions at the national and international levels strive to move slowly toward accomplishing goals of sustainable development. 4. Environmental systems deteriorate, notwithstanding occasional advances and a general decrease in resource and energy usage intensity. 5. The second half of the century will see a moderate slowdown in population growth worldwide. 6. Income disparity is still a problem or is becoming worse slowly, and it is still challenging to make people less vulnerable to societal and environmental alterations.
SSP3	**Regional conflict – "A Rough Ride" (Major obstacles to mitigation and adaptation).** 1. Revived nationalism, concerns about competition and safety, and regional conflicts all compel nations to prioritise internally or, at best, regional matters. 2. Over time, strategies change to become more focused on global and domestic security issues. 3. Nations prioritise fulfilling their regions' energy and food security objectives over broad-based advancement. 4. Decreased expenditures on educational and technological advancement. 5. Economic expansion is gradual, consumption is materialistic, and disparities persist or deteriorate. 6. The growing population is high in emerging nations and low in industrialised countries. 7. Environmental issues are given little international attention, which causes momentous damage to the environment in some areas.
SSP4	**Inequality – "A Divided Road": (Low obstacles to mitigation and high barriers to adaptation).** 1. High differences in human capital investments and expanding gaps in economic opportunities and political influence

	contributed to rising inequality and division between and within nations. 2. Over time, a chasm develops between a globally interconnected civilization that contributes to the global economy's knowledge and capital-intensive sectors and a dispersed collection of low-income. These poorly educated societies operate in a labour-intensive, low-tech economy. 3. As social cohesion declines, conflict and instability are more frequent. 4. The high-tech economy and sectors see rapid technological advancement. 5. The internationally interconnected energy sector diversifies by investing in carbon-intensive fuels, such as coal and unconventional oil, and carbon-free energy alternatives. Environmental policies prioritise local concerns in the middle- and high-income regions.
SSP5	**Fossil-powered development — "Hitting the Road" (Mitigation presents more challenges than adaptation.).** 1. As a means of achieving sustainable development, society increasingly relies on competitive markets, creativity, and participative communities to create speedy technological advancement and human capital growth. 2. International market integration is expanding. 3. Large investments are made in health, education, and organizations to improve quality human resources. 4. The global embrace of resource and energy-intensive lifestyles and the drive for economic and social progress go hand in hand with the extraction of copious fossil fuel resources. 5. All of these variables contribute to worldwide economic expansion, while global population peaks and falls in the 21st century. 6. Air pollution and other local environmental issues are brought under control. 7. If required, there is confidence in managing social and environmental systems effectively, including through geoengineering.

Each SSP produces a matching future projection of GHG emissions and land-use change under the baseline SSP scenario. The SSPs were developed to cooperate with an improved variant of RCPs. Additional climate policy scenarios can be projected on SSPs to demonstrate the effects of various climate policy decisions (such as switching from fossil fuels to renewable energy) and the ease or difficulty of meeting an RCP's end-of-century radiative forcing goal.

Radiative forcing is a measure of the extent to which GHGs in the atmosphere warm or cool the climate, measured in watts per metre squared (Wm-2), with

higher values indicating more important climate warming impacts. A particular set of forcing values was selected to facilitate comparisons between the new scenarios and the RCPs used in CMIP5 and IPCC AR5. There are simulations for various possible SSPs and forcing scenario combinations, but not all are applicable. A low forcing scenario (such as 1.9 Wm-2), which necessitates stricter climate policy and substantial mitigation and consequently low GHG emissions, is incompatible with SSP5, which emphasises fossil-fuel growth and thus produces a future with high emissions. Figure 8.1 depicts the interactions between SSPs and radiative forcing.

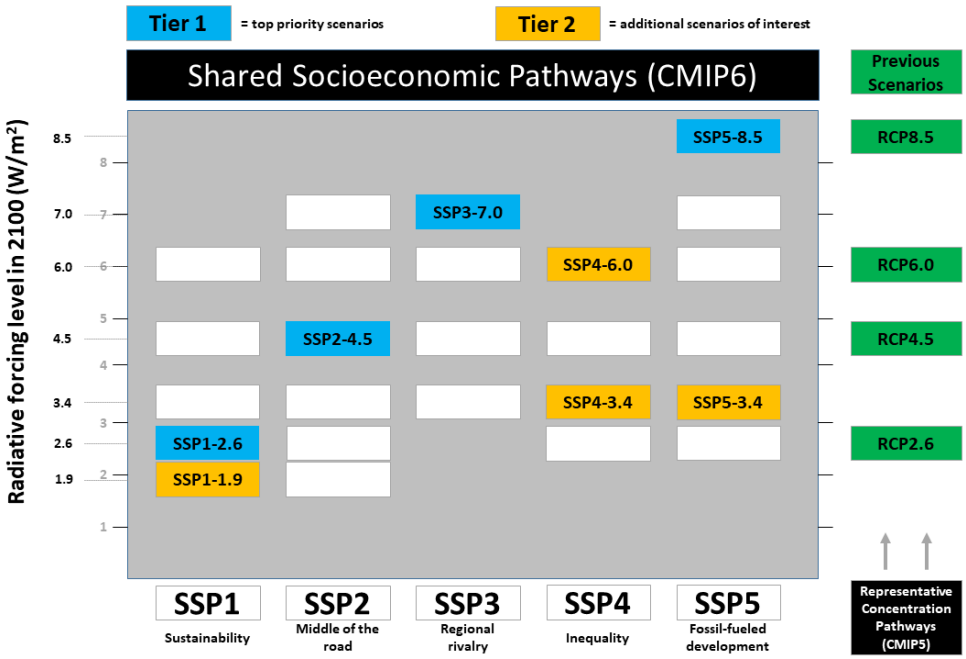


Figure 8.1: Matrix showing Tier 1: Top Priority and Tier 2: Additional Scenarios of interest (O'Neill *et al*., 2016).

8.2.1 Tier 1: Top priority scenario

The IPCC's Sixth Assessment report prioritises scenarios in Tier 1. SSP1-2.6, SSP2-4.5, SSP3-7.0, and SSP5-8.5 are highlighted in blue in Figure 8.1 (O'Neill *et al.*, 2016). Three Tier 1 scenarios are enhanced versions of previous CMIP5 RCP scenarios (RCP2.6, RCP4.5, and RCP8.5). They address various levels of uncertainty about future socioeconomic and climate-forcing paths.

- The SSP1-2.6 scenario corresponds to the previous generation of RCP2.6. The "sustainability" scenario is the SSP1-2.6 "2.0^{o}C scenario," where SSP1

represents the socioeconomic family and has a 2100 nameplate radiative forcing level of 2.6 Wm-2.

- SSP2-4.5 belongs to the SSP2 socioeconomic family and has a notional radiative forcing level of 4.5 Wm-2 by 2100, which is equivalent to the RCP4.5 scenario.
- SSP2-4.5 is a member of the SSP2 socioeconomic family and has a radiative forcing level of 4.5 Wm-2 by 2100, which corresponds to the RCP4.5 scenario.
- The SSP5-8.5 scenario represents the upper end of the SSP scenario spectrum, with the highest reference scenario in a world with high fossil fuel advancement throughout the 21st century.

8.2.2 Tier 2: Additional scenarios of interest

The scenarios in yellow, "Tier 2," are additional scenarios of interest that give concentrations for four more SSP scenarios comprising SSP1-1.9, SSP4-6.0, SSP4-3.4, and SSP5-3.4. The "Tier 2" scenarios include a low reference scenario. The SSP1-1.9 scenario closely reflects the Paris Agreement's 1.5ºC objective. SSP4-6.0 under the socioeconomic setting of an "inequality"-dominated future and its moderate mitigation scenario. SSP4-3.4 and SSP5-3.4 are geophysical fascinating emission "overshoot" scenario that first follows the high-emission SSP5-8.5 scenario until 2030 before demonstrating the sharpest yearly decline rates of all SSP scenario's most essential net harmful emissions by 2100. All other SSP and radiative forcing combinations are either infeasible or not prioritised by Scenario Model Intercomparison Project and are consequently excluded (O'Neill *et al*., 2016). Figures 8.2 and 8.3 presents the data sequence used to generate SSP projections. These comprise population growth (Samir & Lutz, 2016), GDP (Dellink *et al*., 2016), and urbanisation (Jiang & O'Neill, 2016), as well as the assumptions underlying GHG emission concentrations for carbon dioxide (CO_2), methane (CH_4), and nitrous oxide (N_2O) after O'Neill *et al*. (2016). It should be noted that the SSPs provided are baselines, meaning each SSP has no RCP or radiative forcing associated with it. As a result, each SSP represents a future in which no new climate policies are implemented in addition to those already in place, and no new mitigation or adaptation efforts are undertaken (Riahi *et al*., 2017).

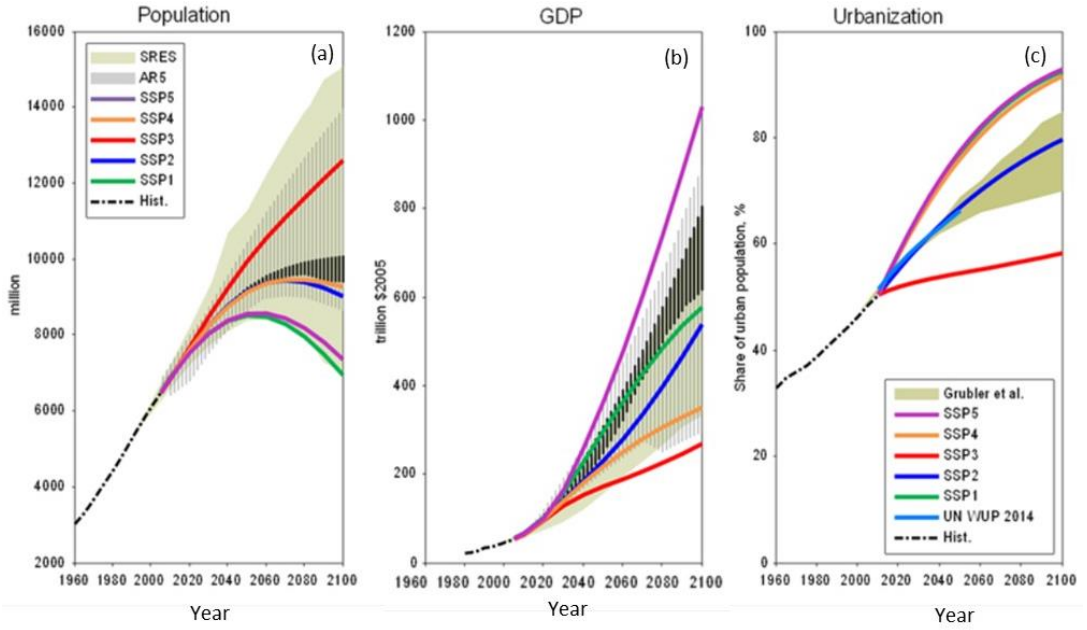


Figure 8.2: The socioeconomic parameters used in SSPs projections based on (a) KC & Lutz (2016), (b) Dellink *et al*. (2016), and (c) Jiang & O'Neill (2016).

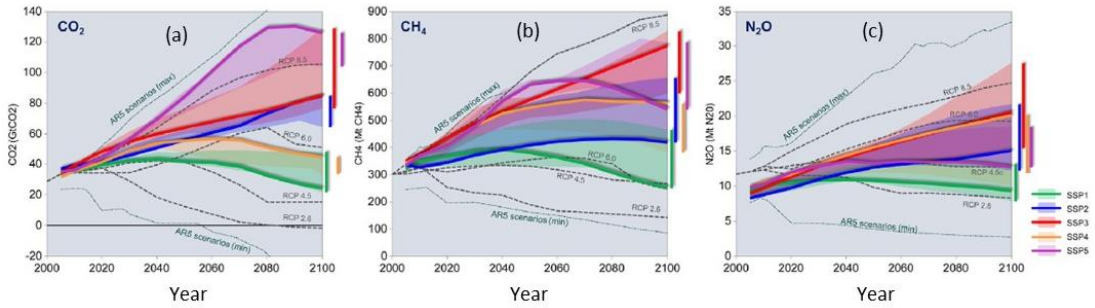


Figure 8.3: Estimates of global GHG emissions and concentrations (O'Neill *et al.*, 2016).

8.3 Representative Concentration Pathways

The Representative Concentration Pathways (RCPs) are used in the CMIP5 projections to provide feasible future scenarios of anthropogenic forcing ranging from a low emissions scenario with active mitigation (RCP2.6) to a high emission scenario (RCP8.5). Each RCP is associated with an appropriate mix of expected population growth, economic activity, energy intensity, and socioeconomic progress. The RCP scenarios were named after the total radiative forcing by (or after) 2100. Table 8.2 presents the summary of the RCP.

Table 8.4: Summary of the RCP scenario storylines after van Vuuren *et al.* (2011).

S/N	RCP Emission scenarios	Radiative forcing
1.	RCP2.6	The radiative force peaks at around 3 Wm-2 in the middle of the 21st century and declines to 2.6 Wm-2 by 2100.
2.	RCP4.5	Radiative force stabilises (without overshoot) at 4.5 Wm-2 after 2100.
3.	RCP6.0	Radiative force stabilises (without overshoot) at 6 Wm-2 after 2100.
4.	RCP8.5	Indicates an increase in radiative forcing to 8.5 Wm-2 in 2100.

The RCP scenarios are inputs for Earth System Models that model the sensitivity of the climate system and the consequent climatic condition. The sequence of data utilised to generate the scenarios is depicted in Figure 8.4.

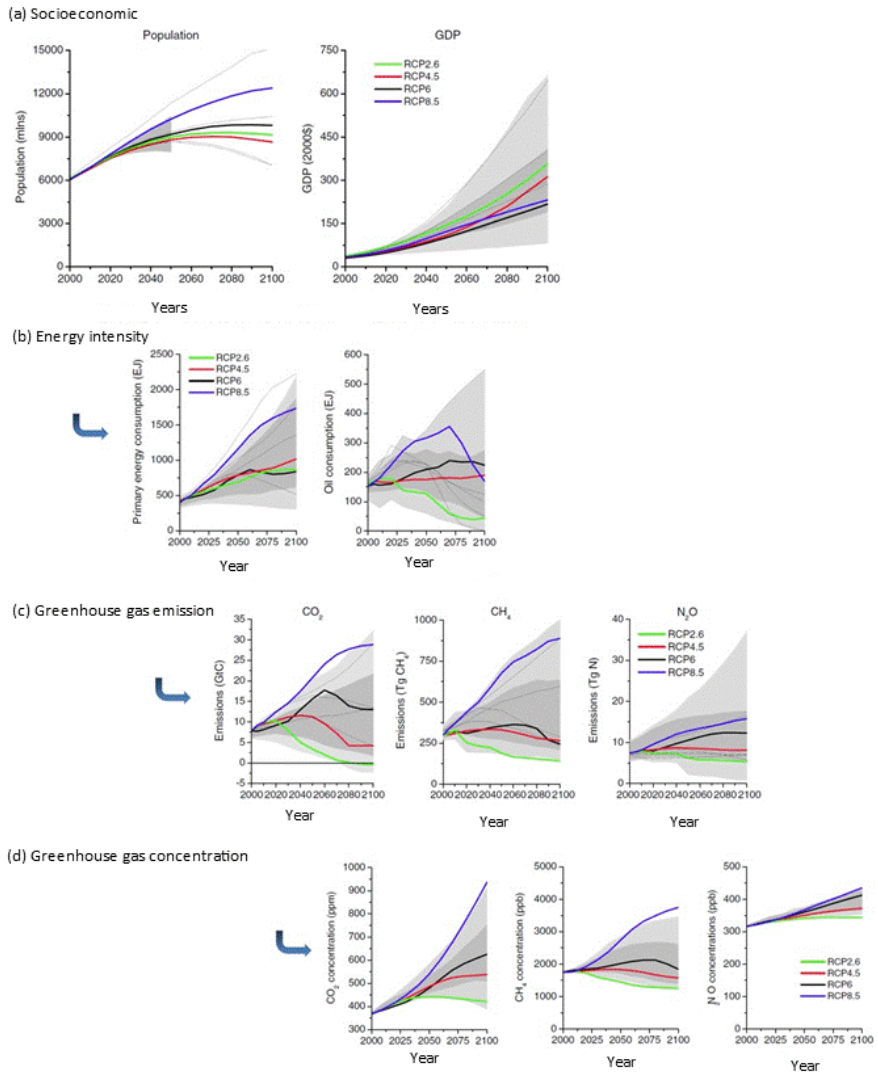


Figure 8.4: Assumptions underlying the RCPs used to drive future climate projections, modified after van Vuuren *et al*. (2011).

8.4 Justification for the choice of Tier 1 (SSP1-2.6 and SSP5-8.5)

Human-caused GHG concentrations increase is the primary cause of long-term climate change. While GHGs appear to be the most prominent human influence on future climate in terms of radiative forcing, anthropogenic aerosols (Hoesly *et al.,* 2018; Jones *et al.,* 2021), land use patterns, aerosol optical properties (Stevens *et al*., 2017; Savage 2021), and natural forces such as solar (Matthes *et al*., 2017) and volcanic impacts (Toohey *et al*., 2016; Beel *et al*., 2020) are also important. CO_2 contributes the most to future warming in SSP scenarios, accounting for between 68 and 85% of GHG radiative forcing by 2100. The second most important contributor to radiative forcing is CH_4 (Meinshausen *et al.,* 2020). As a result, CO_2 and CH_4 concentrations substantially impact future warming caused by GHGs (Rogelj *et al*., 2015; Bertram *et al*., 2021). The radiative forcing in 2100 is projected to be between 8 and 9.7 Wm-2 for CO_2 under the scenario with the highest radiative force, SSP5-8.5. On the low side, the SSP1-1.9 scenario projected a CO_2 radiative forcing of about 1 Wm-2 (van Vuuren *et al*., 2011).

For the higher scenarios, the SSP5-8.5 scenario has meaningfully higher CO_2 concentrations by 2100 than the other scenarios. However, the SSP5-8.5 scenario has a considerably lower CH_4 concentrations by 2100 than the SSP3-7.0 scenario, which has the highest emissions and concentrations of CH_4 and N_2O. The SSP5-8.5 extension, in particular, assumes that land-use-related CH_4 emissions will remain constant by 2100 and that fossil and industrial CH_4 emissions will be phased out by 2250 (Meinshausen *et al*., 2011; O'Neill *et al* 2016). For the lower end of the scenarios, the SSP1-2.6 has higher CO_2 concentrations than the SSP1-1.9, which has the lowest CO_2 concentrations. By the middle of the century, the CH_4 concentrations in these three scenarios are comparable. However, by the end of the century, SSP1-1.9 and SSP1-2.6 scenarios have lowered to 1000 ppb, well below the levels of CH_4. For N_2O, SSP1-1.9 and SSP1-2.6 have nearly identical concentration trajectories (O'Neill *et al* 2016; Tebaldi *et al*., 2021).

8.5 Mean annual temperature projections

The temperature projections in this section are based on the average annual responses to global warming among the five GCMs for low forcing scenarios (SSP 1-2.6) and high forcing scenarios (5-8.5) for 2041-2060 and 2081-2100, respectively. The HadGEM3-GC31-LL model's mean annual warming patterns for the low forcing scenarios (SSP1-2.6) shown in Figure 8.5 indicate an average annual temperature change of 0.4^{o}C for 2041-2060 (1a) and 0.9^{o}C for 2081-2100 (1f). The annual mean temperature change from the HadGEM3-GC31-LL model's high global warming scenarios is 0.9^{o}C for 2041-2060 (2a) and 4.2^{o}C for 2081-2100 (2f). The MPI-ESM1-2-HR model produces less warming than the four models tested in this study for both scenarios and periods. For example, in Figures 8.5(1b) and (1g), the annual mean temperature change for low global warming scenarios (SSP1-2.6) projected warming of 0.2^{o}C between 2041 and 2060 and 0.4^{o}C between 2081 and 2100. As shown in Figures 8.5(2b) and (2g), the MPI-ESM1-2-HR model (SSP5-8.5) projected an annual mean temperature change of 0.3^{o}C between 2041 and 2060 and 1.4^{o}C between 2081 and 2100 under high global warming scenarios.

The output of the MIROC6 model showed no substantial warming between the two low global warming scenarios (SSP1-2.6). Low global warming scenarios (SSP1-2.6), for instance, projected 0.4^{o}C warming between 2041 and 2060 and 0.4^{o}C warming between 2081 and 2100 (Figures 8.5(1c) and (1h)). As depicted in Figures 8.5(2c) and (2h), the MIROC6 model projected a temperature increase of 0.9^{o}C between 2041 and 2060 and 3.3^{o}C between 2081 and 2100 under the high global warming scenarios (SSP5-85). The ACCESS-CSM2 model projected a temperature rise of less than 1.0^{o}C for the low warming scenarios (SSP1-2.6) and 4.4^{o}C for the high warming scenarios (SSP5-8.5). For instance, the low warming scenarios (SSP1-2.6) models presented in Figures 8.5(1d) and (1i) indicate a 0.6^{o}C change in annual mean temperature between 2041 and 2060 and a 0.9^{o}C change between 2081 and 2100. The ACCESS-CSM2 model projected a mean annual temperature increase of 0.8^{o}C from 2041 to 2060 and 4.4^{o}C between 2081 and 2100 for the high global warming scenarios (SSP5-8.5), as shown in Figure 8.5(2d) and 8.5(2i).

For the low global warming scenarios, the mean annual temperature change from the GISS-E2-1-H model output in Figures 8.5(1e) and (1j) indicates a warming of 0.5ºC from 2041-2060 and 0.7ºC between 2081 and 2100 from the low forcing scenarios (SSP1-2.6). The GISS-E2-1-H model output in Figure 8.5(2e) and (2j) show further warming of 0.9ºC from 2041-2060 and 3.1ºC between 2021 and 2100 from the high forcing scenarios (SSP5-8.5). The mean-annual temperature change (°C) across Abuja and its environs from the 5 CMIP6 GCMs included in this study is shown in Table 8.3.

Table 8.5: Mean-annual temperature change (°C) across Abuja and its environs from 5 CMIP6 GCMs for 2041-2060 and 2081-2100 at a spatial resolution of 30 seconds for the low forcing scenario SSP1-2.6 and the strong forcing scenario SSP5-8.5.

Model	**Average annual temperature (ºC)**			
	SSP1-2.6		SSP5-8.5	
	2041-2060	2081-2100	2041-2060	2081-2100
HadGEM3-GC31-LL	0.4	0.9	0.9	4.2
MPI-ESM1-2-HR	0.2	0.4	0.3	1.4
MIROC6	0.4	0.4	0.9	3.3
ACCESS-CSM2	0.6	0.9	0.8	4.4
GISS-E2-1-H	0.5	0.7	0.9	3.1

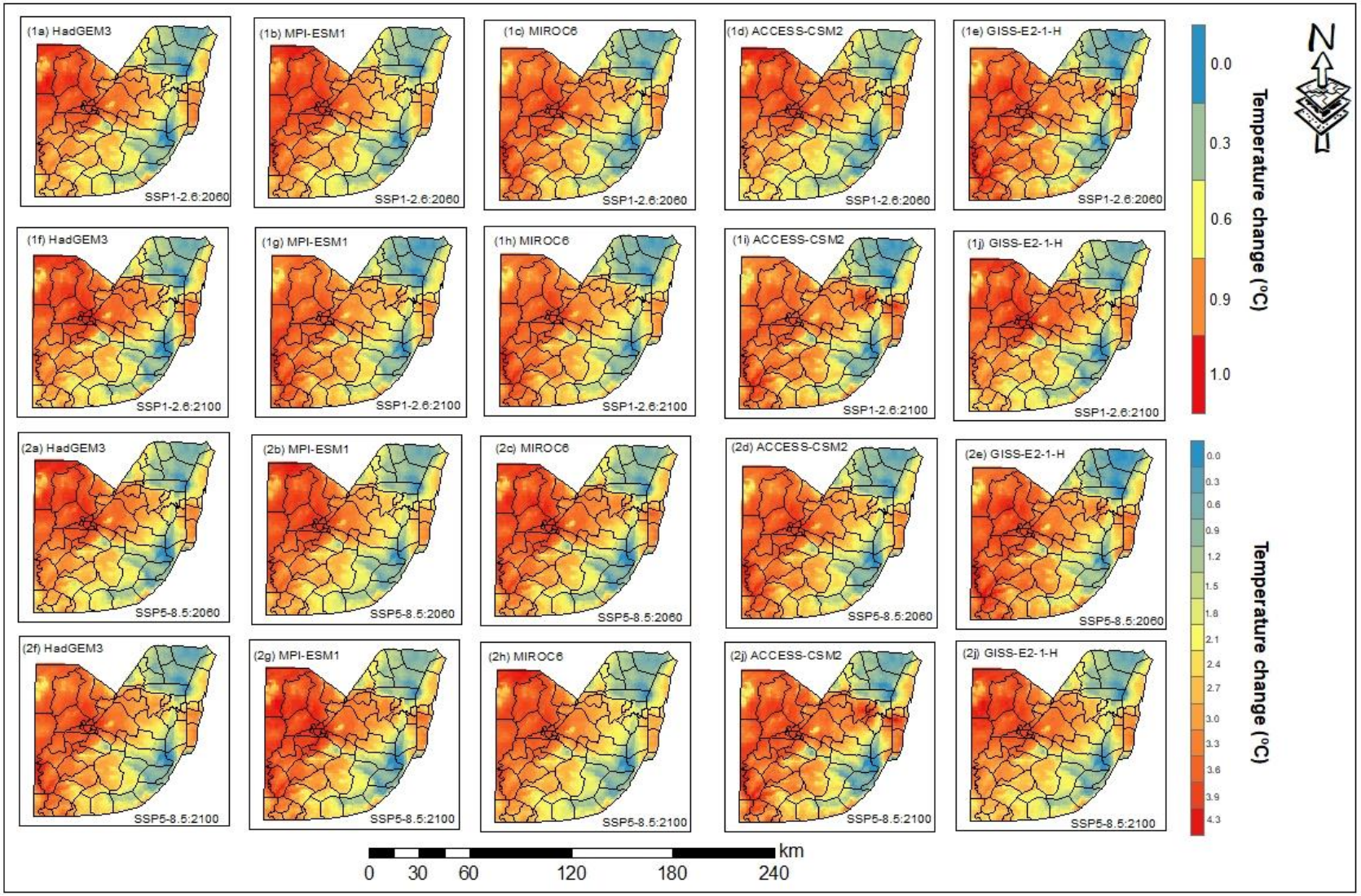


Figure 8.5: Mean annual temperature change (°C) in Abuja and its surrounds from the five selected CMIP6 models for the middle and end of the century, based on the low forcing scenario SSP1-2.6 and the strong forcing scenario SSP5-8.5. Note: The columns represent GCMs and the rows represent scenarios and time periods.

8.6 Monthly average temperature projections

The ensemble of 5 CMIP6 GCMs was used to project the average monthly temperature over Abuja and its surroundings. The aim is to comprehend the monthly change in temperature under the two future SSP scenarios—a low forcing scenario, SSP1-2.6, and an intense forcing scenario, SSP5-8.5, at the beginning and end of the century, respectively.

8.6.1 Monthly average temperature change (ºC) from the low forcing scenario SSP1-2.6

8.6.1.1 The HadGEM3-GC31-LL model

The monthly increases in maximum temperature relative to the reference period of 2001-2020 are shown in the temperature projections for the years 2041-2060 and 2081-2100. For instance, the HadGEM3-GC31-LL's low forcing scenario's (SSP1-2.6) monthly average temperature for the years 2041 to 2060 projects a temperature increase of 0.2°C in January, 0.6°C in February, and 0.5°C in March. A 1.0°C increase in April, a 0.4°C increase in May, and a 0.4°C increase in June are all projected. The projected temperatures for July, August, and September were 0.5°C, 0.1°C, and 0.1°C, respectively. As shown in Table 8.4, the model's output indicates that the monthly temperature change will be 0.2°C in October, 0.1°C in November, and 0.5°C in December. Temperature projections from the HadGEM3-GC31-LL model for the end of the century (2081-2100) under the low forcing scenario (SSP1-2.6) show more substantial warming than in the middle of the century, with 0.9°C, 1.0°C, and 0.8°C rises in January, February, and March, respectively. The average monthly temperature was projected to rise by 1.0°C, 0.8°C, and 0.8°C, respectively, in April, May, and June. The temperature was projected to rise by 0.9°C in July, 0.7°C in August, and 0.7°C in September. Further increases of 1.0°C, 0.4°C, and 1.4°C were projected in October, November, and December, respectively, as shown in Table 8.4.

8.6.1.2 The MPI-ESM1-2-HR model

Under the low forcing scenario (SSP1-2.6) of 2041 - 2060, the MPI-ESM1-2-HR model projects a temperature increase of 0.1°C in January, 0.2°C in February, and 0.2°C in March. Temperatures are projected to rise by 0.3°C in April, 0.8°C in May, and 0.6°C in June. Temperatures were projected to rise by 0.1°C in July, 0.1°C in August, and 0.2°C in September. The model output shows a monthly temperature change of 0.2°C in October, 0.2°C in November, and 0.3°C in December. The MPI-ESM1-2-HR model projected that temperatures will increase by 0.4°C in January, 0.7°C in February, and 0.4°C in March by the end of the century (2081-2100). It is projected that the average monthly temperature will rise by 0.3°C in April, 0.7°C in May, and 0.6°C in June. In July, the average monthly temperature was projected to rise by 0.4°C, August by 0.1°C, and September by 0.3°C. As shown in Table 8.4, the temperature was projected to rise by 0.1°C per month in October, November, and December.

8.6.1.3 The MIROC6 model

The monthly increases in maximum temperature relative to the baseline period 2001-2020 imply a temperature change of 0.3°C in January, 0.4°C in February, and 0.5°C in March based on the MIROC6's low forcing scenario (SSP1-2.6) for 2041-2060. Temperatures are projected to rise by 0.9°C, 0.4°C, and 0.4°C in April, May, and June, respectively. Temperatures are projected to rise by 0.4°C in July, August, and September. The model output shows the monthly temperature change for October at 0.4°C, November at 0.3°C, and December at 0.3°C. January, February, and March will warm by 0.2°C, 0.4°C, and 0.8°C by the end of the century (2081-2100). The projected monthly temperature increases for April, May, and June were 0.9°C, 0.4°C, and 0.4°C, respectively. Temperatures were projected to rise by 0.4°C in July, August, and September, and by 0.5°C, 0.3°C, and 0.2°C in October, November, and December, as shown in Table 8.4.

8.6.1.4 The ACCESS CSM2 model

The ACCESS CSM2 model projected a temperature increase of 0.5°C in January, 0.7°C in February, and 0.7°C in March under the low forcing scenario (SSP1-2.6) of 2041 to 2060. It is projected that temperatures will rise by 0.5°C in April, 0.6°C in May, and 0.7°C in June. The projected temperatures for July, August, and September were 0.7°C, 0.3°C, and 0.7°C, respectively. According to the model's output, October's temperature will increase by 0.8°C, November's by 0.5°C, and December's by 0.4°C. Temperatures will rise by 0.8°C in January, 1.0°C in February, and 1.1°C in March by the end of the century (2081-2100). The monthly average temperature will rise by 0.7°C, 1.0°C, and 1.4°C in April, May, and June, respectively. The average monthly temperature would rise by 0.9°C in July, 0.7°C in August, and 0.8°C in September, according to the model's projections. As shown in Table 8.4, the mean monthly temperature was projected to rise by 1.4°C in October and 1.0°C in November and December.

8.6.1.5 The GISS-E2-1-H model

Based on the GISS-E2-1-H low forcing scenario (SSP1-2.6) for 2041-2060, the monthly increases in maximum temperature relative to the baseline period 2001-2020 imply a temperature change of 0.5°C in January, 0.4°C in February, and 0.4°C in March. In April, May, and June, temperatures are projected to be 0.7°C, 0.5°C, and 0.4°C, respectively. Temperatures were projected to be 0.4°C, 0.4°C, and 0.6°C in July, August, and September, respectively. Table 8.4 displays the model output, which shows the monthly temperature change for October at 0.5°C, November at 0.7°C, and December at 0.6°C. Under the low forcing scenario, the GISS-E2-1-H model's temperature projections for the end of the century (2081-2100) indicate that January, February, and March will warm by 0.7°C, 0.7°C, and 0.9°C, respectively (SSP1-2.6). In April, May, and June, the average monthly temperature is projected to rise by 1.1°C, 0.7°C, and 0.6°C, respectively. July and August temperatures were projected to rise by 0.6°C, while September temperatures will rise by 0.7°C. As shown in Table 8.4, the average monthly temperature will increase by 0.6°C in October, 0.9°C in November, and 0.8°C in December, respectively.

8.6.2 Change in monthly mean temperature (ºC) based on the high forcing scenario SSP5-8.5

8.6.2.1 The HadGEM3-GC31-LL model

According to the model output, temperature increases will be more pronounced in the upper-bound emission scenario (RCP5-8.5). Table 8.4 shows the monthly increases in maximum temperature for 2041-2060 and 2081-2100 relative to the 2001-2020 reference period. For example, the HadGEM3-GC31-LL of 2041-2060 projects a temperature rise of 0.7°C in January, 1.1°C in February, and 0.9°C in March. Temperatures are expected to be 0.7°C, 0.8°C, and 0.3°C in April, May, and June, respectively. Temperatures were projected to be 0.5°C, 0.4°C, and 0.2°C warmer in July, August, and September, respectively. The monthly temperature rise is 0.0°C in October, 0.2°C in November, and 2.1°C in December. Under the strong forcing scenario (SSP5-8.5), HadGEM3-GC31-LL model projections for the end of the century (2081-2100) indicate more substantial warming than in the middle of the century, with January, February, and March experiencing 4.5°C, 4.6°C, and 4.4°C increases, respectively. The average monthly temperature for April, May, and June is projected to rise by 4.6°C, 4.3°C, and 4.2°C, respectively. Figure 8.4 indicated that temperature would increase by 4.1°C in July, 3.5°C in August, and 3.2°C in September before increasing by 4.2°C in October and November and 4.0°C in December.

8.6.2.2 The MPI-ESM1-2-HR model

The MPI-ESM1-2-HR model projects temperature increases of 0.3°C in January, 0.7°C in February, and 0.7°C in March under the high forcing scenario (SSP5-8.5) for 2041 to 2060. April temperatures are projected to rise by 0.3°C, May temperatures by 0.0°C, and June temperatures by 0.2°C. July temperatures were projected to rise by 0.1°C, August by 0.4°C, and September by 0.5°C. The projected temperatures for October, November, and December are 0.3°C, 0.1°C, and 0.1°C, respectively. By the end of the century (2081-2100), temperatures will rise by 1.3°C in January, 0.9°C in February, and 0.5°C in March. The projections call for an increase in the monthly average temperature of 0.8°C in April, 1.8°C in May, and 1.5°C in June. It was further projected that the monthly

average temperature would increase by 1.2°C in July, 1.5°C in August, and 1.8°C in September. The temperature was projected to rise by 1.8°C, 1.6°C, and 1.9°C in October, November, and December, respectively, as shown in Table 8.4.

8.6.2.3 The MIROC6 model

Based on the MIROC6's strong forcing scenario (SSP5-8.5) for 2041-2060, the average monthly increase in maximum temperature relative to the baseline period 2001-2020 indicates a temperature rise of 0.8°C in January, 0.9°C in February, and 1.0°C in March. In April, May, and June, the temperature is projected to rise by 1.1°C, 1.1°C, and 1.0°C, respectively. July, August, and September were projected to experience temperatures rise of 0.7°C, 0.8°C, and 0.8°C, respectively. In addition, the model projects a temperature variation of 0.8°C in October, 0.7°C in November, and 0.9°C in December. According to the temperature projections for the end of the century (2081-2100), January, February, and March will be warmer by 3.1°C, 3.3°C, and 4.1°C, respectively, under the strong forcing scenario (SSP5-8.5). In April, May, and June, the average monthly temperature is projected to rise by 4.2°C, 3.5°C, and 3.3°C, respectively. Temperatures were projected to rise by 3.0°C in July, 3.2°C in August and September, and 2.8°C, 3.2°C, and 3.1°C in October, November, and December, respectively, as shown in Table 8.4.

8.6.2.4 The ACCESS CSM2 model

The ACCESS CSM2 model projects a temperature rise of 1.2°C in January, 1.3°C in February, and 1.2°C in March under the strong forcing scenario (SSP5-8.5) of 2041 to 2060. April temperatures are expected to rise by 1.2°C, May by 0.8°C, and June by 0.6°C. In July, temperatures were projected to rise by 0.8°C, in August by 0.9°C, and in September by 0.7°C. The model projects a change in temperature of 0.5°C in October, 0.7°C in November, and 0.3°C in December. The ACCESS CSM2 model projects that temperatures will rise by 1.0°C in January, 4.7°C in February, and 4.6°C in March by the end of the century (2081-2100). In April, the monthly average temperature will rise by 4.4°C, 4.3°C in May, and 4.6°C in June. The model further projected that the mean monthly

temperature would rise by 4.5°C in July, 4.1°C in August, and 4.7°C in September. Table 8.4 shows that the temperature was projected to rise by 4.6°C in October, 4.2°C in November, and 4.4°C in December.

8.6.2.5 The GISS model

The GISS model projects a 1.0°C temperature rise in January, 0.8°C in February, and 1.0°C in March under the high forcing scenario (SSP5-8.5) for 2041-2060. Temperatures were projected to rise by 1.1℃ in April, 0.8° ℃ in May, and 0.9° ℃ in June. Temperatures were projected to rise further by 0.9℃ in July, 0.8℃ in August, and 1.0℃ in September. The monthly temperature change in October and November is 0.9°C, and 1.1°C in December. Under the high forcing scenario (SSP5-85), the GISS model projects that temperatures will rise by 3.5°C in January, 3.4°C in February, and 3.4°C in March by the end of the century (2081-2100). The average monthly temperature was projected to rise by 3.1°C in April and 2.9°C in May, June, and July. In August, the average monthly temperature was projected to rise by 2.7°C and 2.8°C in September and October. Table 8.4 shows that temperatures were projected to rise by 3.1°C and 3.4°C in November and December, respectively.

Table 8.6: The monthly average maximum temperature changes from the five GCMs chosen. The temperature change was calculated by deducting the projected year (2041-2060 and 2081-2100) from the 20-year average since the turn of the century (2001-2020).

Mean monthly temperature change (°C) from the low forcing scenario SSP1-2.6

	2041-2060												2081-2100											
Model name	Jan	Feb	Mar	Apr	May	June	July	Aug	Sept	Oct	Nov	Dec	Jan	Feb	Mar	Apr	May	June	July	Aug	Sept	Oct	Nov	Dec
HadGEM3	0.2	0.6	0.5	1.0	0.4	0.4	0.5	0.1	0.1	0.2	0.1	0.5	0.9	1.0	0.8	1.0	0.8	0.8	0.9	0.7	0.7	1.0	0.4	1.4
MPI-ESM1	0.1	0.2	0.2	0.3	0.8	0.6	0.1	0.1	0.2	0.2	0.2	0.3	0.4	0.7	0.4	0.3	0.7	0.6	0.4	0.1	0.3	0.1	0.1	0.1
MIRIOC6	0.3	0.4	0.5	0.9	0.4	0.4	0.4	0.4	0.4	0.4	0.3	0.3	0.2	0.4	0.8	0.9	0.4	0.4	0.4	0.4	0.4	0.5	0.3	0.2
ACCESS	0.5	0.7	0.7	0.5	0.6	0.7	0.7	0.3	0.7	0.8	0.5	0.4	0.8	1.0	1.1	0.7	1.0	1.4	0.9	0.7	0.8	1.4	1.0	1.0
GISS-E2	0.5	0.4	0.4	0.7	0.5	0.4	0.4	0.4	0.6	0.5	0.7	0.6	0.7	0.7	0.9	1.1	0.7	0.6	0.6	0.6	0.7	0.6	0.9	0.8

Mean monthly temperature change (°C) from the high forcing scenario SSP5-8.5

	2041-2060												2081-2100											
Model name	Jan	Feb	Mar	Apr	May	June	July	Aug	Sept	Oct	Nov	Dec	Jan	Feb	Mar	Apr	May	June	July	Aug	Sept	Oct	Nov	Dec
HadGEM3	0.7	1.1	0.9	0.7	3.8	0.3	0.5	0.4	0.2	0	0.2	2.1	4.5	4.6	4.4	4.6	4.3	4.2	4.1	3.5	3.2	4.2	4.2	4.0
MPI-ESM1	0.3	0.7	0.7	0.3	0.0	0.2	0.1	0.4	0.5	0.3	0.1	0.1	1.3	0.9	0.5	0.8	1.8	1.5	1.2	1.5	1.8	1.8	1.6	1.9
MIROC6	0.8	0.9	1.0	1.1	1.1	1.0	0.7	0.8	0.8	0.8	0.7	0.9	3.1	3.3	4.1	4.2	3.5	3.3	3.0	3.2	3.2	2.8	3.2	3.1
ACCESS	1.2	1.3	1.2	1.2	0.8	0.6	0.8	0.9	0.7	0.5	0.7	0.3	1.0	4.7	4.6	4.4	4.3	4.6	4.5	4.1	4.7	4.6	4.2	4.4
GISS-E2	1.0	0.8	1.0	1.1	0.8	0.9	0.9	0.8	1.0	0.9	0.9	1.1	3.5	3.4	3.4	3.1	2.9	2.9	2.9	2.7	2.8	2.8	3.1	3.4

8.7 Seasonal temperature change

The seasonal temperature change over Abuja and its environs were calculated by comparing the projected seasonal averages for 2041-2060 and 2081-2100 to the current seasonal average from the turn of the century (2001-2020). Low forcing scenarios (SSP1-2.6) from the HadGEM3-GC31-LL model show an average seasonal temperature change of 0.4^{o}C in DJA, 0.6^{o}C in MAM, 0.3^{o}C in JJA, and 0.6^{o}C in SON for 2041-2060 (Figures 8.6(a), (b), (c) and (d)). Under the low forcing scenario (SSP1-2.6), the HadGEM3-GC31-LL model projects a temperature rise of 1.0°C in DJF, 0.9°C in MAM, 0.8°C in JJA, and 0.0°C in SON for 2081 - 2100, as shown in Figures 8.6(e), (f), (g), and (h). Under the strong forcing scenario (SSP5-8.5), the HadGEM3-GC31-LL model projects a temperature rise of 1.3°C in DJF, 0.7°C in MAM, 0.4°C in JJA, and 0.1°C in SON for 2041-2060 (Figures 8.6(i), (j), (k) and (l)). Temperatures are projected to rise by 4.3°C in DJF, 4.4°C in MAM, 3.9°C in JJA, and 3.9°C in SON under the high forcing scenario (SSP5-8.5) for 2081 - 2100 Figures 8.6(m), (n), (o) and (p)). Table 8.5 presents the projected seasonal temperature change from the HadGEM3-GC31-LL model.

The MPI-ESM1-2-HR model projects that temperatures will rise by 0.2°C in DJF, 0.3°C in MAM, 0.3°C in JJA, and 0.2°C in SON between 2041 and 2060 under the low forcing scenario (SSP1-2.6) (Figures 8.7(a), (b), (c), and (d)). Under the low forcing scenario (SSP1-2.6), seasonal temperatures are projected to rise by 0.3°C in DJF, 0.5°C in MAM, 0.4°C in JJA, and 0.2°C in SON between 2081-2100, as shown in Figure 8.7(e), (f), (g), and (h). Under the strong forcing scenario (SSP5-8.5), the MPI-ESM1-2-HR model projected a seasonal temperature increase of 0.4°C in DJF, 0.3°C in MAM, and 0.2°C in JJA and SON from 2041 to 2060 (Figures 8.7(i), (j), (k), and (l)). Temperatures were projected to rise by 1.4°C in DJF, 1.0°C in MAM, 0.2°C in JJA, and 1.7°C in SON between 2081-2100, as shown in Figures 8.7(m), (n), (o), and (p). The MPI-ESM1-2-HR model's projected seasonal temperature change is shown in Table 8.5.

Figures 8.8(a), (b), (c), and (d) depict the seasonal temperature change relative to the baseline period 2001–2020 under the low forcing scenario (SSP1-2.6) of MIROC6 for 2041–2060. Under the low forcing scenario (SSP1-2.6), the DJF will warm by 0.3°C, the MAM by 0.7°C, the JJA by 0.4°C, and the SON by 0.4°C, as shown in Figure 8.8(e), (f), (g), and (h), respectively. Based on the MIROC6's strong forcing scenario (SSP5-8.5) for 2041-2060, the seasonal temperature increase relative to the baseline period 2001-2020 implies a temperature rise of 0.9°C in DJF, 1.1°C in MAM, 0.8°C in JJA, and 0.3°C in SON (Figure 8.7(i), (j), (k), and (l)). Temperatures are projected to rise by 3.2°C in DJF, 3.9°C in MAM, 3.2°C in JJA, and 3.1°C ASO for the strong forcing scenario (SSP5-8.5) for 2081-2100, as shown in Figure 8.7(m), (n), (o), and (p). Table 8.5 shows the seasonal temperature change projected by the MIROC6 model.

The ACCESS model projects that temperatures will rise by 0.5°C in DJF, 0.6°C in MAM, 0.6°C in JJA, and 0.7°C in SON between 2041 and 2060 under the low forcing scenario (SSP1-2.6) (Figure 8.9(a), (b), (c), and (d)). Under the low forcing scenario (SSP1-2.6), seasonal temperatures are projected to rise by 0.9°C in DJF, 0.9°C in MAM, 1.0°C in JJA, and 1.1°C in SON between 2081-2100, as shown in Figure 8.9(e), (f), (g), and (h). Under the strong forcing scenario (SSP5-8.5), the ACCESS model projected a seasonal temperature increase of 1.2°C in DJF, 0.9°C in MAM, 0.8°C in JJA, and 0.5°C in SON for the years 2041 to 2060 (Figure 8.9 (i), (j), (k), and (l)). As shown in Figures 8.9(m), (n), and (o) and (p), it was projected that seasonal temperatures would increase by 4.6°C in DJF, 4.4°C in MAM, 4.4°C in JJA, and 4.2°C in SON between 2081-2100. The seasonal temperature change projected by the ACCESS model is shown in Table 8.5.

The GISS-EN2 low forcing scenario (SSP1-2.6) for 2041–2060 projects a temperature change of 0.5°C in DJF, 0.5°C in MAM, 0.4°C in JJA, and 0.6°C in SON (Figure 8.10(a), (b), (c), and (d)). According to the GISS-EN2 model's seasonal temperature projections for the end of the century (2081-2100), the DJF

will warm by 0.7°C, the MAM by 0.9°C, the JJA by 0.6°C, and the SON by 0.7°C, respectively (Figure 8.10(e), (f), (g), and (h)). Based on the GISS-EN2 strong forcing scenario (SSP5-8.5) for 2041-2060, the seasonal increase in temperature relative to the baseline period 2001-2020 implies a temperature rise of 1.0°C in DJF, 1.0°C in MAM, 0.9°C in JJA, and 0.9°C in SON (Figure 8.10(i), (j), (k), and (l)). As shown in Figure 8.10(m), (n), and (o), for the strong forcing scenario (SSP5-8.5) for 2081-2100, temperatures are projected to increase by 3.4°C in DJF, 3.1°C in MAM, 2.8°C in JJA, and 2.9°C ASO, respectively (p). Table 8.5 shows the seasonal change in temperature projected by the GISS-EN2 model.

Table 8.7: Projected seasonal temperature changes from the 5 selected GCMs. The temperature change was calculated by subtracting the projected seasonal average (2041-2060 and 2081-2100) from the 20-year seasonal average from the beginning of the 21st century (2001-2020).

The seasonal temperature change from the low forcing scenarios (SSP1-2.6)								
	2040-2060				2081-2100			
Model name	DJF	MAM	JJA	SAN	DJF	MAM	JJA	SON
HadGEM3	0.4	0.6	0.3	0.6	1.0	0.9	0.8	0.0
MPI-ESM1	0.2	0.3	0.3	0.2	0.3	0.5	0.4	0.2
MIROC6	0.3	0.6	0.4	0.4	0.3	0.7	0.4	0.4
ACCESS	0.5	0.6	0.6	0.7	0.9	0.9	1.0	1.1
GISS-E2	0.5	0.5	0.4	0.6	0.7	0.9	0.6	0.7
The seasonal temperature change from the strong forcing scenarios (SSP5-8.5)								
	2040-2060				2081-2100			
Model name	DJF	MAM	JJA	SAN	DJF	MAM	JJA	SON
HadGEM3	1.3	0.7	0.4	0.1	4.3	4.4	3.9	3.9
MPI-ESM1	0.4	0.3	0.2	0.2	1.4	1.0	0.2	1.7
MIROC6	0.9	1.1	0.8	0.3	3.2	3.9	3.2	3.1
ACCESS	1.2	0.9	0.8	0.5	4.6	4.4	4.4	4.2
GISS-E2	1.0	1.0	0.9	0.9	3.4	3.1	2.8	2.9

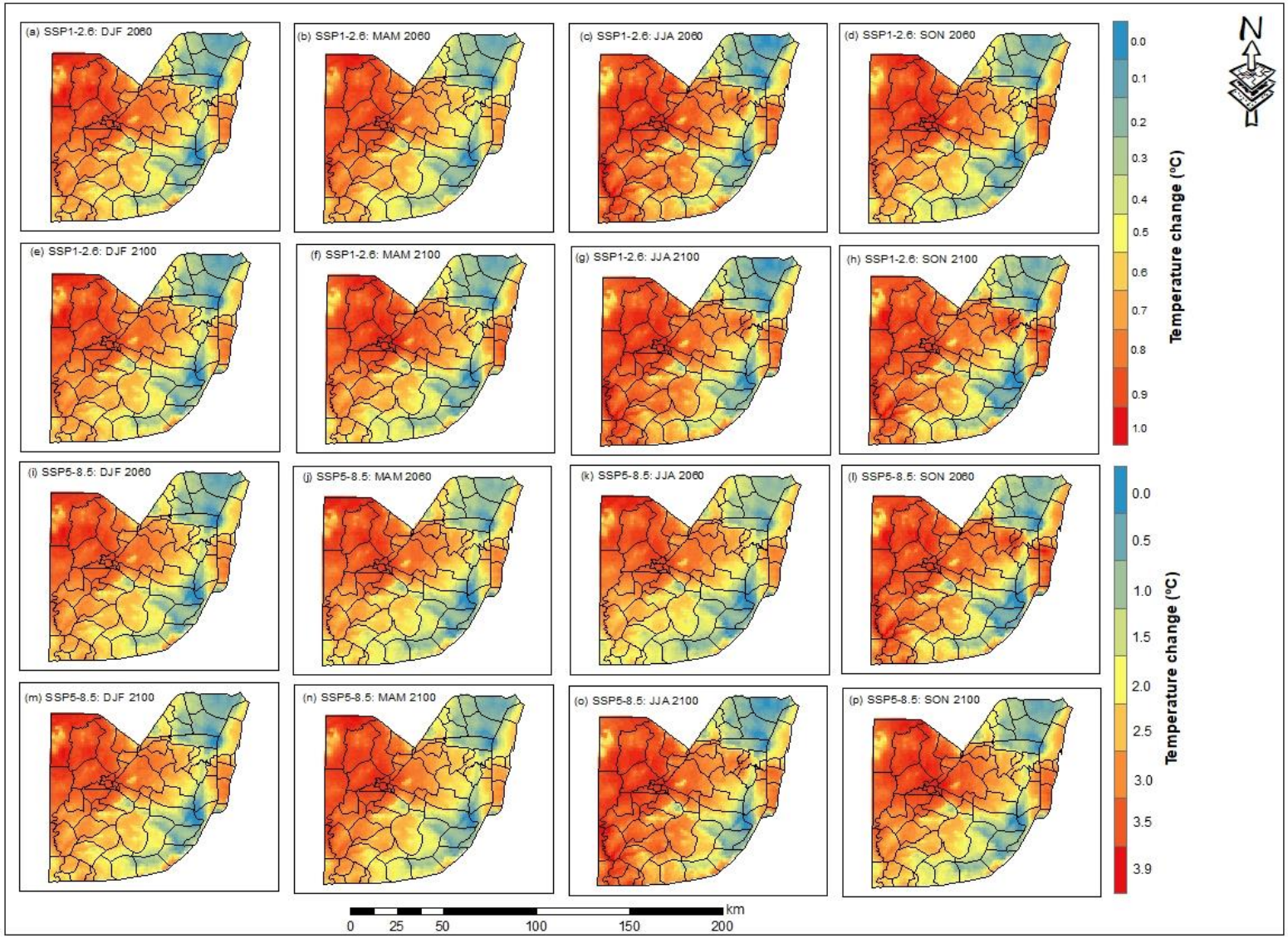


Figure 8.6: Seasonal Temperature change from the CMIP6 downscaled from the HadGEM3-GC31-LL model

It should be noted that the HadGEM3-GC31-LL data at the 30-second spatial resolution for the High-Resolution Model Intercomparison Project (HighResMIP) of the SSP. As depicted in Figure 8.6. (a), (b), (c), and (d) are low forcing scenarios (SSP1-2.6) for the middle of the century (2041-2060), with (a) December, January, and February (DJF); (b) March, April, and May (MAM); (c) June, July, and August (JJA); and (d) September, October, and November. (e), (f), (g), and (h) are the low forcing scenarios (SSP1-2.6) for the end of the century (2081-2100), with (e) representing December, January, and February (DJF); (f) representing March, April, and May (MAM); (g) representing June, July, and August (JJA); and (h) representing September, October, and November.

The high forcing scenarios (SSP5-8.5) for the middle of the century (2041-2060) are represented by (i), (j), (k), and (l), where (i) represents December, January, and February (DJF), (j) represents March, April, and May (MAM), (k) represents June, July, and August (JJA), and (l) represents September, October, and November. The high forcing scenarios (SSP5-8.5) for the end of the century (2081-2100) are represented by (m), (n), (o), and (p), with (m) representing December, January, and February (DJF), (n) representing March, April, and May (MAM), (o) representing June, July, and August (JJA), and (p) representing September, October, and November.

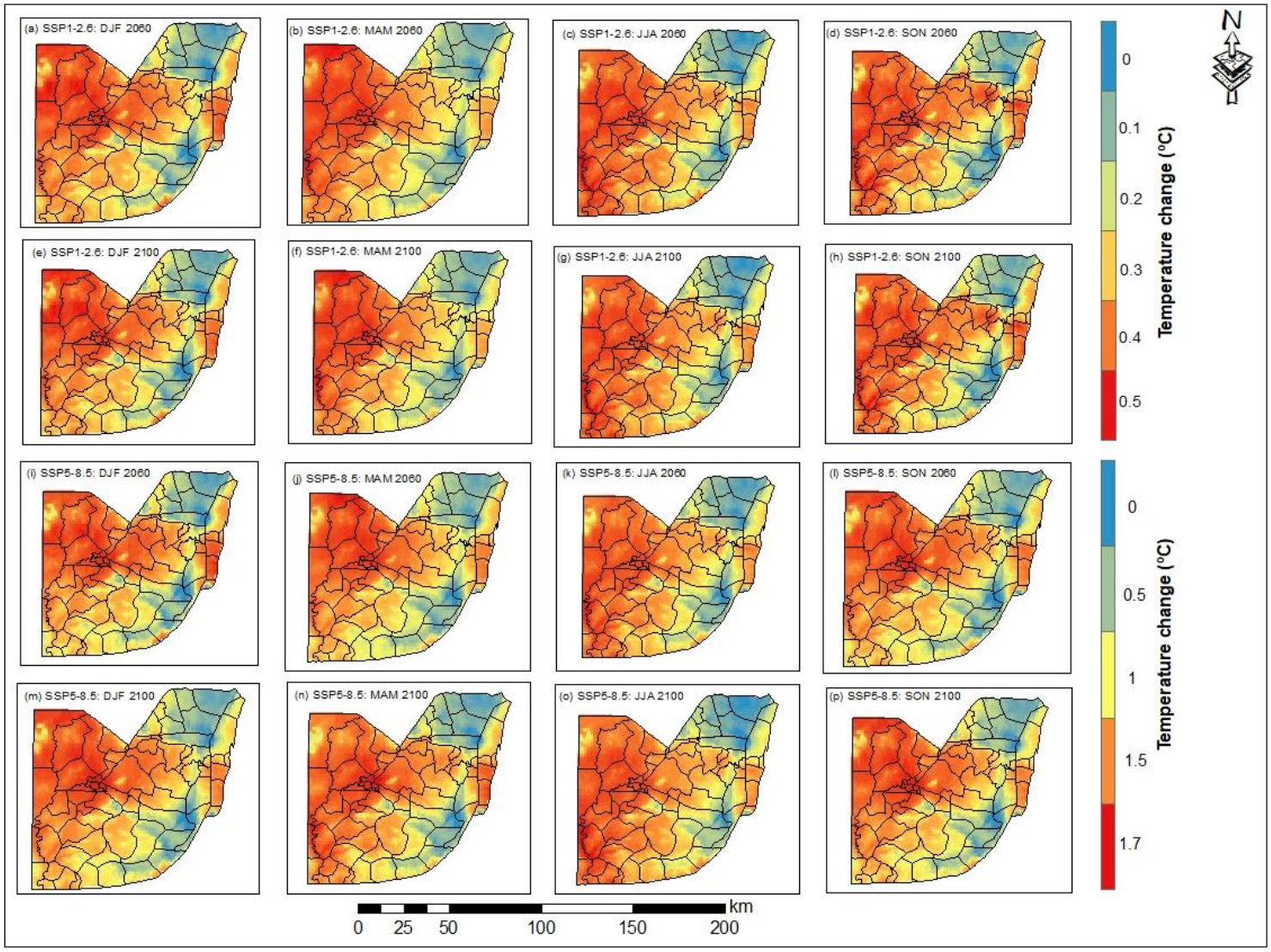


Figure 8.7: Seasonal Temperature change projections from the CMIP6 downscaled from the MPI-ESM1-2-HR model

The MPI-ESMI-2-HR data at a spatial resolution of 30 seconds for the High-Resolution Model Intercomparison Project (HighResMIP) of the SSP. As depicted in Figure 8.7. (a), (b), (c), and (d) are low forcing scenarios (SSP1-2.6) for the middle of the century (2041-2060), with (a) December, January, and February (DJF); (b) March, April, and May (MAM); (c) June, July, and August (JJA); and (d) September, October, and November. (e), (f), (g), and (h) are the low forcing scenarios (SSP1-2.6) for the end of the century (2081-2100), with (e) representing December, January, and February (DJF); (f) representing March, April, and May (MAM); (g) representing June, July, and August (JJA); and (h) representing September, October, and November.

The high forcing scenarios (SSP5-8.5) for the middle of the century (2041-2060) are represented by (i), (j), (k), and (l), where (i) represents December, January, and February (DJF), (j) represents March, April, and May (MAM), (k) represents June, July, and August (JJA), and (l) represents September, October, and November. The high forcing scenarios (SSP5-8.5) for the end of the century (2081-2100) are represented by (m), (n), (o), and (p), with (m) representing December, January, and February (DJF), (n) representing March, April, and May (MAM), (o) representing June, July, and August (JJA), and (p) representing September, October, and November.

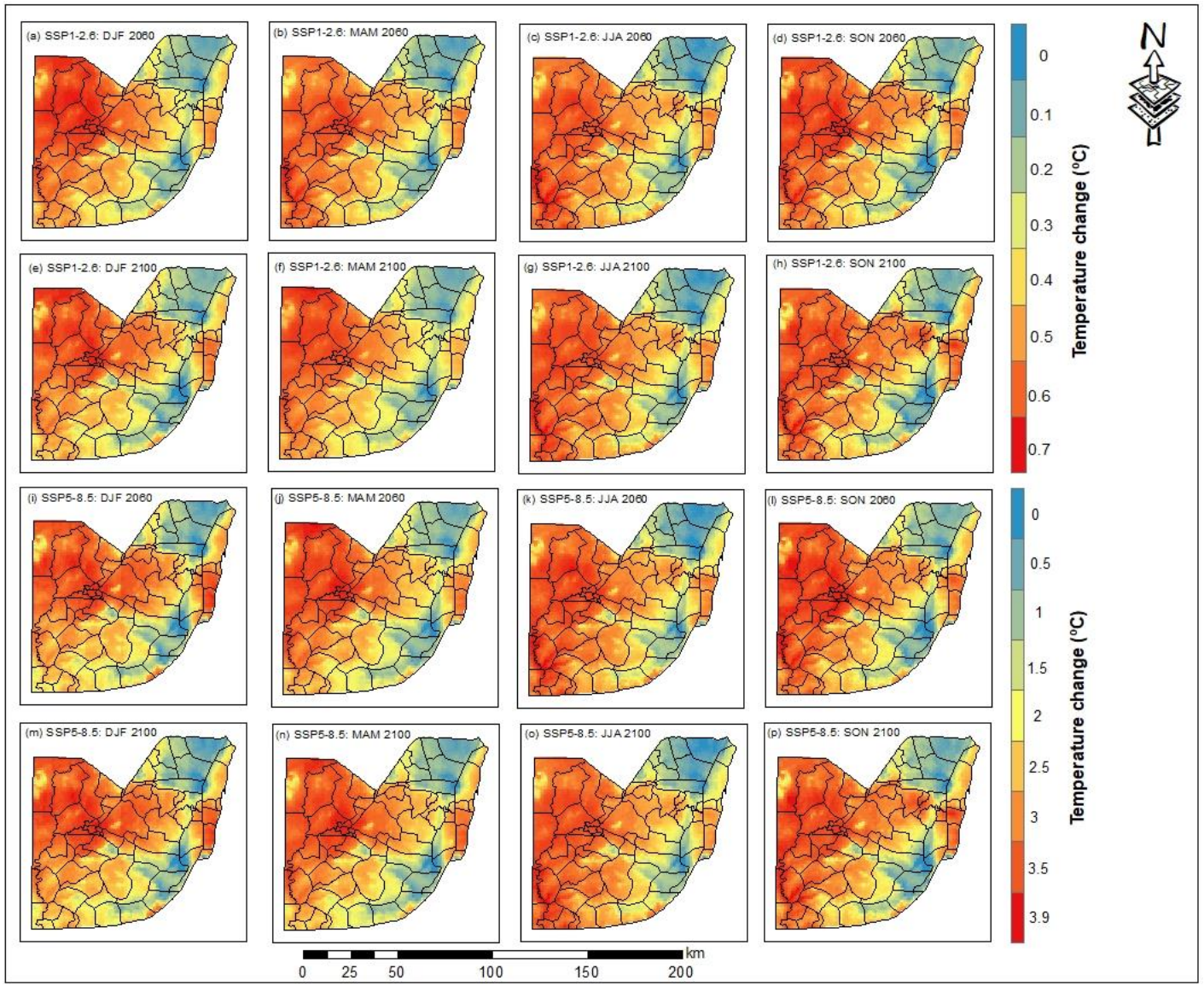


Figure 8.8: Seasonal Temperature change projections from the CMIP6 downscaled from the MIROC6 model

The MIROC6 data at a spatial resolution of 30 seconds for the High-Resolution Model Intercomparison Project (HighResMIP) of the SSP. As depicted in Figure 8.8(a), (b), (c), and (d) are low forcing scenarios (SSP1-2.6) for the middle of the century (2041-2060), with (a) December, January, and February (DJF); (b) March, April, and May (MAM); (c) June, July, and August (JJA); and (d) September, October, and November. (e), (f), (g), and (h) are the low forcing scenarios (SSP1-2.6) for the end of the century (2081-2100), with (e) representing December, January, and February (DJF); (f) representing March, April, and May (MAM); (g) representing June, July, and August (JJA); and (h) representing September, October, and November.

The high forcing scenarios (SSP5-8.5) for the middle of the century (2041-2060) are represented by I (j), (k), and (l), where I represents December, January, and February (DJF), (j) represents March, April, and May (MAM), (k) represents June, July, and August (JJA), and (l) represents September, October, and November. The high forcing scenarios (SSP5-8.5) for the end of the century (2081-2100) are represented by (m), (n), (o), and (p), with (m) representing December, January, and February (DJF), (n) representing March, April, and May (MAM), (o) representing June, July, and August (JJA), and (p) representing September, October, and November.

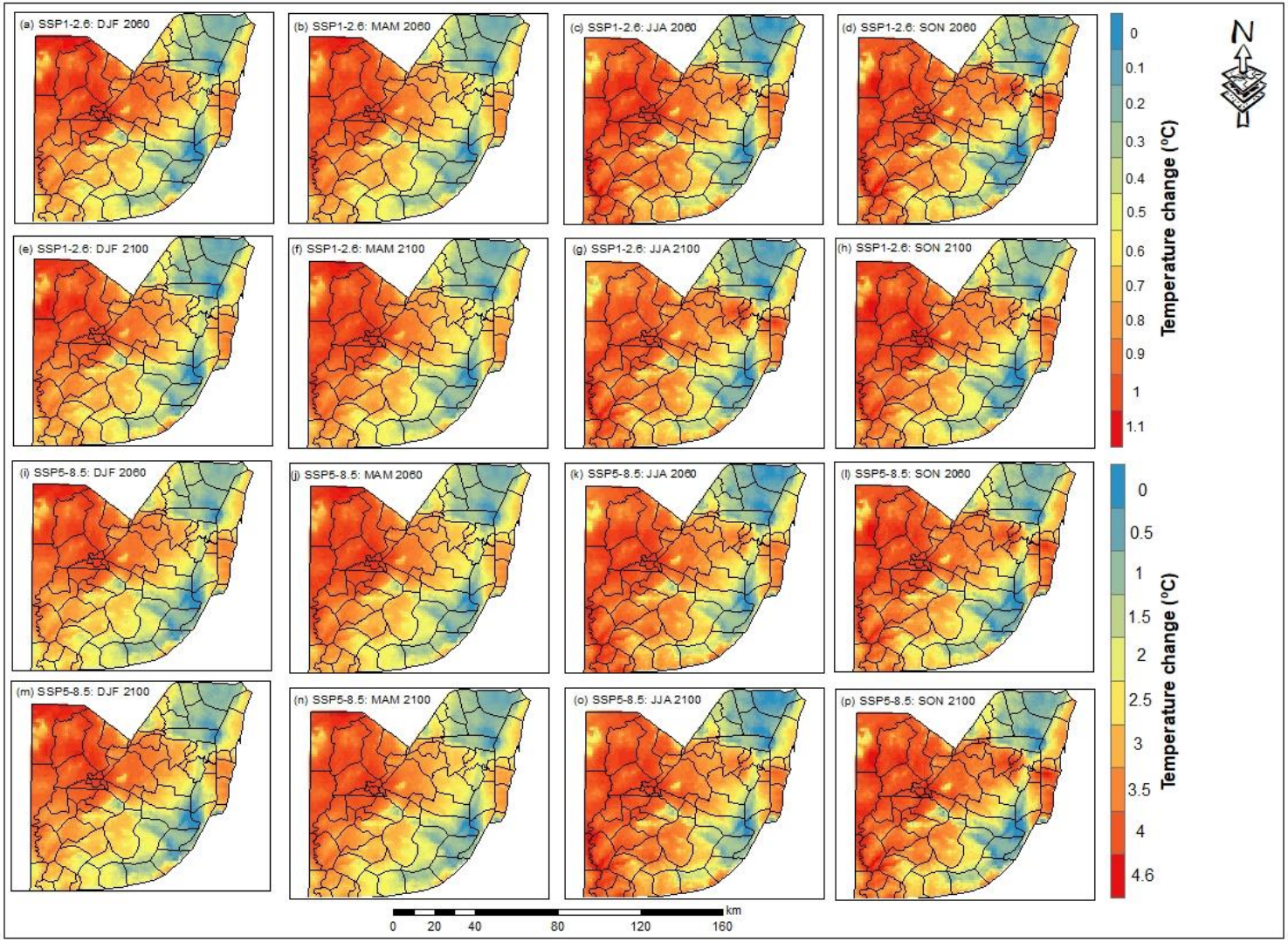


Figure 8.9: Seasonal Temperature change projections from the CMIP6 downscaled from the ACCESS-CSM2 model

The spatial resolution of the ACCESS-CSM2 model used for this study was 30 seconds for the High-Resolution Model Intercomparison Project (HighResMIP) of the SSP. As shown in Figure 8.9(a), (b), (c), and (d) are low forcing scenarios (SSP1-2.6) for the middle of the century (2041-2060), with (a) December, January, and February (DJF); (b) March, April, and May (MAM); and (d) September, October, and November. (e), (f), (g), and (h) are the low forcing scenarios (SSP1-2.6) for the end of the century (2081-2100), where (e) represents December, January, and February (DJF), (f) represents March, April, and May (MAM), (g) represents June, July, and August (JJA), and (h) represents September, October, and November.

The high forcing scenarios (SSP5-8.5) for the middle of the century (2041-2060) are represented by (i), (j), (k), and (l), with (i) representing December, January, and February (DJF), (j) representing March, April, and May (MAM), (k) representing June, July, and August (JJA), and (l) representing September, October, and November. The high forcing scenarios (SSP5-8.5) for the end of the century (2081-2100) are (m), (n), (o), and (p), with (m) representing December, January, and February (DJF), (n) March, April, and May (MAM), (o) June, July, and August (JJA), and (p) September, October, and November.

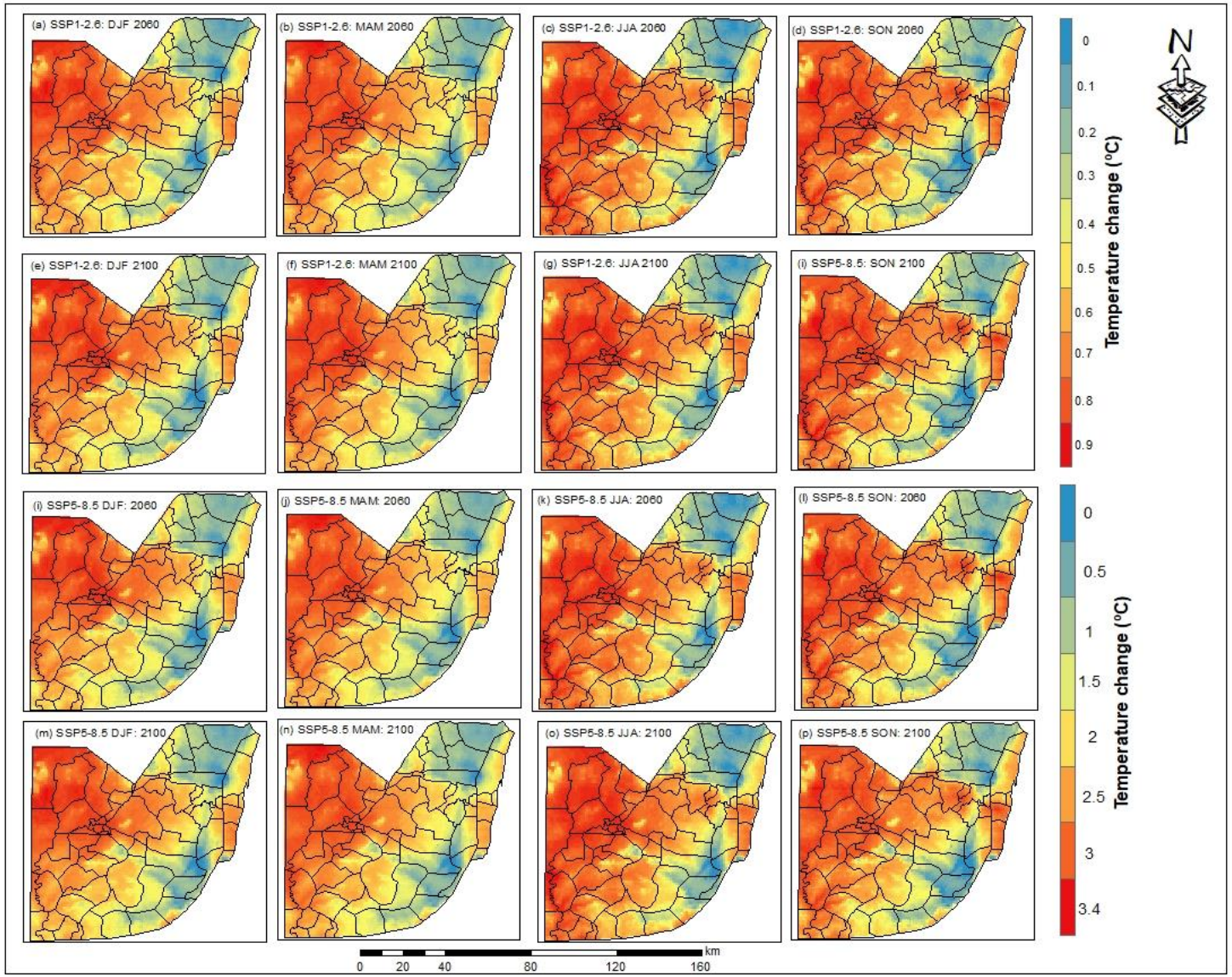


Figure 8.10: Seasonal Temperature change projections from the CMIP6 downscaled from the GISS-E2-1-H model

The GISS-2E-1-H data was obtained at a spatial resolution of 30 seconds for the SSP's High-Resolution Model Intercomparison Project (HighResMIP). As shown in Figure 8.10 the MPI-ESMI-2-HR data at a spatial resolution of 30 seconds for the HighResMIP of the SSP. As depicted in Figure 8.10(a), (b), (c), and (d) are low forcing scenarios (SSP1-2.6) for the middle of the century (2041-2060), with (a) December, January, and February (DJF); (b) March, April, and May (MAM); (c) June, July, and August (JJA); and (d) September, October, and November. (e), (f), (g), and (h) are the low forcing scenarios (SSP1-2.6) for the end of the century (2081-2100), with (e) representing December, January, and February (DJF); (f) representing March, April, and May (MAM); (g) representing June, July, and August (JJA); and (h) representing September, October, and November. Low forcing scenarios (SSP1-2.6) for the middle of the century (2041-2060) are (a), (b), (c), and (d), with (a) December, January, and February (DJF); (b) March, April, and May (MAM); (c) June, July, and August (JJA); and (d) September, October, and November. The low forcing scenarios (SSP1-2.6) for the end of the century (2081-2100) are represented by (e), (f), (g), and (h), with (e) representing December, January, and February (DJF), (f) representing March, April, and May (MAM), (g) representing June, July, and August (JJA), and (h) representing September, October, and November.

The high forcing scenarios (SSP5-8.5) for the middle of the century (2041-2060) are represented by (i), (j), (k), and (l), where (i) represents December, January, and February (DJF), (j) represents March, April, and May (MAM), (k) represents June, July, and August (JJA), and (l) represents September, October, and November. The high forcing scenarios (SSP5-8.5) for the end of the century (2081-2100) are represented by (m), (n), (o), and (p), with (m) representing December, January, and February (DJF), (n) representing March, April, and May (MAM), (o) representing June, July, and August (JJA), and (p) representing September, October, and November.

8.8 Spatial variations of temperature over Abuja and its environs

The spatial changes in maximum temperature over Abuja and its environs may be influenced by the extent of artificial impervious surface and the regional elements such as topography in hilly terrain. Land at high altitudes, such as highlands or plateaus, is typically likely to have lower temperature change than the surroundings due to the environmental lapse rate. To better understand how the current warming in the region varies with the high and low latitudes areas, the spatial variation of maximum temperature in 2022 relative to 1970 and the elevation of Abuja and its surroundings were overlaid. The temperature change and average zonal hills allow for more understanding of the relationship between topography and orographic features of the study area. Figure 8.11 shows how the topography of the study area is overlaid with the average maximum temperature. The closely spaced contour line indicates a steep slope or areas with relatedly high topography whereas, the widely spaced contour line indicates a gentle slope or relatively flat areas.

The orographic influence on temperature change presented in Figure 8.11 demonstrates that the orographic impacts on the northeast temperature gradient are visible, as are the lower temperatures associated with high elevation towards the southeast part of the study area. The topography of Abuja and its environs has a considerable effect on temperature change, with regions with elevations ranging between 607 and 843 metres above sea level (ASL)registering the lowest maximum temperature change (0.0°C - 0.2°C) commonly observed in the north-eastern and south-eastern parts of the study area in all the 5 models. For instance, the highest elevations found in Shere, Dutse, and Bwari, are characterised by various peaks, a cluster of hills, and vast ranges of hills and isolated hills known as inselbergs. These settlements have relatively low-temperature change and are predominantly characterised by orographic kind of precipitation partly due to their elevation and proximity to the windward side of the Jos plateau.

The settlements of Wuse, the city centre, Garki, a portion of Karshi, and Bwari in the central and north-eastern-south-western portion of the research area are

characterised by the temperature change of 0.3°C to 0.5°C. The area has altitudes between 463-606m ASL and is characterised by a rough and undulating topography, with the basement rock erupting as hills and inselbergs. In these sites, the geologic formation consists of foundation complex rocks that form conspicuous hilly physiographic characteristics. Gwagwa, Jiwa, a portion of Gwarimpa, Kabusa, Aso, Karu, and Kabi are among the regions with topographic heights ranging from 331 to 462m ASL. These regions have had a temperature change of 0.6°C and 0.8°C. The northwest-to-southwest portion of Abuja and its environs has the lowest elevation, ranging from 63m to 330m ASL. These regions, including Gurdi, Paiko, Pai, Kwali, Yaba, and Pandagi, had the most significant temperatures change, between 0.9°C and 1.1°C. Figure 8.11 shows the spatial change in temperatures with elevation.

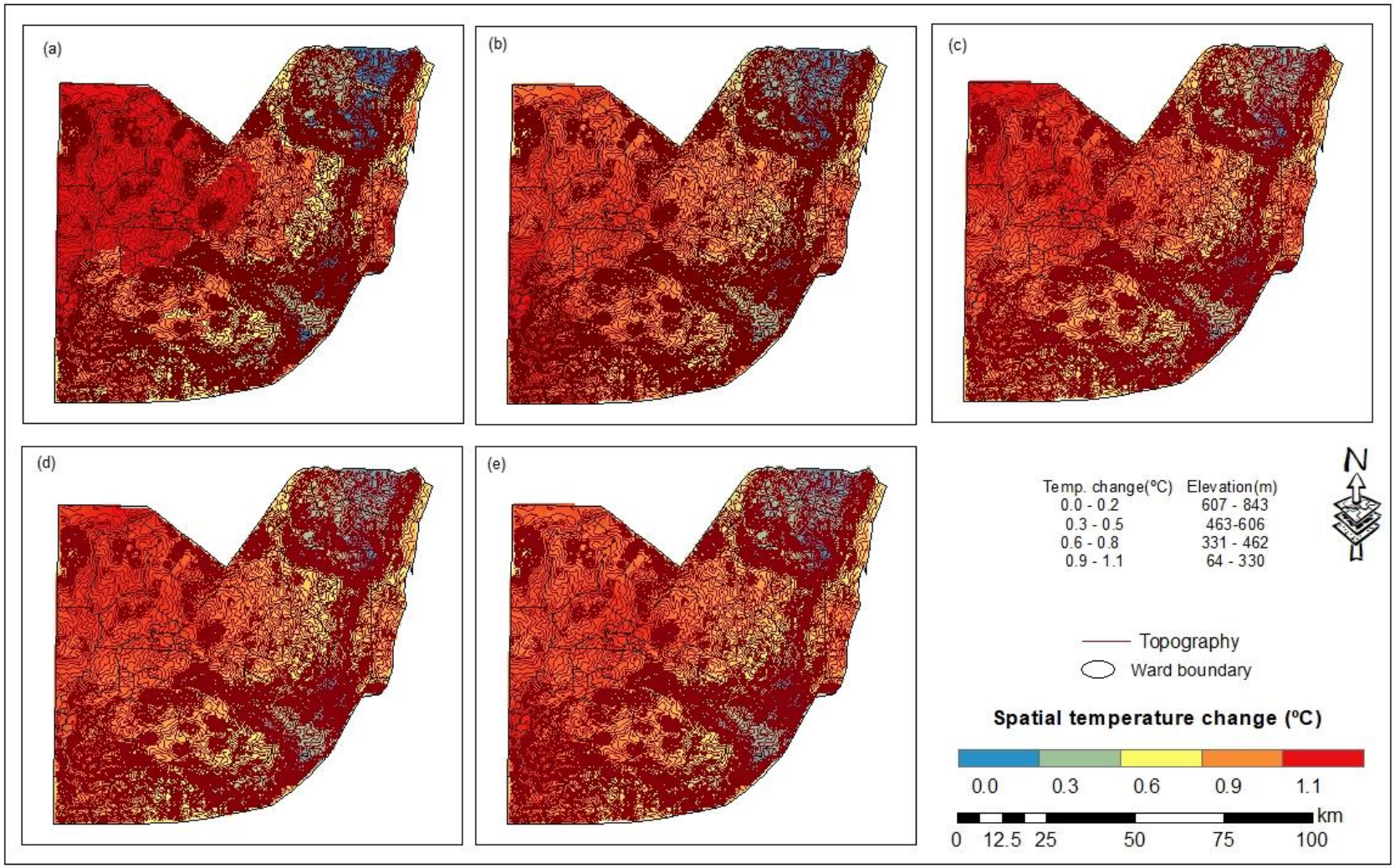


Figure 8.11: Spatial variations in temperature due to the elevations derived from the Shuttle Radar Topography Mission (SRTM) model and the (a), HadGEM3-GC31-LL(b), MPI-ESM1(c), Miroc6 (d), ACCESS-CSM2 and (e) GISS-E2-1-H to highlight the terrain-induced spatial variation in maximum temperatures.

8.9 Heat vulnerability projections

The previous sections of this chapter demonstrated that rising temperatures have exacerbated the UHI phenomenon, which has been worsened by climate change and urbanisation, and that human exposure to dangerous heat is expected to increase residents' vulnerability to heat-related health outcomes. The previous chapter of this research also revealed that demographic and socioeconomic characteristics influence human sensitivity and adaptive capability to harmful heat. Rising poverty is expected to increase inhabitants' vulnerability to heat-related morbidity and mortality. Based on the sensitivity of the Abuja population to temperature and socioeconomic change, this section seeks to make projections of heat vulnerability during the middle and end of the 21st century.

This section includes nine heat vulnerability indicators for the projections of heat vulnerability. These include projected temperature, NDVI, artificial impervious surface, women population, poverty level, literacy rate, dwelling quality, population density, and the vulnerable population, which consists of the younger population under 14 and the elderly population over 65 years old. For the heat vulnerability projections, temperature projections from the 5 GCMs were used to replace the LST indicator. The other eight HVIs could not be projected to the middle and end of the century due to a lack of consistent data. Despite efforts to project each HVI to the middle and end of the century using the C. A. Markov model, time constraints prevented this. Even though the Gross Domestic Product (GDP) is the most commonly used indicator in heat vulnerability studies as a proxy for income level, poverty, and inequality (Geiger, 2018; Wang & Sun, 2022), this study purposefully excluded the GDP projections available for the middle and end of the century due to incompatibility, as the data was not initially included as an indicator in the initial mapping of heat vulnerability. To that purpose, the eight HVIs were at present. This means that the heat vulnerability projections reported in this study are demonstrative rather than realistic or ideal. All the nine HVIs used to construct the heat vulnerability projections for this study were reprojected to a consistent spatial resolution of 30 m.

8.10 Preparation of indicators for the projection of heat vulnerability

The projections of heat vulnerability for this study were developed based on the premise that temperatures would rise while the other eight HVIs would remain unchanged. In this regard, heat vulnerability projections for the middle and end of the century were based on temperature projections from five GCMs under low and strong forcing scenarios. Heat vulnerability projections for each SSP model were constructed using the mean annual temperature change from the low emission scenario (SSP1-2.6) and the high emission scenario (SSP5-8.5) for the middle of the century (2041–2060) and the end of the century (2081-2100), respectively. Table 8.3 presents the mean-annual temperature change (°C) across Abuja and its environs from 5 GCMs for 2041-2060 and 2081-2100 at a spatial resolution of 30 seconds for the low forcing scenario SSP1-2.6 and the strong forcing scenario SSP5-8.5.

Under the scenario of low forcing (SSP1-2.6), the five SSP models projected ten different heat vulnerability maps. Five heat vulnerability maps have been generated for the middle of the century (2041–2060) and five for the end of the century (2081-2100). Heat vulnerability projections for the middle of the century included temperature rises of 0.4^{o}C from the HadGEM3-GC31-LL model, 0.2^{o}C from the MPI-ESM1-2-HR model, 0.4^{o}C from the MIROC6 model, 0.6^{o}C from the ACCESS model, and 0.5^{o}C from the GISS model. Heat vulnerability projections for the end of the century included a temperature increase of 0.9^{o}C for the HadGEM3-GC31-LL model, 0.4^{o}C for the MPI-ESM1-2HR model, 0.4^{o}C for the MIROC6 model, 0.9^{o}C for the ACCESS model, and 0.7^{o}C for the GISS model.

Under the strong forcing scenario (SSP8–8.5), five SSP models projected ten heat vulnerability maps. Five heat vulnerability maps were generated for the middle of the century (2041–2060) and five for the end of the century (2081-2100). The five heat vulnerability projections for the middle of the century (2041-2060) included a temperature rise of 0.9°C for the HadGEM3-GC31-LL Model, 0.3°C for the MPI-ESM1-2-HR Model, 0.9°C for the MIROC6 Model, 0.8°C for the ACCESS model, and 0.9°C for the GISS model. For the end of the century (2081-2100), the HadGEM3-GC31-LL Model projected a 4.2°C

increase in temperature, the MPI-ESM1-2-HR Model projected 1.4°C, the MIROC6 Model projected 3.3°C, and the ACCESS Model projected 4.4°C. The GISS Model projected 3.1°C, which was used for the heat vulnerability projections.

The projections of heat vulnerability were generated using a weighted overlay based on the expert's judgement of the relative influence of nine heat vulnerability indicators. The weighted ranking overlay generated projected heat vulnerability maps based on decile values: very high (9^{th}–10th deciles), high (7^{th}–8^{th} deciles), moderate (5^{th}–6^{th} deciles), low (3^{rd}–4^{th} deciles), and very low (1^{st}–2^{nd} deciles). The spatial change in the projected heat vulnerability maps' areas was calculated compared to the prevailing heat vulnerability map generated in Chapter 7. The projected areas of vulnerability were estimated with the current heat vulnerability map for each of the five models' projected heat vulnerability map areas, as well as the forcing scenario and period (2020). The area of each map indicating a heat vulnerability scale, such as very low, low, moderate, high, and very high, was computed by subtracting the area representing a projected heat vulnerability from each map representing a current heat vulnerability. Tables 8.6 and 8.7 present the spatial variations of heat vulnerability projections from the five GCMs considered in this study. The Tables are based on the low and high forcing scenarios for the middle and end of the 21^{st} century.

Table 8.6: Spatial change in the heat vulnerability area from the low forcing scenarios

Model name	Vulnerability Scale	Present (2020)		SSP1-2.6 (2060)				SSP1-2.6 (2100)			
		Map area (sqkm)	% area	Map area (sqkm)	% area	Change in area	% change in area	Map area (sqkm)	% area	Change in area	% change in area
HadGEM3	Very Low	4405.3	8.1	4058.0	7.5	-347.3	5.2	3061.3	5.6	-1343.9	8.10
	Low	12442.2	23.0	12444.1	23.0	1.8	0.0	8337.4	15.4	-4104.7	24.7
	Moderate	14419.7	26.6	11423.8	21.1	-2995.8	45.6	11514.8	21.3	-2904.8	17.5
	High	16237.4	30.0	18953.0	35.1	2715.6	41.3	18099.1	33.5	1861.7	11.2
	Very High	6595.8	12.1	7105.5	13.1	509.7	7.7	12971.7	24.0	6375.9	38.4
	Total map area	54100.5	100.0	53984.6	100.0	-115.9	100.0	53984.6	100.0	-115.9	100.0
MPI-ESM1	Very Low	4405.3	8.1	4326.2	8.0	-79.1	1.1	3261.8	6.0	-1143.4	11.9
	Low	12442.2	23.0	11262.5	20.8	-1179.6	16.7	10230.7	18.9	-2211.4	23.1
	Moderate	14419.7	26.6	12088.6	22.3	-2331.0	33.0	12930.1	23.9	-1489.6	15.5
	High	16237.4	30.0	16512.8	30.5	275.4	3.9	16854.9	31.2	617.4	6.4
	Very High	6595.8	12.1	9794.3	18.1	3198.5	45.2	10706.9	19.8	4111.1	42.9
	Total map area	54100.5	100.0	53984.6	100.0	-115.9	100.0	53984.6	100.0	-115.9	100.0
MIROC6	Very Low	4405.3	8.1	3765.5	6.9	-639.7	7.4	3265.5	6.0	-1139.7	7.4
	Low	12442.2	23.0	9390.7	17.4	-3051.4	35.3	8590.7	15.9	-3851.4	25.2
	Moderate	14419.7	26.6	13737.8	25.4	-681.9	7.9	11737.8	21.7	-2681.9	17.6
	High	16237.4	30.0	17706.9	32.8	1469.5	17.0	18006.9	33.3	1769.5	11.6
	Very High	6595.8	12.1	9383.4	17.3	2787.6	32.3	12383.4	22.9	5787.6	38.0
	Total map area	54100.5	100.0	53984.6	100.0	-115.9	100.0	53984.6	100.0	-115.9	100.0
ACCESS	Very Low	4405.3	8.1	3038.4	5.6	-1366.8	17.2	3000.8	5.5	-1404.5	10.2
	Low	12442.2	23.0	9778.8	18.1	-2663.4	33.5	7452.8	13.8	-4989.3	36.2
	Moderate	14419.7	26.6	16243.8	30.0	1824.1	22.9	15897.3	29.4	1477.6	10.7
	High	16237.4	30.0	16501.2	30.5	263.8	3.3	15692.9	29.0	-544.4	3.9
	Very High	6595.8	12.1	8422.2	15.6	1826.4	22.9	11940.6	22.1	5344.8	38.8

	Total map area	54100.5	100.0	53984.6	100.0	-115.9	100.0	53984.6	100.0	-115.9	100.0
GISS-E2	Very Low	4405.3	8.1	3821.7	7.0	-583.5	4.4	2873.1	5.3	-1532.1	11.2
	Low	12442.2	23.0	9412.9	17.4	-3029.2	22.8	10267.2	19.0	-2174.9	15.9
	Moderate	14419.7	26.6	11348.3	21.0	-3071.3	23.1	11258.3	20.8	-3161.3	23.2
	High	16237.4	30.0	16903.2	31.3	665.8	5.0	19627.5	36.3	3390.0	24.8
	Very High	6595.8	12.1	12498.2	23.1	5902.3	44.5	9958.3	18.4	3362.5	24.6
	Total map area	54100.5	100.0	53984.6	100.0	-115.9	100.0	53984.6	100.0	-115.9	100.0

Table 8.7: Spatial change in the heat vulnerability area from the high forcing scenarios

Model name	Vulnerability Scale	Present (2020)		SSP5-8.5 (2060)				SSP5-8.5 (2100)			
		Map area (sqkm)	% area	Map area (sqkm)	% area	Change in area	% change in area	Map area (sqkm)	% area	Change in area	% change in area
HadGEM3	Very Low	4405.3	8.1	2331.4	4.3	-2073.9	14.3	198.2	0.3	-4207.0	14.4
	Low	12442.2	23.0	8338.7	15.4	-4103.5	28.4	3863.0	7.1	-8579.1	29.4
	Moderate	14419.7	26.6	13332.6	24.7	-1087.1	7.5	12599.5	23.3	-1820.1	6.2
	High	16237.4	30.0	17746.3	32.8	1508.8	10.4	20351.9	37.7	4114.4	14.1
	Very High	6595.8	12.1	12235.5	22.6	5639.7	39.1	16971.7	31.4	10375.9	35.6
	Total map area	54100.5	100.0	53984.6	100.0	-115.9	100.0	53984.6	100.0	-115.9	100.0
MPI-ESM1	Very Low	4405.3	8.1	3498.3	6.4	-907.0	7.0	1189.5	2.2	-3215.7	11.9
	Low	12442.2	23.0	11064.9	20.4	-1377.2	10.7	2174.2	4.0	-10268.0	38.2
	Moderate	14419.7	26.6	10247.1	18.9	-4172.5	32.6	20614.0	38.1	6194.2	23.0
	High	16237.4	30.0	17952.3	33.2	1714.9	13.4	17857.8	33.0	1620.4	6.0
	Very High	6595.8	12.2	11221.8	20.7	4626.0	36.1	12149.0	22.5	5553.1	20.6
	Total map area	54100.5	100.0	53984.6	100.0	-115.9	100.0	53984.6	100.0	-115.9	100.0
MIROC6	Very Low	4405.3	8.14	2821.7	5.23	-1583.5	9.3	1089.5	2.2	-3215.7	11.9

	Low	12442.2	23.0	9496.2	17.5	-2946.0	17.3	2174.2	4.03	-10268.0	38.2
	Moderate	14419.7	26.6	10410.2	19.2	-4009.4	23.6	14614.0	27.0	194.2	0.7
	High	16237.4	30.0	21406.4	39.6	5168.9	30.4	23857.8	44.1	7620.4	28.3
	Very High	6595.8	12.2	9849.8	18.2	3254.0	19.1	12149.0	22.5	5553.1	20.6
	Total map area	54100.5	100.0	53984.6	100.0	-115.9	100.0	53984.6	100.0	-115.9	100.0
ACCESS	Very Low	4405.3	8.1	3500.8	6.4	-904.5	9.4	40.4	0.0	-4364.9	16.2
	Low	12442.2	23.0	8380.0	15.5	-4062.2	41.1	4018.0	7.4	-8424.1	31.4
	Moderate	14419.7	26.6	16355.7	30.2	1827.8	19.0	13750.0	25.4	-669.6	2.5
	High	16237.4	30.0	18594.7	34.4	2357.4	24.5	20859.4	38.6	4621.9	17.2
	Very High	6595.8	12.2	7153.1	13.2	557.3	5.8	15316.6	28.3	8720.8	32.5
	Total map area	54100.5	100.0	53984.6	100.0	-115.9	100.0	53984.6	100.0	-115.9	100.0
GISS-E2	Very Low	4405.3	8.1	2900.8	5.3	-1504.5	13.9	2740.4	5.0	-1664.9	7.9
	Low	12442.2	23.0	8488.2	15.7	-3953.9	36.6	4958.2	9.1	-7483.9	35.7
	Moderate	14419.7	26.6	16247.5	30.1	1827.8	16.9	13035.6	24.1	-1384.0	6.6
	High	16237.4	30.0	17247.5	31.9	1010.2	9.3	21275.0	39.4	5037.6	24.0
	Very High	6595.8	12.2	9100.3	16.8	2504.6	23.1	11975.2	22.1	5379.3	25.6
	Total map area	54100.5	100.0	53984.6	100.0	-115.9	100.0	53984.6	100.0	-115.9	100.0

8.11 Heat vulnerability projections from the HadGEM3-GC31-LL model

The heat vulnerability projections from the HadGEM3-GC31-LL model for the low forcing scenario (SSP1-2.6) indicate that the very low and low heat vulnerability areas are projected to decrease by 347.3qkm (5.3%) and 1.8sqkm (0.0%) by the middle of the century, and by 1343.9sqkm (8.1%) and -4104.8sqkm (24.7%) by the end of the 21st century, respectively. This change will predominantly impact the eastern portion of the study regions. By the middle of the 21st century, moderate heat vulnerability is projected to decline by 2995.8sqkm (45.6%) and by 2904.8sqkm (17.5%) by the end of the 21st century. This alteration would affect the towns of Kuduru, Usman, Dutse, Gwarimpa, Kutunku, Chibiri, and Karu the most. By the middle of the 21st century, high and very high heat vulnerability areas are expected to increase by 2715.6sqkm (41.3%) and 509.7sqkm (7.8%), and 1861.7sqkm (11.2%) and 6375.9sqkm (38.4%), respectively. As shown in Figure 8.12(b) and (c), the map areas most affected by this change include Kutunku, Wuse, a portion of Kuje and Kwali, Gwarimpa, and Karu.

Results of the heat vulnerability projections from the HadGEM3-GC31-LL model for the high forcing scenarios (SSP5-8.5) further indicated that the very low and low heat vulnerability areas were projected to decrease by 2073.9sqkm (14.4%) and 4103.5sqkm (28.5%) by the middle of 21st century and -4207.1sqkm (14.5%) and -8579.2sqkm (29.5%) by the end of the 21st century. Map areas projected to be very low and low vulnerable to heat include Wuse, the city centre, part of Garki, Shere, Panda and part of Gaube. The moderate heat vulnerability was projected to decrease by 4172.6sqkm (32.6%) by the middle of the 21st century and 6194.3sqkm (23.1%) by the end of the 21st century. Settlements of the study area affected by this change are Gwarimpa, Garki, part of Kuduru and Kabusa. The projected areas of high and very high heat vulnerability for the high forcing scenarios in the middle of the 21st century indicated a projected increase of 1508.8sqkm (10.4%) and 5639.7sqkm (39.1). At the end of the 21st century, the results from this study projected the high and very high heat vulnerability areas to increase by 4114.4sqkm (14.1%) and 10375.9sqkm (35.6%). Areas affected by this increase were Paiko, Kwali, Jiwa,

Zuba, Tunga-Maje, central Abaji and Karu areas. Figure 8.12(d) and (e) present the heat vulnerability projections from the HadGEM3-GC31-LL model.

8.12 Heat vulnerability projections from the MPI model

Results of the heat vulnerability projections from the MPI model for the low forcing scenario (SSP1-2.6) indicated that the areas of very low and low heat vulnerability were projected to decrease by 79.1sqkm (1.1%) by the middle of the century (2060) and 1143.4sqkm (11.9%) by the end of the century (2100). The regions surrounding the northeastern areas of the study area, particularly the settlements at the city centre, are predominantly very low and low vulnerable to heat during this time. The moderate heat vulnerability area was projected to reduce by 2331.0sqkm (33.0%) in the middle of the century and 1489.6sqkm (15.5%) by the end of the century. Among the settlements mostly affected by this change were Gwarimpa, Usman, Garki and part of Kabusa. The middle of the century has most of the moderate vulnerability. Results from the MPI model further indicated that the areas of high and very high heat vulnerability were projected to increase by 275.4sqkm (3.9%) in the middle of the century (2060) and 617.4sqkm (6.4%) by the end of the century (2100). The settlements projected to be affected by this change include Kutunku, Paiko and Zuba in the Gwagwalada area council. Other settlements projected to have high and very high heat vulnerability were Kabusa, Aso Kadope, and part of Gwagwa, Chibiri, Kwali and central Abaji, as shown in Figure 8.13 (b) and (c).

The result of the heat vulnerability projections for the high forcing scenarios (SSP5-8.5) for the middle of the century (2060) indicates that the areas of very low and low heat vulnerability will be reduced by 907.0sqkm (7.0%) and 1377.2sqkm (10.7%) in 2060, and 3215.7sqkm (11.9%) and 10268.0sqkm (38.2%) in 2100. Wuse, the city centre, part of Garki and Karu, Shere, and Gurku Kabusa in the northeastern portion of the research area is where this reduction is projected. Areas of moderate heat vulnerability were projected to decline by 4172.5sqkm (32.6%) by the middle of the century (2060) and 6194.2sqkm (23.0%) by the end of the century (2100). These locations are common throughout the study area, with the most prominent being the easternmost region. Areas of high and very high vulnerability to heat were projected to grow

by 1714.9sqkm (13.4%) and 4626.0sqkm (36.1%) by the middle of the century (2060), and 1620.4sqkm (6.03%) and 5553.1sqkm (20.6%) by the end of the century (2100). Very high and high heat-vulnerable areas can be found throughout the study region, with a particular concentration in the informal settlements of Karu in the northeastern and Zuba in the northern extent of the study area. Quarters in Gwagwalada area council, Kwali, and Chibiri in the southwestern part of the study region also have high and very high vulnerability concentrations, as shown in Figure 8.13(d) and (e).

8.13 Heat vulnerability projections from the MORIC6 model

The results of the heat vulnerability projections from the MIROC6 model for the low forcing scenario (SSP1-2.6) for the middle of the 21st century indicate that the areas of very low and low heat vulnerability were projected to decrease by 639.7sqkm (7.4%) and 3051.4sqkm (35.3%). By the end of the 21st century, the very low and low heat vulnerability was expected to decrease further by 1139.7sqkm (7.4%) and 3851.4sqkm (25.2%). The areas of low and very low vulnerability to heat are more prominent in the north-eastern part of the study area, with pockets of scattered low vulnerable areas in the south-eastern portion of the study area. Bwari, Shere, Dutse, Usman, part of Wuse and Garki are projected to be mostly very low and low vulnerable to heat. Areas of moderate heat vulnerability were projected to decrease by 681.9sqkm in 2060, indicating a 7.9% change and a decrease of 2681.9sqkm by the end of the 21st century, indicating a decrease of 17.6%. Areas of moderate heat vulnerability are scattered throughout the study area with pockets of concentrations at Gwarimpa, part of Karu, Wuse, Orozo, and Kubwa, among other settlements. The areas of high and very high heat vulnerability were projected to increase by 1469.5sqkm (17.0%) and 2787.6sqkm (23.3sqkm) by the middle of the 21st century and a further increase of 1769.5sqkm (11.6%) and 5787.6sqkm (38.0%) by the end of the 21st century. The areas of high and very high vulnerability to heat have concentrations at Kutunku, central Giwa, Chibiri, Municipal Aso Kadope, Orozo, Zuba and Gwagwa settlements, among others, as shown in Figure 8.14(b) and (c).

The results of heat vulnerability projections from the MIROC6 model for the strong forcing scenario (SSP5-8.5) at the middle of the 21st century reveal that the regions of very low and low heat vulnerability were projected to decline by 907.0sqkm (7.0%) and 1377.2sqkm (10.0%) and a further decline by 3215.7sqkm (11.9%) and 10268.0sqkm (38.2%) by the end of the 21st century. Very low and low heat-vulnerable areas are primarily distributed at Wuse, part of the city centre, part of Garki, part of Dutse, Shere, Kawa, Gaube and Karshi areas in the southeastern and northeastern part of the study area. The areas of moderate heat vulnerability are projected to decrease by 4009.4sqkm (23.6%) in the middle of the 21st century and 194.2sqkm, representing a projected reduction of 0.7% by the end of the 21st century. Areas of moderate heat vulnerability are common throughout the study area, with more concentrations at Gwarinpa, part of the Usman, Garki, Kabusa, and Karu areas. The areas of high and very high heat vulnerability were projected to grow by 5168.9sqkm (30.4%) and 3254.0sqkm (19.1%) by the middle of the 21st century and a further increase of 7620.4sqkm (28.3%) and 5553.1sqkm (20.6%) by the end of the 21st century. Areas of high and very high heat vulnerability are scattered throughout the study area, with more concentration in central Abaji, Kwali town centre, Gwako, Aso, municipal and Kutunku in the southern part of the study area. Other settlements with high concentrations of high and very high vulnerability to heat are GUI, Zuba, part of Gwagwa, and Nyanya, in the northern part of the study area. Figure 8.14(d) and (e) present the heat vulnerability projections from the MIROC6 model.

8.14 Projections of heat vulnerability from the ACCESS model

The results of the ACCESS model for the low forcing scenario (SSP1-2.6) for the middle of the century indicate that the areas of very low and low heat vulnerability were projected to decrease by 1366.8sqkm (17.2%) and 2663.4sqkm (33.5%) by the middle of the 21st century. A further decrease of 1404.5sqkm (10.2%) and 4989.3 sqkm (36.2%) in the area of very low to low heat vulnerability was projected by the end of the 21st century. The noticeable area affected by this change is in the city centre, part of Garki, Karu, Dutse, and Bwari. Others include Share, Gurku Kabusa, Karshi and Kawu in the northeastern part of the study area. A few areas of the southeastern region are

also affected by this change. Areas of moderate heat vulnerability were projected to decrease by 681.9sqkm (7.9%) in the middle of the 21st century (2060) and a further decrease by 2681.9sqkm, indicating a projected change of 17.6% by the end 21st century. Most of the map areas during the middle of the century were projected to be covered by moderate heat vulnerability. The end of the century has fewer areas of moderate heat vulnerability, notably in parts of Garki, Orozo, Nyanya, Gwarimpa and Usman. The areas of high and very high heat vulnerability were projected to increase by 263.8qkm (3.3%) and 1826.4sqkm (29.2%) by the middle of the 21st century. The result from this study projected a decrease in areas of low heat vulnerability by 544.4sqkm (3.9%) at the end of the 21st century and an increase in very high heat vulnerability by 5344.8sqkm, signifying a projected increase of (38.8%). The map areas of high and very high vulnerability to heat have higher concentrations at Kutunku, Zuba, Usman, Gwagwa, Kwali, Chibiri, and part of central Abaji during the middle of the century. In addition to these locations are Bagaji, Karu, and Aso Kadope in the northwestern part of the study area during the end of the 21st century, as shown in figure 8.15(b) and (c).

The heat vulnerability projections from the ACCESS model from the high forcing scenarios (SSP5-8.5) for the middle of the 21st century reveal that the regions of very low and low heat vulnerability were projected to decline by 904.5sqkm (9.4%) and 3953.9sqkm (41.1%). Further decline in very low and low heat vulnerability areas by 4364.9sqkm (16.2%) and 8424.1sqkm (31.4%) was projected for the end of the 21st century. Fewer settlements in the part of Wuse, city centre, Usman and Dutse are among the most affected by the change, mainly in the north-eastern region of the study area. Areas of moderate heat vulnerability were projected to decrease by 681.9sqkm by the middle of the 21st century, representing a projected change of 7.9% and a further decrease of 2681.9sqkm (17.6%) by the end of the 21st century. Moderate heat vulnerability areas are distributed all over the study area, with more concentration in the city centre, part of the Garki and Nyanya study area. Areas of high and very high vulnerability to heat were projected to grow by 2357.3sqkm (24.5%) and 557.3sqkm (5.8%) by the middle of the 21st century and a further increase of 4621.9sqkm (17.2%) and 8720.8sqkm (32.2%) by the end of the 21st century.

Areas with very high heat vulnerability are common in the Paiko, GUI, central Giwa, Yangoji, and Aso Kadope, among others, as shown in Figure 8.15(d) and (e).

8.15 Projections of heat vulnerability from the GISS-E2 model

According to the GISS model results for the low forcing scenario (SSP1-2.6), areas with very low and low heat vulnerability are projected to decline by -583.5sqkm (4.4%) and -3029.2sqkm (22.8%) by the middle of the 21st century. By the end of the 21st century, a further reduction of -1532.1sqkm and -2174.9sqkm was projected, indicating a change in the area of 11.2% and 15.9%, respectively. This change is evident on the map in the northeastern region of the research area, notably in urbanised communities. Areas of moderate heat vulnerability are projected to decline by -3071.3sqkm by the middle of the 21st century and by -3161.3sqkm (23.2%) by the end of the 21st century. Many areas in Gwarinpa, Kabusa, Nyanya, Karu, and Orozo are moderately vulnerable to heat, especially in 2060. High and very high heat vulnerability areas were projected to increase by 16237.4sqkm (30.0%) and 6595.8sqkm (12.1%) by the middle of the 21st century, and by 4114.4sqkm (14.1%) and 10375.9sqkm (35.6%) by the end of the 21st century. The southwest and northeastern regions are primarily affected by this alteration, except for the city centre, as seen in Figures 8.16(b) and (c).

The GISS model for the high forcing scenario (SSP5-8.5) in the middle of the 21st century projected the areas of very low and low heat vulnerability to decline by 1504.5sqkm and 3953.9sqkm, implying a projected change of 12.3% and 36.6%. Areas of very low to low heat vulnerability were further projected to decrease by 1664.9sqkm (7.7%) and 7483.9sqkm (35.7%) by the end of the 21st century. Areas mostly affected by this change are the urbanised centre which includes Wuse, the city centre and part of Garki. The moderate heat vulnerability was projected to increase by 1827.8sqkm, representing a projected increase of 16.9% in the map area by the middle of the 21st century and a projected decrease of 1384.0sqkm, representing a decrease of (6.6%). The map areas mostly affected by this change are part of Bwari, Gwarinpa, and Garki. Others include

part of Gaube and Karshi, particularly at the end of the 21st century. The high and very high heat vulnerability for the high forcing scenario was projected to perceive an increase in area by1010.1sqkm and 2504.5sqkm by the middle of the 21st century, representing a projected increase of 9.3% and 23.1%. Further increases in the map areas of high and very high heat vulnerability were projected to 5037.6sqkm (24.0%) and 5379.3sqkm (25.6%) by the end of the 21st century. Except for the settlements of Wuse, Garki, part of Gwarimpa and the northern extent of the study area, the dominant part of the study areas was projected for high vulnerability to heat, as shown in Figure 8.16(d) and (e). Figure 8.17(a) and (b) presents the ensemble of the average change in the heat vulnerability for the low and strong forcing scenarios for the middle and end of the 21st century.

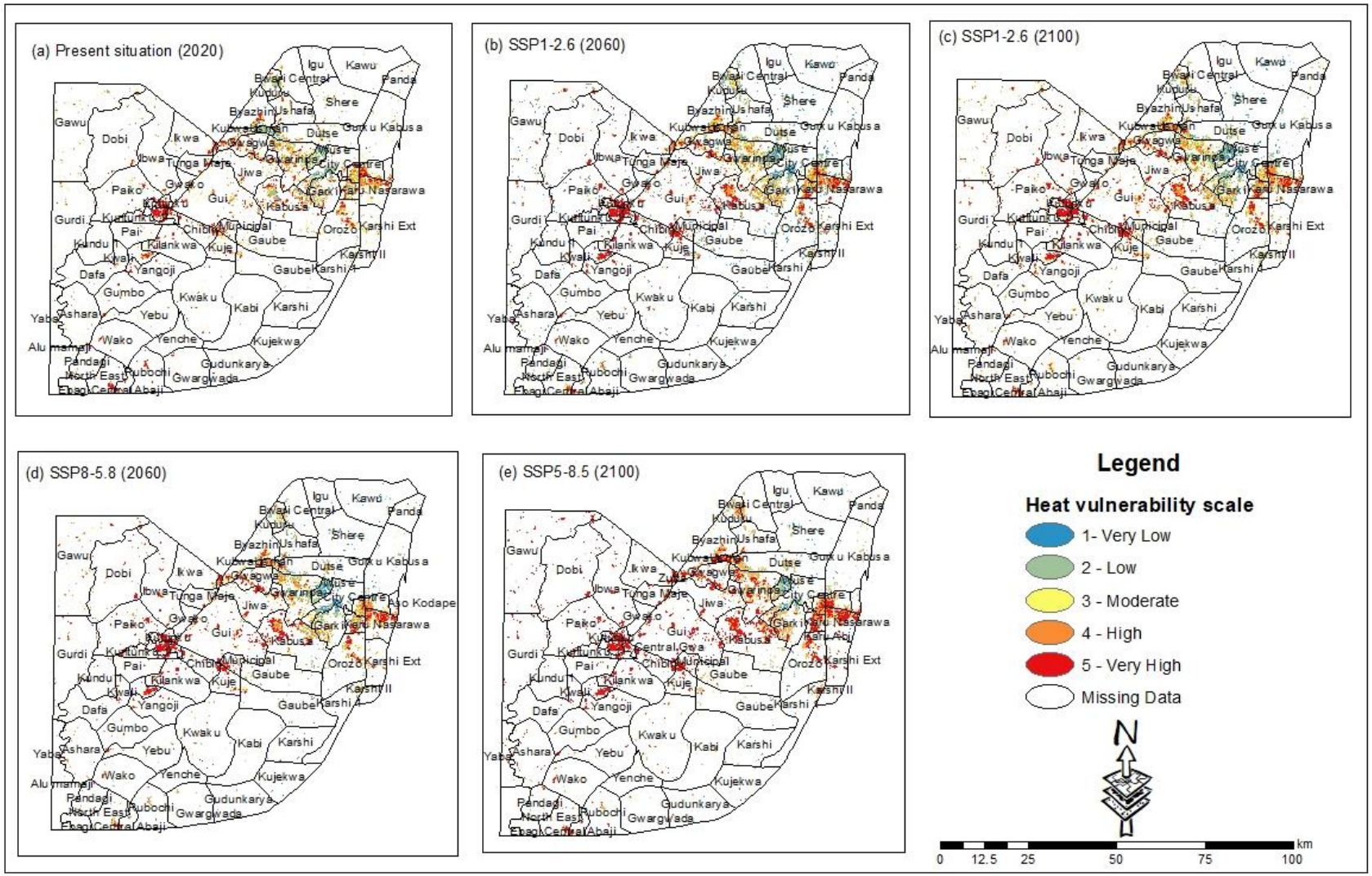


Figure 8.12: Heat vulnerability projections from the HadGEM3-GC31-LL model under low and high forcing scenarios (a) present situation (2020), (b) SSP1-2.6 for 2060, (c) SSP1-2.6 for 2100, and (d) SSP5-8.5 for 2060, and (e) SSP5-8.5 for 2100.

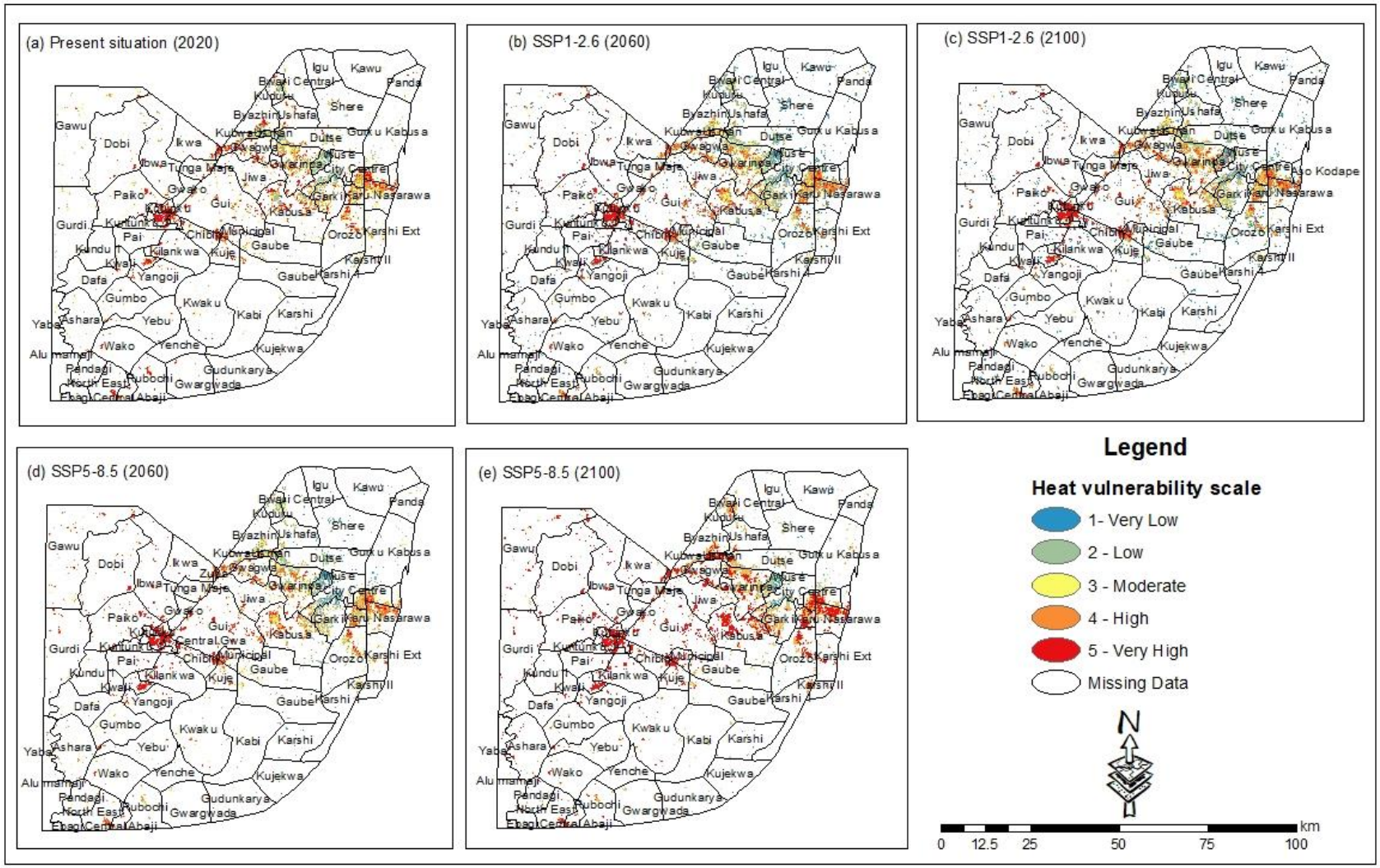


Figure 8.13: Heat vulnerability projections from the MPI model under low and high forcing scenarios (a) present situation (2020) (b) SSP1-2.6 for 2060, (c) SSP1-2.6 for 2100, and (d) SSP5-8.5 for 2060, and (e) SSP5-8.5 for 2100.

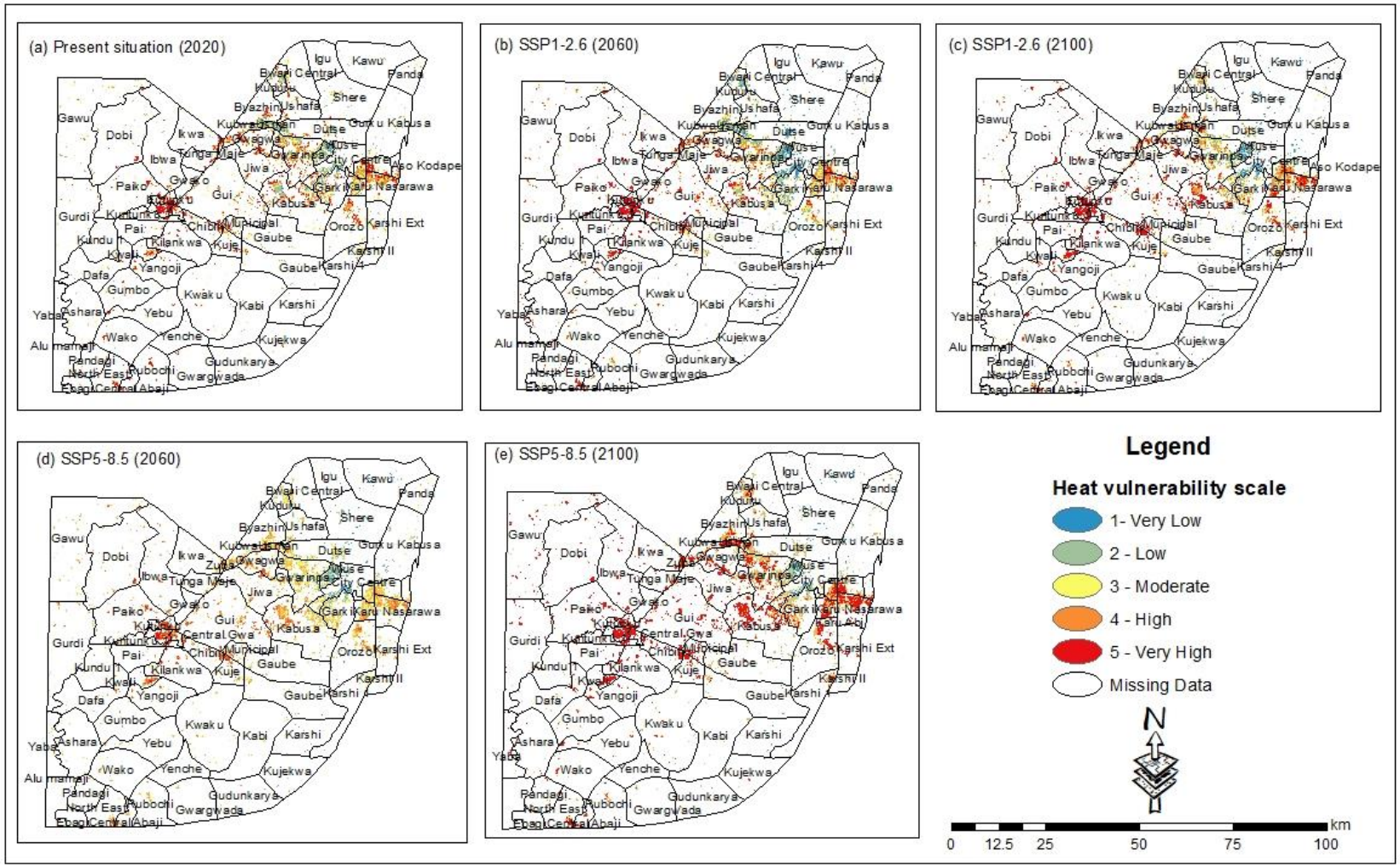


Figure 8.14: Heat vulnerability projections from the MIROC6 model under low and high forcing scenarios (a) present situation (2020), (b) SSP1-2.6 for 2060, (c) SSP1-2.6 for 2100, and (d) SSP5-8.5 for 2060, and (e) SSP5-8.5 for 2100.

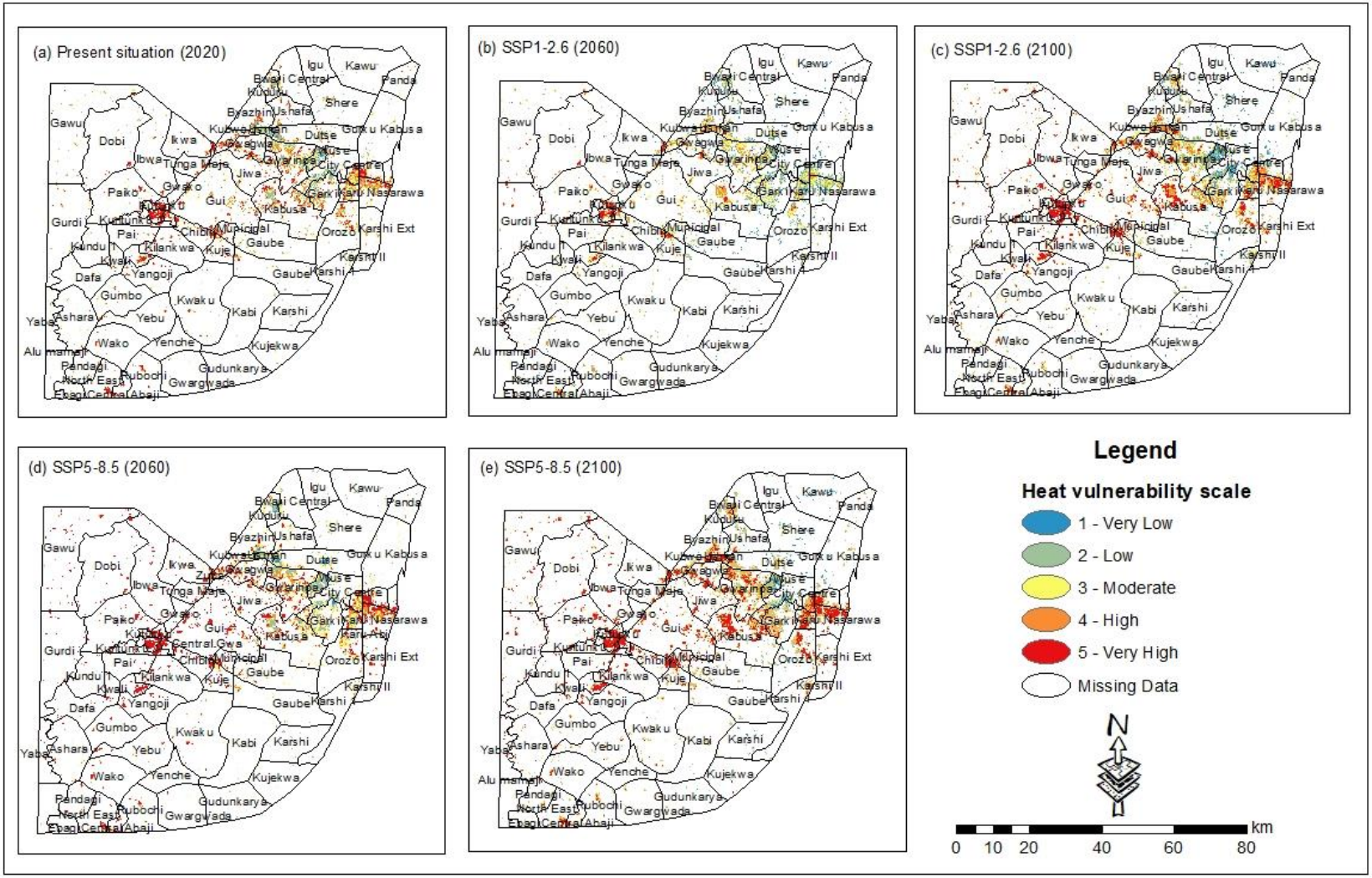


Figure 8.15: Heat vulnerability projections from the ACCESS model under low and high forcing scenarios (a) present situation (2020), (b) SSP1-2.6 for 2060, (c) SSP1-2.6 for 2100, and (d) SSP5-8.5 for 2060, and (e) SSP5-8.5 for 2100.

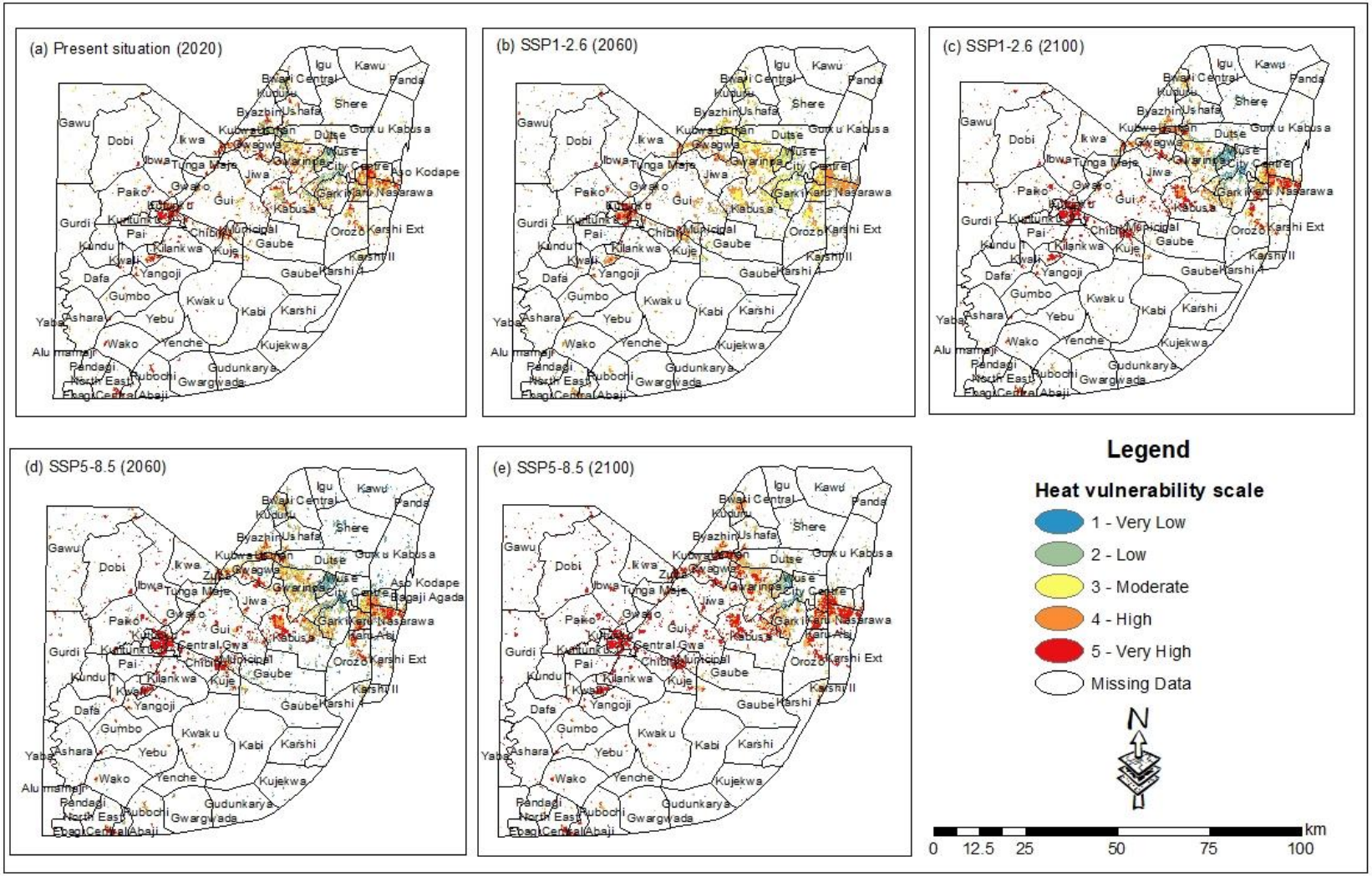


Figure 8.16: Heat vulnerability projections from the GISS-E2 model under low and high forcing scenarios (a) present situation (2020), (b) SSP1-2.6 for 2060, (c) SSP1-2.6 for 2100, and (d) SSP5-8.5 for 2060, and (e) SSP5-8.5 for 2100.

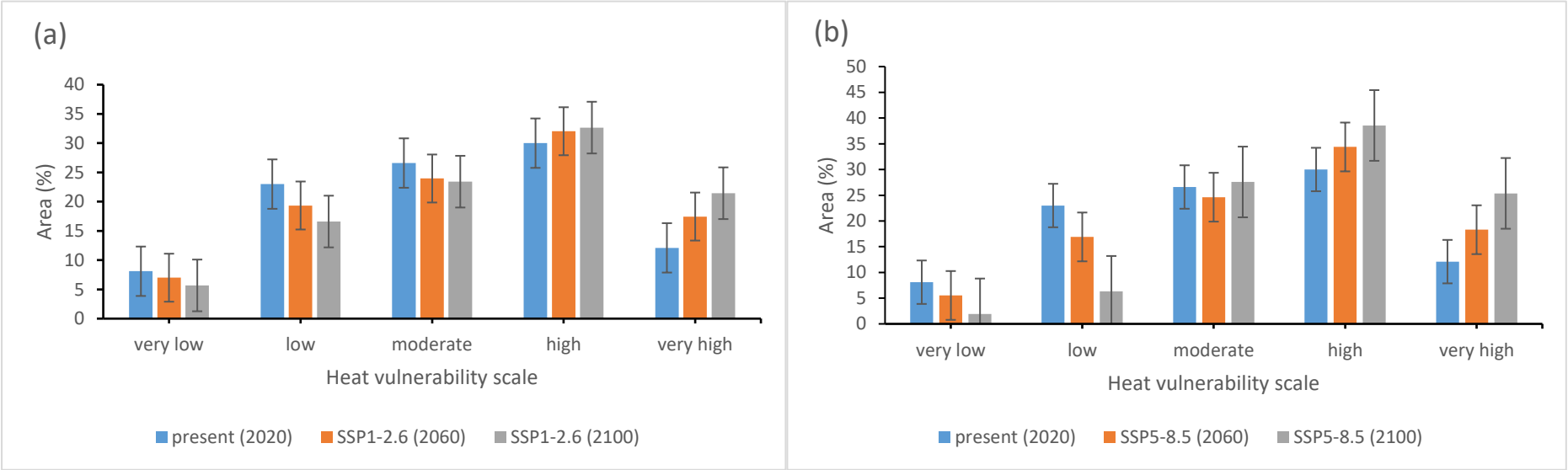


Figure 8.17: Heat vulnerability ensemble for the 5GCMs for low forcing scenarios (a) and high forcing scenarios (b).

8.16 Conclusion

This chapter covers the annual, monthly, seasonal, and spatial variations in temperature from five CMIP6 climate models. Based on the model output reported in this chapter, Abuja and its surroundings are today 1.1°C warmer than they were 40 years ago. Abuja was projected to be warmer by 0.4^{o}C by the middle of the 21st century and 0.7^{o}C by the end of the 21st century under low forcing scenarios. Under the high forcing scenario, Abuja was projected to be 0.7^{o}C warmer by the middle of the century and 3.2^{o}C warmer by the end of the 21^{s}t century. To assess the performance of the models, simulations of five GCMs from the CMIP6 set of experiments were employed. When the performance of the five models was evaluated, the model output from the MPI showed relatively less warming than the model output from the HadGEM3-GC31-LL and ACCESS, which showed more warming. The heat vulnerability projections reported in this chapter are based on temperature projections for the middle and end of the 21st century and low and high forcing scenarios. The heat vulnerability projections in all five GCMs of Abuja and its surroundings indicated an increase in high and very high vulnerability to heat by the end of the 21st century. Even though the study intended to generate separate maps of heat vulnerability projections based on climate and socioeconomic indicators, this aimed to measure the relative contributions of climate change and socioeconomic change to heat vulnerability. This became impossible because the socioeconomic indicators used for heat vulnerability projections remain at present times (2020) due to data problems.

The fundamental assumption of this chapter is that the models are 'faithful to reality' in the absence of validation of model output for a reference period against the same for observations, such as the model for 2000-2029 versus observations for 2000-2019. Validating heat vulnerability maps is essential for ensuring their accuracy and dependability. Validation entails comparing predicted vulnerability patterns to observations or health data from previous heatwave events. It helps identify any inconsistencies, biases, or flaws in the methodology and assumptions of the maps. Through validation, adjustments and

enhancements can be made to enhance the effectiveness of the maps and eliminate biases.

In the absence of validation, warm or cold bias can significantly affect the accuracy and efficacy of heat vulnerability maps. The purpose of heat vulnerability maps is to identify regions that are more prone to heat-related health hazards, such as heat waves. These maps typically consider temperature, humidity, land cover, socioeconomic conditions, and population density to assess vulnerability. However, in the absence of validation, these maps may contain biases. Warm bias describes a circumstance in which vulnerability maps overestimate the risk of heat-related health problems. In this instance, areas that may not be especially susceptible to heatwaves are categorised as high-risk zones. Consequently, resources and interventions may need to be allocated more, focusing on regions that do not require immediate attention while ignoring regions that genuinely require assistance. Warm bias can result in inefficient resource allocation and misunderstanding of vulnerability patterns. In contrast, chill bias occurs when heat-related health issues are underestimated on vulnerability maps. This bias can also be problematic, as it may minimise the vulnerability of vulnerable areas. Therefore, resources and efforts to mitigate the effects of heatwaves may be directed to something other than the areas that would benefit most.

Without validation, fostering data-driven decision-making and scientific rigour is critical to avoid warm or cold bias. Continuous monitoring and evaluation of vulnerability maps and feedback from local communities and stakeholders can help enhance the models and eliminate any potential biases. Collaboration among researchers, public health professionals, and community organisations can help to speed up the validation process and guarantee that vulnerability maps correctly reflect the reality on the ground. To this end, warm or cold bias without validation highlights the need to analyse and refine heat vulnerability maps thoroughly. This allows us to identify better and prioritise locations that require action and effectively deploy resources to safeguard vulnerable populations during heatwave episodes. The following chapter presents a discussion of the results of this study.

CHAPTER NINE: SUMMARY, DISCUSSION, AND CONCLUSION

9.0 Introduction

This chapter summarises the research findings, the limitations of the study, and future research directions. Previous studies have shown that remotely sensed data and GIS techniques can provide a potent tool for scientific explanations of the effects of climate change on human health. The majority of previous research on the effect of heat on human health has been conducted in high-income countries. Most of these investigations focused on the relationship between temperature and heat-related morbidity and. The investigations on heat-human health conducted in the tropical Africa have focused on the impacts of heat as a modifier of morbidity and mortality from infectious diseases. This study mapped heat vulnerability, which could be linked to temperature rise and urban heat island. Extreme heat from the temperature rise is an important indicator of heat exposure that influences heat-related morbidity and mortality. It is well-accepted that urbanisation leads to the growth in the AIS of cities, which is a crucial source of the thermal environment and the associated morbidity and mortality linked with heat.

This research fills a gap in scientific knowledge about the effects of climate change on human health in Abuja and its environs. This study has five main goals (details in section 1.7 of chapter one), which leads to a discussion of outcomes in this chapter organised into five subsections. Firstly, mapping the spatiotemporal change in the study area's AIS was performed to quantify the spatial and temporal changes in the areas of AIS and other land use/cover. This helped to understand the effects of anthropogenic activities such as urbanisation on land use/cover change. Secondly, the investigations of high-resolution spatial and temporal changes in the magnitude of UHI as a result of urbanisation were focussed on understanding the impacts of urbanisation and land use/cover change on the LST and UHI of the study area. Thirdly, the modelling of relationships between maximum temperature and heat-related mortality in the six subregions of Abuja and its environs was focused on understanding the effect

of extreme heat on human health. Fourthly, the spatial mapping of heat vulnerability in the research area was aimed to recognise the spatial locations within the study that are vulnerable to extreme heat. Finally, the study concluded by performing heat vulnerability projections for the middle and end of the 21st century under low and high forcing scenarios. This was aimed to understand the future temperature change; together with demographics and socioeconomic variables, the study intends to understand the spatial extent of heat vulnerability at the middle and end of the 21st century. The following sections present a discussion of the five main goals of this study as follow:

9.1 Research objective 1*:* mapping the spatiotemporal change in the study area's artificial impervious surface

Seven classes of land use/cover were identified for this study. These classes were bare land, shrubland, water bodies, forest land, AIS, grassland, and cropland. While grassland, forest land, and bareland constituted the most prominent land use/cover categories in the study area in 1985, covering over 70% of the total land area, the AIS and cropland were the minor land cover classes during this period, covering less than 30% of the study area. The change in the AIS revealed in this study could be attributed to urban expansion, which impacted the thermal environment of Abuja. Recently, substantial vegetation was destroyed to make way for urban expansion and cultivated land. This has led to considerable growth in AIS and croplands in the study area in 2019. Urban development has further encroached upon many of the territories set aside for environmental protection, intensive farming, and animal husbandry. The findings of this study indicate that cropland has decreased in recent years, which could be attributable to changes in the occupation of the area's labour force. For career opportunities, most people in the area take advantage of the construction activities and widespread commercialization of the local economy for unskilled labour. Youths from this area and other migrants fled to the city to pursue brighter jobs, leaving agricultural work to women and the elderly.

One critical factor responsible for the rise in the population of Abuja and its environs is the search for better living conditions due to the development brought about by the Federal Capital Territory (FCT) movement from Lagos to

Abuja in 1991. This signifies rapid urban growth and the increase in AIS, which comprises housing, shopping malls and plazas, administration structures, infrastructure, and amenities such as schools, hospitals, recreational parks, and gardens. The change detection reported from this study shows that urbanisation and socio-economic activities may have considerably contributed to transforming the natural surfaces into AIS.

This study shows that water bodies comprising streams, lakes, dams, and rivers are decreasing. Climate change and the fast-growing population's need for water for irrigation and other uses may be blamed for declining surface water. The exposed riverbeds are now the construction industry's source of sand and gravel. During the operation, large open shallow pits are left behind, occasionally changed into waste disposal sites or filled with water during the rainy season. The spatial trends of urban expansion detected in this study are connected to the locations of dense informal settlements. The number and size of settlements in Nyanya, Masaka, Koroduma, Kodepe (Auta ba Laifi), and One Man Village have increased dramatically. Between 1985 and 2005, these villages, which were merely farmsteads grew into linear conurbations stretching from Mararaba to Kodepe (Auta ba Laifi) along the Keffi-Abuja motorway. Informal settlements are a physical and spatial manifestation of urban poverty and intra-city inequality.

9.2 Research objective 2: To investigate high-resolution spatial and temporal changes in the magnitude of UHI in the study area as a result of urbanisation

To comprehend the effect of land use/cover change on LST, this study examined the change in the magnitude of UHI as a result of urbanisation. The growth of AIS in Abuja and its environs has severely impacted the natural environment, influencing the thermal environment. This study shows that areas of AIS and bareland recorded the most substantial increase in LST between 1986 and 2019. The spatial variations of the LST show that the northwestern, eastern, and central regions of the study area had the greatest LST. The high LST recorded in these regions could be linked to urban growth and the replacement of natural vegetation with non-evaporative and non-transpiring surfaces such as the AIS.

The prevalence of AIS and the bare surface could influence the LST and contribute to UHI growth in the region. The north-eastern part of the study area is the economic hub, explaining why the high LST was recorded. Due to human pressure on land resources, more vegetation cover is destroyed into built-up and bare surfaces.

The spatial pattern of LST of Abuja and its environs showed a substantial variance between the urban, suburban, and rural settlements, with Gwagwalada, Gwarinpa, Kubwa, and Kuje among the urban area with the highest intensity of UHI, while Kurunduma, Kwali, Abaji among other settlements having the rural characteristics with the lowest temperature. With LST difference of 4.9°C, Maitama urban and Kurunduma rural areas had a meaningful temperature difference. In addition, whereas Gwarinpa metropolitan area and Kurunduma rural area had the peak and lowest LST, respectively, the area with the utmost heat island intensity was between Gwagwalada urban area and Abaji rural area, with an LST differential of 7.2^{o}C. A substantial rise was noted when comparing the LST parameters of 1986 to those of 2019. For instance, between 1986 and 2019, the LST in Area 11, an important economic and administrative centre in Abuja, climbed by 7.6°C. LST differential of 8.7^{o}C was detected between the central business area (CBD) and the Wupa plant, an industrial layout in the FCT. This could be attributed to replacing vegetative cover with non-evaporative with high thermal conductivity, such as concrete and asphalt; urban areas typically have higher LST than adjacent rural areas. This study found an increase in LST over the study area, linked to increased AIS and loss of vegetation cover. In 1986, the average LST difference between Jiwa urban area and Yangoji rural areas was 3.4^{o}C. By 2019, the metropolitan areas had meaningfully expanded, resulting in a 17.1^{o}C increase in LST.

Several rural areas in the southern part of the study area, such as Ashara, Gaube, Pandagi, Gurdi, and Kutunku, had more unusual LST than their urban counterparts, such as part of Gwarimpa, Asokoro Shere, and Garki, with LST variance up to 3^{o}C. UHI development has been linked to an increase of 12.9^{o}C in 2019 in the southern part of the study area. This was due to several factors, including the development of large estates. Between 2003 and 2007, the FCT

minister was tasked with ensuring that the Abuja Master Plan was carried out diligently. This resulted in the demolition of poorly positioned dwellings and communities and the rapid expansion of the Phases. During this time, other ministries were transferred from Lagos to Abuja to continue the relocation of the capital's headquarters. This has led to the rise in LST due to massive urbanisation.

A negative correlation between LST and NDVI for each analysed period shows vegetation is linked to lower LST. The results show that LST and vegetation cover have negative values, while LST and NDBI have positive values. Pixels with low NDBI values are associated with vegetation cover, whereas pixels with high NDBI values are associated with no vegetation cover. The highest NDBI values were recorded in built-up and bareland areas. The positive link between LST and built-up areas is consistent with prior studies, which discovered more variance in LST of impermeable surfaces, such as largely built-up regions and bare surfaces, than in vegetated areas.

9.3 Research objective 3: To determine the effect of maximum temperature on heat-related mortality in the study area

Heat-related illness and death in Abuja and its surroundings are expected to be on the increase due to temperature rise from climate change. This study found that death rates rose for every 1°C rise in maximum temperature above 30°C. This means that death rates could go up on the hottest days. This study demonstrated that the amount of heat-related mortality differs by location in Abuja. In the Gwagwalada, AMAC, Kuje, and Abaji area councils, for example, an average of 10 deaths per 1^{o}C temperature increase was observed at the monthly basis. In contrast, an average of 300 deaths were reported in the Kwali and Karu regions every month.

For temperatures below 32°C, the association appears to be stable, but the rate of change accelerates above this threshold. This means that the temperature at which the heat exposure signal becomes powerful enough to cause rapid increase in heat-related mortality is 32°C. Regression models on the relationship between

maximum temperature and heat-related mortality reveal a considerable relationship in Gwagwalada, Municipal, and Karu areas. A strong association between maximum temperature and total mortality was also identified in the Abuja area councils of Kuje, Kwali, and Abaji. The relative risk for the relationship, on the other hand, varies with geography. For example, the results of this study revealed a high statistical link in the Maraba (Karu region), Kuje, Kwali, and Gwagwalada areas, as opposed to the Municipal and Abaji areas, where the relationship was weaker.

The relatively weak statistical association between maximum temperature and mortality in AMAC and Abaji councils could be attributed to the following explanations. First, because of AMAC's strategic location and the presence of various government institutions, international embassies, organisations, and commercial offices, it has been classified as one of the area councils with a high share of AIS. This could result in the growth of UHI, particularly in adjoining slums and informal settlements. Even though vegetative cover and gardens may meaningfully reduce the intensity of UHI in the city, the poor correlation between maximum temperature and mortality may be related to poverty and inequality. AMAC has the highest proportion of wealthy population who can afford air conditioning and other measures to reduce the effects of extreme heat. The National hospital in AMAC is a well-equipped facility with cutting-edge equipment solely accessible to the privileged populace. The institution's rehabilitation expense is unreasonably expensive for the impoverished who live in the area's informal settlements. Due to the high expense of treatment in AMAC, low-income earners typically seek care at less expensive health centres, which may explain the poor link between excessive temperature and mortality. Furthermore, the hospital's poor data collecting and management practices may have contributed to the unsatisfactory connection.

The Abaji is a bordering area council on Abuja's southern outskirts. It is bounded by the states of Nasarawa, Niger, and Kogi. The Abaji area council's suburban and rural nature, dominated by farming communities, may explain the weak association between maximum temperature and excess mortality in the area. The peculiar aspect of the neighbourhood is distinguished by farming communities

with extensive vegetation cover and relatively small area of AIS. The high relationship between maximum temperature and mortality in the Gwagwalada, Kuje, Kwali, and Karu areas may be linked to the area's thermal environment, characterised by AIS and developed UHIs. The regions are dominated by low and middle-income earners who cannot afford the city's living standards but choose to reside near the city centre. The Karu community, for example, is the closest informal settlement to the city centre, and it houses more than 60% of Abuja's low and middle-income workers. The unplanned nature of these settlements, combined with their high population, has resulted in densely packed buildings with little vegetation and high AIS, enhancing the creation of UHI in the area.

9.4 Research objective 4: To perform spatial mapping of heat vulnerability in the research area

The spatial variation of heat vulnerability in Abuja ranging from very low, low, moderate, high, and very high. The findings from this study show that the spatial distribution of heat vulnerability to human health was uneven, with the northern part of the research area more vulnerable to heat than the southern part. The regional variation in heat vulnerability in the study area could be attributed to various factors related to the degree of heat exposure, sensitivity, and adaptation capacity. They could all considerably influence the spatial variations in heat vulnerability found in Abuja and its environs. The heat exposure index found substantial spatial heterogeneity among Abuja's settlements which could be attributed to the spatial variation in the thermal environment. The spatial variation in heat exposure is related to AIS, LST, and vegetal cover. In recent times, settlements in the northern part of the study area have witnessed a rise in the magnitude of UHI due to the high rate of population growth and urban expansion. The high rate of urbanisation witnessed in the northern part of Abuja, and its environs have replaced the vegetal cover with AIS. The wide range of low vulnerability areas can be observed in the city centre, a highly urbanised area in the northeastern region. For example, heat vulnerability in the city centre, Wuse, and Garki neighbourhoods are substantially low. This disparity may be attributable to a well-developed economy and well-planned layout providing a

park and garden may lead to low heat vulnerability, illustrating the importance of urban vegetation and economic qualities. Even though hot spots of high heat vulnerable areas are more common in the settlements in the north-central region of the research area, a large portion of the region is also moderate to low vulnerable to heat. This could be due to several granite inselbergs that hinder heat from dispersing efficiently in the area. Furthermore, the northern regions saw more economic development than the southern regions, with high proportions of wealthy population resulting in greater adaptability for northern inhabitants. Poverty could be the main reasons most people in the southern region do not utilise air conditioning during the hot season. Air conditioning is one of the most effective ways to reduce heat effects.

The proportion of moderate to low areas vulnerable to heat is high in the southern part of the study area. This could be attributed to the region's low level of urban development. Because suburban to rural areas have low AIS, they are covered by a considerable vegetation. This has led to a low magnitude of UHI. Low concentrations of AIS in the area may also aid in reducing the severity of heat waves. The urban cooling intensity of water bodies in the study area has been demonstrated to a direct impact on the microclimate. The outcomes of this study imply that surface water can help to minimise heat in metropolitan settings by lowering the surrounding environment's LST. Microclimate are affected by changes in biodiversity, water, and radiation budgets. The existence of dam may have contributed to places in Ushafa that were less vulnerable. Because water absorbs more heat than land, the Usman Dam's presence could cause heat to be absorbed during hot days, decreasing temperatures.

The heat sensitivity map for this study demonstrates that the UHI does not always cause high vulnerability areas from urbanisation and AIS. Areas of relatively low socio-economic status in the research area's southern section could be linked to pockets of the region's highly vulnerable areas to heat. Some settlements in the southern region's suburban and rural areas are highly vulnerable to heat. Heat is perilous in the Paiko, the southern part of Kilankwa, the northern half of Dafa, and Gwako. Poverty is a socioeconomic factor in health. The dominant households in the rural and informal settlements in the

study area survive on less than $1.5 per day. The low-income residents are more vulnerable to heat-related disease due to their weak immune systems. A weakened immune system and a high illness burden may compromise efficient thermoregulation, putting people at risk of heat-related morbidity and death. Poor sanitation raises the likelihood of disease, making people more sensitive to heat. Inadequate sanitary conditions and the disease burden could make a community more sensitive to external causes such as shifting climatic circumstances.

The lack of awareness about the impacts of heat on human health is likely to limit heat adaptation. Because the public has poor knowledge of temperature levels, they do not use weather forecasts/reports, limiting their ability to prepare for extreme heat events. There is a need to raise awareness about the harmful effects of heat on human health through social gatherings, such as religious gatherings in churches and mosques, in order to educate the locals who do not have access to information about the effects of heat on human health and who do not understand warnings due to their low educational status. Their illiteracy may have contributed to their poor responsiveness to early-warning systems, heat awareness, and Heat Health Programs. Households outside the city centre and in informal settlements have few heat adaptation alternatives since they have little control over their living and working conditions and cannot afford air conditioning, fans, or freezers. Most informal settlement households are unlikely to have air conditioners due to the residents' poverty. There were also not enough cooling places for residents. Poor ventilation and hot weather were the primary reasons for populations staying outside to cool off throughout the heating season. On the other hand, staying indoors at night may increase heat exposure and the likelihood of people removing mosquito nets.

Poverty played a crucial role in the growth of informal settlements. 70% of Nigerians are currently living below the poverty line. Informal settlements are home to most of the urban poor population. In Abuja, the Federal Capital of Nigeria, informal settlements are among the fastest-expanding informal settlements in tropical Africa (Adepoju *et al*., 2013). These are predominantly

in the area near the city centre, where most offices and businesses are located. The ineffectiveness of development policies has resulted in the fast spread of informal settlements within and outside the capital city, also known as clusters of haphazard development in abandoned sections of towns. These settlements lack essential facilities such as potable drinking water, proper hygiene, proper solid and liquid waste disposal system, and poor sanitation. They also lack access to roadways. In Abuja, over 30 informal settlements areas have been discovered, ranging from high-density, dismal central city tenements to unofficial squatter communities (Ene, 2021). The expanding informal settlements of Abuja could be attributed to poverty and inequality, unaffordable housing for all demographic classes, and social marginalisation. These densely populated informal settlements are distinguished by densely packed communities in mud constructions with rusted roofs. The structures were congested, resulting in minor pedestrian routes preventing cross ventilation. The lack of primary amenities such as health centres, power, roads, water, and schools increase their sensitivity to heat.

9.5 Research objective 5: heat vulnerability projections for the middle and end of the 21st century under low and high forcing scenarios

Extreme heat exacerbates the negative consequences of climate change on human health. The effects of temperature change on a spatial, monthly, seasonal, and annual scale for 2041-2060 and 2081-2100 based on low forcing scenarios (1-2.6) and high forcing scenarios (5-8.5) imply warming in Abuja and its surroundings. The ACCESS model projected the hottest mean annual temperature change in the middle of the century from the low forcing scenarios, according to a comparison of the model output from the 5 GCMs examined in this study (SSP1-2.6). Compared to the output of the HadGEM3-GC31-LL model, MIROC6 models, and the GISS-E2-1-H model. Compared to the other models, the MPI model exhibits the least warming. The HadGEM3-GC31-LL model, the GISS-E2-1-H model, the MIROC6 model, and the ACCESS model all projects warmer mean annual temperature changes at the end of the century. Compared to the other models, the MPI model exhibits the least warming.

The ACCESS and HadGEM3-GC31-LL models projected the hottest mean annual temperature change for the middle of the century under high-forcing scenarios. The MIROC6 and GISS-E2-1-H models likewise projected warmer temperatures compared to the MPI model, which projected the smallest rise in average annual temperature change compared to the other four models included in this study. The CMIP6 model output from the five models in this study indicates that the mean annual temperature over Abuja and its environs will increase by less than 0.5^{o}C for low forcing scenarios and by 0.9^{o}C for high forcing scenarios by the middle of the century. Over most of the study area, the mean changes in an annual temperature range from 0.3^{o}C to less than 1.0°C at the end of the century under low forcing scenarios and from 1^{o}C to over 4°C under high forcing scenarios, which is consistent with the late 20th-century baseline. In the late 21st century, under the SSP5-8.5 scenario, most of the study area experiences mean annual temperature changes of greater than 4.1°C. The northwestern region of the research area suffers more substantial temperature increases than the southeastern and northeastern regions, as indicated by a pattern. This holds for RCP5-8.5 mean annual temperature changes. Under RCP1-2.6, the mid-and late-21st-century mean changes are less than 1.0°C above the late 20th-century baseline. Through the high-forcing scenarios, a similar pattern of annual temperature change was projected for the end of the century.

At the seasonal temperature change, the cold Harmattan season dominates December, January, and February (DJF), which is characterised by dust and haze from the Sahara desert. Maximum temperatures are projected to drop during this season, with January showing the lowest maximum temperatures. It should be stated that the maximum temperature for Abuja and its environs does not always exhibit substantial regional variations presumably because of the interdecadal fluctuation which could influence spatial variations. The rise in maximum temperature in the season often begins in February, when the Harmattan season is winding down, with rising daytime cloud cover and latent heat fluxes that recharge the atmospheric moisture to start the heat/rainy season. The months of March, April, and May (MAM) are critical for the consequences of maximum temperature in the Abuja region, as these are the months in which the effects of maximum temperature are most pronounced. The highest maximum

temperatures change were recorded in the Gawu, Dobi, Paiko, and Kutunku communities in the northwest section of the study area during the MAM season. The MAM is the pre-monsoon season when the cold tropical continental air mass's influence has waned, and the atmosphere has become dry and warm. The season is distinguished by a lack of excessive cloud cover and a lack of suspended dust, both of which could have reduced insolation and raised maximum temperatures. As a result, the month of March sees a momentous rise in air temperatures as a transition month between the cold and hazy Harmattan and the overcast and rainy season. The warm season predominates throughout MAM, implying that March has had maximum temperatures above the long-term average while April and May were projected to experience maximum temperatures within the normal long-term range. Even while maximum temperatures in most of the study region are within the long-term average throughout most of the projection season, several places in the study area will witness temperature anomalies that were approximately above 1.0^{o}C hotter than the present seasonal average between 2041 and 2060 and 4.0^{o}C at the end of the century (2081-2100).

Due to the intensity of monsoon flow, the average maximum temperature during June, July, and August (JJA) was found to be low, JJA detects an increase in precipitation events accompanied by cloud cover, reducing the amount of solar energy reaching the earth's surface and lowering maximum temperatures. The decrease in maximum temperatures measured during this season ranges from 0.5^{o}C to 1^{o}C between 2041 and 2060 to 1.5^{o}C to 2.5^{o}C between 2081-2100, with August being the coldest month and the northwest-to-southwest region of the study area seeing the lowest temperatures. The September, October, and November season (SON) is the transitional season between the wet season and the Harmattan season. SON is characterized by a high amount of rainfall usually accompanied by strong winds and floods. The temperature in this season is generally mild throughout the region.

The terrain of a region influences the geographic variation of temperature change. Hot spots of severe heat predominate over numerous regions in Abuja and its surroundings due to the terrain's effect. For instance, highland areas in

the northeast have been identified as having comparatively low temperatures. The ACCESS and MPI models exhibit the least temperature change compared to the other models in this study regarding the spatial fluctuations of extreme heat. Due to the influence of higher elevation, areas adjacent to highland areas are less prone to experience excessive heat than other low grounds. Furthermore, it is unlikely that Abuja and its surroundings would experience uniform warming; as a result, variations in extreme temperature might be connected to the regional heterogeneity of the projected warming trends.

The variation in the average rate of temperature increase across Abuja and its surroundings was highlighted by the analysis of the average monthly temperature change for the five CMIP 6 models used in this study for the high and low forcing scenarios at the middle and end of the century. Additionally, the research on the topographic relationships between the spatial variations of rising temperatures helped to pinpoint regions, such as the northwest lowlands, where health may be in increased danger due to increases in monthly, seasonal, and yearly temperature change. According to this study's projections, the mean average temperature will rise on an annual, monthly, and seasonal basis, with a relative increase in mean temperature beginning in the middle of the century as opposed to the end. Because of climate change, it is expected that Abuja and its environs will see an increase in the number of days when high heat will considerably impact health. The population's incapacity to adapt to rapid and prolonged temperature increases, such as those projected by climate change in this study, necessitates regional projections of heat vulnerability that include demographic and socioeconomic characteristics in addition to the prevailing temperature projections.

The spatial projections of heat vulnerability can help the health sector better plan for adaptation to the expected increases in perceived temperature to mitigate the associated health impacts. Health stakeholders can utilise these outputs to comprehend the possible danger to human health, its expected magnitude and rate of change, and to identify geographic areas of concern. The identification of "hotspot" areas is a crucial step in the prioritisation of public health risks. In addition, primary data collecting is essential for comprehending the historical

health effects of high temperatures, particularly the formation of the local temperature–mortality association. The historical information from primary data collection and anticipated future risks from regional climate modelling can assist decision-makers in determining if high temperatures provide a health risk and if they will continue to do so, as well as the extent of the possible health impact.

This study shows a spatial heterogeneity in heat vulnerability projections among the five SSPs under low-forcing and high-forcing scenarios for the middle and end of the 21st century. In addition, the comparison of the heat vulnerability projections from this study highlighted the limitation of using projected demographic and socioeconomic variables. This is because the ensembles of heat vulnerability projections for this study show a continued increase in areas of high heat vulnerability throughout the study period for both the low and high forcing scenarios. It was expected that heat vulnerability would decrease as the population's socioeconomic status improved; however, this was not the case in this study. This demonstrates a clear distinction between projections of heat vulnerability in which vulnerability remained stable or decreased with increased adaptation to heat due to improved socioeconomic status and those in which vulnerability was considered dynamic or increasing due to the rise in heat exposure. Depending on the scenario, urban-rural disparities were more severe, and towards the end of the century, differences across all scenarios were projected to increase.

While the findings of this study suggest that heat vulnerability will increase by the middle and end of the 21st century, improvements in socioeconomic activities may emerge to improve adaptability. The SSP1-2-6 heat vulnerability projection has demonstrated a decreased risk of heat vulnerability, whereas the SSP5-8.5 has the highest risk. The SSP1-2.6 inequality scenario, particularly in income and education, confirms this study's disparity-related conclusions. The SSP5-8.5 scenario is the fossil fuel development scenario, which allows for considerable health and education investments and long-term population and economic growth. However, it is based on a high-carbon-energy-intensive lifestyle, which contradicts the findings of this study. As a result, SSP5-8.5 is unlikely and SSP1 -2.6 is the lowest risk, as SSP1-2.6 reduces vulnerability the

most after SSP5. Despite decreasing economic development, this scenario promotes social and environmental sustainability. A rise in area of high heat vulnerability increases heat-related health risks.

9.6 Conclusion

Climate change is expected to increase extreme temperatures as heat waves become more common and persistent. The IPCC (2022) has emphasised the need to limit global warming to 1.5 C, warning that surpassing this threshold could severely affect human health. This study reveals that Abuja and its surroundings have witnessed a temperature rise over the past decades and are anticipated to experience an increase in temperatures if emissions are not reduced, which could cause a high heat-related death rate. These findings highlight the significance of preventative mitigation and adaptive approaches for reducing population sensitivity to climate change-induced increases in extreme heat.

The primary objective of this study was to perform mapping of heat vulnerability to locate heat-vulnerable areas in Abuja and its surroundings. This study began by showing the temporal mapping resulting from an assessment of the effect of settlement expansion on land use/cover change, which is a valuable tool for examining the effects of urbanisation on UHI. The relationship between maximum temperature and heat-related mortality were relevant for examining the heat-human health in the research area. The use of GIS for spatial mapping and statistical analysis to connect the components of this study revealed key relationships between heat exposure, sensitivity, and adaption indices. This study's spatial mapping of heat vulnerability is a valuable tool for locating very highly vulnerable areas, such as Gwagwalada, which are areas of heat risks.

The spatial mapping of heat vulnerability indicated significant regional variance in Abuja and its surroundings. Very high and highly vulnerable areas were found across the research area, with a higher proportion in the north and north-eastern regions than in the southern regions, where moderate to low vulnerable areas predominated. The spatial variation in heat vulnerability could be explained by

heat exposure due to the expansion of AIS, the degradation of vegetation cover, and the disparity in socioeconomic status among the regions. UHIs are expected to increase in the research area due to the continued due to rising urbanisation and AIS. The dwellers in urban informal settlements have the most substantial exposure, sensitivity, and low adaptation capacity to heat. This study shows that rising heat islands in tropical African cities represent a major risk to human health. The spatial mapping of heat vulnerability in tropical Africa is not readily available, which emphasises the need for heat-related human health studies.

Temperature projections indicate a temperature increase through to the end of the 21st century. As shown in this study for Abuja and its environs, climate change and human activity are anticipated to have one of the most critical direct consequences on human health in the coming decades. Many of these characteristics are likely to be encountered in tropical African cities. It becomes vital to emphasise the necessity of heat management, such as urban greening, to minimise the impacts of heat on human health. Responses and strategies that benefit the overall management of heat concerns and provide co-benefits should be promoted. Furthermore, understanding how the government, the health sector, and various stakeholders can fund such research programmes is critical. It is expected that tropical Africa's exponential urbanisation rates will approach climatic health parity. Rapid urbanisation in tropical African cities outstrips the capacity of urban institutions and infrastructure, resulting in widespread urban poverty and the expansion of urban slums. Slums house a large majority of the urban population in tropical Africa. Residents of slum communities, often located in dangerous regions, are exposed to various health risks. Future urban planning needs to incorporate impoverished communities into cities while restricting urban growth. The analysis of this study will provide helpful information for heat health planning, particularly in the context of climate change. Integrating remote sensing data with GIS helps uncover common spatial locations of vulnerable areas to heat and the associated impacts on human health. This dissertation's findings explain GIS approaches for identifying and visualising location-specific vulnerability to heat. Although the significance of evaluating vulnerability at fine scales may seem obvious, the findings of this study can be utilised to inform programmes and policies designed to safeguard

vulnerable groups. Given the threat of heat to human health, productivity, and well-being, this study provides a projections of heat vulnerability to human health in Abuja. The projections of heat vulnerability was aim to improve policy decisions and interventions that safeguard the most vulnerable populations from the current and future effects of high heat. The heat vulnerability projections incorporated demographic, socioeconomic, and environmental components at present, with only temperature projections to the middle and end of the 21st century.

9.7 Recommendations

This study provides valuable information for urban planners, emergency management, hazard reduction, public policy, and community education by mapping heat dangers' existing and future health effects. The study's findings could be used to reduce existing and future UHI magnitude through city planning. The heat exposure maps produced by this research have the potential to serve as a baseline for long-term climate resilience. Among the recommendations made by this study are the following:

1. The first step toward effective and efficient heat mitigation and adaptation techniques in Abuja and its surroundings is to identify high and low heat vulnerability regions. The result of this study will enable stakeholders to identify hazards posed by urban heat to reduce the heat vulnerability in chosen sensitive precincts, either by reducing physical exposure or boosting adaptability within each planning area. Policymakers of the adverse effects of heat on human health require heat mitigation methods. This study's findings can be used to formulate theories on particular attributes that improve heat vulnerability, offer appropriate preventative and reactive tactics, and enhance quantitative research. Plans for Heat Health can be formulated using context-specific knowledge.

2. The heat exposure index of this study demonstrates large and dynamic fluctuations in physical exposure, which require heat mitigation and adaptation tactics. A practice that reduces exposure to the UHI and boosts

cooling strategies to reduce net physical exposure. One suggestion is to increase the amount and connection of green infrastructure in the research region, which lowers daytime temperatures (e.g., through shading from dense tree canopies) and perhaps lowers nocturnal UHI intensities (e.g. from evapotranspiration). Encourage green and cool roofs: vegetal layers on rooftops provide shading and heat removal through evapotranspiration. Cool roofs also aid in the reflection of heat and sunlight. As a result, lowering the surface temperature of the city's rooftops, this method will help to reduce the city's UHI. It will also make a substantial contribution to improving the thermal condition of the urban environment by lowering energy demand. Adopting cool pavements as an alternative to conventional AIS is highly recommended. The use of cool pavements on parking lots, sidewalks, and street ways has the potential to store less heat than conventional paving materials and reduce the city's surface temperature by reflecting more solar energy and increasing water evaporation.

Through the design of urban spaces, the implementation of smart growth techniques can lessen the impact of UHI. This approach encompasses extensive conservative and progressive actions that aim to maintain the natural environment and improve the city's liability. It includes the development of walkable, bike-friendly, transit-oriented, and mixed-use neighbourhoods, all of which are absent in Abuja and its environs. The suggested strategies are consistent with the UHI cooling strategies of the United States Environmental Protection Agency. Consequently, the city's planning authorities may implement these programmes effectively by carefully implementing zoning and other planning regulations.

3. Effective plans should consider the sources of socioeconomic vulnerability to heat and the demographic sensitivity of each affected planning region. Access to medical services could be made easier in highly vulnerable locations such as informal settlements. Community programmes that use public education and understanding of heat vulnerability are critical to lessen social vulnerability. Rising temperatures and the threats associated with global climate change should be conveyed and highlighted through

campaigns, news, educational initiatives, and warning systems. These communication methods should incorporate non-official languages for audiences more vulnerable to UHI, such as Hausa and Pidgin English dialects, which the illiterate population is familiar with.

9.8 Limitations of the research

There are some limitations to this study, which are listed below.

1. There are possibilities of errors related to data uncertainty during the classification of images for this investigation. First, there are discrepancies between the class label generated by the classification and the actual class label. The second form of error in this study pertains to the misclassification pattern depicted by the confusion matrix. Thirdly, nonthematic errors can lead to a distortion of the true precision, which is frequently an underestimation. There are limitations associated with the misregistration of image classification and ground data and the TIR data, which were acquired at a sub-optimal time. Other potential limitations involve the ground reference data - the data sets' size, precision, *etc*. In addition, a 30m pixel size may lose some detail compared to a high-resolution pixel.

2. Since many LMICs do not maintain accurate data records, this study used monthly data to simulate the correlation between maximum temperature and mortality. This study disregards extreme events such as specific heatwave events, despite their occurrences being associated with additional deaths. These occurrences are rare in the majority of tropical African cities. Consequently, this study does not investigate the additional mortality during a particular, extreme occurrence. Instead, only deaths exceeding a specified temperature threshold are examined.

3. From the standpoint of public health, it is critical to identify vulnerable populations and target actions that can lower heat risk. This study suggests that developing tailored interventions to minimise risk may be difficult based on data from a city-specific heat vulnerability index.

4. Only some hospitals supplied heat-related mortality data for the investigation, which hampered the availability of the mortality data utilised to validate the heat vulnerability maps presented in this study. This could influence the reliability of the validation. These constraints may impact the conclusions drawn concerning the heat vulnerability model. Due to patient privacy issues and poor data storage, heat-related mortality datasets are frequently unavailable for in most tropical African nations. This constraint could provide high precision in both spatial (census tracts group) and temporal (day of admission) occurrence of health outcomes. Matching maximum temperatures measured from the nearest weather station to a health centre for spatial analysis does not account for microclimate differences caused by land use/cover heterogeneity that characterises spatial form in cities. In this sense, the amount of under and overestimating local temperatures near a geocoded health centre based on arbitrarily remote measurements will result in erroneous conclusions. Only a few climate models from a large ensemble were employed for this inquiry. Similarly, the expert elicitation exercise in this study had a limited sample size. There was no evaluation of the heat vulnerability map's sensitivity to different weightings. Furthermore, not all of the factors that contribute to heat vulnerability were considered in this study.

5. The spatial and temporal scope of the data, the bias associated with the reporting and accessibility of health data, and the availability of demographic and socioeconomic variables can be used to classify the methodological limitations of datasets. First, the spatial resolution of the heat vulnerability indicators differs; for instance, the LST, AIS and the NDVI have a spatial resolution of 100 and 30m, while the demographic and socioeconomic indicators have a spatial resolution of 100 to 1000m. Variations in the spatial resolution of the datasets necessitated resampling all datasets to a spatial resolution of 30 metres (m). The resampling process may result in the loss of data details and a deterioration of the geographical precision of the spatial locations of data

points. Second, because access to health services in the research area is determined by the severity of diseases and the availability of resources to access medical needs, the health data for each hospital may not represent the actual overall heat-related mortality rate for the region. This means that proximity to the hospital is not always a determinant of accessibility. People from an area council may choose to go to other hospitals in other regions with superior amenities if they can afford it.

6. Similarly, poor techniques of archiving health data, which is primarily analogue, may misrepresent the actual record of heat-related mortality in the area. Similarly, the inability to obtain health data from clinics, dispensaries, and other private institutions in the research area may limit the true nature of the area's heat-related mortality. Third, some heat vulnerability indicators are unavailable, such as the percentage of persons living in hospital and care establishments, families with at least one person with a long-term limiting illness, and crime levels - but only if data for burglary and theft is accessible. Other offences, such as abuse and knife crime, are not included. % Disability/ill health (number of persons with limited daily activity), % people living alone, % unemployed, % English proficiency, % private and social renters (2 datasets must be combined for this), % low-income occupations The veracity of heat sensitive maps may be influenced by open and greenspace.

9.9 Future research direction

This research raises many unsolved questions. The research emphasises the need for more studies on heat-human health in LMIC, particularly in tropical Africa, where rapid urbanisation and climate change may outpace available resources for controlling and mitigating the effects of extreme heat. There are still many questions about heat waves, the heat island, and their effects on human health in tropical African cities. The future research direction for this study is presented based on the research objectives.

Objective 1: More studies of informal settlements should be looked at to determine how exposure to extreme heat may affect the population. Access to cloud-free data in tropical Africa is typically difficult due to image-capturing challenges during the wet season. This renders access to Landsat data for the summer months for this analysis impossible, which has implications for the results on the spatial and temporal variations of LST for this study. The results from this study are only for a micro scale, they show how conventional datasets and modelling techniques can be improved with targeted fieldwork. Future research on UHI must insist on ground-truthing and evaluating numerical models with local, on-site data. This will improve the comprehension of how scientific measurements impact health and policy. Using various observational and modelling techniques, future research can enhance and expand a process-based understanding of how cities heat up. This knowledge could contribute to developing additional strategies to mitigate the effects of heat in warmer climates.

Objective 2: Future research must continue evaluating how well numerical models can respond to queries about UHI and human health by utilising more specific data sets. This study concentrates on LST's spatial and temporal mapping, but the results demonstrate the limitations of using a numerical model for LST mapping. They also demonstrate that more is needed to presume that a model accurately represents the UHI if its bias and error are low. Future research should consider the diurnal characteristics of UHI, which are absent from this investigation.

Objective 3: Inadequate techniques for archiving health data, which is predominantly analogue, may distort the actual record of heat-related mortality in the region. Future research will also need to address the limited spatial coverage of health data. Future research should insist on the development of a scalable method for generating data on heat-related morbidity and mortality. LMICs require more investment in data infrastructure. Future research is urged to employ methodologies that are optimally suited to the available datasets.

Objective 4: The urgent need to constantly update and develop a methodology for identifying populations most vulnerable to heat necessitates critically examining the methods and data utilised to assess the heat-health relationship. Climate change adaptation programmes and policies strongly rely on integrated evaluations, many of which are based on public health research like that provided in this dissertation. Future heat health research must focus on precise techniques to handle the individual and community-level factors contributing to heat vulnerability. More studies, alertness, and legislation on the effects of heat on human health are needed in tropical Africa. As evidenced by the current study, heat levels in Abuja and its environs are already a concern, particularly among residents of informal settlements, which shows that there is a vacuum in heat-human health research at LMICs.

References

Aara'L, Y. Y. (2020). Linkages between Saharan Dust Proxies, *Climate, and Meningitis in West Africa from 2012 to 2017* (Doctoral dissertation, The Pennsylvania State University).

Abdul, E. O., Raimi, K. O., & Ibisola, A. S. (2018). Effects of Abandoned Urban Infrastructure on Environmental Development in Ogun State. *Geomatics and Environmental Engineering*, *12* (7), 3-17.

Abrar, R., Sarkar, S. K., Nishtha, K. T., Talukdar, S., Rahman, A., Islam, A. R. M. T., & Mosavi, A. (2022). Assessing the Spatial Mapping of Heat Vulnerability under Urban Heat Island (UHI) Effect in the Dhaka Metropolitan Area. *Sustainability*, *14* (9), 4945.

Abubakar, I. R. (2014). Abuja city profile. *Cities*, *41*, (3), 81-91.

Adeniyi, M.O. (2009). Determination of heat stress in the tropical urban area of Ibadan, Southwestern Nigeria. *International Journal of Natural and Applied Sciences*, *5* (1), 235-243.

Adeponle, B. J. (2013). The Integrated City as a Tool for Sustainable Development Abuja Master Plan. *Journal of Educational and Social Research*, *3* (5), 145.

Adeyeri, O. E., Akinsanola, A. A., & Ishola, K. A. (2017). Investigating surface urban heat island characteristics over Abuja, Nigeria: Relationship between land surface temperature and multiple vegetation indices. *Remote Sensing Applications: Society and Environment*, *7*, (1), 57-68.

Adger, W. N., & Kelly, P. M. (1999). Social vulnerability to climate change and the architecture of entitlements. *Mitigation and Adaptation Strategies for Global Change*, *4* (3), 253-266.

Adnan, M. S. G., Dewan, A., Botje, D., Shahid, S., & Hassan, Q. K. (2022). Vulnerability of Australia to heatwaves: A systematic review on influencing factors, impacts, and mitigation options. *Environmental Research*, *213* (1), 113703.

Agan, P. N. (2017). Heat Waves Research and Impacts on Human Health: The Need for Studies in Nigeria. *Journal of Earth Science and Climate Change*, *8* (3), 418-427.

Agbelade, A. D., Onyekwelu, J. C., & Oyun, M. B. (2017). Tree species richness, diversity, and vegetation index for Federal Capital Territory, Abuja, Nigeria. *International Journal of Forestry Research*, *7* (1), *20-29*.

Agunleti, Y. S., & Arikawe, E. A. (2014). Groundwater targeting within the basement complex rocks of federal capital territory Abuja using remotely sensed and vertical electrical sounding Data. *International Journal of*

Technology Enhancements and Emerging Engineering Research, 2 (12), 38-47.

Ahmed, M. A., Olowosulu, A. T., Adeogun, B. K., Murana, A. A., Ahmed, H. A., & Sanni, I. M. (2021). Development of Rainfall Intensity-Duration-Frequency (IDF) Curve for Abuja, Nigeria. *Nigerian Journal of Technology, 40* (1), 154-160.

Ajayi, V.O. (2018). Urban land use land cover changes and their effect on urban thermal Pattern: A case study of Nigeria's Federal Capital City. *Journal of Environment and Earth Science, 8* (5), 18-29.

Akomolafe, E. A., Isioye, O. A., & Awulu, J. U. (2020). Geospatial Analysis of Impervious Surfaces and Their Effect on Land Surface Temperature in Abuja, Nigeria. *The International Archives of Photogrammetry, Remote Sensing and Spatial Information Sciences, 44* (1), 5-11.

Akpu, B., Tanko, A. I., Jeb, D. N., & Dogo, B. (2017). Geospatial Analysis of Urban Expansion and Its Impact on Vegetation Cover in Kaduna Metropolis, Nigeria. *Australian Journal of Engineering Education, 3(2)* 31149.

Alaigba, D. B., Fabiyi, O. O., & Akinnawo, O. S. (2018). GIS in the assessment of the impact of microclimatic variables on human comfort in Akure, Nigeria. *South African Journal of Geomatics, 7* (1), 64-74.

Alavipanah, S., Wegmann, M., Qureshi, S., Weng, Q., & Koellner, T. (2015). The role of vegetation in mitigating urban land surface temperatures: A case study of Munich, Germany during the warm season. *Sustainability, 7* (4), 4689-4706.

Alexander, K. A., Carzolio, M., Goodin, D., & Vance, E. (2013). Climate change is likely to worsen the public health threat of diarrheal disease in Botswana. *International Journal of Environmental Research and Public Health, 10* (4), 1202-1230.

Aljazeera news (2019) available at https://www.aljazeera.com/news/2019/4/6/nigeria-suffers-severe-heatwave-with-no-relief-in-sight.

Alkama, R., Forzieri, G., Duveiller, G., Grassi, G., Liang, S., & Cescatti, A. (2022). Vegetation-based climate mitigation in a warmer and greener World. *Nature Communications, 13* (1), 1-10.

Almadrones-Reyes, K. J., & Dagamac, N. H. A. (2022). Land-use/land cover change and land surface temperature in Metropolitan Manila, the Philippines using Landsat imagery. *GeoJournal, 2* (1), 1-12.

Almusaed, A. (2011). The urban heat island phenomenon upon urban components. In *Biophilic and Bioclimatic Architecture, 7* (3), 139-150.

Amano, T., Butt, I., & Peh, K. S. H. (2018). The importance of green spaces to public health: a multi-continental analysis. *Ecological Applications, 28* (6), 1473-1480.

Aminipouri, M., Knudby, A., and Ho, H. C. (2016). Using multiple disparate data sources to map heat vulnerability: Vancouver case study. *The Canadian Geographer*, *60* (3), 356-368.

Andersen, J. E., Jenkins, P., & Nielsen, M. (2015). Who plans the African city? A case study of Maputo: part 1–the structural context. *International Development Planning Review*, *37* (3), 329-351.

Anderson, C. I., Gough, W. A., & Mohsin, T. (2018). Characterization of the urban heat island at Toronto: Revisiting the choice of rural sites using a measure of day-to-day variation. *Urban Climate*, *25* (7), 187-195.

Anyanwu, N. C., & Adefila, J. O. (2014). Nature and management of solid waste in Karu Nasarawa State, Nigeria. *American International Journal of Contemporary Research*, *4* (11), 149-159.

Aondoaseer A. A., Terseer A., & Ibrahim T.Y., (2018). Mitigating Urban Heat Islands in Abuja, Nigeria: Adopting Cool Pavement Technology – A Review. *American Journal of Environmental Policy and Management.* 4, (2), 60-66.

Appiah, D. O., Schröder, D., Forkuo, E. K., & Bugri, J. T. (2017). Application of geo-information techniques in land use and land cover change analysis in a peri-urban district of Ghana. *ISPRS International Journal of Geo-Information*, *4* (3), 1265-1289.

Apriana, M., & Syahrani, E. (2022). Land Surface Temperature and its Relationship to Population Density. *Journal of Applied Geospatial Information*, *6* (1), 569-575.

Arnfield, A. J. (2003). Two decades of urban climate research: A review of turbulence, exchanges of energy and water, and the urban heat island. *International Journal of Climatology: a Journal of the Royal Meteorological Society*, *23* (1), 1-26.

Arsenović, D., Lehnert, M., Fiedor, D., Šimáček, P., Středová, H., Středa, T., & Savić, S. (2019). Heat-waves and mortality in Czech cities: A case study for the summers of 2015 and 2016. *Geographica Pannonica*, *23* (3), 162-172.

Arsiso, B. K., Tsidu, G. M., Stoffberg, G. H., & Tadesse, T. (2018). Influence of urbanization-driven land use/cover change on climate: The case of Addis Ababa, Ethiopia. *Physics and Chemistry of the Earth, Parts A/B/C*, *105* (1), 212-223.

Asamoah, B., Kjellstrom, T., & Östergren, P. O. (2018). Is ambient heat exposure level associated with miscarriage or stillbirths in hot regions? A cross-sectional study using survey data from the Ghana Maternal Health Survey 2007. *International Journal of Biometeorology*, *62* (3), 319-330.

Atkinson, B.W. (2003). Numerical modeling of urban heat-island intensity. *Boundary-Layer Meteorology*, *109* (3), 285-310.

Aubrecht, C., & Özceylan, D. (2013). Identification of heat risk patterns in the US National Capital Region by integrating heat stress and related vulnerability. *Environment International*, *56* (2), 65-77.

Awuh, M. E., Japhets, P. O., & Enete, I. C. (2021). Geospatial Techniques, a Superlative Method to Assess Urban Heat Island Intensity: The Case of Abuja Municipal, Nigeria. *Journal of Geographic Information System*, *13* (01), 52.

Awuh, M. E., Japhets, P. O., Officha, M. C., Okolie, A. O., & Enete, I. C., (2019). A Correlation Analysis of the Relationship between Land Use and Land Cover/Land Surface Temperature in Abuja Municipal, FCT, Nigeria. *Journal of Geographic Information System*, *11* (1), 44-53.

Awuh, M. E., Officha, M. C., Okolie, A. O., & Enete, I. C. (2018). A remote sensing analysis of the temporal and spatial changes of land surface temperature in Calabar metropolis, Nigeria. *Journal of Geographic Information System*, *10* (05), 562.

Ayanlade, A. (2017). Variations in urban surface temperature: an assessment of land use change impacts over Lagos metropolis. *Weather*, *72* (10), 315-319.

Azari, M., Billa, L., & Chan, A. (2022). Multi-temporal analysis of past and future land cover change in the highly urbanized state of Selangor, Malaysia. *Ecological Processes*, *11* (1), 1-15.

Azhar, G., S, S., Ganguly, P., Mavalankar, D., & Madrigano, J. (2017). Heatwave vulnerability mapping for India. *International Journal of Environmental Research and Public Health*, *14* (4), 357.

Azhar, G.S., Mavalankar, D., Nori-Sarma, A., Rajiva, A., Dutta, P., Jaiswal, A and Hess, J.J. (2014). Heat-related mortality in India: Excess all-cause mortality associated with the 2010 Ahmedabad heatwave. *PLoS One, 9* (3), 91831.

Azmi, R., Alami, O. B., Saadane, A. E., Kacimi, I., & Chafiq, T. (2016). A modified and enhanced normalized built-up index using multispectral and thermal bands. *Indian Journal of Science and Technology*, *9* (28), 1-11.

Azongo, D. K., Awine, T., Wak, G., Binka, F. N., & Rexford Oduro, A. (2012). A time-series analysis of weather variables and all-cause mortality in the

Kasena-Nankana Districts of Northern Ghana, 1995–2010. *Global Health Action*, *5* (1), 19073.

Babalola, O., Razzaque, A., & Bishai, D. (2018). Temperature extremes and infant mortality in Bangladesh: Hotter months, lower mortality. *PLoS One*, *13* (1), 17-26.

Bai, L., Woodward, A., & Liu, Q. (2016). County-level heat vulnerability of urban and rural residents in Tibet, China. *Environmental Health*, *15* (1), 1-10.

Balogun, I. A., & Balogun, A. A. (2014). Urban heat island and bioclimatological conditions in a hot-humid tropical city: the example of Akure, Nigeria. *DIE ERDE–Journal of the Geographical Society of Berlin*, *14* (5), 3-15.

Balogun, I. A., & Daramola, M. T. (2019). The outdoor thermal comfort assessment of different urban configurations within Akure City, Nigeria. *Urban Climate*, *29* (3), 100489.

Bambrick, H., Moncada, S., & Briguglio, M. (2015). Climate change and health vulnerability in informal urban settlements in the Ethiopian Rift Valley. *Environmental Research Letters*, *10* (5), 054014.

Basu, R. (2009). High ambient temperature and mortality: a review of epidemiologic studies from 2001 to 2008. *Environmental Health*, *8* (1), 40.

Batté, L., Ardilouze, C., & Déqué, M. (2018). Forecasting West African heat waves at sub seasonal and seasonal time scales. *Monthly Weather Review*, *146* (3), 889-907.

Beel, C. R., Lamoureux, S. F., Orwin, J. F., Pope, M. A., Lafrenière, M. J., & Scott, N. A. (2020). Differential impact of thermal and physical permafrost disturbances on the High Arctic dissolved and particulate fluvial fluxes. *Scientific Reports*, *10* (1), 1-13.

Béguin, A., Hales, S., Rocklöv, J., Åström, C., Louis, V. R., & Sauerborn, R. (2011). The opposing effects of climate change and socio-economic development on the global distribution of malaria. *Global Environmental Change*, *21*(4), 1209-1214.

Beker, B. M., Cervellera, C., De Vito, A., & Musso, C. G. (2018). Human physiology in extreme heat and cold. *International Archives of Clinical. Physiology*, 1 (1), 43-51.

Bell, M. L., O'neill, M. S., Ranjit, N., Borja-Aburto, V. H., Cifuentes, L. A., & Gouveia, N. C. (2008). Vulnerability to heat-related mortality in Latin America: a case-crossover study in Sao Paulo, Brazil, Santiago, Chile and

Mexico City, Mexico. *International Journal of Epidemiology*, *37* (4), 796-804.

Berry, P., Enright, P. M., Shumake-Guillemot, J., Villalobos Prats, E., & Campbell-Lendrum, D. (2018). Assessing health vulnerabilities and adaptation to climate change: a review of international progress. *International Journal of Environmental Research and Public Health*, *15* (12), 2626.

Bertram, C., Riahi, K., Hilaire, J., Bosetti, V., Drouet, L., Fricko, O., & Luderer, G. (2021). Energy system developments and investments in the decisive decade for the Paris Agreement goals. *Environmental Research Letters*, *16* (7), 074020.

Bhattacharjee, S., Gerasimova, E., Imbert, C., Tencar, J., & Rotondo, F. (2019). Assessment of different methodologies for mapping urban heat vulnerability for Milan, Italy. In *IOP Conference Series: Earth and Environmental Science*, *290* (1), 012162.

Bhatti, S. S., & Tripathi, N. K. (2014). Built-up area extraction using Landsat 8 OLI imagery. *GIScience & Remote Sensing*, *51* (4), 445-467.

Bi, P., Williams, S., Loughnan, M., Lloyd, G., Hansen, A., Kjellstrom, T., & Saniotis, A. (2011). The effects of extreme heat on human mortality and morbidity in Australia: implications for public health. *Asia Pacific Journal of Public Health*, *23* (2), 27-36.

Bibby, P., & Shepherd, J. (2004). Developing a new classification of urban and rural areas for policy purposes–the methodology. *London: Defra*.

Binbol, N. L., & Uzochukwu, C. T. (2008). Climate and Human Comfort in Abuja, Nigeria. *Ethiopian Journal of Environmental Studies and Management*, 6, (6) 737-745.

Binita, K. C., Shepherd, J. M., & Gaither, C. J. (2015). Climate change vulnerability assessment in Georgia. *Applied Geography*, *62* (1), 62-74.

Birkmann, J., Böhm, H. R., Buchholz, F., Büscher, D., Daschkeit, A., Ebert, S., & Walkenhorst, O. (2013). *Glossar Klimawandel und Raumentwicklung*, *13* (1), 143-155.

Blaikie, P., Cannon, T., & Wisner, B. (1994). At risk. *Natural Hazards, People's Vulnerability and Disasters*, *1* (4), 14-23.

Bobb, J. F., Peng, R. D., Bell, M. L., & Dominici, F. (2014). Heat-related mortality and adaptation to heat in the United States. *Environmental Health Perspectives*, *122* (8), 811-816.

Bokaie, M., Zarkesh, M. K., Arasteh, P. D., & Hosseini, A. (2016). Assessment of urban heat island based on the relationship between land surface temperature and land use/land cover in Tehran. *Sustainable Cities and Society*, *23* (5), 94-104.

Bondarenko M., Nieves J. J., Stevens F. R., Gaughan A. E., Tatem A. & Sorichetta A. (2020). RFPMS: Random Forests population modeling R scripts, version 0.1.0. *University of Southampton: Southampton, UK*.

Borg, M. A., Xiang, J., Anikeeva, O., Pisaniello, D., Hansen, A., Zander, K., & Bi, P. (2021). Occupational heat stress and economic burden: A review of the global evidence. *Environmental Research*, *195* (1), 110781.

Bornstein, R., & Lin, Q. (2000). Urban heat islands and summertime convective thunderstorms in Atlanta: Three case studies. *Atmospheric Environment*, *34* (3), 507-516.

Bosco, C., Alegana, V., Bird, T., Pezzulo, C., Bengtsson, L., Sorichetta, A., & Tatem, A. J. (2017). Exploring the high-resolution mapping of gender-disaggregated development indicators. *Journal of the Royal Society Interface*, *14* (129), 20160825.

Bosco, N. J., & Thomas, M. (2019). Land Surface Temperature Analysis of Kigali City. *Current Journal of Applied Science and Technology*, *32* (2), 1-11.

Bounoua, L., Nigro, J., Zhang, P., Thome, K., & Lachir, A. (2018). Mapping urbanisation in the United States from 2001 to 2011. *Applied Geography*, *90* (2), 123-133.

Bradford, K., Abrahams, L., Hegglin, M., & Klima, K. (2015). A heat vulnerability index and adaptation solutions for Pittsburgh, Pennsylvania. *Environmental Science and Technology*, *49* (19), 11303-11311.

Braga, A. L., Zanobetti, A., & Schwartz, J. (2002). The effect of weather on respiratory and cardiovascular deaths in 12 US cities. *Environmental Health Perspectives*, *110* (9), 859-863.

Brewster, D., & Greenwood, B. (1993). Seasonal variation of paediatric diseases in the Gambia, West Africa. *Annals of Tropical Paediatrics, 13*, (4), 133-146.

Brundtland, G. H. (1985). World commission on environment and development. *Environmental Policy and Law*, *14* (1), 26-30.

Burkart, K., Khan, M. M. H., Schneider, A., Breitner, S., Langner, M., Kraemer, A., & Endlicher, W. (2014). The effects of season and meteorology on human mortality in tropical climates: a systematic review. *Transactions of the Royal Society of Tropical Medicine and Hygiene*, *108* (7), 393-401.

Buscail, C., Upegui, E., & Viel, J. F. (2012). Mapping heatwave health risk at the community level for public health action. *International Journal of Health Geographics*, *11* (1), 1-9.

Buyantuyev, A., and Wu, J. (2010). Urban heat islands and landscape heterogeneity: linking spatiotemporal variations in surface temperatures to land-cover and socioeconomic patterns. *Landscape Ecology*, *25* (1), 17-33.

Campbell, S., Remenyi, T. A., White, C. J., & Johnston, F. H. (2018). Heatwave and health impact research: A global review. *Health and Place*, *53* (8), 210-218.

Carlson, T. (2007). An overview of the "Triangle method" for estimating surface evapotranspiration and soil moisture from satellite imagery. *Sensors*, *7* (1), 1612–1629.

Carter, T. R., Fronzek, S., Inkinen, A., Lahtinen, I., Lahtinen, M., Mela, H., & Terama, E. (2016). Characterising vulnerability of the elderly to climate change in the Nordic region. *Regional Environmental Change*, *16* (1), 43-58.

Centers for Disease Control & Prevention. (2008). Heat-related deaths among crop workers--the United States, 1992--2006*: Morbidity and Mortality Weekly Report*, *57* (24), 649-653.

Chanana-Nag, N., & Aggarwal, P. K. (2020). Woman in agriculture, and climate risks: hotspots for development. *Climatic Change*, *158* (1), 13-27.

Chang, C. L., Shipley, M., Marmot, M., & Poulter, N. (2004). Lower ambient temperature was associated with an increased risk of hospitalization for stroke and acute myocardial infarction in young women. *Journal of Clinical Epidemiology*, *57* (7), 749-757.

Chen, G., Li, X., Liu, X., Chen, Y., Liang, X., Leng, J., & Huang, K. (2020). Global projections of future urban land expansion under shared socioeconomic pathways. *Nature Communications*, *11* (1), 1-12.

Chen, K., Bi, J., Chen, J., Chen, X., Huang, L., & Zhou, L. (2015). Influence of heat wave definitions to the added effect of heat waves on daily mortality in Nanjing, China. *Science of the Total Environment*, *506* (2), 18-25.

Chen, S., Yu, B., Wu, R., Chen, W., & Song, L. (2021). The dominant North Pacific atmospheric circulation patterns and their relations to Pacific SSTs: historical simulations and future projections in the IPCC AR6 models. *Climate Dynamics*, *56* (3), 701-725.

Chen, T. L., Lin, H., & Chiu, Y. H. (2022). Heat vulnerability and extreme heat risk at the metropolitan scale: A case study of Taipei metropolitan area, Taiwan. *Urban Climate, 41* (7), 101054.

Chersich, M. F., Pham, M. D., Areal, A., Haghighi, M. M., Manyuchi, A., Swift, C. P., & Hajat, S. (2020). Associations between high temperatures in pregnancy and risk of preterm birth, low birth weight, and stillbirths: systematic review and meta-analysis. *British Medical Journal, 371* (3), 132-141.

Chibuike, E. M., Ibukun, A. O., Abbas, A., & Kunda, J. J. (2018). Assessment of green parks cooling effect on Abuja urban microclimate using geospatial techniques. *Remote Sensing Applications: Society and Environment, 11 (3)*, 11-21.

Chithra, S. V., Nair, M. H., Amarnath, A., and Anjana, N. S. (2015). Impacts of impervious surfaces on the environment. *International Journal of Engineering Science Invention*, *4* (5), 27-31.

Chow, W. T., Chuang, W. C., and Gober, P. (2012). Vulnerability to extreme heat in metropolitan Phoenix: Spatial, temporal, and demographic dimensions. *The Professional Geographer, 64* (2), 286-302.

Christenson, M., Geiger, S. D., Phillips, J., Anderson, B., Losurdo, G., & Anderson, H. A. (2017). Heat vulnerability index mapping for Milwaukee and Wisconsin. *Journal of Public Health Management and Practice*, *23* (4), 396-403.

Christian, E. I., & Ugoyibo, O. V. (2013). Mapping Enugu city's urban heat island. *International Journal of Environmental Protection and Policy, 1* (4), 50-58.

Chuang, W. C., & Gober, P. (2015). Predicting hospitalization for heat-related illness at the census-tract level: accuracy of a generic heat vulnerability index in Phoenix, Arizona (USA). *Environmental Health Perspectives, 123* (6), 606-612.

Coates, L., Haynes, K., O'brien, J., McAneney, J., & De Oliveira, F. D. (2014). Exploring 167 years of vulnerability: An examination of extreme heat events in Australia 1844–2010. *Environmental Science and Policy, 42* (4), 33-44.

Cobbinah, P. B., Erdiaw-Kwasie, M. O., & Amoateng, P. (2015). Africa's urbanization: Implications for sustainable development. *Cities, 47* (1), 62-72.

Coffel, E. D., Horton, R. M., & de Sherbinin, A. (2017). Temperature and humidity-based projections of a rapid rise in global heat stress exposure during the 21st century. *Environmental Research Letters, 13* (1), 014001.

Cohen, F., & Dechezleprêtre, A. (2022). Mortality, temperature, and public health provision: evidence from Mexico. *American Economic Journal: Economic Policy*, *14*(2), 161-92.

Conlon, K. C., Mallen, E., Gronlund, C. J., Berrocal, V. J., Larsen, L., & O'neill, M. S. (2020). Mapping human vulnerability to extreme heat: a critical assessment of heat vulnerability indices created using principal components analysis. *Environmental Health Perspectives*, *128* (9), 097001.

Coutts, A. M., Beringer, J., & Tapper, N. J. (2007). Impact of increasing urban density on local climate: Spatial and temporal variations in the surface energy balance in Melbourne, Australia. *Journal of Applied Meteorology and Climatology*, *46* (4), 477-493.

Cresswell, M. P., Morse, A. P., Thomson, M. C., & Connor, S. J. (1999). Estimating surface air temperatures, from Meteosat land surface temperatures, using an empirical solar zenith angle model. *International Journal of Remote Sensing*, *20* (6), 1125–1132.

Cristóbal, J., Jiménez-Muñoz, J. C., Prakash, A., Mattar, C., Skoković, D., & Sobrino, J. A. (2018). An improved single-channel method to retrieve land surface temperature from the Landsat-8 thermal band. *Remote Sensing*, *10* (3), 431.

Cutter, S. L. (1996). Vulnerability to environmental hazards. *Progress in Human Geography*, *20* (4), 529-539.

Cutter, S. L., Boruff, B. J., & Shirley, W. L. (2003). Social vulnerability to environmental hazards. *Social Science Quarterly*, *84* (2), 242-261.

Cutter, S. L., Mitchell, J. T., & Scott, M. S. (2012). Revealing the vulnerability of people and places: A case study of Georgetown County, South Carolina. In *Hazards Vulnerability and Environmental Justice* 23 (3), 111-142). Routledge.

Daniel, O.A. (2015). Urban extreme weather: a challenge for a healthy living environment in Akure, Ondo State, Nigeria. *Climate*, *3* (4), 775-791.

Dapi, L.N., Rocklöv, J., Nguefack-Tsague, G., Tetanye, E., & Kjellstrom, T. (2010). Heat impact on schoolchildren in Cameroon, Africa: Potential health threat from climate change. *Global Health Action*, *3* (1), 56-69.

Dar, M. U. D., Shah, A. I., Bhat, S. A., Kumar, R., Huisingh, D., & Kaur, R. (2021). Blue Green infrastructure as a tool for sustainable urban development. *Journal of Cleaner Production*, *31* (8), 128474.

Das, S., & Angadi, D. P. (2022). Land use land cover change detection and monitoring of urban growth using remote sensing and GIS techniques: a micro-level study. *GeoJournal*, *87* (3), 2101-2123.

Dash, P., Göttsche, F. M., Olesen, F. S., & Fischer, H. (2002). Land surface temperature and emissivity estimation from passive sensor data: Theory and practice-current trends. *International Journal of Remote Sensing*, *23* (13), 2563-2594.

Dawam, P. D. (1994). Urban development and population relocation in Abuja, Nigeria. *Ekistics*, *61* (216), 366-367).

De Cian, E., Pavanello, F., Randazzo, T., Mistry, M. N., & Davide, M. (2019). Households' adaptation in a warming climate. Air conditioning and thermal insulation choices. *Environmental Science & Policy*, *100* (2), 136-157.

de Schrijver, E., Bundo, M., Ragettli, M. S., Sera, F., Gasparrini, A., Franco, O. H., & Vicedo-Cabrera, A. M. (2022). Nationwide analysis of the heat-and cold-related mortality trends in Switzerland between 1969 and 2017: the role of population aging. *Environmental Health Perspectives*, *130* (3), 037001.

de Souza, R. J., Eisen, R. B., Perera, S., Bantoto, B., Bawor, M., Dennis, B. B., ... & Thabane, L. (2016). Best (but oft-forgotten) practices: sensitivity analyses in randomized controlled trials. *The American Journal of Clinical Nutrition*, *103* (1), 5-17.

Deilami, K., Kamruzzaman, M., & Liu, Y. (2018). Urban heat island effect: A systematic review of spatio-temporal factors, data, methods, and mitigation measures. *International Journal of Applied Earth Observation and Geoinformation*, *67* (2), 30-42.

Dellink, R., Chateau, J., Lanzi, E., & Magné, B. (2017). Long-term economic growth projections in the Shared Socioeconomic Pathways. *Global Environmental Change*, *42* (1), 200-214.

Deng, C., Li, C., Zhu, Z., Lin, W., & Xi, L. (2017). Subpixel urban impervious surface mapping: the impact of input Landsat images. *ISPRS Journal of Photogrammetry and Remote Sensing*, *133 (3)*, 89-103.

Depietri, Y., Welle, T., & Renaud, F. G. (2013). Social vulnerability assessment of the Cologne urban area (Germany) to heat waves: Links to ecosystem services. *International Journal of Disaster Risk Reduction*, *6 (2)*, 98-117.

DESA, U. (2018). United Nations Department of Economic and Social Affairs (2018) World population is projected to reach 9.8 billion in 2050, and 11.2 billion in 2100| UN DESA|. United Nations department of economic and social affairs.

Dessai, S., (2002). Heat stress and mortality in Lisbon part I. model construction and validation. *International Journal of Biometeorology*, *47* (1), 6-12.

Deville, P., Linard, C., Martin, S., Gilbert, M., Stevens, F. R., Gaughan, A. E., & Tatem, A. J. (2014). Dynamic population mapping using mobile phone data. *Proceedings of the National Academy of Sciences*, *111* (45), 15888-15893.

Di Leo, N., Escobedo, F. J., & Dubbeling, M. (2016). The role of urban green infrastructure in mitigating land surface temperature in Bobo-Dioulasso, Burkina Faso. *Environment, Development and Sustainability*, *18* (2), 373-392.

Di Napoli, C., Pappenberger, F., & Cloke, H. L. (2018). Assessing heat-related health risk in Europe via the Universal Thermal Climate Index (UTCI). *International Journal of Biometeorology*, *62* (7), 1155-1165.

Diboulo, E., Sie, A., Rocklöv, J., Niamba, L., Ye, M., Bagagnan, C., & Sauerborn, R. (2012). Weather and mortality: A 10-year retrospective analysis of the Nouna Health and Demographic Surveillance System, Burkina Faso. *Global Health Action*, *5* (1), 19-31.

Diouf, I., Deme, A., Ndione, J. A., Gaye, A. T., Rodríguez-Fonseca, B., & Cissé, M. (2013). Climate and health: Observation and modeling of malaria in the Ferlo (Senegal). *Comptes Rendus Biologies*, *336* (56), 253-260.

Dissanayake, D. M. S. L. B., Morimoto, T., Murayama, Y., & Ranagalage, M. (2019). Impact of landscape structure on the variation of land surface temperature in the sub-Saharan region: A case study of Addis Ababa using Landsat data (1986–2016). *Sustainability*, *11* (8), 2257.

Dixon, P. G., & Mote, T. L. (2003). Patterns and causes of Atlanta's urban heat island–initiated precipitation. *Journal of Applied Meteorology*, *42* (9), 1273-1284.

Doick, K. J., Peace, A., & Hutchings, T. R. (2014). The role of one large greenspace in mitigating London's nocturnal urban heat island. *Science of the Total Environment*, *493 (4)*, 662-671.

Dong, W., Liu, Z., Liao, H., Tang, Q., & Li, X. E. (2015). New climate and socio-economic scenarios for assessing global human health challenges due to heat risk. *Climatic Change*, *130* (4), 505-518.

Dong, W., Liu, Z., Zhang, L., Tang, Q., Liao, H., & Li, X. E. (2014). Assessing heat-health risk for sustainability in Beijing's urban heat island. *Sustainability*, *6* (10), 7334-7357.

Dos Santos, M., John, J., Garland, R., Palakatsela, R., Banos, A., Martens, P., & Lenyibi, K. (2022). Climate change and health within the South African context: A thematic content analysis study of climate change and health

expert interviews. *African Journal of Primary Health Care & Family Medicine*, *14* (1), 3203.

Doshi, N., Turakhia, T., Nair, A. S., Pandya, M., & Iyer, R. (2020). Estimating Air Temperature using Land Surface Temperature products of INSAT-3D satellite. In *2020 IEEE India Geoscience and Remote Sensing Symposium 1 (2)*, 177-180.

Driskell, R., & Embry, E. (2007). Poverty and migration in the Black Belt: means of escape? *Michigan Sociological Review*, *7* (21), 9-108.

Du Toit, M. J., Cilliers, S. S., Dallimer, M., Goddard, M., Guenat, S., & Cornelius, S. F. (2018). Urban green infrastructure and ecosystem services in sub-Saharan Africa. *Landscape and Urban Planning*, *180* (4), 249-261.

Dutta, D., Rahman, A., Paul, S. K., & Kundu, A. (2021). Impervious surface growth and its inter-relationship with vegetation cover and land surface temperature in peri-urban areas of Delhi. *Urban Climate*, *37* (2), 100799.

Dutta, D., Rahman, A., Paul, S. K., & Kundu, A. (2021). Impervious surface growth and its inter-relationship with vegetation cover and land surface temperature in peri-urban areas of Delhi. *Urban Climate*, *37 (2)*, 100799.

Ebi, K. L., & Burton, I. (2008). Identifying practical adaptation options: an approach to address climate change-related health risks. *Environmental Science & Policy*, *11* (4), 359-369.

Ebi, K. L., Vanos, J., Baldwin, J. W., Bell, J. E., Hondula, D. M., Errett, N. A., & Berry, P. (2021). Extreme weather and climate change: population health and health system implications. *Annual Review of Public Health*, *42 (1)*, 293.

Efe, S. I., & Eyefia, O. A. (2014). Urban warming in Benin City, Nigeria. *Atmospheric and Climate Sciences*, *2 (14), 21-33*.

Egondi, T., Kyobutungi, C., Kovats, S., Muindi, K., Ettarh, R., & Rocklöv, J. (2012). Time-series analysis of weather and mortality patterns in Nairobi's informal settlements. *Global Health Action*, *5* (1), 19065.

Ekwe, M. C., Joshua, J. K., Igwe, J. E., & Osinowo, A. (2014). Mathematical study of monthly and annual rainfall trends in Nasarawa State, Nigeria. *IOSR Journal of Mathematics*, *10* (1), 56-62.

Elemo, E. O., Ogobor, E. A., Ayantunji, B. G., Mangete, O. E., Alagbe, G. A., Abdulkareem, M. L., & Onuh, B. O. (2021). Relationship between Relative Humidity and the Dew Point Temperature in Abuja, Nigeria. *Open Access Library Journal*, *8* (12), 1-13.

El-Zein, A., & Tonmoy, F. N. (2015). Assessment of vulnerability to climate change using a multi-criteria outranking approach with application to heat stress in Sydney. *Ecological Indicators, 48* (1), 207-217.

EM-DAT (2021) The OFDA/CRED international disaster database. Université Catholique de Louvain, Brussels, Belgium. Available at http://www.emdat.be.

Eneh, O. C. (2021). Abuja slums: development, causes, waste-related health challenges, government response, and way-forward. *Environment, Development, and Sustainability*, *23* (6), 9379-9396.

Enete, I. C., Awuh, M. E., & Ikekpeazu, F. O. (2013). Assessment of urban heat island situation in Douala Metropolis, Cameroon. *Journal of Geography and Earth Sciences*, *2* (1), 55-57.

Engelbrecht, F., Adegoke, J., Bopape, M. J., Naidoo, M., Garland, R., Thatcher, M., & Gatebe, C. (2015). Projections of rapidly rising surface temperatures over Africa under low mitigation. *Environmental Research Letters*, *10* (8), 085004.

Enoguanbhor, E. C. (2022). Geospatial Assessments of Urban Green Space Protection in Abuja City, Nigeria. *Eximia, 5* (1), 177-194.

Enoguanbhor, E. C., Gollnow, F., Nielsen, J. O., Lakes, T., & Walker, B. B. (2019). Land cover change in the Abuja City-Region, Nigeria: Integrating GIS and remotely sensed data to support land use planning. *Sustainability*, *11* (5), 1313.

Enoguanbhor, E. C., Gollnow, F., Walker, B. B., Nielsen, J. O., & Lakes, T. (2020). Simulating Urban Land Expansion in the Context of Land Use Planning in the Abuja City-Region, Nigeria. *GeoJournal*, *2* (1), 1-19.

EPA. (2014). *Reducing Urban Heat Islands: Compendium of Strategies, U.S. Environmental Protection Agency*. Retrieved from https://www.epa.gov/sites /production/files/2014-06/documents/basicscompendium.pdf.

Equere, V., Mirzaei, P. A., & Riffat, S. (2020). Definition of a new morphological parameter to improve prediction of urban heat island. *Sustainable Cities and Society*, *56* (2), 102021.

Ermert, V., Fink, A. H., Morse, A. P., & Paeth, H. (2012). The impact of regional climate change on malaria risk due to greenhouse forcing and land-use changes in tropical Africa. *Environmental Health Perspectives*, *120* (1), 77-84.

Ermida, S. L., Soares, P., Mantas, V., Göttsche, F. M., & Trigo, I. F. (2020). Google earth engine open-source code for land surface temperature estimation from the Landsat series. *Remote Sensing*, *12* (9), 1471.

Etard, J.F., Le Hesran, J.Y., Diallo, A., Diallo, J.P., Ndiaye, J.L., & Delaunay, V. (2004). Childhood mortality and probable causes of death using verbal autopsy in Niakhar, Senegal, 1989–2000. *International Journal of Epidemiology*, *33* (6), 1286-1292.

Eyring, V., Bony, S., Meehl, G. A., Senior, C. A., Stevens, B., Stouffer, R. J., & Taylor, K. E. (2016). Overview of the Coupled Model Intercomparison Project Phase 6 (CMIP6) experimental design and organization. *Geoscientific Model Development*, *9* (5), 1937-1958.

Ezeamaka, C. K., & Oluwole, O. A. (2016). Assessment of Recreational Facilities in Federal Capital City, Abuja, Nigeria. *The Indonesian Journal of Geography*, *48* (1), 21.

Fall (2014) Arc User the Magazine for ESRI Software Users. *Esri 17* (4), 1-9.

Farid, M., Qadri, A., Hayat, U., Shakoor, M. B., Abbas, M., Masood, A., & Raza, N. (2022). Sustainable Urban Forestry, Merits, Demerits, and Mitigation of Climate Change at Global Scale. In *Managing Plant Production Under Changing Environment 3* (2), 375-401.

Farina, A. (2012). Exploring the relationship between land surface temperature and vegetation abundance for urban heat island mitigation in Seville, Spain. *ISPRS International Journal of Geo-Information*, *10* (2), 76.

Fashae, O. A., Adagbasa, E. G., Olusola, A. O., & Obateru, R. O. (2020). Land use/land cover change and land surface temperature of Ibadan and environs, Nigeria. *Environmental monitoring and assessment*, *192* (2), 1-18.

Fatima, S. H., Rothmore, P., Giles, L. C., Varghese, B. M., & Bi, P. (2021). Extreme heat and occupational injuries in different climate zones: A systematic review and meta-analysis of epidemiological evidence. *Environment International*, *148* (2), 106384.

Faye, M., Dème, A., Diongue, A. K., & Diouf, I. (2021). Impact of different heatwave definitions on daily mortality in Bandafassi, Senegal. *PLoS One*, *16* (4), 0249199.

Feyisa, G. L., Dons, K., & Meilby, H. (2014). Efficiency of parks in mitigating urban heat island effect: An example from Addis Ababa. *Landscape and Urban Planning*, *123* (8), 87-95.

Feyissa, G., Zeleke, G., Bewket, W., & Gebremariam, E. (2018). Downscaling of future temperature and precipitation extremes in Addis Ababa under climate change. *Climate*, *6* (3), 58.

Field, C. B., & Barros, V. R. (Eds.). (2014). *Climate change 2014–Impacts, adaptation, and vulnerability: Regional aspects*. Cambridge University Press.

Flanagan BE, Gregory EW, Hallisey EJ, Heitgerd JL, Lewis B. (2011). A social vulnerability index for disaster management. *Journal of Homeland Security and Emergency Management* 8 (1), 17-29.

Flynn, C. M., & Mauritsen, T. (2020). On the climate sensitivity and historical warming evolution in recently coupled model ensembles. *Atmospheric Chemistry and Physics, 20* (13), 7829-7842.

Forget, Y., Shimoni, M., Gilbert, M., & Linard, C. (2021). Mapping 20 years of urban expansion in 45 urban areas of sub-Saharan Africa. *Remote Sensing, 13* (3), 525.

Freire, M., Lall, S., & Leipziger, D. (2015). Africa's urbanization: Challenges and opportunities. *Urban Forum, 21* (3), 187-204.

French, M. (2018). Accuracy of a Heat Vulnerability Index for Estimating Heat Mortality in Dallas, Texas. *Urban Climate 30* (2), 100-128.

French, M., & Gardner, J. (2012). The health of informal settlements: Illness and the internal thermal conditions of informal housing. In *Sustainable Environmental Design in Architecture, 7* (3), 157-171.

Fricko, O., Havlik, P., Rogelj, J., Klimont, Z., Gusti, M., Johnson, N., & Riahi, K. (2017). The marker quantification of the Shared Socioeconomic Pathway 2: A middle-of-the-road scenario for the 21st century. *Global Environmental Change, 42* (1), 251-267.

Frimpong, K., Odonkor, S. T., Kuranchie, F. A., & Nunfam, V. F. (2020). Evaluation of heat stress impacts and adaptations: Perspectives from smallholder rural farmers in Bawku East of Northern Ghana. *Heliyon, 6* (4), 03679.

Frimpong, K., Oosthuizen, J., & Van Etten, E. J. (2014). Recent trends in temperature and relative humidity in Bawku East, Northern Ghana. *The International Journal of Climate Change: Impacts and Responses, 4* (1), 3-12.

Frimpong, K., Van Etten, E., & Oosthuizen, J. (2016). Barriers of adaptation to heat stress in Northeast Ghana. *The International Journal of Climate Change: Impacts and Responses, 8* (2), 53-65.

Fussel HM. (2007). Vulnerability: a generally applicable conceptual framework for climate change research. *Global Environmental Change 17* (2), 155–167.

Gabriel, K. M., & Endlicher, W. R. (2011). Urban and rural mortality rates during heat waves in Berlin and Brandenburg, Germany. *Environmental pollution*, *159* (89), 2044-2050.

Gamble, J., Schmeltz, M., Hurley, B., Hseih, J., Jette, G., & Wagner, H. (2018). Mapping the Vulnerability of Human Health to Extreme Heat in the US. *Urban Climate*, *30*, (1), 100528.

Gandhi, G. M., Parthiban, B. S., Thummalu, N., & Christy, A. (2015). NDVI: Vegetation change detection using Remote Sensing and GIS–A case study of Vellore District. *Procedia Computer Science*, *57* (4), 1199-1210.

Gao, J., Gong, J., Yang, J., Li, J., & Li, S. (2022). Measuring Spatial Connectivity between patches of the heat source and sink (SCSS): A new index to quantify the heterogeneity impacts of landscape patterns on land surface temperature. *Landscape and Urban Planning*, *21*(7), 104260.

Garland, R. M., Matooane, M., Engelbrecht, F. A., Bopape, M. J. M., Landman, W. A., Naidoo, M., & Wright, C. Y. (2015). Regional projections of extreme apparent temperature days in Africa and the related potential risk to human health. *International Journal of Environmental Research and Public Health*, *12* (10), 12577-12604.

Gascon, M., Triguero-Mas, M., Martínez, D., Dadvand, P., Rojas-Rueda, D., Plasència, A., & Nieuwenhuijsen, M. J. (2016). Residential green spaces and mortality: A systematic review. *Environment International*, *86* (1), 60-67.

Gasparrini, A., Guo, Y., Hashizume, M., Lavigne, E., Zanobetti, A., Schwartz, J., & Armstrong, B. (2015). Mortality risk attributable to high and low ambient temperature: a multicountry observational study. *The Lancet*, *386* (9991), 369-375.

Gauer, R. L., & Meyers, B. K. (2019). Heat-related illnesses. *American family physician*, *99* (8), 482-489.

Ghosh, S., Kumar, D., & Kumari, R. (2022). Assessing spatiotemporal dynamics of land surface temperature and satellite-derived indices for new town development and suburbanization planning. *Urban Governance*, *2* (1), 28-41.

Gidden, M. J., Riahi, K., Smith, S. J., Fujimori, S., Luderer, G., Kriegler, E., & Takahashi, K. (2019). Global emissions pathways under different socioeconomic scenarios for use in CMIP6: a dataset of harmonized emissions trajectories through the end of the century. *Geoscientific Model Development*, *12* (4), 1443-1475.

Gillipelli, S. R., Kaye, E. C., Garza, M., Ferrara, G., Rodriguez, M., Soberanis Vasquez, D. J., & Graetz, D. E. (2022). Paediatric Early Warning Systems (PEWS) improve provider-family communication from the provider

perspective in paediatric cancer patients experiencing clinical deterioration. *Cancer Medicine*, *21* (7), 116-127.

Goetz, S. J., Prince, S. D., & Small, J. (2000). Advances in satellite remote sensing of environmental variables for epidemiological applications. *Advances in Parasitology*, *47* (1), 289–307.

Gong, P., Li, X., & Zhang, W. (2019). 40-Year (1978–2017) human settlement changes in China reflected by impervious surfaces from satellite remote sensing. *Science Bulletin*, *64* (11), 756-763.

Gong, P., Li, X., Wang, J., Bai, Y., Chen, B., Hu, T., & Zhou, Y. (2020). Annual maps of global artificial impervious area (GAIA) between 1985 and 2018. *Remote Sensing of Environment*, *236*, 111510.

Goodfellow, T. (2013). Planning and development regulation amid rapid urban growth: Explaining divergent trajectories in Africa. *Geoforum*, *48*, (21), 83-93.

Goshua, A., Gomez, J., Erny, B., Burke, M., Luby, S., Sokolow, S., & Nadeau, K. (2021). Addressing climate change and its effects on human health: A call to action for medical schools. *Academic Medicine*, *96* (3), 324-328.

Gosling, S. N., Lowe, J. A., McGregor, G. R., Pelling, M., & Malamud, B. D. (2009). Associations between elevated atmospheric temperature and human mortality: A critical review of the literature. *Climate change*, *92* (3), 299-341.

Gosling, S.N., McGregor, G.R., & Páldy, A. (2007). Climate change and heat-related mortality in six cities Part 1: model construction and validation. *International Journal of Biometeorology*, *51* (6), 525-540.

Goward, S. N. (1981). Thermal behaviour of urban landscapes and the urban heat island. *Physical Geography*, *2* (1), 19-33.

Grace, K., Davenport, F., Funk, C., & Lerner, A. M. (2012). Child malnutrition and climate in Sub-Saharan Africa: An analysis of recent trends in Kenya. *Applied Geography*, *35* (12), 405-413.

Green, H., Bailey, J., Schwarz, L., Vanos, J., Ebi, K., & Benmarhnia, T. (2019). Impact of heat on mortality and morbidity in low and middle-income countries: a review of the epidemiological evidence and considerations for future research. *Environmental Research*, *171* (1), 80-91.

Grigorescu, I., Mocanu, I., Mitrică, B., Dumitraşcu, M., Dumitrică, C., & Dragotă, C. S. (2021). Socio-economic and environmental vulnerability to heat-related phenomena in Bucharest metropolitan area. *Environmental Research*, *192* (3), 110268.

Gronlund, C. J., Sullivan, K. P., Kefelegn, Y., Cameron, L., & O'Neill, M. S. (2018). Climate change and temperature extremes: A review of heat-and cold-related morbidity and mortality concerns of municipalities. *Maturitas*, *114* (1), 54-59.

Gronlund, C. J., Zanobetti, A., Wellenius, G. A., Schwartz, J. D., & O'Neill, M. S. (2016). Vulnerability to renal, heat, and respiratory hospitalizations during extreme heat among US elderly. *Climatic Change*, *136* (3), 631-645.

Gross, D. (2005). Monitoring Agricultural Biomass Using NDVI Time Series, Food and Agriculture Organization of the United Nations (FAO), Rome, Italy.

Guardaro, M., Hondula, D. M., Ortiz, J., & Redman, C. L. (2022). Adaptive capacity to extreme urban heat: The dynamics of differing narratives. *Climate Risk Management*, *35*, (3), 100415.

Guest, C. S., Willson, K., Woodward, A. J., Hennessy, K., Kalkstein, L. S., Skinner, C., & McMichael, A. J. (1999). Climate and mortality in Australia: a retrospective study, 1979-1990, and predicted impacts in five major cities in 2030. *Climate Research*, *13* (1), 1-15.

Guha, S., Govil, H., & Diwan, P. (2019). Analytical study of seasonal variability in land surface temperature with normalized difference vegetation index, normalized difference water index, normalized difference built-up index, and normalized multiband drought index. *Journal of Applied Remote Sensing*, *13* (2), 024518.

Guo, X., Huang, G., Jia, P., & Wu, J. (2019). Estimating fine-scale heat vulnerability in Beijing through two approaches: spatial patterns, similarities, and divergence. *Remote Sensing*, *11* (20), 2358.

Guo, Y., Gasparrini, A., Armstrong, B. G., Tawatsupa, B., Tobias, A., Lavigne, E., & Tong, S. (2016). Temperature variability and mortality: a multi-country study. *Environmental Health Perspectives*, *124* (10), 1554-1559.

Haase, D., Guneralp, B., Bai, X., Elmqvist, T., Dahiya, B., Fragkias, M., & Gurney, K. (2018). Different pathways of global urbanization. *The Urban Planet: Patterns and Pathways to the Cities We Want*, *2* (1), 17-146.

Haggag, M., Kalisa, J. C., & Abdeldayem, A. W. (2016). Projections of precipitation, air temperature, and potential evapotranspiration in Rwanda under changing climate conditions. *African Journal of Environmental Science and Technology*, *10* (1), 18-33.

Hajat, S., O'Connor, M., & Kosatsky, T. (2010). Health effects of hot weather: from awareness of risk factors to effective health protection. *The Lancet*, *375*, (9717), 856-863.

Halder, B., Bandyopadhyay, J., & Banik, P. (2021). Evaluation of the climate change impact on urban heat islands based on land surface temperature and geospatial indicators. *International Journal of Environmental Research*, *15* (5), 819-835.

Hammer, G.P., Some, F., Muller, O., Kynast-Wolf, G., Kouyate, B., & Becher, H. (2006). The pattern of cause-specific childhood mortality in a malaria-endemic area of Burkina Faso. *Malaria Journal, 5* (1), 47.

Hammer, J., Ruggieri, D. G., Thomas, C., & Caum, J. (2020). Local extreme heat planning: an interactive tool to examine a heat vulnerability index for Philadelphia, Pennsylvania. *Journal of Urban Health*, *97* (2), 519-528.

Han, L., Zhao, J., Gao, Y., & Gu, Z. (2022). Prediction and evaluation of spatial distributions of ozone and urban heat island using a machine learning modified land use regression method. *Sustainable Cities and Society*, *78* (4), 103643.

Han, L., Zhou, W., & Li, W. (2015). The city is a major source area of fine particulate (PM2. 5) in China. *Environmental Pollution*, *206* (8), 183-187.

Hanberry, B. B. (2022). Global population densities, climate change, and the maximum monthly temperature threshold as a potential tipping point for high urban densities. *Ecological Indicators*, *135* (8), 108512.

Harlan, S. L., Brazel, A. J., Jenerette, G. D., Jones, N. S., Larsen, L., Prashad, L., & Stefanov, W. L. (2007). In the shade of affluence: the inequitable distribution of the urban heat island. *Equity and the Environment*, *1* (1), 11-19.

Harlan, S. L., Brazel, A. J., Prashad, L., Stefanov, W. L., & Larsen, L. (2006). Neighborhood microclimates and vulnerability to heat stress. *Social Science & Medicine*, *63* (11), 2847-2863.

Harlan, S. L., Declet-Barreto, J. H., Stefanov, W. L., & Petitti, D. B. (2013). Neighborhood effects on heat deaths: Social and environmental predictors of vulnerability in Maricopa County, Arizona. *Environmental Health Perspectives*, *121* (2), 197-204.

Harrington, L. J., Frame, D. J., Hawkins, E., & Joshi, M. (2017). Seasonal cycles enhance disparities between low-and high-income countries in exposure to monthly temperature emergence with future warming. *Environmental Research Letters*, *12* (11), 114039.

Hayes, A. T., Jandaghian, Z., Lacasse, M. A., Gaur, A., Lu, H., Laouadi, A., & Wang, L. (2022). Nature-Based Solutions (NBS) to Mitigate Urban Heat Island (UHI) Effects in Canadian Cities. *Buildings*, *12* (7), 925.

He, C., Ma, L., Zhou, L., Kan, H., Zhang, Y., Ma, W., & Chen, B. (2019). Exploring the mechanisms of heatwave vulnerability at the urban scale based on the application of big data and artificial societies. *Environment International*, *127* (4), 573-583.

He, W., Zhang, L., & Yuan, C. (2022). Future air temperature projection in high-density tropical cities based on global climate change and urbanization–a study in Singapore. *Urban Climate*, *42* (4), 101115.

Heaton, M. J., Sain, S. R., Greasby, T. A., Uejio, C. K., Hayden, M. H., Monaghan, A. J., & Wilhelmi, O. V. (2014). Characterizing urban vulnerability to heat stress using a spatially varying coefficient model. *Spatial and Spatio-temporal Epidemiology*, *8* (1), 23-33.

Henderson, S. B., Wan, V., & Kosatsky, T. (2013). Differences in heat-related mortality across four ecological regions with diverse urban, rural, and remote populations in British Columbia, Canada. *Health & place*, *23* (5), 48-53.

Henninger, S. (2009). Urban climate and air pollution in Kigali, Rwanda. In *The 7th International Conference on Urban Climate*, *29*, (7), 1038-1041.

Herold, N., Alexander, L., Green, D., & Donat, M. (2017). Greater increases in temperature extremes in low versus high-income countries. *Environmental Research Letters*, *12* (3), 034007.

Hess, J. J., McDowell, J. Z., & Luber, G. (2012). Integrating climate change adaptation into public health practice: using adaptive management to increase adaptive capacity and build resilience. *Environmental Health Perspectives*, *120* (2), 171-179.

Hewitt, K. (2014). *Regions of risk: A geographical introduction to disasters*. *Routledge*, *23* (3), 114-128

Hidayati, I. N., & Suharyadi, R. (2019). A Comparative Study of various Indices for extraction of the urban impervious surface of Landsat 8 OLI. In *Forum Geografi*, *33* (2), 162-172.

Ho, H. C., Knudby, A., & Huang, W. (2015). A spatial framework to map heat-health risks at multiple scales. *International Journal of Environmental Research and Public Health*, *12* (3), 16110-16123.

Ho, H. C., Knudby, A., Chi, G., Aminipouri, M., & Lai, D. Y. F. (2018). Spatiotemporal analysis of regional socio-economic vulnerability change associated with heat risks in Canada. *Applied Geography*, *95* (1), 61-70.

Hoesly, R. M., Smith, S. J., Feng, L., Klimont, Z., Janssens-Maenhout, G., Pitkanen, T., & Zhang, Q. (2018). Historical (1750–2014) anthropogenic emissions of reactive gases and aerosols from the Community Emissions Data System (CEDS). *Geoscientific Model Development*, *11* (1), 369-408.

Hondula, D. M., Davis, R. E., Leisten, M. J., Saha, M. V., Veazey, L. M., & Wegner, C. R. (2012). Fine-scale spatial variability of heat-related mortality in Philadelphia County, USA, from 1983-2008: A case-series analysis. *Environmental Health, 11* (1), 1-11.

Hooker, J., Duveiller, G., & Cescatti, A. (2018). A global dataset of air temperature derived from satellite remote sensing and weather stations. *Scientific Data, 5* (1), 1-11.

Hou, H., Estoque, R. C., & Murayama, Y. (2016). Spatiotemporal analysis of urban growth in three African capital cities: A grid-cell-based analysis using remote sensing data. *Journal of African Earth Sciences, 123* (4), 381-391.

Hu, K., Yang, X., Zhong, J., Fei, F., & Qi, J. (2017). Spatially explicit mapping of heat health risk utilizing environmental and socioeconomic data. *Environmental Science and Technology, 51* (3), 1498-1507.

Huang, G., Zhou, W., & Cadenasso, M. L. (2011). Is everyone hot in the city? Spatial pattern of land surface temperatures, land cover, and neighbourhood socioeconomic characteristics in Baltimore, MD. *Journal of Environmental Management, 92* (7), 1753-1759.

Hulley, G., Shivers, S., Wetherley, E., & Cudd, R. (2019). New ECOSTRESS and MODIS land surface temperature data reveal fine-scale heat vulnerability in cities: A case study for Los Angeles County, California. *Remote Sensing, 11* (18), 2136.

Hummel, D. (2016). Climate change, land degradation, and migration in Mali and Senegal–some policy implications. *Migration and Development, 5* (2), 211-233.

Huynen, M. M., Martens, P., Schram, D., Weijenberg, M. P., & Kunst, A. E. (2001). The impact of heatwaves and cold spells on mortality rates in the Dutch population. *Environmental Health Perspectives, 109* (5), 463-470.

Ibrahim Mahmoud, M., Duker, A., Conrad, C., Thiel, M., & Shaba Ahmad, H. (2016). Analysis of settlement expansion and urban growth modelling using geoinformation for assessing potential impacts of urbanization on climate in Abuja City, Nigeria. *Remote Sensing, 8* (3), 220.

Idoko, M. A., & Bisong, F. E. (2010). Application of geo-information for evaluation of land use change: A case study of federal capital territory-Abuja. *Environmental. Resources. Journal, 4* (2), 140-144.

Iduseri, E. O., Abbas, I. I., & Izunobi, J. U. (2022). Role of Sustainable Development Goals in Combating Youth Unemployment: A Case Study

of the Federal Capital Territory (FCT) Abuja, Nigeria. *Journal of Sustainable Development*, *15* (3), 125-125.

Ifatimehin, O. O., & Ujoh, F. (2014). Application of remotely-sensed data for modeling malaria infection in Lokoja, Nigeria. *International Journal of Tropical Diseases & Health*, *4* (6), 634-644.

Ige, S. O., Ajayi, V. O., Adeyeri, O. E., & Oyekan, K. S. A. (2017). Assessing remotely sensed temperature humidity index as a human comfort indicator relative to land use/cover change in Abuja, Nigeria. *Spatial Information Research*, *25* (4), 523-533.

Ihtisham, M., Liu, S., Shahid, M. O., Khan, N., Lv, B., Sarraf, M., & Chen, Q. (2020). The Optimized N, P, and K Fertilization for Bermudagrass Integrated Turf Performance during the Establishment and Its Importance for the Sustainable Management of Urban Green Spaces. *Sustainability*, *12* (24), 10294.

Ihuma, J. O., Tella, I. O., Madakan, P. S., & Akpan, M. (2016). Socio-ecological survey of parks and gardens in the Federal Capital Territory, Abuja Nigeria. *Journal of Research in Forestry, Wildlife and Environment*, *8* (1), 1-13.

Ike, C. C., Ezeibe, C. C., Anijiofor, S. C., & Daud, N. N. (2018). Solid waste management in Nigeria: problems, prospects, and policies. *The Journal of Solid Waste Technology and Management*, *44* (2), 163-172.

Ingole, V., Sheridan, S. C., Juvekar, S., Achebak, H., & Moraga, P. (2022). Mortality risk attributable to high and low ambient temperature in Pune city, India: A time series analysis from 2004 to 2012. *Environmental Research*, *204* (5), 112304.

Inostroza, L., Palme, M., and de la Barrera, F. (2016). A heat vulnerability index: spatial patterns of exposure, sensitivity and adaptive capacity for Santiago de Chile. *PLoS One*, *11* (9), 0162464.

IPCC. (2013). *Climate Change 2013: The Physical Science Basis. The contribution of Working Group I to the Fifth Assessment Report of the Intergovernmental Panel on Climate Change (WG1 AR5)*. Cambridge, United Kingdom and New York, NY, USA.

Ishola, K. A., Okogbue, E. C., & Adeyeri, O. E. (2016). Dynamics of surface urban biophysical compositions and their impact on the land surface thermal field. *Modeling Earth Systems and Environment*, *2* (4), 1-20.

Jaffar, S., Leach, A., Greenwood, A., Jepson, A., Muller, O., Ota, M., Bojang, K., Obaro, S., & Greenwood, B. (1997). Changes in the pattern of infant and childhood mortality in Upper River Division, The Gambia, from 1989 to 1993. *Tropical Medicine and International Health*, *2* (1), 28-37.

Jagarnath, M., Thambiran, T., & Gebreslasie, M. (2020). Heat stress risk and vulnerability under climate change in Durban metropolitan, South Africa—identifying urban planning priorities for adaptation. *Climatic Change*, *163* (2), 807-829.

Jain, S., Sannigrahi, S., Sen, S., Bhatt, S., Chakraborti, S., & Rahmat, S. (2020). Urban heat island intensity and its mitigation strategies in the fast-growing urban area. *Journal of Urban Management*, *9* (1), 54-66.

Jalalzadeh Fard, B., Mahmood, R., Hayes, M., Rowe, C., Abadi, A. M., Shulski, M., & Bell, J. E. (2021). Mapping heat vulnerability index based on different urbanization levels in Nebraska, USA. *GeoHealth*, *5* (10), 202-224.

Jang, J. D., Viau, A. A., & Anctil, F. (2004). Neural network estimation of air temperatures from AVHRR data. *International Journal of Remote Sensing*, 25, 4541–4554.

Janik, A. (2022). The Psychological Importance of Green Spaces During COVID-19: A comparison between those who had access to. *International Journal of Environmental Research and Public Health 19*, (13), 202- 237.

Jankowska, M. M., Lopez-Carr, D., Funk, C., Husak, G. J., & Chafe, Z. A. (2012). Climate change and human health: Spatial modeling of water availability, malnutrition, and livelihoods in Mali, Africa. *Applied Geography*, *33* (1), 4-15.

Jasim, O. Z., AL-Anbari, R. H., & Mohammed, Z. T. (2020). MODIS and Landsat satellite images comparison for modeling near-surface air temperature. In *IOP Conference Series: Materials Science and Engineering*, *737* (1), 012211.

Jenerette, G. D., Harlan, S. L., Stefanov, W. L., & Martin, C. A. (2011). Ecosystem services and urban heat riskscape moderation: water, green spaces, and social inequality in Phoenix, USA. *Ecological Applications*, *21* (7), 2637-2651.

Jenkins, P. (2009). African cities: Competing claims on urban land. In *African Cities*, 3 (8), 81-107.

Jiang, L., & O'Neill, B. C. (2017). Global urbanization projections for the Shared Socioeconomic Pathways. *Global Environmental Change*, *42* (3), 12-33.

Jiang, S., Zhan, W., Dong, P., Wang, C., Li, J., Miao, S., & Wang, C. (2022). Surface air temperature differences of intra-and inter-local climate zones across diverse timescales and climates. *Building and Environment*, *222* (9), 109396.

Jiménez-Muñoz, J. C., Sobrino, J. A., Mattar, C., Hulley, G., & Göttsche, F. M. (2014). Temperature and emissivity separation from MSG/SEVIRI data. *IEEE Transactions on Geoscience and Remote Sensing*, *52* (9), 5937-5951.

Jin, K., Wang, F., Zong, Q., Qin, P., & Liu, C. (2020). Impact of variations in vegetation on surface air temperature change over the Chinese Loess Plateau. *Science of the Total Environment*, *716* (4), 136967.

Johnson, D. P., & Wilson, J. S. (2009). The socio-spatial dynamics of extreme urban heat events: The case of heat-related deaths in Philadelphia. *Applied Geography*, *29* (3), 419-434.

Johnson, D. P., Stanforth, A., Lulla, V., & Luber, G. (2012). Developing an applied extreme heat vulnerability index utilizing socioeconomic and environmental data. *Applied Geography*, *35* (1-2), 23-31.

Johnson, D. P., Webber, J. J., Urs Beerval Ravichandra, K., Lulla, V., & Stanforth, A. C. (2013). Spatiotemporal variations in heat-related health risk in three Midwestern US cities between 1990 and 2010. *Geocarto International*, *29* (1), 65-84.

Jolliffe, I. T., & Cadima, J. (2016). Principal component analysis: a review and recent developments. *Philosophical Transactions of the Royal Society A: Mathematical, Physical and Engineering Sciences*, *374* (2065), 20150202.

Jones, M. W., Andrew, R. M., Peters, G. P., Janssens-Maenhout, G., De-Gol, A. J., Ciais, P., & Le Quéré, C. (2021). Gridded fossil CO_2 emissions and related O_2 combustion consistent with national inventories 1959–2018. *Scientific Data*, *8* (1), 1-23.

Kabanda, T. H., & Kabanda, T. A. (2019). Urban heat island analysis in Dar es Salaam, Tanzania. *South African Journal of Geomatics*, *8* (1), 98-107.

Kabano, P., Harris, A., & Lindley, S. (2022). Spatiotemporal dynamics of urban climate during the wet-dry season transition in a tropical African city. *International Journal of Biometeorology*, *66* (2), 385-396.

Kabisch, N., Korn, H., Stadler, J., & Bonn, A. (2017). Nature-based solutions to climate change adaptation in urban areas: Linkages between science, policy, and practice. *Springer Nature*, *3* (2), 11-24.

Kafy, A. A., Saha, M., Rahaman, Z. A., Rahman, M. T., Liu, D., Fattah, M. A., & Ahasan, M. A. K. (2022). Predicting the impacts of land use/land cover changes on seasonal urban thermal characteristics using machine learning algorithms. *Building and Environment*, *217* (11*)*, 109066.

Kamali Maskooni, E., Hashemi, H., Berndtsson, R., Daneshkar Arasteh, P., & Kazemi, M. (2021). Impact of spatiotemporal land-use and land-cover

changes on surface urban heat islands in a semiarid region using Landsat data. *International Journal of Digital Earth*, *14* (2), 250-270.

Karakuş, C. B. (2019). The impact of land use/land cover (LULC) changes on land surface temperature in Sivas City Center and its surroundings and assessment of Urban Heat Island. *Asia-Pacific Journal of Atmospheric Sciences*, *55* (4), 669-684.

Karanja, J., Wanyama, D., & Kiage, L. (2022). Weighting mechanics and the spatial pattern of composite metrics of heat vulnerability in Atlanta, Georgia, USA. *Science of the Total Environment, 812 (7),* 151432.

Karimi, M., Nazari, R., Dutova, D., Khanbilvardi, R., & Ghandehari, M. (2018). A conceptual framework for environmental risk and social vulnerability assessment in complex urban settings. *Urban Climate, 26* (8), 161-173.

Kenny, G.P., Yardley, J., Brown, C., Sigal, R.J., & Jay, O., (2010). Heat stress in older individuals and patients with common chronic diseases. *Canadian Medical Association Journal 182* (2), 1053–1060.

Keramitsoglou, I., Kiranoudis, C. T., Maiheu, B., De Ridder, K., Daglis, I. A., Manunta, P., & Paganini, M. (2013). Heatwave hazard classification and risk assessment using artificial intelligence fuzzy logic. *Environmental Monitoring and Assessment*, *185* (10), 8239-8258.

Khan, F., Das, B., & Mishra, R. K. (2022). An automated land surface temperature modelling tool box designed using spatial technique for ArcGIS. *Earth Science Informatics*, *15* (1), 725-733.

Khanal, N., Uddin, K., Matin, M. A., & Tenneson, K. (2019). Automatic detection of spatiotemporal urban expansion patterns by fusing OSM and landsat data in Kathmandu. *Remote Sensing*, *11* (19), 2296.

Kim, D. W., Deo, R. C., Lee, J. S., & Yeom, J. M. (2017). Mapping heatwave vulnerability in Korea. *Natural Hazards*, *89* (1), 35-55.

Kim, H., Gu, D., & Kim, H. Y. (2018). Effects of Urban Heat Island mitigation in various climate zones in the United States. *Sustainable Cities and Society*, *41*(7), 841-852.

Kim, S. (2020). Novel Air Temperature Measurement Using Midwave Hyperspectral Fourier Transform Infrared Imaging in the Carbon Dioxide Absorption Band. *Remote Sensing*, *12* (11), 1860.

Kim, Y., & Joh, S. (2006). A vulnerability study of the low-income elderly in the context of high temperature and mortality in Seoul, Korea. *Science of the Total Environment*, *371* (13), 82-88.

Kim, S. W., & Brown, R. D. (2021). Urban heat island (UHI) variations within a city boundary: A systematic literature review. *Renewable and Sustainable Energy Reviews*, (*148)*, 111256.

Kjellstrom, T., Briggs, D., Freyberg, C., Lemke, B., Otto, M., & Hyatt, O. (2016). Heat, human performance, and occupational health: a key issue for the assessment of global climate change impacts. *Annual Review of Public Health*, *37*, 97-112.

Koko, A. F., Yue, W., Abubakar, G. A., Alabsi, A. A. N., & Hamed, R. (2021). Spatiotemporal influence of land use/land cover change dynamics on surface urban heat island: A case study of Abuja metropolis, Nigeria. *ISPRS International Journal of Geo-Information*, *10* (5), 272.

Köppen, W. (1900). Versuch einer Klassifikation der Klimate, vorzugsweise nachihren Beziehungen zur Pflanzenwelt. *Geographische Zeitschrift, 6*, 593-611.

Kotharkar, R., & Ghosh, A. (2022). Progress in extreme heat management and warning systems: A systematic review of heat-health action plans (1995-2020). *Sustainable Cities and Society*, *76* (4), 103487.

Kottek, M., Grieser, J., Beck, C., Rudolf, B., & Rubel, F. (2006). World Map of the Köppen-Geiger climate classification updated. *Meteorologische Zeitschrift*, *15* (8), 259-263.

Koudahe, K., Koffi, D., Kayode, J., Awokola, S., & Adebola, A. (2018). Impact of climate variability on crop yields in southern Togo. *Environment Pollution and Climate Change*, *2* (1), 1-9.

Kouis, P., Kakkoura, M., Ziogas, K., Paschalidou, A. K. & Papatheodorou, S. I. (2019). The effect of ambient air temperature on cardiovascular and respiratory mortality in Thessaloniki, Greece. *Science of the Total Environment*, *647* (8), 1351-1358.

Krstic, N., Yuchi, W., Ho, H. C., Walker, B. B., Knudby, A. J., & Henderson, S. B. (2017). The Heat Exposure Integrated Deprivation Index (HEIDI): A data-driven approach to quantifying neighbourhood risk during extremely hot weather. *Environment International*, *109* (2), 42-52.

Kumar, D., & Shekhar, S. (2015). Statistical analysis of land surface temperature–vegetation indexes relationship through thermal remote sensing. *Ecotoxicology and Environmental Safety*, *121*(7), 39-44.

Kwasi, F., Oosthuizen, J., & Etten, E. V. (2014). The extent of heat on health and sustainable farming in Ghana–Bawku East. *Sustainable Agriculture Research*, *3,* (526), 2016-37861.

Kynast-Wolf, G., Hammer, G., Müller, O., Kouyaté, B., & Becher, H. (2006). Season of death and birth predict patterns of mortality in Burkina Faso. *International Journal of Epidemiology*, *35* (4), 427-435.

Kynast-Wolf, G., Preuß, M., Sié, A., Kouyaté, B., & Becher, H. (2010). Seasonal patterns of cardiovascular disease mortality of adults in Burkina Faso, West Africa. *Tropical Medicine and International Health*, *15* (1), 1082-1089.

Kyselý, J., & Plavcová, E. (2012). Declining impacts of hot spells on mortality in the Czech Republic, 1986–2009: adaptation to climate change? *Climatic change*, *113* (2), 437-453.

Laburn, H. P. (1996). How does the fetus cope with thermal challenges? *Physiology*, *11* (2), 96-100.

Landreau, A., Juhola, S., Jurgilevich, A., & Räsänen, A. (2021). Combining socio-economic and climate projections to assess heat risk. *Climatic Change*, *167* (1), 1-20.

Landsberg, H.E., (1981). The Urban Climate: *Academic Press*, *New York*, *28* (9), 17-29.

Lapola, D. M., Braga, D. R., Di Giulio, G. M., Torres, R. R., & Vasconcellos, M. P. (2019). Heat stress vulnerability and risk at the (super) local scale in six Brazilian capitals. *Climate Change*, *154* (3), 477-492.

Laranjeira, K., Göttsche, F., Birkmann, J., & Garschagen, M. (2021). Heat vulnerability and adaptive capacities: Findings of a household survey in Ludwigsburg, BW, Germany. *Climatic Change*, *166* (1), 1-19.

Laryea, A. E. N., Oluwaseun, O. O., Kofi, A. S., & Oduro, N. B. (2022). Dust Sources and Impact: A Review. North American Academic Research, *5* (9), 1-13.

Laue, F., Adegun, O. B., & Ley, A. (2022). Heat Stress Adaptation within Informal, Low-Income Urban Settlements in Africa. *Sustainability*, *14* (13), 8182.

Lavoie, C., & Lachance, D. (2006). A new herbarium-based method for reconstructing the phenology of plant species across large areas. *American Journal of Botany*, *93* (4), 512-516.

Lawoyin, T.O. (2001). Risk factors for infant mortality in a rural community in Nigeria. *Journal of the Royal Society for the Promotion of Health*, *121* (2), 114-118.

Lay, C. R., Sarofim, M. C., Zilberg, A. V., Mills, D. M., Jones, R. W., Schwartz, J., & Kinney, P. L. (2021). City-level vulnerability to temperature-related

mortality in the USA and future projections: A geographically clustered meta-regression. *The Lancet Planetary Health, 5* (6), 338-346.

Leal Filho, W., Icaza, L. E., Neht, A., Klavins, M., & Morgan, E. A. (2018). Coping with the impacts of urban heat islands. A literature based study on understanding urban heat vulnerability and the need for resilience in cities in a global climate change context. *Journal of Cleaner Production*, *171*(8), 1140-1149.

Li, H., & Tang, Q. (2019). Joint Extremes in Temperature and Mortality: A Bivariate POT Approach. *Social Science Research Network, 3* (49), 322.

Li, Y., Westlund, H., & Liu, Y. (2019). Why some rural areas decline while some others not: An overview of rural evolution in the world. *Journal of Rural Studies*, *68*, 135-143.

Li, X., Stringer, L. C., Chapman, S., & Dallimer, M. (2021). How urbanisation alters the intensity of the urban heat island in a tropical African city. *PLoS One*, *16* (7), 0254371.

Liao, W., Cai, Z., Feng, Y., Gan, D., & Li, X. (2021). A simple and easy method to quantify the cool island intensity of urban greenspace. *Urban Forestry & Urban Greening*, *62* (9), 127173.

Lillesand, T., Kiefer, R. W., & Chipman, J. (2015). *Remote Sensing and Image Interpretation*. John Wiley & Sons.

Lim, Y. H., Reid, C. E., Mann, J. K., Jerrett, M., & Kim, H. (2015). Diurnal temperature range and short-term mortality in large US communities. *International Journal of Biometeorology*, *59* (9), 1311-1319.

Lin, C. Y., Chen, W. C., Chang, P. L., & Sheng, Y. F. (2011). Impact of the urban heat island effect on precipitation over a complex geographic environment in northern Taiwan. *Journal of Applied Meteorology and Climatology*, *50* (2), 339-353.

Linda, A., & Oluwatola, A. (2015). Impact of land-use change on surface temperature in Ibadan, Nigeria. *International Journal of Environmental and Ecological Engineering*, *9* (3), 235-241.

Lindén, J. (2011). Nocturnal Cool Island in the Sahelian city of Ouagadougou, Burkina Faso. *International Journal of Climatology*, *31* (4), 605-620.

Lindén, J., Grimmond, C. S. B., & Esper, J. (2015). Urban warming in villages. *Advances in Science and Research*, *12* (1), 157-162.

Lindley, S., Kibassa, D., & Cavan, G. (2015). Climate moderation via green infrastructure–the potential of regulating ecosystem services to mitigate

the UHI effect in Dar es Salaam. *ICUC9 - 9th International Conference on Urban Climate jointly with 12th Symposium on the Urban Environment.*

Lissner, T. K., Holsten, A., Walther, C., & Kropp, J. P. (2012). Towards sectoral and standardized vulnerability assessments: the example of heatwave impacts on human health. *Climatic change*, *112* (3), 687-708.

Littaye, A., Boba, M. S., & Cheikh, M. A. O. S. (2018). Temporal Variabilities of the Climate along the Mauritanian Coast over the Last Decades. *Journal of Earth Science and Climate Change*, *9* (442), 1-23.

Liu, S., Su, H., Tian, J., & Wang, W. (2018). An analysis of spatial representativeness of air temperature monitoring stations. *Theoretical and Applied Climatology*, *132* (3), 857-865.

Liu, X., Yue, W., Yang, X., Hu, K., Zhang, W., & Huang, M. (2020). Mapping urban heat vulnerability of extreme heat in Hangzhou via comparing two approaches. *Complexity*, *3* (1), 1-9.

Liu, Z., Lai, J., Zhan, W., Bechtel, B., Voogt, J., Quan, J., & Li, J. (2022). Urban heat islands were significantly reduced by the COVID-19 lockdown. *Geophysical Research Letters*, *49* (2), 17-33.

Longo-Mbenza, B., Phanzu-Mbete, L. B., M'Buyamba-Kabangu, J. R., Tonduangu, K., Mvunzu, M., Muvova, D., & Mpaka, M. (1999). Hematocrit and stroke in black Africans under tropical climate and meteorological influence. *Annales de Médecine Interne*, *150* (3), 171-177.

Lorena, P., Lisa, A., Jessica, L., Christie, G., & Chris, J., (2018). Emerging climate change-related public health challenges: the potential impacts of temperature rise on health outcomes in Dar es Salaam, Tanzania. *Urban Africa Risk Knowledge Briefing, UN-Habitat.*

Loughnan, M. E., Tapper, N. J., Phan, T., & McInnes, J. A. (2014). Can a spatial index of heat-related vulnerability predict emergency service demand in Australian capital cities? *International Journal of Emergency Services*, *3* (91), 6-33.

Loughnan, M., Carroll, M., & Tapper, N. J. (2015). The relationship between housing and heatwave resilience in older people. *International Journal of Biometeorology*, *59* (9), 1291-1298.

Loughnan, M., Nicholls, N., & Tapper, N. J. (2012). Mapping heat-health risks in urban areas. *International Journal of Population Research*, *2* (1), 12-21.

Lucas, R. A., Epstein, Y., & Kjellstrom, T. (2014). Excessive occupational heat exposure: a significant ergonomic challenge and health risk for current and future workers. *Extreme physiology & medicine*, *3* (1), 1-8.

Luque Fernández, M. Á., Bauernfeind, A., Jiménez, J. D., Gil, C. L., Omeiri, N. E., & Guibert, D. H. (2009). Influence of temperature and rainfall on the evolution of cholera epidemics in Lusaka, Zambia, 2003–2006: analysis of a time series. *Transactions of the Royal Society of Tropical Medicine and Hygiene*, *103* (2), 137-143.

Ma, X., & Peng, S. (2022). Research on the spatiotemporal coupling relationships between land use/land cover compositions or patterns and the surface urban heat island effect. *Environmental Science and Pollution Research*, *29* (26), 39723-39742.

Macnee, R. G., & Tokai, A. (2016). Heatwave vulnerability and exposure mapping for Osaka City, Japan. *Environment Systems and Decisions*, *36*, (4), 368-376.

Mahlstein, I., Knutti, R., Solomon, S., & Portmann, R. W. (2011). Early-onset of significant local warming in low latitude countries. *Environmental Research Letters*, *6* (3), 034009.

Maier, G., Grundstein, A., Jang, W., Li, C., Naeher, L. P., & Shepherd, M. (2014). Assessing the performance of a vulnerability index during oppressive heat across Georgia, United States. *Weather, Climate, and Society*, *6* (2), 253-263.

Malik, M. S., & Shukla, J. P. (2019). Assessment of groundwater vulnerability risk in shallow aquifers of Kandaihimmat Watershed, Hoshangabad, Madhya Pradesh. *Journal of the Geological Society of India*, *93* (2), 199-206.

Mallen, E., Stone, B., & Lanza, K. (2019). A methodological assessment of extreme heat mortality modeling and heat vulnerability mapping in Dallas, Texas. *Urban Climate*, *30* (1), 100528.

Mallo, I. Y. Y., & Mgbanyi, L. L. O. (2013). Assessment of soil wash and soil erodibility indices on miniature badlands at Gada Biyu, Abuja, Federal Capital Territory, Nigeria. *Ethiopian Journal of Environmental Studies and Management*, *6* (2), 135-142.

Malmquist, A., Hjerpe, M., Glaas, E., Karlsson, H., & Lassi, T. (2022). Elderly People's Perceptions of Heat Stress and Adaptation to Heat: An Interview Study. *International Journal of Environmental Research and Public Health*, *19* (7), 3775.

Malomo, S., Olorunniwo, M. A., & Ogunsanwo, O. (1983). Engineering geological mapping in terrains of tropical weathering—an example from Abuja, Nigeria. *Engineering Geology*, *19* (2), 133-148.

Manangan, A. P., Uejio, C. K., Saha, S., Schramm, P. J., Marinucci, G. D., Hess, J. J., & Luber, G. (2015). Assessing health vulnerability to climate change. *Centre for Disease Control and Prevention*, *1* (1), 1-23.

Manik, T. K., & Syaukat, S. (2017). Comparative Vulnerability Assessment of Urban Heat Islands in Two Tropical Cities in Indonesia. *International Journal of Environment and Climate Change*, *2* (1), 119-134.

Maragno, D., Dalla Fontana, M. & Musco, F., (2020). Mapping heat stress vulnerability and risk assessment at the neighborhood scale to drive urban adaptation planning. *Sustainability*, *12* (3), 1056.

Marando, F., Heris, M. P., Zulian, G., Udías, A., Mentaschi, L., Chrysoulakis, N., & Maes, J. (2022). Urban heat island mitigation by green infrastructure in European Functional Urban Areas. *Sustainable Cities and Society*, *77*(4), 103564.

März, S. (2018). Assessing the fuel poverty vulnerability of urban neighbourhoods using spatial multi-criteria decision analysis for the German city of Oberhausen. *Renewable and Sustainable Energy Reviews*, *82* (5), 1701-1711.

Matthes, K., Funke, B., Andersson, M. E., Barnard, L., Beer, J., Charbonneau, P., & Versick, S. (2017). Solar forcing for CMIP6. *Geoscientific Model Development*, *10* (6), 2247-2302.

McCarthy, J. J., Canziani, O. F., Leary, N. A., Dokken, D. J., & White, K. S. (Eds.). (2001). *Climate change 2001: impacts, adaptation, and vulnerability: contribution of Working Group II to the third assessment report of the Intergovernmental Panel on Climate Change* (Vol. 2). Cambridge University Press.

McGeehin, M. A., & Mirabelli, M. (2001). The potential impacts of climate variability and change on temperature-related morbidity and mortality in the United States. *Environmental health perspectives*, *109* (2), 185-189.

McGregor, I.A., Billewicz, W.Z., & Thomson, A.M. (1961). Growth and Mortality in Children in an African Village. *British Medical Journal, 2* (1), 1661-1666.

McGregor, G. R., & Vanos, J. K. (2018). Heat: a primer for public health researchers. *Public Health*, (*161)*, 138-146.

McMichael, A. J., Woodruff, R. E., & Hales, S. (2006). Climate change and human health: present and future risks. *The Lancet*, *367* (9513), 859-869.

Meade, R. D., Akerman, A. P., Notley, S. R., McGinn, R., Poirier, P., Gosselin, P., & Kenny, G. P. (2020). Physiological factors characterizing heat-vulnerable older adults: A narrative review. *Environment International*, *144* (8), 105909.

Meinshausen, M., Nicholls, Z. R., Lewis, J., Gidden, M. J., Vogel, E., Freund, M., & Wang, R. H. (2020). The shared socio-economic pathway (SSP)

greenhouse gas concentrations and their extensions to 2500. *Geoscientific Model Development, 13* (8), 3571-3605.

Meinshausen, M., Smith, S. J., Calvin, K., Daniel, J. S., Kainuma, M. L., Lamarque, J. F., & Van Vuuren, D. P. P. (2011). The RCP greenhouse gas concentrations and their extensions from 1765 to 2300. *Climatic Change, 109* (1), 213-241.

Méndez-Lázaro, P., Muller-Karger, F. E., Otis, D., McCarthy, M. J., & Rodríguez, E. (2018). A heat vulnerability index to improve urban public health management in San Juan, Puerto Rico. *International Journal of Biometeorology*, *62* (5), 709-722.

Mensah, E. (2017). Land cover, land surface temperature, and urban heat island effects in tropical sub-Saharan City of Accra. In *Proceedings of the 19th International Conference on Geomatics Engineering*.

Mideksa, T. K., & Kallbekken, S. (2010). The impact of climate change on the electricity market: A review. *Energy Policy, 38* (7), 3579-3585.

Mileti, D. (1999). *Disasters by design: A reassessment of natural hazards in the United States*. Joseph Henry Press.

Ming, T., Liu, W., & Caillol, S. (2014). Fighting global warming by climate engineering: Is the Earth radiation management and solar radiation management any option for fighting climate change? *Renewable and Sustainable Energy Reviews*, *31*, 792-834.

Mortensen, J. W., Heaton, M. J., & Wilhelmi, O. V. (2018). Urban heat risk mapping using multiple point patterns in Houston, Texas. *Journal of the Royal Statistical Society: Series C (Applied Statistics), 67* (1), 83-102.

Moshi, I. R., Ngowo, H., Dillip, A., Msellemu, D., Madumla, E. P., Okumu, F. O., & Manderson, L. (2017). Community perceptions on outdoor malaria transmission in Kilombero Valley, Southern Tanzania. *Malaria Journal*, *16* (1), 1-8.

Mostovoy, G. V., King, R. L., Reddy, K. R., Kakani, V. G., & Filippova, M. G. (2006). A statistical estimation of daily maximum and minimum air temperatures from MODIS Ts data over the state of Mississippi. *GIScience and Remote Sensing*, *43* (1), 78–110.

Mrema, S., Shamte, A., Selemani, M., & Masanja, H. (2012). The influence of weather on mortality in rural Tanzania: a time-series analysis 1999–2010. *Global Health Action*, *5* (1), 19068.

Murage, P., Hajat, S., & Kovats, R. S. (2017). Effect of night-time temperatures on cause and age-specific mortality in London. *Environmental Epidemiology Philadelphia*, *1* (2), 005.

Mushore, T. D., Mutanga, O., Odindi, J., & Dube, T. (2018). Determining extreme heat vulnerability of Harare Metropolitan City using multispectral remote sensing and socio-economic data. *Journal of Spatial Science, 63* (1), 173-191.

Mutai, B. K. (2013). Assessment of population exposure to climate change-induced exceedances of health-based air pollution thresholds in some urban areas in Kenya. *Doctoral Dissertation, University of Nairobi*.

Mutisya, M., Orindi, B., Emina, J., Zulu, E., & Ye, Y. (2010). Is mortality among under-five children in Nairobi slums seasonal? *Tropical Medicine and International Health, 15*, (2), 132-139.

Myers, J., Tucker, T., Young, T., Galloway, M., & Manyike, P. (2011). Responding to climate change in southern Africa-the role of research. *South African Medical Journal*, *101* (11), 820-822.

Naicker, N., Teare, J., Balakrishna, Y., Wright, C. Y., & Mathee, A. (2017). Indoor temperatures in low-cost housing in Johannesburg, South Africa. *International Journal of Environmental Research and Public Health*, *14* (11), 1410.

Naikoo, M. W., Islam, A. R. M. T., Mallick, J., & Rahman, A. (2022a). Land use/land cover change and its impact on surface urban heat island and urban thermal comfort in a metropolitan city. *Urban Climate*, *41* (6), 101052.

Naikoo, M. W., Rihan, M., Peer, A. H., Talukdar, S., Mallick, J., Ishtiaq, M., & Rahman, A. (2022b). Analysis of peri-urban land use/land cover change and its drivers using geospatial techniques and geographically weighted regression. *Environmental Science and Pollution Research, 7* (9), 1-19.

Nayak, S. G., Shrestha, S., Kinney, P. L., Ross, Z., Sheridan, S. C., Pantea, C. I., & Hwang, S. A. (2018). Development of a heat vulnerability index for New York State. *Public Health*, *161* (4), 127-137.

Ncongwane, K. P., Botai, J. O., Sivakumar, V., & Botai, C. M. (2021). A literature review of the impacts of heat stress on human health across Africa. *Sustainability*, *13* (9), 5312.

Ndetto, E. L., & Matzarakis, A. (2013). Basic analysis of climate and urban bio climate of Dar es Salaam, Tanzania. *Theoretical and Applied Climatology*, *114* (1), 213-226.

Nemani, R. R., and Running, J. W. (1989). Estimation of regional surface resistance to evapotranspiration from NDVI and thermal-IR AVHRR data. *Journal of Applied Meteorology*, *28* (2), 276–284.

Ng, S., & Cowling, B. J. (2014). Association between temperature, humidity, and ebola virus disease outbreaks in Africa, 1976 to 2014. *Eurosurveillance*, *19* (35), 20892.

Nguemhe Fils, S. C., Mimba, M. E., Dzana, J. G., Etouna, J., Mounoumeck, P. V., & Hakdaoui, M. (2018). TM/ETM+/LDCM Images for studying land surface temperature (LST) interplay with impervious surface changes over time within the Douala Metropolis, Cameroon. *Journal of the Indian Society of Remote Sensing*, *46* (1), 131-143.

Ngwenya, B., Oosthuizen, J., Cross, M., & Frimpong, K. (2018). Emerging heat-related climate change influences; a public health challenge to health care practitioners and policymakers: insight from Bulawayo, Zimbabwe. *International Journal of Disaster Risk Reduction*, *27* (2), 596-601.

Niang, I., Ruppel, O.C., Abdrabo, M.A., Essel, A., Lennard, C., Padgham, J., & Urquhart, P. (2014). Africa. In: Barros, V.R., Field, C.B., Dokken, D.J., Mastrandrea, M.D., Mach, K.J., Bilir, T.E., Chatterjee, M., Ebi, K.L., Estrada, Y.O., Genova, R.C., Girma, B., Kissel, E.S., Levy, A.N., MacCracken, S., Mastrandrea, P.R., White, L.L. (Eds.), Climate Change 2014: Impacts, Adaptation, and Vulnerability. Part B: Regional Aspects. Contribution of Working Group II to the Fifth Assessment Report of the Intergovernmental Panel on Climate Change. *Cambridge University Press*, Cambridge, United Kingdom, and New York, NY, USA, 1199–1265.

Nigeria Population Commission. (2019). *Nigeria demographic and Health Survey 2018*. NPC, ICF.

Nigerian Meteorological Agency, (2021). State of the Climate in Nigeria. Publication of the Nigerian Meteorological Agency, National Weather Forecasting, and Climate Research Center, Nnamdi Azikwe International Airport, Abuja. 1-46.

Niu, Y., Li, Z., Gao, Y., Liu, X., Xu, L., Vardoulakis, S., & Liu, Q. (2021). A Systematic Review of the Development and Validation of the Heat Vulnerability Index: Major Factors, Methods, and Spatial Units. *Current Climate Change Reports*, *7* (3), 87-97.

Norton, B. A., Coutts, A. M., Livesley, S. J., Harris, R. J., Hunter, A. M., & Williams, N. S. (2015). Planning for cooler cities: A framework to prioritize green infrastructure to mitigate high temperatures in urban landscapes. *Landscape and Urban Planning*, *134* (4), 127-138.

Nse, O. U., Okolie, C. J., & Nse, V. O. (2020). Dynamics of land cover, land surface temperature and NDVI in Uyo City, Nigeria. *Scientific African*, *10* (4), 599.

Ntoumos, A., Hadjinicolaou, P., Zittis, G., Proestos, Y., & Lelieveld, J. (2022). Projected Air Temperature Extremes and Maximum Heat Conditions over the Middle-East-North Africa (MENA) Region. *Earth Systems and Environment*, *6* (2), 343-359.

Nunfam, V. F. (2021). Mixed methods study into social impacts of work-related heat stress on Ghanaian mining workers: A pragmatic research approach. *Heliyon*, *7* (5), 06918.

Nunfam, V. F., Afrifa-Yamoah, E., Adusei-Asante, K., Van Etten, E. J., Frimpong, K., Mensah, I. A., & Oosthuizen, J. (2021). Construct validity and invariance assessment of the social impacts of occupational heat stress scale (SIOHSS) among Ghanaian mining workers. *Science of the Total Environment*, *771* (6), 144911.

Nunfam, V. F., Oosthuizen, J., Adusei-Asante, K., Van Etten, E. J., & Frimpong, K. (2019a). Perceptions of climate change and occupational heat stress risks and adaptation strategies of mining workers in Ghana. *Science of the Total Environment*, *657*, (7), 365-378.

Nunfam, V. F., Van Etten, E. J., Oosthuizen, J., Adusei-Asante, K., & Frimpong, K. (2019b). Climate change and occupational heat stress risks and adaptation strategies of mining workers: perspectives of supervisors and other stakeholders in Ghana. *Environmental Research*, *169* (8), 147-155.

Nurvitasari, P. U., Gunawan, D. S., & Sambodo, H. (2020). Faktor-Faktor yang Mempengaruhi Kemiskinan di Daerah Istimewa Yogyakarta Berdasarkan Perspektif World Poverty Clock. *Prosiding*, *10* (1), 1-19.

Nwilo, P. C., Olayinka, D. N., Okolie, C. J., Emmanuel, E. I., Orji, M. J., & Daramola, O. E. (2020). Impacts of land cover changes on desertification in northern Nigeria and implications on the Lake Chad Basin. *Journal of Arid Environments*, *181*, (2), 104190.

Nwilo, P. C., Umar, A. A., Adepoju, M. O., & Okolie, C. J. (2019). Spatio-temporal assessment of changing land surface temperature and depleting water in the Lake Chad area. *South African Journal of Geomatics*, *8* (2), 144-159.

O'Neill BC, Kriegler E, Ebi KL, Kemp-Benedict E, Riahi K, Rothman DS, Solecki W (2017) The roads ahead: narratives for shared socioeconomic pathways describing world futures in the 21st century. *Global Environmental Change 5* (42), 169–180.

O'Neill, M. S., Zanobetti, A., & Schwartz, J. (2003). Modifiers of the temperature and mortality association in seven US cities. *American Journal of Epidemiology*, *157* (12), 1074-1082.

Obiadi B. N., & Nzewi, N. U. (2018). Population Challenges and the Nebulous Architecture of Abuja, Nigeria: The Problem of Abuja,

Nigeria. *International Journal of Scientific and Technology Research, 7* (7), 191-200.

Obiadi, B. N., & Onochie, A. O. (2018). Abuja, Nigeria Urban Actors, Master Plan, Development Laws and their Roles in the Design and Shaping of Abuja Federal Territory and their Urban Environments. *IIARD International. Journal of Geography and Environmental Management, 4* (2), 23-43.

Obiadi, B. N., Ezezue, A. M., & Uduak, P. U. (2019). Abuja: Nigeria's spatial economic turmoil and urban development disarray. *Current Urban Studies, 7* (3), 371-398.

Obradovich, N., Migliorini, R., Mednick, S. C., & Fowler, J. H. (2017). Nighttime temperature and human sleep loss in a changing climate. *Science Advances, 3* (5), 1601555.

Odongo, S.O., (2016). Urban Heat Island: Investigation of Urban Heat Island Effect of Nairobi. *Department of Meteorology, the University of Nairobi.*

Offerle, B., Jonsson, P., Eliasson, I., & Grimmond, C. S. B. (2005). Urban modification of the surface energy balance in the West African Sahel: Ouagadougou, Burkina Faso. *Journal of Climate, 18* (19), 3983-3995.

Oke, T. R. (1982). The energetic basis of the urban heat island. *Quarterly Journal of the Royal Meteorological Society, 108* (455), 1-24.

Oke, T. R. (2006). Towards better scientific communication in urban climate. *Theoretical and Applied Climatology, 84* (1), 179-190.

Oke, T. R., Johnson, G. T., Steyn, D. G., & Watson, I. D. (1991). Simulation of surface urban heat islands under ideal conditions at night part 2: Diagnosis of causation. *Boundary-layer Meteorology, 56* (4), 339-358.

Oke, T.R., (1987). Boundary Layer Climates, *Methuen and Co. Ltd, London.*

Okundamiya, M. S., & Nzeako, A. N. (2010). Empirical model for estimating global solar radiation on horizontal surfaces for selected cities in the six geopolitical zones in Nigeria. *Research Journal of Applied Sciences, Engineering and Technology, 2* (8), 805-812.

Olanrewaju, A. V. (2018). Urban Land Use Land Cover Changes and Their Effect on Urban Thermal Pattern: Case Study of Nigeria's Federal Capital City. *Urban Land, 8* (5), 16-31.

Olatunde, A.F. (2016). The Intensity and Extent of Thermal Discomfort in Lokoja, Nigeria. *International Journal of Social Sciences, 10* (4), 17-31.

Olofsson, P., Foody, G. M., Herold, M., Stehman, S. V., Woodcock, C. E., & Wulder, M. A. (2014). Good practices for estimating area and assessing the accuracy of land change. *Remote Sensing of Environment, 148,* 42-57.

Olofsson, P., Foody, G. M., Stehman, S. V., & Woodcock, C. E. (2013). Making better use of accuracy data in land change studies: Estimating accuracy and area and quantifying uncertainty using stratified estimation. *Remote Sensing of Environment, 129*, 122-131.

Oloukoi, G., Bob, U., & Jaggernath, J. (2014). Perception and trends of associated health risks with seasonal climate variation in Oke-Ogun region, Nigeria. *Health and Place, 25* (3), 47-55.

Olsson, L., Barbosa, H., Bhadwal, S., Cowie, A., Delusca, K., Flores-Renteria, D., & Stringer, L. (2019). Land degradation: IPCC special report on climate change, desertification, land 5 degradation, sustainable land management, food security, and 6 greenhouse gas fluxes in terrestrial ecosystems. In *IPCC Special Report on Climate Change, Desertification, Land 5 Degradation, Sustainable Land Management, Food Security, and 6 Greenhouse Gas Fluxes in Terrestrial Ecosystems*. Intergovernmental Panel on Climate Change (IPCC).

Omali, T. U. (2020). Ecological evaluation of urban heat island impacts in Abuja Municipal Area of FCT Abuja, Nigeria. *World Academics Journal of Engineering Sciences, 7* (1), 66-72.

Omonijo, A. G. (2017). Assessing seasonal variations in urban thermal comfort and potential health risks using Physiologically Equivalent Temperature: A case of Ibadan, Nigeria. *Urban Climate, 21* (2), 87-105.

Omonijo, A. G., Adeofun, C. O., Oguntoke, O., & Matzarakis, A. (2013). Relevance of thermal environment to human health: a case study of Ondo State, Nigeria. *Theoretical and Applied Climatology, 113* (1), 205-212.

O'Neill, B. C., Ren, X., Jiang, L., & Dalton, M. (2012). The effect of urbanization on energy use in India and China in the iPETS model. *Energy Economics, 34* (7), 339-345.

O'Neill, B. C., Tebaldi, C., Van Vuuren, D. P., Eyring, V., Friedlingstein, P., Hurtt, G., & Sanderson, B. M. (2016). The scenario model intercomparison project (ScenarioMIP) for CMIP6. *Geoscientific Model Development, 9* (9), 3461-3482.

Orisakwe, I. C., Nwofor, O. K., Njoku, C. C., and Ezedigboh, U. O. (2017). On the analysis of the changes in the temperatures over Abuja, Nigeria. *Journal of Physical Science and Environmental Studies, 3,* (1), 8-17.

Osima, S., Indasi, V. S., Zaroug, M., Endris, H. S., Gudoshava, M., Misiani, H. O., & Dosio, A. (2018). The projected climate over the Greater Horn of

Africa under 1.5 C and 2 C global warming. *Environmental Research Letters*, *13* (6), 065004.

Oyewole, M. O., Ojutalayo, A. A., & Araloyin, F. M. (2019). Developers' willingness to invest in green features in Abuja, Nigeria. *Smart & Sustainable Built Environment*, *2* (7), 112-138.

Pal, S., & Ziaul, S. K. (2017). Detection of land use and land cover change and land surface temperature in English Bazar urban center. *The Egyptian Journal of Remote Sensing and Space Science*, *20* (1), 125-145.

Park, J., Kim, J. H., Sohn, W., & Lee, D. K. (2021). Urban cooling factors: Do small greenspaces outperform building shade in mitigating urban heat island intensity? *Urban Forestry & Urban Greening*, *64* (7), 127256.

Parsons, K. (2007). *Human thermal environments: the effects of hot, moderate, and cold environments on human health, comfort and performance*. CRC press.

Pasquini, L., van Aardenne, L., Godsmark, C. N., Lee, J., & Jack, C. (2020). Emerging climate change-related public health challenges in Africa: A case study of the heat-health vulnerability of informal settlement residents in Dar es Salaam, Tanzania. *Science of the Total Environment*, *747* (3), 141355.

Paz, S. (2009). Impact of temperature variability on cholera incidence in southeastern Africa, 1971–2006. *Ecohealth*, *6* (3), 340-345.

Pateman, T. (2011). Rural and urban areas: comparing lives using rural/urban classifications. *Regional trends*, *43*, 11-86.

Pezzulo, C., Hornby, G. M., Sorichetta, A., Gaughan, A. E., Linard, C., Bird, T. J., & Tatem, A. J. (2017). Sub-national mapping of population pyramids and dependency ratios in Africa and Asia. *Scientific Data*, *4* (1), 1-15.

Pörtner, H. O., Roberts, D. C., Adams, H., Adler, C., Aldunce, P., Ali, E., & Birkmann, J. (2022). Climate change 2022: Impacts, adaptation and vulnerability. *IPCC Sixth Assessment Report*, 37-118.

Prihodko, L., & Goward, S.N. (1997). Estimation of air temperature from remotely sensed surface observations. *Remote Sensing of Environment*, 60, (8), 335–346.

Prosdocimi, D., & Klima, K. (2020). Health effects of heat vulnerability in Rio de Janeiro: A validation model for policy applications. *Applied Sciences*, *2* (12), 1-11.

Prudent, N., Houghton, A., & Luber, G. (2016). Assessing climate change and health vulnerability at the local level: Travis County, Texas. *Disasters, 40* (4), 740-752.

Qiu, K., & Jia, B. (2020). The roles of landscape both inside the park and the surroundings in park cooling effect. *Sustainable Cities and Society, 52* (9), 101864.

Ragatoa, D. S., Ogunjobi, K. O., Okhimamhe, A.A., Klutse, N.A.B., & Lamptey, B.L. (2018). A predictive study of heatwave characteristics and their Spatio-temporal trends in climatic zones of Nigeria. *Modeling Earth Systems and Environment, 4* (3), 1125-1151.

Raihan, A., & Tuspekova, A. (2022). Nexus between emission reduction factors and anthropogenic carbon emissions in India. *Anthropocene Science, 1* (2), 295-310.

Ramyar, R., Ackerman, A., & Johnston, D. M. (2021). Adapting cities for climate change through urban green infrastructure planning. *Cities, 117* (7), 103316.

Rathi, S. K., Chakraborty, S., Mishra, S. K., Dutta, A., & Nanda, L. (2021). A heat vulnerability index: spatial patterns of exposure, sensitivity and adaptive capacity for urbanites of four cities of India. *International Journal of Environmental Research and Public Health, 19* (1), 283.

Rayco-Solon, P., Moore, S.E., Fulford, A.J., & Prentice, A.M. (2004). Fifty-year mortality trends in three rural African villages. *Tropical Medicine & International Health, 9* (3), 1151-1160.

Reckien, D. (2018). What is in an index? Construction method, data metric, and weighting scheme determine the outcome of composite social vulnerability indices in New York City. *Regional Environmental Change, 18* (5), 1439-1451.

Rehan, R. M. (2016). Cool city as a sustainable example of heat island management case study of the coolest city in the world. *HBRC journal, 12* (2), 191-204.

Reid, C. E., Mann, J. K., Alfasso, R., English, P. B., King, G. C., Lincoln, R. A., & Balmes, J. R. (2012). Evaluation of a heat vulnerability index on abnormally hot days: An environmental public health tracking study. *Environmental Health Perspectives, 120* (5), 715-720.

Reid, C. E., O'neill, M. S., Gronlund, C. J., Brines, S. J., Brown, D. G., Diez-Roux, A. V., & Schwartz, J. (2009). Mapping community determinants of heat vulnerability. *Environmental Health Perspectives, 117* (11), 1730-1736.

Reis-Mansur, M. C. P. P., da Luz, B. G., & dos Santos, E. P. (2023). Consumer Behavior, Skin Phototype, Sunscreens, and Tools for Photoprotection: A Review. *Cosmetics, 10*(2), 39.

Revich, B. A., Shaposhnikov, D. A., Avaliani, S. L., Rubinshtein, K. G., Emelina, S. V., Shiriaev, M. V., & OIu, K. (2015). Hazard assessment of the impact of high temperature and air pollution on public health in Moscow. *Gigiena i Sanitariia*, *94* (1), 36-40.

Rey, G., Fouillet, A., Bessemoulin, P., Frayssinet, P., Dufour, A., Jougla, E., & Hémon, D. (2009). Heat exposure and socio-economic vulnerability as synergistic factors in heat-wave-related mortality. *European Journal of Epidemiology*, *24* (9), 495-502.

Reyburn, R., Kim, D. R., Emch, M., Khatib, A., Von Seidlein, L., & Ali, M. (2011). Climate variability and the outbreaks of cholera in Zanzibar, East Africa: A time series analysis. *The American Journal of Tropical Medicine and Hygiene*, *84* (6), 862.

Riahi K, Van Vuuren DP, Kriegler E, Edmonds J, O'neill BC, Fujimori S, Tavoni M (2017) The shared socioeconomic pathways and their energy, land use, and greenhouse gas emissions implications: an overview. *Global Environmental Change*, *42* (1), 153–168.

Rikko, L.S & Wapwera, S.D. (2016). Perception and Conditions of the Urban Poor in Greater Karu Urban Area, Nasarawa, Nigeria. *IOSR Journal of Humanities and Social Science, 21* (2), 80-87.

Rinner, C., Patychuk, D., Bassil, K., Nasr, S., Gower, S., & Campbell, M. (2010). The role of maps in neighbourhood-level heat vulnerability assessment for the city of Toronto. *Cartography and Geographic Information Science*, *37* (1), 31-44.

Robinson, P. J. (2001). On the definition of a heatwave. *Journal of Applied Meteorology and Climatology*, *40* (4), 762-775.

Rogelj, J., Luderer, G., Pietzcker, R. C., Kriegler, E., Schaeffer, M., Krey, V., & Riahi, K. (2015). Energy system transformations for limiting end-of-century warming to below 1.5 C. *Nature Climate Change*, *5* (6), 519-527.

Rohat G, Flacke J, Dosio A, Pedde S, Dao H, Van Maarseveen M (2019a) Influence of changes in socioeconomic and climatic conditions on future heat-related health challenges in Europe. *Glob Planet Change 172* (9), 45–59.

Rohat, G., Wilhelmi, O., Flacke, J., Monaghan, A., Gao, J., Dao, H., & van Maarseveen, M. (2019b). Characterizing the role of socioeconomic pathways in shaping future urban heat-related challenges. *Science of the Total Environment*, *695*, (8), 133941.

Roy, M., Shemdoe, R., Hulme, D., Mwageni, N., & Gough, A. (2018). Climate change and declining levels of green structures: Life in informal

settlements of Dar es Salaam, Tanzania. *Landscape and Urban Planning*, *180* (17), 282-293.

Royé, D., Sera, F., Tobías, A., Lowe, R., Gasparrini, A., Pascal, M., & Teixeira, J. P. (2021). Effects of hot nights on mortality in southern Europe. *Epidemiology*, *32* (4), 487-498.

Russo, S., Marchese, A. F., Sillmann, J., & Immé, G. (2016). When will unusual heat waves become normal in a warming Africa? *Environmental Research Letters*, *11* (5), 054016.

Ryti, N. R., Guo, Y., & Jaakkola, J. J. (2016). Global association of cold spells and adverse health effects: a systematic review & meta-analysis. *Environmental Health Perspectives*, *124* (1), 12-22.

Sabrin, S., Karimi, M., & Nazari, R. (2020). Developing Vulnerability Index to Quantify Urban Heat Islands Effects Coupled with Air Pollution: A Case Study of Camden, NJ. *ISPRS International Journal of Geo-Information*, *9* (6), 349.

Sabrin, S., Karimi, M., Fahad, M. G. R., & Nazari, R. (2020). Quantifying environmental and social vulnerability: Role of urban Heat Island and air quality, a case study of Camden, NJ. *Urban Climate*, *34* (7), 100699.

Sadiya, T. B., Ibrahim, O., Asma, T. F., Mamfe, V., Nsofor, C. J., Oyewmi, A. S., & Ozigis, M. S. (2014). Mineral Detection and Mapping Using Band Rationing & Crosta Technique in Bwari Area Council, Abuja Nigeria. *International Journal of Scientific and Engineering Research*, *5* (12), 1100-1108.

Salmamza, Y. M., Onywere, S. M., & Letema, S. C. (2022). Geospatial dimensions of land cover transitions and land surface temperature in abuja city, nigeria. *The International Archives of Photogrammetry, Remote Sensing and Spatial Information Sciences*, *43* (5), 699-704.

Samir, K. C., & Lutz, W. (2017). The human core of the shared socioeconomic pathways: Population scenarios by age, sex and level of education for all countries to 2100. *Global Environmental Change*, *42* (9), 181-192.

Sankoh, O.A., Kynast-Wolf, G., Kouyaté, B., & Becher, H. (2003). Patterns of adult and old-age mortality in rural Burkina Faso. *Journal of Public Health*, *25* (4), 372-376.

Santacroce, L., Dellaripa, P. F., Costenbader, K. H., Collins, J., & Feldman, C. H. (2022). Association of Area-Level Heat and Social Vulnerability with Recurrent Hospitalizations among Individuals with Rheumatic Conditions. *Arthritis Care and Research*, 4 (11), 123-143.

Santamouris, M., Cartalis, C., Synnefa, A., & Kolokotsa, D. (2015). On the impact of urban heat island and global warming on the power demand and

electricity consumption of buildings—A review. *Energy and buildings*, *98* (12), 119-124.

Savage, C. W. (2021). *The measurement of sensation: A critique of perceptual psychophysics*. University of California Press, 1 (12), 1288.

Scaramuzza, P., & Barsi, J. (2005). Landsat 7 scan line corrector-off gap-filled product development. In *Proceeding of Pecora*, *16* (2), 23-27).

Scheelbeek, P. F., Dangour, A. D., Jarmul, S., Turner, G., Sietsma, A. J., Minx, J. C., & Berrang-Ford, L. (2021). The effects on public health of climate change adaptation responses: a systematic review of evidence from low- and middle-income countries. *Environmental Research Letters*, *16* (7), 073001.

Schinasi, L. H., Benmarhnia, T., & De Roos, A. J. (2018). Modification of the association between high ambient temperature and health by urban microclimate indicators: A systematic review and meta-analysis. *Environmental Research*, *161* (4), 168-180.

Schneeweiss, S. (2006). Sensitivity analysis and external adjustment for unmeasured confounders in epidemiologic database studies of therapeutics. *Pharmacoepidemiology and Drug Safety*, *15*(5), 291-303.

Schulte, P. A., & Chun, H. (2009). Climate change and occupational safety and health: establishing a preliminary framework. *Journal of Occupational and Environmental Hygiene*, *6* (9), 542-554.

Scott, A. A., Misiani, H., Okoth, J., Jordan, A., Gohlke, J., Ouma, G, & Waugh, D. W. (2017). Temperature and heat in informal settlements in Nairobi. *PLoS One*, *12* (1), 11.

Scott, R. W., & Huff, F. A. (1996). Impacts of the Great Lakes on regional climate conditions. *Journal of Great Lakes Research*, *22* (4), 845-863.

Seto, K. C., Reenberg, A., Boone, C. G., Fragkias, M., Haase, D., Langanke, T., & Simon, D. (2012). Urban land teleconnections and sustainability. *Proceedings of the National Academy of Sciences*, *109* (20), 7687-7692.

Sharma, R., Humphrey, J. L., Frueh, L., Kinnee, E. J., Sheffield, P. E., & Clougherty, J. E. (2023). Neighborhood violence and socioeconomic deprivation influence associations between acute air pollution and temperature on childhood asthma in New York City. *Environmental research*, *231*, 116235.

Shen, X., Wang, X., Zhang, Z., Lu, Z., & Lv, T. (2019). Evaluating the effectiveness of land use plans in containing urban expansion: An integrated view. *Land Use Policy*, *80* (7), 205-213.

Sheridan, S. C., & Allen, M. J. (2015). Changes in the frequency and intensity of extreme temperature events and human health concerns. *Current Climate Change Reports*, *1* (3), 155-162.

Sheridan, S. C., & Allen, M. J. (2018). Temporal trends in human vulnerability to excessive heat. *Environmental Research Letters*, *13* (4), 043001.

Sherwood, S. C., & Huber, M. (2010). An adaptability limit to climate change due to heat stress. *Proceedings of the National Academy of Sciences*, *107* (21), 9552-9555.

Shih, W. Y., Lung, S. C. C., & Hu, S. C. (2022). Perceived heat impacts and adaptive behaviours in different socio-demographic groups in the subtropics. *International Journal of Disaster Risk Reduction*, *71* (19), 102799.

Shindell, D., Ru, M., Zhang, Y., Seltzer, K., Faluvegi, G., Nazarenko, L., & Glick, A. (2021). Temporal and spatial distribution of health, labour, and crop benefits of climate change mitigation in the United States. *Proceedings of the National Academy of Sciences*, *118* (46), 2104061118.

Simwanda, M., Ranagalage, M., Estoque, R. C., & Murayama, Y. (2019). Spatial analysis of surface urban heat islands in four rapidly growing African cities. *Remote Sensing*, *11* (14), 1645.

Snyder, A. R., McLaughlin, D. K., & Findeis, J. (2006). Household composition and poverty among women-headed households with children: Differences by race and residence. *Rural Sociology*, *71* (4), 597-624.

Solecki, W., Seto, K. C., & Marcotullio, P. J. (2013). It's time for an urbanization science. *Environment: Science and Policy for Sustainable Development*, *55* (1), 12-17.

Song, J., Huang, B., Kim, J. S., Wen, J., & Li, R. (2020). Fine-scale mapping of an evidence-based heat health risk index for high-density cities: Hong Kong as a case study. *Science of the Total Environment*, *718* (3), 137226.

Srivastava, P. K., Han, D., Rico-Ramirez, M. A., Bray, M., & Islam, T. (2012). Selection of classification techniques for land use/land cover change investigation. *Advances in Space Research*, *50* (9), 1250-1265.

Steele, W., Hussey, K., & Dovers, S. (2017). What's critical about critical infrastructure? *Urban Policy and Research*, *35* (1), 74-86.

Stehman, S. V., & Foody, G. M. (2019). Key issues in rigorous accuracy assessment of land cover products. *Remote Sensing of Environment*, *231*, 111199.

Stephenne, N., Beaumont, B., Hallot, E., Lenartz, F., Lefebre, F., Lauwaet, D., & Wolff, E. (2017). Exposure and vulnerability geospatial analysis using earth observation data in the city of Liege, Belgium. *ISPRS Annals of the Photogrammetry, Remote Sensing and Spatial Information Sciences, 4* (4), 149.

Stern, N., & Stiglitz, J. E. (2021). *The social cost of carbon, risk, distribution, market failures: An alternative approach*. Cambridge, MA, USA: *National Bureau of Economic Research*, (1) 5, 11-23.

Stevens, B., Fiedler, S., Kinne, S., Peters, K., Rast, S., Müsse, J., & Mauritsen, T. (2017). MACv2-SP: A parameterization of anthropogenic aerosol optical properties and an associated Twomey effect for use in CMIP6. *Geoscientific Model Development, 10* (1), 433-452.

Stevens, F. R., Gaughan, A. E., Linard, C., & Tatem, A. J. (2015). Disaggregating census data for population mapping using random forests with remotely-sensed and ancillary data. *PLoS One, 10* (2), 0107042.

Stewart, I. D., & Oke, T. R. (2012). Local climate zones for urban temperature studies. *Bulletin of the American Meteorological Society, 93* (12), 1879-1900.

Stewart, I. D., Krayenhoff, E. S., Voogt, J. A., Lachapelle, J. A., Allen, M. A., & Broadbent, A. M. (2021). Time evolution of the surface urban heat island. *Earth's Future, 9* (10), 2178.

Stisen, S., Sandholt, I., Norgaard, A., Fensholt, R., & Eklundh, L. (2007). Estimation of diurnal air temperature using MSG SEVIRI data inWest Africa. *Remote Sensing of Environment, 10* (2), 262–274.

Strathearn, M., Osborne, N. J., & Selvey, L. A. (2022). Impact of low-intensity heat events on mortality and morbidity in regions with hot, humid summers: a scoping literature review. *International Journal of Biometeorology, 6* (11), 1-17.

Streutker, D. R. (2002). A remote sensing study of the urban heat island of Houston, Texas. *International Journal of Remote Sensing, 23* (13), 2595-2608.

Sulyman, A. O., & Danladi, A. A. (2021). Appraisal of Informal Access to Land for Housing Delivery in Karu Urban Area of Nasarawa State, Nigeria. *International Journal of Tropical Geography, 2* (7) 112-132.

Sun, Y., Li, Y., Ma, R., Gao, C., & Wu, Y. (2022). Mapping urban socio-economic vulnerability related to heat risk: A grid-based assessment framework by combing the geospatial big data. *Urban Climate, 43* (11), 101169.

Sy, I., Cissé, B., Ndao, B., Touré, M., Diouf, A. A., Sarr, M. A., & Ndione, J. A. (2022). Heat waves and health risks in the northern part of Senegal: analysing the distribution of temperature-related diseases and associated risk factors. *Environmental Science and Pollution Research*, *9* (1), 1-13.

Tafesse, B. (2021). Role of Pastoralists' Indigenous Knowledge in Drought Risk Reduction: Implications for Early Warning System and Adaptation Practices in Borana, Southern Ethiopia. *Ethiopian Journal of Agricultural Sciences*, *31* (3), 41-52.

Tan, J. (2008). Commentary: People's vulnerability to a heatwave. *International Journal of Epidemiology*, *37* (2), 318-320.

Tan, J., Yu, D., Li, Q., Tan, X., & Zhou, W. (2020). Spatial relationship between land-use/land-cover change and land surface temperature in the Dongting Lake area, China. *Scientific Reports*, *10* (1), 1-9.

Tan, J., Zheng, Y., Song, G., Kalkstein, L. S., Kalkstein, A. J., & Tang, X. (2007). Heat wave impacts on mortality in Shanghai, 1998 and 2003. *International Journal of Biometeorology*, *51* (3), 193-200.

Tan, J., Zheng, Y., Tang, X., Guo, C., Li, L., Song, G., & Chen, H. (2010). The urban heat island and its impact on heat waves and human health in Shanghai. *International Journal of Biometeorology*, *54* (1), 75-84.

Tang, R. L., Li, Z. L., & Tang, B. H. (2010). An application of the Ts-VI triangle method with enhanced edges determination for evapotranspiration estimation from MODIS data in arid and semi-arid regions: Implementation and validation. *Remote Sensing of Environment, 114* (95), 540–551.

Tarawally, M., Xu, W., Hou, W., & Mushore, T. D. (2018). Comparative analysis of responses of land surface temperature to long-term land use/cover changes between a coastal and Inland City: A case of Freetown and Bo Town in Sierra Leone. *Remote Sensing*, *10* (1), 112.

Tatem, A. J., Garcia, A. J., Snow, R. W., Noor, A. M., Gaughan, A. E., Gilbert, M., & Linard, C. (2013). Millennium development health metrics: where do Africa's children and women of childbearing age live? *Population Health Metrics*, *11* (1), 1-11.

Tebaldi, C., Debeire, K., Eyring, V., Fischer, E., Fyfe, J., Friedlingstein, P., & Ziehn, T. (2021). Climate model projections from the scenario model intercomparison project (ScenarioMIP) of CMIP6. *Earth System Dynamics*, *12* (1), 253-293.

Tewari, S., & Vinay, D. (2022). Workplace Heat Stress and Its Effect on Worker's Health Employed in Glass Manufacturing Unit. In *Technology Enabled Ergonomic Design*, *6* (9), 491-500.

Tian, L., Li, Y., Lu, J., & Wang, J. (2021). Review on urban heat island in China: Methods, its impact on buildings energy demand and mitigation strategies. *Sustainability*, *13* (2), 762.

Tomlinson, C. J., Chapman, L., Thornes, J. E., & Baker, C. J. (2011). Including the urban heat island in spatial heat health risk assessment strategies: a case study for Birmingham, UK. *International Journal of Health Geographics*, *10* (1), 1-14.

Toohey, R. C., Herman-Mercer, N. M., Schuster, P. F., Mutter, E. A., & Koch, J. C. (2016). Multidecadal increases in the Yukon River Basin of chemical fluxes as indicators of changing flow paths, groundwater, and permafrost. *Geophysical Research Letters*, *43* (23), 12-120.

Trærup, S. L., Ortiz, R. A., & Markandya, A. (2011). The costs of climate change: A study of cholera in Tanzania. *International Journal of Environmental Research and Public Health*, *8* (12), 4386-4405.

Tran, D. N., Van Quang, D., Nguyen, V. T., Khan, A., Thai, P. K., Huang, C., & Dung, P. (2020). Spatial patterns of health vulnerability to heatwaves in Vietnam. *International Journal of Biometeorology*, *64* (5), 863-872.

Turner, B. L., Matson, P. A., McCarthy, J. J., Corell, R. W., Christensen, L., Eckley, N., & Tyler, N. (2003). Illustrating the coupled human-environment system for vulnerability analysis: three case studies. *Proceedings of the National Academy of Sciences*, *100* (14), 8080-8085.

Tusting, L. S., Bisanzio, D., Alabaster, G., Cameron, E., Cibulskis, R., Davies, M., & Bhatt, S. (2019). Mapping changes in housing in sub-Saharan Africa from 2000 to 2015. *Nature*, *568* (7752), 391-394.

Tzavali, A., Paravantis, J. P., Mihalakakou, G., Fotiadi, A., & Stigka, E. (2015). Urban heat island intensity: A literature review. *Fresenius Environmental Bulletin*, *24* (12), 4537-4554.

Uddin, M. N., Islam, A. S., Bala, S. K., Islam, G. T., Adhikary, S., Saha, D., ... & Akter, R. (2019). Mapping of climate vulnerability of the coastal region of Bangladesh using principal component analysis. *Applied Geography*, *102* (7), 47-57.

Uejio, C. K., Wilhelmi, O. V., Golden, J. S., Mills, D. M., Gulino, S. P., & Samenow, J. P. (2011). Intra-urban societal vulnerability to extreme heat: the role of heat exposure and the built environment, socioeconomics, and neighborhood stability. *Health and place*, *17* (2), 498-507.

Ujoh, F., Kwabe, I. D., & Ifatimehin, O. O. (2011). Urban expansion and vegetal cover loss in and around Nigeria's Federal Capital City. *Journal of Ecology and the Natural Environment*, *3* (1), 1-10.

Umar, U. M., & Kumar, J. S. (2014). Spatial and temporal changes of urban heat island in Kano Metropolis, Nigeria. *International Journal of Engineering, Science and Technology*, *1* (3), 1-9.

UNFCCC. (2010). *United Nations Framework Convention on Climate Change: Full Text of the Convention*. United Nations Framework Convention on Climate Change. Bonn. Retrieved from http://unfccc.int/essential_background/convention/background/items/2536.php

UN-Habitat (United Nations Human Settlements Programme). (2014). The State of African Cities 2014. United Nations Human Settlements Programme, Nairobi, Kenya.

UN-Habitat. (2012). Planning and Design for Sustainable Urban Mobility: Global Report on Human Settlements. *Earth scan UN-HABITAT, Abingdon, and Oxon*, *3* (12), 13452.

United Nations. Framework Convention on Climate Change. Subsidiary Body for Scientific and Technological Advice. 46th session. Nairobi work programme on impacts, vulnerability and adaptation to climate change. Human health and adaptation: understanding climate impacts on health and opportunities for action. (2017). https://unfccc.int/sites/default/files/resource/docs/2017/sbsta/eng/02.pdf

USAID. Heat waves and human health: emerging evidence and experience to inform risk management in a warming world. (2019). https://www.climatelinks.org/sites/default/files/asset/document/2019_USAID-ATLAS_Heat-Waves-and-Human-Health.pdf.

Usmani, G., & Ahmad, N. (2018). Health status in India: A study of urban slum and non-slum population. *Journal of Nursing Research and Practice*, *2* (1), 09-14.

Uzzoli, A., Szilágyi, D., & Bán, A. (2018). Climate vulnerability regarding heat waves–A case study in Hungary. *DETUROPE: Central European Journal of Tourism and Regional Development*, *10* (3), 53-69.

Van Der Hoeven, F., & Wandl, A. (2015). Amsterdam: Mapping the land use, health, and energy-efficiency implications of the Amsterdam urban heat island. *Building Services Engineering Research and Technology*, *36* (1), 67-88.

Van Vuuren, D. P., Edmonds, J., Kainuma, M., Riahi, K., Thomson, A., Hibbard, K., & Rose, S. K. (2011). The representative concentration pathways: an overview. *Climatic change*, *109* (1), 5-31.

Van Vuuren, D. P., Stehfest, E., Gernaat, D. E., Doelman, J. C., Van den Berg, M., Harmsen, M., & Tabeau, A. (2017). Energy, land-use and greenhouse

gas emissions trajectories under a green growth paradigm. *Global Environmental Change*, *42* (9), 237-250.

Vancutsem, C., Ceccato, P., Dinku, T., & Connor, S. J. (2010). Evaluation of MODIS land surface temperature data to estimate air temperature in different ecosystems over Africa. *Remote Sensing of Environment*, *114* (3), 449–465.

Vani, M., & Prasad, P. (2020). Assessment of spatio-temporal changes in land use and land cover, urban sprawl, and land surface temperature in and around Vijayawada city, India. *Environment, Development, and Sustainability*, *22* (4), 3079-3095.

Vanos, J. K., Baldwin, J. W., Jay, O., & Ebi, K. L. (2020). Simplicity lacks robustness when projecting heat-health outcomes in a changing climate. *Nature Communications*, *11* (1), 1-5.

Vescovi, L., Rebetez, M., & Rong, F. (2005). Assessing public health risk due to extremely high-temperature events: climate and social parameters. *Climate Research*, *30* (1), 71-78.

Viana, C. M., Oliveira, S., Oliveira, S. C., & Rocha, J. (2019). Land use/land cover change detection and urban sprawl analysis. In *Spatial modeling in GIS and R for the earth and environmental sciences*, *11* (6), 621-651.

Voelkel, J., Hellman, D., Sakuma, R., & Shandas, V. (2018). Assessing vulnerability to urban heat: A study of disproportionate heat exposure and access to the refuge by socio-demographic status in Portland, Oregon. *International Journal of Environmental Research and Public Health*, *15* (4), 640.

Wang, J., Xue, P., Pringle, W., Yang, Z., & Qian, Y. (2022). Impacts of Lake Surface Temperature on the Summer Climate over the Great Lakes Region. *Journal of Geophysical Research: Atmospheres*, *2* (21), 36231.

Wang, L., & Chen, W. (2014). A CMIP5 multimodel projection of future temperature, precipitation, and climatological drought in China. *International Journal of Climatology*, *34* (6), 2059-2078.

Wang, R., Voogt, J., Ren, C., & Ng, E. (2022). Spatial-temporal variations of surface urban heat island: An application of local climate zone into large Chinese cities. *Building and Environment*, *222* (11), 109378.

Wang, Y., Li, X., Zhang, C., & He, W. (2022). Influence of spatiotemporal changes of impervious surface on the urban thermal environment: A case of Huai'an central urban area. *Sustainable Cities and Society*, *79* (4), 103710.

Wang, Y., Zhan, Q., & Ouyang, W. (2019). How to quantify the relationship between the spatial distribution of urban water bodies and land surface temperature? *Science of the Total Environment, 671* (1), 1-9.

Wang, Z., Meng, Q., Allam, M., Hu, D., Zhang, L., & Menenti, M. (2021). Environmental and anthropogenic drivers of surface urban heat island intensity: A case-study in the Yangtze River Delta, China. *Ecological Indicators, 128* (8), 107845.

Watkins, L. E., Wright, M. K., Kurtz, L. C., Chakalian, P. M., Mallen, E. S., Harlan, S. L., & Hondula, D. M. (2021). Extreme heat vulnerability in Phoenix, Arizona: A comparison of all-hazard and hazard-specific indices with household experiences. *Applied Geography, 131* (5), 102430.

Weber, S., Sadoff, N., Zell, E., & de Sherbinin, A. (2015). Policy-relevant indicators for mapping the vulnerability of urban populations to extreme heat events: A case study of Philadelphia. *Applied Geography, 63* (2), 231-243.

Weeramanthri, T. S., Quilty, S., & Campbell, S. (2021). Climate, extreme heat, and human health: risks and lessons for Australia. *Medical Journal of Australia, 3* (1), 1-3.

Wheeler, B. W., Lovell, R., Higgins, S. L., White, M. P., Alcock, I., Osborne, N. J., & Depledge, M. H. (2015). Beyond greenspace: an ecological study of population general health and indicators of natural environment type and quality. *International Journal of Health Geographics, 14* (1), 1-17.

Wilby, R. L., & Perry, G. L. (2006). Climate change, biodiversity, and the urban environment: a critical review based on London, UK. *Progress in Physical Geography, 30* (1), 73-98.

Williams, A. A., Spengler, J. D., Catalano, P., Allen, J. G., & Cedeno-Laurent, J. G. (2019). Building vulnerability in a changing climate: Indoor temperature exposures and health outcomes in older adults living in public housing during an extreme heat event in Cambridge, MA. *International Journal of Environmental Research and Public Health, 16* (13), 2373.

Wilson, B., & Chakraborty, A. (2019). Mapping vulnerability to extreme heat events: Lessons from metropolitan Chicago. *Journal of Environmental Planning and Management, 62* (6), 1065-1088.

Wiru, K., Oppong, F. B., Agyei, O., Zandoh, C., Nettey, O. E., Adda, R., & Asante, K. P. (2020). The influence of apparent temperature on mortality in the Kintampo Health and Demographic Surveillance area in the Middle Belt of Ghana: A retrospective time-series analysis. *Journal of Environmental and Public Health,* 2 (1), 1-9.

Wolf, T., & McGregor, G. (2013). The development of a heatwave vulnerability index for London, United Kingdom. *Weather and Climate Extremes*, *1* (1), 59-68.

Wolf, T., McGregor, G., & Analitis, A. (2014). Performance assessment of a heat wave vulnerability index for Greater London, United Kingdom. *Weather, Climate, and Society*, *6*, (1), 32-46.

World Bank. (2022). Sub-Saharan Africa-Macro Poverty Outlook: Country-by-Country Analysis and Projections for the Developing World, April 2022.

World Health Organization. (2020). *Report of the ninth meeting of the European Environment and Health Task Force. Bonn, 9–10 December 2019* (No. WHO/EURO: 2020-1392-41142-55939). World Health Organization. Regional Office for Europe.

Wright, C. Y., Kapwata, T., Du Preez, D. J., Wernecke, B., Garland, R. M., Nkosi, V., & Norval, M. (2021). Major climate change-induced risks to human health in South Africa. *Environmental Research*, *196* (11), 110973.

Wu, Z., Man, W., & Ren, Y. (2022). Influence of tree coverage and micro-topography on the thermal environment within and beyond a green space. *Agricultural and Forest Meteorology*, *316* (7), 108846.

Xian, G., & Crane, M. (2006). An analysis of urban thermal characteristics and associated land cover in Tampa Bay and Las Vegas using Landsat satellite data. *Remote Sensing of Environment*, *104* (2), 147-156.

Yahia, M. W., Johansson, E., Thorsson, S., Lindberg, F., & Rasmussen, M. I. (2018). Effect of urban design on microclimate and thermal comfort outdoors in warm-humid Dar es Salaam, Tanzania. *International Journal of Biometeorology*, *62* (3), 373-385.

Yang, J., Yin, P., Sun, J., Wang, B., Zhou, M., Li, M., & Liu, Q. (2019). Heatwave and mortality in 31 major Chinese cities: definition, vulnerability and implications. *Science of the Total Environment*, *649* (8), 695-702.

Yang, Z., Yang, J., Zhou, M., Yin, P., Chen, Z., Zhao, Q., & Ou, C. Q. (2021). Hourly temperature variability and mortality in 31 major Chinese cities: Effect modification by individual characteristics, season and temperature zone. *Environment International, 156* (1),106746.

Yao, N., Huang, C., Yang, J., Konijnendijk van den Bosch, C. C., Ma, L., & Jia, Z. (2020). Combined effects of impervious surface change and large-scale afforestation on the surface urban heat island intensity of Beijing, China based on remote sensing analysis. *Remote Sensing*, *12* (23), 3906.

Yao, X., Yu, K., Zeng, X., Lin, Y., Ye, B., Shen, X., & Liu, J. (2022). How can urban parks be planned to mitigate the urban heat island effect in "Furnace cities"? An accumulation perspective. *Journal of Cleaner Production, 330* (8), 129852.

Ye, Y., Zulu, E., Mutisya, M., Orindi, B., Emina, J., & Kyobutungi, C. (2009). Seasonal pattern of pneumonia mortality among under-five children in Nairobi's informal settlements. *The American Journal of Tropical Medicine and Hygiene, 81* (3), 770-775.

Yu, J., Castellani, K., Forysinski, K., Gustafson, P., Lu, J., Peterson, E., & Brauer, M. (2021). Geospatial indicators of exposure, sensitivity, and adaptive capacity to assess neighborhood variation in vulnerability to climate change-related health hazards. *Environmental Health, 20* (1), 1-20.

Yu, X., Guo, X., & Wu, Z. (2014). Land surface temperature retrieval from Landsat 8 TIRS—Comparison between radiative transfer equation-based method, split window algorithm and single channel method. *Remote sensing, 6* (10), 9829-9852.

Yue, W., Liu, X., Zhou, Y., & Liu, Y. (2019). Impacts of urban configuration on urban heat island: An empirical study in China mega-cities. *Science of the Total Environment, 671* (11), 1036-1046.

Yunus, S., & Adamu, F. (2018). Spatio-temporal dynamics of urban growth and its impact on the environment of the Federal Capital City of Nigeria (Abuja). *Dutse Journal of Pure and Applied Sciences, 4* (1), 130-142.

Zelinka, M. D., Myers, T. A., McCoy, D. T., Po-Chedley, S., Caldwell, P. M., Ceppi, P., & Taylor, K. E. (2020). Causes of higher climate sensitivity in CMIP6 models. *Geophysical Research Letters, 47* (1), 85782.

Zha, Y., Gao, J., & Ni, S. (2003). Use of normalized difference built-up index in automatically mapping urban areas from TM imagery. *International Journal of Remote Sensing, 24* (3), 583-594.

Zhang, M., Wang, H., Jin, W., & Dijk, M. P. V. (2019). Assessing heatwave vulnerability in Beijing and its districts, using a three-dimensional model. *International Journal of Global Warming, 17* (3), 297-314.

Zhang, W., McManus, P., & Duncan, E. (2018). A raster-based subdividing indicator to map urban heat vulnerability: A case study in Sydney and Australia. *International Journal of Environmental Research and Public Health, 15,* (11), 2516.

Zhang, W., Zheng, C., & Chen, F. (2019). Mapping heat-related health risks of elderly citizens in a mountainous area: A case study of Chongqing, China. *Science of the Total Environment, 663* (4), 852-866.

Zhang, X., Estoque, R. C., & Murayama, Y. (2017). An urban heat island study in Nanchang City, China-based on land surface temperature and social-ecological variables. *Sustainable Cities and Society*, *32* (2), 557-568.

Zhang, X., Li, Y., Cheng, Y., Wang, Y., Wang, Y., & Yao, X. (2021). Assessment of Regional Health Vulnerability to Extreme Heat. *China Centre for Disease Control, Weekly*, *3* (23), 490-494.

Zhang, Z., He, G., Wang, M., Long, T., Wang, G., Zhang, X., & Jiao, W. (2016). Towards an operational method for land surface temperature retrieval from Landsat 8 data. *Remote Sensing Letters*, *7* (3), 279-288.

Zhao, H., Tan, J., Ren, Z., & Wang, Z. (2020). Spatiotemporal characteristics of urban surface temperature and its relationship with landscape metrics and vegetation cover in rapid urbanization region. *Complexity*, *2 (2), 1-9*.

Zhao, Q., Guo, Y., Ye, T., Gasparrini, A., Tong, S., Overcenco, A., & Li, S. (2021). Global, regional, and national burden of mortality associated with non-optimal ambient temperatures from 2000 to 2019: a three-stage modelling study. *The Lancet Planetary Health*, *5* (7), 415-425.

Zhou, L., Dickinson, R. E., Tian, Y., Vose, R. S., & Dai, Y. (2007). Impact of vegetation removal and soil aridation on diurnal temperature range in a semiarid region: Application to the Sahel. *Proceedings of the National Academy of Sciences*, *104* (46), 17937-17942.

Zhou, X., & WANG, Y. C. (2011). Dynamics of land surface temperature in response to land-use/cover change. *Geographical Research*, *49* (1), 23-36.

Zhu, Q., Liu, T., Lin, H., Xiao, J., Luo, Y., Zeng, W., & Ma, W. (2014). The spatial distribution of health vulnerability to heatwaves in Guangdong Province, China. *Global Health Action*, *7* (1), 25051.

Zhu, X. X., Qiu, C., Hu, J., Shi, Y., Wang, Y., Schmitt, M., & Taubenböck, H. (2022). The urban morphology on our planet–Global perspectives from space. *Remote Sensing of Environment*, *269* (6), 112794.

Zhu, X., Song, X., Leng, P., Li, X., Gao, L., Guo, D., & Cai, S. (2021). A Framework for Generating High Spatiotemporal Resolution Land Surface Temperature in Heterogeneous Areas. *Remote Sensing*, *13* (19), 3885.

Zhu, Z., Zhou, Y., Seto, K. C., Stokes, E. C., Deng, C., Pickett, S. T., & Taubenböck, H. (2019). Understanding an urbanizing planet: Strategic directions for remote sensing. *Remote Sensing of Environment*, *228* (91), 164-182.

Zubair, O. A., Ojigi, L. M., & Mbih, R. A. (2015). Urbanization: A catalyst for the emergence of squatter settlements and squalor in the vicinities of the

federal capital city of Nigeria. *Journal of Sustainable Development*, *8* (2), 134.